

Chunquan Sheng · Gunda I. Georg
Editors

Targeting Protein-Protein Interactions by Small Molecules

 Springer

Targeting Protein-Protein Interactions by Small Molecules

Chunquan Sheng · Gunda I. Georg
Editors

Targeting Protein-Protein Interactions by Small Molecules

 Springer

Editors

Chunquan Sheng
School of Pharmacy
Second Military Medical University
Shanghai, China

Gunda I. Georg
College of Pharmacy
University of Minnesota
Minneapolis, MN, USA

ISBN 978-981-13-0772-0 ISBN 978-981-13-0773-7 (eBook)
<https://doi.org/10.1007/978-981-13-0773-7>

Library of Congress Control Number: 2018942928

© Springer Nature Singapore Pte Ltd. 2018

This work is subject to copyright. All rights are reserved by the Publisher, whether the whole or part of the material is concerned, specifically the rights of translation, reprinting, reuse of illustrations, recitation, broadcasting, reproduction on microfilms or in any other physical way, and transmission or information storage and retrieval, electronic adaptation, computer software, or by similar or dissimilar methodology now known or hereafter developed.

The use of general descriptive names, registered names, trademarks, service marks, etc. in this publication does not imply, even in the absence of a specific statement, that such names are exempt from the relevant protective laws and regulations and therefore free for general use.

The publisher, the authors and the editors are safe to assume that the advice and information in this book are believed to be true and accurate at the date of publication. Neither the publisher nor the authors or the editors give a warranty, express or implied, with respect to the material contained herein or for any errors or omissions that may have been made. The publisher remains neutral with regard to jurisdictional claims in published maps and institutional affiliations.

Printed on acid-free paper

This Springer imprint is published by the registered company Springer Nature Singapore Pte Ltd. The registered company address is: 152 Beach Road, #21-01/04 Gateway East, Singapore 189721, Singapore

Preface

Protein-protein interactions (PPIs) regulate a number of biological processes both in normal and disease states, providing a rich source of drug targets for the development of new generation of clinical therapeutics. However, the discovery and development of selective and drug-like small-molecule inhibitors are rather challenging as compared to traditional targets, due to large, flat, and hydrophobic features of the PPI interfaces. Despite the challenges, important progress has been made in the design strategies and clinical development of small-molecule PPI inhibitors. In recent years, with better understanding of the structural biology of PPIs, particularly the “hot spots” as critical interaction components for inhibitor design, the identification of drug-like PPIs inhibitors has been greatly accelerated. The development of PPI inhibitors as novel therapeutics is coming into reality. Bcl-2 inhibitor venetoclax and LFA-1/ICAM-1 inhibitor lifitegrast have been approved by the US FDA for clinical use, and a number of other small-molecule PPI inhibitors are currently under clinical evaluation. To summarize recent advances and guide future research, this book will comprehensively introduce state-of-the-art strategies of PPI-based drug discovery focusing on the developments of new methodologies. Moreover, representative case studies will illustrate how these technologies are applied in the discovery of small-molecule PPI inhibitors.

This book consists of two parts with twelve chapters. The first part deals with various discovery strategies of small-molecule PPI inhibitors, such as high throughput screening, hot spot-based design, computational approaches, and fragment-based drug design. The second part introduces recent advances made with small-molecule inhibitors focusing on clinical candidates and new PPI targets (*e.g.*, β catenin/T-cell factor, Keap1-Nrf2, and small GTPases). In every chapter, in-depth discussions and perspectives will be provided to inspire future research in this field. Also, a number of examples are from the contributions of the authors.

While several books have been published that cover PPI-based drug discovery, we felt that very few had been written from a medicinal chemist’s perspective. In this book, the medicinal chemistry efforts in the discovery of drug-like PPI inhibitors are highlighted. Also, a number of novel PPI targets and the newest case

studies are introduced for the first time. The authors of our chapters are highly experienced medicinal chemists in this field, and it is our hope that the readers of this book will gain an overview of discovery strategies and successful examples of small-molecule PPI inhibitors. Also, we hope that this book holds broad appeal and significant interest for the pharmaceutical science and medicinal chemistry communities.

As last time, we are very grateful to all chapter authors for their excellent work of assembling such a unique collection of important topics. Last but not least, we thank the publisher Wiley-VCH, in particular Heather Feng and June Tang, for their valuable contributions to this book.

Shanghai, China
Minneapolis, USA
February 2018

Chunquan Sheng
Gunda I. Georg

Contents

Part I Current Strategies for the Discovery of Small-Molecule Inhibitors of Protein-Protein Interactions

1 Overview of Protein-Protein Interactions and Small-Molecule Inhibitors Under Clinical Development	3
Guoqiang Dong and Chunquan Sheng	
2 High-Throughput Screening in the Discovery of Small-Molecule Inhibitors of Protein-Protein Interactions	29
Chunlin Zhuang and Chunquan Sheng	
3 Hot Spot-Based Design of Small-Molecule Inhibitors for Protein-Protein Interactions	53
Haitao Ji	
4 Computational Methods Applicable to the Discovery of Small-Molecule Inhibitors of Protein-Protein Interactions	73
Li Han and Renxiao Wang	
5 Experimental Methods Used for Identifying Small-Molecule Inhibitors of Protein-Protein Interaction	95
Mi Zhou, Qing Li, Wenna Kong and Renxiao Wang	
6 Fragment-Based Drug Discovery for Developing Inhibitors of Protein-Protein Interactions	135
Bing Xiong, Qi Wang and Jingkang Shen	

Part II Case Studies of Small-Molecule Inhibitors of Protein-Protein Interactions

- 7 Small Molecule Inhibitors Targeting New Targets of Protein-Protein Interactions** 179
Liyan Yue, Wei Wan, Pan Xu, Linjuan Li, Chen Wang,
Yuanyuan Zhang, Heng Xu, Rukang Zhang, Junchi Hu, Wenchao Lu,
Hao Jiang and Cheng Luo
- 8 The Development of New Spirooxindoles Targeting the p53–MDM2 Protein-Protein Interactions for Cancer Therapy** 213
Bin Yu and Hong-Min Liu
- 9 Small-Molecule Inhibitors for the β -Catenin/T Cell Factor Protein-Protein Interaction** 239
Yongqiang Zhang and Wei Wang
- 10 Discovery and Development of Keap1-Nrf2 Protein-Protein Interaction Inhibitors** 249
Zhengyu Jiang and Qidong You
- 11 BRDT Inhibitors for Male Contraceptive Drug Discovery: Current Status** 287
Zhenyuan Miao, Xianghong Guan, Jiewei Jiang and Gunda I. Georg
- 12 Targeting Protein-Protein Interactions in Small GTPases** 317
Jiahui Liu, Ning Kang, Yaxue Zhao and Mingyan Zhu

Contributors

Guoqiang Dong Department of Medicinal Chemistry, School of Pharmacy, Second Military Medical University, Shanghai, China

Gunda I. Georg Department of Medicinal Chemistry and Institute for Therapeutics Discovery and Development, University of Minnesota, Minneapolis, MN, USA

Xianghong Guan Department of Medicinal Chemistry and Institute for Therapeutics Discovery and Development, University of Minnesota, Minneapolis, MN, USA

Li Han State Key Laboratory of Bioorganic and Natural Products Chemistry, Shanghai Institute of Organic Chemistry, Chinese Academy of Sciences, Shanghai, People's Republic of China

Junchi Hu State Key Laboratory of Drug Research, Shanghai Institute of Materia Medica, Chinese Academy of Sciences, Shanghai, China

Haitao Ji Drug Discovery Department, H. Lee Moffitt Cancer Center and Research Institute, Tampa, FL, USA; Departments of Oncologic Sciences and Chemistry, University of South Florida, Tampa, FL, USA

Hao Jiang State Key Laboratory of Drug Research, Shanghai Institute of Materia Medica, Chinese Academy of Sciences, Shanghai, China

Jiewei Jiang Department of Medicinal Chemistry and Institute for Therapeutics Discovery and Development, University of Minnesota, Minneapolis, MN, USA

Zhengyu Jiang Jiangsu Key Laboratory of Drug Design and Optimization, Department of Medicinal Chemistry, School of Pharmacy, China Pharmaceutical University, Nanjing, Jiangsu, People's Republic of China

Ning Kang School of Pharmacy, Shanghai Jiao Tong University, Shanghai, People's Republic of China

Wenna Kong State Key Laboratory of Bioorganic and Natural Products Chemistry, Shanghai Institute of Organic Chemistry, Chinese Academy of Sciences, Shanghai, People's Republic of China

Linjuan Li State Key Laboratory of Drug Research, Shanghai Institute of Materia Medica, Chinese Academy of Sciences, Shanghai, China

Qing Li State Key Laboratory of Bioorganic and Natural Products Chemistry, Shanghai Institute of Organic Chemistry, Chinese Academy of Sciences, Shanghai, People's Republic of China

Hong-Min Liu Ministry of Education, Key Laboratory of Advanced Drug Preparation Technologies, Zhengzhou University, Zhengzhou, Henan, China; Co-innovation Center of Henan Province for New Drug Research & Development and Preclinical Safety, School of Pharmaceutical Sciences, Zhengzhou University, Zhengzhou, Henan, China

Jiahui Liu School of Pharmacy, Shanghai Jiao Tong University, Shanghai, People's Republic of China

Wenchao Lu State Key Laboratory of Drug Research, Shanghai Institute of Materia Medica, Chinese Academy of Sciences, Shanghai, China

Cheng Luo State Key Laboratory of Drug Research, Shanghai Institute of Materia Medica, Chinese Academy of Sciences, Shanghai, China

Zhenyuan Miao Second Military Medical University, Shanghai, China

Jingkang Shen Shanghai Institute of Materia Medica, Chinese Academy of Sciences, Shanghai, China

Chunquan Sheng Department of Medicinal Chemistry, School of Pharmacy, Second Military Medical University, Shanghai, China

Wei Wan State Key Laboratory of Drug Research, Shanghai Institute of Materia Medica, Chinese Academy of Sciences, Shanghai, China

Chen Wang State Key Laboratory of Drug Research, Shanghai Institute of Materia Medica, Chinese Academy of Sciences, Shanghai, China

Qi Wang Shanghai Institute of Materia Medica, Chinese Academy of Sciences, Shanghai, China

Renxiao Wang State Key Laboratory of Bioorganic and Natural Products Chemistry, Shanghai Institute of Organic Chemistry, Chinese Academy of Sciences, Shanghai, People's Republic of China; State Key Laboratory of Quality Research in Chinese Medicine, Macau Institute for Applied Research in Medicine and Health, Macau University of Science and Technology, Macau, People's Republic of China

Wei Wang School of Pharmacy, East China University of Science & Technology, Shanghai, China; Department of Chemistry & Chemical Biology, University of New Mexico, Albuquerque, NM, USA

Bing Xiong Shanghai Institute of Materia Medica, Chinese Academy of Sciences, Shanghai, China

Heng Xu State Key Laboratory of Drug Research, Shanghai Institute of Materia Medica, Chinese Academy of Sciences, Shanghai, China

Pan Xu State Key Laboratory of Drug Research, Shanghai Institute of Materia Medica, Chinese Academy of Sciences, Shanghai, China

Qidong You Jiangsu Key Laboratory of Drug Design and Optimization, Department of Medicinal Chemistry, School of Pharmacy, China Pharmaceutical University, Nanjing, Jiangsu, People's Republic of China

Bin Yu Ministry of Education, Key Laboratory of Advanced Drug Preparation Technologies, Zhengzhou University, Zhengzhou, Henan, China; Co-innovation Center of Henan Province for New Drug Research & Development and Preclinical Safety, School of Pharmaceutical Sciences, Zhengzhou University, Zhengzhou, Henan, China

Liyun Yue State Key Laboratory of Drug Research, Shanghai Institute of Materia Medica, Chinese Academy of Sciences, Shanghai, China

Rukang Zhang State Key Laboratory of Drug Research, Shanghai Institute of Materia Medica, Chinese Academy of Sciences, Shanghai, China

Yongqiang Zhang School of Pharmacy, East China University of Science & Technology, Shanghai, China

Yuanyuan Zhang State Key Laboratory of Drug Research, Shanghai Institute of Materia Medica, Chinese Academy of Sciences, Shanghai, China

Yaxue Zhao School of Pharmacy, Shanghai Jiao Tong University, Shanghai, People's Republic of China

Mi Zhou State Key Laboratory of Bioorganic and Natural Products Chemistry, Shanghai Institute of Organic Chemistry, Chinese Academy of Sciences, Shanghai, People's Republic of China

Mingyan Zhu School of Pharmacy, Shanghai Jiao Tong University, Shanghai, People's Republic of China

Chunlin Zhuang Department of Medicinal Chemistry, School of Pharmacy, Second Military Medical University, Shanghai, China

Part I
Current Strategies for the Discovery of
Small-Molecule Inhibitors of Protein-
Protein Interactions

Chapter 1

Overview of Protein-Protein Interactions and Small-Molecule Inhibitors Under Clinical Development



Guoqiang Dong and Chunquan Sheng

1.1 Introduction

Protein-protein interactions (PPIs) regulate a number of biological processes both in normal and disease states [1]. It is estimated that human interactome, the complex network of PPIs, contains about 130,000–650,000 types of PPI [2, 3]. The pivotal importance of PPIs makes them a rich source of targets for the development of novel therapeutic drugs. There are several ways to modulate PPI complexes including inhibition, stabilization, direct binding, and allosteric binding. A direct PPI modulator binds to the interaction surface of one protein, thereby sterically preventing or stabilizing the binding to its protein partner. In contrast, an allosteric modulator binds at a distant region outside of the protein interaction interface and remotely acts on the protein binding by triggering conformational change. For the type of binding effect, PPI inhibitors compete with one of the protein partners and prevent its binding, which represent a major approach in current PPI-based drug discovery. Another way to interfere with the PPI-associated biological functions is the stabilization of PPI complexes. PPI stabilizers bind to the regions at or near the PPI interface and promote the binding without competing with any of the protein partners [4]. Also, the therapeutic effects of PPI stabilizers are attracting increasing research interests [4–6]. Currently, most PPI modulators in clinical development are small-molecule inhibitors [7] and this chapter will mainly focus on design strategies and case studies of small-molecule PPI inhibitors.

G. Dong · C. Sheng (✉)

Department of Medicinal Chemistry, School of Pharmacy, Second Military Medical University, 325 Guohe Road, Shanghai 200433, China
e-mail: shengcq@smmu.edu.cn

© Springer Nature Singapore Pte Ltd. 2018

C. Sheng and G. I. Georg (eds.), *Targeting Protein-Protein Interactions by Small Molecules*, https://doi.org/10.1007/978-981-13-0773-7_1

1.2 Challenges in the Discovery of Small-Molecule PPI Inhibitors

Although PPIs represent promising targets for the development of new generation of clinical therapeutics, the design of selective and potent small-molecule inhibitors is rather challenging as compared to that for traditional targets (e.g., proteinase, kinases, G protein-coupled receptors) [8–10]. The nature of the PPI interfaces is significantly different from that of traditional drug targets, which have well-defined pockets for binding small molecules [11]. The PPI interface is generally large (about 1,500–3,000 Å²), flat (often exposed to solvent) [12], and dominated with hydrophobic and charged characteristics [13, 14]. Such features bring difficulties to discover small molecules that can effectively interrupt PPIs. First, a potent PPI inhibitor is required to have large molecular weight (MW) and high hydrophobicity so that it can cover a large and hydrophobic surface area. However, such a binder may have poor solubility and face pharmacokinetic problems. Second, the natural binder of a specific PPI interface is the protein counterpart itself, whose amino acids involved in PPIs are not contiguous. Thus, the protein or peptide involved in PPI cannot be used as a good starting point for the design and identification of small-molecule inhibitors. Third, existing compound libraries are mainly collected or constructed for traditional drug targets, which cannot effectively cover the chemical space of PPI inhibitors. Therefore, it is highly challenging to find a high-quality hit or lead through high-throughput screening (HTS) of PPI inhibitors. Moreover, validation of a PPI inhibitor from artifactual binding requires more biological assays than that for traditional targets.

1.3 Structures and Classifications of PPIs

Despite these challenges, remarkable progress has been achieved in the discovery and development of small-molecule PPI inhibitors [15–17]. The knowledge of the topological features of PPI interfaces is critically important for the identification of small-molecule inhibitors. Generally, PPI interface consists of a core region and a rim region [18]. According to the PPI buried surface area and binding affinity, PPI interfaces can be generally classified into four categories: “tight and wide,” “tight and narrow,” “loose and narrow,” and “loose and wide” [19]. The properties and examples of the four classes of PPIs are depicted in Table 1.1 and Fig. 1.1. Among them, the “narrow and tight” PPIs are more druggable to design small-molecule inhibitors, whereas the “loose and wide” is the most difficult to be targeted by small molecules.

In Arkin’s review, PPIs can be classified into primary peptide epitopes, secondary structure epitopes, and tertiary structural epitopes according to the complexity of epitopes (Table 1.2) [20]. The difficulties in identifying small-molecule inhibitors increase as the interface becomes more complex (from primary to tertiary

Table 1.1 Features of four classes of PPI interfaces according to the contact area and binding affinity

PPI type	Contact area (Å ²)	Affinity (K _d , nM)	Examples	Description
Tight and wide	>2500	<200	β-Catenin/Tcf4 Hsp70/NEF RGS4/Gα cMyc/Max	Large buried and convoluted (or discontinuous) contact areas with tight affinities. Difficult to be targeted by small-molecule inhibitors
Tight and narrow	<2500	<200	IL-2/IL-2Rα MDM2/p53 Bcl-2/BH3 XIAP/caspase 9	High affinity binding in a relatively small surface area. Deep pockets engaged by less than five hot spot residues. Excellent druggability
Loose and narrow	<2500	>200	Hsp70/Hsp40 Hsp90/TPR ZipA/FtsZ	Weak binding but relatively small contact areas. Transient interactions, relatively shallow binding pockets and difficult to obtain structural data. Challenging targets for small-molecules binding
Loose and wide	>2500	>200	Ras/SOS	Large surface areas and weak affinities. Particularly challenging for discovering small-molecule inhibitors

Abbreviations Tcf4, transcription factor 4; Hsp70, heat shock protein 70; NEF, nucleotide exchange factor; RGS4, G protein signaling 4; MAX, MYC-associated factor X; IL-2, interleukin-2; IL-2R, interleukin-2 receptor; MDM2, mouse double minute 2; Bcl, B-cell lymphoma; BH3, BCL-2 homology domain 3; XIAP, X-linked inhibitor of apoptosis protein; TPR, tetratricopeptide repeat; ZipA, cell division protein ZipA; FtsZ, filamenting temperature-sensitive mutant Z; Ras, a small GTP-binding protein; SOS, a guanine nucleotide exchange factor

epitopes). The primary peptide epitope consists of a primary linear protein as one side of the interface sequence. This type of PPI interface is particularly amenable to be targeted by drug-like small molecules. The secondary structure epitopes mainly include α-helix, β-sheet, and extended peptides. Key residues on the peptide are not continuous in the primary sequence, which are centered on two to three subpockets. The secondary structural epitopes have also been proven tractable to small-molecule inhibition. Tertiary structural epitopes require multiple sequences with discontinuous binding sites, which are the most challenging targets with limited successful examples.

More recently, Skidmore et al. divided PPIs into a series of structural classes including globular protein–globular protein interactions, globular protein–peptide interactions, and peptide–peptide interactions [21]. These structural classes can be further differentiated depending on whether the peptides have continuous epitope or

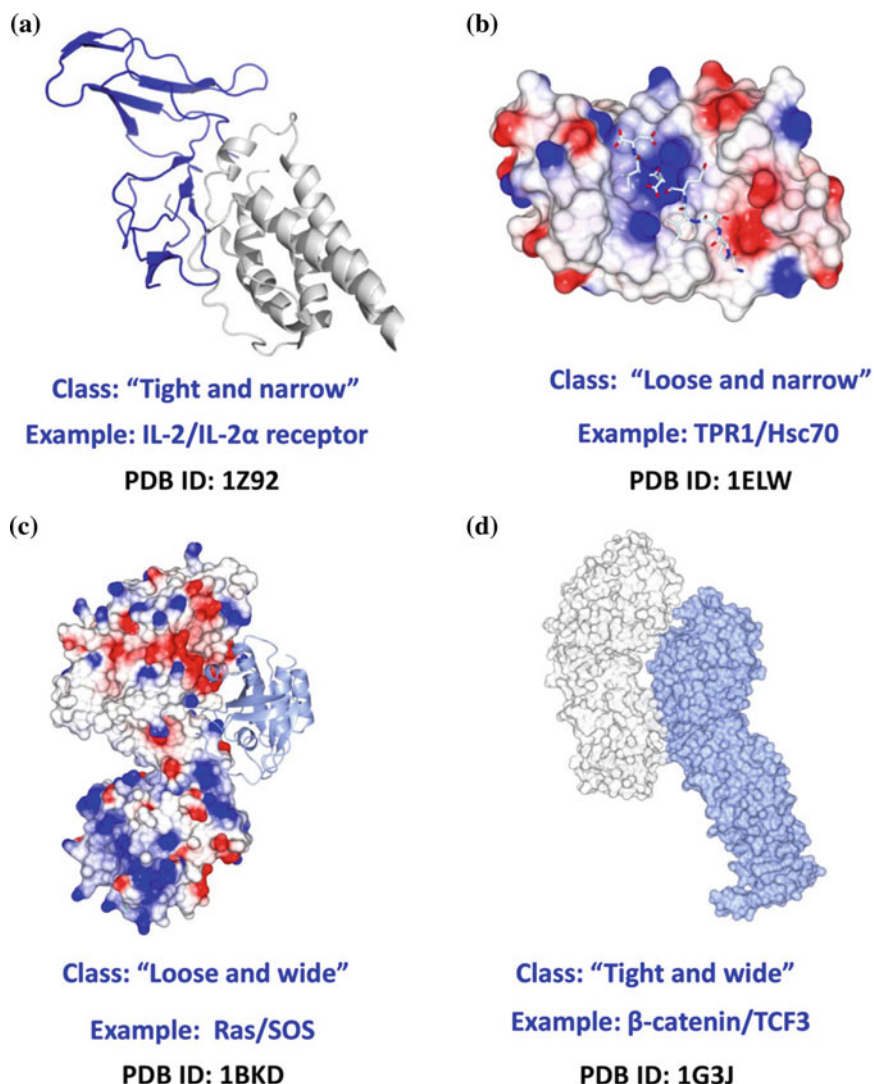


Fig. 1.1 Topological features of four classes of PPIs according to the PPI contact area and binding affinity

undergo substantial conformational changes upon binding (Fig. 1.2). PPIs between globular proteins are highly challenging for small-molecule drug discovery [22]. In contrast, globular protein–peptide interactions have been proven to be more drug-gable. The difficulty in targeting peptide–peptide interactions depends on whether there is a defined binding site.

1.4 “Hot Spots” as Structural Basis for the Design of Small-Molecule PPI Inhibitors

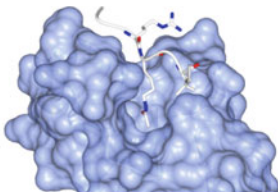
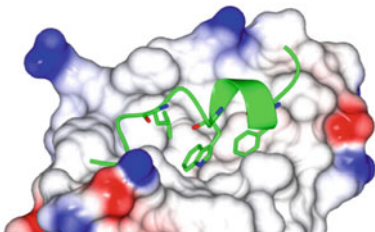
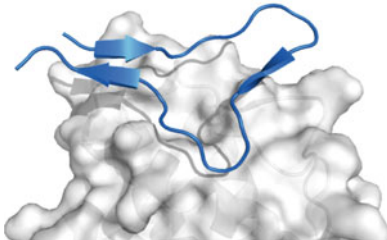
The concept of “hot spots” in PPI interfaces was introduced by Clackson and Wells in 1995 [23], which means a few key residues are responsible for the majority of the binding free energy in PPI [18, 23]. Notably, the surface area of “hot spots” is significantly smaller than the entire PPI interface [24]. Recent studies indicated that the existence of “hot spots” was prevalent in PPI interfaces [18]. They account for an average of 9.5% of the interfacial residues and are generally located in the core regions [25]. Another important feature of “hot spots” is the conformational change upon binding small molecules [26, 27]. When a small molecule binds to the PPI interface, the opening of so-called transient pockets that facilitate the ligand binding can be observed [28, 29]. “Hot spot” residues are highly adaptive with low energy barriers for conformational changes. The flexibility of “hot spots” for small-molecules binding has been observed in a number of PPI targets such as IL-2 receptor α (IL-2R α) [28], Bcl-X_L [30], HDM2 [31], and HPV-18-E2 [32]. “Hot spot” residues are often enriched in tryptophan (21%), arginine (13.3%), and tyrosine (12.3%), which allow adaptive conformational change and form various interactions to accommodate small molecules [25]. The existence and dynamic features of “hot spots” offer an opportunity to underscore the challenge to identify small-molecule PPI inhibitors.

The “hot spots” of PPI interfaces can be determined by alanine scanning mutagenesis [23, 25, 33] in combination with structural biology studies. The former can measure the contribution of each residue to the binding affinity with the partner protein by serially mutating each residue to alanine. Moreover, X-ray crystallography enables to provide key structural information about the distribution and orientation of these hot spot residues in PPI interfaces. Also, solving crystal structures of the target protein in free state and in complex with different ligands is helpful to understand the dynamic properties of the “hot spots,” which is highly valuable for inhibitor design. Computational methods, such as molecular dynamics (MD) simulations, are complementary tools to investigate the dynamic features of the “hot spots” [34–39].

1.5 Overview of Strategies for the Design of Small-Molecule PPI Inhibitors

Recently, important progress has been made in the discovery and development of small-molecule PPI inhibitors [20, 39–51]. Herein, state-of-the-art strategies of PPI-based drug discovery will be briefly introduced. More details about the advantages and limitations of the methodologies and successful examples can refer to our recent review [52]. The first step for the discovery of small-molecule PPI inhibitors is to determine the structure of the PPI interface (Fig. 1.3) [53]. Due to

Table 1.2 Properties and examples of primary, secondary, and tertiary epitopes

PPI Type	Description	Examples
Primary peptide epitopes	 <p>Example: Bromodomain/histone (PDB ID: 2WP1)</p> <p>Description: Short, continuous and linear peptides.</p>	LFA1/ICAM1 cIAP/SMAC Bromodomain/histone Integrase/LEDGF VHL/HIF1 α
Secondary structural epitopes	 <p>Example: MDM2/p53 (PDB ID: 1YCR)</p> <p>Description: α-Helix, β-sheet, and extended peptides</p>	Bel family/BH3 MDM2/p53 PDK1/PIF-tide Menin/MLL p300 CH1 domain/HIF1a
Tertiary structural epitopes	 <p>Example: IL-2/IL-2R (PDB: 1Z92)</p> <p>Description: discontinuous binding sites, and larger and shallower interfaces.</p>	IL-2/IL-2R α HPV11 E1/E2

the flexibility of PPI interface, the availability of structures from different statuses (unbound protein, protein-protein complex, protein-inhibitors complex) can significantly improve the efficiency of inhibitor design. Then, druggability assessment

Abbreviations LFA1, leukocyte function-associated molecule 1; ICAM1, intercellular adhesion molecule 1; IAP, inhibitor of apoptosis proteins; SMAC, second mitochondrial activator of caspases; LEDGF, lens endothelial growth factor; VHL, Von Hippel-Lindau disease tumor suppressor; HIF1 α , hypoxia-inducible factor 1 α ; PDK1, 3-phosphoinositide-dependent protein kinase-1; PIF-tide, PDK1-interacting fragment; menin, a tumor suppressor associated with multiple endocrine neoplasia type 1; MLL, mixed lineage leukemia; CH1, cysteine-histidine-rich 1; HPV11, human papilloma virus-11; E1, a kind of replication initiation factor; E2, a kind of transcription factor

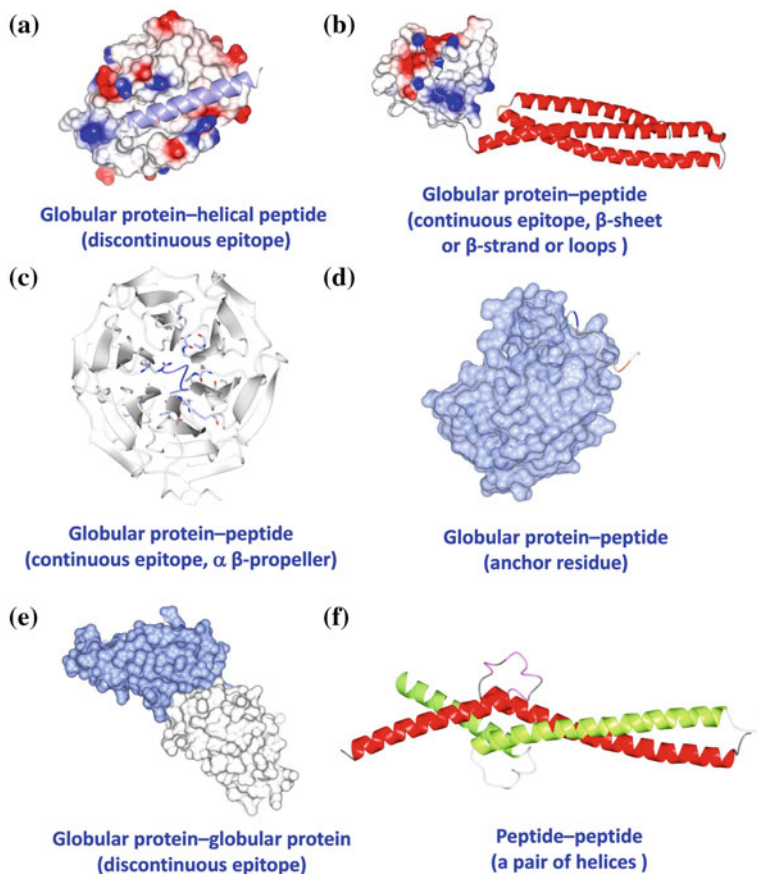


Fig. 1.2 Classification of PPIs and examples. **a** Bcl-X_L-BAD (PDB ID: 2XA0); **b** XIAP-SMAC (PDB ID: 1G73); **c** KEAP1 (Kelch-like ECH-associated protein 1)-NRF2 (nuclear factor erythroid 2-related factor 2) (PDB ID: 2DYH); **d** bromodomains (PDB ID: 3UVW); **e** IL-2-IL-2R (PDB ID: 1Z92); **f** MYC-MAX (PDB ID: 1NKP)

is necessary to evaluate whether the protein has well-defined binding sites or pockets to accommodate small molecules because the success in designing PPI inhibitors largely depends on the target type [54]. The next important step is the

identification of the “hot spots” on the PPI interface [55, 56]. After establishing assays for biological evaluation, the strategy to discover initial hits depends on the properties of PPI hot spots. Currently, screening strategies, designing strategies, and synthetic strategies represent three major methods for small-molecule PPI inhibitor discovery. Screening strategies mainly include HTS, fragment screening, and virtual screening [39], which aim to discover PPI inhibitors from known compound libraries. Among them, fragment screening in combination with fragment-based drug design (FBDD) has the advantages of higher hit rate and better ligand efficiency (LE). Designing strategies focus on building novel small molecules to mimic the key interactions of the hot spot residues, which are used as the starting points for substructure search, bioisostere design, and de novo design. Besides hot spot residues, key secondary structure motif (i.e., α -helix, β -turn, and β -strand) involved in PPI interface can also be for inhibitor design. A new scaffold decorated with the side chains of hot spot residues is designed to mimic spatial orientation and interactions of the original secondary structure. Synthetic strategies aim to explore new chemical space for PPI inhibitor screening by developing efficient synthetic methods to construct new libraries with chemical diversity and complexity. When initial hits are available, validation studies are necessary to exclude false positives. Secondary assays to determine the kinetic and thermodynamic parameters (e.g., association and dissociation rates) as well as solving the structures of protein–hit complexes are important for selecting suitable hits for further optimization. Structural optimization of the hits and leads aims to improve the binding affinity, therapeutic effects, and drug-likeness, and the strategies are similar to those for traditional targets. Finally, drug candidates can be obtained for preclinical and clinical trials until they are marked for therapeutic application.

1.6 Small-Molecule PPI Inhibitors Under Clinical Development

The discovery and development of PPIs inhibitors have been greatly accelerated with better understanding of the structure and functions of PPIs and numerous medicinal chemistry efforts in this field [57]. Up to now, a great number of highly potent small-molecule PPI inhibitors have been identified and several of them are marketed or under different stages of clinical evaluations. According to a recent review by Abell and Skidmore [21], small-molecule PPI inhibitors in clinical development are summarized in Table 1.3. On April 11, 2016, venetoclax (ABT-199) was approved by FDA for the treatment of chronic lymphocytic leukemia (CLL) with 17p deletion, which represents the first marketed small-molecule PPI inhibitor [58]. Subsequently, lifitegrast (SAR 1118) [59], a small-molecule inhibitor of LFA-1/ICAM-1, was approved for the treatment of dry eye syndrome on July 11, 2016. Here, the drug discovery and medicinal chemistry optimization process of venetoclax and lifitegrast were briefly introduced.

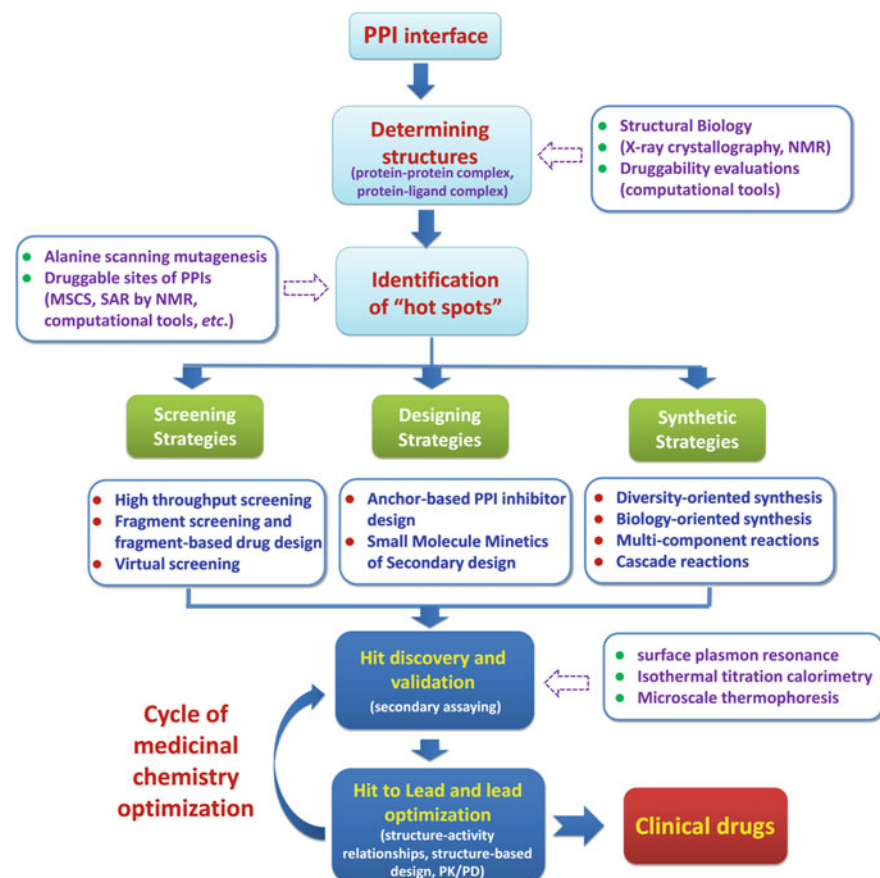


Fig. 1.3 Current strategies for the design and development of small-molecule PPI inhibitors

1.6.1 Fragment-Based Discovery of Bcl-2 Inhibitor Venetoclax

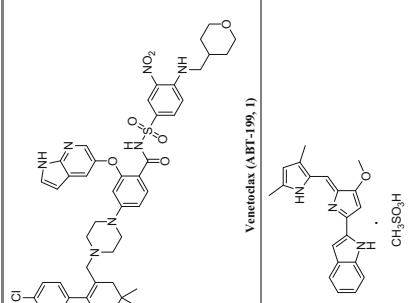
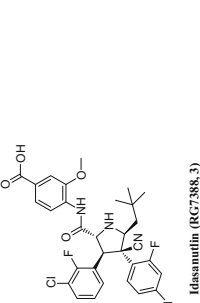
The discovery and development of Bcl-2 inhibitor venetoclax represent one of the most successful examples of PPI-based drug discovery [91]. Bcl (B-cell lymphoma) family of proteins (e.g., Bcl-X_L, Bcl-2, Bcl-w, and Mcl-1) is anti-apoptotic proteins, whose interactions with pro-apoptotic proteins such as Bak, Bax, and Bad play key roles in both normal and abnormal apoptotic processes [92]. Initial drug discovery efforts were focused on the non-selective Bcl-2/Bcl-X_L/Bcl-w inhibitor navitoclax (ABT-263) [93]. NMR structural studies revealed that the Bcl-X_L/BAK interface was a long and hydrophobic groove [94]. The “hot spots” include several hydrophobic and charged residues (e.g., Ile85, Leu78, and Asp83). ABT-263 was discovered by a combination of NMR-based fragment screening, parallel synthesis

and structure-based design and ADME optimization. Initially, the research group from Abbot screened a library containing 10,000 fragments using ^{15}N HSQC NMR spectroscopy [95]. Weak fragment hits **31** ($K_i = 300 \mu\text{M}$) and **32** ($K_i = 4,300 \mu\text{M}$) were found to occupy two different subsites of Bcl- X_L (Fig. 1.4) [96]. Guided by the structural information of Bcl- X_L /fragment complexes, the two fragment hits were linked by the acylsulfonamide group to maintain the key interactions and followed by optimization of the substitution of acylsulfonamide to yield inhibitor **33** ($K_i = 36 \mu\text{M}$) with improved affinity with Bcl- X_L . Further structure-based optimization of lead compound **33** led to the discovery of ABT-737 (**34**) as a highly potent Bcl- X_L inhibitor ($K_i \leq 1 \text{ nM}$), which successfully mimicked the α -helical BH3 domain of BAK [30, 97, 98]. However, ABT-737 is not orally bioavailable and subsequent medicinal chemistry optimizations generated clinical candidate ABT-263 (**35**) [99]. ABT-263 showed subnanomolar affinities for Bcl-2, Bcl-XL, and Bcl-W with improved bioavailability [100]. Surprisingly, ABT-263 performed poorly in clinical trials probably due to its non-selective profile. Thus, further clinical evaluations were performed on the selective Bcl-2 inhibitor venetoclax [101, 102]. Venetoclax selectively blocks Bcl-2 protein, leading to programmed cell death of CLL cells.

1.6.2 Discovery of LFA-1/ICAM-1 Inhibitor Lifitegrast for the Treatment of Dry Eye Syndrome

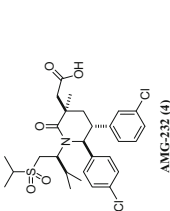
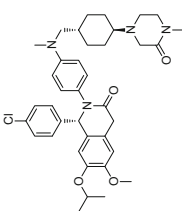
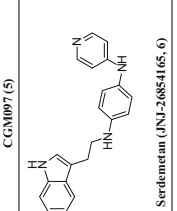
The PPI between LFA-1 and ICAM-1 is essential in lymphocyte and immune system function. Small-molecule LFA-1/ICAM-1 inhibitors can be used to develop novel drugs for the treatment of dry eye. The ICAM-1 epitope containing discontinuous residues Glu34, Lys39, Met64, Tyr66, Asn68, and Gln73 was identified as “hot spots.” Gadek et al. designed compounds **36** ($\text{IC}_{50} = 47 \text{ nM}$) and **37** ($\text{IC}_{50} = 1.4 \text{ nM}$) as potent LFA-1 inhibitors. Their structures were embedded with the carboxylic acid, sulfide, phenol, and carboxamide groups to mimic the ICAM-1 hot spots (Fig. 1.5) [103]. Structure–activity relationship (SAR) analysis revealed that the inhibitors shared a “left-wing”–“central scaffold”–“right-wing” structural mode. Based on this assumption, Zhong et al. designed bicyclic tetrahydroisoquinoline (THIQ) as the central scaffold and discovered a highly active LFA-1 inhibitor **38** ($\text{IC}_{50} = 9 \text{ nM}$) with good in vivo efficacy [104]. Further optimization studies were focused on improving pharmacokinetic profiles and successfully discovered lifitegrast (**9**) as a new drug for the treatment of dry eye [59, 105].

Table 1.3 Overview of representative small-molecule PPI inhibitors in clinical application or clinical development

Compound name and chemical structures	MW	Target (activity)	Therapeutic area	Status	Discovery strategy	References
 <p>Venetoclax (ABT-199, 1)</p> <p>Obatoclax mesylate (GX15-070, 2)</p>	868.44	Bcl protein family Bcl-2 ($K_i \leq 0.01$ nM) Bcl-xL ($K_i = 48$ nM) Bcl-w ($K_i = 245$ nM) Mcl-1 ($K_i > 4444$ nM)	Cancer	Approved	FBDD	[60]
 <p>Idasanutlin (RC7388, 3)</p>	616.48	MDM2-p53 MDM2 ($K_i = 30$ nM)	Cancer	Phase 3	HTS	[62]

(continued)

Table 1.3 (continued)

Compound name and chemical structures	MW	Target (activity)	Therapeutic area	Status	Discovery strategy	References
 AMG-232 (4)	568.55	MDM2-p53 MDM2 ($K_i = 0.045$ nM)	Cancer	Phase 2	SBDD	[63]
 CGM097 (5)	659.26	MDM2-p53 MDM2 ($K_i = 1.6$ nM)	Cancer	Phase 1	Virtual screening	[64]
 Sildenafil (JNJ-26854165, 6)	328.41	MDM2-p53 (no activity reported)	Cancer	Phase 1	Virtual screening	[65, 66]
 RG7112 (7)	726.80	MDM2 ($K_i = 10.7$ nM)	Cancer	Phase 1 (discontinued)	HTS	[67, 68]

(continued)

Table 1.3 (continued)

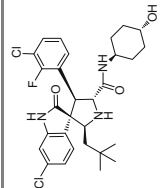
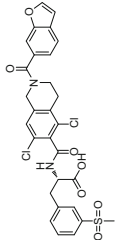
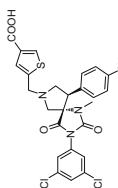
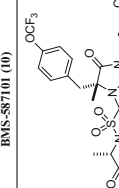
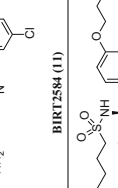
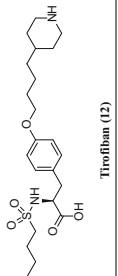
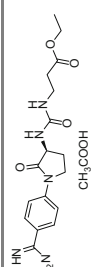
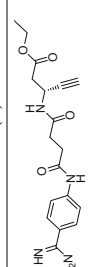
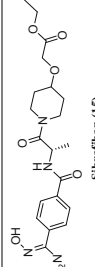
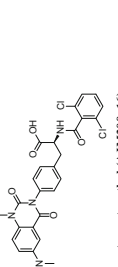
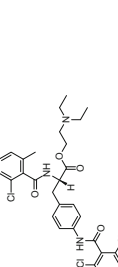
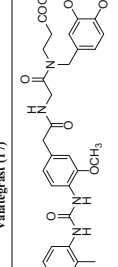
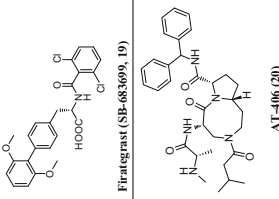
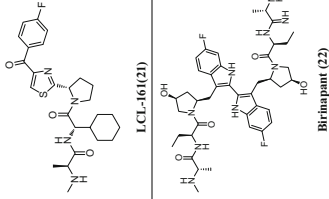
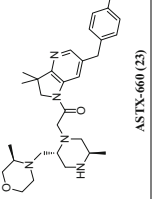
Compound name and chemical structures	MW	Target (activity)	Therapeutic area	Status	Discovery strategy	References
 SAR-405838 (8)	562.50	MDM2 ($K_i = 0.88$ nM)	Cancer	Phase 1 (discontinued)	SBDD	[69]
 LFA1-ICAMI LFA-1	615.48	LFA1-ICAMI LFA-1 ($IC_{50} = 9$ nM)	Dry eye	Approved	SBDD	[65]
 Liffitegrast (SAR 1118, 9)	555.43	LFA-1 ($IC_{50} = 20$ nM)	Psoriasis	Phase 2 (discontinued)	SBDD	[70, 71]
 BMS-587101 (10)	606.40	LFA-1 ($K_i < 10$ μ M)	Psoriasis	Phase 2 (discontinued)	SBDD	[72]
 BIRT2584 (11)	440.60	α IIb β 3 ($IC_{50} = 32$ nM)	Cardiovascular	Approved	Virtual screening	[73]
 Tirofiban (12)						(continued)

Table 1.3 (continued)

Compound name and chemical structures	MW	Target (activity)	Therapeutic area	Status	Discovery strategy	References
 Orbioflan (13)	421.45	α IIb β 3 (IC ₅₀ = 80 nM)	Cardiovascular area	Phase 3 (discontinued)	Peptidomimetics and SBDD	[74]
 Xenifiban (14)	358.39	α IIb β 3 (IC ₅₀ = 67 nM)	Cardiovascular	Phase 3 (discontinued)	Peptidomimetics and SBDD	[75]
 Sibrafiban (15)	420.46	α IIb β 3 (IC ₅₀ = 38 nM)	Cardiovascular	Phase 3 (discontinued)	Peptidomimetics and SBDD	[76]
 Carotegrast methyl (AJM300, 16)	555.41	α 4 β 1/ α 4 β 7 (IC ₅₀ range: 0.94 nM ~ 26 nM)	Ulcerative colitis	Phase 3	Peptidomimetics	[77]
 Valategrast (17)	604.95	α 2 β 1 (IC ₅₀ = 0.214 μ M)	Asthma	Phase 2 (discontinued)	Virtual screening	[78]
 IVL-745 (18)	592.64	α 4 β 1 (IC ₅₀ < 100 nM)	Asthma	Phase 2 (discontinued)	Virtual screening	[79, 80]

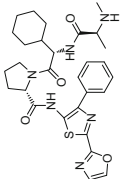
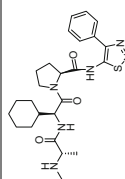
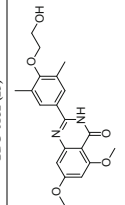
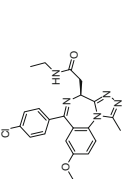
(continued)

Table 1.3 (continued)

Compound name and chemical structures	MW	Target (activity)	Therapeutic area	Status	Discovery strategy	References
 <p>Firazegran (SB-683609, 19)</p> <p>AT-406 (20)</p>	474.33	<p>α4β7-CS1 (IC₅₀ = 0.077 μM)</p> <p>α4β1-CS1 (IC₅₀ = 0.85 μM)</p> <p>IAPs</p> <p>c-IAP1 (K_i = 1.9 nM)</p> <p>c-IAP2 (K_i = 5.1 nM)</p> <p>XIAP (K_i = 66.4 nM)</p>	Multiple sclerosis	Phase 2 (discontinued)	Peptidomimetics	[81]
 <p>LCL-161 (21)</p> <p>Birinapant (22)</p>	500.63	<p>IAPs (no activity reported)</p> <p>IAPs</p> <p>c-IAP1 (K_i < 1 nM)</p> <p>c-IAP2 (K_i = 36 nM)</p> <p>XIAP (K_i = 45 nM)</p>	Cancer	Phase 2	Peptidomimetics and SBDD	[83]
 <p>ASTX-660 (23)</p>	509.66	<p>IAPs</p> <p>c-IAP1 (EC₅₀ = 0.32 nM), XIAP (EC₅₀ = 5.1 nM)</p>	Cancer	Phase 2	SBDD and virtual screening	[84]

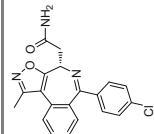
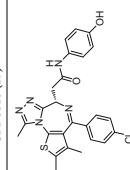
(continued)

Table 1.3 (continued)

Compound name and chemical structures	MW	Target (activity)	Therapeutic area	Status	Discovery strategy	References
 <p>CLDC-427 (24)</p>	564.7	IAPs c-IAP1, c-IP2 and XIAP ($K_i < 60$ nM)	Cancer	Phase 1	SBDD	[85]
 <p>GDC-0152 (25)</p>	498.64	IAPs c-IAP1 ($K_i = 17$ nM) c-IAP2 ($K_i = 43$ nM) XIAP ($K_i = 28$ nM) ML-IAP ($K_i = 14$ nM)	Cancer	Phase 1 (discontinued)	SBDD	[86]
 <p>Apabetalone (RXX-208, 26)</p>	370.4	BET BRD—bromodomain BRD2-4 (IC_{50} range: 1.9–7.7 nM)	Cardiovascular	Phase 3	Screening	[87]
 <p>GSK525762 (27)</p>	423.9	BET BRD—bromodomain BRD2-4 (IC_{50} range: 32.5–42.5 nM)	Cancer	Phase 2	Screening	[88]

(continued)

Table 1.3 (continued)

Compound name and chemical structures	MW	Target (activity)	Therapeutic area	Status	Discovery strategy	References
 CPI-0610 (29)	365.81	BET BRD—bromodomain BRD4 (IC ₅₀ = 39 nM)	Cancer	Phase 1	FBDD	[89]
 OTX015 (MK-8628, 30)	491.99	BET BRD—bromodomain BRD2-4 (IC ₅₀ range: 10–19 nM)	Cancer	Phase 1	SBDD	[90]

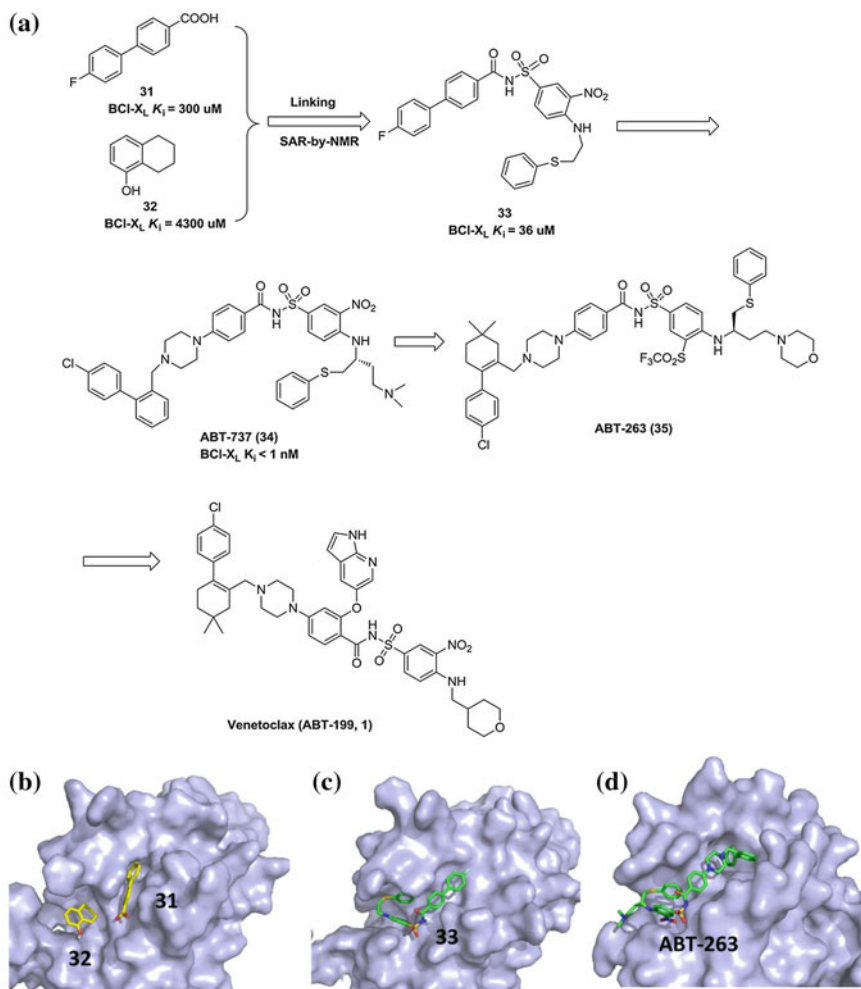


Fig. 1.4 Fragment-based design of Bcl-2 inhibitor venetoclax (a). The binding modes of the Bcl-X_L inhibitors (b–d) were generated from the crystal structures in PDB database (PDB codes: 1YSG, 1YSI, and 2YXJ)

1.7 Conclusions

With the progress of structural biology studies of PPIs, the identification of “hot spots” for inhibitor design as well as numerous medicinal chemistry efforts, the development of small-molecule PPI inhibitors has come into reality with two marketed drugs and a number of clinical candidates. The encouraging success has attracted increasing interests and activities from both pharmaceutical industry and academia. Deeper understanding of the structures, functions, and dynamics of PPIs

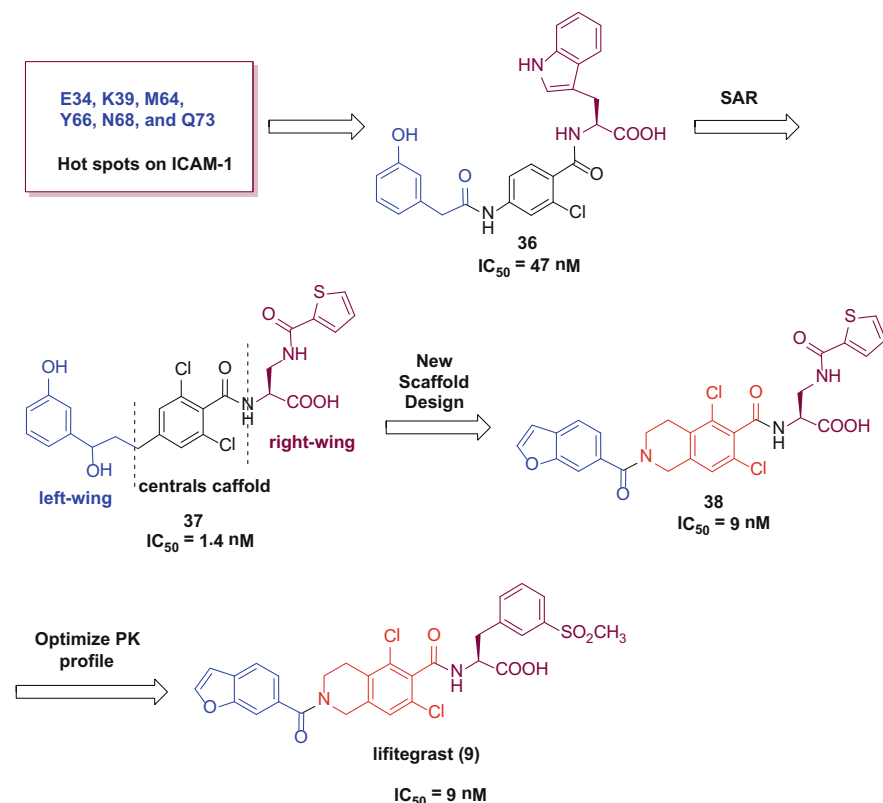


Fig. 1.5 Drug design process of LFA-1/ICAM-1 inhibitor lifitegrast

is highly desirable to improve the efficiency of PPI-based drug discovery. Also, the drug design principles and drug-like criteria for PPI inhibitors need to be further investigated. Taken together, with increasing knowledge and experience gained for small-molecule PPI inhibitors, more challenging PPI targets will become accessible to drug discovery. It is expected that more PPI inhibitors will come into clinical application in the near future.

References

1. Arkin MR, Wells JA (2004) Small-molecule inhibitors of protein-protein interactions: progressing towards the dream. *Nat Rev Drug Discov* 3(4):301–317
2. Stumpf MP, Thorne T, de Silva E, Stewart R, An HJ, Lappe M, Wiuf C (2008) Estimating the size of the human interactome. *Proc Natl Acad Sci USA* 105(19):6959–6964
3. Venkatesan K, Rual JF, Vazquez A, Stelzl U, Lemmens I, Hirozane-Kishikawa T, Hao T, Zenkner M, Xin X, Goh KI, Yildirim MA, Simonis N, Heinzmann K, Gebreab F,

- Sahalie JM, Cevik S, Simon C, de Smet AS, Dann E, Smolyar A, Vinayagam A, Yu H, Szeto D, Borick H, Dricot A, Klitgord N, Murray RR, Lin C, Lalowski M, Timm J, Rau K, Boone C, Braun P, Cusick ME, Roth FP, Hill DE, Tavernier J, Wanker EE, Barabasi AL, Vidal M (2009) An empirical framework for binary interactome mapping. *Nat Methods* 6 (1):83–90
4. Thiel P, Kaiser M, Ottmann C (2012) Small-molecule stabilization of protein-protein interactions: an underestimated concept in drug discovery? *Angew Chem Int Ed Engl* 51 (9):2012–2018
 5. Milroy LG, Bartel M, Henen MA, Leysen S, Adriaans JM, Brunsveld L, Landrieu I, Ottmann C (2015) Stabilizer-Guided Inhibition of Protein-Protein Interactions. *Angew Chem Int Ed Engl* 54(52):15720–15724
 6. Zarzycka B, Kuenemann MA, Miteva MA, Nicolaes GA, Vriend G, Sperandio O (2016) Stabilization of protein-protein interaction complexes through small molecules. *Drug Discov Today* 21(1):48–57
 7. Mullard A (2012) Protein-protein interaction inhibitors get into the groove. *Nat Rev Drug Discov* 11(3):173–175
 8. Whitty A, Kumaravel G (2006) Between a rock and a hard place? *Nat Chem Biol* 2(3):112–118
 9. Chene P (2006) Drugs targeting protein-protein interactions. *ChemMedChem* 1(4):400–411
 10. Fry DC (2008) Drug-like inhibitors of protein-protein interactions: a structural examination of effective protein mimicry. *Curr Protein Pept Sci* 9(3):240–247
 11. Cheng AC, Coleman RG, Smyth KT, Cao Q, Soulard P, Caffrey DR, Salzberg AC, Huang ES (2007) Structure-based maximal affinity model predicts small-molecule druggability. *Nat Biotechnol* 25(1):71–75
 12. Blundell TL, Burke DF, Chirgadze D, Dhanaraj V, Hyvonen M, Innis CA, Parisini E, Pellegrini L, Sayed M, Sibanda BL (2000) Protein-protein interactions in receptor activation and intracellular signalling. *Biol Chem* 381(9–10):955–959
 13. Jones S, Thornton JM (1996) Principles of protein-protein interactions. *Proc Natl Acad Sci USA* 93(1):13–20
 14. Lo Conte L, Chothia C, Janin J (1999) The atomic structure of protein-protein recognition sites. *J Mol Biol* 285(5):2177–2198
 15. Wells JA, McClendon CL (2007) Reaching for high-hanging fruit in drug discovery at protein-protein interfaces. *Nature* 450(7172):1001–1009
 16. Buchwald P (2010) Small-molecule protein-protein interaction inhibitors: therapeutic potential in light of molecular size, chemical space, and ligand binding efficiency considerations. *IUBMB Life* 62(10):724–731
 17. Jubb H, Higuero AP, Winter A, Blundell TL (2012) Structural biology and drug discovery for protein-protein interactions. *Trends Pharmacol Sci* 33(5):241–248
 18. Moreira IS, Fernandes PA, Ramos MJ (2007) Hot spots—a review of the protein-protein interface determinant amino-acid residues. *Proteins* 68(4):803–812
 19. Smith MC, Gestwicki JE (2012) Features of protein-protein interactions that translate into potent inhibitors: topology, surface area and affinity. *Expert Rev Mol Med* 14:e16
 20. Arkin MR, Tang Y, Wells JA (2014) Small-molecule inhibitors of protein-protein interactions: progressing toward the reality. *Chem Biol* 21(9):1102–1114
 21. Scott DE, Bayly AR, Abell C, Skidmore J (2016) Small molecules, big targets: drug discovery faces the protein-protein interaction challenge. *Nat Rev Drug Discov* 15(8):533–550
 22. Jubb H, Blundell TL, Ascher DB (2015) Flexibility and small pockets at protein-protein interfaces: new insights into druggability. *Prog Biophys Mol Biol* 119(1):2–9
 23. Clackson T, Wells JA (1995) A hot spot of binding energy in a hormone-receptor interface. *Science* 267(5196):383–386
 24. Keskin O, Gursoy A, Ma B, Nussinov R (2008) Principles of protein-protein interactions: what are the preferred ways for proteins to interact? *Chem Rev* 108(4):1225–1244

25. Bogan AA, Thorn KS (1998) Anatomy of hot spots in protein interfaces. *J Mol Biol* 280 (1):1–9
26. DeLano WL, Ultsch MH, de Vos AM, Wells JA (2000) Convergent solutions to binding at a protein-protein interface. *Science* 287(5456):1279–1283
27. Atwell S, Ultsch M, De Vos AM, Wells JA (1997) Structural plasticity in a remodeled protein-protein interface. *Science* 278(5340):1125–1128
28. Arkin MR, Randal M, DeLano WL, Hyde J, Luong TN, Oslob JD, Raphael DR, Taylor L, Wang J, McDowell RS, Wells JA, Braisted AC (2003) Binding of small molecules to an adaptive protein-protein interface. *Proc Natl Acad Sci USA* 100(4):1603–1608
29. Eyrisch S, Helms V (2009) What induces pocket openings on protein surface patches involved in protein-protein interactions? *J Comput Aided Mol Des* 23(2):73–86
30. Bruncko M, Oost TK, Belli BA, Ding H, Joseph MK, Kunzer A, Martineau D, McClellan WJ, Mitten M, Ng SC, Nimmer PM, Oltersdorf T, Park CM, Petros AM, Shoemaker AR, Song X, Wang X, Wendt MD, Zhang H, Fesik SW, Rosenberg SH, Elmore SW (2007) Studies leading to potent, dual inhibitors of Bcl-2 and Bcl-xL. *J Med Chem* 50(4):641–662
31. Grasberger BL, Lu T, Schubert C, Parks DJ, Carver TE, Koblisch HK, Cummings MD, LaFrance LV, Milkiewicz KL, Calvo RR, Maguire D, Lattanze J, Franks CF, Zhao S, Ramachandren K, Bylebyl GR, Zhang M, Manthey CL, Petrella EC, Pantoliano MW, Deckman IC, Spurlino JC, Maroney AC, Tomczuk BE, Molloy CJ, Bone RF (2005) Discovery and cocrystal structure of benzodiazepinedione HDM2 antagonists that activate p53 in cells. *J Med Chem* 48(4):909–912
32. Wang Y, Coulombe R, Cameron DR, Thauvette L, Massariol MJ, Amon LM, Fink D, Titolo S, Welchner E, Yoakim C, Archambault J, White PW (2004) Crystal structure of the E2 transactivation domain of human papillomavirus type 11 bound to a protein interaction inhibitor. *J Biol Chem* 279(8):6976–6985
33. Cunningham BC, Wells JA (1989) High-resolution epitope mapping of hGH-receptor interactions by alanine-scanning mutagenesis. *Science* 244(4908):1081–1085
34. Kozakov D, Hall DR, Chuang GY, Cencic R, Brenke R, Grove LE, Beglov D, Pelletier J, Whitty A, Vajda S (2011) Structural conservation of druggable hot spots in protein-protein interfaces. *Proc Natl Acad Sci USA* 108(33):13528–13533
35. Beglov D, Hall DR, Brenke R, Shapovalov MV, Dunbrack RL Jr, Kozakov D, Vajda S (2012) Minimal ensembles of side chain conformers for modeling protein-protein interactions. *Proteins* 80(2):591–601
36. Yang CY, Wang S (2011) Hydrophobic binding hot spots of Bcl-xL protein-protein interfaces by cosolvent molecular dynamics simulation. *ACS Med Chem Lett* 2(4):280–284
37. Klepeis JL, Lindorff-Larsen K, Dror RO, Shaw DE (2009) Long-timescale molecular dynamics simulations of protein structure and function. *Curr Opin Struct Biol* 19(2):120–127
38. Fuller JC, Burgoyne NJ, Jackson RM (2009) Predicting druggable binding sites at the protein-protein interface. *Drug Discov Today* 14(3–4):155–161
39. Villoutreix BO, Bastard K, Sperandio O, Fahraeus R, Poyet JL, Calvo F, Deprez B, Miteva MA (2008) In silico-in vitro screening of protein-protein interactions: towards the next generation of therapeutics. *Curr Pharm Biotechnol* 9(2):103–122
40. Zinzalla G, Thurston DE (2009) Targeting protein-protein interactions for therapeutic intervention: a challenge for the future. *Future Med Chem* 1(1):65–93
41. Meireles LM, Mustata G (2011) Discovery of modulators of protein-protein interactions: current approaches and limitations. *Curr Top Med Chem* 11(3):248–257
42. Jin L, Wang W, Fang G (2014) Targeting protein-protein interaction by small molecules. *Annu Rev Pharmacol Toxicol* 54:435–456
43. Aeluri M, Chamakuri S, Dasari B, Guduru SK, Jimmidi R, Jogula S, Arya P (2014) Small molecule modulators of protein-protein interactions: selected case studies. *Chem Rev* 114 (9):4640–4694
44. Milroy LG, Grossmann TN, Hennig S, Brunsveld L, Ottmann C (2014) Modulators of protein-protein interactions. *Chem Rev* 114(9):4695–4748

45. Higuero AP, Jubb H, Blundell TL (2013) Protein-protein interactions as druggable targets: recent technological advances. *Curr Opin Pharmacol* 13(5):791–796
46. Villoutreix BO, Labbe CM, Lagorce D, Laconde G, Sperandio O (2012) A leap into the chemical space of protein-protein interaction inhibitors. *Curr Pharm Des* 18(30):4648–4667
47. Valkov E, Sharpe T, Marsh M, Greive S, Hyvonen M (2012) Targeting protein-protein interactions and fragment-based drug discovery. *Top Curr Chem* 317:145–179
48. Azzarito V, Long K, Murphy NS, Wilson AJ (2013) Inhibition of alpha-helix-mediated protein-protein interactions using designed molecules. *Nat Chem* 5(3):161–173
49. London N, Raveh B, Schueler-Furman O (2013) Druggable protein-protein interactions—from hot spots to hot segments. *Curr Opin Chem Biol* 17(6):952–959
50. Ivanov AA, Khuri FR, Fu H (2013) Targeting protein-protein interactions as an anticancer strategy. *Trends Pharmacol Sci* 34(7):393–400
51. Nero TL, Morton CJ, Holien JK, Wielens J, Parker MW (2014) Oncogenic protein interfaces: small molecules, big challenges. *Nat Rev Cancer* 14(4):248–262
52. Sheng C, Dong G, Miao Z, Zhang W, Wang W (2015) State-of-the-art strategies for targeting protein-protein interactions by small-molecule inhibitors. *Chem Soc Rev* 44(22):8238–8259
53. Guo W, Wisniewski JA, Ji H (2014) Hot spot-based design of small-molecule inhibitors for protein-protein interactions. *Bioorg Med Chem Lett* 24(11):2546–2554
54. Wanner J, Fry DC, Peng Z, Roberts J (2011) Druggability assessment of protein-protein interfaces. *Future Med Chem* 3(16):2021–2038
55. Eyrich S, Helms V (2007) Transient pockets on protein surfaces involved in protein-protein interaction. *J Med Chem* 50(15):3457–3464
56. Villoutreix BO, Kuenemann MA, Poyet JL, Bruzzoni-Giovanelli H, Labbe C, Lagorce D, Sperandio O, Miteva MA (2014) Drug-Like protein-protein interaction modulators: challenges and opportunities for drug discovery and chemical biology. *Mol Inform* 33(6–7):414–437
57. Berg T (2008) Small-molecule inhibitors of protein-protein interactions. *Curr Opin Drug Discov Devel* 11(5):666–674
58. Ashkenazi A, Fairbrother WJ, Levenson JD, Souers AJ (2017) From basic apoptosis discoveries to advanced selective BCL-2 family inhibitors. *Nat Rev Drug Discov* 16(4):273–284
59. Zhong M, Hanan EJ, Shen W, Bui M, Arkin MR, Barr KJ, Evanchik MJ, Hoch U, Hyde J, Martell JR, Oslob JD, Paulvannan K, Prabhu S, Silverman JA, Wright J, Yu CH, Zhu J, Flanagan WM (2011) Structure-activity relationship (SAR) of the alpha-amino acid residue of potent tetrahydroisoquinoline (THIQ)-derived LFA-1/ICAM-1 antagonists. *Bioorg Med Chem Lett* 21(1):307–310
60. Cervantes-Gomez F, Lamothe B, Woyach JA, Wierda WG, Keating MJ, Balakrishnan K, Gandhi V (2015) Pharmacological and protein profiling suggests venetoclax (ABT-199) as optimal partner with ibrutinib in chronic lymphocytic leukemia. *Clin Cancer Res* 21(16):3705–3715
61. Konopleva M, Watt J, Contractor R, Tsao T, Harris D, Estrov Z, Bornmann W, Kantarjian H, Viallet J, Samudio I, Andreeff M (2008) Mechanisms of antileukemic activity of the novel Bcl-2 homology domain-3 mimetic GX15-070 (obatoclax). *Cancer Res* 68(9):3413–3420
62. Ding Q, Zhang Z, Liu JJ, Jiang N, Zhang J, Ross TM, Chu XJ, Bartkovitz D, Podlaski F, Janson C, Tovar C, Filipovic ZM, Higgins B, Glenn K, Packman K, Vassilev LT, Graves B (2013) Discovery of RG7388, a potent and selective p53-MDM2 inhibitor in clinical development. *J Med Chem* 56(14):5979–5983
63. Sun D, Li Z, Rew Y, Gribble M, Bartberger MD, Beck HP, Canon J, Chen A, Chen X, Chow D, Deignan J, Duquette J, Eksterowicz J, Fisher B, Fox BM, Fu J, Gonzalez AZ, Gonzalez-Lopez De Turiso F, Houze JB, Huang X, Jiang M, Jin L, Kayser F, Liu JJ, Lo MC, Long AM, Lucas B, McGee LR, McIntosh J, Mihalic J, Oliner JD, Osgood T, Peterson ML, Roveto P, Saiiki AY, Shaffer P, Toteva M, Wang Y, Wang YC, Wortman S, Yakowec P,

- Yan X, Ye Q, Yu D, Yu M, Zhao X, Zhou J, Zhu J, Olson SH, Medina JC (2014) Discovery of AMG 232, a potent, selective, and orally bioavailable MDM2-p53 inhibitor in clinical development. *J Med Chem* 57(4):1454–1472
64. Jeay S, Gaulis S, Ferretti S, Bitter H, Ito M, Valat T, Murakami M, Ruetz S, Guthy DA, Rynn C, Jensen MR, Wiesmann M, Kallen J, Furet P, Gessier F, Holzer P, Masuya K, Wurthner J, Halilovic E, Hofmann F, Sellers WR, Graus Porta D (2015) A distinct p 53 target gene set predicts for response to the selective p53-HDM2 inhibitor NVP-CGM097. *eLife* e06498
 65. Perez VL, Pflugfelder SC, Zhang S, Shojaei A, Haque R (2016) Lifitegrast, a novel integrin antagonist for treatment of dry eye disease. *Ocul Surf* 14(2):207–215
 66. Tabermero J, Dirix L, Schoffski P, Cervantes A, Lopez-Martin JA, Capdevila J, van Beijsterveldt L, Platero S, Hall B, Yuan Z, Knoblauch R, Zhuang SH (2011) A phase I first-in-human pharmacokinetic and pharmacodynamic study of serdemetan in patients with advanced solid tumors. *Clin Cancer Res* 17(19):6313–6321
 67. Vu B, Wovkulich P, Pizzolato G, Lovey A, Ding Q, Jiang N, Liu JJ, Zhao C, Glenn K, Wen Y, Tovar C, Packman K, Vassilev L, Graves B (2013) Discovery of RG7112: a small-molecule MDM2 inhibitor in clinical development. *ACS Med Chem Lett* 4(5):466–469
 68. Tovar C, Graves B, Packman K, Filipovic Z, Higgins B, Xia M, Tardell C, Garrido R, Lee E, Kolinsky K, To KH, Linn M, Podlaski F, Wovkulich P, Vu B, Vassilev LT (2013) MDM2 small-molecule antagonist RG7112 activates p53 signaling and regresses human tumors in preclinical cancer models. *Cancer Res* 73(8):2587–2597
 69. Wang S, Sun W, Zhao Y, McEachern D, Meaux I, Barriere C, Stuckey JA, Meagher JL, Bai L, Liu L, Hoffman-Luca CG, Lu J, Shangary S, Yu S, Bernard D, Aguilar A, Dos-Santos O, Besret L, Guerif S, Pannier P, Gorge-Bernat D, Debussche L (2014) SAR405838: an optimized inhibitor of MDM2-p53 interaction that induces complete and durable tumor regression. *Cancer Res* 74(20):5855–5865
 70. Potin D, Launay M, Monatik F, Malabre P, Fabreguettes M, Fouquet A, Maillet M, Nicolai E, Dorgeret L, Chevallier F, Besse D, Dufort M, Caussade F, Ahmad SZ, Stetsko DK, Skala S, Davis PM, Balimane P, Patel K, Yang Z, Marathe P, Postelneck J, Townsend RM, Goldfarb V, Sheriff S, Einspahr H, Kish K, Malley MF, DiMarco JD, Gougoutas JZ, Kadiyala P, Cheney DL, Tejwani RW, Murphy DK, McIntyre KW, Yang X, Chao S, Leith L, Xiao Z, Mathur A, Chen BC, Wu DR, Traeger SC, McKinnon M, Barrish JC, Robl JA, Iwanowicz EJ, Suchard SJ, Dhar TG (2006) Discovery and development of 5-[(5S,9R)-9-(4-cyanophenyl)-3-(3,5-dichlorophenyl)-1-methyl-2,4-dioxo-1,3,7-triazaspiro[4.4]non-7-yl-methyl]-3-thiophenecarboxylic acid (BMS-587101)—a small molecule antagonist of leukocyte function associated antigen-1. *J Med Chem* 49(24):6946–6949
 71. Watterson SH, Xiao Z, Dodd DS, Tortolani DR, Vaccaro W, Potin D, Launay M, Stetsko DK, Skala S, Davis PM, Lee D, Yang X, McIntyre KW, Balimane P, Patel K, Yang Z, Marathe P, Kadiyala P, Tebben AJ, Sheriff S, Chang CY, Ziemba T, Zhang H, Chen BC, DelMonte AJ, Aranibar N, McKinnon M, Barrish JC, Suchard SJ, Murali Dhar TG (2010) Small molecule antagonist of leukocyte function associated antigen-1 (LFA-1): structure-activity relationships leading to the identification of 6-((5S,9R)-9-(4-cyanophenyl)-3-(3,5-dichlorophenyl)-1-methyl-2,4-dioxo-1,3,7-triazaspiro[4.4]nonan-7-yl)nicotinic acid (BMS-688521). *J Med Chem* 53(9):3814–3830
 72. Kelly TA, Kim JML, R.M. (2004) Preparation of [6,7-dihydro-5H-imidazo[1,2-a]imidazole-3-sulfonylamino]propionamide derivatives for treatment of inflammatory disease. *WO* 2004041827
 73. Polishchuk PG, Samoylenko GV, Khristova TM, Krysko OL, Kabanova TA, Kabanov VM, Kornilov AY, Klimchuk O, Langer T, Andronati SA, Kuz'min VE, Krysko AA, Varnek A (2015) Design, virtual screening, and synthesis of antagonists of alphaIIb beta3 as antiplatelet agents. *J Med Chem* 58(19):7681–7694

74. Gowda RM, Khan IA, Vasavada BC, Sacchi TJ (2004) Therapeutics of platelet glycoprotein IIb/IIIa receptor antagonism. *Am J Ther* 11(4):302–307
75. Zablocki JA, Rico JG, Garland RB, Rogers TE, Williams K, Schretzman LA, Rao SA, Bovy PR, Tjoeng FS, Lindmark RJ et al (1995) Potent in vitro and in vivo inhibitors of platelet aggregation based upon the Arg-Gly-Asp sequence of fibrinogen. (Aminobenzamidino)succinyl (ABAS) series of orally active fibrinogen receptor antagonists. *J Med Chem* 38(13):2378–2394
76. Feldstein CA (1999) Sibrafiban (Genentech). *IDrugs* 2(5):460–465
77. Sugiura T, Kageyama S, Andou A, Miyazawa T, Ejima C, Nakayama A, Dohi T, Eda H (2013) Oral treatment with a novel small molecule alpha 4 integrin antagonist, AJM300, prevents the development of experimental colitis in mice. *J Crohns Colitis* 7(11):e533–e542
78. Halland N, Blum H, Buning C, Kohlmann M, Lindenschmidt A (2014) Small macrocycles as highly active integrin alpha2beta1 antagonists. *ACS Med Chem Lett* 5(2):193–198
79. Davenport RJ, Munday JR (2007) Alpha4-integrin antagonism—an effective approach for the treatment of inflammatory diseases? *Drug Discov Today* 12(13–14):569–576
80. Astles PC, Harris NV, Morley AD (1999) Preparation of substituted β -alanines as integrin-mediated cell adhesion inhibitors. *WO* 9933789
81. Sircar I, Gudmundsson KS, Martin R, Liang J, Nomura S, Jayakumar H, Teegarden BR, Nowlin DM, Cardarelli PM, Mah JR, Connell S, Griffith RC, Lazarides E (2002) Synthesis and SAR of N-benzoyl-L-biphenylalanine derivatives: discovery of TR-14035, a dual alpha (4)beta(7)/alpha(4)beta(1) integrin antagonist. *Bioorg Med Chem* 10(6):2051–2066
82. Cai J, Hu Y, Li W, Li L, Li S, Zhang M, Li Q (2011) The neuroprotective effect of propofol against brain ischemia mediated by the glutamatergic signaling pathway in rats. *Neurochem Res* 36(10):1724–1731
83. Derakhshan A, Chen Z, Van Waes C (2017) Therapeutic small molecules target inhibitor of apoptosis proteins in cancers with deregulation of extrinsic and intrinsic cell death pathways. *Clin Cancer Res* 23(6):1379–1387
84. Benetatos CA, Mitsuchi Y, Burns JM, Neiman EM, Condon SM, Yu G, Seipel ME, Kapoor GS, Laporte MG, Rippin SR, Deng Y, Hendi MS, Tirunahari PK, Lee YH, Haimowitz T, Alexander MD, Graham MA, Weng D, Shi Y, McKinlay MA, Chunduru SK (2014) Birinapant (TL32711), a bivalent SMAC mimetic, targets TRAF2-associated cIAPs, abrogates TNF-induced NF-kappaB activation, and is active in patient-derived xenograft models. *Mol Cancer Ther* 13(4):867–879
85. Wong H, Gould SE, Budha N, Darbonne WC, Kadel EE 3rd, La H, Alicke B, Halladay JS, Erickson R, Portera C, Tolcher AW, Infante JR, Mamounas M, Flygare JA, Hop CE, Fairbrother WJ (2013) Learning and confirming with preclinical studies: modeling and simulation in the discovery of GDC-0917, an inhibitor of apoptosis proteins antagonist. *Drug Metab Dispos* 41(12):2104–2113
86. Flygare JA, Beresini M, Budha N, Chan H, Chan IT, Cheeti S, Cohen F, Deshayes K, Doerner K, Eckhardt SG, Elliott LO, Feng B, Franklin MC, Reisner SF, Gazzard L, Halladay J, Hymowitz SG, La H, LoRusso P, Maurer B, Murray L, Plise E, Quan C, Stephan JP, Young SG, Tom J, Tsui V, Um J, Varfolomeev E, Vucic D, Wagner AJ, Wallweber HJ, Wang L, Ware J, Wen Z, Wong H, Wong JM, Wong M, Wong S, Yu R, Zobel K, Fairbrother WJ (2012) Discovery of a potent small-molecule antagonist of inhibitor of apoptosis (IAP) proteins and clinical candidate for the treatment of cancer (GDC-0152). *J Med Chem* 55(9):4101–4113
87. Bailey D, Jahagirdar R, Gordon A, Hafiane A, Campbell S, Chatur S, Wagner GS, Hansen HC, Chiacchia FS, Johansson J, Krimbou L, Wong NC, Genest J (2010) RVX-208: a small molecule that increases apolipoprotein A-I and high-density lipoprotein cholesterol in vitro and in vivo. *J Am Coll Cardiol* 55(23):2580–2589
88. Nicodeme E, Jeffrey KL, Schaefer U, Beinke S, Dewell S, Chung CW, Chandwani R, Marazzi I, Wilson P, Coste H, White J, Kirilovsky J, Rice CM, Lora JM, Prinjha RK, Lee K, Tarakhovsky A (2010) Suppression of inflammation by a synthetic histone mimic. *Nature* 468(7327):1119–1123

89. Albrecht BK, Gehling VS, Hewitt MC, Vaswani RG, Cote A, Leblanc Y, Nasveschuk CG, Bellon S, Bergeron L, Campbell R, Cantone N, Cooper MR, Cummings RT, Jayaram H, Joshi S, Mertz JA, Neiss A, Normant E, O'Meara M, Pardo E, Poy F, Sandy P, Supko J, Sims RJ 3rd, Harmange JC, Taylor AM, Audia JE (2016) Identification of a Benzoisoxazoloazepine Inhibitor (CPI-0610) of the Bromodomain and Extra-Terminal (BET) family as a candidate for human clinical trials. *J Med Chem* 59(4):1330–1339
90. Boi M, Gaudio E, Bonetti P, Kwee I, Bernasconi E, Tarantelli C, Rinaldi A, Testoni M, Cascione L, Ponzoni M, Mensah AA, Stathis A, Stussi G, Riveiro ME, Herait P, Inghirami G, Cvitkovic E, Zucca E, Bertoni F (2015) The BET Bromodomain Inhibitor OTX015 affects pathogenetic pathways in preclinical B-cell tumor models and synergizes with targeted drugs. *Clin Cancer Res* 21(7):1628–1638
91. Schenk RL, Strasser A, Dewson G (2017) BCL-2: long and winding path from discovery to therapeutic target. *Biochem Biophys Res Commun* 482(3):459–469
92. Adams JM, Cory S (1998) The Bcl-2 protein family: arbiters of cell survival. *Science* 281(5381):1322–1326
93. Rudin CM, Hann CL, Garon EB, Ribeiro de Oliveira M, Bonomi PD, Camidge DR, Chu Q, Giaccone G, Khaira D, Ramalingam SS, Ranson MR, Dive C, McKeegan EM, Chyla BJ, Dowell BL, Chakravarty A, Nolan CE, Rudersdorf N, Busman TA, Mabry MH, Krivoshik AP, Humerickhouse RA, Shapiro GI, Gandhi L (2012) Phase II study of single-agent navitoclax (ABT-263) and biomarker correlates in patients with relapsed small cell lung cancer. *Clin Cancer Res* 18(11):3163–3169
94. Sattler M, Liang H, Nettesheim D, Meadows RP, Harlan JE, Eberstadt M, Yoon HS, Shuker SB, Chang BS, Minn AJ, Thompson CB, Fesik SW (1997) Structure of Bcl-xL-Bak peptide complex: recognition between regulators of apoptosis. *Science* 275(5302):983–986
95. Oltersdorf T, Elmore SW, Shoemaker AR, Armstrong RC, Augeri DJ, Belli BA, Bruncko M, Deckwerth TL, Dinges J, Hajduk PJ, Joseph MK, Kitada S, Korsmeyer SJ, Kunzer AR, Letai A, Li C, Mitten MJ, Nettesheim DG, Ng S, Nimmer PM, O'Connor JM, Oleksijew A, Petros AM, Reed JC, Shen W, Tahir SK, Thompson CB, Tomaselli KJ, Wang B, Wendt MD, Zhang H, Fesik SW, Rosenberg SH (2005) An inhibitor of Bcl-2 family proteins induces regression of solid tumours. *Nature* 435(7042):677–681
96. Petros AM, Dinges J, Augeri DJ, Baumeister SA, Betebenner DA, Bures MG, Elmore SW, Hajduk PJ, Joseph MK, Landis SK, Nettesheim DG, Rosenberg SH, Shen W, Thomas S, Wang X, Zanze I, Zhang H, Fesik SW (2006) Discovery of a potent inhibitor of the antiapoptotic protein Bcl-xL from NMR and parallel synthesis. *J Med Chem* 49(2):656–663
97. Wendt MD, Shen W, Kunzer A, McClellan WJ, Bruncko M, Oost TK, Ding H, Joseph MK, Zhang H, Nimmer PM, Ng SC, Shoemaker AR, Petros AM, Oleksijew A, Marsh K, Bauch J, Oltersdorf T, Belli BA, Martineau D, Fesik SW, Rosenberg SH, Elmore SW (2006) Discovery and structure-activity relationship of antagonists of B-cell lymphoma 2 family proteins with chemopotential activity in vitro and in vivo. *J Med Chem* 49(3):1165–1181
98. Park CM, Oie T, Petros AM, Zhang H, Nimmer PM, Henry RF, Elmore SW (2006) Design, synthesis, and computational studies of inhibitors of Bcl-XL. *J Am Chem Soc* 128(50):16206–16212
99. Park CM, Bruncko M, Adickes J, Bauch J, Ding H, Kunzer A, Marsh KC, Nimmer P, Shoemaker AR, Song X, Tahir SK, Tse C, Wang X, Wendt MD, Yang X, Zhang H, Fesik SW, Rosenberg SH, Elmore SW (2008) Discovery of an orally bioavailable small molecule inhibitor of prosurvival B-cell lymphoma 2 proteins. *J Med Chem* 51(21):6902–6915
100. Tse C, Shoemaker AR, Adickes J, Anderson MG, Chen J, Jin S, Johnson EF, Marsh KC, Mitten MJ, Nimmer P, Roberts L, Tahir SK, Xiao Y, Yang X, Zhang H, Fesik S, Rosenberg SH, Elmore SW (2008) ABT-263: a potent and orally bioavailable Bcl-2 family inhibitor. *Cancer Res* 68(9):3421–3428
101. Souers AJ, Levenson JD, Boghaert ER, Ackler SL, Catron ND, Chen J, Dayton BD, Ding H, Enschede SH, Fairbrother WJ, Huang DC, Hymowitz SG, Jin S, Khaw SL, Kovar PJ, Lam LT, Lee J, Maecker HL, Marsh KC, Mason KD, Mitten MJ, Nimmer PM, Oleksijew A,

- Park CH, Park CM, Phillips DC, Roberts AW, Sampath D, Seymour JF, Smith ML, Sullivan GM, Tahir SK, Tse C, Wendt MD, Xiao Y, Xue JC, Zhang H, Humerickhouse RA, Rosenberg SH, Elmore SW (2013) ABT-199, a potent and selective BCL-2 inhibitor, achieves antitumor activity while sparing platelets. *Nat Med* 19(2):202–208
102. Anderson MA, Deng J, Seymour JF, Tam C, Kim SY, Fein J, Yu L, Brown JR, Westerman D, Si EG, Majewski IJ, Segal D, Heitner Enschede SL, Huang DC, Davids MS, Letai A, Roberts AW (2016) The BCL2 selective inhibitor venetoclax induces rapid onset apoptosis of CLL cells in patients via a TP53-independent mechanism. *Blood* 127(25):3215–3224
103. Gadek TR, Burdick DJ, McDowell RS, Stanley MS, Marsters JC Jr, Paris KJ, Oare DA, Reynolds ME, Ladner C, Zioncheck KA, Lee WP, Gribling P, Dennis MS, Skelton NJ, Tumas DB, Clark KR, Keating SM, Beresini MH, Tilley JW, Presta LG, Bodary SC (2002) Generation of an LFA-1 antagonist by the transfer of the ICAM-1 immunoregulatory epitope to a small molecule. *Science* 295(5557):1086–1089
104. Zhong M, Shen W, Barr KJ, Arbitrario JP, Arkin MR, Bui M, Chen T, Cunningham BC, Evanchik MJ, Hanan EJ, Hoch U, Huen K, Hyde J, Kumer JL, Lac T, Lawrence CE, Martell JR, Oslob JD, Paulvannan K, Prabhu S, Silverman JA, Wright J, Yu CH, Zhu J, Flanagan WM (2010) Discovery of tetrahydroisoquinoline (THIQ) derivatives as potent and orally bioavailable LFA-1/ICAM-1 antagonists. *Bioorg Med Chem Lett* 20(17):5269–5273
105. Zhong CX, Wu JX, Liang JX, Wu QH (2012) Laparoscopic and gasless laparoscopic sigmoid colon vaginoplasty in women with vaginal agenesis. *Chin Med J (Engl)* 125(2):203–208

Chapter 2

High-Throughput Screening in the Discovery of Small-Molecule Inhibitors of Protein-Protein Interactions



Chunlin Zhuang and Chunquan Sheng

2.1 Introduction

Protein-protein interactions (PPIs) govern various key biological processes in normal and disease states including cell division, adaption, or response to extracellular signals [1]. Thus, PPIs offer attractive targets for therapeutic potentials. However, the discovery of drug-like small molecules that modulate PPIs is generally considered to be a challenging task because of relatively large and flat surface areas involved in PPI interfaces [2, 3]. While natural small-molecule PPI binders are generally unavailable, high-throughput screening (HTS) became an important tool to discover initial hits or starting points for PPI-based drug discovery [4].

A workflow for HTS of small-molecule PPI inhibitors is depicted in Fig. 2.1. The availability of HTS compatible assays and suitable compounds libraries is of key importance for successful identification of PPI inhibitors. There are several commercial compound libraries available, such as Specs, Enamine, Maybridge, Chembridge, ChemDiv, ZINC. [5]. Besides, a number of combinatorial chemical libraries have been developed by highly efficient synthetic chemistry. HTS is a well-established tool for drug discovery based on traditional drug targets (e.g., enzymes and receptors). Nonetheless, discovery of PPI inhibitors by HTS still remains challenging. First, compound libraries for HTS are mainly collected or designed for conventional drug targets, which cannot significantly cover the chemical space of PPI inhibitors. New chemical space suitable for PPIs is highly desirable to be constructed. Second, the PPI interface is large and shallow, resulting in low affinity (generally in micromolar range) of initial hits from HTS campaigns. Thus, compound screening generally should be performed at high concentrations ($>10 \mu\text{M}$), which always leads to low hit rates and high false-positive rates.

C. Zhuang · C. Sheng (✉)

Department of Medicinal Chemistry, School of Pharmacy, Second Military Medical University, 325 Guohe Road, Shanghai 200433, China
e-mail: shengcq@smmu.edu.cn

© Springer Nature Singapore Pte Ltd. 2018

C. Sheng and G. I. Georg (eds.), *Targeting Protein-Protein Interactions by Small Molecules*, https://doi.org/10.1007/978-981-13-0773-7_2

To address these bottlenecks, a number of reliable and robust assays have been established. Fluorescence polarization (FP) assay, fluorescence resonance energy transfer (FRET) assay, and AlphaScreen (amplified luminescent proximity homogeneous assay screen) have been widely and successfully applied in discovering PPI inhibitors [6]. In the post-screening stage, low-throughput assays such as surface plasmon resonance (SPR), isothermal titration calorimetry (ITC), and microscale thermophoresis (MST) are extensively employed in hit validation [7]. Binding parameters obtained from these assays such as dissociation constant (K_d), the binding kinetics (K_{on} and K_{off}) and stoichiometry are also important for the selection of hits for structural optimization. In the stage of hit optimization, well-accepted medicinal chemistry strategies including structure-activity relationship (SAR), structure-based drug design (SBDD), and pharmacokinetic (PK)/pharmacodynamics (PD) optimization are similar to those for traditional drug targets. Notably, the structural information of PPI hotspots and binding complex are invaluable to improve the efficiency and success rate of drug discovery [4].

The success of a HTS campaign largely depends on the choice of target and assay and the size and diversity of the compound library. Currently, HTS is prevalent in identifying initial hits targeting PPIs, particularly in the pharmaceutical industry [8]. Encouragingly, a large portion of the PPI inhibitors under clinical trials have originated from HTS campaigns [8]. Moreover, a number of HTS assays

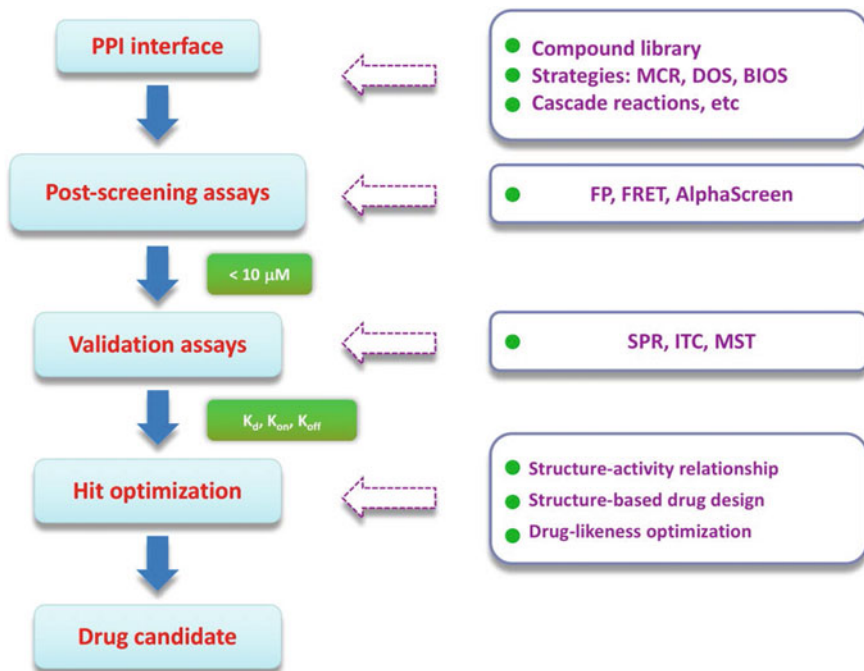


Fig. 2.1 A workflow for HTS of small-molecule PPI inhibitors

compatible with PPI inhibitor screening have been developed recently [9]. Herein, construction of compound libraries, establishment of assays as well as successful examples of HTS of PPI inhibitors will be introduced.

2.2 Compound Libraries for HTS of PPI Inhibitors

The selection of an appropriate chemical library plays an important role in the success of HTS. PPI inhibitors generally have higher molecular weight and more structural complexity as compared with traditional drug-like molecules. Thus, compound libraries are required to be expanded into new chemical space to achieve better sampling of PPI inhibitors. Despite that current HTS mainly relies on the compound collections in pharmaceutical industry, innovative construction of new and biological relevant libraries with improved diversity and complexity is becoming an important area for screening PPI inhibitors. The development of highly efficient synthetic chemistry, such as multi-component reactions (MCRs), diversity-oriented synthesis (DOS), biology-oriented synthesis (BIOS), and domino (or cascade) reactions were powerful tools to construct focused compound libraries for targeting PPIs [4].

2.2.1 MCR-Inspired Compound Library

MCR is an efficient synthetic strategy, which utilizes “one-step, one-pot” reaction of three or more reactants to form a single product. MCR has been extensively used for the rapid generation of compound libraries [10]. PPIs inhibitors such as p53/MDM2 (mouse double minute 2) [11], Bcl2 [11], and HIV-1/gp414 [12] inhibitors have been discovered by screening MCR-derived compounds. Despite high efficiency of MCR in compound synthesis, molecular, and stereo-diversity of MCR library remains to be further improved [10].

Dömling’s group reported a series of PPI inhibitors by screening of MCR-derived compound libraries (Fig. 2.2). Compound **1**, a MCR-derived imidazole analog, was identified as a selective inhibitor of Bcl-w/BH3 peptide interaction ($IC_{50} = 8.09 \mu\text{M}$) [11]. Notably, this compound also showed potent cellular antitumor activity against the HL-60 leukemia cancer cell line ($GI_{50} = 9.43 \mu\text{M}$) by inducing apoptosis.

Dömling et al. also developed a new strategy that combines anchor-based design, MCR-inspired construction of focused virtual libraries, virtual screening, chemical synthesis, and biological screening to discover PPI inhibitors. The anchor mimics the “hotspot” residue in PPI interface and MCR was used to build an anchor-based virtual library, which takes the advantages of both HTS and SBDD. For example, inhibitors of Bir3 domain of XIAP (X-linked inhibitor of apoptosis) were successfully discovered by this strategy (compound **2**, $IC_{50} = 4.9 \mu\text{M}$) [13].

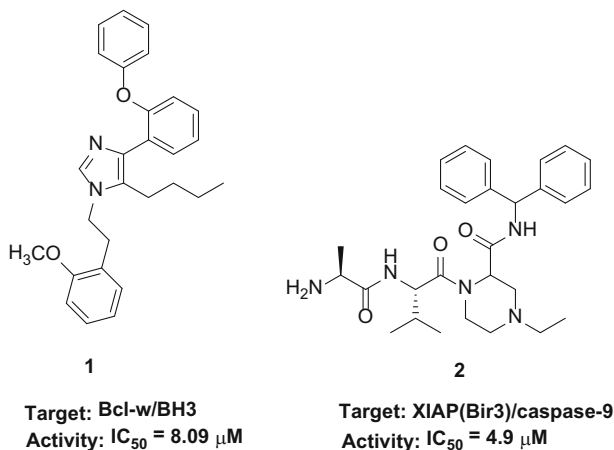


Fig. 2.2 MCR-inspired PPI inhibitors

More recently, the MCR approach was used to discover p53–MDM2/MDM4 inhibitors [14–17]. Trp23, a hotspot residue in p53–MDM2 interaction, was used as an anchor to construct virtual libraries by indole-based MCRs (Fig. 2.3). After initial screen by molecular docking, the highest-ranking compounds were selected for chemical synthesis and biological assays based on the binding mode, structural diversity, and synthetic feasibility. On the basis of the strategy, several new classes of p53–MDM2 inhibitors were identified. For example, inhibitor **3** had a K_d value

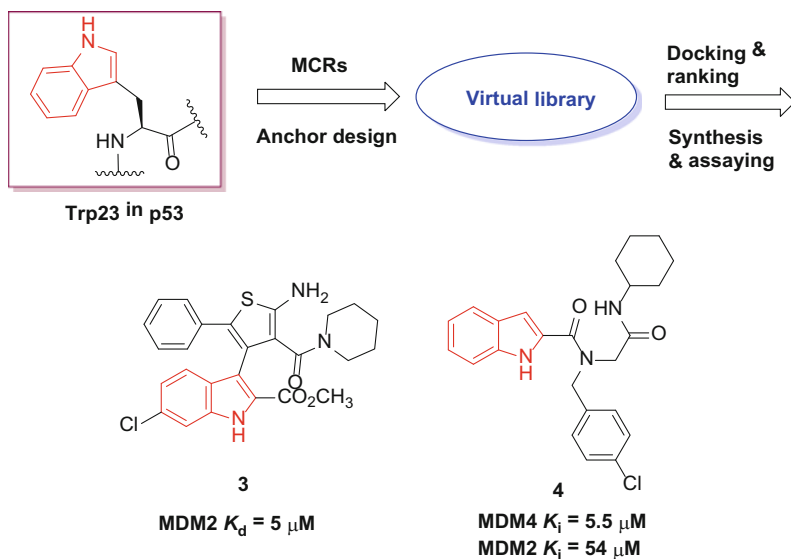


Fig. 2.3 MCR-inspired p53/MDM2 inhibitors

of 5 μM toward MDM2 [15]. In another study, Ugi four-component reaction containing an indole fragment was used to discover selective MDM4 inhibitors. By a similar strategy, compound **4** showed good selectivity for MDM4 ($K_i = 5.5 \mu\text{M}$) over MDM2 ($K_i = 54 \mu\text{M}$) [14].

2.2.2 DOS-Inspired Compound Library

DOS is an efficient synthetic strategy to investigate drug-like chemical space focusing on generating compound libraries with scaffold diversity, structural complexity and stereo-diversity [16, 18]. These features were proven to be useful in improving the hit rate and hit quality of HTS [19]. Up to now, a number of bioactive compounds have been identified from DOS-inspired compound libraries [20, 21]. In the field of PPI-based drug discovery, DOS mainly contributed to highly efficient construction of macrocycle libraries [22, 23], whose structural features show good potential as PPI inhibitors [24]. Macrocycles are conformational pre-organized and have restricted conformational flexibility. Thus, they can serve as potential mimics for interactions with hotspots and bind to topologically defined PPI surfaces without major entropic loss. Moreover, macrocycles possess better cellular penetration as compared with peptide PPI inhibitors.

Several examples of PPI inhibitors derived from DOS libraries are described in Fig. 2.4. Schreiber's group screened a DOS library for inhibitors of the interaction between sonic hedgehog (Shh) and Patched (Ptch1), an important kind of PPI in the hedgehog signaling pathway [25]. Macrocycle hit **5** was identified as the first example of small-molecule ShhN inhibitor (*N*-terminal construct of Shh) [26]. Hit optimization of inhibitor **5** led to the discovery of 12-membered macrocycle robotnikinin (**6**) with increased binding affinity ($K_d = 3.1 \mu\text{M}$) [26]. Marcaurelle et al. designed and

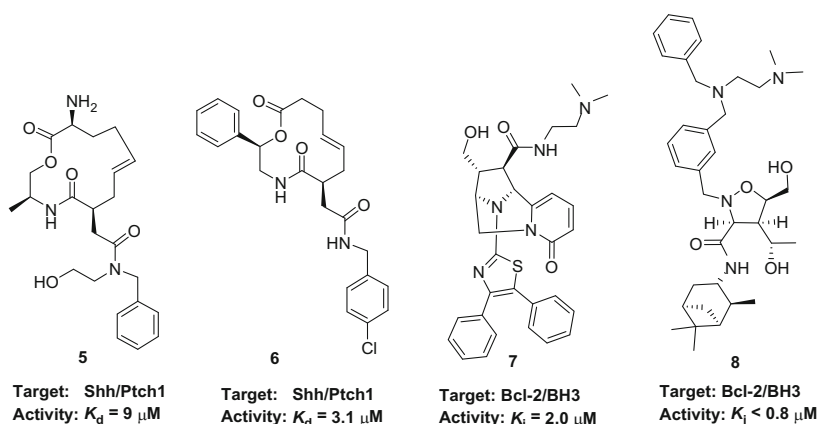


Fig. 2.4 DOS-inspired PPI inhibitors

synthesized a natural product-inspired DOS library containing 15,000 compounds with four types of chiral cytosine-inspired scaffolds [27]. After biological screening, a series of new Bcl-2 (hit rate: 1.1%) and Bcl-xL (hit rate: 0.2%) inhibitors were identified. For example, the bridged bicyclic pyridone scaffold **7** showed similar activity against Bcl-2 ($K_i = 2.0 \mu\text{M}$) and Bcl-xL ($K_i = 5.7 \mu\text{M}$) [27]. Another screen of a DOS library discovered a selective Bcl-2 inhibitor. Compound **8** showed good selectivity between Bcl-2 ($K_i < 0.8 \mu\text{M}$) and Bcl-xL ($K_i > 100 \mu\text{M}$), which also revealed potent in vitro and in vivo antitumor activities [18].

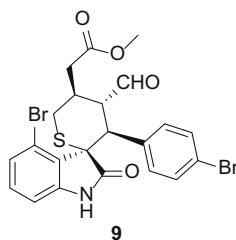
2.2.3 Cascade Reaction-Inspired Compound Library

Cascade reactions are powerful tools to facilitate assembly of diverse and complex scaffolds in one-pot manner. Our group developed the divergent organocatalytic cascade approach (DOCA) strategy by merging the advantages of organocatalysis, cascade reactions, divergent synthesis, and drug-likeness [28]. A “privileged sub-structure”-based compound library was constructed by the DOCA strategy and novel bioactive molecules were identified [28, 29]. Recently, our group constructed a focused library containing a novel spiro-tetrahydrothiopyran–oxindole scaffold by organocatalytic enantioselective Michael–Michael cascade reaction of drug-like tetrahydrothiopyran and oxindole motifs (Fig. 2.5) [29]. After biological screening, the new scaffold was confirmed as a new type of p53–MDM2 inhibitor (**9**), which also displayed good antitumor activity [30].

2.2.4 BIOS-Inspired Compound Library

Natural products-inspired compound libraries are considered to be a rich source of PPI inhibitors. Inspired by the idea, BIOS aims to synthesize compound libraries enriched in bioactivity by embedding structural information and underlying scaffolds in complex natural products [31, 32]. A typical BIOS-derived compound library generally contains 200–500 compounds with an hit rate ranging from 0.2 to

Fig. 2.5 Cascade reaction-inspired p53/MDM2 inhibitors



9

MDM2 $K_D = 2.2 \mu\text{M}$

A549 Lung Cancer Cell Line $IC_{50} = 1.67 \mu\text{M}$

1.5% [32]. BIOS have been applied in medicinal chemistry and chemical biology [33–35]. Although examples of BIOS in the discovery of PPI inhibitors are rare, the BIOS libraries provide the basis for screening PPI inhibitors.

2.3 Assays for HTS of PPI Inhibitors

The discovery of compounds that modulate PPIs is a challenging task because of the following reasons: (1) these interactions are wider and shallower than classical small-molecule binding sites on proteins [3, 36]; (2) the design of small-molecule PPI inhibitors is often based on mimicking a fairly large peptide structure at the PPI interface [2]; (3) the success of any HTS campaign will depend on the choice of target(s), the size and diversity of the chemical library screened [6, 37]; (4) typically, there is no facile enzymatic readout associated with protein-protein binding [6]. Therefore, the selection of a suitable assay plays a critical role in the success of HTS. The following sections detail the utility of several popular technologies in HTS. FP assay, time-resolved fluorescence resonance energy transfer (TR-FRET)

Table 2.1 Recent examples of small-molecule PPI inhibitors identified by HTS^a

Compound	Target	Assay	Activity	Hit rate	References
10	ZipA/FtsZ	FP	K_i : 12 μ M	0.01%	[40]
11	CBP/ β -Catenin	Cell-based Luciferase Assay	IC ₅₀ : 3.0 μ M	0.06%	[41]
12	EGFR/p85	Cell-based Luciferase Assay	IC ₅₀ : 5 μ M	0.005%	[37]
13	JIP/JNK	FP	IC ₅₀ : 5.7 μ M	0.0001%	[42]
14	JNK/JIP	TR-FRET	IC ₅₀ : 0.28 μ M	Not reported	[43]
15	p53/GST	ELISA	IC ₅₀ : 10 μ M	0.3%	[44]
16	Atg8/Atg3	SPR	IC ₅₀ : 18.16 μ M	1.5%	[45]
17	Keap1/ Nrf2	FP	IC ₅₀ : 3 μ M	0.002%	[46]
18	Keap1/ Nrf2	2D-FIDA	IC ₅₀ : 118 μ M	0.007%	[47]

^aAbbreviations ZipA/FtsZ, cell division protein ZipA/filamenting temperature-sensitive mutant Z; CBP/ β -catenin, β -catenin/CREB-binding protein; EGFR/p85, epidermal growth factor receptor/p85 protein; JIP/JNK, JNK-interacting protein/c-Jun N-terminal kinase; Plk1/PBD, polo-like kinase 1/polo-box domain; p53/GST, p53 protein/ glutathione s-transferase; Atg8/Atg3, Atg8 is a ubiquitin-like protein; and Atg3 is a E2-like conjugating enzyme. Keap1/Nrf2, Kelch-like ECH-associated protein 1/nuclear factor erythroid 2-related factor 2. 2D-FIDA, two-dimensional fluorescence intensity distribution analysis

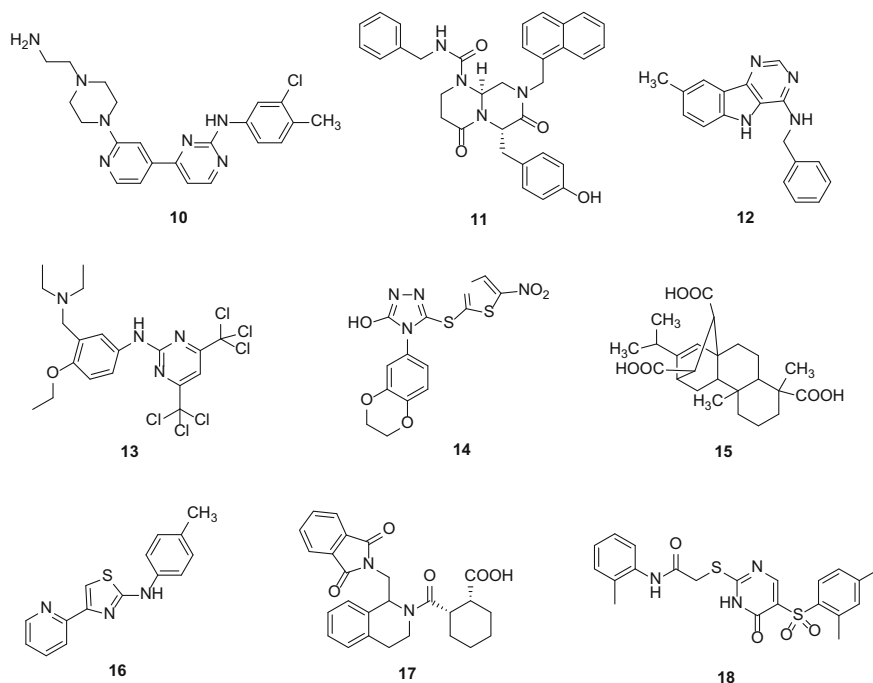


Fig. 2.6 Chemical structures of small-molecule PPI inhibitors identified by HTS

assay, bioluminescence resonance energy transfer (BRET), and AlphaScreen have been widely and successfully applied in discovering PPI inhibitors [6, 7, 9, 38, 39] and will be discussed herein. Recent examples of HTS-derived small-molecule PPI inhibitors (10–18) are listed in Table 2.1 and Fig. 2.6.

2.3.1 FP Assay

FP, also named fluorescence anisotropy, is a technique using a basic principal that the light emitted by a fluorophore has unequal intensities along different axes of polarization [48]. Perrin first described this phenomenon in 1926 [49]. Gregorio Weber, Andreas Albrecht, and other early pioneers contributed significantly in the field [50–52]. Now, it has been widely applied in solution to investigate PPIs, DNA–protein interactions, DNA–DNA interactions, and small-molecule–protein interactions. It is measured using the relative rates of rotation in solution of a complex of fluorescent-tagged macromolecule or peptide and the protein [9, 53, 54]. Briefly, the linear polarized light enters the complex and becomes partly depolarized. The degree of polarization of the emission light is the difference in the intensity of the emission light (parallel and perpendicular) relative to the excitation

light plane. The size of the fluorescent-labeled probe has a great influence on the degree of depolarization of the initial polarized light after entering the sample. A green or red fluorescent-tagged peptide containing key residues is often designed to mimic the binding mode of the protein-binding partners in PPI study. The peptide will rotate fast and depolarize the initial polarized light in a strong way as it is relatively much smaller than the protein. The free peptide depolarizes the initially polarized light in the solution, resulting in low polarization signal. After the interaction, the complex becomes more rigid and rotates more slowly than the free fluorescent-tagged peptide. The reduced rotation behavior decreases the amount of depolarization. Therefore, the interaction with its protein partner causes a decreased depolarization, resulting in high polarization signal. The above two states are used to characterize the molecular interaction. For a third small molecule, it disrupts the complex and releases the faster rotating fluorescent-labeled peptide and subsequently increase depolarization, resulting in decreased polarization. This technique can be easily realized using standard 96-, 384-, and 1536-well plates and data can be collected using commercially available fluorescence readers. In addition, fluorescent-tagged peptides can be easily synthesized and the proteins as well, making this assay ideal for PPI modulator screens. This technique is widely used for HTS as it is affordable to different proteins and to use a very simple procedure without separation or washing steps to obtain the different signals [55, 56]. More importantly, this method needs the minimal modification of the protein as only a small peptide needs labeling. However, the limitation of the method cannot be ignored: (1) The change of polarization is dependent on the affinity between the two proteins and their complex needs a sufficient overall change in mass to affect the rotation of the fluorescent peptide. It is recommended to have tenfold mass difference between the peptide and its protein partner [57]. (2) Auto-fluorescence and light scattering exist to disturb signal detection. (3) False positives are difficult to recognize when using high concentrations of small molecules. Non-specific interaction between the fluorescent peptide and small molecule aggregates at high concentration can induce abnormal signal [58]. FP technique has been successfully applied to identify small-molecule inhibitors of PPIs, such as ZipA/FtsZ [40, 59], p53/MDM2 [60–64], c-Myc/Max [65], Bcl-xL/Bak [66], eIF4E/eIF4G [67].

2.3.2 FRET Assay

FRET, also referred to Förster resonance energy transfer, was refined into theory by Förster in 1946 [68]. It is a method testing non-radioactive energy transfer from one donor fluorophore to an acceptor fluorophore. Energy is transferred and absorbed into the acceptor fluorophore when a donor fluorophore is located close to an acceptor and electronically excited. Thus, the distance between the two fluorophores plays a critical role in the energy transfer. It is reported that the energy transfers only when the distance is in a range of 10–100 Å [69]. FRET has been applied in HTS for enzymatic, peptide-binding and PPI assays [70]. For PPIs, cyan

fluorescent protein (CFP) and yellow fluorescent protein (YFP) are typically fused with each partner [71]. FRET is detected after the two fusion protein interacts. The fluorescence increases when PPI is blocked by a small molecule and energy transfer is decreased. However, this assay has its inherent drawbacks: (1) FRET requires tagging of proteins and peptides with FRET donors and acceptors that is not easy to be realized. (2) This assay is less sensitive than other fluorescence-based assays. The FRET signal can be apparently disturbed by the auto-fluorescence background of the fluorophore as energy transfer and fluorophore need similar emission wavelength. Thus, it is not easy to distinguish weak interactions and the background signal. (3) Photobleaching over time depends on the fluorophores used, which has high influence on the FRET signal. (4) Moreover, fluorescent emission wavelengths of small-molecule mirror that of common FRET donors [6]. TR-FRET and BRET have been developed to address this problem [39, 72].

TR-FRET relies on the use of rare earth lanthanides (Europium or Terbium). Their signal is easy to be distinguished from the short fluorescence lifetimes of most organic molecules and eliminate auto-fluorescence from small molecules, microplates, and buffers. Taken Europium as an example, it is excited at 340 nm and emits at 615/620 nm. Then, the emission wavelength of Europium (615/620 nm) is transferred to a far-red dye leading to its excitation and in turn emits at ~665 nm [56, 72]. Now, three main TR-FRET assays (Cisbio, HTRF), PerkinElmer (LANCER[®]) and Life Technologies (LanthaScreen[™]) are commercially available. TR-FRET technique has been successfully applied to identify small-molecule inhibitors of PPIs, such as 14-3-3/Bad [73], Myc/Max [74], Jun/Fos [75].

BRET, minor modification of the TR-FRET, uses bioluminescent enzyme as the energy donor and converts its substrate into light emission. It has several advantages in screening of PPI inhibitors over other FRET methods [76]: (1) monochromatic light in FRET excites the donor fluorophore and concomitantly excites the acceptor to harden the readout; (2) photobleaching of the donor and cell auto-fluorescence are promoted by excitatory light in FRET; (3) BRET signal/noise ratio is tenfold higher than FRET. This is helpful to use less amount of protein (<40-fold) to reach the same readout level of FRET. However, FRET still needs further optimizations [39]: (1) The percentage of donor/acceptor complexes versus the donor alone decides the BRET signal. It is difficult to detect when the percentage is low. Substrate trapping is one of the main strategies to enhance the monitoring. (2) Variants of luciferases or fluorescent acceptors are applied to develop new BRET. The BRET method is well suitable to identify PPI inhibitors and this technology has been applied to validate compounds disrupting MDM2/p53 [77], TEM8/PA [78], YAP/TEAD [79].

2.3.3 *AlphaScreen*

AlphaScreen, developed by PerkinElmer, is a bead-based assay technology used to study biomolecular interactions in a microplate format. The acronym “Alpha” refers

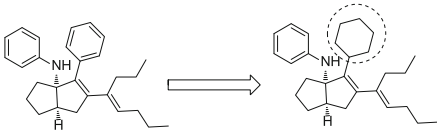
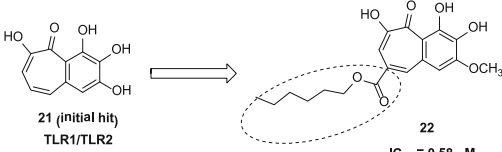
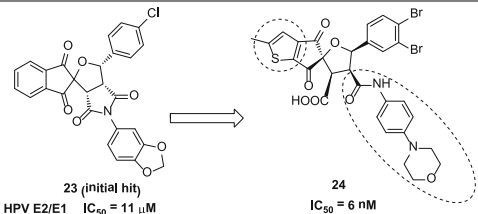
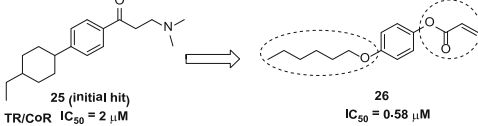
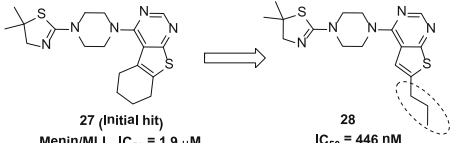
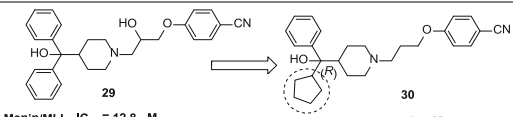
to amplified luminescent proximity homogeneous assay. As the name implies, the key features of the technology are non-radioactive, homogeneous proximity assays. Similar to FRET, this method uses the energy transferring from one bead to the other and detects the produced luminescent or fluorescent signal. Two bead types are required: donor beads and acceptor beads. Different tags, such as biotin, are accepted to attach on the beads. Donor beads contain a photosensitizer and generate a molecular oxygen with a single excited electron after excitation at 680 nm. It can diffuse to the acceptor beads within a distance of approximately 200 nm in solution within its 4 μ sec half-life. Finally, it leads to a chemical reaction cascade inside the acceptor beads and arises emission of light at 520–620 nm. If no acceptor bead is available, no signal is produced with the singlet oxygen falls to ground state [7, 9, 72, 80–82]. The principal is also applied in PPI inhibitor screening. Two interacting proteins are linked to the donor beads and the acceptor beads, respectively. For example, a biotinylated protein is attached to Streptavidin-coated donor beads, and a GST-fused partner protein is attached to anti-GST-conjugated acceptor beads.

Excitation of the donor bead will generate a signal when the two proteins interact. Disrupting the PPI by a small molecule leads to the loss of the emission signal. Compared with the FRET assay, this assay detects the interaction between two proteins at a much longer distance (200 nm vs. 10 nm). It is convenient and can be easily performed in a microplate format without any wash or filtration steps. However, the disadvantages are unavoidable [7, 9]: (1) A specialized reader is necessary. It is not suitable to detect the signal using standard fluorimeters and luminometers. (2) The signal is temperature sensitive. Room temperature has to be maintained during the signal detection. (3) Based on the principle of the assay, the signal is produced by chemical reaction, leading to many false positives. This HTS technology has previously been successfully applied to identify a KRAS/PDE δ inhibitor [83].

2.4 Hit Validation and Optimization

A large proportion of the initial hits from HTS are often false positives. Different assays have their own advantages and inherent limitations. Thus, multiple/orthogonal assays are required in the preliminary stage of a PPI study to authenticate each other and validate the hits. Representative examples of structural optimization of HTS hits are listed in Table 2.2. It can be found that minor modification of the initial hits could lead to substantial improvement of the activity. Importantly, structural optimization guided by SBDD to form favorable interactions with the “hotspots” can efficiently accelerate the process of hit-to-lead.

Table 2.2 Selected examples of structural optimization of HTS hits as PPI inhibitors^a

Entry	Optimization process and biological activity	References
1	 <p>19 (initial hit) LRH-1 EC₅₀ = 0.43 μM SF-1 EC₅₀ = 0.054 μM</p> <p>20 LRH-1 EC₅₀ = 0.012 μM SF-1 EC₅₀ = 0.010 μM</p>	[84]
2	 <p>21 (initial hit) TLR1/TLR2 IC₅₀ = 2.45 μM</p> <p>22 IC₅₀ = 0.58 μM</p>	[85]
3	 <p>23 (initial hit) HPV E2/E1 IC₅₀ = 11 μM</p> <p>24 IC₅₀ = 6 nM</p>	[86, 87]
4	 <p>25 (initial hit) TR/CoR IC₅₀ = 2 μM</p> <p>26 IC₅₀ = 0.58 μM</p>	[88]
5	 <p>27 (Initial hit) Menin/MLL IC₅₀ = 1.9 μM</p> <p>28 IC₅₀ = 446 nM</p>	[89]
6	 <p>29 Menin/MLL IC₅₀ = 12.8 μM</p> <p>30 IC₅₀ = 56 nM</p>	[90]

^aAbbreviations TLR1/TLR2, toll-like receptor 1/toll-like receptor 2; HPV E2/E1, human papilloma virus transcription factor E2/helicase E1; TR/CoR, thyroid hormone receptor/coregulator; LRH-1/SF-1, liver receptor homolog-1/steroidogenic factor-1; Menin/MLL, menin/mixed lineage leukemia

2.5 Case Studies

2.5.1 Discovery and Optimization of p53–MDM2 Inhibitors

So far, the most successful case of application of HTS in identification of PPI inhibitors is the discovery of nutlins and benzodiazepinediones [91] as p53–MDM2 inhibitors (Fig. 2.7a). The p53–MDM2 PPI represents a promising target for the development of new generation of antitumor agents. The crystal structure of MDM2 in complex with the α -helix of p53 (PDB code: 1T4F) reveals that there are three hotspots on MDM2 (namely Phe19, Trp23, and Leu26 pocket) suitable for small-molecule binding (Fig. 2.7b) [92]. Researchers at Roche discovered nutlins

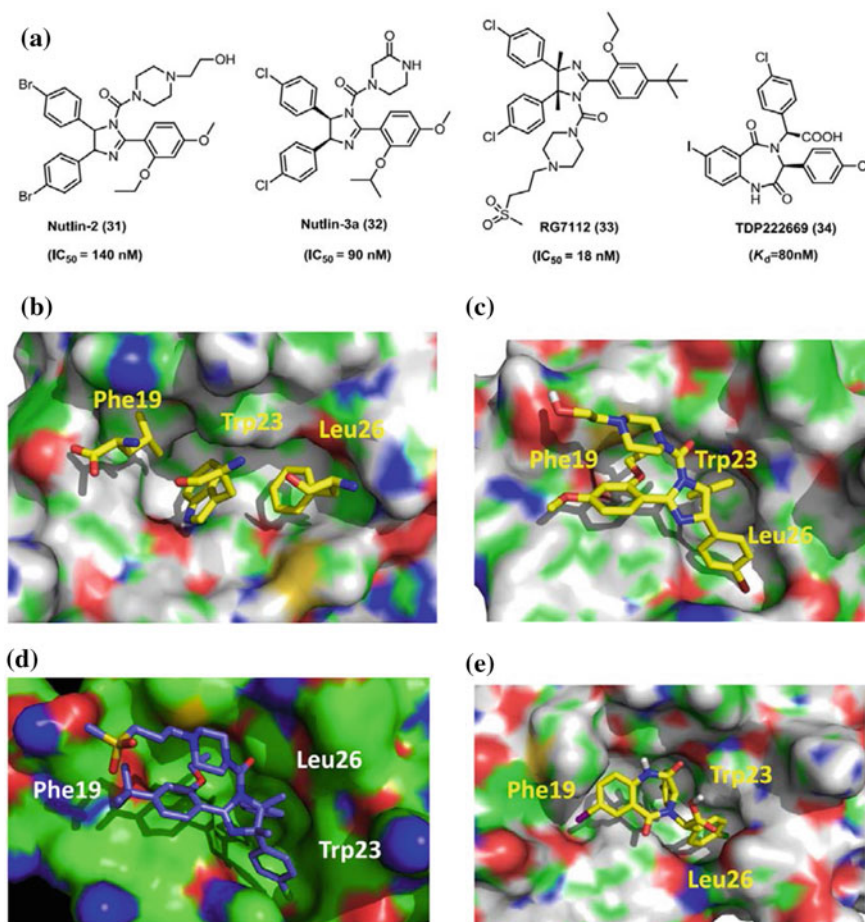


Fig. 2.7 a Chemical structures of nutlin-2, nutlin-3a, RG7112, and TDP222669; b the hotspots of p53–MDM2 interaction; c the binding mode of nutlin-2 with MDM2; d the binding mode of RG7112 with MDM2; e the binding mode of TDP222669 with MDM2

(*cis*-imidazoline analogs **31–32**) as potent small-molecule p53–MDM2 inhibitors (Fig. 2.7c) through HTS [93]. The crystal structure of the human MDM2–Nutlin-2 complex shows that the ligand binds to the three hotspots and mimics their interactions to a high degree (Fig. 2.7c). The imidazoline scaffold replaces the helical backbone of the peptide and is able to direct the side chains to the proper position. The two bromophenyl moieties occupy the Trp23 pocket and Leu26 pocket, respectively, and the ethyl ether side chain is located in the Phe19 pocket. Moreover, excellent anti-tumor potency of nutlin-3 was validated by a series of cellular and in vivo assays [93]. Notably, subsequent medicinal efforts of nutlins led to the discovery of a clinical candidate RG7112 (formerly RO5045337, **33**, Fig. 2.7d), which is under phase II clinical trial for the treatment of leukemias and solid tumors [94–96].

Another example from Johnson & Johnson also reported a HTS study of p53–HMD2 (a homology of MDM2) inhibitors [91]. A combinatorial library containing more than 338,000 compounds was screened using a temperature-dependent protein-unfolding assay [91]. A novel series of benzodiazepinedione inhibitors of the p53–HDM2 interaction was identified. TDP222669 (**34**) had a K_D value of 80 nM and showed potent in vitro and in vivo antitumor activities [97]. Further medicinal efforts of TDP222669 from our group led to the significant improvement of the in vitro antitumor activity [63, 64]. The bound conformation of TDP222669 is also similar to the α -helix of p53 peptide. Its core phenyl moiety, side chain chlorophenyl, and chlorobenzyl group interacted with the Phe19, Trp23, and Leu26 pocket, respectively (Fig. 2.7e). The above two examples indicate the usefulness of HTS in identifying PPI inhibitors. Also, the feasibility of PPI hotspots for drug design is validated. Moreover, clinical development of p53–MDM2 inhibitor RG7112 provides a proof-of-concept for the druggability of PPI targets.

2.5.2 Discovery and Structure-Based Optimization of PDE δ –KRAS Inhibitors

Oncogenic RAS signaling is an important antitumor target. Inhibition of the binding of mammalian PDE δ to KRAS by small molecules provides a novel opportunity to impair Ras localization and signaling, and discover novel antitumor agents [98]. Waldmann's group identified benzimidazole fragment **35** as a novel PDE δ –KRAS inhibitor by AlphaScreen HTS of about 150,000 in-house compounds (Fig. 2.8a) [83]. Compound **35** binds to the farnesyl-binding pocket of PDE δ and has a K_D value of 165 nM. Co-crystallization of PDE δ with compound **35** reveals that two molecules of **35** bind to the different sites of the protein, which form two hydrogen bonds with Arg61 and Tyr149, respectively (Fig. 2.8b). Structure-based approaches were used to optimize hit **35** [99]. First, the two benzimidazole hits were covalently linked by an ether bond and the resulting dimeric compound **36** showed significantly increased activity ($K_D = 39$ nM). Crystal structure of PDE δ in complex with linked bis-benzimidazole **36** indicates that the original orientation and

hydrogen-binding interaction of the two benzimidazoles are retained (Fig. 2.8c). Also, the crystal complex reveals that the allyl group can be replaced by a larger moiety. Guided by the binding mode, compound **37** with more steric cyclohexyl substitution showed improved activity ($K_D = 16$ nM). Another chiral piperidine derivative **37** (named deltarasin, $K_D = 38$ nM) was only comparable to **37**, but it has favorable solubility and membrane permeability. Further optimization of the phenyl ether linker discovered piperidine 4-carboxylic acid ester **38** with increased activity ($K_D = 10$ nM). Crystal structure of **38** in complex with PDE δ confirms the hydrogen-bonding interaction between the piperidine nitrogen and the backbone carbonyl of Cys56 (Fig. 2.8d). Considering the hydrolytic stability and physico-chemical properties, deltarasin was further evaluated in a number of assays. Deltarasin showed potent in vitro and in vivo anti-proliferative activity against human pancreatic ductal adenocarcinoma cells by inhibiting oncogenic RAS signaling. At the dose of 10 mg/kg (twice per day), deltarasin could almost completely inhibited in vivo growth of xenografted pancreatic carcinoma in nude mice.

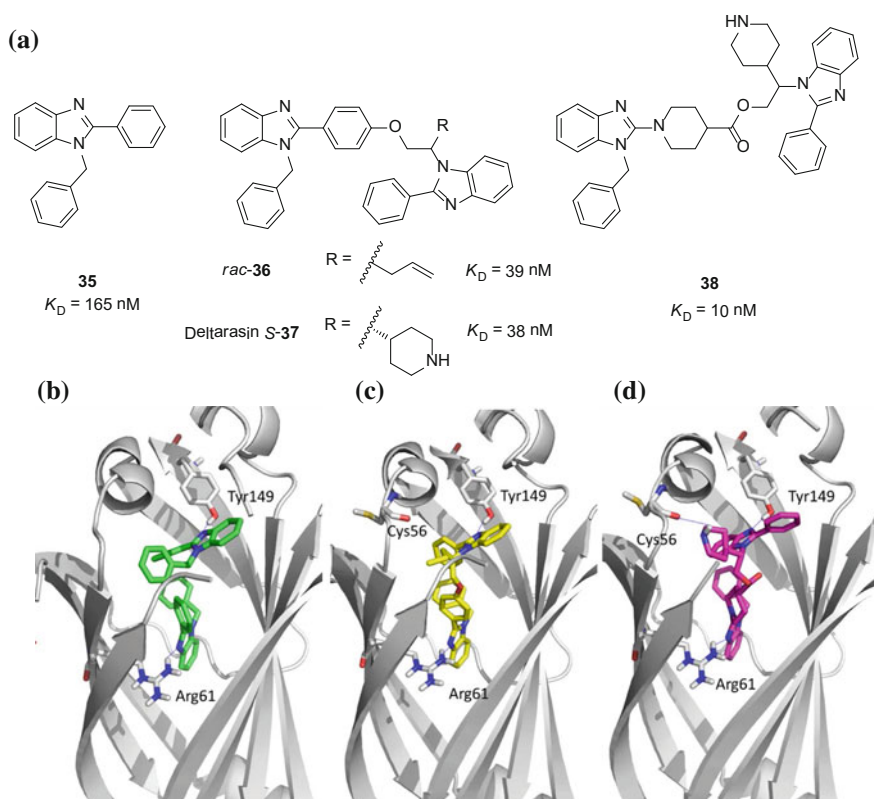


Fig. 2.8 Discovery and optimization of benzimidazole PDE δ -KRAS inhibitors. **a** Structures and binding affinities of benzimidazole PDE δ inhibitors. The binding modes of inhibitors **35** (**b**), **36** (**c**), and **37** (**d**) with PDE δ were generated from the crystal structures in PDB database (PDB codes: 4JV6, 4JVB, and 4JVF)

In 2016, Waldmann's group identified pyrazolopyridazinone (Fig. 2.9a, **39**, $K_D = 5$ nM) as the ligand of the prenyl-binding pocket of PDE δ from the same in-house library employing AlphaScreen HTS [100]. A co-crystal structure of compound **39** and PDE δ protein (Fig. 2.9b, PDB code: 5E80) revealed a deltarasin-type binding mode. The heterocycle of **39** forms H-bonds with Arg61 and Tyr149 for binding to PDE δ and the C-3 linker between the two hydrogen-bonding groups is important, which was kept for further optimization. Guided by the binding mode, deltazone (**40**) was obtained with a K_D value of 8 nM. This compound could decrease RAS-mediated signaling through PDE δ inhibition. However, its rapid metabolism in mice made it unsuitable for in vivo experiments.

Very recently, Waldmann and co-workers reported a novel bis-sulfonamide (Fig. 2.10a, **41**, $K_D = 13$ nM) through AlphaScreen HTS of the in-house compound library (increased to 200 K compounds) [101]. Co-crystal structure revealed that compound **41** formed three H-bonds to Arg61, Gln78, and Tyr149 and two additional interactions with the aromatic rings of Trp32 and Trp90 (Fig. 2.10b, PDB code: 5ML2). Further optimization obtained compound **42** ($K_D = 8$ nM) forming an additional H-bond with the carbonyl group of Cys56 (Fig. 2.10c, PDB code: 5ML8). Compound **43** (deltasonamide 1) was designed to form two water molecule-mediated H-bonds to the Glu88 side chain and the amide proton of Met118 (Fig. 2.10d, PDB code: 5ML3). The biochemical potency of the seven-hydrogen-bonding compound was increased to picomolar level ($K_D = 203$ pM). Introducing a 4-aminocyclohexane moiety obtained an analog (**44**, deltasonamide 2) exhibiting picomolar affinity ($K_D = 385$ pM). In the oncogenic KRAS-dependent Panc-Tu-1 and MiaPaCa-2 cells, the IC_{50} value of compound **44**

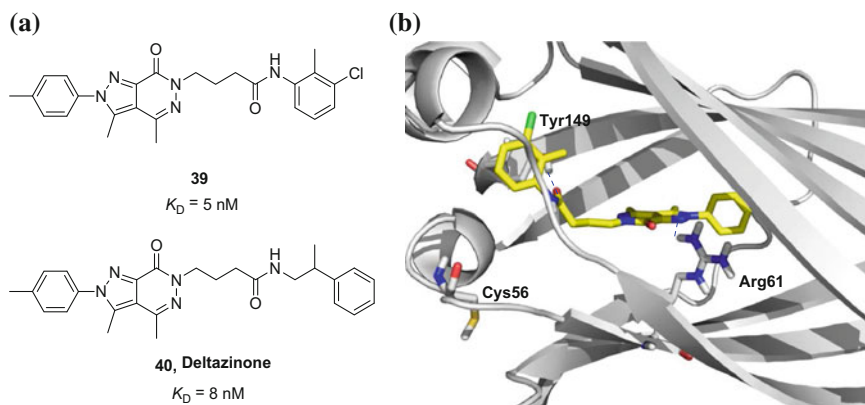


Fig. 2.9 Discovery and optimization of pyrazolopyridazinone PDE δ -KRAS inhibitors. **a** Structures and binding affinities of pyrazolopyridazinone PDE δ inhibitors. **b** The binding modes of inhibitor **39** with PDE δ were generated from the crystal structures in PDB database (PDB codes: 5E80)

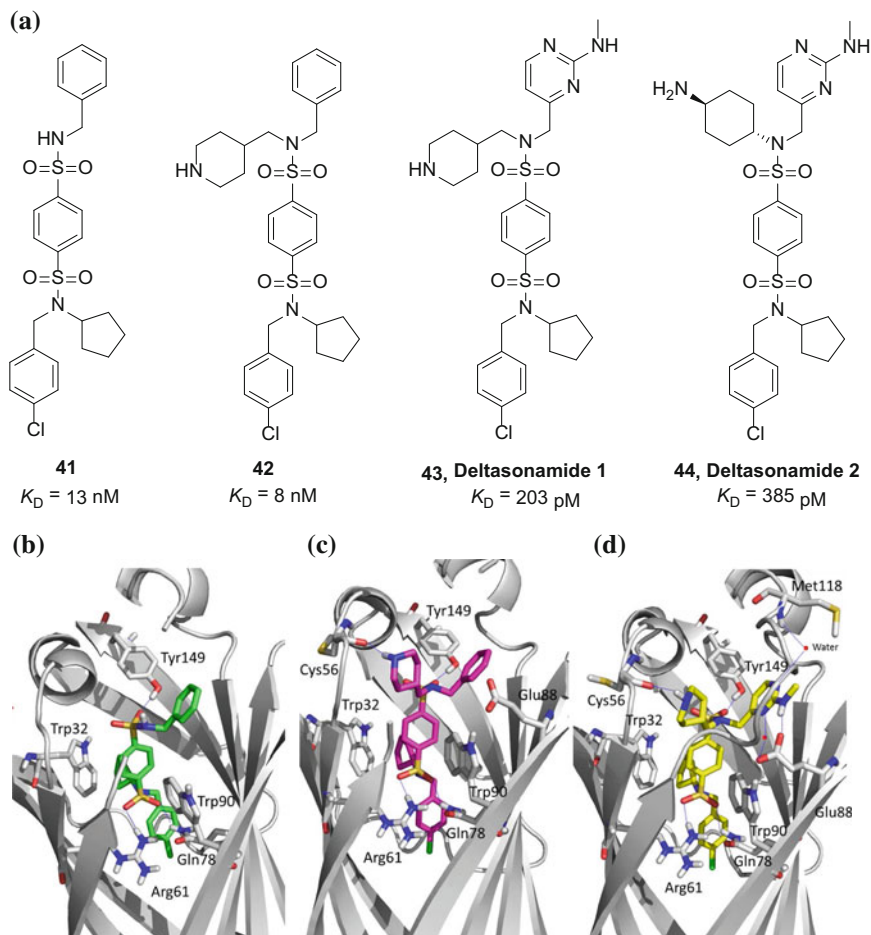


Fig. 2.10 Discovery and optimization of benzimidazole PDE δ -KRAS inhibitors. **a** Structures and binding affinities of benzimidazole PDE δ inhibitors. The binding modes of inhibitors **41** (**b**), **42** (**c**), and **43** (**d**) with PDE δ protein were generated from the crystal structures in PDB database (PDB codes: 5ML2, 5ML8, 5ML3)

was 750 nM and 1500 nM, respectively. However, for the KRas-independent Panc-1 cells, both of them showed reduced activity.

2.6 Conclusions

HTS is an important strategy in the discovery of small-molecule PPI inhibitors particularly prevalent in pharmaceutical industries, which has led to several clinical candidates. New chemical space compatible with PPI inhibitors remains to be

constructed. Highly efficient synthetic methods, such as MCR, DOS, and BIOS, will contribute to build high-quality compound libraries and increase the hit rate of HTS. Moreover, new HTS assays with improved sensitivity and reliability are highly desirable to reduce the false positives and identify drug-like hits or leads. Validation of HTS hits and subsequent medicinal chemistry optimization are necessary to improve the efficiency of PPI-based drug development.

References

1. Arkin MR, Wells JA (2004) Small-molecule inhibitors of protein-protein interactions: progressing towards the dream. *Nat Rev Drug Discov* 3(4):301–317
2. Fry DC (2008) Drug-like inhibitors of protein-protein interactions: a structural examination of effective protein mimicry. *Curr Protein Pept Sci* 9(3):240–247
3. Whitty A, Kumaravel G (2006) Between a rock and a hard place? *Nat Chem Biol* 2(3):112–118
4. Sheng C, Dong G, Miao Z, Zhang W, Wang W (2015) State-of-the-art strategies for targeting protein-protein interactions by small-molecule inhibitors. *Chem Soc Rev* 44(22):8238–8259
5. Cheng T, Li Q, Zhou Z, Wang Y, Bryant SH (2012) Structure-based virtual screening for drug discovery: a problem-centric review. *AAPS J* 14(1):133–141
6. Heeres JT, Hergenrother PJ (2011) High-throughput screening for modulators of protein-protein interactions: use of photonic crystal biosensors and complementary technologies. *Chem Soc Rev* 40(8):4398–4410
7. Gul S, Hadian K (2014) Protein-protein interaction modulator drug discovery: past efforts and future opportunities using a rich source of low- and high-throughput screening assays. *Expert Opin Drug Discov* 9(12):1393–1404
8. Adler-Moore JP, Gangneux JP, Pappas PG (2016) Comparison between liposomal formulations of amphotericin B. *Med Mycol* 54(3):223–231
9. Choi S, Choi KY (2017) Screening-based approaches to identify small molecules that inhibit protein-protein interactions. *Expert Opin Drug Discov* 12(3):293–303
10. Ruijter E, Scheffelaar R, Orru RV (2011) Multicomponent reaction design in the quest for molecular complexity and diversity. *Angew Chem Int Ed Engl* 50(28):6234–6246
11. Antuch W, Menon S, Chen QZ, Lu Y, Sakamuri S, Beck B, Schauer-Vukasinovic V, Agarwal S, Hess S, Domling A (2006) Design and modular parallel synthesis of a MCR derived alpha-helix mimetic protein-protein interaction inhibitor scaffold. *Bioorg Med Chem Lett* 16(6):1740–1743
12. Xu Y, Lu H, Kennedy JP, Yan X, McAllister LA, Yamamoto N, Moss JA, Boldt GE, Jiang S, Janda KD (2006) Evaluation of “credit card” libraries for inhibition of HIV-1 gp41 fusogenic core formation. *J Comb Chem* 8(4):531–539
13. Monfardini I, Huang JW, Beck B, Cellitti JF, Pellicchia M, Domling A (2011) Screening multicomponent reactions for X-linked inhibitor of apoptosis-baculoviral inhibitor of apoptosis protein repeats domain binder. *J Med Chem* 54(3):890–900
14. Boltjes A, Huang Y, van de Velde R, Rijke L, Wolf S, Gaugler J, Lesniak K, Guzik K, Holak TA, Domling A (2014) Fragment-based library generation for the discovery of a peptidomimetic p53-Mdm4 inhibitor. *ACS Comb Sci* 16(8):393–396
15. Czarna A, Beck B, Srivastava S, Popowicz GM, Wolf S, Huang Y, Bista M, Holak TA, Domling A (2010) Robust generation of lead compounds for protein-protein interactions by computational and MCR chemistry: p53/Hdm2 antagonists. *Angew Chem Int Ed Engl* 49(31):5352–5356
16. Schreiber SL (2009) Organic chemistry: molecular diversity by design. *Nature* 457(7226):153–154

17. Koes D, Khoury K, Huang Y, Wang W, Bista M, Popowicz GM, Wolf S, Holak TA, Domling A, Camacho CJ (2012) Enabling large-scale design, synthesis and validation of small molecule protein-protein antagonists. *PLoS ONE* 7(3):e32839
18. Cj OC, Beckmann HS, Spring DR (2012) Diversity-oriented synthesis: producing chemical tools for dissecting biology. *Chem Soc Rev* 41(12):4444–4456
19. Kim J, Kim H, Park SB (2014) Privileged structures: efficient chemical “navigators” toward unexplored biologically relevant chemical spaces. *J Am Chem Soc* 136(42):14629–14638
20. Nielsen TE, Schreiber SL (2008) Towards the optimal screening collection: a synthesis strategy. *Angew Chem Int Ed Engl* 47(1):48–56
21. Galloway WR, Isidro-Llobet A, Spring DR (2010) Diversity-oriented synthesis as a tool for the discovery of novel biologically active small molecules. *Nat Commun* 1:80
22. Grossmann A, Bartlett S, Janecek M, Hodgkinson JT, Spring DR (2014) Diversity-oriented synthesis of drug-like macrocyclic scaffolds using an orthogonal organo- and metal catalysis strategy. *Angew Chem Int Ed Engl* 53(48):13093–13097
23. Beckmann HS, Nie F, Hagerman CE, Johansson H, Tan YS, Wilcke D, Spring DR (2013) A strategy for the diversity-oriented synthesis of macrocyclic scaffolds using multidimensional coupling. *Nat Chem* 5(10):861–867
24. Marsault E, Peterson ML (2011) Macrocycles are great cycles: applications, opportunities, and challenges of synthetic macrocycles in drug discovery. *J Med Chem* 54(7):1961–2004
25. Rubin LL, de Sauvage FJ (2006) Targeting the Hedgehog pathway in cancer. *Nat Rev Drug Discov* 5(12):1026–1033
26. Stanton BZ, Peng LF, Maloof N, Nakai K, Wang X, Duffner JL, Taveras KM, Hyman JM, Lee SW, Koehler AN, Chen JK, Fox JL, Mandinova A, Schreiber SL (2009) A small molecule that binds Hedgehog and blocks its signaling in human cells. *Nat Chem Biol* 5(3):154–156
27. Marcaurelle LA, Johannes C, Yohannes D, Tillotson BP, Mann D (2009) Diversity-oriented synthesis of a cytosine-inspired pyridone library leading to the discovery of novel inhibitors of Bcl-2. *Bioorg Med Chem Lett* 19(9):2500–2503
28. Zhang Y, Wang S, Wu S, Zhu S, Dong G, Miao Z, Yao J, Zhang W, Sheng C, Wang W (2013) Facile construction of structurally diverse thiazolidinedione-derived compounds via divergent stereoselective cascade organocatalysis and their biological exploratory studies. *ACS Comb Sci* 15(6):298–308
29. Zhang Y, Wu S, Wang S, Fang K, Dong G, Liu N, Miao Z, Yao J, Li J, Zhang W, Sheng C, Wang W (2015) Divergent cascade construction of skeletally diverse “Privileged” pyrazole-derived molecular architectures. *Eur J Org Chem* 9:2030–2037
30. Wang S, Jiang Y, Wu S, Dong G, Miao Z, Zhang W, Sheng C (2016) Meeting organocatalysis with drug discovery: asymmetric synthesis of 3,3'-Spirooxindoles fused with tetrahydrothiopyrans as novel p53-MDM2 inhibitors. *Org Lett* 18(5):1028–1031
31. Bon RS, Waldmann H (2010) Bioactivity-guided navigation of chemical space. *Acc Chem Res* 43(8):1103–1114
32. Wetzel S, Bon RS, Kumar K, Waldmann H (2011) Biology-oriented synthesis. *Angew Chem Int Ed Engl* 50(46):10800–10826
33. Svenda J, Sheremet M, Kremer L, Maier L, Bauer JO, Strohmam C, Ziegler S, Kumar K, Waldmann H (2015) Biology-oriented synthesis of a withanolide-inspired compound collection reveals novel modulators of hedgehog signaling. *Angew Chem Int Ed Engl* 54(19):5596–5602
34. Antonchick AP, Gerding-Reimers C, Catarinella M, Schurmann M, Preut H, Ziegler S, Rauh D, Waldmann H (2010) Highly enantioselective synthesis and cellular evaluation of spirooxindoles inspired by natural products. *Nat Chem* 2(9):735–740
35. Duckert H, Pries V, Khedkar V, Menninger S, Bruss H, Bird AW, Maliga Z, Brockmeyer A, Janning P, Hyman A, Grimme S, Schurmann M, Preut H, Hubel K, Ziegler S, Kumar K, Waldmann H (2011) Natural product-inspired cascade synthesis yields modulators of centrosome integrity. *Nat Chem Biol* 8(2):179–184

36. Wells JA, McClendon CL (2007) Reaching for high-hanging fruit in drug discovery at protein-protein interfaces. *Nature* 450(7172):1001–1009
37. Zhao HF, Kiyota T, Chowdhury S, Purisima E, Banville D, Konishi Y, Shen SH (2004) A mammalian genetic system to screen for small molecules capable of disrupting protein-protein interactions. *Anal Chem* 76(10):2922–2927
38. Makley LN, Gestwicki JE (2013) Expanding the number of ‘druggable’ targets: non-enzymes and protein-protein interactions. *Chem Biol Drug Des* 81(1):22–32
39. Couturier C, Deprez B (2012) Setting up a bioluminescence resonance energy transfer high throughput screening assay to search for protein/protein interaction inhibitors in mammalian cells. *Front Endocrinol (Lausanne)* 3:100
40. Kenny CH, Ding W, Kelleher K, Benard S, Dushin EG, Sutherland AG, Mosyak L, Kriz R, Ellestad G (2003) Development of a fluorescence polarization assay to screen for inhibitors of the FtsZ/ZipA interaction. *Anal Biochem* 323(2):224–233
41. Emami KH, Nguyen C, Ma H, Kim DH, Jeong KW, Eguchi M, Moon RT, Teo JL, Kim HY, Moon SH, Ha JR, Kahn M (2004) A small molecule inhibitor of beta-catenin/CREB-binding protein transcription. *Proc Natl Acad Sci USA* 101(34):12682–12687
42. Chen T, Kablaoui N, Little J, Timofeevski S, Tschantz WR, Chen P, Feng J, Charlton M, Stanton R, Bauer P (2009) Identification of small-molecule inhibitors of the JIP-JNK interaction. *Biochem J* 420(2):283–294
43. Stebbins JL, De SK, Machleidt T, Becattini B, Vazquez J, Kuntzen C, Chen LH, Cellitti JF, Riel-Mehan M, Emdadi A, Solinas G, Karin M, Pellecchia M (2008) Identification of a new JNK inhibitor targeting the JNK-JIP interaction site. *Proc Natl Acad Sci USA* 105(43):16809–16813
44. Glanzer JG, Liu S, Oakley GG (2011) Small molecule inhibitor of the RPA70 N-terminal protein interaction domain discovered using in silico and in vitro methods. *Bioorg Med Chem* 19(8):2589–2595
45. Hain AU, Bartee D, Sanders NG, Miller AS, Sullivan DJ, Levitskaya J, Meyers CF, Bosch J (2014) Identification of an Atg8-Atg3 protein-protein interaction inhibitor from the medicines for Malaria Venture Malaria Box active in blood and liver stage *Plasmodium falciparum* parasites. *J Med Chem* 57(11):4521–4531
46. Hu L, Magesh S, Chen L, Wang L, Lewis TA, Chen Y, Khodier C, Inoyama D, Beamer LJ, Emge TJ, Shen J, Kerrigan JE, Kong AN, Dandapani S, Palmer M, Schreiber SL, Munoz B (2013) Discovery of a small-molecule inhibitor and cellular probe of Keap1-Nrf2 protein-protein interaction. *Bioorg Med Chem Lett* 23(10):3039–3043
47. Marcotte D, Zeng W, Hus JC, McKenzie A, Hession C, Jin P, Bergeron C, Lugovskoy A, Enyedy I, Cuervo H, Wang D, Atmanene C, Roecklin D, Vecchi M, Vivat V, Kraemer J, Winkler D, Hong V, Chao J, Lukashev M, Silvan L (2013) Small molecules inhibit the interaction of Nrf2 and the Keap1 Kelch domain through a non-covalent mechanism. *Bioorg Med Chem* 21(14):4011–4019
48. Jameson DM, Ross JA (2010) Fluorescence polarization/anisotropy in diagnostics and imaging. *Chem Rev* 110(5):2685–2708
49. Perrin F (1926) Polarisation of fluorescence and mean life of excited molecules. *J Phys Radium* 7(12):390–401
50. Albrecht AC (1961) Polarizations and assignments of transitions: the method of photoselection. *J Mol Spectrosc* 6:84–108
51. Weber G (1953) Rotational Brownian motion and polarization of the fluorescence of solutions. *Adv Protein Chem* 8:415–459
52. Perrin F (1936) Brownian motion of an ellipsoid. II. Free rotation and depolarisation of fluorescence: Translation and diffusion of ellipsoidal molecules. *J Phys Radium* 7(1):1–11
53. Moerke NJ (2009) Fluorescence Polarization (FP) assays for monitoring peptide-protein or nucleic acid-protein binding. *Curr Protoc Chem Biol* 1(1):1–15
54. Lodge JM, Rettenmaier TJ, Wells JA, Pomerantz WC, Mapp AK (2014) FP tethering: a screening technique to rapidly identify compounds that disrupt protein-protein interactions. *MedChemCommun* 5(3):370–375

55. Lea WA, Simeonov A (2011) Fluorescence polarization assays in small molecule screening. *Expert Opin Drug Discov* 6(1):17–32
56. Owicki JC (2000) Fluorescence polarization and anisotropy in high throughput screening: perspectives and primer. *J Biomol Screen* 5(5):297–306
57. Gribbon P, Sewing A (2003) Fluorescence readouts in HTS: no gain without pain? *Drug Discov Today* 8(22):1035–1043
58. Shoichet BK (2006) Screening in a spirit haunted world. *Drug Discov Today* 11(13–14):607–615
59. Rush TS 3rd, Grant JA, Mosyak L, Nicholls A (2005) A shape-based 3-D scaffold hopping method and its application to a bacterial protein-protein interaction. *J Med Chem* 48(5):1489–1495
60. Zhuang C, Miao Z, Zhu L, Dong G, Guo Z, Wang S, Zhang Y, Wu Y, Yao J, Sheng C, Zhang W (2012) Discovery, synthesis, and biological evaluation of orally active pyrrolidone derivatives as novel inhibitors of p53-MDM2 protein-protein interaction. *J Med Chem* 55(22):9630–9642
61. Zhuang C, Miao Z, Wu Y, Guo Z, Li J, Yao J, Xing C, Sheng C, Zhang W (2014) Double-edged swords as cancer therapeutics: novel, orally active, small molecules simultaneously inhibit p53-MDM2 interaction and the NF-kappaB pathway. *J Med Chem* 57(3):567–577
62. Lu Y, Nikolovska-Coleska Z, Fang X, Gao W, Shangary S, Qiu S, Qin D, Wang S (2006) Discovery of a nanomolar inhibitor of the human murine double minute 2 (MDM2)-p53 interaction through an integrated, virtual database screening strategy. *J Med Chem* 49(13):3759–3762
63. Guo Z, Zhuang C, Zhu L, Zhang Y, Yao J, Dong G, Wang S, Liu Y, Chen H, Sheng C, Miao Z, Zhang W (2012) Structure-activity relationship and antitumor activity of thio-benzodiazepines as p53-MDM2 protein-protein interaction inhibitors. *Eur J Med Chem* 56:10–16
64. Zhuang C, Miao Z, Zhu L, Zhang Y, Guo Z, Yao J, Dong G, Wang S, Liu Y, Chen H, Sheng C, Zhang W (2011) Synthesis and biological evaluation of thio-benzodiazepines as novel small molecule inhibitors of the p53-MDM2 protein-protein interaction. *Eur J Med Chem* 46(11):5654–5661
65. Kiessling A, Sperl B, Hollis A, Eick D, Berg T (2006) Selective inhibition of c-Myc/Max dimerization and DNA binding by small molecules. *Chem Biol* 13(7):745–751
66. Degterev A, Lugovskoy A, Cardone M, Mulley B, Wagner G, Mitchison T, Yuan J (2001) Identification of small-molecule inhibitors of interaction between the BH3 domain and Bcl-xL. *Nat Cell Biol* 3(2):173–182
67. Moerke NJ, Aktas H, Chen H, Cantel S, Reibarkh MY, Fahmy A, Gross JD, Degterev A, Yuan J, Chorev M, Halperin JA, Wagner G (2007) Small-molecule inhibition of the interaction between the translation initiation factors eIF4E and eIF4G. *Cell* 128(2):257–267
68. Förster T (1946) Th. Energiewanderung und Fluoreszenz. *Naturwissenschaften* 33:166–175
69. Wu P, Brand L (1994) Resonance energy transfer: methods and applications. *Anal Biochem* 218(1):1–13
70. Ma L, Yang F, Zheng J (2014) Application of fluorescence resonance energy transfer in protein studies. *J Mol Struct* 1077:87–100
71. Schaap M, Hancock R, Wilderspin A, Wells G (2013) Development of a steady-state FRET-based assay to identify inhibitors of the Keap1-Nrf2 protein-protein interaction. *Protein Sci* 22(12):1812–1819
72. Degorce F, Card A, Soh S, Trinquet E, Knapik GP, Xie B (2009) HTRF: a technology tailored for drug discovery—a review of theoretical aspects and recent applications. *Curr Chem Genomics* 3:22–32
73. Du Y, Fu RW, Lou B, Zhao J, Qui M, Khuri FR, Fu H (2013) A time-resolved fluorescence resonance energy transfer assay for high-throughput screening of 14-3-3 protein-protein interaction inhibitors. *Assay Drug Dev Technol* 11(6):367–381

74. Berg T, Cohen SB, Desharnais J, Sonderegger C, Maslyar DJ, Goldberg J, Boger DL, Vogt PK (2002) Small-molecule antagonists of Myc/Max dimerization inhibit Myc-induced transformation of chicken embryo fibroblasts. *Proc Natl Acad Sci USA* 99(6):3830–3835
75. Mathis G (1995) Probing molecular interactions with homogeneous techniques based on rare earth cryptates and fluorescence energy transfer. *Clin Chem* 41(9):1391–1397
76. Arai R, Nakagawa H, Tsumoto K, Mahoney W, Kumagai I, Ueda H, Nagamune T (2001) Demonstration of a homogeneous noncompetitive immunoassay based on bioluminescence resonance energy transfer. *Anal Biochem* 289(1):77–81
77. Mazars A, Fahraeus R (2010) Using BRET to study chemical compound-induced disruptions of the p53-HDM2 interactions in live cells. *Biotechnol J* 5(4):377–384
78. Cryan LM, Habeshian KA, Caldwell TP, Morris MT, Ackroyd PC, Christensen KA, Rogers MS (2013) Identification of small molecules that inhibit the interaction of TEM8 with anthrax protective antigen using a FRET assay. *J Biomol Screen* 18(6):714–725
79. Guo L, Teng L (2015) YAP/TAZ for cancer therapy: opportunities and challenges (review). *Int J Oncol* 46(4):1444–1452
80. Glickman JF, Wu X, Mercuri R, Illy C, Bowen BR, He Y, Sills M (2002) A comparison of ALPHAScreen, TR-FRET, and TRF as assay methods for FXR nuclear receptors. *J Biomol Screen* 7(1):3–10
81. Schorpp K, Rothenaigner I, Salmina E, Reinshagen J, Low T, Brenke JK, Gopalakrishnan J, Tetko IV, Gul S, Hadian K (2014) Identification of small-molecule frequent hitters from AlphaScreen high-throughput screens. *J Biomol Screen* 19(5):715–726
82. Hou Y, McGuinness DE, Prongay AJ, Feld B, Ingravallo P, Ogert RA, Lunn CA, Howe JA (2008) Screening for antiviral inhibitors of the HIV integrase-LEDGF/p75 interaction using the AlphaScreen luminescent proximity assay. *J Biomol Screen* 13(5):406–414
83. Zimmermann G, Papke B, Ismail S, Vartak N, Chandra A, Hoffmann M, Hahn SA, Triola G, Wittinghofer A, Bastiaens PI, Waldmann H (2013) Small molecule inhibition of the KRAS-PDEdelta interaction impairs oncogenic KRAS signalling. *Nature* 497(7451):638–642
84. Whitby RJ, Dixon S, Maloney PR, Delerive P, Goodwin BJ, Parks DJ, Willson TM (2006) Identification of small molecule agonists of the orphan nuclear receptors liver receptor homolog-1 and steroidogenic factor-1. *J Med Chem* 49(23):6652–6655
85. Cheng K, Wang X, Zhang S, Yin H (2012) Discovery of small-molecule inhibitors of the TLR1/TLR2 complex. *Angew Chem Int Ed Engl* 51(49):12246–12249
86. Goudreau N, Cameron DR, Deziel R, Hache B, Jakalian A, Malenfant E, Naud J, Ogilvie WW, O'Meara J, White PW, Yoakim C (2007) Optimization and determination of the absolute configuration of a series of potent inhibitors of human papillomavirus type-11 E1-E2 protein-protein interaction: a combined medicinal chemistry, NMR and computational chemistry approach. *Bioorg Med Chem* 15(7):2690–2700
87. Yoakim C, Ogilvie WW, Goudreau N, Naud J, Hache B, O'Meara JA, Cordingley MG, Archambault J, White PW (2003) Discovery of the first series of inhibitors of human papillomavirus type 11: inhibition of the assembly of the E1-E2-Origin DNA complex. *Bioorg Med Chem Lett* 13(15):2539–2541
88. Arnold LA, Estebanez-Perpina E, Togashi M, Jouravel N, Shelat A, McReynolds AC, Mar E, Nguyen P, Baxter JD, Fletterick RJ, Webb P, Guy RK (2005) Discovery of small molecule inhibitors of the interaction of the thyroid hormone receptor with transcriptional coregulators. *J Biol Chem* 280(52):43048–43055
89. Grembecka J, He S, Shi A, Purohit T, Muntean AG, Sorenson RJ, Showalter HD, Murai MJ, Belcher AM, Hartley T, Hess JL, Cierpicki T (2012) Menin-MLL inhibitors reverse oncogenic activity of MLL fusion proteins in leukemia. *Nat Chem Biol* 8(3):277–284
90. He S, Senter TJ, Pollock J, Han C, Upadhyay SK, Purohit T, Gogliotti RD, Lindsley CW, Cierpicki T, Stauffer SR, Grembecka J (2014) High-affinity small-molecule inhibitors of the menin-mixed lineage leukemia (MLL) interaction closely mimic a natural protein-protein interaction. *J Med Chem* 57(4):1543–1556

91. Grasberger BL, Lu T, Schubert C, Parks DJ, Carver TE, Koblisch HK, Cummings MD, LaFrance LV, Milkiewicz KL, Calvo RR, Maguire D, Lattanze J, Franks CF, Zhao S, Ramachandren K, Bylebyl GR, Zhang M, Manthey CL, Petrella EC, Pantoliano MW, Deckman IC, Spurlino JC, Maroney AC, Tomczuk BE, Molloy CJ, Bone RF (2005) Discovery and cocrystal structure of benzodiazepinedione HDM2 antagonists that activate p53 in cells. *J Med Chem* 48(4):909–912
92. Kussie PH, Gorina S, Marechal V, Elenbaas B, Moreau J, Levine AJ, Pavletich NP (1996) Structure of the MDM2 oncoprotein bound to the p53 tumor suppressor transactivation domain. *Science* 274(5289):948–953
93. Vassilev LT, Vu BT, Graves B, Carvajal D, Podlaski F, Filipovic Z, Kong N, Kammlott U, Lukacs C, Klein C, Fotouhi N, Liu EA (2004) In vivo activation of the p53 pathway by small-molecule antagonists of MDM2. *Science* 303(5659):844–848
94. Vu B, Wovkulich P, Pizzolato G, Lovey A, Ding Q, Jiang N, Liu JJ, Zhao C, Glenn K, Wen Y, Tovar C, Packman K, Vassilev L, Graves B (2013) Discovery of RG7112: a small-molecule MDM2 inhibitor in clinical development. *ACS Med Chem Lett* 4(5):466–469
95. Tovar C, Graves B, Packman K, Filipovic Z, Higgins B, Xia M, Tardell C, Garrido R, Lee E, Kolinsky K, To KH, Linn M, Podlaski F, Wovkulich P, Vu B, Vassilev LT (2013) MDM2 small-molecule antagonist RG7112 activates p53 signaling and regresses human tumors in preclinical cancer models. *Cancer Res* 73(8):2587–2597
96. Ray-Coquard I, Blay JY, Italiano A, Le Cesne A, Penel N, Zhi J, Heil F, Rueger R, Graves B, Ding M, Geho D, Middleton SA, Vassilev LT, Nichols GL, Bui BN (2012) Effect of the MDM2 antagonist RG7112 on the P53 pathway in patients with MDM2-amplified, well-differentiated or dedifferentiated liposarcoma: an exploratory proof-of-mechanism study. *Lancet Oncol* 13(11):1133–1140
97. Koblisch HK, Zhao S, Franks CF, Donatelli RR, Tominovich RM, LaFrance LV, Leonard KA, Gushue JM, Parks DJ, Calvo RR, Milkiewicz KL, Marugan JJ, Raboisson P, Cummings MD, Grasberger BL, Johnson DL, Lu T, Molloy CJ, Maroney AC (2006) Benzodiazepinedione inhibitors of the Hdm2:p53 complex suppress human tumor cell proliferation in vitro and sensitize tumors to doxorubicin in vivo. *Mol Cancer Ther* 5(1):160–169
98. Baker NM, Der CJ (2013) Cancer: drug for an ‘undruggable’ protein. *Nature* 497(7451):577–578
99. Zimmermann G, Schultz-Fademrecht C, Kuchler P, Murarka S, Ismail S, Triola G, Nussbaumer P, Wittinghofer A, Waldmann H (2014) Structure guided design and kinetic analysis of highly potent benzimidazole inhibitors targeting the PDEdelta prenyl binding site. *J Med Chem* 57(12):5435–5448
100. Papke B, Murarka S, Vogel HA, Martin-Gago P, Kovacevic M, Truxius DC, Fansa EK, Ismail S, Zimmermann G, Heinelt K, Schultz-Fademrecht C, Al Saabi A, Baumann M, Nussbaumer P, Wittinghofer A, Waldmann H, Bastiaens PI (2016) Identification of pyrazolopyridazinones as PDEdelta inhibitors. *Nat Commun* 7:11360
101. Martín-Gago P, Fansa EK, Klein CH, Murarka S, Janning P, Schürmann M, Metz M, Ismail S, Schultz-Fademrecht C, Baumann M, Bastiaens PIH, Wittinghofer A, Waldmann H (2017) A PDE6 δ -KRas inhibitor chemotype with up to seven H-bonds and picomolar affinity that prevents efficient inhibitor release by Arl2. *Angew Chem Int Ed Engl* 56(9):2423–2428

Chapter 3

Hot Spot-Based Design of Small-Molecule Inhibitors for Protein-Protein Interactions



Haitao Ji

3.1 Introduction

Protein-protein interactions (PPIs) play a pivotal role in most biological processes. The interface between two proteins typically has an area of 1500–3000 Å² with approximately 750–1500 Å² of surface area buried in each protein [1–3]. The formation of a protein-protein complex is largely driven by hydrophobic effects [4], which occur between the nonpolar regions of protein residues through van der Waals contacts. Electrostatic complementarity of the interacting protein surfaces between two proteins promotes the formation and lifetime of the complex. For some interfaces, hydrogen bonding and electrostatic interaction play a major role in steering one protein to dock onto the binding site of the second protein.

3.2 Characteristics of Hot Spots and Hot Regions

The residues on the protein-protein interface do not contribute equally to PPIs. A small subset of residues contributes to the majority of the binding free energy; they are called hot spots [5]. A hot spot is defined as a residue which substitution by an alanine leads to a significant decrease in the free energy of binding ($\Delta\Delta G_{\text{binding}} > 1.5$ kcal/mol) [5]. The experiment that involves individually mutat-

H. Ji (✉)

Drug Discovery Department, H. Lee Moffitt Cancer Center and Research Institute,
12902 Magnolia Drive, MRC room 4047,
Tampa, FL 33612-9416, USA
e-mail: Haitao.Ji@moffitt.org

H. Ji

Departments of Oncologic Sciences and Chemistry, University of South Florida, Tampa, FL,
USA

© Springer Nature Singapore Pte Ltd. 2018

C. Sheng and G. I. Georg (eds.), *Targeting Protein-Protein Interactions
by Small Molecules*, https://doi.org/10.1007/978-981-13-0773-7_3

ing interface residues to alanine, eliminating side chain atoms beyond C_{β} , and then measuring the effect of individual side chain on binding affinity is called alanine scanning. A survey of alanine scanning data indicated that the amino acid composition of hot spots was enriched in tryptophan (W), arginine (R), and tyrosine (Y) [6]. This trend of residue enrichment was also reproduced by a different surface analysis approach using clustered interface families [7]. Energetic hot spots from alanine scanning correlate with structurally conserved residues [8]. The number of the structurally conserved residues, in particular the energetic hot spots, increases with the expansion of the interacting surface area. Typically, hot spot density on the protein-protein interface composes 10% of the binding site residues [9].

The free energy of binding between two proteins is not a simple summation of the contribution from individual hot spots. Hot spots tend to occur in clusters. Within the cluster, the tightly packed hot spots are in contact with each other and form a network of conserved interactions called hot regions [10]. One example of hot regions in a protein-protein interface is shown in Fig. 3.1 [11]. The contributions of hot spots within one hot region are cooperative to stabilize PPIs. Hot regions are networked and contribute dominantly to the stability of PPIs. The energetic contributions between two hot regions can be additive [12] or cooperative [13].

The protruding hot region of one protein packs against the concave hot region of the other protein [4, 14]. Figure 3.2 illustrates a typical arrangement of hot spot and hot region. Residues 1–4 in Fig. 3.2 constitute the top hot region for the interactions between proteins A and B while residues 5–8 form the bottom hot region. For the

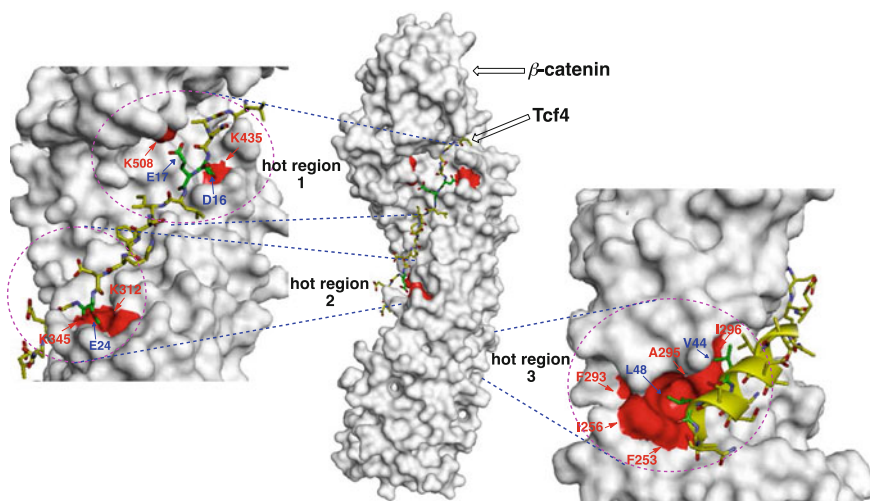


Fig. 3.1 Crystal structure of β -catenin in complex with T cell factor (Tcf) shows three hot regions (PDB IDs, 1G3J, and 2GL7). Hot region 1 includes K435 and K508 of β -catenin and D16 and E17 of Tcf4. Hot region 2 includes K312 and K345 of β -catenin and E24 and E29 of Tcf4. Hot region 3 includes F253, I256, F293, A295, and I296 of β -catenin and V44 and L48 of Tcf4. Reprinted from Ref. [11]

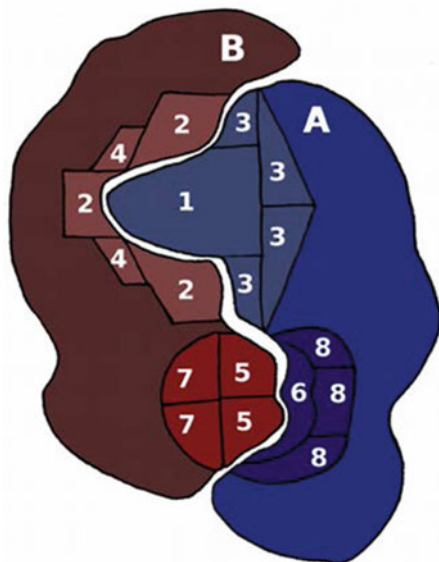


Fig. 3.2 Illustration of hot spots and hot regions in the protein-protein interface (adapted from Fig. 3.8 of Ref. [14]. Reprinted with the permission from Ref. [14]. Copyright 2011 American Chemical Society). The top hot region has a projecting hot spot, **1**, from protein A. This projecting residue binds to a complementary surface pocket of protein B, which is lined by residues that are labeled **2**. The residues on protein A that help to orient projecting hot spot **1** are labeled **3**. The residues on protein B that help to form the concave hot region are labeled **4**. The bottom hot region has two projecting hot spots from protein B that are labeled **5**. The concave surface pocket residue of protein A is labeled **6**. The residues in protein B that support the projecting hot spot are labeled **7**. The residues in protein A that support the formation of the concave hot region are labeled **8**. Reprinted from Ref. [11]

top hot region, residues 1 and 3 make a protruding hot region, and residues 2 and 4 create a concave hot region. The projecting hot spot, residue 1 in Fig. 3.2, makes a direct contact with hot spot 2 in the concave hot spot pocket. Residue 3 organizes the orientation of projecting hot spot 1, and 4 supports the structure of the hot spot pocket. Not only the alanine mutations of hot spots 1 and 2 but also the mutations of residues 3 and 4 would greatly affect the free energy of binding between proteins A and B. Therefore, residues 1–4 are all called energetic hot spots in the alanine scanning experiments. The projecting hot spots, 1 and 5 in Fig. 3.2, are also named anchor residues if the change of their solvent accessible surface areas (SASA) upon binding is $>0.5 \text{ \AA}^2$ [15, 16].

The concave hot regions are usually pre-organized in the unbound state prior to protein complexation [15, 17], as demonstrated in Fig. 3.3. The existence of such ready-made recognition motifs implies that the binding pathway can avoid kinetically costly structural rearrangement at the core of the binding interface, allowing for a relatively smooth recognition process. Once the protruding hot region is

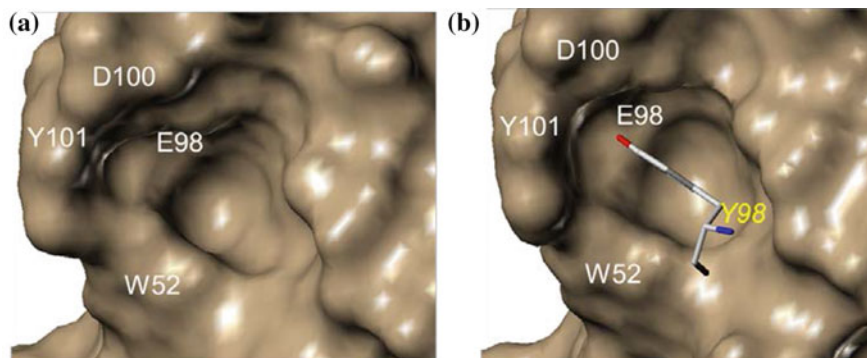


Fig. 3.3 Pre-organization of the concave hot region in the protein-protein interface. The anti-hen egg white lysozyme antibody D1.3/anti-idiotypic antibody E5.2 complex was used as an example [17]. Examination of the two structures reveals that the concave region of D1.3 is formed in both the absence and presence of E5.2. **a** The crystal structure of the apo antibody D1.3 (PDB id, 1VFB). **b** The crystal structure of the complex of antibodies D1.3 and E5.2 (PDB id, 1DVF). Reprinted from Ref. [11]

docked to the concave hot region, an induced fit process could further contribute to the formation of the final high-affinity complex.

Alanine scanning experiments to unravel hot spots are relatively time-consuming and labor-intensive. In some cases, the results of the alanine scanning experiments could be inconclusive. For example, the alanine mutation of residues that participate in forming concave hot regions likely gives rise to nonadditive $\Delta\Delta G_{\text{binding}}$ values. The alanine mutations could affect the free energy of binding by a mechanism unrelated to the PPIs at the interface, e.g., by destabilizing the unbound state of the protein or altering its conformation. Therefore, hot spots identified by alanine scanning experiments could be false positives in the sense that they do not reflect energetically important binding interactions with the partner protein. In addition, alanine scans could miss a binding hot spot that mostly involves interaction of backbone rather than side chain atoms. Computational methods have been developed to predict hot spots. These methods are complementary to the alanine scanning experiments and provide valuable insights into the nature of protein-protein complexation [18]. Some computational methods calculate the changes of free energy of binding upon mutation using calibrated free energy functions, such as Robetta [19] and FOLDEF [20]. A second group of computational methods incorporates molecular dynamics simulations in computational alanine scanning [21, 22]. The third group covers knowledge-based methods that learn the relationship between hot spots and various residue features from training data and then predict new hot spots [23–27]. Also, hybrid approaches that integrate the strengths of the machine learning and energy-based methods have been developed and applied to predict protein hot spots [28, 29].

Solvation also plays an important role in protein-protein association. Hot spots are often surrounded by energetically less important residues that shape like an

O-ring to occlude bulk water molecules from the hot spot [6]. The affinity of a hot region depends not only on the energetically critical hot spots located near the center of a hot region but also on the surrounding seal of contacting residues that establish the correct solvation environment. The O-ring structure results in a lower local dielectric constant environment and an enhancement of specific electrostatic and hydrogen bond interactions for the polar and ionizable hot spots. The further development of the O-ring structure led to the “double water exclusion” hypothesis. This hypothesis not only recognizes the existence of the hydrophobic O-ring structure but also assumes some hot spots themselves are water-free [30, 31]. Both the O-ring theory [32, 33] and the “double water exclusion” hypothesis [30, 31, 34] explain certain PPIs.

3.3 Druggable Hot Spot Pockets

Protein-protein interfaces have been recognized as biologically appealing targets for designing small-molecule chemical probes and/or therapeutic agents. However, the discovery of such small molecules with desired potency, selectivity, and physico-chemical properties has proven challenging [2, 3]. Protein-protein interfaces tend to be flat, featureless, and rather large (typically 1500–3000 Å²), while the surface of a protein often displays complex dynamic behavior. In contrast to enzymes or receptors that have one or two disproportionately large substrate-binding pockets with an average volume of 260 Å³, protein-protein interfaces are characterized by several shallow small pockets with an average volume of 54 Å³ for each pocket [35]. These features make the discovery of potent PPI inhibitors difficult. Nevertheless, the preexistence of the concave hot spot region on the unbound protein surface and the complementary packing of two hot regions from two interacting proteins provide impetus to search for small-molecule PPI inhibitors. A small-molecule PPI inhibitor should target 3–5 small pockets in the protein-protein surface and take advantage of protein adaptability [35]. The conformational adaptivity of a protein surface has frequently been observed when binding with a second protein or a small molecule [3]. It is possible that the protein surface adjacent to a concave hot region undergoes induced fit to accommodate small-molecule PPI inhibitors.

Hot spot pockets for PPIs are distinguishable from the other regions of protein surface due to their concave topology combined with a pattern of hydrophobic and polar functionality. This combination of properties confers on concave hot regions a tendency to bind small organic compounds possessing some polar functionality decorating a largely hydrophobic scaffold. In other words, concave hot regions on PPI surfaces are not simply the sites that are complementary to a particular organic functionality but rather possess a general tendency to bind organic compounds with a variety of structures. This property of hot regions has been observed in multiple solvent crystal structures (MSCS) [36] and structure–activity relationship by nuclear magnetic resonance (SAR by NMR) [37]. MSCS determines the X-ray

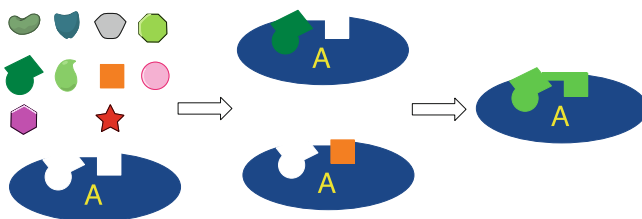


Fig. 3.4 Schematic diagram for SAR by NMR. The binding modes of a collection of fragments with target protein are studied by two-dimensional NMR spectra. The fragment hits from the NMR-based screen are then linked or evolved into drug-like molecules. Reprinted from Ref. [11]

structures of a target protein in aqueous solutions containing high concentrations of organic co-solvents and then superimposes the obtained crystal structures. Consensus binding sites have been observed from these crystal structures. A consensus binding site typically accommodates a number of different organic probes binding in well-defined orientations. SAR by NMR screens a library of fragments using NMR and identifies the specific binding pocket for each fragment hit, guiding the synthesis of larger molecules from the fragments that bind at multiple binding sites (Fig. 3.4). A fragment here is defined as a small organic molecule that follows the “rule of three” (the molecular weight of the compound ≤ 300 , $\text{ClogP} \leq 3$, the number of H-bond donors ≤ 3 , the number of H-bond acceptors ≤ 3 , the number of rotatable bonds ≤ 3 , and polar surface area (PSA) $\leq 60 \text{ \AA}^2$) [38]. The SAR by NMR studies observed the existence of consensus binding sites that were capable of binding a variety of small organic molecules. Further, studies of MSCS and SAR by NMR demonstrated that these consensus binding sites were often overlapped with energetic hot regions discovered through alanine scanning. Starting on a different path, protein phage display studies demonstrated that short peptides with entirely different structural scaffolds bound to the concave hot region and mimicked the binding mode for native PPIs [39]. These observations provide strong support for the efforts to discover small-molecule PPI inhibitors.

One should bear in mind that in identifying hot spots, alanine scanning experiments examine the contributions to the mutual interaction energy between two proteins, investigating both the concave and convex PPI regions. In contrast, the “consensus binding site” derived from MSCS or SAR by NMR is a property of a single protein, usually the concave PPI surface [40]. The energetically favored region identified by fragment screening is not necessarily a PPI hot region as its binding is determined simply by the concavity of the surface pocket and the chemical complementarity with fragment probes. If the structure of the protein-protein complex and the protruding hot spots are known, the relationship between the consensus binding sites identified by fragment screening and the concave hot regions can be established. FTMap, a computational solvent mapping program based on the fast Fourier transform correlation approach, has been used to predict the consensus binding site for 16 common solvents/small organic molecules [41].

The mapping results of FTMap have a high agreement with those derived from the X-ray crystallography and NMR studies [40, 42, 43]. FTMap is also able to rank the relative importance of the identified consensus binding sites.

Inspired by the results of MSCS, SAR by NMR, and computational solvent mapping, fragment screening has been used to identify new hits for PPI targets [44]. The libraries for fragment screening contain hundreds to thousands of low-molecular-weight fragments, which are screened at high concentrations. The binding affinities of commercially available fragments to protein targets are typically low. Highly sensitive biophysical methods are required to identify the fragments with weak binding affinities. The common techniques for fragment screening include NMR, X-ray crystallography, cysteine engineering-based tethering [45, 46], surface plasmon resonance (SPR), thermal shift [47], and confocal fluorescence correlation spectroscopy-based assays [48]. These methods can also be used in a synergistic way [49]. Dozens of potent PPI inhibitors with novel scaffolds have been reported by use of fragment screening coupled with structure-based optimization. Some well-known examples are the inhibitors for anti-apoptotic protein BCL-X_L/pro-apoptotic protein BAD interactions (Fig. 3.5a) [50], tumor necrosis factor α (TNF- α)/tumor necrosis factor receptor 1 (TNFR1) interactions [51], and interleukin-2 (IL-2)/interleukin-2 α receptor (IL-2R α) interactions [46]. It is worth noting that without structural and biochemical validation the fragments identified by fragment screening are not always useful for developing PPI inhibitors. If a fragment binds to the protein pocket outside the hot region, it may have no use. Carelessly evolving a fragment hit or linking two fragment hits might lead to a small molecule that tightly binds to the target protein but has no effect on disrupting PPIs. The prior knowledge of hot spots and hot regions derived from biochemical and crystallographic studies is essential for the success of fragment screening. An alternative of experimental fragment screening is hot spot-based virtual screening using a database of fragment-size molecules. One example is the discovery of **4** in Fig. 3.5b as an inhibitor for interferon- α (IFN- α)/type I interferon receptor (IFNAR) interactions [52]. NMR and SPR experiments confirm the direct binding of **4** with IFN- α .

The characteristics of a druggable PPI hot region have been investigated [58, 59]. The druggability of a pocket increases logarithmically with total surface area and apolar contact area, while it decreases logarithmically with polar contact area. The polar groups in the druggable binding site play a decisive role in recognizing drug-like small molecules [60]. There is an optimal size and composition of a protein pocket that is best suited for interacting with small organic molecules. The druggability of a protein pocket increases linearly with surface roughness [61]. Pocket shape also has a significant influence on druggability. The optimal value for pocket compactness (defined as pocket volume divided by pocket surface area) is ~ 0.4 . Large values, corresponding to more spherical shapes, or small values, corresponding to more elongated shapes, have a decreased contribution toward druggability. The amino acid composition around druggable PPI pockets is markedly different from that in the other areas on the protein surface. A higher frequency of aromatic residues and methionine has been observed in druggable PPI pockets

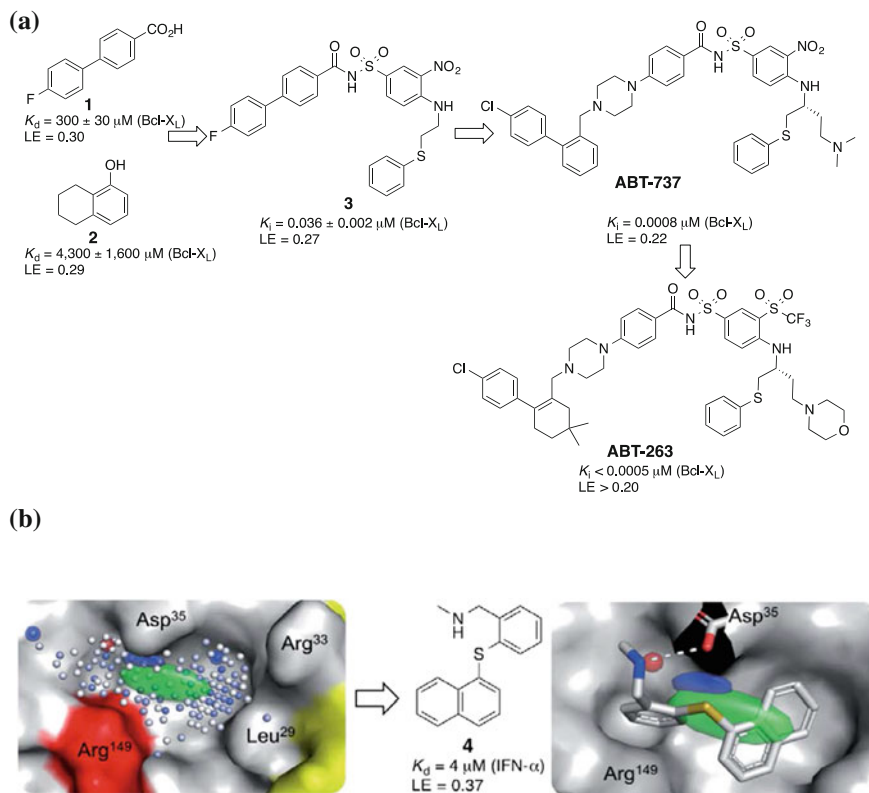


Fig. 3.5 Fragment-based screen to discover PPI inhibitors. **a** The discovery of BCL- X_L /BAD inhibitors. Fragments **1** and **2** were identified by SAR by NMR. They bind at two proximal subpockets on the BCL- X_L surface. Medicinal chemistry optimization yielded **3** with a K_i value of 3.6 nM for disrupting BCL- X_L /BAD interactions [53]. Subsequent lead optimization aimed at removing the binding to human serum albumin [54] and increasing potency to other BCL family proteins [55], which led to ABT-737 [50]. Further, optimization was centered to improve oral pharmacokinetics and resulted in the discovery of ABT-263 [56]. **b** Hot spot-based virtual screening identified **4** as an inhibitor for IFN- α /IFNAR interactions [52]. Pharmacophore model (green, lipophilic center; blue, hydrogen bond donor; red, hydrogen bond acceptor) inside the binding pocket of IFN- α and a docking pose of **4** in IFN- α were provided. LE, ligand efficiency; it is defined as free energy of ligand binding ($\Delta\Delta G = -RT \ln K_d$ or $\Delta\Delta G = -RT \ln K_i$, R: gas constant, T, Kelvin temperature used in the assays) divided by the number of non-hydrogen atoms of the tested compound [57]. Reprinted from Ref. [11]

[62, 63]. The molecular interplay between amino acids at a given hot region is also worth attention when identifying druggable PPI pockets. An increasing number of charged residues were reported to have a negative impact on the druggability of a pocket [58]. Furthermore, the conformational fluctuations of the areas adjacent to hot regions due to inherent thermal motions of a protein could open up transient pockets [64] that are important for accommodating a PPI inhibitor with drug-like

dimensions [65]. It was reported that druggable sites on PPIs are more predisposed than the rest of protein surface and more likely to accommodate drug-like molecules [66]. Indeed, mapping surface pockets by FTMap with a side chain conformer generator successfully identified druggable sites in the protein-protein interfaces [67].

3.4 Case Study 1

Due to the facts that: (1) the hot regions of PPIs are pre-organized on the protein surface and complementarily packed between two proteins; (2) the hot spots in the concave hot regions are deeply buried; and (3) the conformational transition to open up a new pocket for drug-like inhibitors has little energetic cost, and it is arguable that hot spot-based design could be an efficient approach in discovering drug-like PPI inhibitors. Wang and co-workers have used hot spot-based design to discover a series of spirooxindole-containing inhibitors for murine double minute 2 (MDM2)/tumor suppressor p53 interactions (Fig. 3.6). The inhibition of MDM2/p53 interactions by small molecules can restore the level of wild-type p53 and represents an appealing strategy for anticancer therapy. Crystallographic and biochemical studies revealed that three hydrophobic residues, F19, W23, and L26 from an α -helix in p53, form a hot region to interact with a concave hydrophobic hot region in MDM2.

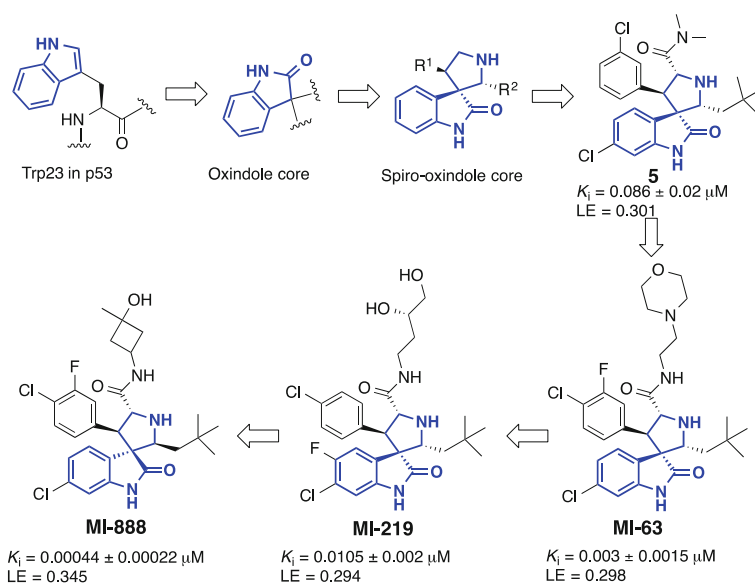


Fig. 3.6 Hot spot-based design of spirooxindole-containing MDM2/p53 PPI inhibitors. LE, ligand efficiency. Reprinted from Ref. [11]

The indole ring of p53 W23 was used as the starting point for inhibitor design, and the spirooxindole structure was used to build the inhibitor scaffold [68]. The oxindole moiety of the spirooxindole core was designed to mimic the binding mode of the side chain of p53 W23. Two hydrophobic substituents on the spirooxindole core, R¹ and R², were designed to mimic the binding mode of the side chains of F19 and L26, respectively. After the synthesis, compound **5** was found to have a K_i value of 0.086 ± 0.02 for disrupting MDM2/p53 PPIs. The optimization resulted in the discovery of MI-63 with a K_i value of 3 nM [69]. Consistent with its mode of action, MI-63 inhibits the growth of cancer cells with wild-type p53. Derivation to increase oral bioavailability and in vivo activity led to MI-219 [70] and MI-888 [71, 72]. MI-888 exhibits a K_i value of 0.00044 ± 0.00022 μM for disrupting MDM2/p53 interactions. This compound induces tumor regression in two xenograft models in a complete and durable manner.

3.5 Case Study 2

Dömling, Camacho, and co-workers also performed hot spot-based design to discover MDM2/p53 PPI inhibitors (Fig. 3.7). Residue W23 of p53 was again used as the starting point to initiate the design. 6-chloroindole and 4-chlorobenzene were defined as anchor fragments to mimic the indole ring of p53 W23. Multicomponent reactions (MCRs) were used to produce diverse scaffolds containing the 6-chloroindolyl or 4-chlorophenyl group [73]. The van Leusen three-component reaction was used to synthesize WK23, which exhibited a K_i value of 0.916 μM . The crystallographic analysis of MDM2 in complex with WK23 demonstrated that the 6-chloroindole moiety of WK23 was located at the same position as the side chain of p53 W23. The 6-chlorine atom of WK23 is positioned toward the very bottom of this concave hot region [74]. The nitrogen atom of 6-chloroindole forms a hydrogen bond with L54 carbonyl oxygen of MDM2 and mimics the binding mode of the indole nitrogen of p53 W23. The 4-chlorobenzyl group and the phenyl rings of WK23 occupy the L26 and F19 binding sites of p53, respectively. Further, modification of the WK23 structure led to the generation of WK298 exhibiting a K_i value of 0.109 μM . The Ugi four-component reaction was used to generate KK271 [75], YH239 [76], and **6** [77] which had K_i values of 1.2, 0.4, and 0.25 μM , respectively. A crystallographic analysis revealed a conformational change of the aromatic residues around the p53 F19/W23/L26 binding site [78]. The 4-chlorobenzyl group was introduced to YH119 to generate YH300 with a K_i value of 0.6 μM .

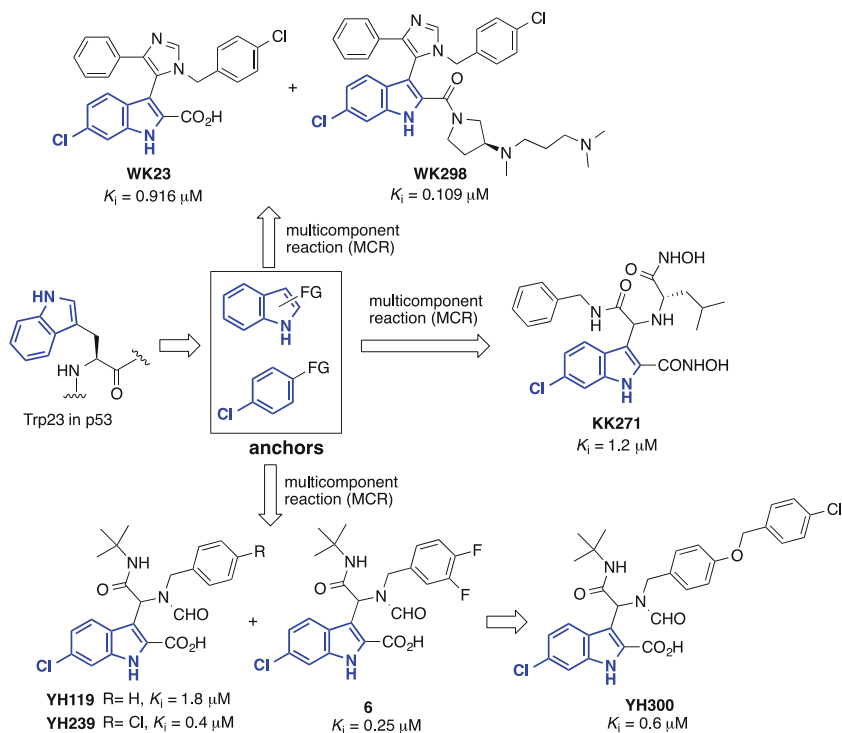


Fig. 3.7 Anchor-oriented design of chloroindole-containing MDM2/p53 PPI inhibitors. Reprinted from Ref. [11]

3.6 Case Study 3

Crews, Ciulli, and co-workers designed inhibitors for von Hippel–Lindau (VHL)/hypoxia-inducible factor 1 α (HIF1 α) interactions (Fig. 3.8) [79, 80]. The VHL protein is a component of the E3 ligase. The formation of the VHL/HIF1 α complex promotes the ubiquitination and degradation of HIF1 α by the proteasome. The accumulation of HIF1 α upregulates the genes that are involved in hypoxic response, and VHL/HIF1 α inhibitors can potentially be used to treat chronic anemia. 3-Hydroxy-L-proline (Hyp) 564 of HIF1 α is a hot spot for interacting with VHL. This residue was used as a starting point to design new inhibitors with the assistance of the de novo design software BOMB [81]. Compound **8** was discovered to exhibit an IC_{50} value of $117 \pm 10 \mu\text{M}$. The isoxazole moiety of **8** was designed to interact with a crystallographic water observed in the VHL/HIF1 α complex. The benzyl group of **8** was designed to stack with the side chain of Y98. An oxazole ring was then introduced to the *para* position of the benzyl group, resulting in **9** with an IC_{50} value of $4.1 \pm 0.4 \mu\text{M}$. Crystallographic analysis showed that the nitrogen atom of the oxazole ring formed an H-bond with R107 of VHL, and the

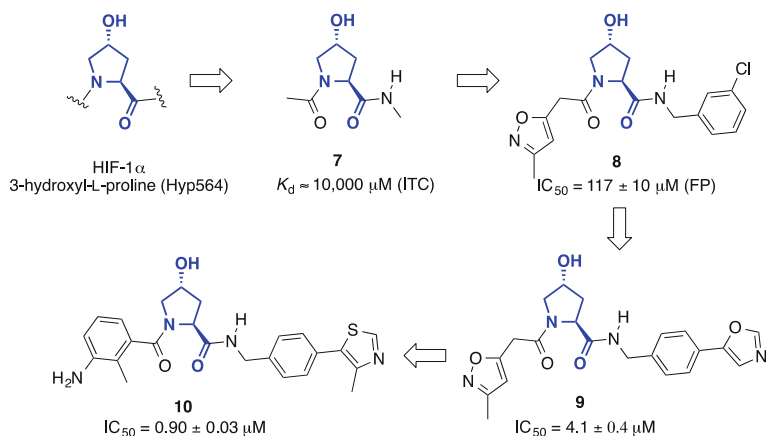


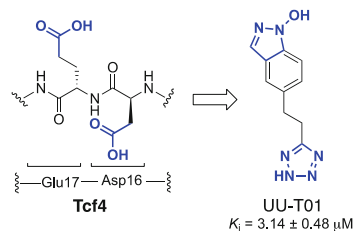
Fig. 3.8 Hot spot-based design of hydroxyproline-containing VHL/HIF1 α PPI inhibitors. Reprinted from Ref. [11]

C–H at position 2 of the oxazole ring in **9** formed a nonclassical H-bond with the carboxyl oxygen of P99. Further, optimization led to the generation of **10**. In this compound, the 4-methylthiazole ring replaced the oxazole ring, resulting in better interactions with a hydrophobic pocket in VHL. A substituted aniline was used to replace the isoxazolmethyl moiety. Crystallographic analysis showed that the aniline ring lay adjacent to the side chain of W88 and made a water-mediated H-bond with Q96 of VHL. This compound exhibited improved potency, with an IC_{50} value of $0.90 \pm 0.03 \mu\text{M}$ [82].

3.7 Case Study 4

Ji et al. used fragment hopping [83–85] to initiate the design of potent and selective PPI inhibitors. Fragment hopping requires the extraction of key binding elements based on the binding mode between the projecting hot spots and the concave hot spot pocket. The bioisosteric replacement technique is then used to design new fragments that match the proposed critical binding elements and generate new inhibitor structures with the chemotypes that do not exist in hot spots. As the first case study for PPI targets, this approach was employed to design small-molecule inhibitors for β -catenin/Tcf cell factor (Tcf) interactions (Fig. 3.9) [86]. The β -catenin/Tcf protein-protein complex is a key downstream effector of the canonical Wnt signaling pathway. The aberrant formation of this protein-protein complex overactivates Wnt target genes that cause the initiation and progression of many cancers and fibroses. The previous crystallographic and biochemical studies revealed three hot regions for β -catenin/Tcf PPIs, as shown in Fig. 3.1. The contribution of each hot region was quantitatively evaluated, and the D16/K435 and

Fig. 3.9 Bioisosteric replacement technique to design β -catenin/T cell factor PPI inhibitor, UU-T01. Reprinted from Ref. [11]



E17/K508 interactions were identified essential for the formation of the β -catenin/Tcf complex. Bioisosteres were used to mimic the binding mode of side chain carboxylic acids of Tcf4 D16 and E17, which led to UU-T01 with a K_i value of $3.14 \pm 0.48 \mu\text{M}$. This compound completely disrupts β -catenin/Tcf interactions and is two orders of magnitude more potent than dipeptide D–E. The binding mode of the designed inhibitors was evaluated by site-directed mutagenesis and structure–activity relationship (SAR) studies.

3.8 Epilogue

The discovery of small-molecule PPI inhibitors has been difficult. The low success rate for discovering PPI inhibitors was primarily ascribed to: (1) the overall characteristic of the protein–protein interface, which is large, flat, and featureless. The amount of buried surface area upon the formation of the protein–protein complex greatly exceeds the potential binding area of a small molecule, which highlights the value of rational design of PPI inhibitors and the need for new techniques to detect transient pockets; (2) the compound libraries used in HTS and virtual screening. The currently available compound collections were traditionally synthesized for enzyme and receptor targets, which contain binding sites drastically different from those in the protein–protein surfaces. The compound survey studies indicate that PPI inhibitors tend to be larger, more hydrophobic, more rigid, and contain multiple aromatic rings [87, 88]; (3) the difficulty to attain reliable HTS assays for some PPI targets, in particular for the weak PPIs with large contact surfaces [89, 90]; and (4) the flexibility of the protein surface around hot regions, which accounts for some failures of virtual screening. Hot spot-based design of PPI inhibitors is a valuable strategy for discovering PPI inhibitors. The hot spots and hot regions of PPIs can be identified and quantitatively evaluated by biochemical and crystallographic studies. Biologically important and druggable concave hot regions can be identified from the protein–protein interface. Sometimes, energetic cooperativity exists between two hot regions. The potency of a PPI inhibitor that targets a cooperative hot region can be amplified relative to the inhibitor that targets a hot region that is strictly additive. Fragment-size inhibitors can be designed and synthesized to mimic the binding mode of hot spots in a specified hot region that contributes most to the free energy of binding. Fragment hopping can play an

important role in designing such anchor fragments with new chemotypes. An O-ring structure can further be built into inhibitor structures to complement the concave hot region of PPIs when enlarging an anchor fragment.

Protein adaptability has frequently been observed for the structures around the hot regions of PPIs. Taking into account, protein adaptability in the process of generating drug-like PPI inhibitors is critical; this is also the advantage of hot spot-based design. After the design and validation of an anchor fragment for one concave hot region, this anchor fragment can be evolved into a drug-like PPI inhibitor with the consideration of protein adaptability.

Cellular proteins often use the same surface to bind with a structurally diverse set of proteins in different organelles or cellular environments. Inside of the cell, there is a complex network of PPIs [91]. With the mapping of the drug–target network [92], the evaluation and leverage of the selectivity/specificity of PPI inhibitors has become an emerging field. Hot spot-based design matches well with the need to discover PPI inhibitors with high selectivity/specificity because the hot spots that are essential for different binding partners could be located in different hot regions when more than one hot region exists on the protein surface [9]. For the proteins that use one identical hot region for interacting with multiple protein partners, the key binding elements for PPI selectivity often reside in the protein-protein interface adjacent to the concave hot region [93–96]. Indeed, hot spot-based inhibitor design for PPI target is still at its beginning stage, and few examples have been reported. More techniques need to be developed, and a surge of research in this field can be expected in the coming years.

References

1. Lo Conte L, Chothia C, Janin J (1999) The atomic structure of protein–protein recognition sites. *J Mol Biol* 285(5):2177–2198
2. Arkin MR, Wells JA (2004) Small-molecule inhibitors of protein-protein interactions: progressing towards the dream. *Nat Rev Drug Discov* 3(4):301–317
3. Wells JA, McClendon CL (2007) Reaching for high-hanging fruit in drug discovery at protein–protein interfaces. *Nature* 450(7172):1001–1009
4. Keskin O, GURSOY A, Ma B, Nussinov R (2008) Principles of protein-protein interactions: what are the preferred ways for proteins to interact? *Chem Rev* 108(4):1225–1244
5. Clackson T, Wells JA (1995) A hot spot of binding energy in a hormone-receptor interface. *Science* 267(5196):383–386
6. Bogan AA, Thorn KS (1998) Anatomy of hot spots in protein interfaces. *J Mol Biol* 280(1):1–9. doi:
7. Hu Z, Ma B, Wolfson H, Nussinov R (2000) Conservation of polar residues as hot spots at protein interfaces. *Proteins* 39(4):331–342
8. Ma B, Elkayam T, Wolfson H, Nussinov R (2003) Protein–protein interactions: structurally conserved residues distinguish between binding sites and exposed protein surfaces. *Proc Natl Acad Sci USA* 100(10):5772–5777
9. Carbonell P, Nussinov R, del Sol A (2009) Energetic determinants of protein binding specificity: insights into protein interaction networks. *Proteomics* 9(7):1744–1753

10. Keskin O, Ma B, Nussinov R (2005) Hot regions in protein–protein interactions: the organization and contribution of structurally conserved hot spot residues. *J Mol Biol* 345 (5):1281–1294
11. Guo W, Wisniewski JA, Ji H (2014) Hot spot-based design of small-molecule inhibitors for protein–protein interactions. *Bioorg Med Chem Lett* 24(11):2546–2554
12. Reichmann D, Rahat O, Albeck S, Meged R, Dym O, Schreiber G (2005) The modular architecture of protein–protein binding interfaces. *Proc Natl Acad Sci USA* 102(1):57–62
13. Moza B, Buonpane RA, Zhu P, Herfst CA, Rahman AKMN-u, McCormick JK, Kranz, DM, Sundberg EJ (2006) Long-range cooperative binding effects in a T cell receptor variable domain. *Proc Natl Acad Sci USA* 103(26):9867–9872
14. Golden MS, Cote SM, Sayeg M, Zerbe BS, Villar EA, Beglov D, Sazinsky SL, Georgiadis RM, Vajda S, Kozakov D, Whitty A (2013) Comprehensive experimental and computational analysis of binding energy hot spots at the NF- κ B essential modulator/IKK β protein–protein interface. *J Am Chem Soc* 135(16):6242–6256
15. Rajamani D, Thiel S, Vajda S, Camacho CJ (2004) Anchor residues in protein–protein interactions. *Proc Natl Acad Sci USA* 101(31):11287–11292
16. Meireles LMC, Dömling AS, Camacho CJ (2010) ANCHOR: a web server and database for analysis of protein–protein interaction binding pockets for drug discovery. *Nucleic Acids Res* 38:W407–W411
17. Li X, Keskin O, Ma B, Nussinov R, Liang J (2004) Protein–protein interactions: hot spots and structurally conserved residues often locate in complemented pockets that pre-organized in the unbound states: implications for docking. *J Mol Biol* 344(3):781–795
18. Morrow JK, Zhang S (2012) Computational prediction of protein hot spot residues. *Curr Pharm Des* 18(9):1255–1265
19. Kortemme T, Baker D (2002) A simple physical model for binding energy hot spots in protein–protein complexes. *Proc Natl Acad Sci USA* 99(22):14116–14121
20. Guerois R, Nielsen JE, Serrano L (2002) Predicting changes in the stability of proteins and protein complexes: a study of more than 1000 mutations. *J Mol Biol* 320(2):369–387
21. Massova I, Kollman PA (1999) Computational alanine scanning to probe protein–protein interactions: a novel approach to evaluate binding free energies. *J Am Chem Soc* 121 (36):8133–8143
22. Moreira IS, Fernandes PA, Ramos MJ (2007) Computational alanine scanning mutagenesis–an improved methodological approach. *J Comput Chem* 28(3):644–654
23. Darnell SJ, LeGault L, Mitchell JC (2008) KFC Server: interactive forecasting of protein interaction hot spots. *Nucleic Acids Res* 36:W265–W269
24. Tuncbag N, Gursoy A, Keskin O (2009) Identification of computational hot spots in protein interfaces: combining solvent accessibility and inter-residue potentials improves the accuracy. *Bioinformatics* 25(12):1513–1520
25. Cho K-I, Kim D, Lee D (2009) A feature-based approach to modeling protein-protein interaction hot spots. *Nucleic Acids Res* 37(8):2672–2687
26. Xia J-F, Zhao X-M, Song J, Huang D-S (2010) APIS: accurate prediction of hot spots in protein interfaces by combining protrusion index with solvent accessibility. *BMC Bioinform* 11:174
27. Zhu X, Mitchell JC (2011) KFC2: a knowledge-based hot spot prediction method based on interface solvation, atomic density, and plasticity features. *Proteins* 79(9):2671–2683
28. Masso M, Vaisman II (2008) Accurate prediction of stability changes in protein mutants by combining machine learning with structure based computational mutagenesis. *Bioinformatics* 24(18):2002–2009
29. Lise S, Archambeau C, Pontil M, Jones DT (2009) Prediction of hot spot residues at protein-protein interfaces by combining machine learning and energy-based methods. *BMC Bioinform* 10:365
30. Li J, Liu Q (2009) ‘Double water exclusion’: a hypothesis refining the O-ring theory for the hot spots at protein interfaces. *Bioinformatics* 25(6):743–750

31. Liu Q, Li J (2010) Protein binding hot spots and the residue-residue pairing preference: a water exclusion perspective. *BMC Bioinform* 11:244
32. Moreira IS, Fernandes PA, Ramos MJ (2007) Hot spot occlusion from bulk water: a comprehensive study of the complex between the lysozyme HEL and the antibody FVD1.3. *J Phys Chem B* 111(10):2697–2706
33. Moreira IS, Ramos RM, Martins JM, Fernandes PA, Ramos MJ (2014) Are hot-spots occluded from water? *J Biomol Struct Dyn* 32(2):186–197
34. Li Z, Li J (2010) Geometrically centered region: a “wet” model of protein binding hot spots not excluding water molecules. *Proteins* 78(16):3304–3316
35. Fuller JC, Burgoyne NJ, Jackson RM (2009) Predicting druggable binding sites at the protein–protein interface. *Drug Discov Today* 14(3–4):155–161
36. Mattos C, Ringe D (1996) Locating and characterizing binding sites on proteins. *Nat Biotechnol* 14(5):595–599
37. Shuker SB, Hajduk PJ, Meadows RP, Fesik SW (1996) Discovering high-affinity ligands for proteins: SAR by NMR. *Science* 274(5292):1531–1534
38. Congreve M, Carr R, Murray C, Jhoti H (2003) A ‘rule of three’ for fragment base discovery. *Drug Discov Today* 8(19):876–877
39. DeLano WL, Ultsch MH, de Vos AM, Wells JA (2000) Convergent solutions to binding at a protein–protein interface. *Science* 287(5456):1279–1283
40. Zerbe BS, Hall DR, Vajda S, Whitty A, Kozakov D (2012) Relationship between hot spot residues and ligand binding hot spots in protein–protein interfaces. *J Chem Inf Model* 52(8):2236–2344
41. Brenke R, Kozakov D, Chuang G-Y, Beglov D, Hall D, Landon MR, Mattos C, Vajda S (2009) Fragment-based identification of druggable ‘hot spots’ of proteins using Fourier domain correlation techniques. *Bioinformatics* 25(5):621–627
42. Buhman G, O’Connor C, Zerbe B, Kearney BM, Napoleon R, Kovrigina EA, Vajda S, Kozakov D, Kovrigin EL, Mattos C (2011) Analysis of binding site hot spots on the surface of Ras GTPase. *J Mol Biol* 413(4):773–789
43. Hall DH, Grove LE, Yueh C, Ngan CH, Kozakov D, Vajda S (2011) Robust identification of binding hot spots using continuum electrostatics: application to hen egg-white lysozyme. *J Am Chem Soc* 133(51):20668–20671
44. Winter A, Higuero AP, Marsh M, Sigurdardottir A, Pitt WR, Blundell TL (2012) Biophysical and computational fragment-based approaches to targeting protein–protein interactions: applications in structure-guided drug discovery. *Q Rev Biophys* 45(4):383–426
45. Erlanson DA, Braisted AC, Raphael DR, Randal M, Stroud RM, Gordon EM, Wells JA (2000) Site-directed ligand discovery. *Proc Natl Acad Sci USA* 97(17):9367–9372
46. Braisted AC, Oslob JD, Delano WL, Hyde J, McDowell RS, Waal N, Yu C, Arkin MR, Raimundo BC (2003) Discovery of a potent small molecule IL-2 inhibitor through fragment assembly. *J Am Chem Soc* 125(13):3714–3715
47. Scott DE, Ehebauer MT, Pukala T, Marsh M, Blundell TL, Venkitaraman AR, Abell C, Hyvönen M (2013) Using a fragment-based approach to target protein–protein interactions. *ChemBioChem* 14(3):332–342
48. Mikuni J, Kato M, Taruya S, Tsuganezawa K, Mori M, Ogawa N, Honma T, Yokoyama S, Kojima H, Okabe T, Nagano T, Tanaka A (2010) A fluorescence correlation spectroscopy-based assay for fragment screening of slowly inhibiting protein-peptide interaction inhibitors. *Anal Biochem* 402(1):26–31
49. Davis BJ, Erlanson DA (2013) Learning from our mistakes: the ‘unknown knowns’ in fragment screening. *Bioorg Med Chem Lett* 23(10):2844–2852
50. Oltersdorf T, Elmore SW, Shoemaker AR, Armstrong RC, Augeri DJ, Belli BA, Bruncko M, Deckwerth TL, Dinges J, Hajduk PJ, Joseph MK, Kitada S, Korsmeyer SJ, Kunzer AR, Letai A, Li C, Mitten MJ, Nettesheim DG, Ng S, Nimmer PM, O’Connor JM, Oleksijew A, Petros AM, Reed JC, Shen W, Tahir SK, Thompson CB, Tomaselli KJ, Wang B, Wendt MD, Zhang H, Fesik SW, Rosenberg SH (2005) An inhibitor of Bcl-2 family proteins induces regression of solid tumours. *Nature* 435(7042):677–681

51. He MM, Smith AS, Oslob JD, Flanagan WM, Braisted AC, Whitty A, Cancilla MT, Wang J, Lugovskoy AA, Yoburn JC, Fung AD, Farrington G, Eldredge JK, Day ES, Cruz LA, Cachero TG, Miller SK, Friedman JE, Choong IC, Cunningham BC (2005) Small-molecule inhibition of TNF- α . *Science* 310(5750):1022–1025
52. Geppert T, Bauer S, Hiss JA, Conrad E, Reutlinger M, Schneider P, Weisel M, Pfeiffer B, Altmann K-H, Waibler Z, Schneider G (2012) Immunosuppressive small molecule discovered by structure-based virtual screening for inhibitors of protein–protein interactions. *Angew Chem Int Ed* 51(1):258–261
53. Petros AM, Dinges J, Augeri DJ, Baumeister SA, Betebenner DA, Bures MG, Elmore SW, Hajduk PJ, Joseph MK, Landis SK, Nettesheim DG, Rosenberg SH, Shen W, Thomas S, Wang X, Zanze I, Zhang H, Fesik SW (2006) Discovery of a potent inhibitor of the antiapoptotic protein Bcl-xL from NMR and parallel synthesis. *J Med Chem* 49(2):656–663
54. Wendt MD, Shen W, Kunzer A, McClellan WJ, Bruncko M, Oost TK, Ding H, Joseph MK, Zhang H, Nimmer PM, Ng S-C, Shoemaker AR, Petros AM, Oleksijew A, Marsh K, Bauch J, Oltersdorf T, Belli BA, Martineau D, Fesik SW, Rosenberg SH, Elmore SW (2006) Discovery and structure-activity relationship of antagonists of B-cell lymphoma 2 family proteins with chemopotential activity in vitro and in vivo. *J Med Chem* 49(3):1165–1181
55. Bruncko M, Oost TK, Belli BA, Ding H, Joseph MK, Kunzer A, Martineau D, McClellan WJ, Mitten M, Ng S-C, Nimmer PM, Oltersdorf T, Park C-M, Petros AM, Shoemaker AR, Song X, Wang X, Wendt MD, Zhang H, Fesik SW, Rosenberg SH, Elmore SW (2007) Studies leading to potent, dual inhibitors of Bcl-2 and Bcl-xL. *J Med Chem* 50(4):641–662
56. Park C-M, Bruncko M, Adickes J, Bauch J, Ding H, Kunzer A, Marsh KC, Nimmer P, Shoemaker AR, Song X, Tahir SK, Tse C, Wang X, Wendt MD, Yang X, Zhang H, Fesik SW, Rosenberg SH, Elmore SW (2008) Discovery of an orally bioavailable small molecule inhibitor of pro-survival B-cell lymphoma 2 proteins. *J Med Chem* 51(21):6902–6915
57. Hopkins AL, Groom CR, Alex A (2004) Ligand efficiency: a useful metric for lead selection. *Drug Discov Today* 9(10):430–431
58. Hajduk PJ, Huth JR, Fesik SW (2005) Druggability indices for protein targets derived from NMR-based screening data. *J Med Chem* 48(7):2518–2525
59. Cheng AC, Coleman RG, Smyth KT, Cao Q, Soulard P, Caffrey DR, Salzberg AC, Huang ES (2007) Structure-based maximal affinity model predicts small-molecule druggability. *Nat Biotechnol* 25(1):71–75
60. Schmidtke P, Barril X (2010) Understanding and predicting druggability. A high-throughput method for detection of drug binding sites. *J Med Chem* 53(15):5858–5867
61. Pettit FK, Bowie JU (1999) Protein surface roughness and small molecular binding sites. *J Mol Biol* 285(4):1377–1382
62. Soga S, Shirai H, Kobori M, Hirayama N (2007) Use of amino acid composition to predict ligand-binding sites. *J Chem Inf Model* 47(2):400–406
63. Li Y, Liu Z, Han L, Li C, Wang R (2013) Mining the characteristic interaction patterns on protein–protein binding interfaces. *J Chem Inf Model* 53(9):2437–2447
64. Metz A, Pfeleger C, Kopitz H, Pfeiffer-Marek S, Baringhaus K-H, Gohlke H (2012) Hot spots and transient pockets: predicting the determinants of small-molecule binding to a protein–protein interface. *J Chem Inf Model* 52(1):120–133
65. Eyrich S, Helms V (2007) Transient pockets on protein surfaces involved in protein–protein interaction. *J Med Chem* 50(15):3457–3464
66. Johnson DK, Karanicolas J (2013) Druggable protein interaction sites are more predisposed to surface pocket formation than the rest of the protein surface. *PLoS Comput Biol* 9(3): e1002951
67. Kozakov D, Hall DR, Chuang G-Y, Cencic R, Brenke R, Grove LE, Beglov D, Pelletier J, Whitty A, Vajda S (2011) Structural conservation of druggable hot spots in protein–protein interfaces. *Proc Natl Acad Sci USA* 108(33):13528–13533

68. Ding K, Lu Y, Nikolovska-Coleska Z, Qiu S, Ding Y, Gao W, Stuckey J, Krajewski K, Roller PP, Tomita Y, Parrish DA, Deschamps JR, Wang S (2005) Structure-based design of potent non-peptide MDM2 inhibitors. *J Am Chem Soc* 127(29):10130–10131
69. Ding K, Lu Y, Nikolovska-Coleska Z, Wang G, Qiu S, Shangary S, Gao W, Qin D, Stuckey J, Krajewski K, Roller PP, Wang S (2006) Structure-based design of spiro-oxindoles as potent, specific small-molecule inhibitors of the MDM2–p53 interaction. *J Med Chem* 49(12):3432–3435
70. Shangary S, Qin D, McEachern D, Liu M, Miller RS, Qiu S, Nikolovska-Coleska Z, Ding K, Wang G, Chen J, Bernard D, Zhang J, Lu Y, Gu Q, Shah RB, Pienta KJ, Ling X, Kang S, Guo M, Sun Y, Yang D, Wang S (2008) Temporal activation of p53 by a specific MDM2 inhibitor is selectively toxic to tumors and leads to complete tumor growth inhibition. *Proc Natl Acad Sci USA* 105(10):3933–3938
71. Zhao Y, Liu L, Sun W, Lu J, McEachern D, Li X, Yu S, Bernard D, Ochsenbein P, Ferey V, Carry J-C, Deschamps JR, Sun D, Wang S (2013) Diastereomeric spirooxindoles as highly potent and efficacious MDM2 inhibitors. *J Am Chem Soc* 135(19):7223–7234
72. Zhao Y, Yu S, Sun W, Liu L, Lu J, McEachern D, Shangary S, Bernard D, Li X, Zhao T, Zou P, Sun D, Wang S (2013) A potent small-molecule inhibitor of the MDM2–p53 interaction (MI-888) achieved complete and durable tumor regression in mice. *J Med Chem* 56(13):5553–5561
73. Czarna A, Beck B, Srivastava S, Popowicz GM, Wolf S, Huang Y, Bista M, Holak TA, Dömling A (2010) Robust generation of lead compounds for protein–protein interactions by computational and MCR chemistry: p53/Hdm2 antagonists. *Angew Chem Int Ed* 49(31):5352–5356
74. Popowicz GM, Czarna A, Wolf S, Wang K, Wang W, Dömling A, Holak TA (2010) Structures of low molecular weight inhibitors bound to MDMX and MDM2 reveal new approaches for p53-MDMX/MDM2 antagonist drug discovery. *Cell Cycle* 9(6):1104–1111
75. Koes D, Khoury K, Huang Y, Wang W, Bista M, Popowicz GM, Wolf S, Holak TA, Dömling A, Camacho CJ (2012) Enabling large-scale design, synthesis and validation of small molecule protein–protein antagonists. *PLoS ONE* 7(3):e32839
76. Huang Y, Wolf S, Beck B, Köhler L-M, Khoury K, Popowicz GM, Goda SK, Subklewe M, Twarda A, Holak TA, Dömling A (2014) Discovery of highly potent p53-MDM2 antagonists and structural basis for anti-acute myeloid leukemia activities. *ACS Chem Biol* 9(3):802–811
77. Huang Y, Wolf S, Koes D, Popowicz GM, Camacho CJ, Holak TA, Dömling A (2012) Exhaustive fluorine scanning toward potent p53–Mdm2 antagonists. *ChemMedChem* 7(1):49–52
78. Bista M, Wolf S, Khoury K, Kowalska K, Huang Y, Wrona E, Arciniega M, Popowicz GM, Holak TA, Dömling A (2013) Transient protein states in designing inhibitors of the MDM2–p53 interaction. *Structure* 21(12):2143–2151
79. Buckley DL, Van Molle I, Gareiss PC, Tae HS, Michel J, Noblin DJ, Jorgensen WL, Ciulli A, Crews CM (2012) Targeting the von Hippel-Lindau E3 ubiquitin ligase using small molecules to disrupt the VHL/HIF-1 α interaction. *J Am Chem Soc* 134(10):4465–4468
80. Van Molle I, Thomann A, Buckley DL, So EC, Lang S, Crews CM, Ciulli A (2012) Dissecting fragment-based lead discovery at the von Hippel-Lindau protein:hypoxia inducible factor 1 α protein–protein interface. *Chem Biol* 19(10):1300–1312
81. Jorgensen WL (2009) Efficient drug lead discovery and optimization. *Acc Chem Res* 42(6):724–733
82. Buckley DL, Gustafson JL, Van Molle I, Roth AG, Tae HS, Gareiss PC, Jorgensen WL, Ciulli A, Crews CM (2012) Small-molecule inhibitors of the interaction between the E3 ligase VHL and HIF1 α . *Angew Chem Int Ed* 51(46):11463–11467
83. Ji H, Stanton BZ, Igarashi J, Li H, Martásek P, Roman LJ, Poulos TL, Silverman RB (2008) Minimal pharmacophoric elements and fragment hopping, an approach directed at molecular diversity and isozyme selectivity. Design of selective neuronal nitric oxide synthase inhibitors. *J Am Chem Soc* 130(12):3900–3914

84. Ji H, Li H, Martásek P, Roman LJ, Poulos TL, Silverman RB (2009) Discovery of highly potent and selective inhibitors of neuronal nitric oxide synthase by fragment hopping. *J Med Chem* 52(3):779–797
85. Teuscher KB, Ji H (2015) Protocol for fragment hopping. *Methods Mol Biol* 1289:57–73
86. Yu B, Huang Z, Zhang M, Dillard DR, Ji H (2013) Rational design of small-molecule inhibitors for β -catenin/T-cell factor protein–protein interactions by bioisostere replacement. *ACS Chem Biol* 8(3):524–529
87. Reynès C, Host H, Camproux A-C, Laconde G, Leroux F, Mazars A, Deprez B, Fahraeus R, Villoutreix BO, Sperandio O (2010) Designing focused chemical libraries enriched in protein-protein interaction inhibitors using machine-learning methods. *PLoS Comput Biol* 6(3):e1000695
88. Hamon V, Brunel JM, Combes S, Basse MJ, Roche P, Morelli X (2013) 2P2Ichem: focused chemical libraries dedicated to orthosteric modulation of protein–protein interactions. *MedChemComm* 4(5):797–809
89. Smith MC, Gestwicki JE (2012) Features of protein-protein interactions that translate into potent inhibitors: topology, surface area and affinity. *Expert Rev Mol Med* 14:e16
90. Cesa LC, Patury S, Komiyama T, Ahmad A, Zuiderweg ERP, Gestwicki JE (2013) Inhibitors of difficult protein-protein interactions identified by high-throughput screening of multiprotein complexes. *ACS Chem Biol* 8(9):1988–1997
91. (a) Venkatesan K, Rual J-F, Vazquez A, Stelzl U, Lemmens I, Hirozane-Kishikawa T, Hao T, Zenkner M, Xin X, Goh K-I, Yildirim MA, Simonis N, Heinzmann K, Gebreab F, Sahalie JM, Cevik S, Simon C, de Smet A-S, Dann E, Smolyar A, Vinayagam A, Yu H, Szeto D, Borick H, Dricot A, Klitgord N, Murray RR, Lin C, Lalowski M, Timm J, Rau K, Boone C, Braun P, Cusick ME, Roth FP, Hill DE, Tavernier J, Wanker EE, Barabási A-L, Vidal M (2009) An empirical framework for binary interactome mapping. *Nat Methods* 6(1):83–90; (b) Zhang QC, Petrey D, Deng L, Qiang L, Shi Y, Thu CA, Bisikirska B, Lefebvre C, Accili D, Hunter T, Maniatis T, Califano A, Honig B (2012) Structure-based prediction of protein-protein interactions on a genome-wide scale. *Nature* 490(7421):556–560
92. Yildirim MA, Goh K-I, Cusick ME, Barabási A-L, Vidal M (2007) Drug-target network. *Nat Biotechnol* 25(10):1119–1126
93. Huang Z, Zhang M, Burton SD, Katsakhyan LN, Ji H (2014) Targeting the Tcf4 G¹³ANDE¹⁷ binding site to selectively disrupt β -catenin/T-cell factor protein–protein interactions. *ACS Chem Biol* 9(1):193–201
94. Levin KB, Dym O, Albeck S, Magdassi S, Keeble AH, Kleanthous C, Tawfik DS (2009) Following evolutionary paths to protein-protein interactions with high affinity and selectivity. *Nat Struct Mol Biol* 16(10):1049–1055
95. Meenan NA, Sharma A, Fleishman SJ, Macdonald CJ, Morel B, Boetzel R, Moore GR, Baker D, Kleanthous C (2010) The structural and energetic basis for high selectivity in a high-affinity protein-protein interaction. *Proc Natl Acad Sci USA* 107(22):10080–10085
96. Kosloff M, Travis AM, Bosch DE, Siderovski DP, Arshavsky VY (2011) Integrating energy calculations with functional assays to decipher the specificity of G protein-RGS protein interactions. *Nat Struct Mol Biol* 18(7):846–853

Chapter 4

Computational Methods Applicable to the Discovery of Small-Molecule Inhibitors of Protein-Protein Interactions



Li Han and Renxiao Wang

4.1 Background

Protein-protein interactions (PPIs) are implicated in a wide range of biological processes such as hormone-receptor binding, antigen-antibody recognition, signal transduction, and protease inhibition, and they are vital for regulating cellular functions [1–3]. Thus, the central role of PPIs in biological functions makes them a large family of potential targets for drug discovery [4, 5]. Small-molecule inhibitors may be used to disrupt the interaction between two protein molecules. However, this approach is yet to be fully explored. The total number of PPIs associated with the human proteome is estimated to be between 130,000 and 650,000 [6, 7]. However, a network of only $\sim 3,200$ interaction pairs among 1,705 proteins has been determined by automated yeast two-hybrid (Y2H) experiments [8]. Among these hundreds of thousands PPIs, only a few dozen have been considered as molecular targets for drug discovery efforts [9].

Drug discovery based on PPI targets is more challenging than that based on conventional targets. Conventional drug targets, such as enzymes and G protein-coupled receptors, usually have well-defined cavities on their molecular surfaces that can accommodate small-molecule binders. However, the binding interfaces of protein-protein complexes lack this feature, because they are typically wider and flatter. The surface area of protein-protein binding interfaces ranges

L. Han · R. Wang (✉)

State Key Laboratory of Bioorganic and Natural Products Chemistry, Shanghai Institute of Organic Chemistry, Chinese Academy of Sciences, 345 Lingling Road, Shanghai 200032, People's Republic of China
e-mail: wangrx@mail.sioc.ac.cn

R. Wang

State Key Laboratory of Quality Research in Chinese Medicine, Macau Institute for Applied Research in Medicine and Health, Macau University of Science and Technology, Macau, People's Republic of China

© Springer Nature Singapore Pte Ltd. 2018

C. Sheng and G. I. Georg (eds.), *Targeting Protein-Protein Interactions by Small Molecules*, https://doi.org/10.1007/978-981-13-0773-7_4

between 1,000 and 4,000 Å², whereas the surface areas of conventional drug target binding pockets are typically smaller than 1,000 Å² [10]. Another distinct feature of protein-protein binding interfaces is that they often consist of discontinuous regions, making it difficult for small-molecule binders to block the entire interface [11]. Despite these difficulties, significant advances in experimental techniques in recent years, as described in other chapters in this book, have led to the discovery of potent small-molecule inhibitors for previously intractable targets. Notable examples include the discovery of potent small-molecule inhibitors of the PPIs exhibited by anti-apoptotic Bcl-2 family proteins [12–23] and MDM2/p53 interactions [24–40].

Experimental methods such as high-throughput screening (HTS) are indispensable for drug discovery projects. However, they are often associated with high cost and problematic issues such as false positives [41]. Computational methods provide a complementary, and sometimes decisive, approach to the discovery of small-molecule PPI inhibitors (Fig. 4.1). Owing to the unique features of PPIs mentioned above, computational methods applicable to this task are also different

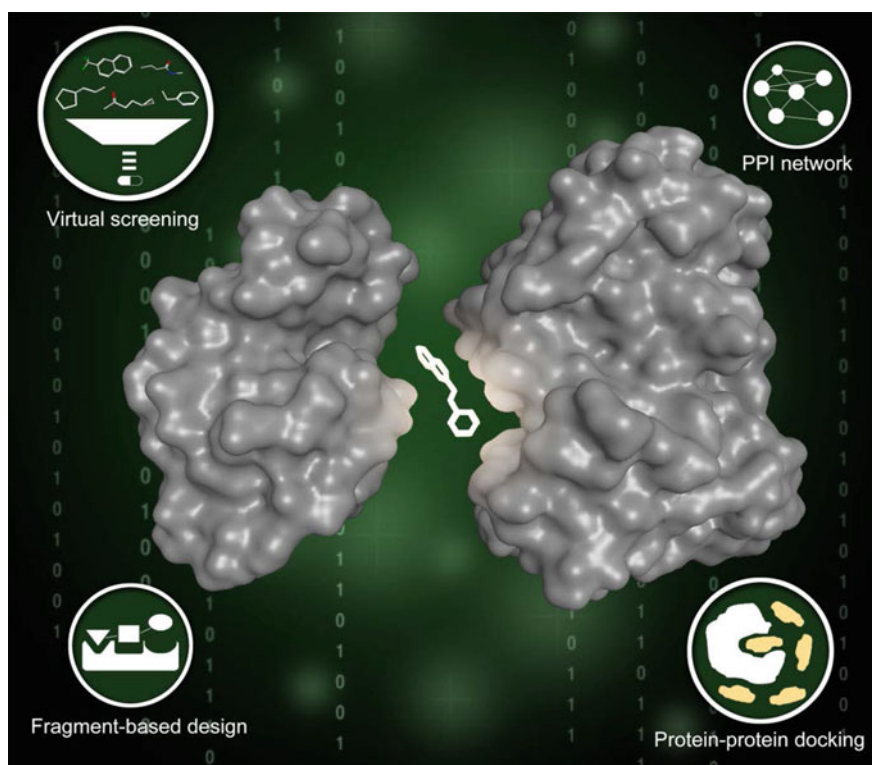


Fig. 4.1 Small-molecule compounds can be used to regulate protein-protein interactions and thus have important pharmaceutical implications. A range of computational methods are helpful for the discovery of such compounds

from those applicable to conventional drug targets. Depending on the possible application of such methods, they can be grouped into two categories: The first contains methods developed for characterizing PPIs, which are used to select worthwhile PPI targets, derive protein-protein complex structural models, and identify hot spots on protein-protein binding interfaces; the second contains methods developed for deriving small-molecule PPI inhibitors. For example, virtual screening is a widely applied method for identifying novel lead compounds in commercial compound libraries. Fragment-based design offers an alternative strategy for assembling molecular structures from simple fragment-like compounds. This chapter reviews several typical computational methods applicable to the workflow of discovering small-molecule PPI inhibitors, and several pertinent works published in recent years are briefly described as examples.

4.2 Computational Methods Used for Characterizing PPIs

4.2.1 *Selecting a PPI Target*

Usually, the first aim of a drug discovery project is to select a suitable target. For this aim, knowledge of the PPI network along the relevant biological pathway is critical. The topological structure of a PPI network is one of the most important indicators to determine the target type [42]. In most interaction networks, nodes with high connectivity, also known as hubs, are closely related to pathway regulation, making them promising drug targets. However, these hubs are always involved in multiple functional processes; therefore, their inhibition may induce undesired effects and express toxicity. Thus, knowledge of network dynamics can provide important information for selecting reasonable PPI targets. Using mathematical methods, static network topologies can be transformed into dynamic network models. By simulating and analyzing these models, the interactions between nodes can be described quantitatively or semiquantitatively, and the nonlinear dynamic properties of complicated PPI networks can be determined.

The developments of high-throughput experiments and computational prediction methods have led to the identification of a huge number of PPIs, resulting in the development of many PPI databases for different purposes (Table 4.1) [43–64]. PPI databases can be categorized into two types: pathway databases and interaction databases. The KEGG pathway database [44] is a collection of manually drawn pathway maps representing information on molecular interactions and reaction networks (Fig. 4.2a). The latest version of the KEGG pathway database, which was updated in March 2017, contains 504,349 pathway maps for various organismal systems and cellular processes. These maps provide important information for establishing PPI networks. Reactome [43] is another pathway database. The newest

Table 4.1 Details of a selection of current PPI databases

Database	Number of interactions	Experimental verification	Computational prediction	Graphically visualization	Features
KEGG	504,349 pathways	+	+	+	Pathway database
Reactome	22,833 pathways	+	–	+	Pathway database
MetaCyc	2,491	+	+	–	Metabolic pathways
IntAct	720,711	+	–	+	
BioGRID	1,421,025	+	–	–	
DIP	81,731	+	–	+	
STRING	184 mio	+	+	+	
MINT	125,464	+	+	+	
HPRD	41,327	+	–	–	Human species
PIPs	37,606	+	+	–	Human species

Reactome database (v60) describes 22,833 pathway maps of 131,417 proteins from 19 organisms (Fig. 4.2b). Along with visible pathway maps, Reactome also provides a report for each query that contains all the data and the original literature for related signaling pathways. Some databases, such as IntAct [45] and BioGRID [46], collect primary experimental data, while other databases, such as STRING [47] and MINT, also include computationally predicted interactions. MINT is a database designed to store data on functional interactions between proteins. Each PPI in MINT (Fig. 4.2c) is assigned a confidence score, which is based on the number of interaction sites, experiment type, and number of citations. It is an important criterion for assessing the reliability of the corresponding PPI. There are several subdatabases of MINT, such as HomoMINT, which contains interactions of human proteins, and VirusMINT, which contains human-viral protein interactions. STRING is another well-known database that incorporates both experimentally demonstrated and computationally predicted protein interactions. It is one of the largest PPI databases. STRING (v10.0) contains more than 900 million interactions between more than 9 million proteins from 2,031 organisms (Fig. 4.2d). It is noteworthy that STRING also provides a confidence score to each predicted association. This score is derived by benchmarking the performance of the predictions against known interactions. Thus, the confidence score generally corresponds to the probability of finding the interaction in real systems. The databases mentioned above (and several other databases, as presented in Table 4.1) can be used to graphically visualize interaction networks, and this can give users an intuitive overview of the topologies of PPI networks.

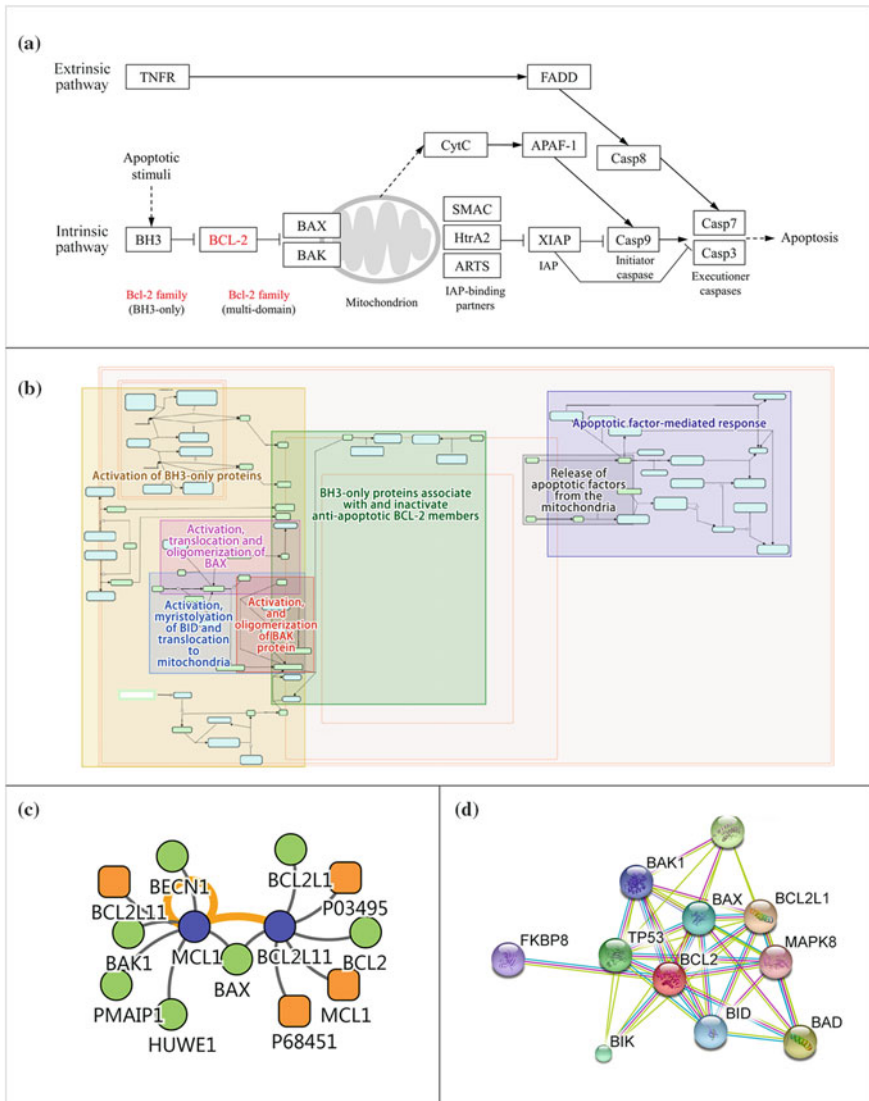


Fig. 4.2 Outputs returned by four selected PPI databases upon using the keyword “Bcl-2” as the query. KEGG (a) and Reactome (b) provide information primarily regarding biological pathways, whereas MINT (c) and STRING (d) provide information regarding interaction networks

4.2.2 Homology Modeling of Protein Structures

High-resolution structures are highly valuable for structure-based drug design. However, the number of protein-protein complex structures currently available is

insufficient. As mentioned above, there are hundreds of thousands of estimated PPIs between human proteins, but there are only $\sim 20,000$ non-redundant protein complex structures in the Protein Data Bank (PDB) [65]. In the absence of experimental structures, homology models often provide complementary information. Several theoretical tools have been developed to predict the structures of protein-protein complexes.

Homology modeling refers to constructing an atomic-resolution model of a target protein from its amino acid sequence and an experimental three-dimensional (3D) structure of a template protein. Homology modeling starts from the identification of one or more known protein structures likely to resemble the structure. Then, these structures are aligned to generate a template. Finally, the homology models are produced by threading the novel sequence along the backbone of the template structures.

A widely used Web-based tool for homology modeling is I-TASSER [66], which is an integrated platform for automated protein structure and function prediction. Using this tool, homology modeling can be achieved by means of a sequence-to-structure strategy. I-TASSER firstly makes multiple threading alignments and detects structure templates from the PDB [65]. Then, full-length structure models are constructed by reassembling structural fragments using replica exchange Monte Carlo simulations. By comparing the 3D structure of the homology models with those of other known proteins, the function of the model proteins can be predicted. I-TASSER has achieved great success in community-wide critical assessment of structure prediction (CASP) experiments. Another well-known tool for homology modeling is SWISS-MODEL [67], which is a Web server that performs homology modeling and an annotated database of previously constructed homology models. SWISS-MODEL provides several modes for structure prediction. Users can build a 3D structure either from an amino acid sequence or from a user-defined template. For professional users, a “project mode” is available for complex modeling tasks.

4.2.3 Protein-Protein Molecular Docking

Molecular docking is used to predict the native position, orientation, and conformation of a small-molecule ligand within the binding site of a target macromolecule. The aim of protein-protein docking is to predict the final complex structure from the unbound structures of two interacting protein molecules, which is an important and challenging task in current computational structural biology. Dozens of protein-protein docking software packages have been developed [68–75]. Protein-protein docking is not only critical in designing PPI inhibitors, but also indispensable for improving our understanding of the rules of protein interactions.

Protein-protein docking involves assembling two separate protein components into their biologically relevant complex structure. Docking can be described as a combination of a searching algorithm and a scoring function. The searching

algorithm aims to suggest possible binding poses. In protein-protein docking, several different strategies have been used to search conformation spaces, such as matching surface position [76], application of real space [77], and applying the fast Fourier transform (FFT) algorithm [75], which is the most widely used strategy. The scoring function is concerned with obtaining the global minimum structure of the complex using energy functions. The scoring functions implemented in protein-protein docking can be divided into three major categories: knowledge-based, empirical, and force-field-based. Knowledge-based scoring functions use interatomic interaction potentials obtained by a reverse-Boltzmann analysis of the occurrence of different atom contacts in known structures. Empirical scoring functions are based on the idea that binding free energies can be calculated by several uncorrelated energy terms [78]. These scoring functions are largely dependent on experimental data [79]. Conversely, force-field-based scoring functions are composed of universal and physical energy terms, such as van der Waals and electrostatic interactions.

Usually, protein-protein docking algorithms, such as DOT [80], ClusPro [81], and FTDock [82], are based on a rigid-body treatment of the molecules and do not take into account conformational changes during the binding process. Thus, this procedure can yield incorrect solutions if the interacting molecular structures acquire different conformations for binding. During binding, both component proteins adapt their conformations to each other. For protein-protein systems, owing to their large number of atoms and conformational degrees of freedom, it is necessary to consider molecular flexibility. However, it is impossible to search all the binding poses possible in conformational space. Consequently, flexibility is introduced to docking procedures mainly in two ways. First, some methods accommodate flexibility using “soft” scoring functions. Soft docking treats the molecular surface and volume as a cube, which allows conformational changes by means of size and shape complementarity, close packing, and liberal steric overlap [83]. For example, BIGGER [77] is one of the methods that allows soft docking. Other flexible or semiflexible software packages explicitly include backbone or side-chain flexibility in docking. Secondly, flexibility can be introduced by combining molecular dynamics (MD) simulation and some kind of rigid-body docking. For example, HADDOCK [68] starts with a randomization of orientations. After rigid-body energy minimization, the protein can be docked to ensembles of receptor structures, which are generated by a short MD simulation. Finally, both the side chain and backbone can be refined by steepest descent minimization and MD simulation. There are some other strategies to deal with the flexibility of proteins. For example, RosettaDock [84] uses real-space Monte Carlo minimization on both the rigid-body and side chain to obtain the lowest free energy binding mode of a protein complex. Furthermore, the key-lock model can successfully predict binding modes that undergo minimal conformation changes, and it is included in ZDOCK [85] and RosettaDock.

The Critical Assessment of PRedicted Interactions (CAPRI) exercise, which is a community-wide experiment in modeling the molecular structure of protein complexes, acts as an influential promoter for the development of protein-protein

docking algorithms [86]. CAPRI is a blind test of the capacity of prediction methods to produce protein binding models. In each round of a CAPRI exercise, several unpublished X-ray structures of protein complexes are solicited as targets. A necessary condition for the targets is that there should be no homologous complexes reported (or the binding modes of any homologous structure should be totally different). Unbound coordinates of at least one component should be publicly available. Participants may submit up to 100 predicted models to the organizing committee. All submitted models are evaluated according to the number of correct protein-protein contacts as well as root-mean-square (RMS) deviations. Since 2001, 39 rounds of the CAPRI exercise have been conducted with a total of 124 targets. In recent years, each round of the CAPRI exercise has attracted dozens of participants, and hundreds of predictions have been submitted for each target. The CAPRI exercise has evolved into a remarkable benchmark in the field of protein-protein interaction prediction. It not only evaluates the performance of protein docking algorithms [87], but also establishes CAPRI criteria, such as $f(\text{nat})$, L-rms, and I-rms, for assessing the quality of docking models [88] and provides benchmarks for docking and scoring protein complexes [89].

Since 2005, a scoring test has been introduced into CAPRI exercises [90]. For each target involved in a scoring test, participants of docking experiments are asked to submit not only 10 models for the docking test, but also a set of 100 models that contains both correct and incorrect models, which is used to compose a decoy for the scoring test. The “scorer” groups are invited to evaluate decoy-predicted models using their own scoring functions and to identify their own best scoring ones. Since this scoring experiment decouples the conformational sampling process from the scoring process, it provides an objective evaluation of the quality of scoring functions per se. In recently reported CAPRI exercises [87], participants performed quite differently in the scoring tests. Some scoring functions improved the prediction models significantly, while some other methods failed to predict any correct models for an easy target, for which many correct models were contained in the decoy set. In 2014, Lensink et al. published a scoring benchmark named “score_set,” which contains 15 targets and their decoys used in the CAPRI scoring test [89].

4.2.4 Identifying Hot Spots on PPI Interfaces

As mentioned above, PPI interfaces are relatively large. Furthermore, some protein complexes possess extended interfaces [91], which means that the interacting residues are diffused over the entire surface. In general, not all residues within the interface are equally important. Thus, it is possible to induce the concept of hot spots to identify closely interacting regions. Hot spots are defined as areas that provide a disproportionately large contribution to protein-protein binding affinity [92]. The residues involved in hot spots are directly responsible for the stabilization of a complex and confer most of the binding energy to the interaction. Typically,

they are defined as residues contributing at least 2 kcal/mol to the total binding energy [93].

Alanine scanning involves mutating a residue to alanine so that the contribution of the residue side chain to the protein-protein interface can be determined [93]. As indicated by a decrease in the free energy of binding ($\Delta\Delta G$), alanine scanning can be used to detect residues that may be involved in PPI hot spots. According to a database that contains $\Delta\Delta G$ values for 2325 alanine mutants, three amino acids, tryptophan, tyrosine, and arginine, are energetically important residues [94]. However, alanine scanning experiments are time-consuming and costly. Furthermore, the results may provide false positives and negatives. For example, the changes of $\Delta\Delta G$ can not only reflect energetically important residues for protein-protein binding, but are also related to changes in protein structure. Moreover, alanine scanning can provide false negatives when backbone atoms instead of side-chain atoms are involved in PPIs. Several kinds of computational methods have been developed to complement alanine scanning experiments. Some computational methods calculate $\Delta\Delta G$ using calibrated free energy functions [95, 96] or by incorporating MD simulation [97, 98]. Another strategy is to generate hot spot maps with specific molecular probes.

Existing methods predict hot spots in a variety of ways. Some computational methods can predict hot spots using only amino acid sequence information, such as ISIS [99] and PPIcons [100]. It is notable that these sequence-based methods are not as accurate as strategies that use structural information. Some computational methods that require protein structures predict atomic hot spots by placing atomic probes on the surface of proteins. For example, GRID [101] and SuperStar [102] are widely used programs. GRID generates a 3D grid over the surface of a protein and calculates the binding energies of small-molecule probes on each grid point with a force field to determine favorable binding positions. SuperStar predicts hot spots using a knowledge-based strategy in which the relationship between hot spots and residue features is obtained from the Cambridge Structural Database (CSD) [103] to give a prediction for probes on each grid point. The second group of computational methods predicts hot spots by detecting the binding ability between proteins and a variety of chemically diverse probes. FTMap, which is based on the FFT correlation approach [104], predicts the binding sites of 16 solvents or small-molecule probes. All subpockets are ranked according to the number of probes, resulting in a consensus hot spot. The third group employs MD simulations. MDMix [105] uses three MD simulations with three kinds of solvents. The difference between this method and those above is that the prediction results from MDMix are able to demonstrate the effect of water dissociation. Furthermore, several strategies have been developed by extending classic methods of hot spot mapping. For example, a workflow for generating fragment hot spot maps has been developed in which the atomic hot spots are weighed by surface exposure and the fragment hot spot map is generated by calculating the probe scores of grid points [106].

4.3 Computational Methods Used for Designing PPI Inhibitors

4.3.1 *Virtual Screening*

Either HTS or virtual screening can be employed in discovering lead compounds for small-molecule inhibitors, and it is obvious that the latter is more efficient and economical. Virtual screening has had a dramatic effect on the pharmaceutical industry. This is not just because it is faster; more importantly, virtual screening broadens search spaces considerably. Furthermore, in recent years, several other computational approaches, such as fragment-based methods (discussed later), have been developed based on virtual screening methods.

Virtual screening approaches have been traditionally divided into two main methods [107–109]: ligand-based screening and structure-based screening. In ligand-based virtual screening, the chemical structures or molecular descriptors of known inhibitors are used as templates to retrieve other compounds from a database. Ligand-based virtual screening methods can be further divided into several subgroups, according to different strategies for seeking similar molecules. These include descriptor-based methods, graph-based methods, and pharmacophore-based methods. Among them, pharmacophore-based virtual screening is widely used in designing PPI inhibitors. Although pharmacophores are mainly used to align and compare ligands sharing the same target [110], the same concept can be easily applied to PPIs in which one partner is the “receptor” and the second is the “ligand.” Several tools, including LigandScout [111], Discovery Studio [112], and Pocket Query [113], can be directly used to map PPI pharmacophores onto protein-protein X-ray structures.

Structure-based virtual screening is probably the most straightforward application of docking algorithms. For structure-based screening, compounds from a database are docked into a binding site and are ranked using one or several scoring functions. Theoretically, all docking approaches can be used in docking-based virtual screening of PPI targets. However, it should be noted that there are important differences between protein–ligand and protein-protein interfaces. Several groups have made effort to verify the authenticity of docking methods for PPI targets. As is reported, conventional docking and scoring methods perform well for PPI systems. The predictive accuracy drop is only about 10% compared to that for regular binding sites [114]. Thus, structure-based screening can assist the design of PPI inhibitors. Importantly for PPI inhibitor design, structure-based screening can be carried out on homology models or on low-resolution structures [115].

4.3.2 *Fragment-Based Design*

In recent years, fragment-based drug design (FBDD) has emerged as an attractive complement to HTS methods. FBDD aims at building molecules piece-by-piece with well-chosen fragments that bind into separate positions of binding pockets. Then, these fragments are linked by a variety of methods. Compared with the HTS method, FBDD has several advantages. Firstly, FBDD allows sampling with a much larger chemical diversity using a much smaller number of starting molecules. Secondly, FBDD leads to higher hit rates because the fragments are generally smaller than the molecules used in HTS experiments and the probability of a protein–ligand interaction decreases exponentially with the size and complexity of the molecule [96].

In most experimental FBDD studies, only hundreds to thousands of fragments can be screened. However, at least 250,000 fragments are commercially available [116], leaving a large portion of fragment libraries untested. Development of computational fragment-based methods may address this shortfall. However, docking and scoring strategies involved in fragment-based methods are still underdeveloped owing to several factors. Firstly, fragments are small in size. Therefore, during docking calculations, a number of interaction sites on a protein surface that accommodate a fragment might be found, which can lead to false docking positions or incorrect binding modes [117]. Secondly, interactions between fragments and receptors are generally weak. Thus, current scoring functions are not accurate enough to differentiate an active fragment among many non-active ones because most scoring functions have been developed and optimized on the basis of larger drug-like molecules [118]. Several improved fragment-based strategies have been developed to overcome these problems.

Present docking methodologies simulate only one single ligand at a time during the docking process. In reality, especially for PPI systems, the molecular recognition process always involves multiple molecular species, such as substrates, cofactors, ligands, and metal ions. To simulate real molecular binding processes, Li's group proposed a novel multiple-ligand simultaneous docking (MLSD) strategy [119]. In this strategy, an improved Lamarckian genetic algorithm (LGA) [120] and hybrid particle swarm optimization (PSO) algorithms are engaged. LGA is a stochastic population-based sampling optimization algorithm. PSO is used to handle the increased degrees of freedom for multi-ligand translation and rotation. The MLSD strategy is implemented in AutoDock4 [121]. In a MLSD job, the ligands can “dance” simultaneously and independently. However, when it comes to computing the total interaction energy at each step, a ligand can “sense” the existence of others. This methodology has been proved to be robust through systematic testing against several diverse model systems including an *E. coli* purine nucleoside phosphorylase (PNP) complex with two substrates, a SHP2NSH2 complex with two peptides, and a Bcl-xL complex with ABT-737 fragments. In all cases, correct docking poses and relative binding free energies were obtained.

Generally, in a virtual screening work, only a small number of molecules are selected as hit compounds, while the rest participants are abandoned. Therefore, it would be of enormous benefit if the huge number of virtual screening results could be reused. For this purpose, Wang's group developed the automatic tailoring and transplanting (AutoT&T) program [122], which was developed primarily for performing lead optimization in structure-based drug design. AutoT&T uses information on a lead compound as the starting point. In addition, a docking-driven virtual screening against the given target protein is conducted. AutoT&T identifies suitable fragments on the screened molecules based on their binding modes derived from molecular docking. Then, these selected fragments are transplanted onto the lead compound to form new ligand molecules with higher binding affinities. In this way, the outcomes of virtual screening are effectively "recycled" in lead optimization. AutoT&T has been tested on different targets, and the results showed that this program is able to produce rational predictions. Furthermore, the results from AutoT&T are more diverse and exhibit better binding scores.

4.4 Example Applications of Computational Methods for PPI Inhibitor Discovery

4.4.1 Case 1: A Pharmacophore-Based Strategy Used in the Design of p53-MDM2 Inhibitors

Protein 53 (p53) is important in multi-cellular organisms, where it regulates the cell cycle and thus functions as a tumor suppressor. In a normal cell, p53 is inactivated by its negative regulator, MDM2. The p53-MDM2 interaction regulates the transcriptional activity of tumor cells in the human body [29]. However, this complex is deemed to be a challenging target because of its relatively large and flat interface, which is not conducive for small-molecule binding.

Xue et al. designed a series of p53-MDM2 inhibitors starting from a consensus pharmacophore-based virtual screening strategy [123]. First, they built structure-based pharmacophores with 15 p53-MDM2 crystal complex structures. The resulting 15 pharmacophores were aligned and the most common features were reserved to constitute a structure-based pharmacophore, which consisted of six pharmacophore features. Then, similar procedures were performed upon 10 MDM2-non-peptide complex structures to generate a receptor-ligand-based pharmacophore model, which contained seven pharmacophore features. Next, the common features of these two models were extracted to form an ensemble pharmacophore model, which consisted of a hydrogen-bond donor, two aromatic rings, and two hydrophobic cores (Fig. 4.3a). With this pharmacophore model, a collection of 21,287 molecules was screened by the fast flexible search method in Discovery Studio 3.0 (Accelrys Software, Inc.). Subsequently, the 75 hit molecules from virtual screening were further screened by a cascade docking process, and 15

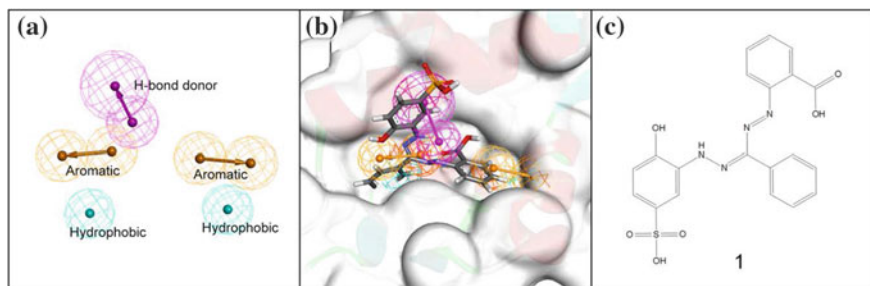


Fig. 4.3 **a** Common pharmacophore model for MDM2 inhibitors described by Xue et al. [123], which was derived through a combination of receptor-based and ligand-based approaches. **b** Predicted binding mode of compound 1 with MDM2 and how it overlaps with the pharmacophore model. **c** Chemical structure of compound 1

final hits were obtained. The binding affinities of these molecules toward MDM2 were determined by fluorescence polarization assay, and six of them exhibited micromolar binding affinity to MDM2. Among them, compound 1 (Fig. 4.3b, c) exhibited a K_i of 180 nM.

4.4.2 Case 2: Discovery of uPA–uPAR Inhibitors Through a Docking-Based Virtual Screening

The interaction of the urokinase receptor (uPAR) and urokinase-type plasminogen activator (uPA) is involved in tissue reorganization events such as wound healing and tumor progression. Several peptides and antibodies inhibit the uPA–uPAR interaction [124], but not with sufficient binding affinities. Besides the common challenges associated with PPI interfaces, the flexibility of the uPA–uPAR interface presents particular difficulties for inhibitor design.

Khanna et al. used a workflow that combined docking-based virtual screening and MD simulation to design uPA–uPAR inhibitors [125]. First, two X-ray structures of uPAR were used as receptors in docking-based virtual screening. Approximately 5,000,000 compounds from the ZINC database were docked to the receptors using AutoDock4 [121], and the docked complexes were rescored by a set of scoring functions, including ChemScore [126], GoldScore [126], and X-score [127]. Approximately 10,000 compounds were reserved for the subsequent steps. Then, 10 parallel MD simulations were performed on uPAR, and 50 conformations were selected as receptors for second-round docking. The 10,000 hits selected in the previous step were further docked, also with AutoDock, and the 500 top-ranked hits were retained. These 500 compounds were then docked into the 50 receptor conformers using Glide 5.5 (Schrodinger Inc.), leading to 250 top-ranked hits. Finally, these compounds were clustered and the first-ranked compound of the top 50 clusters was reserved for in vitro experiment. According to biochemical tests,

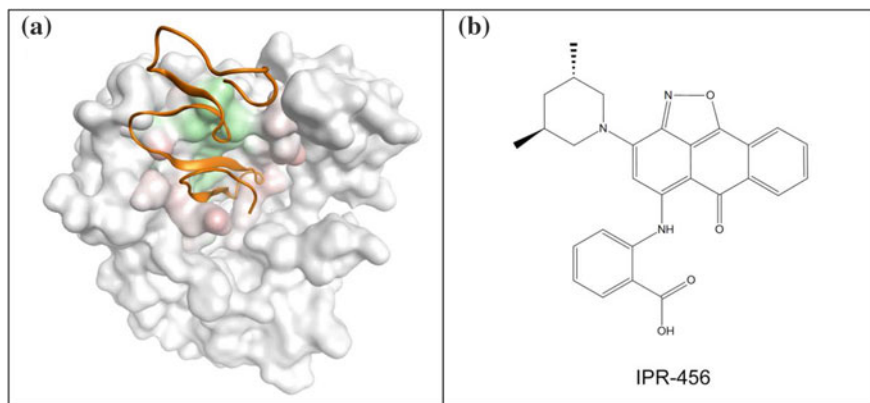


Fig. 4.4 **a** uPA–uPAR complex structure (PDB code: 2FD6), where uPAR is rendered as a gray molecular surface and the growth factor-like domain of uPA is rendered as orange ribbons. **b** Chemical structure of compound IPR-456 reported by Khanna et al. [125]

IPR-456 (Fig. 4.4b) could bind to uPAR ($K_d = 310$ nM) and inhibit the uPA–uPAR interaction ($IC_{50} = 10$ mM). This work demonstrates that combining docking-based virtual screening and MD simulation is an effective strategy for targeting flexible PPIs.

4.4.3 Case 3: Discovery of IL-6/GP130 Interaction Inhibitors Through Multi-fragment Docking

Li et al. discovered a set of inhibitors that regulate the interaction between interleukin-6 (IL-6) and glycoprotein 130 (GP130) [119] with the previously discussed MLSD strategy [127]. As mentioned above, MLSD is a computational method that can dock multiple fragments into a single protein pocket. In this work, the MLSD method was employed as follows: First, a set of fragment scaffolds was prepared for MLSD docking. MDL-A is a known inhibitor of GP130. Consequently, MDL-A and its analogs were fragmented and used as templates. Two databases, the US Food and Drug Administration (FDA) approved and extended drugs [79] and DrugBank [80], were screened according to the template fragments, and two fragment pools were obtained (Fig. 4.5a). Second, fragment scaffolds from these two pools were docked to GP130 using the MLSD method. Fragments that possess higher binding energy than MDL-A were reserved for the following steps. Third, these fragments were linked by various types of tethers, and the resulting virtual compounds were optimized and re-docked to GP130. Finally, using SMILES encoding and Tanimoto similarity coefficient indicators, similarity searches were performed in DrugBank and PubChem to obtain virtual compound

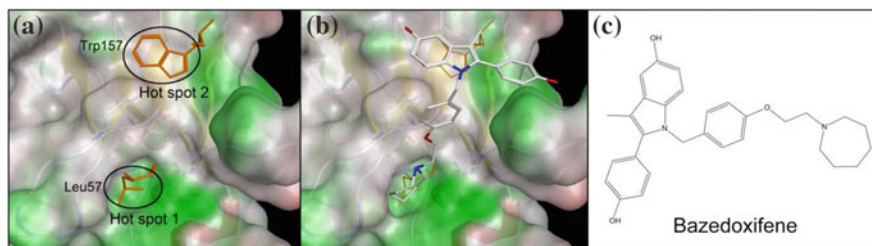


Fig. 4.5 **a** Location of the two main hot spots on the binding interface of GP130, as described by Li et al. [119]. **b** Predicted binding mode of Bazedoxifene to GP130. **c** Chemical structure of Bazedoxifene

hits. With this method, Bazedoxifene was discovered as a promising inhibitor of IL-6/GP130 interaction with an IC_{50} value of 25 μ M (Fig. 4.5b, c).

4.4.4 Case 4: Development of a Bcl-2 Inhibitor via a Fragment-Based De Novo Design

Apoptosis plays a central role in many life-threatening diseases, such as cancer and several cardiovascular, neurological, and autoimmune conditions [128]. Apoptosis is related to the equilibrium of the Bcl-2 protein family. The Bcl-2 protein family can be divided into three subsets: the anti-apoptotic subset (Bcl-2, Bcl-x_L, Mcl-1 and so on), the apoptotic subset (Bax and Bak), and BH3-only proteins. Anti-apoptotic members can bind to apoptotic proteins and prevent apoptosis processes. BH3-only proteins can either inhibit Bcl-2 subfamily or activate Bax and Bak. The overexpression of the Bcl-2 subfamily may induce tumor generation and growth. Therefore, the inhibition of pro-survival proteins is a promising strategy in cancer therapy [17].

Ding et al. designed a set of Bcl-2 and Mcl-1 inhibitors using a computational strategy based on mining characteristic interaction patterns (CIPs) [129]. CIPs are used to describe protein-protein interfaces. As presented in Fig. 4.6a, a CIP is a cluster of four interacting residues, three of which are from the protein and the other from the binding partner. In order to design small-molecule inhibitors of PPIs, the CIPs of target protein-protein interfaces can be used as “anchors.” For a known protein–ligand complex, the ligand can be dissected into certain fragments. If the CIPs of the receptor–fragment interface are comparable with the template CIPs, the fragment can be reserved as a candidate for targeting PPIs.

In this work, two series of complexes, Bcl-x_L/BH3-only complexes and Mcl-1/BH3-only complexes, were selected to generate anchor CIPs. Over 25,000 protein–ligand crystal structures from the PDB [65] were processed, and their ligands were dissected into fragments with an in-house program. The CIPs of the receptor–fragment interface were generated and compared with anchor CIPs. The top 30 hits

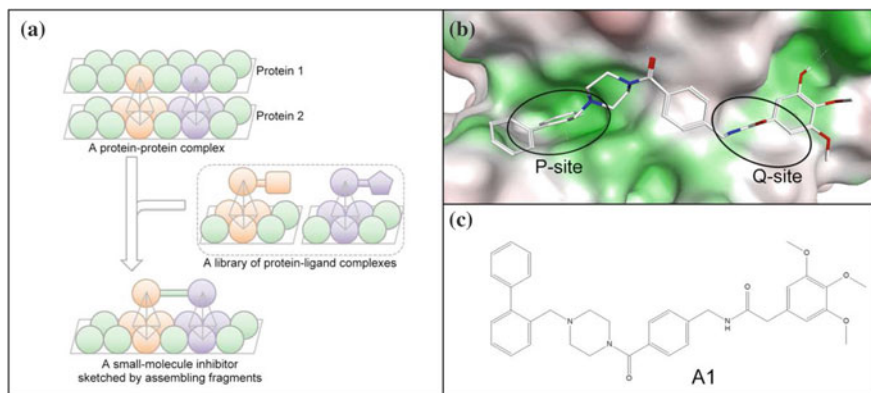


Fig. 4.6 **a** Workflow of the fragment-based de novo design of the Mcl-1 inhibitor reported by Ding et al. [129]. First, the conserved residue clusters on the Mcl-1 binding interface were identified. Then, the protein-ligand complexes in PDB were analyzed to search for chemical fragments that form similar interactions. Finally, small-molecule inhibitors were designed by assembling the chemical fragments obtained. **b** Predicted binding mode of compound A1 to Mcl-1. **c** Chemical structure of A1

for each query were reserved, and 15 fragments were chosen as candidates. These fragments were linked with synthetically feasible tethers, and four series of molecules were finally obtained. Some of these molecules exhibited micromolar or submicromolar affinities toward Bcl-x_L or Mcl-1. Among them, compound A1 (Fig. 4.6b, c) selectively binds to Mcl-1 with a K_i value of 180 nM.

4.5 Conclusion

In the past few decades, computational methods have proven their value in drug discovery and are widely applied in both academia and the pharmaceutical industry. It is no surprise then that they are also useful for drug discovery efforts targeting PPIs. As described in this chapter, computational methods have been employed for various tasks including target characterization, lead discovery, and lead optimization. Nevertheless, given the unique features of protein-protein binding interfaces, computational methods that were originally developed to deal with conventional targets must undergo appropriate modifications before they can be applied to PPI targets. Even so, some technical issues associated with PPI targets remain challenging. For example, it is common for a protein molecule involved in PPI to undergo conformational rearrangement upon binding to a small-molecule ligand instead of the original partner protein. This effect makes reliably predicting the binding mode and the binding affinity of small-molecule ligands much more challenging.

With continuous progress in all disciplines of biological science, knowledge of new PPIs as well as their biological functions will continue to expand. This will facilitate the elucidation of suitable drug targets more precisely by, for example, network pharmacology analysis. In the future, the computational design of small-molecule PPI inhibitors will benefit from more advanced theoretical models, such as next-generation force fields and new solvation models, and much more extensive molecular simulations on increasingly powerful computer hardware. Hopefully, significant improvements will also be made to computational/informatics methods dedicated to the assessment of toxicity, pharmacokinetic, and metabolic properties. Having witnessed the extraordinary advances made in the field of computer-aided drug design thus far, we are optimistic that computational methods will play an even bigger role in accelerating drug discovery efforts targeting PPIs.

Acknowledgements The authors are grateful for the financial support from the National Natural Science Foundation of China (Grant No. 81430083, 21472227, 21673276 to Prof. R. Wang and Grant No. 21402230 to Dr. L. Han), the Ministry of Science and Technology of China (National Key R&D Program of China Grant No. 2016YFA0502302 to Prof. R. Wang), the Chinese Academy of Sciences (Strategic Priority Research Program, Grant No. XDB20000000, No. XDB20020200), and the Science and Technology Development Foundation of Macao SAR (Grant No. 055/2013/A2 to Prof. R. Wang).

References

1. Keskin O, Gursoy A, Ma B et al (2008) Principles of protein–protein interactions: what are the preferred ways for proteins to interact? *Chem Rev* 108:1225–1244
2. Pawson T, Nash P (2000) Protein-protein interactions define specificity in signal transduction. *Gene Dev* 14:1027–1047
3. Wilson IA, Stanfield RL (1994) Antibody-antigen interactions: new structures and new conformational changes. *Curr Opin Struct Biol* 4:857–867
4. Zinzalla G, Thurston DE (2009) Targeting protein–protein interactions for therapeutic intervention: a challenge for the future. *Future Med Chem* 1:65–93
5. Wells JA, McClendon CL (2007) Reaching for high-hanging fruit in drug discovery at protein-protein interfaces. *Nature* 450:1001–1009
6. Venkatesan K, Rual JF, Vazquez A et al (2009) An empirical framework for binary interactome mapping. *Nat Methods* 6:83–90
7. Stumpf MP, Thorne T, de Silav E et al (2008) Estimating the size of the human interactome. *Proc Natl Acad Sci USA* 105:6959–6964
8. Stelzl U, Worm U, Lalowski M et al (2005) A human protein-protein interaction network: a resource for annotating the proteome. *Cell* 122:957–968
9. Bienstock RJ (2012) Computational drug design targeting protein-protein interactions. *Curr Pharm Des* 18:1240–1254
10. Jones S, Thornton JM (1996) Principles of protein-protein interactions. *Proc Natl Acad Sci USA* 93:13–20
11. Jochim AL, Arora PS (2010) Systematic analysis of helical protein interfaces reveals targets for synthetic inhibitors. *ACS Chem Biol* 5:919–923

12. Wei J, Kitada S, Rega MF et al (2009) Apogossypol derivatives as pan-active inhibitors of antiapoptotic B-Cell Lymphoma/Leukemia-2 (Bcl-2) family proteins. *J Med Chem* 52:4511–4523
13. Wang G, Nikolovska-Coleska Z, Yang CY et al (2006) Structure-based design of potent small-molecule inhibitors of anti-apoptotic Bcl-2 proteins. *J Med Chem* 49:6139–6142
14. Yin H, Lee GI, Sedey KA et al (2005) Terphenyl-Based Bak BH3 alpha-helical proteomimetics as low-molecular-weight antagonists of Bcl-xL. *J Am Chem Soc* 127:10191–10196
15. Park CM, Bruncko M, Adickes J et al (2008) Discovery of an orally bioavailable small molecule inhibitor of prosurvival B-cell lymphoma 2 proteins. *J Med Chem* 51:6902–6915
16. Wang JL, Liu D, Zhang ZJ et al (2000) Structure-based discovery of an organic compound that binds Bcl-2 protein and induces apoptosis of tumor cells. *Proc Natl Acad Sci USA* 97:7124–7129
17. Bodur C, Basaga H (2012) Bcl-2 inhibitors: emerging drugs in cancer therapy. *Curr Med Chem* 19:1804–1820
18. Pan R, Hogdal LJ, Benito JM et al (2014) Selective BCL-2 inhibition by ABT-199 causes on target cell death in acute myeloid leukemia. *Cancer Discov* 4:362–375
19. Levenson JD, Zhang H, Chen J et al (2015) Potent and selective small-molecule MCL-1 inhibitors demonstrate on-target cancer cell killing activity as single agents and in combination with ABT-263 (navitoclax). *Cell Death Dis* 6:e1590–e1590
20. Brady RM, Vom A, Roy MJ et al (2014) De-novo designed library of benzoylureas as inhibitors of BCL-XL: synthesis, structural and biochemical characterization. *J Med Chem* 57:1323–1343
21. Pelz NF, Bian X, Zhao B et al (2016) Discovery of 2-indole-acylsulfonamide Myeloid Cell Leukemia 1 (Mcl-1) inhibitors using fragment-based methods. *J Med Chem* 59:2054–2066
22. Wertz IE, Kusam S, Lam C et al (2011) Sensitivity to antitubulin chemotherapeutics is regulated by MCL1 and FBW7. *Nature* 471:110–114
23. Wei SH, Dong K, Lin F et al (2008) Inducing apoptosis and enhancing chemosensitivity to gemcitabine via RNA interference targeting Mcl-1 gene in pancreatic carcinoma cell. *Cancer Chemoth Pharm* 62:1055–1064
24. Bowman AL, Nikolovska-Coleska Z, Zhong H et al (2007) Small molecule inhibitors of the MDM2-p53 interaction discovered by ensemble-based receptor models. *J Am Chem Soc* 129:12809–12814
25. Ding K, Lu Y, Nikolovska-Coleska Z et al (2005) Structure-based design of potent non-peptide MDM2 inhibitors. *J Am Chem Soc* 127:10130–10131
26. Yang Y, Ludwig RL, Jensen JP et al (2005) Small molecule inhibitors of HDM2 ubiquitin ligase activity stabilize and activate p53 in cells. *Cancer Cell* 7:547–559
27. Vogelstein B, Lane D, Levine AJ (2000) Surfing the p53 network. *Nature* 408:307–310
28. Vazquez A, Bond EE, Levine AJ et al (2008) The genetics of the p53 pathway, apoptosis and cancer therapy. *Nat Rev Drug Discov* 7:979–987
29. Chène P (2003) Inhibiting the p53–MDM2 interaction: an important target for cancer therapy. *Nat Rev Cancer* 3:102–109
30. Khoo KH, Verma CS, Lane DP (2014) Drugging the p53 pathway: understanding the route to clinical efficacy. *Nat Rev Drug Discov* 13:217–236
31. Kussie PH, Gorina S, Marechal V et al (1996) Structure of the MDM2 oncoprotein bound to the p53 tumor suppressor transactivation domain. *Science* 274:948–953
32. Gessier F, Kallen J, Jacoby E et al (2015) Discovery of dihydroisoquinolinone derivatives as novel inhibitors of the p53-MDM2 interaction with a distinct binding mode. *Bioorg Med Chem Lett* 25:3621–3625
33. Holzer P, Masuya K, Furet P et al (2015) Discovery of a dihydroisoquinolinone derivative (NVP-CGM097) - a highly potent and selective MDM2 inhibitor undergoing phase I clinical trials in p53wt tumors. *J Med Chem* 58:6348–6358
34. Rew Y, Sun D (2014) Discovery of a small molecule MDM2 inhibitor (AMG 232) for treating cancer. *J Med Chem* 57:6332–6341

35. Ferri E, Petosa C, McKenna CE (2016) Bromodomains: Structure, function and pharmacology of inhibition. *Biochem Pharmacol* 106:1–18
36. Dey A, Chitsaz F, Abbasi A et al (2003) The double bromodomain protein Brd4 binds to acetylated chromatin during interphase and mitosis. *Proc Natl Acad Sci USA* 100:8758–8763
37. Wyce A, Ganji G, Smitheman KN et al (2013) BET inhibition silences expression of MYCN and BCL2 and induces cytotoxicity in neuroblastoma tumor models. *PLoS ONE* 8:e72967–e72967
38. Albrecht BK, Gehling VS, Hewitt MC et al (2016) Identification of a Benzoisoxazoloazepine Inhibitor (CPI-0610) of the Bromodomain and Extra-Terminal (BET) family as a candidate for human clinical trials. *J Med Chem* 59:1330–1339
39. Seal J, Lamotte Y, Donche F et al (2012) Identification of a novel series of BET family bromodomain inhibitors: binding mode and profile of I-BET151 (GSK1210151A). *Bioorg Med Chem Lett* 22:2968–2972
40. Ran X, Zhao Y, Liu L et al (2015) Structure-based design of γ -carboline analogues as potent and specific BET bromodomain inhibitors. *J Med Chem* 58:4927–4939
41. Gribbon P, Sewing A (2003) Fluorescence readouts in HTS: no gain without pain? *Drug Discov Today* 8:1035–1043
42. Zhang QC, Petrey D, Deng L et al (2012) Structure-based prediction of protein-protein interactions on a genome-wide scale. *Nature* 490:556–560
43. Croft D, O’Kelly G, Wu G et al (2011) Reactome: a database of reactions, pathways and biological processes. *Nucleic Acids Res* 39:D691–D697
44. Kanehisa M, Goto S, Furumichi M et al (2010) KEGG for representation and analysis of molecular networks involving diseases and drugs. *Nucleic Acids Res* 38:D355–D360
45. Kerrien S, Aranda B, Breuza L et al (2012) The IntAct molecular interaction database in 2012. *Nucleic Acids Res* 40:D841–D846
46. Chatr-Aryamontri A, Breitkreutz BJ, Oughtred R et al (2015) The BioGRID interaction database: 2015 update. *Nucleic Acids Res* 43:D470–D478
47. Szklarczyk D, Morris JH, Cook H et al (2017) The STRING database in 2017: quality-controlled protein–protein association networks, made broadly accessible. *Nucleic Acids Res* 45:D362–D368
48. Warde-Farley D, Donaldson SL, Comes O et al (2010) The GeneMANIA prediction server: biological network integration for gene prioritization and predicting gene function. *Nucleic Acids Res* 38:W214–W220
49. Basse MJ, Betzi S, Bourgeas R et al (2013) 2P2Idb: a structural database dedicated to orthosteric modulation of protein–protein interactions. *Nucleic Acids Res* 41:D824–D827
50. Thorn KS, Bogan AA (2001) ASEdb: a database of alanine mutations and their effects on the free energy of binding in protein interactions. *Bioinformatics* 17:284–285
51. Hendlich M, Bergner A, Günther J et al (2003) Relibase: Design and development of a database for comprehensive analysis of protein–ligand interactions. *J Mol Biol* 326:607–620
52. Higuero AP, Jubb H, Blundell TL (2013) TIMBAL v2: update of a database holding small molecules modulating protein–protein interactions. *Database* 2013:bat039–bat039
53. Zhang QC, Petrey D, Garzón JI et al (2013) PrePPI: a structure-informed database of protein–protein interactions. *Nucleic Acids Res* 41:D828–D833
54. Fong JH, Shoemaker BA, Garbuzynskiy SO et al (2009) Intrinsic disorder in protein interactions: Insights from a comprehensive structural analysis. *PLoS Comput Biol* 5:e1000316–e1000316
55. Cukuroglu E, Gursoy A, Nussinov R et al (2014) Non-redundant unique interface structures as templates for modeling protein interactions. *PLoS ONE* 9:e86738–e86738
56. Sugaya N, Kanai S, Furuya T (2012) Dr. PIAS 2.0: an update of a database of predicted druggable protein–protein interactions. *Database* 2012:bas034–bas034
57. Kumar MDS, Gromiha MM (2006) PINT: protein–protein interactions thermodynamic database. *Nucleic Acids Res* 34:D195–D198

58. Moal IH, Fernández-Recio J (2012) SKEMPI: a structural kinetic and energetic database of mutant protein interactions and its use in empirical models. *Bioinformatics* 28:2600–2607
59. Gong W, Zhou D, Ren Y et al (2008) PepCyber:P~PEP: a database of human protein–protein interactions mediated by phosphoprotein-binding domains. *Nucleic Acids Res* 36: D679–D683
60. Lo YS, Chen YC, Yang JM (2010) 3D-interologs: an evolution database of physical protein–protein interactions across multiple genomes. *BMC Genom* 11:S7–S7
61. Apweiler R, Bairoch A, Wu CH et al (2004) UniProt: the universal protein knowledgebase. *Nucleic Acids Res* 32:D115–D119
62. Koes DR, Camacho CJ (2012) PocketQuery: protein–protein interaction inhibitor starting points from protein–protein interaction structure. *Nucleic Acids Res* 40:W387–W392
63. Bergey CM, Watkins AM, Arora PS (2013) HippDB: a database of readily targeted helical protein–protein interactions. *Bioinformatics* 29:2806–2807
64. Watkins AM, Arora PS (2014) Anatomy of β -Strands at protein–protein interfaces. *ACS Chem Biol* 9:1747–1754
65. Berman HM, Westbrook J, Feng Z et al (2000) The protein data bank. *Nucleic Acids Res* 28:235–242
66. Yang J, Yan R, Roy A et al (2015) The I-TASSER Suite: protein structure and function prediction. *Nat Methods* 12:7–8
67. Arnold K, Bordoli L, Kopp J et al (2006) The SWISS-MODEL workspace: a web-based environment for protein structure homology modelling. *Bioinformatics* 22:195–201
68. de Vries SJ, van Dijk AD, Krzeminski M et al (2007) HADDOCK versus HADDOCK: new features and performance of HADDOCK2.0 on the CAPRI targets. *Proteins* 69:726–733
69. Pierce BG, Wiehe K, Hwang H et al (2014) ZDOCK server: interactive docking prediction of protein–protein complexes and symmetric multimers. *Bioinformatics* 30:1771–1773
70. Cheng TM, Blundell TL, Fernandez-Recio J (2007) pyDock: electrostatics and desolvation for effective scoring of rigid-body protein–protein docking. *Proteins* 68:503–515
71. Gray JJ, Moughon S, Wang C et al (2003) Protein–protein docking with simultaneous optimization of rigid-body displacement and side-chain conformations. *J Mol Biol* 331:281–299
72. Andrusier N, Nussinov R, Wolfson H (2007) FireDock: fast interaction refinement in molecular docking. *Proteins* 69:139–159
73. Mashiah E, Nussinov R, Wolfson HJ (2010) FiberDock: Flexible induced-fit backbone refinement in molecular docking. *Proteins* 78:1503–1519
74. Torchala M, Moal IH, Chaleil RA et al (2013) SwarmDock: a server for flexible protein–protein docking. *Bioinformatics* 29:807–809
75. Katchalski-Katzir E, Sharif I, Eisenstein M et al (1992) Molecular surface recognition: determination of geometric fit between proteins and their ligands by correlation techniques. *Proc Natl Acad Sci USA* 89:2195–2199
76. Shoichet BK, Kuntz ID (1991) Protein docking and complementarity. *J Mol Biol* 221:327–346
77. Palma PN, Krippahl L, Wampler JE et al (2000) BiGGER: a new (soft) docking algorithm for predicting protein interactions. *Proteins* 39:372–384
78. Eldridge MD, Murray CW, Auton TR et al (1997) Empirical scoring functions: I. The development of a fast empirical scoring function to estimate the binding affinity of ligands in receptor complexes. *J Comput Aid Mol Des* 11:425–445
79. Zou XQ, Kuntz ID (1999) Inclusion of solvation in ligand binding free energy calculations using the generalized-born model. *J Am Chem Soc* 121:8033–8043
80. Mandell JG, Roberts VA, Pique ME et al (2001) Protein docking using continuum electrostatics and geometric fit. *Protein Eng* 14:105–113
81. Comeau SR, Gatchell DW, Vajda S et al (2004) ClusPro: an automated docking and discrimination method for the prediction of protein complexes. *Bioinformatics* 20:45–50
82. Gabb HA, Jackson RM, Sternberg MJE (1997) Modelling protein docking using shape complementarity, electrostatics and biochemical information. *J Mol Biol* 272:106–120

83. Jiang F, Kim SH (1991) "Soft docking": matching of molecular surface cubes. *J Mol Biol* 219:79–102
84. Lyskov S, Gray JJ (2008) The RosettaDock server for local protein-protein docking. *Nucleic Acids Res* 36:W233–W238
85. Mintseris J, Pierce B, Wiehe K et al (2007) Integrating statistical pair potentials into protein complex prediction. *Proteins* 69:511–520
86. Janin J, Henrick K, Moult J et al (2003) CAPRI: a Critical Assessment of PRedicted Interactions. *Proteins* 52:2–9
87. Lensink MF, Wodak SJ (2013) Docking, scoring, and affinity prediction in CAPRI. *Proteins* 81:2082–2095
88. Méndez R, Leplae R, Lensink MF et al (2005) Assessment of CAPRI predictions in rounds 3–5 shows progress in docking procedures. *Proteins* 60:150–169
89. Lensink MF, Wodak SJ (2014) Score_set: a CAPRI benchmark for scoring protein complexes. *Proteins* 82:3163–3169
90. Lensink MF, Méndez R, Wodak SJ (2007) Docking and scoring protein complexes: CAPRI 3rd Edition. *Proteins* 69:704–718
91. Watkins AM, Arora PS (2014) Structure-based inhibition of protein-protein interactions. *Eur J Med Chem* 94:480–488
92. Hajduk PJ, Huth JR, Fesik SW (2005) Druggability indices for protein targets derived from NMR-based screening data. *J Med Chem* 48:2518–2525
93. Clackson T, Wells J (1995) A hot spot of binding energy in a hormone-receptor interface. *Science* 267:383–386
94. Bogan AA, Thorn KS (1998) Anatomy of hot spots in protein interfaces. *J Mol Biol* 280:1–9
95. Kortemme T, Baker D (2002) A simple physical model for binding energy hot spots in protein-protein complexes. *Proc Natl Acad Sci USA* 99:14116–14121
96. Guerois R, Nielsen JE, Serrano L (2002) Predicting changes in the stability of proteins and protein complexes: a study of more than 1000 mutations. *J Mol Biol* 320:369–387
97. Kortemme T, Kim DE, Baker D (2004) Computational alanine scanning of protein-protein interfaces. *Sci STKE* 2004:pl2–pl2
98. Fogolari F, Brigo A, Molinari H (2003) Protocol for MM/PBSA molecular dynamics simulations of proteins. *Biophys J* 85:159–166
99. Ofra Y, Rost B (2007) ISIS: interaction sites identified from sequence. *Bioinformatics* 23:e13–e16
100. Sriwastava BK, Basu S, Maulik U et al (2013) PPIcons: identification of protein-protein interaction sites in selected organisms. *J Mol Model* 19:4059–4070
101. Goodford PJ (1985) A computational procedure for determining energetically favorable binding sites on biologically important macromolecules. *J Med Chem* 28:849–857
102. Verdonk ML, Cole JC, Taylor R (1999) SuperStar: a knowledge-based approach for identifying interaction sites in proteins. *J Mol Biol* 289:1093–1108
103. Allen FH (2002) The Cambridge Structural Database: a quarter of a million crystal structures and rising. *Acta Crystallogr B* 58:380–388
104. Brenke R, Kozakov D, Chuang GY et al (2009) Fragment-based identification of druggable 'hot spots' of proteins using Fourier domain correlation techniques. *Bioinformatics* 25:621–627
105. Alvarez-Garcia D, Barril X (2014) Molecular simulations with solvent competition quantify water displaceability and provide accurate interaction maps of protein binding sites. *J Med Chem* 57:8530–8539
106. Radoux CJ, Olsson TS, Pitt WR et al (2016) Identifying interactions that determine fragment binding at protein hotspots. *J Med Chem* 59:4314–4325
107. Jain AN (2004) Virtual screening in lead discovery and optimization. *Curr Opin Drug Discov Devel* 7:396–403
108. Zhu T, Cao S, Su PC et al (2013) Hit identification and optimization in virtual screening: practical recommendations based on a critical literature analysis. *J Med Chem* 56:6560–6572

109. Rester U (2008) From virtuality to reality—virtual screening in lead discovery and lead optimization: a medicinal chemistry perspective. *Curr Opin Drug Discov Devel* 11:559–568
110. Leach AR, Gillet VJ, Lewis RA et al (2010) Three-dimensional pharmacophore methods in drug discovery. *J Med Chem* 53:539–558
111. Wolber G, Langer T (2005) LigandScout: 3-D pharmacophores derived from protein-bound ligands and their use as virtual screening filters. *J Chem Inf Model* 45:160–169
112. Meslamani J, Li J, Sutter J et al (2012) Protein-ligand-based pharmacophores: generation and utility assessment in computational ligand profiling. *J Chem Inf Model* 52:943–955
113. Koes DR, Camacho CJ (2012) PocketQuery: protein–protein interaction inhibitor starting points from protein–protein interaction structure. *Nucleic Acids Res* 40:W387–W392
114. Krüger DM, Jessen G, Gohlke H (2012) How good are state-of-the-art docking tools in predicting ligand binding modes in protein–protein interfaces? *J Chem Inf Model* 52:2807–2811
115. Cavasotto CN, Phatak SS (2009) Homology modeling in drug discovery: current trends and applications. *Drug Discov Today* 14:676–683
116. Irwin JJ, Shoichet BK (2005) ZINC—a free database of commercially available compounds for virtual screening. *J Chem Inf Model* 45:177–182
117. Noyal M, Honig B (2006) On the nature of cavities on protein surfaces: application to the identification of drug-binding sites. *Proteins* 63:892–906
118. Leach AR, Shoichet BK, Peishoff CE (2006) Prediction of protein-ligand interactions. Docking and scoring: successes and gaps. *J Med Chem* 49:5851–5855
119. Li H, Li C (2010) Multiple ligand simultaneous docking: orchestrated dancing of ligands in binding sites of protein. *J Comput Chem* 31:2014–2022
120. Morris GM, Goodsell DS, Halliday RS et al (2015) Automated docking using a Lamarckian genetic algorithm and an empirical binding free energy function. *J Comput Chem* 19:1639–1662
121. Morris GM, Huey R, Lindstrom W et al (2009) AutoDock4 and AutoDockTools4: automated docking with selective receptor flexibility. *J Comput Chem* 30:2785–2791
122. Li Y, Zhao Y, Liu Z et al (2011) Automatic tailoring and transplanting: a practical method that makes virtual screening more useful. *J Chem Inf Model* 51:1474–1491
123. Xue X, Wei JL, Xu LL et al (2013) Effective screening strategy using ensembled pharmacophore models combined with cascade docking: application to p53-MDM2 interaction inhibitors. *J Chem Inf Model* 53:2715–2729
124. Mazar AP (2008) Urokinase plasminogen activator receptor choreographs multiple ligand interactions: implications for tumor progression and therapy. *Clin Cancer Res* 14:5649–5655
125. Khanna M, Wang F, Jo I et al (2011) Targeting multiple conformations leads to small molecule inhibitors of the uPAR uPA protein–protein interaction that block cancer cell invasion. *ACS Chem Biol* 6:1232–1243
126. Verdonk ML, Chessari G, Cole JC et al (2005) Modeling water molecules in protein–ligand docking using GOLD. *J Med Chem* 48:6504–6515
127. Wang R, Lai L, Wang S (2002) Further development and validation of empirical scoring functions for structure-based binding affinity prediction. *J Comput Aid Mol Des* 16:11–26
128. Favalaro B, Allocati N, Graziano V et al (2012) Role of apoptosis in disease. *Aging (Milano)* 4:330–349
129. Ding X, Li Y, Lv L et al (2013) De novo design, synthesis and evaluation of benzylpiperazine derivatives as highly selective binders of Mcl-1. *ChemMedChem* 8:1986–2014

Chapter 5

Experimental Methods Used for Identifying Small-Molecule Inhibitors of Protein-Protein Interaction



Mi Zhou, Qing Li, Wenna Kong and Renxiao Wang

5.1 Introduction

In the postgenomic era, proteomics that focuses on the study of the expression, structure, and function of large numbers of proteins has become an important research field. It has been estimated that human genome consists of 19,000 genes encoding for ~500,000 proteins. Over 80% of proteins do not operate alone, but rather interact with one another in complexes [1]. Protein-protein interactions (PPIs) play key roles in numerous biological processes, such as signal transduction, cellular organization, metabolism, transport, immune recognition, cell cycle control, and gene transcription [2]. Aberrant PPIs may contribute to the pathogenesis of various human diseases, which makes PPIs as an emerging class of drug targets for therapeutic intervention.

Compared with the design of small molecules that bind to enzyme active sites, modulating PPIs with small-molecule inhibitors remains enormously challenging. The intractability lies in the fact that PPI contact surface areas are typically large (with a buried area of approximately 1500–3000 Å² per side), less conserved, often flat or more shallow, with a lack of well-defined binding sites and “druggable” cavities [3]. And because of this, PPIs had been previously considered “undruggable.” However, in recent years, mutational analysis of protein interfaces found that not all residues at the PPI interface, but rather a small number of residues,

M. Zhou · Q. Li · W. Kong · R. Wang (✉)
State Key Laboratory of Bioorganic and Natural Products Chemistry,
Shanghai Institute of Organic Chemistry, Chinese Academy of Sciences,
345 Lingling Road, Shanghai 200032, People’s Republic of China
e-mail: wangrx@mail.sioc.ac.cn

R. Wang
State Key Laboratory of Quality Research in Chinese Medicine,
Macau Institute for Applied Research in Medicine and Health,
Macau University of Science and Technology, Macau, People’s Republic of China

so-called hot spots, are directly responsible for the PPI. They appear to be clustered in tightly packed regions in the center of the interface, account for most of the binding energy and can be covered by a small molecule [4, 5]. Nowadays, more than 40 PPIs implicated in cancer, virology, cardiovascular, and immunology have been targeted, including Bcl-2/Bcl-x_L-Bax/Bak [6], p53-MDM2 [7], CCR5-HIV-1 gp120 [8], fibrinogen-GPIIb/IIIa [9], CD80-CD28 [10], offering the opportunity to develop novel drugs for the treatment of the corresponding disease. In fact, a dozen PPI inhibitors have reached clinical trials [11]. In 2016, an inhibitor of Bcl-2-Bim interaction, venetoclax (ABT-199), was approved by Food and Drug Administration (FDA) of USA for the treatment of chronic lymphocytic leukemia (CLL), becoming the first PPI inhibitor drug [12].

Similar to the drug discovery efforts by shooting other types of molecular targets, identification of PPI inhibitors also relies on certain experimental methods. A variety of experimental methods based on biophysical, biochemical, or genetic principles have been developed for this purpose (Table 5.1). Those methods are employed to obtain important information about binding affinity, kinetics, structure, or cellular function of PPI inhibitors when they bind to protein-protein interfaces. This chapter will describe some widely applied experimental methods for characterizing PPI inhibitors, summarizing the principles, strengths and limitations, and applications of each type of method.

5.2 Biophysical Methods

5.2.1 Fluorescence Polarization (FP)

The theory of fluorescence polarization (FP), first described in 1926, provides information on the rotational mobility of fluorophores in solution [13]. When a fluorophore is excited by plane polarized light, it emits light with a degree of polarization that is inversely proportional to its molecular rotation. Typically, larger molecule rotates slowly and emits highly polarized light, whereas smaller molecule rotates faster and emits depolarized light [14] (Fig. 5.1a). By measuring the extent of fluorescence polarization, FP can be applied to study biomolecular interactions if one of the binding molecules is relatively small and labeled with a fluorescent probe. Commonly used probes include fluorescein isothiocyanate (FITC), fluorescein amidite (FAM), tetramethylrhodamine (TAMRA), boron-dipyrromethene (BODIPY), cyanine-5 (Cy5) dyes, Texas Red, Alexa 488 [15]. Complex formation leads to an increase in FP signal (in millipolarization units, mP), which can be measured by a microplate reader equipped with polarizing optics.

The FP method has been applied extensively to the analysis of molecular interactions including protein-protein, protein-ligand, and protein-nucleic acid interactions [16–18]. With adequate experimental design, it can also be adapted to a high-throughput format for identification of PPI inhibitors. As PPIs are often

Table 5.1 Comparison of experimental methods for identifying PPI inhibitors

Methods	General mechanism	Strengths	Weaknesses	Examples
Fluorescence polarization (FP)	Based on the rotational mobility of fluorophores in solution	Low cost; mix-and-read format; high throughput	Suffers from interference from auto-fluorescence, quenching, and light scattering	[20–23]
Surface plasmon resonance (SPR)	Detects small changes in refractive index very close to a sensor surface	Label-free; small sample consumption; real-time kinetic measurement	Suffers from interfering effect such as nonspecific interaction between the sensor surface and analyte; surface immobilization may affect the binding event	[30–33]
Bio-layer interferometry (BLI)	Analyzes the interference pattern of the reflected light from two surfaces at the tip of a glass fiber	Label-free; dip-and-read format; real-time kinetic measurement	Suffers from interfering effect such as nonspecific binding of analytes to the biosensor; buffer containing detergents is incompatible	[31, 38, 39]
Isothermal titration calorimetry (ITC)	Quantifies the heat change in a reaction at constant temperature	Label-free; provides thermodynamic parameters	High sample consumption; low throughput; suffers from the artifacts generated by mismatched buffer components	[45–48]
Differential scanning fluorimetry (DSF)	Quantifies the change in thermal denaturation temperature of a protein under varying conditions	High throughput; small sample consumption	Suffers from interferences from auto-fluorescent compounds and interactions between compounds and fluorescent dye	[54–56]
Nuclear magnetic resonance (NMR) spectroscopy	Based on the phenomenon that magnetically active nuclei in a strong magnetic field absorb and re-emit electromagnetic radiation	High structural resolution generates less false positives or false negatives in protein-observed NMR experiment; needs small amounts of protein in ligand-observed NMR experiment	Needs larger amounts of protein and longer acquisition time in protein-observed NMR experiment	[30, 46, 60, 61, 63, 66–71]

(continued)

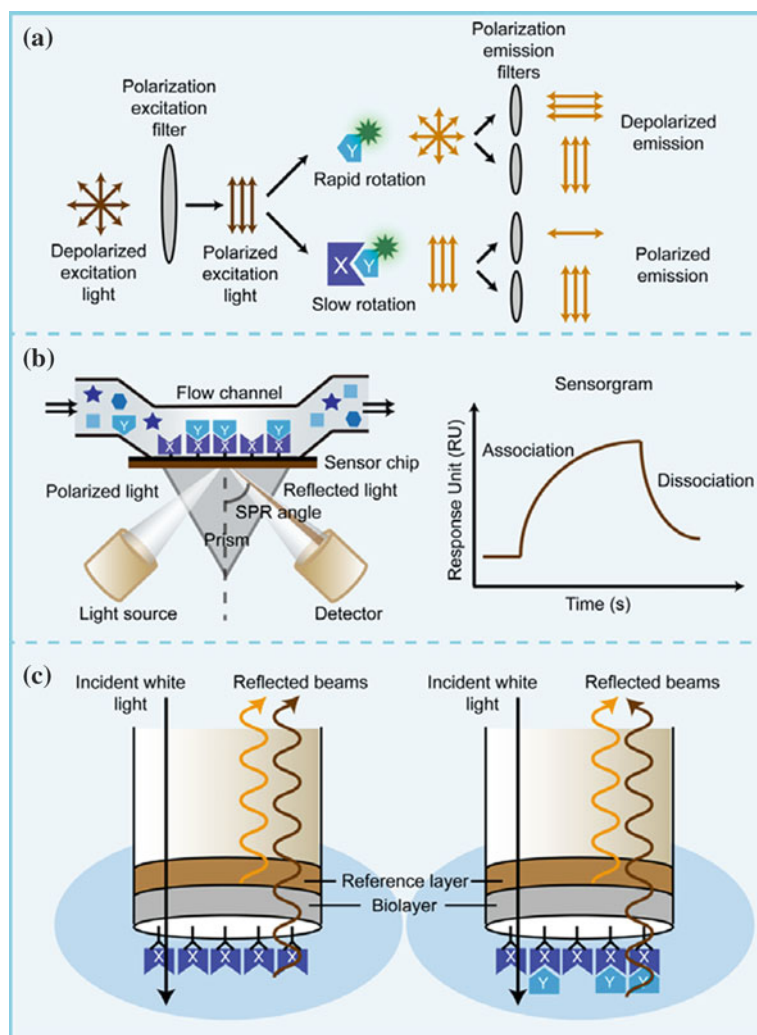
Table 5.1 (continued)

Methods	General mechanism	Strengths	Weaknesses	Examples
X-ray crystallography	Determines the atomic and molecular structure of a crystal, in which atoms scatter the X-ray into a pattern of reflections that is collected for structure determination	High experimental resolution; fewer false positives; no limitations on the size and complexity of the protein	Fairly costly; time-consuming	[30, 56, 77–79]
Microscale thermophoresis (MST)	Monitors the directed movement of molecules in a microscopic temperature gradient	Easy setting; fast measurement; low sample consumption	Requires the labeling of the protein with a fluorophore for typical MST	[84–86]
Capillary electrophoresis (CE)	Based on the separation of analytes within a capillary according to their different electrophoretic mobility	Short analysis time; little sample consumption; ease of automation; high separation efficiency	Requires the labeling of the protein with a fluorophore for typical CE	[91–93]
Fluorescence resonance energy transfer (FRET)	Refers to the nonradiative energy transfer from a donor fluorophore upon excitation to an acceptor fluorophore	High throughput	Suffers from interference like background fluorescence from buffer, proteins, chemical compounds, and cell lysate	[97–101]
Bioluminescence resonance energy transfer (BRET)	Refers to the nonradiative energy transfer from a bioluminescent enzyme upon excitation to a fluorescent protein	High throughput; high signal-to-noise ratio	Sometimes microscopic imaging for BRET is limited due to its low level of light emission from bioluminescent reactions	[115–118]
AlphaScreen	Refers to a bead-based proximity assay which measures the interaction of two molecules conjugated to donor and acceptor beads	Ease of use; broad energy transfer distance; high signal-to-noise ratio	Light- and temperature-sensitive; suffers from interference from blue/green compounds	[45, 123–127]

(continued)

Table 5.1 (continued)

Methods	General mechanism	Strengths	Weaknesses	Examples
Protein-fragment complementation assay (PCA)	Detects the interaction between two proteins that are each fused to fragments of a reporter protein	High throughput	Use of fusion proteins may alter the folding or structure of the protein of interest	[132, 134–137]
Pull-down	Enables to probe interactions between a protein of interest expressed with a fusion tag and the potential interacting partners	Many proteins can be expressed at high yields in soluble form when fused to GST	Potential steric hindrance caused by the large fusion tag	[46, 142]
Co-immunoprecipitation (Co-IP)	Uses bait-specific antibody to coprecipitate the bait and bait-interacting proteins	Easy to perform	Requires specific antibodies or tagging of the proteins	[38, 125, 143, 144]
Enzyme-linked immunosorbent assay (ELISA)	Refers to a plate-based assay applied for detecting the presence of an antigen or an antibody in sample solution	High sensitivity due to signal amplification	Multiple incubation and washing steps are time-consuming and can disrupt weak interactions	[142, 145, 146]
Proximity ligation assay (PLA)	Analyzes endogenous single protein and PPIs via an amplifiable DNA reporter with high specificity and sensitivity	Allows visualization of protein complexes in situ; provides powerful signal amplification	Only detects the proximity of proteins within a few tens of nanometers	[153–156]
Phage display	Selects peptides, proteins or antibodies with high affinity and specificity toward wide range of targets from a phage library	High sensitivity due to multi-round selection and amplification steps	The size of the protein that can be expressed on the surface is limited to shorter peptides	[163]
Yeast two-hybrid (Y2H) system	Detects the interactions between two proteins which are fused to DNA-binding and activation domain of a transcriptional activator in yeast GAL4, respectively	Interactions are detected in vivo; allows the detection of weak or transient interactions	Unsuitable for membrane proteins or proteins localized in other subcellular compartment; unsuitable for proteins that cannot efficiently fold or be post-translationally modified in the yeast nucleus; cannot detect PPIs involving transcriptional activators	[167–170]



governed by a small binding epitope referred as a hot spot, utilizing truncated peptides containing such epitopes mimics the interactions between two complete protein molecules and thus facilitates experimental measurements. Hence, FP assay for PPI inhibitors screening tend to be carried out in a competitive inhibition mode, identifying compounds that compete with smaller fluorescent peptide for binding to larger target protein. The binding affinity constants (K_i values) of inhibitors can be calculated using mathematical equations [19]. Such FP assay has been developed to screen inhibitors of interactions between antiapoptotic Bcl-2 proteins and proapoptotic BH3-only proteins [20, 21], MDM2 and p53 [22], and Keap1 and Nrf2 [23].

◀**Fig. 5.1** Illustration of some biophysical methods for identifying PPI inhibitors. **a** Fluorescence polarization (FP). Upon excitation by polarized lights, a fluorescently labeled molecule emits lights with a certain degree of polarization that is inversely proportional to its rotation rate. A smaller molecule rotates faster, so the emitted lights are depolarized, whereas a larger complex rotates more slowly, so the emitted lights remain polarized. **b** Surface plasmon resonance (SPR). One of the interacting proteins X is immobilized on the gold surface of a sensor chip, while a solution containing the other protein Y flows over the sensor surface. An incident light beam then hits a prism on the opposite side of the sensor chip to excite the surface plasmon. Any perturbation on the gold surface, such as binding of Y to X, results in a shift of the SPR angle. This change is detected in real time and is presented in a sensorgram containing both association and dissociation phases of the interaction. **c** Bio-layer interferometry (BLI). White light travels down the glass fiber and is reflected back up from two interfaces at the tip, including a reference layer and a bio-layer immobilized with protein X. When protein Y binds to the immobilized protein X, the thickness variation of the bio-layer causes a shift of the interference pattern of the reflected light

The technical advantages of the FP assay include low cost, simple mix-and-read format with no separation by washing, and high-throughput screening (HTS) capacity when carried out in a microwell plate (96-, 384-, or 1,536-cell). On the other hand, its drawbacks include interference from auto-fluorescence, quenching, and light scattering [15, 24]. Counter screens should be performed to distinguish interference compounds among hits in primary screens. Furthermore, using longer wavelength (red-shifted) fluorophores are viable options for reducing fluorescence interference and light scattering [25].

5.2.2 Surface Plasmon Resonance (SPR)

Surface plasmon resonance (SPR) is an optical technique to detect small changes in refractive index very close to a sensor surface. When a polarized light hits a prism covered by thin layer of metal (typically a gold film) at a particular angle of incidence, free electrons at the metal surface absorb light photons and generate electron charge density waves called surface plasmons that propagate along the metal surface. Under this resonance condition, the reflected light exhibits a sharp attenuation. The angle of incidence at which minimum reflection occurs is defined as the SPR angle, which is strongly dependent on the refractive index of the material near the metal surface. The main application of SPR is to enable real-time detection of molecular interactions. A slight change in the refractive index (e.g., due to the binding of molecules in solution to surface-immobilized molecules) may be monitored as a shift in SPR angle [26, 27]. Since the first commercial SPR-based analytical instrument was launched by Biacore AB in 1990, many SPR biosensors have been developed to become standard instruments in academic institutions and pharmaceutical companies [28].

In a SPR assay to analyze a binary interaction, the target protein is firstly immobilized onto the sensor chip. Immobilization can be performed by covalent coupling depending on the available reactive groups of target protein such as amine

($-\text{NH}_2$), thiol ($-\text{SH}_2$), and aldehyde ($-\text{COOH}$), or by high affinity capture based on interactions between antibodies and specific fusion tags. A variety of robust and reproducible sensor chips are commercially available [29]. Then the solution containing analytes (i.e., interacting proteins, peptides, or compounds) are flown in a microfluidic channel over the chip surface. The accumulation of analytes on the sensor surface due to a binding event causes a proportional increase in refractive index and SPR angle shift. Increasing response defined in resonance or response units (RU) is recorded in a sensorgram in real time. When the analyte is replaced by buffer, the response begins to decrease. Fitting the sensorgram data to a suitable binding model allows for determination of kinetic rate constants ($k_{\text{on}}/k_{\text{off}}$) and equilibrium constants (K_{D}) of the interaction [26] (Fig. 5.1b). Characterization of PPI inhibitors can be carried out in such a direct binding assay, with inhibitors injected over the sensor chip immobilized with target protein [30, 31]. It can also be performed in a competition assay format, wherein a serial dilution of inhibitor is incubated with a fixed concentration of a competitor, followed by passing over the surface immobilized with target protein. IC_{50} value can be determined using a dose-response curve fit [32, 33].

SPR biosensor technology has various technical advantages including label-free format, small sample consumption (micro- to sub-micrograms), real-time measurement of kinetic association and dissociation rate constants, and high sensitivity to detect small molecular weight (<500 Da) analytes and low-affinity interactions ($K_{\text{D}} > 1$ mM) [28]. However, it may suffer from interfering effects such as non-specific interaction between the sensor surface and analyte or changes in the refractive index of the solution [34]. Additionally, surface immobilization may affect the binding event, e.g., covalent coupling makes target protein attach to the chip in random orientations with some of its binding site inaccessible to the analyte. The SPR technique has traditionally been used in low-throughput studies as standard SPR biosensor only contains three to four flow cells on one sensor chip. A recent development of SPR imaging (SPRI) allows to evaluate hundreds or thousands of samples on protein assays simultaneously and has been successfully applied for HTS of PPI inhibitors [35].

5.2.3 *Bio-layer Interferometry (BLI)*

Bio-layer interferometry (BLI) is another optical technique, based on optical interferometry. It allows real-time monitoring the binding events occurring on the tip of a glass fiber. In a BLI-based biosensor, such as Octet system (FortéBio Inc.), target protein is immobilized through various interactions (e.g., amine-coupling, biotin/streptavidin, antibody/anti-Fc, His-tag/Ni-NTA) onto the tip of a fiber-optic biosensor to form a bio-layer. The biosensor is then dipped into a solution of the analyte. White light is sent down the glass fiber and is reflected from two surfaces at the tip: an internal reference layer and an external bio-layer of immobilized protein. Binding of the analyte to the immobilized protein causes an increase in optical

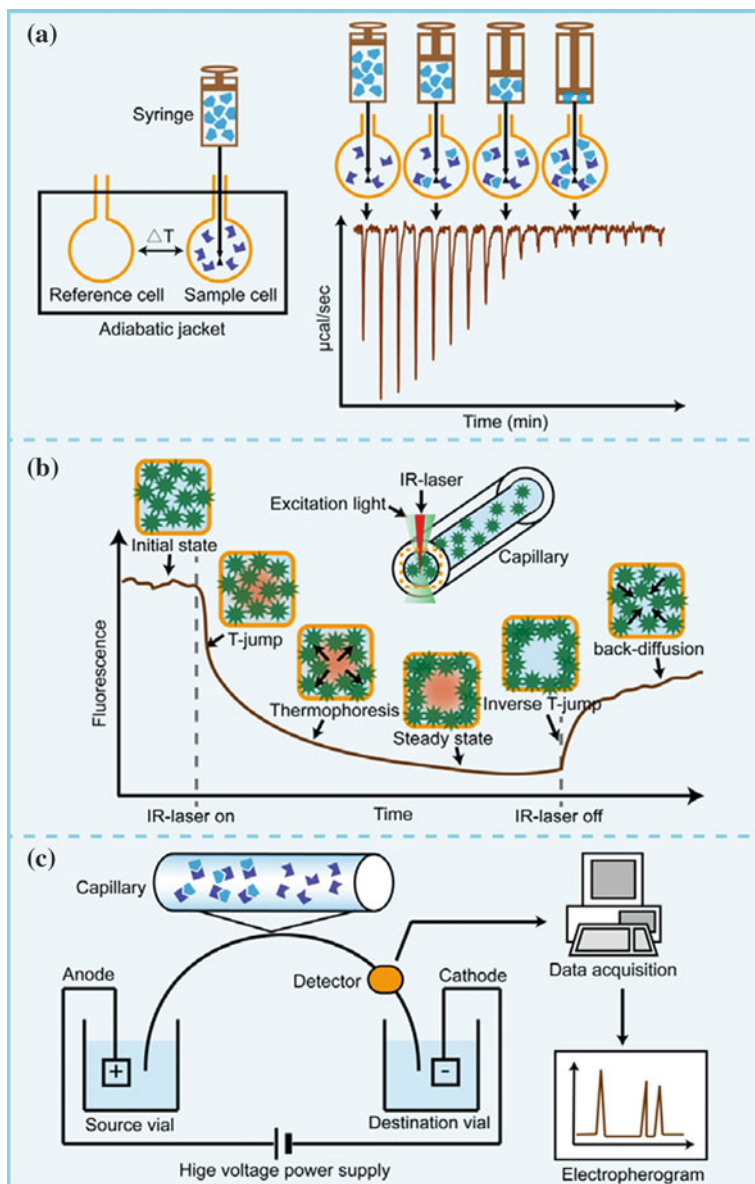
thickness at the biosensor tip, and the interference pattern of the reflected light shifts to higher wavelength (Fig. 5.1c). This wavelength shift ($\Delta\lambda$) is captured by a spectrometer and reported in relative intensity units (nm). When the biosensor is transferred to a solution containing buffer, the dissociation phase is monitored [36, 37]. A BLI-based biosensor can analyze samples in 96- or 384-well plates and enables to measure the binding of analytes with molecular weight as low as 150 Da and affinity ranging from millimolar to picomolar [37]. Hence, it is adaptive to screen compounds or fragments targeting PPIs. Kinetic parameters ($k_{\text{on}}/k_{\text{off}}$) and equilibrium constants (K_{D}) are obtainable via real-time measurement of responses during the association and dissociation phase [31, 38, 39].

As an alternative method to SPR, BLI allows label-free and real-time measurement and generates results similar to SPR. Meanwhile, it has unique properties such as dip-and-read format that eliminates the need for microfluidics. Unbound molecules or changes in the refractive index of the solution do not affect the interference pattern. Cautions should be paid on nonspecific binding of analytes to the biosensor. Furthermore, buffer containing detergents is incompatible with BLI measurements, as detergents may form heterogeneous micelles and lead to a nonuniform “thickening” of the bio-layer [37].

5.2.4 Isothermal Titration Calorimetry (ITC)

A protein–ligand interaction typically involves changes including short-range bond formation (hydrogen bonding, van der Waal’s interaction, pi–cation interactions, etc.) between the protein and the ligand, conformational change of the protein, displacement of water and any cosolutes (buffer, salts, etc.) from the part the protein’s and ligand’s surface, rearrangement of the water adjacent to the protein–ligand interface. All these changes are reflected in the reaction enthalpy and entropy, resulting in an overall change in the Gibbs energy of the system [40]. Calorimetric measurements can help to characterize a given interaction by directly determining thermodynamic parameters associated with the interaction. A main calorimetric technique applied for investigation of protein–ligand interactions including the binding of PPI inhibitors to their target protein is isothermal titration calorimetry (ITC).

ITC directly quantifies the heat change in a reaction at constant temperature or heat capacity at multiple temperatures. A typical commercially available ITC instruments is composed of two identical cells, a sample cell and a reference cell, contacted via sensitive thermopile/thermocouple circuits to detect temperature differences between them. For ligand–protein interaction analysis, the ligand placed in a syringe is injected in small amount at regular intervals into the sample cell containing target protein. The change in heat associated with binding (endothermic or exothermic) results in a change in temperature in the sample cell. The differential heat effects between the sample and reference cell can be measured directly with sufficient sensitivity (in the order of several hundred nanojoules) [41] (Fig. 5.2a).



The main parameters extracted from ITC experiment include Gibbs free energy change (ΔG), enthalpy change (ΔH), entropy change (ΔS), equilibrium binding constant (K_d), reaction stoichiometry (n), and heat capacity change (ΔC_p) [42]. ITC does not suffer from constraints of protein size, shape, or chemical constitution. Neither is there any need for immobilization nor modification of protein [43].

◀**Fig. 5.2** Illustration of some biophysical methods for identifying PPI inhibitors. **a** Isothermal titration calorimetry (ITC). An ITC instrument contains a reference cell and a sample cell, which are surrounded by an adiabatic jacket. When protein Y loaded in the syringe is titrated into the sample cell containing its interacting partner X, X-Y interaction results in heat changes in the sample cell, which can be quantified by the electric power required to maintain equal temperatures between two cells. **b** Microscale thermophoresis (MST). An IR laser is used to generate microscopic temperature gradients within a capillary filled with fluorescent molecules. Changes of fluorescence intensity due to the motions of fluorescent molecules along temperature gradients, including initial state, *T*-jump, thermophoresis, steady state, inverse *T*-jump, and back-diffusion, can be measured. **c** Capillary electrophoresis (CE). CE is performed in a capillary with each end placed in a buffer solution. Separations are driven by a high voltage applied across the capillary after introduction of sample at inlet side. Detection of separated molecules is monitored by a detector near the outlet end of the capillary and is presented in an electropherogram

However, large amounts of protein (~ 0.5 mg) are required for each experiment. Extreme care must be taken in the use of a buffer in an ITC experiment, that is, both in the sample cell as well as the syringe should be dialyzed in an identical buffer to minimize the artifacts generated by mismatched buffer components [44]. Many literatures have reported the use of ITC in validating the activity of PPI inhibitors toward target proteins by measuring their K_D values [45–48]. Reliable measurement range of K_D is 1–100 μM . A displacement assay can be performed to assess interactions with a lower K_D down to picomolar range [49].

5.2.5 Differential Scanning Fluorimetry (DSF)

Differential scanning fluorimetry (DSF), also known as ThermoFluor, is a thermal shift assay, which quantifies the change in thermal denaturation temperature of a protein under varying conditions including through binding to small-molecule inhibitors. In a DSF experiment, target protein is incubated with a fluorescent dye (e.g., SYPRO Orange) which is highly fluorescent upon binding nonspecifically to hydrophobic surfaces of the protein and is quenched in an aqueous environment. As the temperature rises, the protein undergoes thermal unfolding. More exposure of hydrophobic parts of the protein leads to an increase in fluorescence plotted as a function of temperature. A gradual decrease of fluorescence is then observed owing to protein precipitation and aggregation. The midpoint of the protein unfolding transition is defined as the melting temperature (T_m). The stabilizing effect of ligand that binds to the protein will increase the T_m . This thermal shift (ΔT_m) is semi-quantitatively related to ligand binding affinity, with higher affinity ligands generating larger shift [50–52].

DSF can be performed using a conventional real-time PCR instrument in a high-throughput 384-well format. A large number of samples can be analyzed simultaneously with relatively small amounts of protein (~ 2 μg per reaction) [53]. Therefore, it is applicable for both primary screening and hit validation. By using DSF as a screening tool, a novel series of benzodiazepinedione antagonists of the

HDM2-p53 interaction was discovered from a 338,000 compound library [54]. DSF has also been used in a fragment screen to identify fragments against BRCA2-RAD51 interaction [55]. Furthermore, by comparing the ΔT_m induced by several Smac-mimetic compounds targeting Smac-XIAP interaction, the stabilization effects of these compounds on XIAP were analyzed [56]. Intrinsic limitations of this method are interferences from auto-fluorescent compounds and interactions between compounds and fluorescent dye. Detergents in buffer may increase background noise dramatically through binding to lots of dyes, whereas using the dye 1-anilinonaphthalene-8-sulfonic acid (ANS) can minimize such effect [57].

5.2.6 Nuclear Magnetic Resonance (NMR) Spectroscopy

Nuclear magnetic resonance (NMR) is a physical phenomenon in which magnetically active nuclei in a strong magnetic field absorb and re-emit electromagnetic radiation at specific resonance frequencies. Various parameters providing distance, angular, or orientation data can be obtained from NMR experiments, such as nuclear Overhauser effect (NOE), chemical shift, paramagnetic relaxation enhancement (PRE), and residual dipolar coupling (RDC). They give detail information about the structure, dynamics, and interactions of biomolecules [58, 59]. By assessing protein–ligand interactions, NMR spectroscopy has evolved as a powerful tool in drug discovery for hit identification and lead optimization including guiding the design of PPI inhibitors [60, 61]. Protein-observed or ligand-observed NMR experiment can be employed to analyze the binding of single compound or a mixture of 10–50 compounds to target protein by comparing NMR parameters of the free and bound states of the molecules.

In protein-observed NMR experiments, the NMR spectra of protein are recorded in the absence and presence of the ligand. Chemical shift perturbations of protein resonances are typical parameters observed upon ligand addition. The simplest measurement is 1D ^1H -*aliph* NMR spectra (usually below 0.7 ppm). This spectral region contains resonances from protein's methyl groups and is rarely populated by signals from small molecules [62]. Another 1D ^1H NMR approach is Trp side chain $^1\text{H}^\epsilon$ resonances (usually above 10 ppm). These two approaches are applicable for target protein with low molecular masses (less than 30 kDa). Indeed, most protein-observed NMR experiments often rely on the detection of 2D [^1H , ^{15}N] or 2D [^1H , ^{13}C] spectra by using isotopically labeled protein. 2D heteronuclear single quantum correlation (HSQC) experiment, which gives 2D heteronuclear chemical shift correlation map between directly bound ^1H and ^{13}C -or ^{15}N -heteronuclei, is a primarily used strategy. It allows to determine dissociation constant of protein-inhibitor complex in titration experiments and to roughly identify the inhibitor-binding site [30, 46, 63]. In general, protein-observed approach generates less false positives or false negatives than other biophysical methods such as SPR or ITC, shows high sensitivity to detect weaker binders, and meanwhile provides structural information about the binding site. However, it needs larger amounts of

protein (sometimes requires isotopic labeling) and longer acquisition time, and costs great effort into resonance assignment [60].

In ligand-observed NMR experiments, the NMR spectra of ligand are monitored in the absence and presence of target protein. This approach is more diverse than protein-observed approach. Widely used methods include relaxation-edited NMR experiments (e.g., $T_{1\rho}$ experiment), diffusion-edited NMR experiments, saturation transfer difference (STD) spectroscopy, water-ligand observed via gradient spectroscopy (WaterLOGSY), Transferred-NOE spectroscopy (tr-NOESY), NOE pumping, interligand NOE (ILOE) experiment, INPHARMA experiment, fluorine chemical shift anisotropy and exchange for screening (FAXS), and three fluorine atoms for biochemical screening (3-FABS) [61, 64, 65]. Many instances demonstrate the use of ligand-observed NMR experiments in identification of PPI inhibitors, e.g., STD spectroscopy was used to identify inhibitors targeting interactions between uPAR-uPA [66], S100B-p53 [67], and p53-MDM2 [68] and helps to map out the binding epitope of the inhibitor for binding to the target protein. WaterLOGSY was employed to validate hit that inhibits Nef-SH3Hck interaction [46] and to screen fragment library for compounds against the gp41 intramolecular PPI [69] and S100-p53 interaction [70]. By detecting a pair of ligands that bind simultaneously in adjacent sites on the protein surface, ILOE experiment was applied for the rational design of compounds targeting Bcl-x_L and Mcl-1 [71]. Overall, ligand-observed approaches are easier to implement. Minimal amounts of protein are needed with no isotope labeling and no protein size limitation. However, they are not immune to false positives hence do not provide the same level of reliability and unambiguity as protein-observed approaches [61].

5.2.7 *X-Ray Crystallography*

X-ray crystallography is a powerful method for investigating the 3D structure of proteins at the atomic level. There are three major steps involved in its procedure [72–75]. Firstly, protein crystallization. Since X-ray diffraction from a single molecule is too weak to detect, a crystal made up of many ordered protein molecules in identical orientations is needed, which helps to produce a strong diffraction for structure determination. Various conditions should be screened in an attempt to obtain a diffraction-quality crystal, such as pH, ionic strength, temperature, protein concentration, the presence of various salts or additives, the type of precipitant, and the crystallization method (e.g., vapor diffusion in either hanging drop or sitting drop format) to use. With the advent of miniaturized crystallization plates, robot systems, and commercial crystallization kits, one can quickly find suitable crystallization conditions. Secondly, data collection. The crystal is mounted and exposed in a monochromatic X-ray beam using a laboratory X-ray generator or a high brilliance synchrotron source. During the exposure, atoms in the crystal scatter the X-ray into a pattern of reflections. As the crystal orientation is gradually rotated, each diffraction pattern corresponding to a different crystal orientation is collected

by a charge-coupled device (CCD) detector. Thirdly, structure solution. The recorded series of 2D diffraction patterns are converted into a 3D model of the electron density. With an electron density map of sufficient resolution, an atomic model of protein can be obtained by manual or automatic methods. This initial model is then optimized to best fit the experimental diffraction data and prior chemical information after multiple cycles of refinement and validation [76].

Technological advancements have been made in protein crystallization, data collection, and high-resolution structural determinations, contributing to a rapid increase in the number of 3D structures of proteins and protein-protein complexes deposited in the Protein Data Bank (PDB). These structures can facilitate the study of small-molecule inhibitors targeting PPIs. For this, a protein-inhibitor complex crystal is firstly formed by either soaking or cocrystallization. In soaking, a fully grown protein crystal is soaked in a solution containing single inhibitor or a cocktail of inhibitors which can rapidly diffuse into the protein crystal. In cocrystallization, the inhibitor is included in the crystallization solution together with the protein. Once the protein model is sufficiently well refined, automatic procedures are applied to fit the inhibitor to the electron density map of protein-inhibitor complex [73]. Many structures of protein-inhibitor complexes have been reported, providing a detailed view of inhibitor-binding sites and binding modes, and paving the way for structure-based ligand optimization [30, 56, 77–79].

Advantages in this technique include high experimental resolution usually ranging from 1 to 3 Å, fewer false positives, and no limitations on the size and complexity of the protein. However, it is fairly costly and time-consuming, since obtaining a diffraction-quality crystal is a trial and error procedure. Compared with NMR, X-ray crystallography only gives static structural information, and the binding affinities cannot be quantitatively assessed. Sometimes crystallization may change the protein conformation due to packing interactions [73].

5.2.8 *Microscale Thermophoresis (MST)*

Microscale thermophoresis (MST) is a recently developed method that monitors the directed movement of molecules in a microscopic temperature gradient. It is particularly suitable for protein-protein or protein-ligand interaction analysis as thermophoresis is highly sensitive to binding-induced changes in size, charge, conformation, or hydration shell of the protein [80]. In a standard MST experiment, protein of interest is fluorescently labeled by either fusing to a fluorescent protein such as green fluorescent protein (GFP) or using N-hydroxysuccinimide (NHS) dye. An infrared (IR) laser is focused into a capillary containing the fluorescent protein to the exact spot where fluorescence is excited and detected before, during, and after the IR laser is turned on. Before heating, the initial fluorescence is recorded at a constant level. Once the IR laser is turned on, the fluorescent protein moves away from the heated spot because of the effect termed thermophoresis, leading to an abrupt decrease in fluorescence (temperature jump or

T-jump). After that, the fluorescence decreases slowly (thermophoresis) until reaching a steady state in which thermodiffusion is counterbalanced by mass diffusion. When the IR laser is turned off, the fluorescence increases suddenly (inverse *T*-jump) and then increases gradually until achieving a steady state (back-diffusion) [81–83] (Fig. 5.2b). As binding events will cause a difference in the protein's thermophoresis, MST enables to measure binding affinity of biomolecular interactions via a titration where a constant concentration of fluorescent protein and varying concentrations of its binder are applied. The K_D value can be derived from analyzing the fluorescence change in both *T*-jump and thermophoresis process. Some recent researches have proven the application of MST in studying the binding of PPI inhibitors to their target proteins [84–86].

MST possesses several advantages including easy setting, fast measurement (binding affinity is determined in 10 min), low sample consumption (a few microliters at nanomolar concentrations), diversity of analytical solution, and determination of K_D in broad range (picomole to millimole) [81, 83]. Typically, MST requires the labeling of the protein with a fluorophore. It can be performed in a label-free manner alternatively, in which aromatic amino acids are regarded as the intrinsic fluorophore with fluorescence detected in the UV range [82, 87].

5.2.9 Capillary Electrophoresis (CE)

Capillary electrophoresis (CE) is an analytical technique that separates analytes within a capillary based on their different electrophoretic mobility. A typical CE instrument consists of a sample introduction system, a narrow-bore capillary (25–75 μm internal diameter), a high voltage power supply, a detector, and an output device. In CE experiment, the capillary is filled with a flowing electrolyte solution, and a high voltage (typically 5–30 kV) is applied to induce an electric field through the capillary. Analytes are introduced at one extreme of the capillary, which migrate toward the electrode of opposite charge by electroosmotic flow (EOF), and are separated on the basis of their mass to charge ratio. Separated analytes are detected by a UV or laser-induced fluorescence (LIF) detector near the outlet end of the capillary. The data output is displayed as an electropherogram which is a plot of migration time versus detector response (UV-visible absorbance or fluorescence). Hence, separated analytes appear as peaks with different migration time in the electropherogram [88] (Fig. 5.2c). CE has several advantages that make it suitable for detecting biomolecular interactions, such as short analysis time, little sample consumption, ease of automation, and high separation efficiency. Different modes of CE for the study of biomolecular interactions have been developed, e.g., capillary zone electrophoresis (CZE), vacancy peak (VP), vacancy affinity CE (VACE), Hummel–Dreyer (HD), mobility shift (MS), and CE-frontal analysis (CE-FA) [89, 90]. Some of them have been applied in a competitive mode for identifying small-molecule inhibitors of PPIs [91–93].

Houston et al. utilized a MS-based CE assay to identify new scaffolds that bind to the p53-interaction site of MDM2 [91]. MS assay was performed with injection solution containing fluorescent competitive ligand (i.e., fluorescence-labeled p53 peptide) and separation solution containing target protein (i.e., MDM2). The migration time of the injected ligand was detected. When a potential PPI inhibitor was added in varying concentrations to the separation solution, the mobility of the fluorescent ligand will shift between the mobility of its free form and the mobility of the ligand–protein complex. This change in migration time was used to calculate the percentage inhibition (%) of the PPI inhibitor and IC_{50} value.

Rauch et al. developed a CZE assay for library screening of inhibitors against Hsp70-Bag3 interaction [92]. CZE assay was performed with injection solution containing pre-equilibrated fluorescent target protein (i.e., fluorescence-labeled Hsp70), competitive ligand (i.e., Bag3), and a potential PPI inhibitor. Free and ligand-bound fluorescent proteins were observed as separate peaks with different migration time in the electropherogram. The peak area ratio (bound to free Hsp70) was used to identify putative inhibitors.

Recently, Xu et al. developed a CE-FA method for screening inhibitors that block Bcl- x_L -Bid interaction [93]. Similar to CZE, CE-FA is also based on the separation of the free and bound species. In CE-FA, a relatively large volume of injection solution containing pre-equilibrated target protein (i.e., Bcl- x_L), fluorescent competitive ligand (i.e., fluorescence-labeled Bid peptide) and a potential PPI inhibitor was introduced into the capillary. An electropherogram consisting of plateau peaks of free and bound ligand was reported, with the height of the free ligand plateau being proportional to the free ligand concentration. IC_{50} and K_i values can be determined by mathematical equations. Compared to CZE, CE-FA is more robust as the plateau height and the corresponding concentration is not affected by changes in migration times, EOF, length of capillary or applied voltage, therefore is highly recommended for affinity studies [94, 95].

5.3 Biochemical Methods

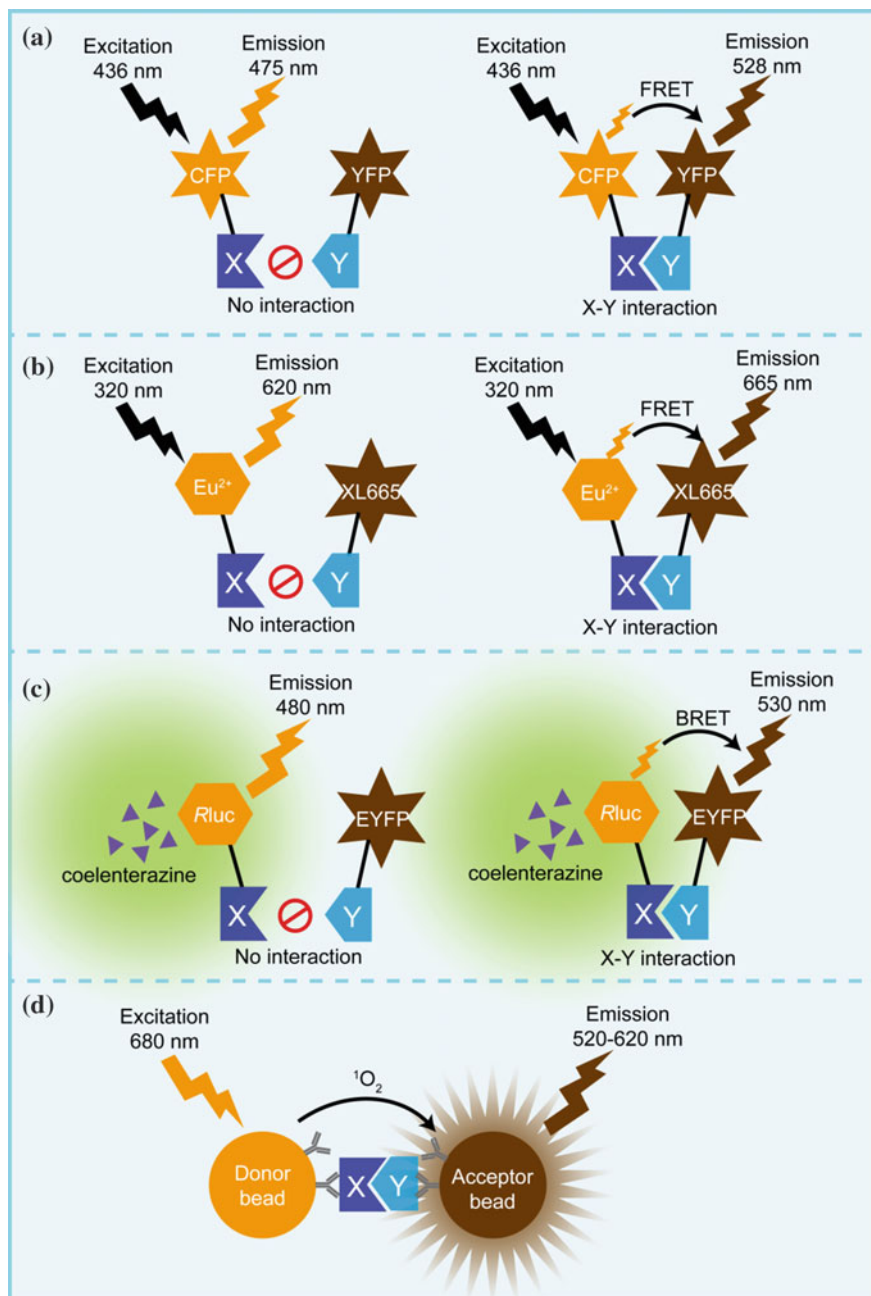
5.3.1 *Fluorescence and Bioluminescence Resonance Energy Transfer (FRET and BRET)*

Fluorescence resonance energy transfer (FRET) refers to the nonradiative (dipole–dipole) energy transfer from a donor fluorophore upon excitation to an acceptor fluorophore [96]. The efficiency of this energy transfer is inversely proportional to the sixth power of the distance between donor and acceptor. Owing to the strong distance dependence, FRET is highly sensitive to detect PPIs and to screen PPI inhibitors both in vitro and in vivo [97–101]. For this, one protein is labeled with donor and the other with acceptor. FRET only occurs when two proteins are engaged in complex formation that brings donor and acceptor in very close

proximity within 1–10 nm range (Fig. 5.3a). Additionally, the emission spectrum of the donor has to overlap with the excitation spectrum of the acceptor. Commonly used FRET pairs with fluorescent proteins or small organic dyes as fluorophores include cyan fluorescent protein (CFP)-yellow fluorescent protein (YFP) [99], CyPet-YPet [102], mVenus-mStrawberry [103], Alexa Fluor 488-Alexa Fluor 546 [97], Alexa Fluor 568-Alexa Fluor 647 [97]. After performing FRET experiment with optimal donor–acceptor pairs, FRET efficiency is measured and used to assess binding degree or disruption of PPIs. For in vitro assay, FRET efficiency can be simply quantified by measuring either the decreased donor emission or the increased acceptor emission. For cellular studies performed with microscopy imaging, several strategies have been developed for measuring FRET efficiency including sensitized emission, acceptor photobleaching, fluorescence lifetime imaging microscopy (FLIM), spectral imaging, and fluorescence polarization imaging [104].

Since FRET sometimes suffers from interference like background fluorescence from buffer, proteins, chemical compounds, and cell lysate, time-resolved FRET (TR-FRET) has been developed, which uses long-life emission fluorophores (lanthanides such as europium and terbium) as donors and allows the elimination of short-lived background fluorescence. As a TR-FRET-based technology, homogeneous time-resolved fluorescence (HTRF) makes further improvements and provides higher sensitivity and stability in detecting biomolecular interactions, as well as HTS of PPI inhibitors in vitro [86, 105–107]. The donor used in HTRF is europium or terbium cryptate in which europium or terbium ion is embedded in a macrocyclic structure for energy collection and transfer. Since the HTRF donor has longer emission lifetime (1–2 ms) compared with conventional fluorophores (1–50 ns), it permits a time delay of ~ 50 –150 μ s between the donor excitation and fluorescence measurement, thus decreasing interference from short-life background fluorescence. One of HTRF acceptors is XL665, which is a chemically modified allophycocyanin of 105 kDa. The other is d2, which is an organic motif of approximately 1,000 Da with photophysical properties close to XL655. As a much smaller fluorophore, d2 limits the steric hindrance problems sometimes suspected in XL655-based systems. The HTRF ratio, which is the ratio of fluorescence measured at 665 nm (acceptor) and 620 nm (donor), is calculated to reflect binding degree or disruption of PPIs [108, 109] (Fig. 5.3b).

Bioluminescence resonance energy transfer (BRET) is analogous to FRET except that the energy donor is a bioluminescent enzyme, typically luciferase. Upon oxidation of its substrate, the donor converts the substrate into light emission, promoting energy transfer with a compatible acceptor, typically a fluorescent protein [110] (Fig. 5.3c). Several versions of BRET donor–acceptor pairs with different substrates have been developed, such as *Renilla* luciferase (*Rluc*)-enhanced YFP (EYFP) [111], *Rluc*-GFP² (a blue-shifted variant of GFP) [112], and firefly luciferase (*Fluc*)-dsRed [113]. As BRET does not require extrinsic excitation by a light source, thereby avoiding some drawbacks associated with FRET, such as auto-fluorescence, photobleaching, and simultaneous excitation of both donor and acceptor [114]. Furthermore, the signal-to-noise ratio of BRET is tenfold higher



than that of FRET, thus allowing the use of 40-fold less amount of protein than FRET. These advantages make BRET a suitable technique for cellular PPI studies.

◀**Fig. 5.3** Illustration of some biochemical methods for identifying PPI inhibitors. **a** Fluorescence resonance energy transfer (FRET). Proteins X and Y are fused with FRET donor CFP and acceptor YFP, respectively. If X and Y do not interact, excitation of CFP results in light emission by CFP (475 nm) only. When X-Y interaction occurs, CFP and YFP are brought into proximity, resulting in energy transfer from CFP to YFP and the detection of YFP emission at 528 nm. **b** Homogenous time-resolved fluorescence (HTRF). Protein X and Y are fused with HTRF donor europium cryptate and acceptor XL665, respectively. If X and Y do not interact, excitation at 320 nm results in donor emission (620 nm) only. When X-Y interaction occurs, energy is transferred from the donor to the acceptor, generating XL665 emission at 665 nm. **c** Bioluminescence resonance energy transfer (BRET). Protein X and Y are fused with BRET donor *Rluc* and acceptor EYFP, respectively. If X and Y do not interact, only blue-emitting spectrum of *Rluc* (480 nm) can be detected. When X-Y interaction occurs, bioluminescence energy generated by *Rluc* is transferred to EYFP, generating EYFP emission at 530 nm. **d** AlphaScreen. Two interacting protein X and Y are linked to donor and acceptor beads, respectively. Upon excitation at 680 nm, a photosensitizing agent on the donor bead converts ambient oxygen to singlet oxygen which initiates a cascade of energy transfer steps in the acceptor bead, finally resulting in the generation of light emission at 520–620 nm

Many literatures have demonstrated the application of BRET in HTS of PPI inhibitors in yeast and mammalian cells [115–118]. The strength of PPI is indicated by BRET ratio and BRET signal. The BRET ratio is defined as the light intensity of the acceptor emission to the donor emission. The BRET signal is calculated by subtracting the measured BRET ratio with a background BRET ratio (obtained when the donor protein is expressed alone). Hence, a decrease in BRET signal is expected upon the addition of a PPI inhibitor [119].

5.3.2 *AlphaScreen*

Amplified luminescent proximity homogenous assay screen (AlphaScreen) is a bead-based proximity assay developed from luminescent oxygen channeling immunoassay (LOCI) [120]. The key components of AlphaScreen are two bead types, donor beads and acceptor beads. The donor beads contain a photosensitizer, phthalocyanine, which converts ambient oxygen into a singlet state upon irradiation at 680 nm. Within its 4 microsecond half-life, singlet oxygen can diffuse to a maximum distance of about 200 nm. The acceptor beads contain three chemical dyes, thioxene, anthracene, and rubrene. If it is located in close proximity (<200 nm) to the donor beads, singlet oxygen initially reacts with thioxene to produce light energy that is transferred to anthracene and then to rubrene, resulting in a broad emission from 520 to 620 nm. If donor and acceptor beads are not in close proximity, singlet oxygen falls to ground state and no signal is produced [121, 122] (Fig. 5.3d).

AlphaScreen is commonly used to study biomolecular interactions in a microplate format. It is also superior in evaluating PPI inhibitors through HTS [45, 123–127]. AlphaScreen possesses a few advantages over other screening technologies. First, ease of use. AlphaScreen is homogeneous with no wash steps and can be

performed in 96-, 384-, or 1536-well formats. Many types of pre-coated beads are available for conjugating biomolecules to the bead surface. Second, broad energy transfer distance. The distance between donor and acceptor beads to generate signal can be very large (200 nm) compared with FRET or HTRF (~ 10 nm), which enables the measurement of a large protein-protein complex. Third, high signal-to-noise ratio. Excitation of each donor beads generates about 60,000 oxygen singlets per second, leading to exceptionally high signal amplification upon interaction with acceptor beads. Combined with low background, AlphaScreen offers outstanding signal-to-noise ratio, which can reach several hundreds in some cases [121, 128]. Nevertheless, AlphaScreen has some intrinsic drawbacks. First, the donor beads are light-sensitive. Direct sunlight and intense artificial light can activate donor beads and reduce signal strength. Second, the signal is temperature-dependent. As temperature may affect the rate of generation and diffusion of singlet oxygen, it is necessary to keep incubation temperatures and plate-read temperatures consistent. Third, blue/green compounds that absorb light at 520–620 nm are interfering in AlphaScreen.

5.3.3 *Protein-Fragment Complementation Assay (PCA)*

Protein-fragment complementation assay (PCA) is a method designed for the identification of PPIs. In the general PCA strategy, a reporter protein is rationally dissected into two fragments, and each is fused to one of the hypothetical binding partners. Interaction between the binding partners brings the split reporter fragments close enough to reconstitute the reporter protein owning its native structure and activity. Commonly used reporter proteins include dihydrofolate reductase (DHFR), β -lactamase, β -galactosidase, TEV protease, ubiquitin, GFP and its variants, luciferase. According, the signal readout can be absorbance, cell survival, reporter gene activation, fluorescence, and luminescence [129, 130]. Besides employed in global organization of PPI networks in yeast or eukaryotes, PCAs using different split systems have been applied for the identification of PPI inhibitors both in vitro and in vivo.

Split-DHFR PCA is a survival-selection assay based on a mutant of murine DHFR that is insensitive to its inhibitor methotrexate or trimethoprim but retains catalytic activity. Formation of PPIs leads to cellular growth on media supplemented with methotrexate or trimethoprim, which can be analyzed through cell survival or fluorescence (in the presence of fluorogenic substrate methotrexate) [131]. Mai et al. established a HTS platform using murine DHFR reporter fragments [F(1,2) and F(3)] to screen for inhibitors against DevR-DevR interaction in mycobacterial cells [132]. Split-DHFR PCA offers advantage that readout signals can be amplified through generations, allowing detecting small changes in PPIs.

Split- β -lactamase PCA is an enzyme-based assay, in which PPIs can be characterized by detecting the β -lactamase activity through colorimetric measurement for in vitro studies or fluorometric measurement for in vivo studies. The

colorimetric assay is performed with nitrocefin as the substrate of β -lactamase. The β -lactamase activity is detected by observing the color change of nitrocefin from yellow to red under hydrolysis, with absorbance measurement at 492 nm. The fluorometric assay is performed with CCF2/AM as the substrate. Upon excitation at 409 nm, formation of PPIs leads to blue fluorescence emission at 447 nm, whereas disruption of PPIs leads to green fluorescence emission at 520 nm [133]. Remy et al. developed an application of split- β -lactamase PCA for HTS of inhibitors against Toll-like receptor 4 (TLR4)-MyD88 interaction from a 16,000 compound library in HeLa cells [134].

PCA based on the reconstitution of a fluorescent protein is also called bimolecular fluorescence complementation (BiFC). Formation of PPIs leads to an increase in fluorescence emission, which can be easily measured and analyzed by microplate reader, fluorescence microscopy, and flow cytometry. Therefore, BiFC cannot only provide an efficient way for in vitro HTS, but also offer a good platform for in vivo imaging, e.g., Hashimoto et al. utilized monomeric Kusabira-GFP (mKG) as a reporter protein and conducted in vitro screening of inhibitors against PAC3 homodimerization from a 123,599 natural product library [135]. Chen et al. designed a new near-infrared BiFC system from a bacterial phytochrome for visualizing the inhibition of HIV-1 integrase (IN)-LEDGF/p75 interaction by drugs in live cells [136]. BiFC sometimes encounters with self-aggregation and folding interference problem of fluorescent reporters. Additionally, the formation of the fluorescent reporter is irreversible that prevents analysis of complex dissociation, but this limitation can be circumvented by adding PPI inhibitors before protein expression.

Split-luciferase PCA utilizes firefly, *Renilla*, or Gaussia luciferase as a reporter protein which can catalyze the oxidation of its substrate (e.g., D-luciferin and coelenterazine) and produce bioluminescence. Major advantages are its superior sensitivity due to low cellular background luminescence and reversible reassembly, allowing in vivo imaging with a high signal-to-noise ratio and detection of kinetic and equilibrium aspects of the formation and disruption of PPIs [130]. Yang et al. adopted a split-luciferase PCA based on firefly luciferase to identify inhibitors of epidermal growth factor (EGF) receptor dimerization [137].

5.3.4 Affinity Chromatography

Affinity chromatography is a biochemical separation technique for purification of a specific molecule from complex mixtures, based on highly specific interactions between two molecules (e.g., enzyme and substrate, receptor and ligand, antibody and antigen). It not only provides an efficient way for protein purification, but also offers a technology platform to study PPIs and PPI inhibitors. Such methods include pull-down, co-immunoprecipitation (Co-IP), and enzyme-linked immunosorbent assay (ELISA).

Pull-down enables to probe interactions between a protein of interest expressed with a fusion tag (bait) and the potential interacting partners (prey). In the original pull-down assay devised by Kaelin et al. [138], the bait protein fused to glutathione S-transferase (GST) was expressed in bacteria, immobilized on glutathione-coupled beads, and incubated with a cell lysate. Proteins binding to the bait (prey) could be captured and “pulled down” with a series of wash and elution steps. Finally, bait–prey complexes were evaluated by sodium dodecyl sulfate-polyacrylamide gel electrophoresis (SDS-PAGE) (Fig. 5.4a). Alternative fusion tags such as polyhistidine [139], HaloTag (a modified dehalogenase) [140], and biotin [141] can also be used to express or label the bait protein with subsequent capture by Ni-NTA agarose, HaloLink resin, and streptavidin magnetic beads, respectively. GST pull-down assay is a commonly used strategy to assess the inhibitory activities of compounds on defined PPIs [46, 142]. In such experiment, purified GST-tag bait is immobilized on glutathione-coupled beads and incubated with a mixture of purified prey and a potential PPI inhibitor. After washing away nonbound prey, the amount of prey bound to GST-tag bait can be detected by western blotting using anti-prey antibody, which reflects the disruption of bait–prey interaction.

Co-IP is similar in methodology to pull-down that purifies interacting proteins by means of beaded support. The difference in co-IP is that it uses bait-specific antibody instead of affinity-tagged bait. In this method, a cell lysate or protein mixture is incubated with anti-bait antibody, followed by adding protein A or G which is covalently attached to agarose beads and can specifically bind to the antibody. So that both bait (i.e., the antigen) and prey are captured or precipitated on the beaded support. After washing and elution from the antibody, bait–prey complexes are subjected to SDS-PAGE and analyzed by western blotting with anti-prey antibody [1] (Fig. 5.4b). Both monoclonal and polyclonal antibodies can be used in co-IP and have their own advantages in different applications. Monoclonal antibodies recognized a single epitope on antigen with highly specificity to decrease background noise and cross-reactivity, whereas polyclonal antibodies recognized multiple epitopes, providing more robust detection and giving stronger signals. Co-IP enables to investigate the inhibitory effects of compounds on defined PPIs under physiological conditions *in vitro*, in which a potential PPI inhibitor is administered to cells before harvest and the change in the amount of bait–bound prey is detected [38, 125, 143, 144]. It can be performed with cells transfected with a plasmid encoding bait with a fusion tag or performed with cells expressing endogenous proteins. The latter approach is capable of avoiding artificial effects such as overexpression or modification of the protein of interacts.

ELISA is a plate-based assay applied as a diagnostic tool for detecting the presence of an antigen or an antibody in sample solution. Its assay format can be used to measure the formation of PPI and thus to measure the disruption of PPIs by inhibitors [142, 145, 146]. To measure a PPI in the direct ELISA format, the protein of interest is noncovalently coated to a polystyrene microwell plate through passive adsorption. After washing away excess free protein, the remaining available binding surfaces of the wells are blocked with nonreacting protein such as bovine serum albumin (BSA). Then the sample solution containing the binding partner is added to

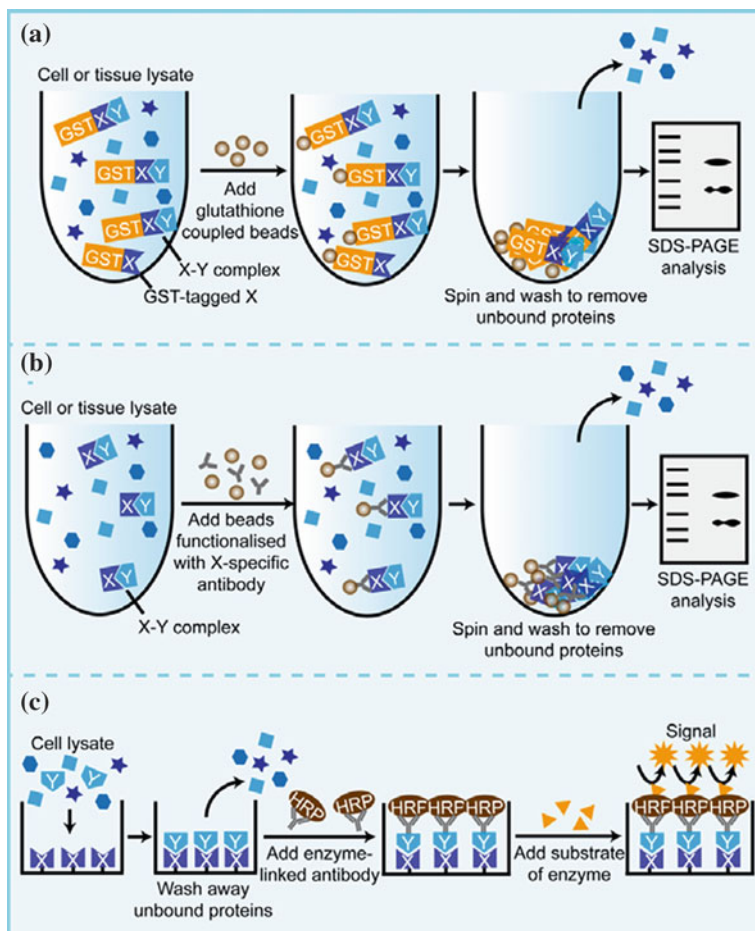


Fig. 5.4 Illustration of some biochemical methods for identifying PPI inhibitors. **a** GST pull-down assay. Protein X is expressed as a GST-fused protein and is incubated with cell or tissue lysate containing its interacting partner Y. GST-X-Y complexes are captured by glutathione-coupled beads and eluted for SDS-PAGE analysis. **b** Co-immunoprecipitation (Co-IP). X-Y complexes in cell or tissue lysate are captured by beads functionalized with X-specific antibody, followed by co-precipitation, washing, elution and SDS-PAGE analysis. **c** ELISA. Protein X is immobilized on a microwell plate and then incubated with cell lysate containing its interacting partner Y. After washing away unbound proteins, X-Y complexes are detected by an HRP-conjugated antibody against protein Y and finally generate detectable fluorescence- or absorbance-based signal upon addition of a substance of the HRP enzyme

the wells and incubated to interact with the immobilized protein. After another washing step, a primary antibody against the binding partner conjugated with an enzyme, such as horseradish peroxidase (HRP) or alkaline phosphatase (AP), is applied as a detection antibody. Finally, a substrate for the enzyme is added, eliciting a chromogenic or fluorescent signal upon enzymatic reaction. The amount

of the binding partner bound to the immobilized protein is quantified through absorbance- or fluorescence-based readout [147] (Fig. 5.4c). For PPI inhibitors characterization, the IC_{50} value can be calculated according to a dose-dependent reduction in readout signal. ELISA can also be performed in an indirect format in which the binding partner is detected by a primary antibody and an enzyme-linked secondary antibody, or in a sandwich format in which the protein of interest is coated to the plate through a pre-coated “capture” antibody. Generally, ELISA exhibits superior sensitivity due to signal amplification through enzymatic oxidation or hydrolysis of substrates to produce enhanced color or fluorescence [148].

5.3.5 Proximity Ligation Assay (PLA)

Proximity ligation assay (PLA) is a novel technique first described by Fredriksson et al. in 2002, allowing to analyze endogenous single protein and PPIs via an amplifiable DNA reporter with high specificity and sensitivity [149]. In the case of PPI characterization, two target proteins are first detected by corresponding two primary antibodies raised in different species and subsequently recognized by a pair of PLA probes consisting of species-specific secondary antibodies, each with an oligonucleotide sequence attached to it. Two other circle-forming DNA oligonucleotides, termed connector oligonucleotides, are then introduced. Upon interaction between target proteins, PLA probes are brought in close proximity (<40 nm). Two oligonucleotides on PLA probes can be hybridized to the connector oligonucleotides, leading to the formation of a circular DNA strand upon ligase incubation. This circular DNA template is further amplified via rolling circle amplification (RCA) upon addition of DNA polymerase, yielding a long concatemeric copy of the template. After the amplification reaction, complementary fluorophore-labeled oligonucleotides are added to interact with the RCA product and generate a fluorescent signal easily detected by fluorescence microscopy [150–152] (Fig. 5.5). Hence, PLA is a powerful technology employed in detection, visualization, and quantification of endogenous PPIs in situ in fixed tissue and cell samples. Likewise, this proximity ligation in situ assay (P-LISA) can be performed to observe the disruption of PPIs by inhibitors [153–156].

P-LISA possesses several advantages over other biochemical methods. Unlike co-IP, it does not require tremendous amount of cells. Compared to fluorescence-based assays such as FRET, BRET, and BiFC, it enables to detect endogenous proteins without being affected by overexpression. Besides, it provides powerful signal amplification via RCA as the protein complex becomes labeled by several hundred copies of the fluorophore and can be imaged as a brightly fluorescent spot [157]. Nevertheless, it should be noted that PLA only detects the proximity of proteins within a certain distance, typically up to a few tens of nanometers, rather than physical molecular interaction [152].

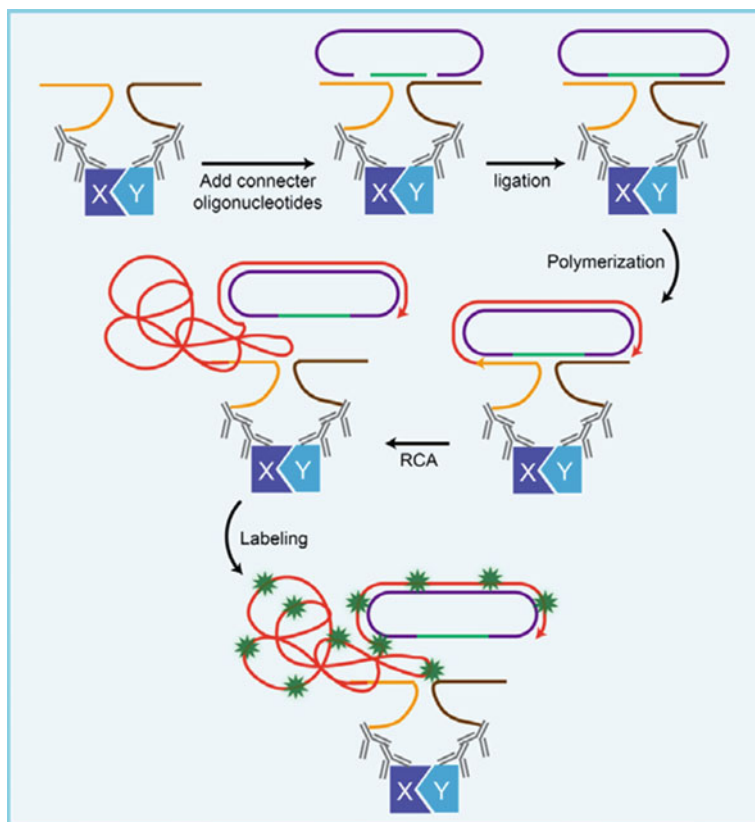


Fig. 5.5 Illustration of proximity ligation assay (PLA). Proteins X and Y are first immuno labeled with two primary antibodies and then with secondary antibodies conjugated to single-stranded oligonucleotides. When the X-Y interaction occurs, the oligonucleotides of the PLA probes will hybridize and ligate with two additional connector oligonucleotides to form a continuous circular DNA template, which is subsequently amplified by DNA polymerase through rolling circle amplification (RCA). The resulting RCA product will be labeled with fluorescent probes for further detection

5.4 Genetic Methods

5.4.1 Phage Display

Phage display was first described by Smith in 1985, who demonstrated the display of the peptide on surface of phage particles by inserting a foreign DNA encoding the peptide into filamentous phage gene III [158]. Since then, this technique has been widely used for selecting peptides, proteins or antibodies with high affinity and specificity toward wide range of targets (e.g., proteins, viruses, cancer cells, bacteria, ions, small molecules, etc.) from a phage library contain up to 10^{10}

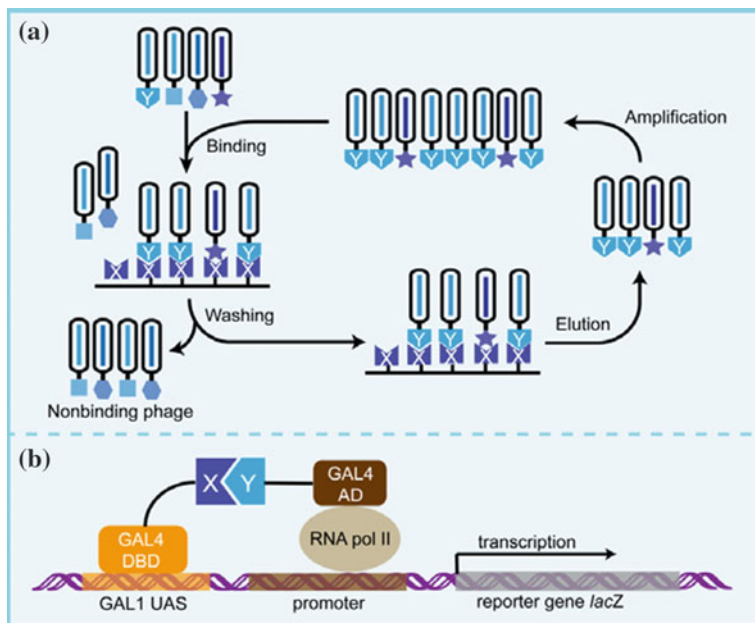


Fig. 5.6 Illustration of some genetic methods for identifying PPI inhibitors. **a** Phage display. A phage library is added to a plate immobilized with protein X. After incubation, nonbinding phages are washed away, while bound phages (i.e., phages displaying X-interacting partner Y) are eluted, amplified by infecting *E. coli* cells, and enriched in the “panning” process. **b** Yeast two-hybrid (Y2H) system. Protein X and Y are fused to the binding domain (BD) and activation domain (AD) of the transcription factor GAL4, respectively. When X-Y interaction occurs, BD and AD are brought into proximity to reconstitute an active transcription factor that finally activates the transcription of a downstream reporter gene *lacZ*

different variants. In the case of screening peptides binding to a target protein, the gene encoding the displayed peptide is packaged within the phage and expressed in fusion with phage coat protein, providing a direct linkage between the genotype and the phenotype. By using filamentous phage M13, DNA sequence encoding the peptide is inserted into the *pIII* or *pVIII* gene encoding minor or major coat protein, respectively. Other preferred systems used for phage display include lambda, T4 and T7 phage. Pools of phages exposing various peptides are incubated with target protein immobilized on a solid surface. Nonspecifically bound phages are washed off, whereas bound phages get captured and then eluted. Eluted phages are amplified by infection of *E. coli* and enriched more than 1000-fold over ordinary phages in a successive rounds of a process called “panning,” and finally identified by sequencing the phage DNA [159–162] (Fig. 5.6a). The great advantage of phage display originates in the incorporation of the protein and genetic information into a single phage particle, allowing fast determination of selected phages. Moreover, multi-round selection and amplification steps make it more sensitive in identifying target binding peptides or proteins.

Even though phage display is a common method to screen protein-binding peptide from a phage library, Ishiet al. established a microwell plate assay by using T7 phage display to screen for candidate inhibitors of p53-MDM2 interactions [163]. In this so-called “reverse phage display,” p53 gene encoding residues 12–36 was fused to the C-terminus of the T7 coat protein 10B to create p53 displaying phage particles, which were then added along with potential PPI inhibitors to a 96-well plate immobilized with GST-MDM2. After incubation and removing nonspecifically bound phages, the bound phages were eluted. Upon infection of *E. coli*, T7 phage particles could form plaques after only 3 h. The number of phage particles in each well was determined by counting the plaques formed on the dishes or plates using a plaque assay method, which reflects the binding between immobilized GST-MDM2 and p53 displayed on T7 phage particles. Therefore, compounds that caused a decrease in the number of eluted phage particles were defined as active inhibitors. Application of this T7 phage display method for HTS of a natural product library identified dehydroaltenusin as a candidate inhibitor of p53-MDM2 interactions.

5.4.2 *Yeast Two-Hybrid (Y2H) System and Other Two-Hybrid Systems*

Yeast two-hybrid (Y2H) pioneered by Fields and Song in 1989 was designed to study PPIs by taking advantage of the properties of a transcriptional activator in yeast GAL4 [164]. The GAL4 protein contains two separable and functionally essential domains, a binding domain (BD) which is responsible for binding to the upstream activating sequence (USA) of GAL1, and an activating domain (AD) which is responsible for the activation of transcription. BD and AD independently are nonfunctional as a transcription factor, but reconstitute a functional GAL4 transcription factor when they are in close proximity [165]. For the study of the interaction between two proteins of interest, one protein is fused to BD and the other is fused to AD. Protein interactions lead to the reassembly of the transcription factor GAL4 which then drives reporter gene expression (Fig. 5.6b). The most popular reporter gene is lacZ, which encodes the enzyme β -galactosidase and allows screening yeast in a colorimetric assay. Other commonly used reporter genes are auxotrophic markers (e.g., HIS3, ADE2, LEU2, LYS2, URA3) whose expression lead to growth on a synthetic medium lacking the cognate nutrient [166]. Y2H is a powerful technique for identifying and analyzing PPIs *in vivo*. Meanwhile, it has been applied successfully to screen for PPI inhibitors [167–170]. However, as Y2H requires the translation of the interacting proteins into the nucleus, it is not suitable for membrane proteins or proteins localized in other subcellular compartment. Neither is it suitable for proteins that cannot efficiently fold or be post-translationally modified in the yeast nucleus. Moreover, Y2H cannot detect PPIs involving transcriptional activators, which produce spontaneous

activation of the transcription of the reporter gene [171]. To circumvent these limitations, a number of variant two-hybrid systems have been established [172].

The repressed transactivator (RTA) system is developed for detection of PPIs involving transcriptional activators, in which an auto-activating protein is fused to BD of GAL4 whereas its interacting partner is fused to the repression domain (RD) of a transcription repressor TUP1. Hence, protein interactions cause repression of a reporter gene, while disruption of the PPI results in reactivation the reporter gene. Joshi et al. devised modification of this system for discovery of PPI inhibitors targeting GV-TGF β -R-FKBP12, ATF4-p300/CBP, Nrf2-p300/CBP, and TR-Ncor1 interactions in HTS [173].

Reverse two-hybrid system is an upside-down version of Y2H, in which disruption of protein interactions decrease the expression of a counter-selectable reporter gene, providing a selective advantage for cell growth. Huang et al. utilized this system to select inhibitors against R1-FKBP12 interaction by using URA3 as a reporter gene. Compounds that caused cell survival in medium containing pro-toxin 5-fluoroorotic acid (5-FOA) were selected as active inhibitors [174]. Young et al. described a HTS based on this reverse two-hybrid system to identify compounds disrupting PPI between α 1B and β 3 subunits of the human N-type calcium channel. CYH2 was adapted as a reporter gene, and compounds that rescued yeast cell growth in the medium containing cycloheximide were selected as active inhibitors [175]. Gunde et al. developed a novel reverse two-hybrid system by using GAL1 as a reporter gene, based on the toxicity of intracellular galactose-1-phosphate. This derivative of galactose accumulates to levels that are toxic to cell metabolism in cells lacking GAL7 function but carrying a galactokinase-encoding GAL1 gene. By using this strategy, compounds against Myc-Max interaction were characterized, which decreased GAL1 reporter gene expression upon dissociation of Myc-Max interaction, reduced intracellular galactose-1-phosphate concentration and restored cell growth under selective conditions [176].

Mammalian protein-protein interaction trap (MAPPIT) is a mammalian two-hybrid system, allowing of the studies of interactions of proteins in native physiological context with proper folding and post-translational modifications. It is dependent on the signal transduction of cytokine receptor and the JAK pathway. In MAPPIT, two interacting proteins are linked to signaling deficient cytokine receptor chimeras. Protein interactions restore functional JAK-STAT signaling and finally induce transcription of a reporter gene coupled to a STAT-dependent promoter [177]. This approach and its reverse format have been well validated for identification of inhibitors targeting Bcl-2-Bid and p53-MDM2 interactions [178, 179].

5.5 Conclusions

Characterizing a small-molecule PPI inhibitor is often technically more challenging than characterizing a small-molecule enzyme inhibitor. Nevertheless, a wide variety of experimental methods have been developed for this purpose. Due to their

different natures, those methods are employed in different applications. Some are more suitable for high-throughput screening jobs, such as FP, FRET, AlphaScreen, and Y2H. Some allow detailed evaluation of binding affinity and binding kinetics of PPI inhibitors at the molecular level, such as ITC, SPR, and BLI. Some can provide additional structural information, such as NMR and X-ray crystallography. Besides, some methods can be used to visualize the disruption of PPIs by small-molecules in living cells, such as FRET, PLA, and BiFC. It is important to note that all methods have their own limitations that may lead to false positives and false negatives in experiments. Therefore, validation by using another method based on a different principle is recommended for obtaining reliable results. Significant advances are made constantly to such experimental methods, which certainly will benefit the identification of small-molecule inhibitors targeting PPIs in the future.

Acknowledgements The authors are grateful for the financial supports from the National Natural Science Foundation of China (Grant No. 81430083, 21472227, 21673276 to Prof. R. Wang), the Ministry of Science and Technology of China (National Key R&D Program of China Grant No. 2016YFA0502302 to Prof. R. Wang), Chinese Academy of Sciences (Strategic Priority Research Program, Grant No. XDB20000000, No. XDB20020200), and the Science and Technology Development Foundation of Macao SAR (Grant No. 055/2013/A2 to Prof. R. Wang).

References

1. Berggard T, Linse S, James P (2007) Methods for the detection and analysis of protein-protein interactions. *Proteomics* 7:2833–2842
2. Braun P, Gingras AC (2012) History of protein-protein interactions: from egg-white to complex networks. *Proteomics* 12:1478–1498
3. Choi S, Choi KY (2017) Screening-based approaches to identify small molecules that inhibit protein-protein interactions. *Expert Opin Drug Discov* 12:293–303
4. Thangudu RR, Bryant SH, Panchenko AR, Madej T (2012) Modulating protein-protein interactions with small molecules: the importance of binding hotspots. *J Mol Biol* 415:443–453
5. Arkin MR, Tang Y, Wells JA (2014) Small-molecule inhibitors of protein-protein interactions: progressing toward the reality. *Chem Biol* 21:1102–1114
6. Tse C, Shoemaker AR, Adickes J, Anderson MG, Chen J, Jin S, Johnson EF, Marsh KC, Mitten MJ, Nimmer P, Roberts L, Tahir SK, Xiao Y, Yang X, Zhang H, Fesik S, Rosenberg SH, Elmore SW (2008) ABT-263: a potent and orally bioavailable Bcl-2 family inhibitor. *Cancer Res* 68:3421–3428
7. Vu BT, Vassilev L (2011) Small-molecule inhibitors of the p53-MDM2 interaction. *Curr Top Microbiol Immunol* 348:151–172
8. Dorr P, Westby M, Dobbs S, Griffin P, Irvine B, Macartney M, Mori J, Rickett G, Smith-Burchnell C, Napier C, Webster R, Armour D, Price D, Stammen B, Wood A, Perros M (2005) Maraviroc (UK-427,857), a potent, orally bioavailable, and selective small-molecule inhibitor of chemokine receptor CCR5 with broad-spectrum anti-human immunodeficiency virus type 1 activity. *Antimicrob Agents Chemother* 49:4721–4732
9. Peerlinck K, De Lepeleire I, Goldberg M, Farrell D, Barrett J, Hand E, Panebianco D, Deckmyn H, Vermynen J, Arnout J (1993) MK-383 (L-700,462), a selective nonpeptide platelet glycoprotein IIb/IIIa antagonist, is active in man. *Circulation* 88:1512–1517

10. Uvebrant K, da Graca Thrige D, Rosen A, Akesson M, Berg H, Walse B, Bjork P (2007) Discovery of selective small-molecule CD80 inhibitors. *J Biomol Screen* 12:464–472
11. Fischer G, Rossmann M, Hyvonen M (2015) Alternative modulation of protein-protein interactions by small molecules. *Curr Opin Biotechnol* 35:78–85
12. Souers AJ, Levenson JD, Boghaert ER, Ackler SL, Catron ND, Chen J, Dayton BD, Ding H, Enschede SH, Fairbrother WJ, Huang DC, Hymowitz SG, Jin S, Khaw SL, Kovar PJ, Lam LT, Lee J, Maecker HL, Marsh KC, Mason KD, Mitten MJ, Nimmer PM, Oleksijew A, Park CH, Park CM, Phillips DC, Roberts AW, Sampath D, Seymour JF, Smith ML, Sullivan GM, Tahir SK, Tse C, Wendt MD, Xiao Y, Xue JC, Zhang H, Humerickhouse RA, Rosenberg SH, Elmore SW (2013) ABT-199, a potent and selective BCL-2 inhibitor, achieves antitumor activity while sparing platelets. *Nat Med* 19:202–208
13. Perrin F (1926) Polarization of light of fluorescence, average life of molecules. *J Phys Radium* 7:390–401
14. Du Y (2015) Fluorescence polarization assay to quantify protein-protein interactions in an HTS format. *Methods Mol Biol* 1278:529–544
15. Matthew DH, Adam Y, Tyler P, John CB, Ajit J, Anton S, Nathan PC (2016) Fluorescence polarization assays in high-throughput screening and drug discovery: a review. *Methods and Applications in Fluorescence* 4:022001
16. Weil J, Hershey JW (1982) The binding of fluorescein-labeled protein synthesis initiation factor 2 to *Escherichia coli* 30 S ribosomal subunits determined by fluorescence polarization. *J Biol Chem* 257:1215–1220
17. Kim YT, Tabor S, Churchich JE, Richardson CC (1992) Interactions of gene 2.5 protein and DNA polymerase of bacteriophage T7. *J Biol Chem* 267:15032–15040
18. Wang Z, Bhattacharya A, Ivanov DN (2015) Identification of small-molecule inhibitors of the HuR/RNA interaction using a fluorescence polarization screening assay followed by NMR validation. *PLoS ONE* 10:e0138780
19. Nikolovska-Coleska Z, Wang R, Fang X, Pan H, Tomita Y, Li P, Roller PP, Krajewski K, Saito NG, Stuckey JA, Wang S (2004) Development and optimization of a binding assay for the XIAP BIR3 domain using fluorescence polarization. *Anal Biochem* 332:261–273
20. Hassig CA, Zeng FY, Kung P, Kiankarimi M, Kim S, Diaz PW, Zhai D, Welsh K, Morshedjian S, Su Y, O'Keefe B, Newman DJ, Rusman Y, Kaur H, Salomon CE, Brown SG, Baire B, Michel AR, Hoye TR, Francis S, Georg GI, Walters MA, Divlianska DB, Roth GP, Wright AE, Reed JC (2014) Ultra-high-throughput screening of natural product extracts to identify proapoptotic inhibitors of Bcl-2 family proteins. *J Biomol Screen* 19:1201–1211
21. Zhai D, Godoi P, Sergienko E, Dahl R, Chan X, Brown B, Rascon J, Hurder A, Su Y, Chung TDY, Jin C, Diaz P, Reed JC (2012) High-throughput fluorescence polarization assay for chemical library screening against anti-apoptotic Bcl-2 family member Bfl-1. *J Biomol Screen* 17:350–360
22. Knight SM, Umezawa N, Lee HS, Gellman SH, Kay BK (2002) A fluorescence polarization assay for the identification of inhibitors of the p53-DM2 protein-protein interaction. *Anal Biochem* 300:230–236
23. Inoyama D, Chen Y, Huang X, Beamer LJ, Kong AN, Hu L (2012) Optimization of fluorescently labeled Nrf2 peptide probes and the development of a fluorescence polarization assay for the discovery of inhibitors of Keap1-Nrf2 interaction. *J Biomol Screen* 17:435–447
24. Owicki JC (2000) Fluorescence polarization and anisotropy in high throughput screening: perspectives and primer. *J Biomol Screen* 5:297–306
25. Turek-Etienne TC, Small EC, Soh SC, Xin TA, Gaitonde PV, Barrabee EB, Hart RF, Bryant RW (2003) Evaluation of fluorescent compound interference in 4 fluorescence polarization assays: 2 kinases, 1 protease, and 1 phosphatase. *J Biomol Screen* 8:176–184
26. Nguyen HH, Park J, Kang S, Kim M (2015) Surface plasmon resonance: a versatile technique for biosensor applications. *Sensors (Basel)* 15:10481–10510
27. Abdulhalim I, Zourob M, Lakhtakia A (2008) Surface plasmon resonance for biosensing: a mini-review. *Electromagnetics* 28:214–242

28. McDonnell JM (2001) Surface plasmon resonance: towards an understanding of the mechanisms of biological molecular recognition. *Curr Opin Chem Biol* 5:572–577
29. Rich RL, Myszka DG (2000) Advances in surface plasmon resonance biosensor analysis. *Curr Opin Biotechnol* 11:54–61
30. Fry DC, Wartchow C, Graves B, Janson C, Lukacs C, Kammloft U, Belunis C, Palme S, Klein C, Vu B (2013) Deconstruction of a nutlin: dissecting the binding determinants of a potent protein-protein interaction inhibitor. *ACS Med Chem Lett* 4:660–665
31. Wartchow CA, Podlaski F, Li S, Rowan K, Zhang X, Mark D, Huang KS (2011) Biosensor-based small molecule fragment screening with biolayer interferometry. *J Comput Aided Mol Des* 25:669–676
32. Hain AU, Bartee D, Sanders NG, Miller AS, Sullivan DJ, Levitskaya J, Meyers CF, Bosch J (2014) Identification of an Atg8-Atg3 protein-protein interaction inhibitor from the medicines for Malaria Venture Malaria Box active in blood and liver stage *Plasmodium falciparum* parasites. *J Med Chem* 57:4521–4531
33. Iozzi S, Remelli R, Lelli B, Diamanti D, Pileri S, Bracci L, Roncarati R, Caricasole A, Bernocco S (2012) Functional characterization of a small-molecule inhibitor of the DKK1-LRP6 interaction. *ISRN Mol Biol* 2012:823875
34. Homola J (2003) Present and future of surface plasmon resonance biosensors. *Anal Bioanal Chem* 377:528–539
35. Jung SO, Ro HS, Kho BH, Shin YB, Kim MG, Chung BH (2005) Surface plasmon resonance imaging-based protein arrays for high-throughput screening of protein-protein interaction inhibitors. *Proteomics* 5:4427–4431
36. Concepcion J, Witte K, Wartchow C, Choo S, Yao D, Persson H, Wei J, Li P, Heidecker B, Ma W, Varma R, Zhao LS, Perillat D, Carricato G, Recknor M, Du K, Ho H, Ellis T, Gamez J, Howes M, Phi-Wilson J, Lockard S, Zuk R, Tan H (2009) Label-free detection of biomolecular interactions using BioLayer interferometry for kinetic characterization. *Comb Chem High Throughput Screening* 12:791–800
37. Sultana A, Lee JE (2015) Measuring protein-protein and protein-nucleic acid interactions by biolayer interferometry. *Curr Protoc Protein Sci* 79:19 25 11–19 25 26
38. Gogate PN, Ethirajan M, Kurenova EV, Magis AT, Pandey RK, Cance WG (2014) Design, synthesis, and biological evaluation of novel FAK scaffold inhibitors targeting the FAK-VEGFR3 protein-protein interaction. *Eur J Med Chem* 80:154–166
39. Jiang ZY, Lu MC, Xu LL, Yang TT, Xi MY, Xu XL, Guo XK, Zhang XJ, You QD, Sun HP (2014) Discovery of potent Keap1-Nrf2 protein-protein interaction inhibitor based on molecular binding determinants analysis. *J Med Chem* 57:2736–2745
40. Falconer RJ (2016) Applications of isothermal titration calorimetry—the research and technical developments from 2011 to 2015. *J Mol Recogn: JMR* 29:504–515
41. Falconer RJ, Penkova A, Jelesarov I, Collins BM (2010) Survey of the year 2008: applications of isothermal titration calorimetry. *J Mol Recogn: JMR* 23:395–413
42. Roselin LS, Lin MS, Lin PH, Chang Y, Chen WY (2010) Recent trends and some applications of isothermal titration calorimetry in biotechnology. *Biotechnol J* 5:85–98
43. Ababou A, Ladbury JE (2007) Survey of the year 2005: literature on applications of isothermal titration calorimetry. *J Mol Recogn: JMR* 20:4–14
44. Pierce MM, Raman CS, Nall BT (1999) Isothermal titration calorimetry of protein-protein interactions. *Methods* 19:213–221
45. Voter AF, Manthei KA, Keck JL (2016) A high-throughput screening strategy to identify protein-protein interaction inhibitors that block the Fanconi anemia DNA repair pathway. *J Biomol Screen* 21:626–633
46. Betzi S, Restouin A, Opi S, Arold ST, Parrot I, Guerlesquin F, Morelli X, Collette Y (2007) Protein protein interaction inhibition (2P2I) combining high throughput and virtual screening: application to the HIV-1 Nef protein. *Proc Natl Acad Sci USA* 104:19256–19261
47. Winkel AF, Engel CK, Margerie D, Kannt A, Szillat H, Glombik H, Kallus C, Ruf S, Gussregen S, Riedel J, Herling AW, von Knethen A, Weigert A, Brune B, Schmol D (2015)

- Characterization of RA839, a noncovalent small molecule binder to Keap1 and selective activator of Nrf2 signaling. *J Biol Chem* 290:28446–28455
48. Gal M, Bloch I, Shechter N, Romanenko O, Shir OM (2016) Efficient isothermal titration calorimetry technique identifies direct interaction of small molecule inhibitors with the target protein. *Comb Chem High Throughput Screen* 19:4–13
 49. Krainer G, Keller S (2015) Single-experiment displacement assay for quantifying high-affinity binding by isothermal titration calorimetry. *Methods* 76:116–123
 50. Cummings MD, Farnum MA, Nelen MI (2006) Universal screening methods and applications of ThermoFluor. *J Biomol Screen* 11:854–863
 51. Simeonov A (2013) Recent developments in the use of differential scanning fluorimetry in protein and small molecule discovery and characterization. *Expert Opin Drug Discov* 8:1071–1082
 52. Niesen FH, Berglund H, Vedadi M (2007) The use of differential scanning fluorimetry to detect ligand interactions that promote protein stability. *Nat Protoc* 2:2212–2221
 53. Vivoli M, Novak HR, Littlechild JA, Harmer NJ (2014) Determination of protein-ligand interactions using differential scanning fluorimetry. *J Vis Exp: JoVE*:51809
 54. Grasberger BL, Lu T, Schubert C, Parks DJ, Carver TE, Koblish HK, Cummings MD, LaFrance LV, Milkiewicz KL, Calvo RR, Maguire D, Lattanze J, Franks CF, Zhao S, Ramachandren K, Bylebyl GR, Zhang M, Manthey CL, Petrella EC, Pantoliano MW, Deckman IC, Spurlino JC, Maroney AC, Tomczuk BE, Molloy CJ, Bone RF (2005) Discovery and cocrystal structure of benzodiazepinedione HDM2 antagonists that activate p53 in cells. *J Med Chem* 48:909–912
 55. Scott DE, Ehebauer MT, Pukala T, Marsh M, Blundell TL, Venkitaraman AR, Abell C, Hyvönen M (2013) Using a fragment-based approach to target protein-protein interactions. *ChemBioChem* 14:332–342
 56. Cossu F, Milani M, Mastrangelo E, Vachette P, Servida F, Lecis D, Canevari G, Delia D, Drago C, Rizzo V, Manzoni L, Seneci P, Scolastico C, Bolognesi M (2009) Structural basis for bivalent Smac-mimetics recognition in the IAP protein family. *J Mol Biol* 392:630–644
 57. Kohlstaedt M, von der Hocht I, Hilbers F, Thielmann Y, Michel H (2015) Development of a ThermoFluor assay for stability determination of membrane proteins using the Na(+)/H(+) antiporter NhaA and cytochrome c oxidase. *Acta Crystallogr D Biol Crystallogr* 71:1112–1122
 58. Marion D (2013) An introduction to biological NMR spectroscopy. *Mol Cell Proteomics* 12:3006–3025
 59. O’Connell MR, Gamsjaeger R, Mackay JP (2009) The structural analysis of protein-protein interactions by NMR spectroscopy. *Proteomics* 9:5224–5232
 60. Wu B, Barile E, De SK, Wei J, Purves A, Pellicchia M (2015) High-Throughput Screening by Nuclear Magnetic Resonance (HTS by NMR) for the identification of PPIs antagonists. *Curr Top Med Chem* 15:2032–2042
 61. Barile E, Pellicchia M (2014) NMR-based approaches for the identification and optimization of inhibitors of protein-protein interactions. *Chem Rev* 114:4749–4763
 62. Wu B, Zhang Z, Noberini R, Barile E, Giulianotti M, Pinilla C, Houghten RA, Pasquale EB, Pellicchia M (2013) HTS by NMR of combinatorial libraries: a fragment-based approach to ligand discovery. *Chem Biol* 20:19–33
 63. D’Silva L, Ozdowy P, Krajewski M, Rothweiler U, Singh M, Holak TA (2005) Monitoring the effects of antagonists on protein-protein interactions with NMR spectroscopy. *J Am Chem Soc* 127:13220–13226
 64. Ludwig C, Guenther UL (2009) Ligand based NMR methods for drug discovery. *Front Biosci (Landmark Ed)* 14:4565–4574
 65. Cala O, Guillièrè F, Krimm I (2014) NMR-based analysis of protein-ligand interactions. *Anal Bioanal Chem* 406:943–956
 66. Mani T, Wang F, Knabe WE, Sinn AL, Khanna M, Jo I, Sandusky GE, Sledge GW Jr, Jones DR, Khanna R, Pollok KE, Meroueh SO (2013) Small-molecule inhibition of the

- uPAR/uPA interaction: synthesis, biochemical, cellular, in vivo pharmacokinetics and efficacy studies in breast cancer metastasis. *Bioorg Med Chem* 21:2145–2155
67. Charpentier TH, Wilder PT, Liriano MA, Varney KM, Zhong S, Coop A, Pozharski E, MacKerell AD Jr, Toth EA, Weber DJ (2009) Small molecules bound to unique sites in the target protein binding cleft of calcium-bound S100B as characterized by nuclear magnetic resonance and X-ray crystallography. *Biochemistry* 48:6202–6212
 68. Angulo J, Goffin SA, Gandhi D, Searcey M, Howell LA (2016) Unveiling the “Three-Finger Pharmacophore” required for p53-MDM2 inhibition by Saturation-Transfer Difference (STD) NMR initial growth-rates approach. *Chemistry* 22:5858–5862
 69. Chu S, Gochin M (2013) Identification of fragments targeting an alternative pocket on HIV-1 gp41 by NMR screening and similarity searching. *Bioorg Med Chem Lett* 23:5114–5118
 70. Arendt Y, Bhaumik A, Del Conte R, Luchinat C, Mori M, Porcu M (2007) Fragment docking to S100 proteins reveals a wide diversity of weak interaction sites. *ChemMedChem* 2:1648–1654
 71. Rega MF, Wu B, Wei J, Zhang Z, Cellitti JF, Pellicchia M (2011) SAR by inter ligand nuclear overhauser effects (ILOEs) based discovery of acylsulfonamide compounds active against Bcl-x(L) and Mcl-1. *J Med Chem* 54:6000–6013
 72. Smyth MS, Martin JH (2000) X-ray crystallography. *Mol Pathol* 53:8–14
 73. Caliendo R, Belviso DB, Aresta BM, de Candia M, Altomare CD (2013) Protein crystallography and fragment-based drug design. *Future Med Chem* 5:1121–1140
 74. Deschamps JR (2010) X-ray crystallography of chemical compounds. *Life Sci* 86:585–589
 75. Blundell TL, Patel S (2004) High-throughput X-ray crystallography for drug discovery. *Curr Opin Pharmacol* 4:490–496
 76. Adams PD, Afonine PV, Grosse-Kunstleve RW, Read RJ, Richardson JS, Richardson DC, Terwilliger TC (2009) Recent developments in phasing and structure refinement for macromolecular crystallography. *Curr Opin Struct Biol* 19:566–572
 77. Lee EF, Czabotar PE, Smith BJ, Deshayes K, Zobel K, Colman PM, Fairlie WD (2007) Crystal structure of ABT-737 complexed with Bcl-xL: implications for selectivity of antagonists of the Bcl-2 family. *Cell Death Differ* 14:1711–1713
 78. Cheng L, Pettersen D, Ohlsson B, Schell P, Karle M, Evertsson E, Pahlen S, Jonforsen M, Plowright AT, Bostrom J, Fex T, Thelin A, Hilgendorf C, Xue Y, Wahlund G, Lindberg W, Larsson LO, Gustafsson D (2014) Discovery of the fibrinolysis inhibitor AZD6564, acting via interference of a protein-protein interaction. *ACS Med Chem Lett* 5:538–543
 79. Agamennone M, Cesari L, Lalli D, Turlizzi E, Del Conte R, Turano P, Mangani S, Padova A (2010) Fragmenting the S100B-p53 interaction: combined virtual/biophysical screening approaches to identify ligands. *ChemMedChem* 5:428–435
 80. Wienken CJ, Baaske P, Rothbauer U, Braun D, Duhr S (2010) Protein-binding assays in biological liquids using microscale thermophoresis. *Nat Commun* 1:100
 81. Mao Y, Yu L, Yang R, Qu LB, Harrington Pde B (2015) A novel method for the study of molecular interaction by using microscale thermophoresis. *Talanta* 132:894–901
 82. Seidel SA, Dijkman PM, Lea WA, van den Bogaart G, Jerabek-Willemsen M, Lazić A, Joseph JS, Srinivasan P, Baaske P, Simeonov A, Katritch I, Melo FA, Ladbury JE, Schreiber G, Watts A, Braun D, Duhr S (2013) Microscale thermophoresis quantifies biomolecular interactions under previously challenging conditions. *Methods* 59:301–315
 83. Jerabek-Willemsen M, Wienken CJ, Braun D, Baaske P, Duhr S (2011) Molecular interaction studies using microscale thermophoresis. *Assay Drug Dev Technol* 9:342–353
 84. Welsch ME, Kaplan A, Chambers JM, Stokes ME, Bos PH, Zask A, Zhang Y, Sanchez-Martin M, Badgley MA, Huang CS, Tran TH, Akkiraju H, Brown LM, Nandakumar R, Cremers S, Yang WS, Tong L, Olive KP, Ferrando A, Stockwell BR (2017) Multivalent small-molecule Pan-RAS inhibitors. *Cell* 168(878–889):e829
 85. Wang X, Wu X, Zhang A, Wang S, Hu C, Chen W, Shen Y, Tan R, Sun Y, Xu Q (2016) Targeting the PDGF-B/PDGFR-beta interface with Destruxin A5 to selectively block PDGF-BB/PDGFR-beta signaling and attenuate liver fibrosis. *EBioMedicine* 7:146–156

86. Fan X, Wei J, Xiong H, Liu X, Benichou S, Gao X, Liu L (2015) A homogeneous time-resolved fluorescence-based high-throughput screening for discovery of inhibitors of Nef-sdAb19 interaction. *Int J Oncol* 47:1485–1493
87. Seidel SAI, Wienken CJ, Geissler S, Jerabek-Willemsen M, Dühr S, Reiter A, Trauner D, Braun D, Baaske P (2012) Label-free microscale thermophoresis discriminates sites and affinity of protein-ligand binding. *Angew Chem* 51:10656–10659
88. Espada A, Molina-Martin M (2012) Capillary electrophoresis and small molecule drug discovery: a perfect match? *Drug Discov Today* 17:396–404
89. Busch MH, Carels LB, Boelens HF, Kraak JC, Poppe H (1997) Comparison of five methods for the study of drug-protein binding in affinity capillary electrophoresis. *J Chromatogr A* 777:311–328
90. He X, Ding Y, Li D, Lin B (2004) Recent advances in the study of biomolecular interactions by capillary electrophoresis. *Electrophoresis* 25:697–711
91. Houston DR, Yen LH, Pettit S, Walkinshaw MD (2015) Structure- and ligand-based virtual screening identifies new scaffolds for inhibitors of the oncoprotein MDM2. *PLoS ONE* 10: e0121424
92. Rauch JN, Nie J, Buchholz TJ, Gestwicki JE, Kennedy RT (2013) Development of a capillary electrophoresis platform for identifying inhibitors of protein-protein interactions. *Anal Chem* 85:9824–9831
93. Xu M, Liu C, Zhou M, Li Q, Wang R, Kang J (2016) Screening of Small-molecule inhibitors of protein-protein interaction with capillary electrophoresis frontal analysis. *Anal Chem* 88:8050–8057
94. Ostergaard J, Heegaard NH (2003) Capillary electrophoresis frontal analysis: principles and applications for the study of drug-plasma protein binding. *Electrophoresis* 24:2903–2913
95. Ostergaard J, Hansen SH, Jensen H, Thomsen AE (2005) Pre-equilibrium capillary zone electrophoresis or frontal analysis: advantages of plateau peak conditions in affinity capillary electrophoresis. *Electrophoresis* 26:4050–4054
96. Forster T (1948) Intermolecular energy migration and fluorescence. *Ann Physik (Leipzig)* 2:55–75
97. Rogers MS, Cryan LM, Habeshian KA, Bazinet L, Caldwell TP, Ackroyd PC, Christensen KA (2012) A FRET-based high throughput screening assay to identify inhibitors of anthrax protective antigen binding to capillary morphogenesis gene 2 protein. *PLoS ONE* 7:e39911
98. Schaap M, Hancock R, Wilderspin A, Wells G (2013) Development of a steady-state FRET-based assay to identify inhibitors of the Keap1-Nrf2 protein-protein interaction. *Protein Sci: A Publ Protein Soc* 22:1812–1819
99. Soderholm JF, Bird SL, Kalab P, Sampathkumar Y, Hasegawa K, Uehara-Bingen M, Weis K, Heald R (2011) Importazole, a small molecule inhibitor of the transport receptor importin-beta. *ACS Chem Biol* 6:700–708
100. Song Y, Liao J (2012) An in vitro Förster resonance energy transfer-based high-throughput screening assay for inhibitors of protein-protein interactions in SUMOylation pathway. *Assay Drug Dev Technol* 10:336–343
101. Roszik J, Toth G, Szollosi J, Vereb G (2013) Validating pharmacological disruption of protein-protein interactions by acceptor photobleaching FRET imaging. *Methods Mol Biol* 986:165–178
102. Song Y, Madahar V, Liao J (2011) Development of FRET assay into quantitative and high-throughput screening technology platforms for protein-protein interactions. *Ann Biomed Eng* 39:1224–1234
103. Adjobo-Hermans MJ, Goedhart J, Gadella TW Jr (2006) Plant G protein heterotrimers require dual lipidation motifs of Galpha and Ggamma and do not dissociate upon activation. *J Cell Sci* 119:5087–5097
104. Piston DW, Kremers GJ (2007) Fluorescent protein FRET: the good, the bad and the ugly. *Trends Biochem Sci* 32:407–414

105. Benicchi T, Iozzi S, Svahn A, Axelsson H, Mori E, Bernocco S, Cappelli F, Caramelli C, Fanti P, Genesio E, Maccari L, Markova N, Micco I, Porcari V, Schultz J, Fecke W (2012) A homogeneous HTRF assay for the identification of inhibitors of the TWEAK-Fn14 protein interaction. *J Biomol Screen* 17:933–945
106. Gonzalez AZ, Li Z, Beck HP, Canon J, Chen A, Chow D, Duquette J, Eksterowicz J, Fox BM, Fu J, Huang X, Houze J, Jin L, Li Y, Ling Y, Lo MC, Long AM, McGee LR, McIntosh J, Oliner JD, Osgood T, Rew Y, Saiki AY, Shaffer P, Wortman S, Yakowec P, Yan X, Ye Q, Yu D, Zhao X, Zhou J, Olson SH, Sun D, Medina JC (2014) Novel inhibitors of the MDM2-p53 interaction featuring hydrogen bond acceptors as carboxylic acid isosteres. *J Med Chem* 57:2963–2988
107. Gonzalez AZ, Eksterowicz J, Bartberger MD, Beck HP, Canon J, Chen A, Chow D, Duquette J, Fox BM, Fu J, Huang X, Houze JB, Jin L, Li Y, Li Z, Ling Y, Lo MC, Long AM, McGee LR, McIntosh J, McMinn DL, Oliner JD, Osgood T, Rew Y, Saiki AY, Shaffer P, Wortman S, Yakowec P, Yan X, Ye Q, Yu D, Zhao X, Zhou J, Olson SH, Medina JC, Sun D (2014) Selective and potent morpholinone inhibitors of the MDM2-p53 protein-protein interaction. *J Med Chem* 57:2472–2488
108. Degorce F (2006) HTRF(R): pioneering technology for high-throughput screening. *Expert Opin Drug Discov* 1:753–764
109. Degorce F, Card A, Soh S, Trinquet E, Knapik GP, Xie B (2009) HTRF: a technology tailored for drug discovery—a review of theoretical aspects and recent applications. *Curr Chem Genomics* 3:22–32
110. Bacart J, Corbel C, Jockers R, Bach S, Couturier C (2008) The BRET technology and its application to screening assays. *Biotechnol J* 3:311–324
111. Xu Y, Piston DW, Johnson CH (1999) A bioluminescence resonance energy transfer (BRET) system: application to interacting circadian clock proteins. *Proc Natl Acad Sci USA* 96:151–156
112. Ramsay D, Kellett E, McVey M, Rees S, Milligan G (2002) Homo- and hetero-oligomeric interactions between G-protein-coupled receptors in living cells monitored by two variants of bioluminescence resonance energy transfer (BRET): hetero-oligomers between receptor subtypes form more efficiently than between less closely related sequences. *Biochem J* 365:429–440
113. Arai R, Nakagawa H, Kitayama A, Ueda H, Nagamune T (2002) Detection of protein-protein interaction by bioluminescence resonance energy transfer from firefly luciferase to red fluorescent protein. *J Biosci Bioeng* 94:362–364
114. Boute N, Jockers R, Issat T (2002) The use of resonance energy transfer in high-throughput screening: BRET versus FRET. *Trends Pharmacol Sci* 23:351–354
115. Corbel C, Wang Q, Bousserouel H, Hamdi A, Zhang B, Lozach O, Ferandin Y, Tan VB, Gueritte F, Colas P, Couturier C, Bach S (2011) First BRET-based screening assay performed in budding yeast leads to the discovery of CDK5/p25 interaction inhibitors. *Biotechnol J* 6:860–870
116. Corbel C, Sartini S, Levati E, Colas P, Maillet L, Couturier C, Montanini B, Bach S (2017) Screening for protein-protein interaction inhibitors using a bioluminescence resonance energy transfer (BRET)-based assay in yeast. *SLAS Discov*:2472555216689530
117. Normandin K, Lavallee JF, Futter M, Beautrait A, Duchaine J, Guiral S, Marinier A, Archambault V (2016) Identification of Polo-like kinase 1 interaction inhibitors using a novel cell-based assay. *Sci Rep* 5:37581
118. Mazars A, Fahraeus R (2010) Using BRET to study chemical compound-induced disruptions of the p53-HDM2 interactions in live cells. *Biotechnol J* 5:377–384
119. Sun S, Yang X, Wang Y, Shen X (2016) In vivo analysis of protein-protein interactions with bioluminescence resonance energy transfer (BRET): progress and prospects. *Int J Mol Sci* 17
120. Ullman EF, Kirakossian H, Singh S, Wu ZP, Irvin BR, Pease JS, Switchenko AC, Irvine JD, Dafforn A, Skold CN et al (1994) Luminescent oxygen channeling immunoassay: measurement of particle binding kinetics by chemiluminescence. *Proc Natl Acad Sci USA* 91:5426–5430

121. Eglen RM, Reisine T, Roby P, Rouleau N, Illy C, Bosse R, Bielefeld M (2008) The use of AlphaScreen technology in HTS: current status. *Curr Chem Genomics* 1:2–10
122. Yasgar A, Jadhav A, Simeonov A, Coussens NP (2016) AlphaScreen-based assays: ultra-high-throughput screening for small-molecule inhibitors of challenging enzymes and protein-protein interactions. *Methods Mol Biol* 1439:77–98
123. Cochran JN, Diggs PV, Nebane NM, Rasmussen L, White EL, Bostwick R, Maddry JA, Suto MJ, Roberson ED (2014) AlphaScreen HTS and live-cell bioluminescence resonance energy transfer (BRET) assays for identification of Tau-Fyn SH3 interaction inhibitors for Alzheimer disease. *J Biomol Screen* 19:1338–1349
124. Zhang M, Wisniewski JA, Ji H (2015) AlphaScreen selectivity assay for beta-catenin/B-cell lymphoma 9 inhibitors. *Anal Biochem* 469:43–53
125. Catrow JL, Zhang Y, Zhang M, Ji H (2015) Discovery of selective small-molecule inhibitors for the beta-Catenin/T-Cell factor protein-protein interaction through the optimization of the acyl hydrazone moiety. *J Med Chem* 58:4678–4692
126. Ungermannova D, Lee J, Zhang G, Dallmann HG, McHenry CS, Liu X (2013) High-throughput screening AlphaScreen assay for identification of small-molecule inhibitors of ubiquitin E3 ligase SCFSkp2-Cks1. *J Biomol Screen* 18:910–920
127. Harrison AT, Kriel FH, Papathanasopoulos MA, Mosebi S, Abrahams S, Hewer R (2015) The evaluation of statins as potential inhibitors of the LEDGF/p75-HIV-1 integrase interaction. *Chem Biol Drug Des* 85:290–295
128. Glickman JF, Wu X, Mercuri R, Illy C, Bowen BR, He Y, Sills M (2002) A comparison of ALPHAScreen, TR-FRET, and TRF as assay methods for FXR nuclear receptors. *J Biomol Screen* 7:3–10
129. Morell M, Ventura S, Aviles FX (2009) Protein complementation assays: approaches for the in vivo analysis of protein interactions. *FEBS Lett* 583:1684–1691
130. Wehr MC, Rossner MJ (2016) Split protein biosensor assays in molecular pharmacological studies. *Drug Discov Today* 21:415–429
131. Remy I, Michnick SW (1999) Clonal selection and in vivo quantitation of protein interactions with protein-fragment complementation assays. *Proc Natl Acad Sci U S A* 96:5394–5399
132. Mai D, Jones J, Rodgers JW, Hartman JLt, Kutsch O, Steyn AJ (2011) A screen to identify small molecule inhibitors of protein-protein interactions in mycobacteria. *Assay Drug Dev Technol* 9:299–310
133. Remy I, Ghaddar G, Michnick SW (2007) Using the beta-lactamase protein-fragment complementation assay to probe dynamic protein-protein interactions. *Nat Protoc* 2:2302–2306
134. Lee HK, Brown SJ, Rosen H, Tobias PS (2007) Application of beta-lactamase enzyme complementation to the high-throughput screening of toll-like receptor signaling inhibitors. *Mol Pharmacol* 72:868–875
135. Hashimoto J, Watanabe T, Seki T, Karasawa S, Izumikawa M, Iemura S, Natsume T, Nomura N, Goshima N, Miyawaki A, Takagi M, Shin-Ya K (2009) Novel in vitro protein fragment complementation assay applicable to high-throughput screening in a 1536-well format. *J Biomol Screen* 14:970–979
136. Chen M, Li W, Zhang Z, Liu S, Zhang X, Zhang XE, Cui Z (2015) Novel near-infrared BiFC systems from a bacterial phytochrome for imaging protein interactions and drug evaluation under physiological conditions. *Biomaterials* 48:97–107
137. Yang RY, Yang KS, Pike LJ, Marshall GR (2010) Targeting the dimerization of epidermal growth factor receptors with small-molecule inhibitors. *Chem Biol Drug Des* 76:1–9
138. Kaelin WG Jr, Pallas DC, DeCaprio JA, Kaye FJ, Livingston DM (1991) Identification of cellular proteins that can interact specifically with the T/E1A-binding region of the retinoblastoma gene product. *Cell* 64:521–532
139. Shao H, Xu X, Jing N, Twardy DJ (2006) Unique structural determinants for Stat3 recruitment and activation by the granulocyte colony-stimulating factor receptor at phosphotyrosine ligands 704 and 744. *J Immunol* 176:2933–2941

140. Krol E, van Kessel SP, van Bezouwen LS, Kumar N, Boekema EJ, Scheffers DJ (2012) *Bacillus subtilis* SepF binds to the C-terminus of FtsZ. *PLoS ONE* 7:e43293
141. Mochizuki Y, Kohno F, Nishigaki K, Nemoto N (2013) A pull-down method with a biotinylated bait protein prepared by cell-free translation using a puromycin linker. *Anal Biochem* 434:93–95
142. Olesen SH, Ingles DJ, Zhu JY, Martin MP, Betzi S, Georg GI, Tash JS, Schonbrunn E (2015) Stability of the human Hsp90-p 50Cdc37 chaperone complex against nucleotides and Hsp90 inhibitors, and the influence of phosphorylation by casein kinase 2. *Molecules (Basel, Switzerland)* 20:1643–1660
143. Yang C, Wang W, Li GD, Zhong HJ, Dong ZZ, Wong CY, Kwong DW, Ma DL, Leung CH (2017) Anticancer osmium complex inhibitors of the HIF-1 α and p300 protein-protein interaction. *Sci Rep* 7:42860
144. Xiang J, Wang Z, Liu Q, Li X, Sun J, Fung KP, Liu F (2017) DMFC (3,5-dimethyl-7H-furo [3,2-g]chromen-7-one) regulates Bim to trigger Bax and Bak activation to suppress drug-resistant human hepatoma. *Apoptosis Int J Program Cell Death* 22:381–392
145. Uesato S, Matsuura Y, Matsue S, Sumiyoshi T, Hirata Y, Takemoto S, Kawaratani Y, Yamai Y, Ishida K, Sasaki T, Enari M (2016) Discovery of new low-molecular-weight p53-Mdmx disruptors and their anti-cancer activities. *Bioorg Med Chem* 24:1919–1926
146. Muratore G, Goracci L, Mercorelli B, Foeglein A, Digard P, Cruciani G, Palu G, Loregian A (2012) Small molecule inhibitors of influenza A and B viruses that act by disrupting subunit interactions of the viral polymerase. *Proc Natl Acad Sci USA* 109:6247–6252
147. Biesiadecki BJ, Jin JP (2011) A high throughput solid phase microplate protein binding assay to investigate interactions between myofibrillar proteins. *J Biomed Biotechnol* 2011:1–8
148. Meng Y, High K, Antonello J, Washabaugh MW, Zhao Q (2005) Enhanced sensitivity and precision in an enzyme-linked immunosorbent assay with fluorogenic substrates compared with commonly used chromogenic substrates. *Anal Biochem* 345:227–236
149. Fredriksson S, Gullberg M, Jarvius J, Olsson C, Pietras K, Gustafsdottir SM, Ostman A, Landegren U (2002) Protein detection using proximity-dependent DNA ligation assays. *Nat Biotechnol* 20:473–477
150. Bellucci A, Fiorentini C, Zaltieri M, Missale C, Spano P (2014) The “in situ” proximity ligation assay to probe protein-protein interactions in intact tissues. *Methods Mol Biol* 1174:397–405
151. Soderberg O, Gullberg M, Jarvius M, Ridderstrale K, Leuchowius KJ, Jarvius J, Wester K, Hydbring P, Bahram F, Larsson LG, Landegren U (2006) Direct observation of individual endogenous protein complexes in situ by proximity ligation. *Nat Methods* 3:995–1000
152. Leuchowius KJ, Weibrecht I, Landegren U, Gedda L, Soderberg O (2009) Flow cytometric in situ proximity ligation analyses of protein interactions and post-translational modification of the epidermal growth factor receptor family. *Cytometry A* 75:833–839
153. Kanthala S, Gauthier T, Satyanarayananjois S (2014) Structure-activity relationships of peptidomimetics that inhibit PPI of HER2-HER3. *Biopolymers* 101:693–702
154. Kanthala S, Banappagari S, Gokhale A, Liu YY, Xin G, Zhao Y, Jois S (2015) Novel peptidomimetics for inhibition of HER2:HER3 heterodimerization in HER2-positive breast cancer. *Chem Biol Drug Des* 85:702–714
155. Kang MA, Kim MS, Kim JY, Shin YJ, Song JY, Jeong JH (2015) A novel pyrido-thieno-pyrimidine derivative activates p53 through induction of phosphorylation and acetylation in colorectal cancer cells. *Int J Oncol* 46:342–350
156. Muller I, Larsson K, Frenzel A, Olynyk G, Zirath H, Prochownik EV, Westwood NJ, Henriksson MA (2014) Targeting of the MYCN protein with small molecule c-MYC inhibitors. *PLoS ONE* 9:e97285
157. Soderberg O, Leuchowius KJ, Gullberg M, Jarvius M, Weibrecht I, Larsson LG, Landegren U (2008) Characterizing proteins and their interactions in cells and tissues using the in situ proximity ligation assay. *Methods* 45:227–232

158. Smith GP (1985) Filamentous fusion phage: novel expression vectors that display cloned antigens on the virion surface. *Science* 228:1315–1317
159. Paschke M (2006) Phage display systems and their applications. *Appl Microbiol Biotechnol* 70:2–11
160. Kuzmicheva GA, Belyavskaya VA (2016) Peptide phage display in biotechnology and biomedicine. *Biomeditsinskaia khimiia* 62:481–495
161. Bazan J, Calkosinski I, Gamian A (2012) Phage display—a powerful technique for immunotherapy: 1. Introduction and potential of therapeutic applications. *Hum Vaccines Immunotherapeutics* 8:1817–1828
162. Tan Y, Tian T, Liu W, Zhu Z, J Yang C (2016) Advance in phage display technology for bioanalysis. *Biotechnol J* 11:732–745
163. Ishi K, Sugawara F (2008) A facile method to screen inhibitors of protein-protein interactions including MDM2-p53 displayed on T7 phage. *Biochem Pharmacol* 75:1743–1750
164. Fields S, Song O (1989) A novel genetic system to detect protein-protein interactions. *Nature* 340:245–246
165. Keegan L, Gill G, Ptashne M (1986) Separation of DNA binding from the transcription-activating function of a eukaryotic regulatory protein. *Science* 231:699–704
166. Stynen B, Tournu H, Tavernier J, Van Dijck P (2012) Diversity in genetic in vivo methods for protein-protein interaction studies: from the yeast two-hybrid system to the mammalian split-luciferase system. *Microbiol Mol Biol Rev* 76:331–382
167. Khazak V, Eyrisch S, Kato J, Tamanoi F, Golemis EA (2013) A two-hybrid approach to identify inhibitors of the RAS-RAF interaction. *The Enzymes* 33 Pt A:213–248
168. Kato-Stankiewicz J, Hakimi I, Zhi G, Zhang J, Serebriiskii I, Guo L, Edamatsu H, Koide H, Menon S, Eckl R, Sakamuri S, Lu Y, Chen QZ, Agarwal S, Baumbach WR, Golemis EA, Tamanoi F, Khazak V (2002) Inhibitors of Ras/Raf-1 interaction identified by two-hybrid screening revert Ras-dependent transformation phenotypes in human cancer cells. *Proc Natl Acad Sci USA* 99:14398–14403
169. Yin X, Giap C, Lazo JS, Prochownik EV (2003) Low molecular weight inhibitors of Myc-Max interaction and function. *Oncogene* 22:6151–6159
170. Lin Y, Li Y, Zhu N, Han Y, Jiang W, Wang Y, Si S, Jiang J (2014) The antituberculosis antibiotic capreomycin inhibits protein synthesis by disrupting interaction between ribosomal proteins L12 and L10. *Antimicrob Agents Chemother* 58:2038–2044
171. Hamdi A, Colas P (2012) Yeast two-hybrid methods and their applications in drug discovery. *Trends Pharmacol Sci* 33:109–118
172. Zhou M, Li Q, Wang R (2016) Current experimental methods for characterizing protein-protein interactions. *ChemMedChem* 11:738–756
173. Joshi PB, Hirst M, Malcolm T, Parent J, Mitchell D, Lund K, Sadowski I (2007) Identification of protein interaction antagonists using the repressed transactivator two-hybrid system. *Biotechniques* 42:635–644
174. Huang J, Schreiber SL (1997) A yeast genetic system for selecting small molecule inhibitors of protein-protein interactions in nanodroplets. *Proc Natl Acad Sci USA* 94:13396–13401
175. Young K, Lin S, Sun L, Lee E, Modi M, Hellings S, Husbands M, Ozenberger B, Franco R (1998) Identification of a calcium channel modulator using a high throughput yeast two-hybrid screen. *Nat Biotechnol* 16:946–950
176. Gunde T, Tanner S, Auf der Maur A, Petrascheck M, Barberis A (2004) Quenching accumulation of toxic galactose-1-phosphate as a system to select disruption of protein-protein interactions in vivo. *Biotechniques* 37:844–852
177. Eyckerman S, Verhee A, der Heyden JV, Lemmens I, Ostade XV, Vandekerckhove J, Tavernier J (2001) Design and application of a cytokine-receptor-based interaction trap. *Nat Cell Biol* 3:1114–1119

178. Lievens S, Caligiuri M, Kley N, Tavernier J (2012) The use of mammalian two-hybrid technologies for high-throughput drug screening. *Methods* 58:335–342
179. Eyckerman S, Lemmens I, Catteuw D, Verhee A, Vandekerckhove J, Lievens S, Tavernier J (2005) Reverse MAPPIT: screening for protein-protein interaction modifiers in mammalian cells. *Nat Methods* 2:427–433

Chapter 6

Fragment-Based Drug Discovery for Developing Inhibitors of Protein-Protein Interactions



Bing Xiong, Qi Wang and Jingkang Shen

After the completion of human genome sequencing at the beginning of twenty-first century, post-genomic research and systems biology study revolutionized our view of the biology to an extraordinary complex level. The importance of the complex network of direct interactions between proteins—known as the interactome—to both biological systems and the development of disease states is widely recognized [1–3]. Despite its dominance in past drug development, simply targeting regulatory sites of enzymes and receptors is not enough to precisely module the biochemical network. Instead, an increasingly popular approach is to target protein-protein interactions (PPIs) that participate in cell signaling, growth, and survival. Although the exact number of human PPIs is unknown, estimates range from hundreds of thousands to around a million. Several databases have been created to aid the study of PPIs. STRING [4] is a database of predicted and known PPIs, TIMBAL [5] provides small-molecule inhibition data, and 2P2I_{DB} [6], PICCOLO [7] and others provide structural information and analysis. Overall, PPIs provided a substantial amount of drug targets to treat the diseases in the selective and elegant way [8, 9].

However, modulation of PPIs for therapeutic intervention also posed significant challenges to medicinal chemists, as the protein-protein interfaces are generally flat and large ($\sim 2000 \text{ \AA}^2$), making the design of small molecule a daunting task. Therefore, many considered PPIs ‘undruggable.’ It has been recapitulated that the interfaces are predominantly hydrophobic with flanked polar residues, and the interfaces could be classified on the basis of complexity of the binding epitopes. A critical development in the understanding of PPIs was the realization that the interactions driving the affinity of a pair of proteins are not distributed evenly across their surfaces, and with the experiment called alanine scanning analysis some critical residues at the interface could be found to contribute a large portion of

B. Xiong (✉) · Q. Wang · J. Shen
Shanghai Institute of Materia Medica, Chinese Academy of Sciences,
Shanghai 201203, China
e-mail: bxiong@simm.ac.cn

binding affinity [10]. Identifying these hot-spot residues is an initial step for designing antagonists of PPIs [11, 12]. Then different approaches can be applied to tackle the challenges of discovering lead compounds, which include peptide-mimics, high-throughput screening, computational virtual screening as well as fragment-based drug discovery.

6.1 Fragment-Based Drug Discovery

The invention of combinatorial chemistry in the late 1980s dramatically expanded the number of compounds in chemical collections, leading to the advent of high-throughput screening (HTS). This random screening approach is essential to the targets with no or little ligand information, and with serendipity it is perhaps the most venerable way to identify new ligands. In parallel to the development of HTS, computer graphics, macromolecular NMR technology and X-ray crystallography were integrated into drug design field to enable the application of structure-based drug discovery (SBDD) to accelerate the lead optimization phase and therefore speed up and lower the cost of the drug development. These two methods are complementary, as the HTS could be utilized for discovering the hit compounds and SBDD could be applied to the optimization of the identified hits. Although HTS remains an important method for hunting the bioactive compounds, the low efficiency and high cost associated with each HTS campaign hinder its usage. To combine the advantages of random screening and rational design, fragment-based drug discovery was proposed in later 1990s to early 2000s [13–16]. Rather than screening millions of compounds to find drug-sized starting points, fragment-based drug discovery takes a different approach to screen much smaller collections of low molecular weight compounds, which dramatically alleviates the burden on common HTS studies, such as compound collection, library maintenance, screening costs. The origins of FBDD can be traced back to the publication by Jencks [17], in which he proposed that ‘fragment’ can form high-quality interactions that can be optimized into highly potent larger molecules. In 1992, Verlinde et al. also mentioned using a link-fragment approach to discover lead compounds for trypanosomiasis [18]. However, the methodology was firmly established only until the studies at Abbott using ‘SAR by NMR’ [19] and at Astex using directed X-ray crystallography as screening method [20, 21]. Over two decades of development, fragment-based methods are now being used worldwide in many pharmaceutical companies and research laboratories as a very efficient tool for lead discovery. Practically, FBDD involved three components, namely fragment library, fragment screening and fragment optimization. In this chapter, we will first introduce the fragment-based drug discovery, then the case studies of applying FBDD in the development of PPI inhibitors. The overall process of developing PPIs, especially with the FBDD method, is illustrated in Fig. 6.1.

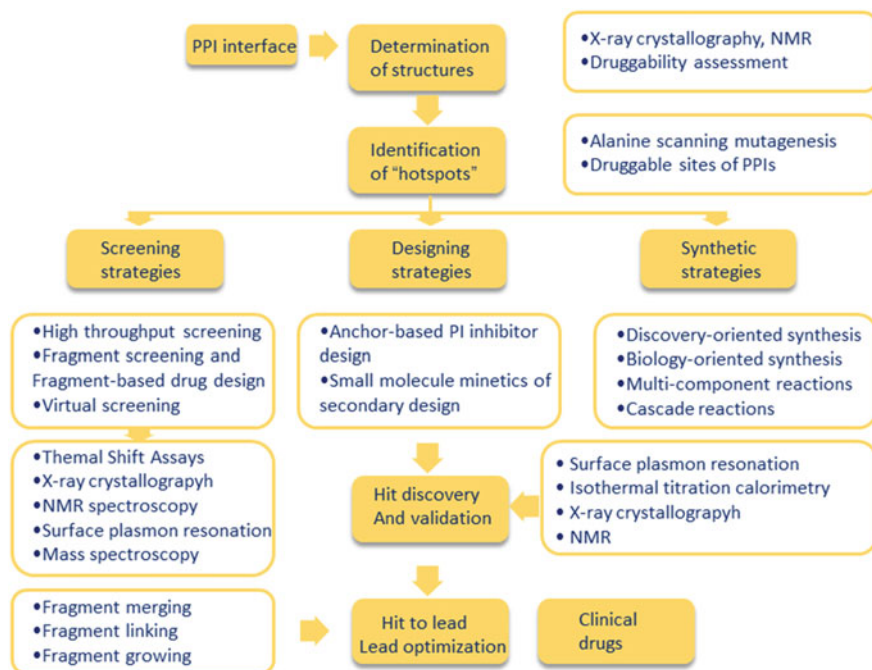


Fig. 6.1 Overview of the current strategies of developing PPI inhibitors

6.1.1 Fragment Library

Constructing fragment library is the critical step for the successful application of FBDD, as the fragment hits are inevitably coming from the library. Reymond et al. [22] in silico enumerated all possible molecules up to 17 heavy atoms and found that sampling of the chemical space is much more efficient with fragments than with larger molecules. Their analysis indicated that adding one heavy atom roughly increases one order of magnitude to number of possible compounds. If the average fragment has 15 heavy atoms and the average optimized compounds have 28 heavy atoms, it means the chemical space of leads is at least 13 orders of magnitude larger than the chemical space of fragments. And in reality, most fragment libraries contain a few thousand molecules, which are about three orders of magnitude smaller than a common HTS collection. Besides of this sampling advantage, fragments have been considered more druggable in the view of bioactivity and pharmaceutical properties such as pharmacokinetics and toxicity. In 2001, Hann and colleagues [23] in GSK proposed a concept of ‘molecular complexity,’ a term measuring the molecular size and chemical features. They noted that, as molecules become more complex, they have more possible interactions with a protein target, both favorable and unfavorable interactions, which sometimes difficult to separate. Therefore, larger molecules will bind fewer targets and will be difficult to optimize.

As a contrast, fragments have few but essential interactions, enabling them to interact with many protein targets and leaving them more direction to optimize the binding affinity as well as the drug-like properties.

To design a valuable fragment library, many have provided guidelines, and good reviews have been written on this topic [24–26]. Generally, most libraries consist of molecules that adhere to the ‘rule of three’: Compounds have a molecular weight below 300 Da, fewer than three hydrogen-bond donors and acceptors, less than three rotatable bonds and the value of ClogP smaller than 3 [27]. Other criteria including solubility and stability are also emphasized in many studies. Molecular weight is a primary property of fragments, as it usually limits other properties. There is a trend in recent years to even use smaller fragments, probably the MW around 200–250 Da. The solubility is critical to fragment screening. Because fragments have few interactions with the targets and showed low to moderate affinity with the IC_{50} range from 1 mM to 10 μ M, the concentration used in these screenings will be high, which requires the fragments with good solubility in aqueous solution. This information can be easily obtained alongside the purity assessment using NMR spectroscopy.

Perhaps the most important issue related to library construction is to avoid compounds known as ‘bad actors,’ which include reactive covalent modifiers, chelators, nonspecific binders, and the compounds fond of aggregation. Baell et al. [28] have compiled a list of substructure to filter such pan assay interference compounds (PAINS), which can be used for excluding bad fragments. The reactive groups such as Michael receptors, alkyl halides or epoxides can be easily detected and removed from the library. Hush et al. also provided an NMR-based method—ALARM NMR—to rapidly and robustly detect reactive fragments [29].

Recently, the 3D features of fragments were considered as a new criterion for assessing the quality of library. Morley et al. argued that current fragment libraries suffered from the limitation of containing too many planar fragments that did not have the capability to bind to difficult targets [30]. They established ‘3D Fragment Consortium’ to enhance the 3D characteristics of fragment libraries and, therefore, to increase the probability of finding fragments interacting with complex binding sites, such as in PPIs. On the contrary, as implied by Hann’s investigation of molecular complexity, increasing 3D features of fragments will lower the hit rates of the library. Then one needs to balance between complexity, size, and diversity of the fragments to ensure the general utility of the fragment library.

6.1.2 *Fragment Screening*

Fragment hits make small number but high-quality interactions with the target, and typically, their binding affinities are in the range of 0.01–1 mM; while HTS assays often identify compounds with a stronger affinity (10 μ M is a typical lower limit). Thus, the screening methodology used for fragment screening must be compatible with the smaller size, reduced complexity and consequently lower affinity of

fragments, needing to provide 100- to 1000-fold higher sensitivity than in HTS. Currently, fragment screening generally utilizes sensitive biophysical technologies [13, 31], including NMR-ligand spectroscopy [32], surface plasmon resonance [33], fluorescence-based thermal shift [34], mass spectrometry [35], NMR-protein spectroscopy [36], and X-ray crystallography [37]. These screening methods are usually used in cascade way: applying the high-throughput methods first and following with more time-consuming techniques to validate the hits.

Thermal shift (TS) Fluorescence-based thermal shift probably is the quickest method for fragment screening [34], as it can be set up in the plate-based format. This technique detects the compounds that increase the melting temperature (T_m) of the target protein by monitoring the unfolding process via a hydrophobic-sensitive fluorescence dye. Because fragment binding is weak, the shift of the melting temperature (ΔT_m) is small, usually in the range of 0.5–1.5 °C. And the size of the protein is the important factor of the temperature shift, being the larger the protein is, usually the smaller the change in temperature. Giving the thermal shift experiments are not always reproducible, screening with this method should be seen as the enrichment process. And some more accurate methods, e.g., NMR screen, should be used to assess the fragment hits from TS experiment. Murry et al. [38] at Astex performed a fragment-based screen against DDR1, a unique receptor tyrosine kinase activated by extracellular collagen. Approximately 1500 compounds from the Astex fragment library were screened against DDR1 using a protein thermal shift assay. Then hits from this assay were progressed with crystal soaking to determine the X-ray structures. A unique fragment containing a urea moiety was selected for optimization, as it binds to the back pocket rather than the typical hinge part of ATP site. Finally, a potent and selective DDR1/2 inhibitor was discovered with IC_{50} value about 3 nM. Laesson and his coworkers used a fragment-based ligand design strategy to find the inhibitors targeting TNKS2 [39]. Initially, a thermal shift assay-based fragment screen method called differential scanning fluorimetry (DSF) was applied to the hit characterization from a 500-compound fragment library. Two compounds gave melting curves distinct from that of the DMSO control, stabilizing TNKS2 and one compound was chosen for the further modification by analyzing the crystal structures of the fragments. As a result, cycles of optimization led a set of compounds with high affinities (IC_{50} values in the low nanomolar range) and with other favorable properties including good solubility, high PARP-selectivity, and high ligand efficiency.

Surface Plasmon Resonance (SPR) Surface plasmon resonance is the resonant oscillation occurring when polarized light strikes an electrically conducting surface at the interface between two media. This generates electron charge density waves called plasmons, which could reduce the intensity of reflected light at a specific angle (known as the resonance angle) in proportion to the mass on a sensor surface. In SPR fragment screening, usually the target protein is covalently linked to the gold surface of an SPR biosensor chip, and solutions of fragments are sequentially passed over it. If the fragments bind to the immobilized target, the increase in the surface mass is detected with the change of the resonance angle in real time. Since the SPR experiment can measure the time-dependent fragment association–

dissociation response, the binding kinetics can be obtained as well as the binding affinity [33, 40, 41]. Mitogen-activated protein kinase kinase kinase 4 (MAP4K4) is a serine/threonine kinase implicated in the regulation of many biological processes. Crawford conducted a screen of diverse fragment library using SPR technique to identify a suitable hit for MAP4K4 [42]. Detailedly, a screening of 2361 fragments at 100 μM as singletons using SPR led to 225 confirmed hits with $LE > 0.35$. They followed up on multiple fragment hits initially and settled on two fragments (pyrrolotriazine and oxazole series) for full optimization. By utilizing crystal structures, molecular modeling, and scaffold hopping methods, compound G495 with excellent potency, kinase selectivity, and mouse PK profile was discovered. Navratilova et al. [43] used a novel SPR protocol as the primary fragment screening method to discover novel bromodomain scaffolds by overcome the presence of DMSO interference. They followed with X-ray crystallography to obtain the binding modes of fragments, providing clear clues about how to aid the development of potent and selective inhibitors of PCAF, CREBBP, and BRD4.

Mass Spectrometry (MS) The advances in mass spectrometry techniques enable it to be a complementary fragment screening method. Protein-fragment mixtures are ionized by soft electrospray ionization (ESI), and the binding can be observed by the increase in the mass of the bimolecular ion corresponding to that of a bound fragment. In principle, it is possible to assay the cocktails of fragments, but due to the soft ionization techniques necessary to see non-covalent binding, it is difficult to detect fragment binding directly with MS techniques.

Nevertheless, MS offers a rapid, sensitive, and high-throughput method for fragment screening. And the amount of protein needed depends on its intrinsic ionization efficiency, the type, and concentration of buffer used and the instrumental conditions. Heat shock protein 90 (HSP90) is a molecular chaperone that plays important functional roles in cells and was considered as an anticancer drug target. Fogliatto and coworkers used ESI-MS to investigate the interaction of ligands to the HSP90 [44]. A set of chemically divergent compounds, with a broad range of dissociation constants from 40 pM to 100 μM , were tested to access the reliability of ESI-MS for the study of protein/ligand complexes. A good agreement was found between the values measured with a fluorescence polarization displacement assay and those determined by mass spectrometry. Poulsen et al. use three fragment screening methods (ESI-MS, X-ray crystallography, and SPR) to demonstrate that there is a tremendous opportunity to apply native state mass spectrometry as a complementary fragment screening method to accelerate drug discovery [45]. Specifically, the study was conducted in two stages: Initial screening against a 720-member fragment library was performed by SPR; then the seven identified hits were confirmed by native MS and X-ray crystallography. The screening results showed that three screening methods are in excellent agreement.

NMR Spectroscopy Based on the object of NMR spectra in fragment screening, it can be classified as ligand-detected one-dimensional (1D) or protein-detected two-dimensional (2D) NMR. Ligand-detected NMR methods, including Carr–Purcell–Meiboom–Gill (CPMG), saturation transfer difference (STD), water-ligand-observed via gradient spectroscopy (waterLOGSY), are frequently used in fragment

screening. CPMG experiment measures the relaxation dispersion parameter of fragment, and when the fragment bound to the slow tumbling protein, the intensity of proton signals of the fragment will decrease. In the waterLOGSY and STD experiments, an irradiation pulse is applied at either the resonance frequency of bulk water or the specific protons in protein targets. Then due to the transfer of magnetization via the binding of fragment to the target, the resonance signals of binding will be different with the original non-binding signals, which could be used to obtain the fragment hits. The acquisition of 1D spectra is relatively fast (less than 15 min), and the experiments also can apply to the ‘cocktail’ solution—mixing several fragments in one stock solution, making these ligand-detected NMR methods ideal for fragment screening.

Since proposed by scientists in Abbott, 2D bimolecular-detected ^1H - ^{15}N HSQC experiment was commonly used for fragment screening [19]. This experiment monitors the difference of chemical shifts in the ^1H - ^{15}N cross-peaks of the ^{15}N -labeled target protein during the process of adding fragments. Although the method is time-consuming, it can provide information about the binding site of fragment/target complex.

The BET family of bromodomain-containing proteins have been potential targets for blocking proliferation in a variety of cancer cell lines. Wang et al. [46] initiated a protein-based NMR-fragment screen carried out against the second bromodomain of BRD4 and found that a phenylpyridazinone fragment showed a strong spectral shift in the NMR screen is a novel small molecule not previously reported. This weak binding fragment was then elaborated by medicinal chemistry efforts and X-ray structure-based design. Several analogs exhibited single-digit nanomolar potency in both biochemical and cell assays and showed high exposures in PK studies and significant tumor growth inhibition efficacy.

Activated factor XI (FXIa) inhibitors are anticipated to combine anticoagulant and profibrinolytic effects with a low bleeding risk. Linda Öster and his coworkers [47] used ligand-detected 1D NMR spectroscopy as the primary fragment screening tool to identify 50 neutral or weakly basic fragment hits from 1800 structures that are selected from the docking study on 65,000 fragments. Finally, two prioritized fragment hits as novel FXIa fragments were chosen for the further study. Sequent work combining the X-ray crystallography and structure-guided linking and expansion work derived a potent and selective FIXa inhibitor with IC_{50} of 1.0 nM.

X-ray Crystallography X-ray crystallography was heavily used in structure-based drug discovery, as it can provide the details of binding interactions. Along the development of facilities and software in crystallography, the X-ray crystallographic screening gets popular in nowadays because it can simultaneously validate the fragment hits and give the binding information for later optimization [37, 48–50]. To speed up the screening, the cocktails of fragments can be soaked into the crystallized apo-protein. To achieve this, the protein crystal must be robust and have a solvent-exposed binding site in the crystal lattice. For other difficult cases, the co-crystallization with cocktails of fragments will be the better option.

Screening of fragment libraries using X-ray crystallography has been an effective method to sample chemical space, to reveal previously unobserved pockets and to illustrate ligand binding modes. Jhoti et al. reported on the successful application of

fragment screening using X-ray crystallography for identifying secondary, allosteric, sites for three separate targets (the viral protease-helicase protein HCV NS3 [51], the p38 MAP kinase [52], and human soluble adenylate cyclase [53]). In 2015, he also reported their analyses of in-house data of 24 previous fragment-based drug discovery campaigns against a wide variety of protein targets, indicating that the majority proteins contain secondary binding sites that could bind with fragments [54]. This provided strong implications of applying FBDD method to generate new chemical tools probing unexploited biological mechanisms.

6.1.3 Fragment Optimization

Before investing time and resources to elaborate fragments, we should select the optimal fragment based on the potency and synthetic tractability of the fragment. Besides, the optimal fragment may require minor chemical modification to determine the scaffold.

In the guidance of structural binding information and quantitative affinity data, validated fragment hits are elaborated to improve potency in an iterative process of rational design and chemical synthesis. Generally, there are three main approaches to increasing the potency of compounds derived from fragments: fragment merging, linking, and growing (Fig. 6.2).

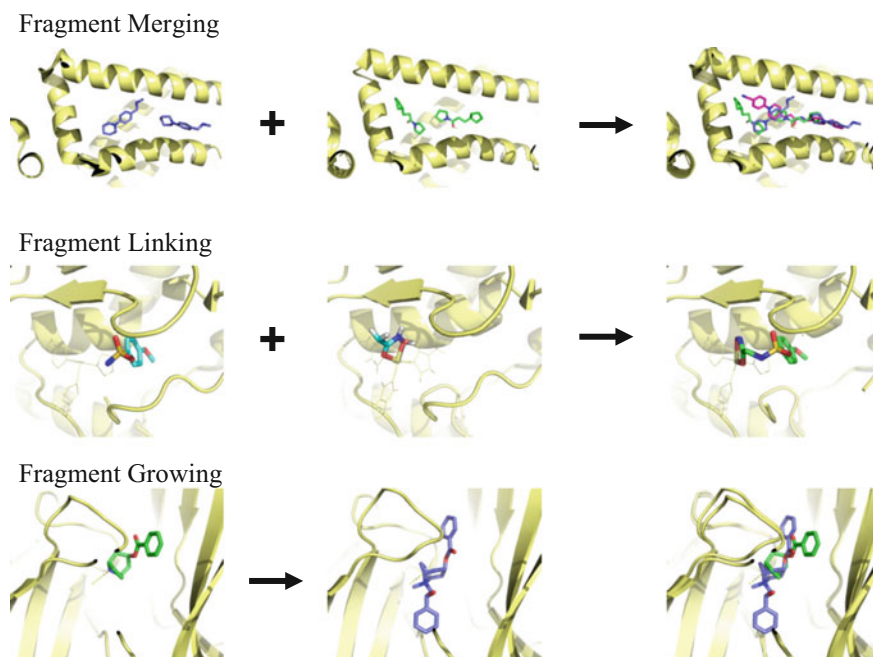


Fig. 6.2 Three methods of fragment optimization

Fragment merging is to incorporate structural portions of other overlapping molecules into a fragment, based on superimposed complexes of the same target bound with other fragments, substrates, and known ligands. Structure–activity relationship from different series can be used to identify important interactions and pharmacophores, and this information can be used to produce a hybrid series. Nikiforov et al. applied such a fragment merging strategy to develop inhibitors against EthR [55], a novel target in tuberculosis. Initially, multiple techniques were used to screen a 1250-member fragment library. Then, two partially overlapped fragments were optimized with merging approach, giving eightfold increase in binding affinity.

Fragment linking is conceptually the most appealing strategy for fragment optimization. It requires the efficient joining of two fragments that are known to bind at non-overlapping sites. In theory, a compound derived from linking fragments with an ideal linker is expected to have a Gibbs free energy of binding that is better than the sum of the individual fragment binding energies, and such favorable contribution mainly attributes to the entropic factor. Borsi et al. investigated this by using ITC experiments to measure the thermodynamic parameters of two fragments and their linking molecule on MMP-12 protein [56]. Although the binding free energy of two fragments is only -3.01 and -3.85 kcal/mol, the linked inhibitor showed the binding free energy -10.50 kcal/mol. And the difference in entropic contribution is -4.3 kcal/mol, which totally accounting for the improvement in binding. An ideal linker not only allows the linked fragments to recapitulate the conformation of the individual fragments and add the favorable entropic contribution, but also may make additional favorable interactions with the protein and provide little additional enthalpic energy. However, in practice, fragment linking can be challenging, because slight length or geometric deficiencies in the linker can have a dramatically negative effect on binding. Moreover, linked compounds are often larger than ideal.

More frequently, a fragment that binds at a single site is discovered and gradually ‘grown’ through adding chemical groups to explore further interactions. The choice of which direction of optimization to pursue will be influenced not only by potency but also by ligand efficiency that is defined simply as the free energy of binding of a ligand divided by the number of non-hydrogen atoms it has (ligand efficiency $LE = \Delta G/N_{\text{heavy_atoms}}$). In general, optimized ligands with a ligand efficiency of more than 0.3 kcal/mol/atom is considered as promising as it maintains the binding without making fat molecules, which leaves large room for medicinal chemists to simultaneously optimize the potency and the druggability. In discovering inhibitors of acetylcholine-binding protein, Edink et al. reported a study of optimization with fragment growing method [57]. After fragment screening, a fragment with good LE (0.43 kcal/mol/atom) was co-crystallized with Ac-AchBP, a representative acetylcholine-binding protein. Based on the crystal structure of the complex, they modified the fragment by gradually adding ethylbenzene motif and increased the binding affinity up to 150-fold. Pin1 is an emerging oncology target related in Ras and ErbB2-mediated tumorigenesis. Potter et al. from Vernalis use structure-based method to evolve a 5-pyridinyl pyrazole-3-carboxylate fragment

into a series of 5-aryl-carbamoyl-3-phenyl-imidazole-4-carboxylates and improve the activity against Pin1 from IC_{50} about 360 μ M of the initial fragment to 0.52 μ M of the best-optimized inhibitor [58].

6.2 FBDD in PPI

Protein-protein interactions are central to all biological processes and are often dysregulated in disease, therefore providing a vast class of therapeutic targets for drug discovery. The last two decades has seen amazing progress in tackling challenging PPI targets with small molecules. Extensive studies have revealed that, although PPIs have many shapes and sizes, most of the inhibitors target PPIs at the essential small binding pockets termed as hot spot. In the mid-1990s, Dagmar Ringe proposed a method of multiple solvent crystal structure determination (MSCS), which is to soak small organic solvent molecules into protein crystals to map out their binding sites experimentally [59]. Similarly, Vajda et al. implemented a computational method called FTMAP to identify the hot spots [60, 61]. In order to design small molecules that interfere with CDK9–cyclin T1 interactions, Randjelovic and colleagues applied the FTMAP to find the low energy binding site and discovered a series of 2-amino-8-hydroxyquinoline inhibitors of CDK9–cyclin T1 interactions [62]. Based on the characteristics of PPI interfaces, Arkin et al. [63] classified the PPIs into four groups, and the classes as well as some examples are listed in Table 6.1. This classification provides insights for designing the small molecular drugs targeting the PPIs. Briefly, the PPI from class I usually is difficult to find potent inhibitors and the interface tends to be much more dynamic than PPIs from other classes. While for PPIs of class II, design approaches have focused on both the binding pocket and the partner peptide. Mapping the hot spot and then focusing on the spot to design small molecules have proved the success with several clinical testing drugs. But the most prevailing drug development of PPIs is coming from class III and class IV, which largely attributes to containing a primary hot spot at the interface. The fragments or pharmacophores bound to this hot spot can dramatically low the binding energy and eventually lead to nanomolar inhibitors. The fragment-based drug discovery has played an important role in the design and developing these drugs, such as ABT199, a drug targeting BCL-2 has been reached to the market for cancer treatment, and several BET bromodomain inhibitors that have entered into clinical trials for various diseases. These successful case studies highlight the importance of FBDD in PPIs.

6.2.1 FBDD Application

Giving the importance of PPIs in drug discovery and prevalence of FBDD, researchers worldwide, either in big pharmaceutical companies or in small research

Table 6.1 The four classes of PPIs and associated examples

PPI Class	Description	Examples
Class I Globular protein-globular protein	Two globular proteins form a large interface, requiring tertiary structure on both sides. For each protein, the residues participate in the interactions are discontinuous in sequences. And usually, there is no primary hot spot that can dominate the interactions	Interleukin-17 IL12-IL2R TNF-TNF E2-E1
Class II Globular protein-peptide with continuous epitope	One globular protein interacts with a secondary structure from another protein like α -helix, β -sheet, and extended peptide. And usually, the first globular protein has a groove-shaped binding site making extensive but individually weak interactions with the second protein	XIAP-SMAC HIV-integrase-LEDGF Integrins RAD51-BRCA2 PDZ domains NRP-1-VEGFA Menin-MLL KEAP1-NRF2 WDR5-MLL
Class III Globular protein— short (<4 aa) peptide	One globular protein interacts with a short peptide (<4 amino acids) from another protein, and the interface usually contains a primary hot spot, which contributes large portion of binding free energy of the complex	MDM2-p53 BCLXL-BAD BCLXL-BAK ZipA-FtsZ S100B-p53 β -catenin-TCF-3-TCF-4 MCL1-BH3 SUR2-ESX
Class IV Globular protein-peptide, anchor residue	The globular protein interacts with a modified residue (acetyl, methyl, phosphate, etc.) or a penetrated residue from another protein. The subpocket of this residue usually is a sole and essential hot spot for the binding	Bromodomains PDE- δ -KRAS SH2 domain PLK1PDB-peptide VHL-HIF1 α

laboratories, utilize this high efficient technique to find the small molecules blocking the PPIs. In this chapter, we cannot provide the throughout review for enormous applications in this field. Instead, we will divide the examples into several groups according to the biological function of targets, which are most appealing or known to the authors. We hope this particular perspective can accelerate readers to grasp the advance in this territory, and we encourage the readers to survey other journal articles for more case studies.

6.2.1.1 Targeting PPIs in Apoptosis Process

Apoptosis, also known as type I programmed cell death, is a naturally occurring process that is crucial for tissue homeostasis. As estimated, between 50 and 70 billion cells die each day due to apoptosis in the average human adult. Because

apoptosis is so important, it is a highly regulated process. There are at least two broad pathways that lead to apoptosis, an extrinsic pathway and an intrinsic pathway. The molecular mechanisms underlying the intrinsic and extrinsic apoptotic pathways have been extensively investigated and found that the extrinsic pathway is activated in response to the binding of death-inducing ligands to cell-surface death receptors and cell-intrinsic apoptotic stimuli include DNA damage, growth factor deprivation and oxidative stress. Defective apoptosis processes have been implicated in a wide variety of diseases, such as cancer, a phenomenon resulting from an insufficient amount of apoptosis [64, 65]. In the efforts to modulate the dysregulated apoptosis process, three types of protein-protein interactions were identified as essential components in the signaling pathway for designing small molecular drugs (Fig. 6.3), which involves BCL-2 family proteins [66, 67], IAP proteins [68], and p53–Mdm2 interaction [69].

Bcl-2 and Bcl-X_L Bcl-2 is located to the out membrane of mitochondria, where it functions as anti-apoptotic factor, and plays an important role in promoting the cellular survival by interacting with pro-apoptosis proteins, such as BAX and BAK. Upregulation of Bcl-2 and its relatives Bcl-X_L and Mcl-1 is an important mechanism through which cancer cells avoid cell death in the face of signal dysregulation,

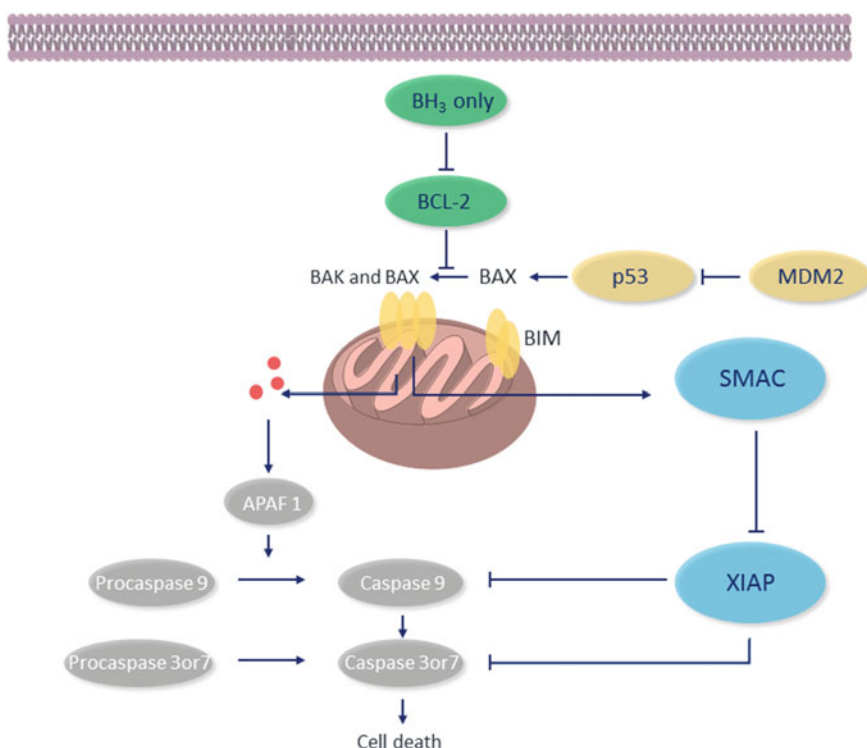


Fig. 6.3 Three important PPIs in the apoptosis signaling pathway

radiation, and chemotherapy. Inspecting the structures of Bcl-X_L bound with BAX peptide or with BAK peptide elucidated that the binding site of Bcl-X_L is an extended hydrophobic groove, of ~20 Å in length, interacts with a critical alpha helix in BH3 domain of the pro-apoptosis proteins. In mid-2000s, Oltschewski and his coworkers [70] applied a high-throughput NMR-based method called ‘SAR by NMR’—a technology based on the linkage of proximal fragments to achieve high-affinity binding—to screen a chemical library to identify small molecules that bind to the hydrophobic BH3-binding groove of Bcl-X_L. Initially, two compounds **6-1** and **6-2** were discovered that bind to distinct but proximal subsites within this cleft (Fig. 6.4a), with affinities of approximately 0.3 mM and 4.0 mM, respectively. Substitution of an acyl-sulfonamide for biphenyl carboxyl group maintained the correct position in site 1 while providing an optimal trajectory to another site. Site-directed parallel synthesis led to compound **6-3** ($K_i = 36$ nM to Bcl-X_L) in which 3-nitro-4-(2-phenylthioethyl) aminophenyl group spans the binding sites and efficiently occupies site 2 (Fig. 6.4b). Later study showed that compound **6-3** tightly bound to domain III of human serum albumin (HSA), which dramatically reduced the binding affinity in vivo study. To reduce binding to HSA, the NMR structure of the thioethylamino-2,4-dimethylphenyl analog of compound 1 complexed with domain III of HSA was compared to the structure of compound **6-3** bound to Bcl-X_L and revealed that portions of the ligand at the solvent-exposed part in Bcl-X_L can be modified with polar substituents to achieve the selectivity. And their efforts finally resulted ABT-737 that binds with high affinity ($K_i \leq 1$ nM) to Bcl-X_L and Bcl-2 (Fig. 6.4c). The subsequent optimization aimed to overcome the poor oral absorption created the second-generation analog, navitoclax [67]. However, concomitant on-target thrombocytopenia caused by Bcl-X_L inhibition limits the efficacy achievable with navitoclax. Subsequent efforts led to the development of the first highly selective inhibitor of Bcl-2, venetoclax, approved in 2016 for the treatment of patients with chronic lymphocytic leukemia (CLL).

Mcl-1 Mcl-1 is a related protein in Bcl-2 family, which is also upregulated in many cancer cells. But Mcl-1 is distinct from Bcl-2 and Bcl-X_L as it binds to different BH3 peptides. Friberg et al. described the discovery of potent and selective Mcl-1 inhibitors using fragment-based method [71]. Firstly, 132 hits (93 inhibited Mcl-1 with $K_i < 500$ μM) was resulted from the screening of their fragment library (>138,000 compounds) by recording SOFAST ¹H-¹⁵N HMQC spectra of Mcl-1 incubated with mixtures of 12 fragments. On the basis of the affinity and distinct chemical characteristics, two classes of compounds (**6-4** and **6-5**, Fig. 6.5) were selected for follow-up experiments. Secondly, to determine how the two class of fragments bind to Mcl-1, they performed NMR-based structural studies on Mcl-1/fragment hit complexes. Using double-labeled (¹⁵N, ¹³C) Mcl-1 protein, they acquired NOE-derived distance restraints and used these to dock representative fragments into a previously determined Mcl-1/Bim BH3 peptide complex. The fragments of the two classes exhibited different patterns of protein-ligand NOEs, confirming that they bind to different regions of Mcl-1. Thirdly, they found the attachment of class II aromatic groups with a two- to four-atom linker to the 3-position of the class I 6,5-fused heterocycles would lead to merged compounds

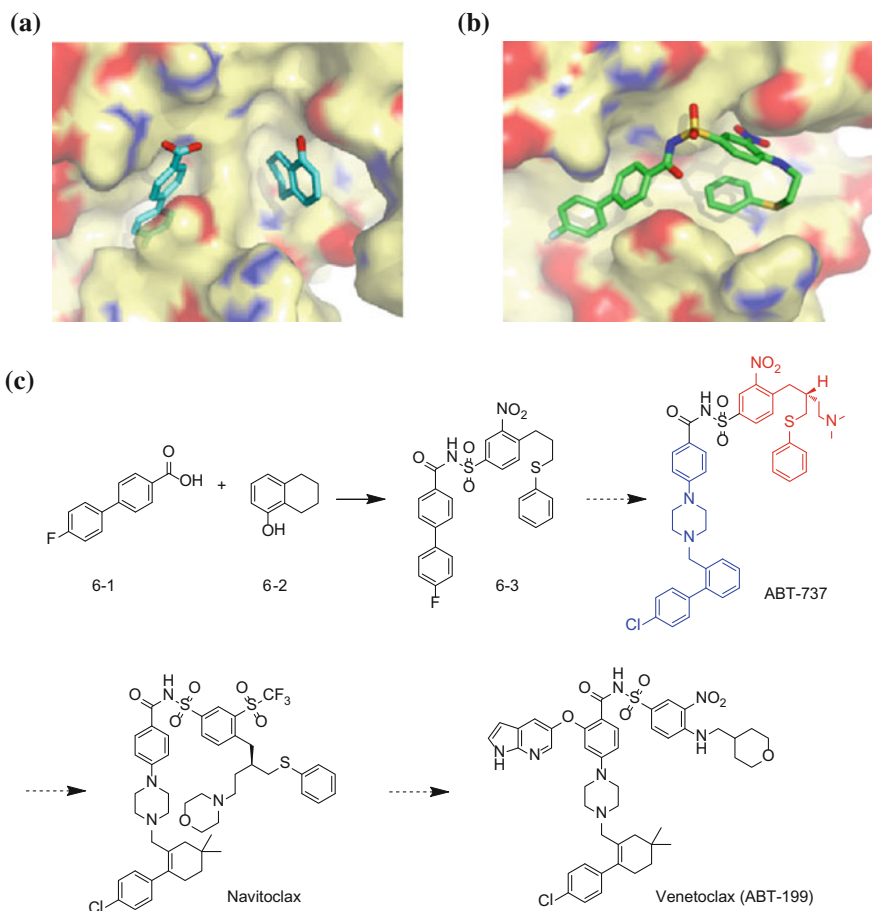


Fig. 6.4 The development of inhibitors of Bcl-2 and Bcl-X_L. **a** Two fragments in two distinct sites of Bcl-X_L (PDB code: 1YSG); **b** co-crystal structure of compound **6-1** bound to Bcl-X_L (PDB code: 1YSI); **c** the development route to marketed drug Venetoclax

that could maintain the favorable hydrophobic contacts of both fragments to Mcl-1 as well as the interaction between the common carboxylic acid and R263 of Mcl-1. With these efforts, they discovered that the four-atom linked compounds as compound **6-6** yielded the most potent Mcl-1 inhibitors in the series, displaying sub-micromolar dissociation constants. Moreover, these compounds exhibited selectivity for Mcl-1 over Bcl-xL and Bcl-2.

Sun's group described using the FBDD method to accelerate the discovery of a novel Mcl-1 inhibitor from two distinct structural classes [72]. An initial NMR-based fragment screen was conducted by employing the protein-based NMR-screening method. In this method, recombinant human Mcl-1 protein labeled with ¹³C at the methyl groups of isoleucine, leucine, valine, and methionine was

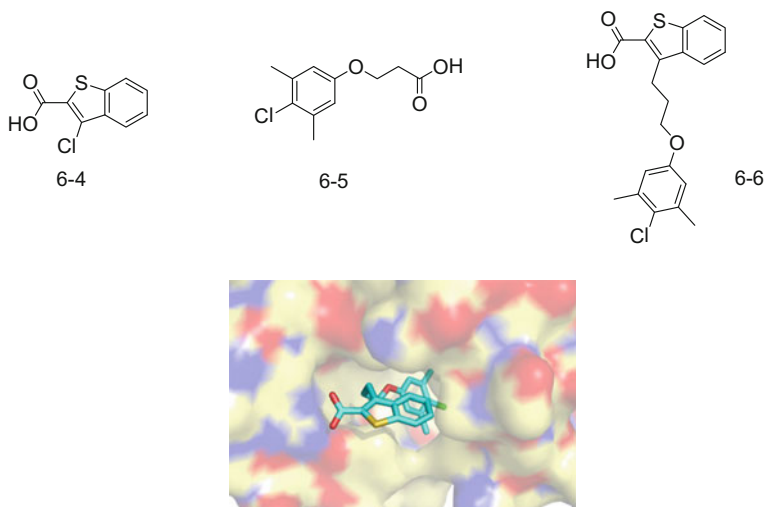


Fig. 6.5 The development of Mcl-1 inhibitor 6-6. Co-crystal structure of compound 6-6 bound to Mcl-1 (PDB code: 4HW3) was depicted as stick and surface model

expressed in *Escherichia coli* and purified. By monitoring the changes in the ^{13}C -HSQC spectrum of this methyl-labeled protein upon addition of approximately 17,000 fragments, they found that Mcl-1 is amenable to small-molecule inhibitions demonstrated by a high hit rate of the screening. In this screening method, two compounds (the aryl sulfonamide and salicylic acid as compounds 6-7 and 6-8, shown in Fig. 6.6) were chosen for the further study. Due to the unavailability of co-crystals of Mcl-1 with the fragment hit, NOE-driven docking of the fragment onto the crystal structure of human Mcl-1 was adopted to illustrate the binding mode of the compounds. Based on the NMR-derived model, the optimization of 6-7 and 6-8 fragments yielded compound 6-9 with an IC_{50} of 30 nM against Mcl-1.

IAPs-SMAC Inhibitor of apoptosis proteins (IAPs), including cIAP1, cIAP2, and XIAP, are important regulators in the apoptosis. They bind to caspases to prevent the activation of apoptosis and often overexpressed in cancer cells. An endogenous inhibitor of IAPs, called second mitochondrial activator of caspases (Smac), competes with caspase binding to BIR domains of IAPs and thereby stimulates apoptosis. Since Smac peptide motif, Ala-Val-Pro-Ile (AVPI), binds tightly to two adjacent subpockets on BIR domains of XIAP, it provides a template for designing small molecules to mimic the binding features of the tetra-peptide.

Pellecchia and his coworkers [73] reported on the utility of the NMR-based approach by deriving novel and effective SMAC mimetics targeting the anti-apoptotic protein XIAP. Initially, they designed a virtual library of L-alanine derivatives coupled with 578 primary and 815 secondary, low molecular weight, amines. Fifteen potential fragments predicted by molecular docking were further checked experimentally by protein-observed NMR for their ability to bind to the

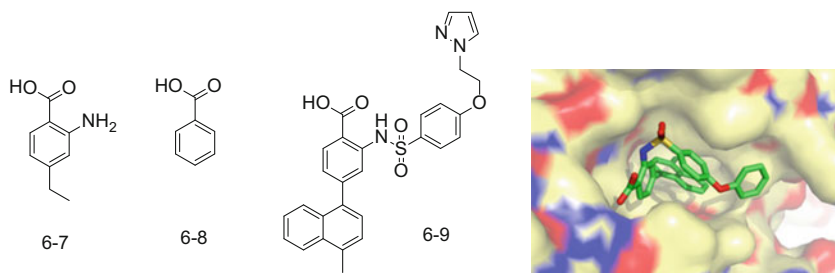


Fig. 6.6 The development of Mcl-1 inhibitor 6-9. Representative binding conformation of aryl sulfonamides (PDB code: 4OQ5)

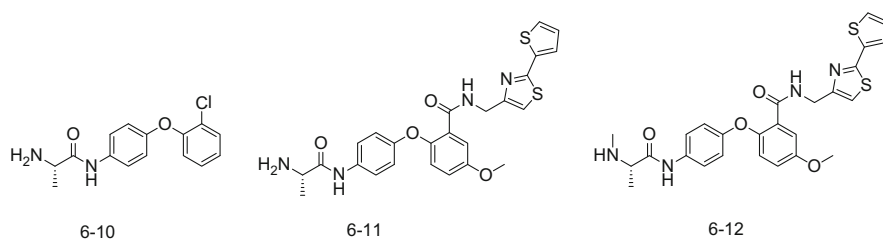


Fig. 6.7 The development of XIAP inhibitor 6-12

Bir3 domain of XIAP. By comparing the differences of chemical shift perturbations on Bir3 in the presence of the selected putative SMAC mimics, compound **6-10** stands out as a weak binder ($K_d = 200 \mu\text{M}$) for the Bir3 domain (Fig. 6.7). Based on the crystal structure, it was predicted that, if compound 1 was modified at position 2 of the 4-phenoxybenzene scaffold, it may provide more interactions with the P2 subpocket, similar to the isoleucine residue of AVPI. Then a second virtual library of derivatives of compound **6-11** (about 900 compounds) was designed, and compound 5 the out from top scoring in the docking study were synthesized and tested by the NMR method with ^{15}N labeled Bir3. Finally, compound **6-12**, an analog of **6-11**, was discovered to be the tightest binding affinity among the tested compounds with a K_d value of $1.2 \mu\text{M}$ to Bir3 domain of XIAP.

In 2015, Chessari et al. at Astex, using fragment-based drug discovery method, discovered a non-alanine lead series with dual activity against cIAP1 and XIAP [74]. Initial screen with ligand-detected NMR methods, such as LOGSY or STD-NMR, were found to be relatively insensitive for XIAP-BIR3 due to the small size of the protein (11.8 kDa). Therefore, protein ^1H NMR was used as a primary screen to detect fragment binding. A protein concentration of $200 \mu\text{M}$ was used in the protein ^1H -NMR spectrum and the chemical shifts and line widths of XIAP-BIR3 ^1H signals was monitored with threshold $\delta < 0.4$ ppm and the range δ 9.8–10.4 ppm (the ranges were expected to be sensitive to fragments binding in the

canonical AVPI pocket). In the second step, an X-ray-based fragment screen of XIAP-BIR3 was applied to the identified fragment hits by soaking crystals of XIAP-BIR3 (residues 250–354) with the fragments for 24–72 h either as singletons (at 50–100 mM fragment, 5–10% DMSO) or doublets (2×50 mM, 10% DMSO). Screened from the 1151 fragments with relatively high LE for both XIAP and cIAP1, four fragment hits contained the small primary or secondary aliphatic amines were confirmed, which is consistent with the known binding preference of N-terminal alanine-containing peptides. One compound (**6-13**) of them was chosen as a starting hit and optimized into a potent non-alanine IAP antagonist (**6-14**), which is structurally distinct from all IAP antagonists reported previously (Fig. 6.8).

p53-Mdm2 The transcription factor p53 is a master tumor suppressor that regulates cell-fate decisions such as senescence, cell-cycle arrest, and apoptosis. Mutations in p53, resulting in reduction or loss of p53 function, are presented in $\sim 50\%$ of human cancers. In other tumors, the p53 pathway is inactivated by upregulation of p53 inhibitors, such as the mouse double minute proteins (Mdm2 and MdmX), or by downregulation of p53 cooperators, such as ARF. In the past decades, extensive efforts of biochemical, structural studies have provided clear picture about function of the p53–Mdm2 interactions. Mdm2 functions as an inhibitor of the N-terminal transactivation domain (TAD) of p53 and promotes p53 degradation through the ubiquitin–proteasome system (E3 ligase activity). On the other hand, MdmX can downregulate p53 by inhibition of the TAD domain and it can upregulate Mdm2. Then the use of Mdm2 antagonists in cancer cells expressing wild-type (WT) p53 should activate p53, resulting in effective antitumor activity. Scrutiny of the Mdm2/p53 complex shows that the p53–Mdm2 interaction can be minimized to an α helix from the TAD domain of p53 that binds into a pocket on the surface of the N-terminal domain of Mdm2 and therefore is druggable by small molecules based on a buried surface area of ~ 700 Å². At the interface, the interacted helix of TAD domain is only two turns and contains three critical hot-spot residues (Phe19, Trp23, and Leu26) pointed toward a deep pocket in the center of the peptide-binding groove of Mdm2 [75].

To dissect the interaction features of the binding site of p53–Mdm2, Fry et al. [76] adopted a fragment-based approach to screen a small focused library generated by deconstructing a potent inhibitor RG7112 into 10 small pieces (compounds 6-15 to 6-24) (Fig. 6.9). The results show that the fragment containing three substituents

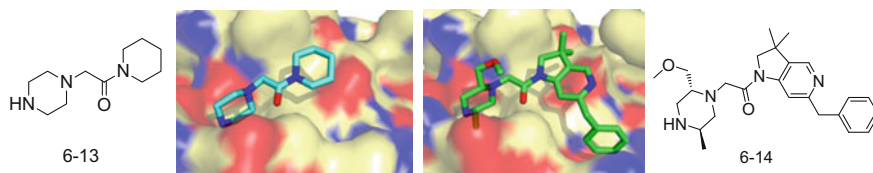
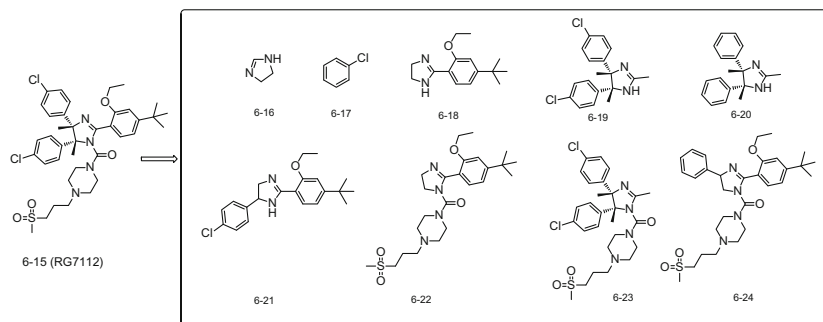


Fig. 6.8 The development of XIAP inhibitor 6-14. **a** Fragment **6-13** bound to XIAP (PDB: 5C3H); **b** structure of compound **6-14** bound to XIAP (PDB code: 5C83)

on the core structure, in any combination, is capable of binding to Mdm2. X-ray structures of compounds **6-23** and **6-24** bound to Mdm2 showed that these fragments attain a position as expected based on the RG7112 binding paradigm, exhibiting the same orientation and utilizing the same subpocket-filling strategy as the parent compound. The binding of fragments that retained only two of the four attached groups was more varied, indicating the combination of attached groups have a dramatic influence on activity, causing affinities to range from an undetectable level to a K_d of 26 μM (Fig. 6.9). This study supports the notion that p53–Mdm2 interaction systems should be highly amenable to a fragment-based lead discovery approach, although these systems will likely require some specialized choice of library composition, as exemplified by a report of Boltjes et al. on the library generation for the discovery of p53-Mdm4 inhibitor [77].

6.2.1.2 Targeting PPIs in Ras Signaling Pathway

Mutational activation of the RAS oncogene products (HRAS, NRAS, and KRAS) is a frequent event in human cancers. Ras belongs to the family of small GTPases and functions as molecular switches in controlling of extracellular growth signal transduction in many vital cellular processes such as cell differentiation, proliferation, and survival [78–80]. By conformational transformation from an inactive GDP-bound to an active GTP-bound state, RAS proteins relay the signals from extracellular kinase receptors and interact with various downstream effectors such as Raf, PI3K, and Ral-GDS, therefore triggering further cellular activities



Comp.	1	2	3	4	5	6	7	8	9	10	11
NMR Binding	Yes	No	No	No	Yes	No	Yes	No	Yes	Yes	Yes
SPR Binding	0.22	No	No	No	26	No	No	No	20	14	1000
LE	0.18				0.31				0.19	0.18	0.10

Fig. 6.9 The deconstruction of RG7112 and result of binding assay

(Fig. 6.10). After the discovery of activated RAS genes in cancers in 1982, targeting the mutated RAS remains as a promising anticancer strategy for more than three decades. However, mutated Ras has proven to be an extremely difficult target for drug development. Ras proteins bind GDP and GTP with high affinity in pM range. Moreover, the cellular concentrations of GDP and GTP are at μM level, which further hinder the pharmacological modulation through the development of GDP/GTP competitive inhibitors for Ras. The activities of Ras proteins are regulated by guanine nucleotide exchange factors (GEFs, e.g., SOS1) and GTPase-activating proteins (GAPs, e.g., neurofibromin) [81]. Ras signaling strongly depends on the intracellular localization of Ras at the plasma membrane [82]. After post-translational modified at the C-terminal hypervariable region of Ras protein at endomembrane, Ras needs shuttling factor PDE δ to bind the farnesyl moiety and dissociate it from endomembranes, therefore enhancing its diffusion throughout the cell. With the help of G-protein Arl2, the Ras protein released from PDE δ and relocalized to the plasma membrane through the electrostatic interaction and hydrophobic interaction.

SOS1-Ras In order to identify and characterize small-molecule binders to KRas, Maurer and Wang [83] carried out a fragment-based lead discovery campaign. Initially, a ligand-detected NMR screen identified 266 fragments from a library of 3285 diverse compounds. Then protein-detected NMR using isotopically labeled KRas protein was applied for hit validation and binding site characterization. A consensus site of fragment binding was revealed and confirmed by X-ray

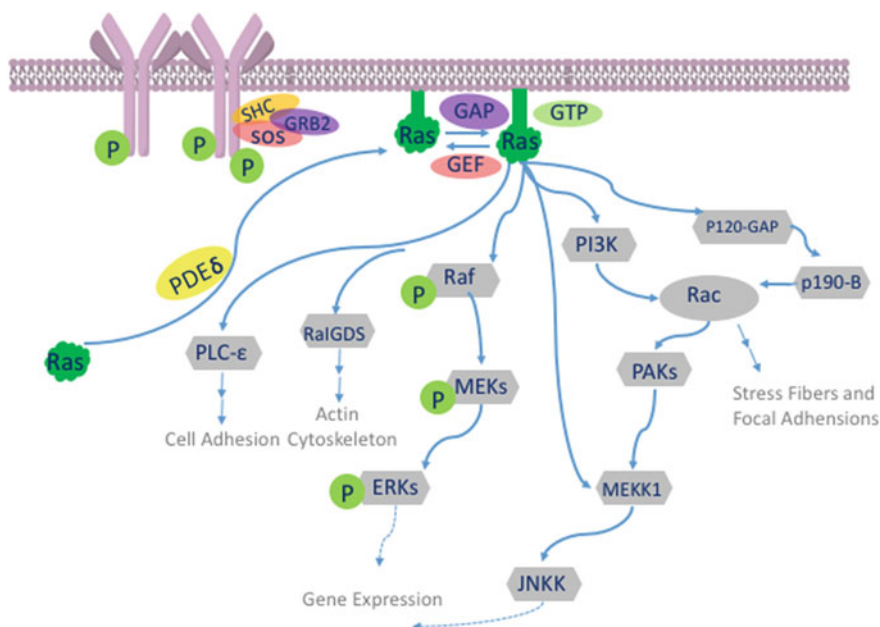


Fig. 6.10 Simplified Ras signaling pathway

crystallography study on KRas protein bound with several hits. The consensus site comprises a shallow hydrophobic pocket, which was expanded upon the fragment binding. The binding site is proximal to the protein-protein interface, especially at the SOS1 binding pocket.

In 2012, Maurer et al. [84] reported their effort for the discovery of a small-molecule blocking Ras–SOS interactions. They applied the NMR-based saturation transfer difference (STD) assay to screen a 3000-compound library (using pools of up to six fragments each), resulting in 240 primary hits. These hits were further validated by 2D 1H15N HSQC NMR method. By comparing the HSQC spectra, 25 compounds produced chemical shift perturbations that can be mapped to a contiguous site on the KRasm structure and were thus classified as confirmed hits. The complexes of KRasm with benzamidine (BZDN), benzimidazole (BZIM), or 4,6-dichloro-2-methyl-3-aminoethyl-indole (DCAI) were obtained by soaking the confirmed fragment hits into the KRasm crystals, indicating they all bind to a similar site surrounded by residues K5, L6, V7, I55, L56, and T74 (Fig. 6.11a). Detailed investigation showed that DCAI, binding at RAS–SOS interface, inhibits SOS-mediated nucleotide exchange and release for Ras with IC_{50} of 342 and 155 μM , respectively.

Another attempt to discover small molecules binding to Ras/SOS complex was reported by Winter and coworkers in 2015 [85]. A library of 1160 fragments organized into four-compound cocktails was screened with X-ray crystallography method. Three interesting fragments bound to distinct sites on the complex were elucidated from co-crystal structures, but none of these compounds were sufficiently potent to show functional activity in the Ras–Raf HTRF assay. Simple modifications on these fragment hits were unsuccessful to improve the activity. Inspecting the complex found a nearby cysteine residue (Cys118) which could be utilized for designing covalent binding molecules. Therefore, a library of 400 compounds containing potentially reactive functional groups was screened, finding

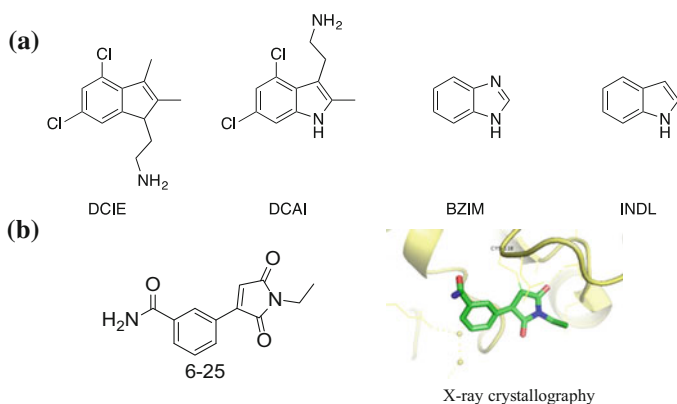


Fig. 6.11 Fragment hits of RAS–SOS. **a** Four fragments identified by Maurer et al. [84]; **b** crystal structure of compound 6-25 bound to SOS (PDB code: 4US2)

the reactive N-ethylmaleimide (NEM) group as an ideal electrophilic ‘warhead’ to bind to Cys118. Further optimization resulted an irreversible inhibitor **6-25** (shown in Fig. 6.11b) that shows a time-dependent inhibitory activity against both wild-type and mutant KRas, opening the way to a new strategy to target aberrant Ras signaling by intervening in the SOS-mediated activation of Ras.

PDE δ -Ras Despite downstream interactions with GEF, GAP proteins, as mentioned before, Ras protein needs transfer to the plasma membrane to execute its oncogenic activity. The shuttle protein PDE δ was found to act as a solubilizing factor that facilitates the transit of RAS proteins to either the Golgi or the recycling endosomes to the plasma membrane. Waldmann’ group carried out drug discovery based on this RAS–PDE δ interactions, and so far, obtained three chemotypes of PDE δ inhibitors: deltarasin, deltazone, and deltasonamide [86–88]. Different from their method of high-throughput screening, we applied fragment-based drug discovery to identify several fragment hits from ligand-observed STD and CPMG NMR screening (unpublished work). By solving the co-crystal structure of PDE δ bound with a tetrazole fragment **6-26**, the binding mode was revealed as shown below, which supports our structure-based lead optimization and finally obtains a potent PDE δ inhibitor compound **6-27** with IC₅₀ value about 27 nM in the FP assay (Fig. 6.12).

6.2.1.3 Targeting PPIs Related Histone Post-translational Modifications

Epigenetic regulation of gene expression is currently the focus of intensive research in post-genomic era. At the molecular level, epigenetic regulation involves dynamic and reversible modification of DNA and the proteins that package DNA. Histones, the core proteins within chromatin structure, are subjected to a range of post-translational modifications (PTMs), mainly including acetylation, methylation, phosphorylation, and ubiquitination (Fig. 6.13). The combinatorial characterized covalent modification on the histone tails is coined as ‘histone code,’ which is believed to be key to understanding the gene expression pattern and many heritable changes in phenotype that are not encoded in the underlying DNA sequences. This histone code hypothesis has led to the presumption that there must be protein families for specifically adding, removing, and recognizing the PTM marks. In recent years, all three types of proteins have been identified for histones.

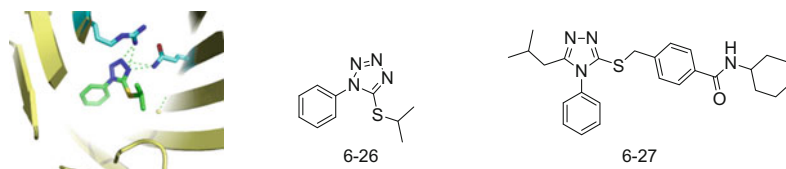


Fig. 6.12 Fragment hit and optimized inhibitor of RAS–PDE δ interactions (unpublished work)

Taking acetylation as an example, histone acetyltransferases (HATs) act as a writer to transfer the acetyl group from acetyl CoA to form an ϵ -N-acetyllysine, whereas histone deacetylases (HDACs) work as an eraser to remove the acetyl group from the histone tail. The proteins containing bromodomains could bind to the acetylated lysine (KAc) and are playing just as readers for signaling transduction of the lysine acetylation states of histone. The aberrant events involving in writer-reader-eraser processes have been associated with many human diseases, especially certain cancers [89–91].

Lysine methyltransferase Histone methyltransferases (HMTs) are a class of enzymes that introduce methyl marks on lysines and arginines of histone proteins using the cofactor *S*-adenosyl methionine (SAM) as methyl source [92, 93]. DOT1L, especially lysine methyltransferase (KMT) responsible for methylations of lysine K79 on histone H3, distinguishes itself from the other KMTs by the absence of the common SET domain and is more closely related to the protein arginine methyltransferase (PRMT) class. Until 2016, the reported DOT1L inhibitors are all SAM-mimic. And due to its unique structure, the optimized inhibitors can achieve high potency and selectivity among the histone methyltransferases, as represented by the clinical candidate EPZ-5676 that was discovered by researchers at Epizyme. The scientists at Novartis took a different approach by applying the fragment-based drug discovery method [94]. They screened the fragment library using surface plasmon resonance (SPR) with an immobilized DOT1L construct containing the catalytic domain. Compound **6-28** was identified as a weak binder with an estimated equilibrium binding constant of $K_d \approx 50 \mu\text{M}$ (Fig. 6.14). Further, the compound was confirmed by the biochemical scintillation proximity assay and

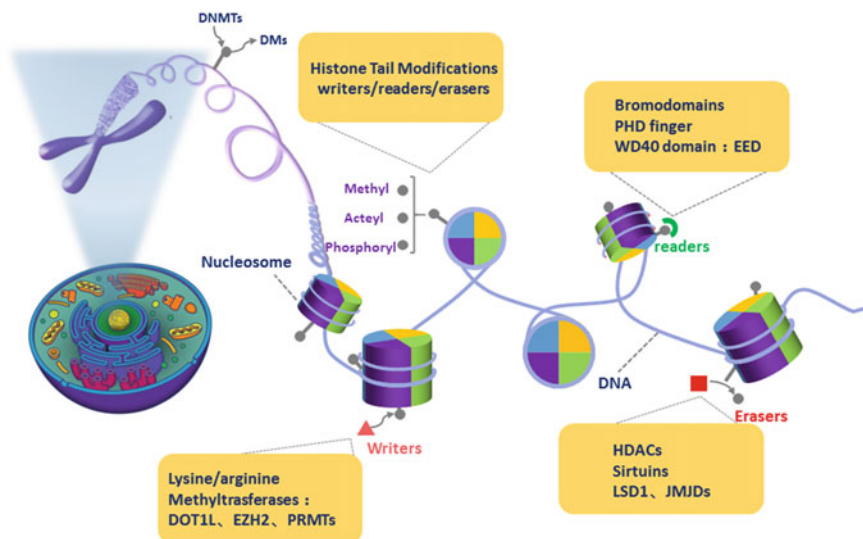


Fig. 6.13 Drug targets in epigenetics

protein-observed NMR experiments. After solving the co-crystal structure of fragment **1** bound DOT1L, the details of binding mode were revealed. The 2,6-dichlorophenyl moiety of fragment **1** acts as a hydrophobic anchor occupying a hydrophobic cavity formed by side chain movements of Met147, Leu143, Phe239, and Tyr312. The 3-(2-*N*-methylaminocarbonyl) pyrrolyl moiety is sandwiched between Phe243, Pro130, and Phe131 engaging the flexible lid loop of the SAM pocket in a novel conformation by π - π stacking. Although the initial fragment has a moderate ligand efficiency (LE = 0.25) and binds to an induced plastic pocket, the authors carried on the optimization with fragment growing method. As shown below, after extensive modification and under the guidance of co-crystal structures, they finally discovered a high-potent DOT1L inhibitor **6-29**, with IC₅₀ value of 14 nM, increased affinity by more than 4 orders of magnitude.

Arginine Methyltransferase Histone arginine methyltransferases using the cofactor S-adenosyl-l-methionine (SAM) transfer a methyl group to the terminal guanidino nitrogens of arginine on histone. Like lysine methyltransferases, they play important roles in histone post-translational modifications and govern essential cellular processes that affect cell growth, proliferation, and differentiation. Therefore, deregulation of these enzymes was implicated in the pathogenesis of several different diseases, including cancer. In mammalian cells total nine protein arginine methyltransferases were identified and can be divided into three types according to the degree and position of methylation. Freitas et al. [95] selected three high-potent PRMT inhibitors and deconstructed them into three fragments containing the essential amine group. From the biochemical assay, all three fragments demonstrated a good ligand efficiency (LE \geq 0.68). This initial result encouraged them to expand the study to screen a commercial fragment library of 2040 compounds. Finally, they obtained 14 confirmed fragment hits. Among them, fragment **7** was in detail characterized with the ITC experiment and found that this fragment shows a signature of favorable enthalpic free energy ($\Delta G = -8.2$ kcal/mol and $\Delta H = -17.2$ kcal/mol). Further tests indicated that fragment **6-33** is substrate-competitive inhibitor of PRMT6, and it could be served as warheads for developing class I PRMT inhibitors (Fig. 6.15).

EED Polycomb repressive complex 2 (PRC2) is a protein complex functioning as a H3K27 methyltransferase and playing a major role in diverse biological processes such as chromatin remodeling and epigenetic silencing. The core of the PRC2 complex is composed of four proteins: EZH2, EED, Suz12, and RBAP48

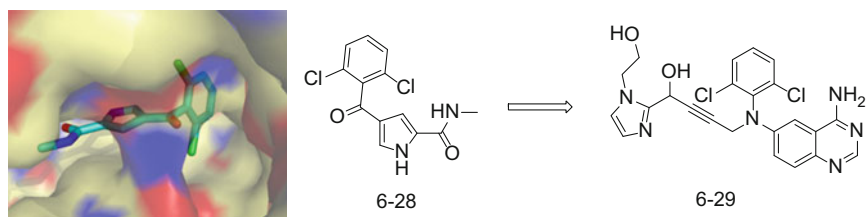
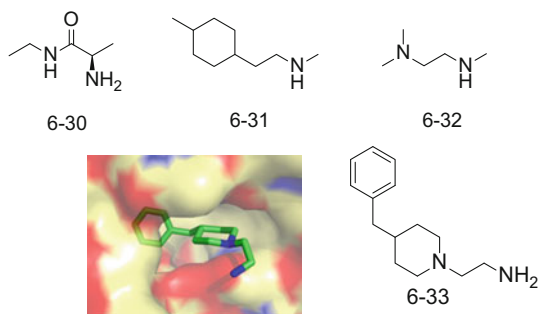


Fig. 6.14 The development of DOT1L inhibitor

Fig. 6.15 The development of PRMT6 inhibitor 6-33. Co-crystal structure of fragment 6-33 bound to PRMT6 (PDB:5EGS)



[96]. The catalytic activity is originated in protein EZH2, which contains the SET domain. Gain-of-function mutations and overexpression of EZH2 are well documented to be involved in various cancer types. In addition to EZH2, EED was shown to be required for enzymatic activity, and its binding mechanism was revealed by structural studies on entire human PRC2 and the minimal core of the PRC2 containing only three proteins: EZH2, EED, and Suz12, visualizing the three proteins forming an intertwined complex in which the catalytic center is formed by EZH2 but is stabilized by domains of EED and Suz12. Moreover, H3K27me3 recognition by EED is essential in stimulating basal PRC2 activity in vitro and propagating H3K27 methylation in repressive chromatin for gene silencing in vivo. Giving the important roles of EED in PRC2 complex, Lingel et al. [97] at Novartis Institutes for BioMedical Research initialized a project of developing EED–histone interaction inhibitor. They conducted a biochemical high-throughput screening campaign and identified compound 1 showing inhibition of PRC2 activity with a single-digit micromolar IC_{50} (2.5 μ M). 2D HSQC NMR spectroscopy was used to assess the binding of 1 to EED protein, and dose-dependent chemical shift perturbations of several ^{13}C -labeled methionine methyl resonances were observed. The binding mode was revealed by the co-crystal structure of **6-34** with EED, showing the compound bound in the trimethyllysine pocket, which is consistent with the biochemical study that is a competitive inhibitor with respect to H3K27Me3 peptide (Fig. 6.16). Since compound **6-34** has large molecular weight and is difficult to perform chemical modification, the authors employed an ingenious approach of ligand deconstruction to identify the minimal fragments (compound **6-35**). The co-crystal structure of **6-35** with EED shows that the interactions made with the protein are very similar to the ones observed for the parent compound **6-34**. Based on this crystal structure, a series of amino-imidazole compounds were synthesized and characterized. Finally, several EED–histone interaction inhibitors (such as **6-36**) with submicromolar activity and favorable drug-like properties were discovered, enabling further optimization and studying the biology of EED-mediated inhibition of PRC2 activity.

Bromdomain Acetylation of histone lysine residues is one of the most widely studied post-translational modifications (PTMs) that regulate chromatin structure and gene expression in the cell. Acetylated histones are recognized by ‘readers,’

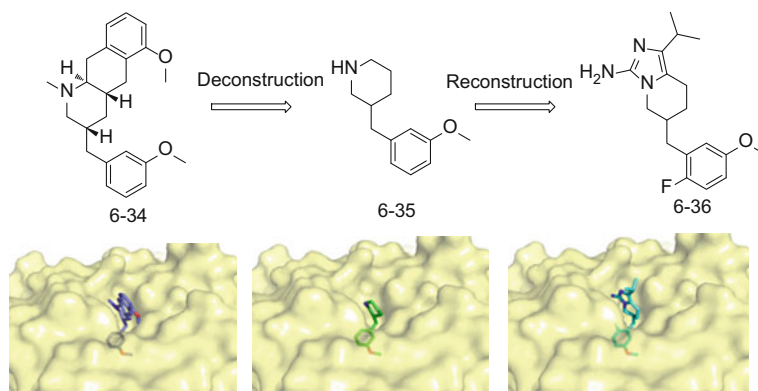


Fig. 6.16 The development of EED inhibitors. Co-crystal structure of compounds **6-34**, **6-35**, and **6-36** (PDB codes: 5U17, 5U5K, 5U5H)

which are typically found in chromatin- and transcription-associated proteins that partake in many protein-protein interactions, facilitating the formation of the protein complexes that drive active transcription. So far, there are three readers (bromodomain, double PHD finger, and pleckstrin homology domain) which recognized acetylated lysine (KAc) and the bromodomain is the most thoroughly characterized of the three. The bromodomain was identified to function as lysine acetylation reader in the early 1990s in the *brahma* gene from *Drosophila melanogaster*. After analysis of human genome, it was found that 46 different nuclear and cytoplasmic proteins contain 61 bromodomains. These proteins include HATs and HAT-associated proteins, histone methyltransferases, helicases, ATP-dependent chromatin remodeling complexes, transcriptional co-activators, TBP-associated factors, and nuclear scaffolding proteins. Despite having large sequence variations, bromodomain modules share a conserved fold that comprises a left-handed bundle of four α -helices (namely, αZ , αA , αB , and αC) that are linked by diverse loop regions of variable charge and length (known as ZA and BC loops) which surround a central acetylated lysine binding site [98, 99].

Initial fragment-like bromodomain inhibitors were described in the literature in 2005 [100], but potent inhibitors were not developed until 2009. The discovery of the first potent BET inhibitor (+)-JQ-1 [101] was reported in 2010 (Fig. 6.17). (+)-JQ1 was widely used as chemical probe to study the function of BET proteins in physiology as well as in many diseases. Similar to (+)-JQ1, I-BET-762 is also a selective BET inhibitor and now in a phase II clinical trial for nuclear protein in testis (NUT) midline carcinoma [102]. Since the first reports of BET inhibitors, the field of bromodomain inhibitor development has evolved rapidly, and many new scaffolds were discovered to interact with acetylated lysine binding site, especially through the fragment-based techniques [103–105]. Taking the first such application as an example, in 2012, Chung et al. [103] reported an attempt to discover the bromodomain inhibitor with the FBDD method. Based on the analysis of solved

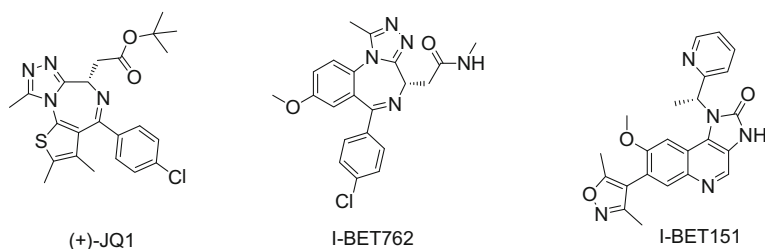


Fig. 6.17 The representative BET inhibitors

bromodomain co-crystal structures, they assembled a focus fragment library and screened with high-throughput biochemical assay and directed X-ray crystallography. The binding modes of over 40 fragment hits were elucidated, which provided invaluable information for bromodomain inhibitor development. Their follow-up study focused on the optimization of dimethyl isoxazole scaffold, and eventually led to several potent inhibitors of BRD2, as represented by well-known inhibitor I-BET151. Besides, the 3,5-dimethyl-isoxazole template was proved to be a war-head of KAc binding pocket, being adopted into several chemical series for diversified bromodomains, including BRD4, CREBBP, and P300 proteins.

Recently, a study exploring the druggability of the entire family of bromodomains has paved the way for developing inhibitors for other important bromodomains [106]. For example, Harner et al. [107] from Vanderbilt University reported a fragment-based screening of bromodomain ATAD2, a protein that possesses both AAA+ATPase (ATPases associated with various cellular activities) and bromodomain functionalities, which has been linked to poor prognosis in prostate, lung, and triple-negative breast cancers, as well as in hepatocellular carcinoma. They rely on the use of protein-observed NMR spectroscopy, as this method could not only measure the ligand binding affinity but also detect the binding site. Totally, 13,800 fragments were screened and ^1H - ^{15}N SOFAST-HMQC NMR spectra were recorded on uniformly ^{15}N -labeled ATAD2 in the presence of mixtures containing 12 fragments. Then, hit mixtures were deconvoluted as singletons to isolate the hit fragments, resulting in a total of 65 fragment hits. Based on the chemical features and the novelty of scaffold, the fragment hits were clustered into three groups (compounds from 6-37 to 6-39 shown in Fig. 6.18). Detailed binding modes were characterized with the aid of co-crystal structures. Together with the published data from the SGC, they proposed several strategies to improve ligand binding affinities toward the design of a chemical probe to examine the biological impact of ATAD2 inhibition.

PHD finger Methyllysine and methylarginine ‘readers’ are proteins with domains that can recognize and bind to methylation marks. They are responsible for conveying the methylation signal downstream, and they do so either by having their own catalytic functions or by recruiting other proteins to sites of action through the formation of multiprotein complexes. The major families of methyl reader domains are the plant homeodomain (PHD) fingers, WD40 repeat domains, chromatin

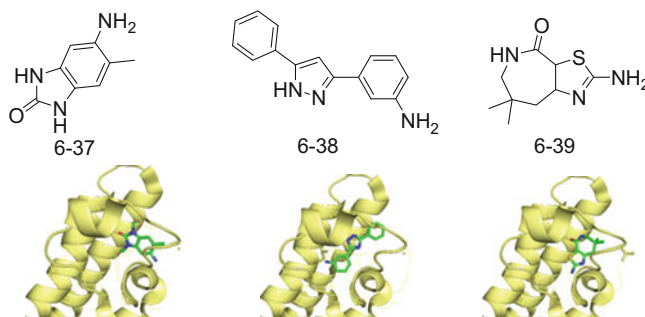


Fig. 6.18 The ATAD2 fragment hits: 6-37, 6-38, and 6-39. Co-crystal structure of compounds bound to ATAD2 bromodomain (PDB: 4TYL,4TZ2,4TZ8)

organization modifier domains (chromodomains), Tudor domains, Agenet domains, proline-tryptophan-tryptophan-proline (PWWP) domains, and malignant brain tumor (MBT) domains.

In 2014 Miller et al. [108] reported an application of NMR-fragment screen to identify small molecules that bound to the pocket of the Pygo PHD finger, which participates in the interaction between Pygo-BCL9 complex and oncogenic β -catenin. In detail, the armadillo repeats domain (ARD) of β -catenin interacts with BCL9 adaptor proteins, which in turn interact with the rear of Pygo PHD fingers through a BCL9 adaptor domain called HD1. This interaction induces a change in the binding module of the PHD finger, which promotes binding to methylated H3K4 and finally translating the signaling to downstream factors. Since inhibition of β -catenin has proved challenging, inhibitors disrupting the PHD finger–BCL9 interactions will be valuable for testing the hypothesis of cancer treatment.

Interaction between the Pygo PHD finger and H3K4me is mediated by two deep binding pockets: one pocket anchoring the N-terminal alanine residue, and the second pocket binding to the mono-methylated side chain of lysine 4 (H3K4me). Firstly, a library of commercially available compounds was screened in silico, and 313 possible hits were tested by protein-observed 2D NMR spectroscopy with a purified ^{15}N -labeled PHD–HD1 complex. Three fragments (6-40 to 6-42) proved to be positive, and elicited several weak chemical shift perturbations (CSPs) of the same PHD residues, indicating they target to same histone binding pocket (Fig. 6.19). To identify compounds with improved solubility and ligand efficiency, they conducted another three consecutive virtual screens and identified 32 additional hits confirmed by NMR spectra. Finally, a fragment containing benzothiazole scaffold (6-43) was analyzed in co-crystal structure, providing the fragment bound the K4me binding pocket of the PHD–HD1 protein with weak affinity (2.5 mM) but unique interaction mode of making a hydrogen bond to Asp380 of PHD. The fragments discovered demonstrate the ability to inhibit the Pygo PHD finger and could lead to future small-molecule inhibitors of the PHD/HD1 complex and other PHD-containing proteins.

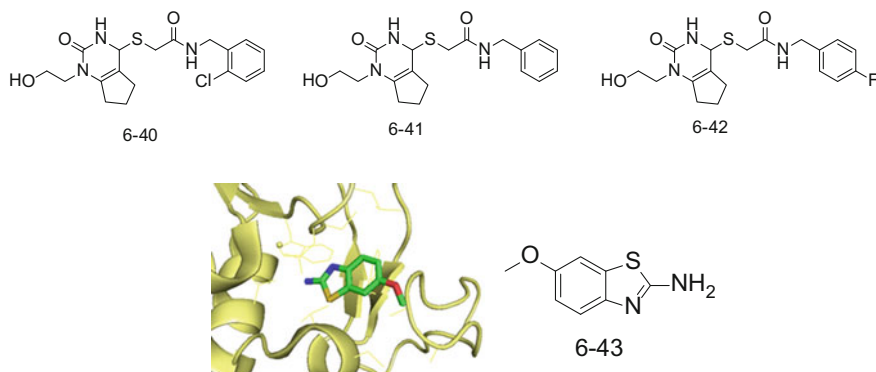


Fig. 6.19 The development of PHD finger inhibitors. Co-crystal structure of benzothiazole scaffold **6-43** (PDB:4UP5)

6.2.2 Targeting PPIs for Antibacterial and Antiviral Treatment

The treatment of bacterial infections through the administration of chemotherapeutic agents, which began in the 1930s, was one of the most profound medical advances of the twentieth century. Unfortunately, the emergence of antibiotic-resistant bacteria has presented a great challenge to humanity. In the past 40 years only two new structural types, daptomycin and linezolid, have been introduced to the clinic following their discovery using empirical screening methods. However, the determination of complete bacterial genome sequences and the parallel development of other techniques such as proteomics inspired a new genomics-based approach to antibacterial drug discovery. Therefore, many new targets were proposed and structure-based or fragment-based drug discovery methods were applied in developing antibiotics. Here we illustrated the fragment-based approach with two recent examples.

FtsZ–ZipA Cell wall division in *E. coli* involves a series of events, in which the first step involves the generation of the Z-ring, a circular polymeric structure formed by the cytosolic protein FtsZ. FtsZ is required for cell division in both Gram– and Gram+ bacteria and is highly conserved among different species. The assembly dynamics of FtsZ is regulated in cooperation with other proteins, such as ZipA. Impeding the FtsZ–ZipA interaction was found to block the cell division leading to long filamentous bacteria and consequently bacterial cell death. Thus, the inhibition of interaction between FtsZ and ZipA has become an important strategy for finding a new class of antibacterial drugs. Mosyaket al. [109] attempted to use the NMR-fragment screening method to discover the novel inhibitors of the ZipA/FtsZ protein-protein interaction. Firstly, an NMR library composed of 825 compounds was built up based on the structural diversity and promising physical properties. The screen was initially conducted by monitoring the ligand binding against ZipA

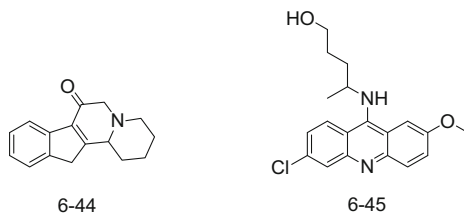
with the ^1H - ^{15}N HSQC experiment and resulted in 16 compounds bound to ZipA. Subsequent research found that seven of the compounds showed perturbations in the ^1H - ^{15}N HSQC peaks corresponding to residues that are involved in interaction with FtsZ and compound **6-44** showing the largest perturbations in the ^1H - ^{15}N HSQC spectrum of ZipA was selected as the hit for further optimization (Fig. 6.20).

The further exploration for the SAR of compound **6-44** was started with a high-quality X-ray crystal structure of ZipA. Eighty-seven compounds structurally similar to compound 6-17 were chosen for testing in the FP assay and evaluation by ^1H - ^{15}N HSQC experiments. Six compounds with possessed better solubility displayed the largest HSQC perturbations, suggesting that they were the better binding analogs. X-ray co-crystallization experiments for the six compounds and structure-based design led to compound **6-45**.

Sliding clamp The bacterial sliding clamp (SC), also known as the DNA polymerase III (Pol III) β subunit, is a torus-shaped homo-dimeric protein that is conserved across bacterial species. The SC serves as a scaffold protein to form large DNA/protein complex, playing a pivotal role in bacterial DNA replication and repair. Proteins that interact with the SC recognize a surface binding pocket that consists of two subsites (I and II), with one pocket located on each of the SC monomers. A consensus LM sequence, QLX₁LX₂F/L (S/D preferred at x₁; x₂ may be absent), has been identified that interacts with the SC LM-binding pocket. In 2014, Yin et al. [110] applied X-ray crystallography as a primary screen to identify fragment hits against the *E. coli* SC. A total of 352 fragment compounds from the First Pass Screen (Zenobia Fragment Libraries) were soaked into *E. coli* SC crystals as 4-in-1 cocktails and screened using X-ray crystallography, resulting in four fragments, 3,4-difluorobenzamide(6-46), 5-chloroisatin(6-47), 6-nitrobenzopyrazole (6-48), and 5-nitroindole (6-49), bound in subsite I of the binding pocket of SC (Fig. 6.21). Compound 6-50, an analog of 6-46, was measured using the FP assay (280 μM). And a co-crystal structure of 6-50 bound SC was solved, showing compound 6-50 fully occupied subsite I, with its fluoroaryl ring adopting a binding pose similar to that of 6-46. Then the ZINC library was subsequently searched for compounds displaying structural similarity to fragments, which led to the identification of additional moderate-active SC inhibitors, providing novel scaffolds for further drug development.

HIV-Integrase Antiviral drugs, like antibiotics, face similar situation of resistance due to fast evolution of viruses. Therefore, constant needs for new antiviral drugs are posed to the whole drug discovery community, especially for treating the

Fig. 6.20 The development of ZipA inhibitors



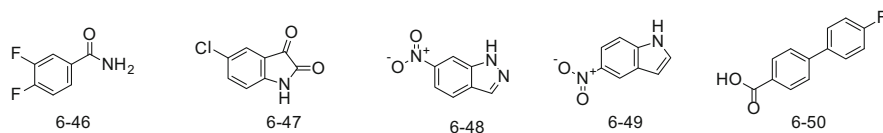
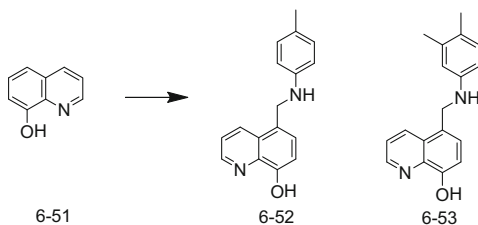


Fig. 6.21 Fragment hits of the sliding clamp protein

infections caused by HIV, HBV, and HCV. As summarized by Latham et al. [111], there are many drug discovery programs aimed at finding novel HIV-1 reverse transcriptase and integrase inhibitors by using the fragment-based approach, such as the work reported by Serrao and his coworkers [112]. Based on an initial molecular modeling study, they found 8-hydroxyquinoline (**6-51**) bound to HIV-1 integrase (IN) at the IN–lens epithelium-derived growth factor/p75 (LEDGF/p75) interface (Fig. 6.22). Then they developed a set of modified 8-hydroxyquinoline fragments demonstrating micromolar IC_{50} values for inhibition of the IN–LEDGF/p75 interaction. Further modifications at the C5 and C7 carbons of the 8-hydroxyquinoline core improved potency, while only modifications at the C5 position ultimately yielded potent inhibitors with low cytotoxicity. Two of these particular compounds, 5-((*p*-tolylamino) methyl) quinolin-8-ol (**6-52**) and 5-(((3,4-dimethylphenyl) amino) methyl) quinolin-8-ol (**6-53**), inhibited viral replication in MT-4 cells with low micromolar EC_{50} , providing evidence for 8-hydroxyquinolines as novel inhibitors of the IN–LEDGF/p75 interaction.

HCV NS3 In 2012, the researchers at Astex reported a potent HCV NS3 allosteric inhibitor identified by fragment screening and structure-guided design [51]. They performed a fragment-based screen using crystals of the HCV NS3–NS4a full-length genotype 1b holoenzyme. From the co-crystal structures of a series of fragment hits, they identified a new binding site at the interface of the two domains. This novel binding site is relatively hydrophobic, with residues Met485, Val524, Cys525, Gln526, and Val630 from the helicase domain and His57, Val78, Asp79, Asp81, and Arg155 from the protease domain making key van der Waals contacts with the fragments. One of the fragment hits (**6-54**), having a half-maximal inhibitory concentration (IC_{50}) $\sim 500 \mu\text{M}$, was selected for further elaboration with the structure-based approach (Fig. 6.23). By introducing an ethylamino side chain, the ligand (**6-55**) achieved additional affinity by forming further interactions with the pocket formed by residues Asp79, Thr519, and Leu522, finally leading to

Fig. 6.22 The development of HIV IN inhibitors



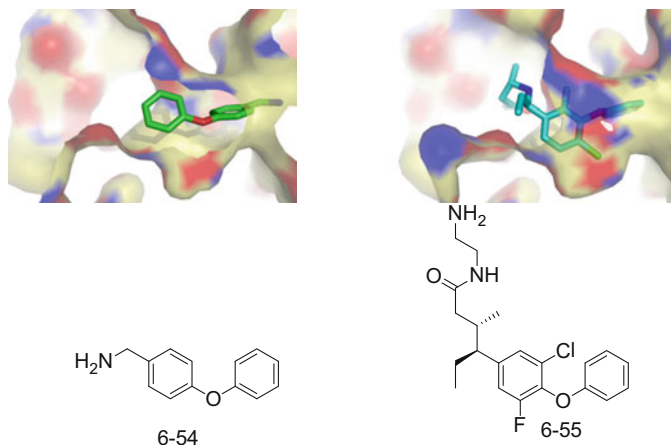


Fig. 6.23 HCV NS3 inhibitors. Co-crystal structure of **6-54** bound to NS3 (PDB code: 4B6F); co-crystal structure of **6-55** bound to NS3 (PDB code: 4B74)

an improvement in potency over four orders of magnitude ($K_d = 0.022 \mu\text{M}$, $\text{IC}_{50} < 0.01 \mu\text{M}$, $\text{LE} \sim 0.39$ kcal per heavy atom).

6.2.3 Other PPIs

CXCL12-CXCR4 Chemokines are small soluble proteins that activate G-protein-coupled receptors (GPCRs) and are involved in many physiological processes including cell trafficking, angiogenesis, and embryogenesis. Of the chemokine receptors, CXCR4 is the only one that is expressed by the majority of cancer types (at least 23 different cancers), functions as a sensor to chemokine ligand 12 (CXCL12) gradients in distant tissues to promoting the migration of the cancer cell. Ziareket al. [113] adopted a fragment-based approach to find a better starting molecule without using traditional hit-to-lead optimization strategy. A5-substituted-1H-tetrazole group, a bioisostere of the carboxylic acid, was chosen to bind the sY21 subpocket of CXCL12. Based on the tetrazole group, a fragment library contains only 9 compounds through altering the length of the linker and the substitution pattern of the phenyl. 2D protein-observed NMR was employed to study the fragment-induced CXCL12 chemical shift perturbations and determine the binding affinity of the synthesized fragments. The result showed that all molecules produced a subset of chemical shift changes indicative of a specific binding interaction. Three compounds were docked against total 21 structure models in order to account for protein flexibility and capture the best conformation. With these efforts, they found a compound as a novel hit binding to the sY21 site of

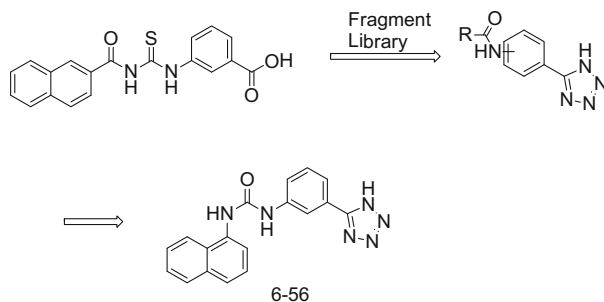


Fig. 6.24 The deconstruction of CXCR4 inhibitors

CXCL12, and subsequent research led a lead compound **6-56** with improvement in affinity, efficiency, and potency (Fig. 6.24).

pVHL-HIF1 α Ciulli et al. [114] dissected small molecular inhibitors (6-57 to 6-60) targeting the pVHL-HIF-1 α interaction to fragments and analyzed the implication of fragment-based approaches in the discovery of PPIs inhibitors (Fig. 6.25). Firstly, they deconstructed three targeting molecules into nine fragments (6-61 to 6-69) as a small library. To monitor the fragment binding, they initially selected DSF, NMR spectroscopy, and FP for the first-line screening, but they were unable to unambiguously detect fragment binding directly in any of these experiments except compound 6-69, which showed a very weak signal in the CPMG and Water LOGSY NMR spectra. To address the question of which size and structural complexity would be required to detect and characterize fragment binding, the promising fragment derivatives (6-70 to 6-73) were synthesized. Evidence of binding of 6-71 was only observed by NMR but not by DSF and FP. In contrast, it was able to detect binding of fragment 6-72 and fragment 6-73 in DSF and NMR and to characterize their binding affinities by FP and ITC. This result indicated of the requirement of fragments of the starting inhibitors to form favorable interactions in at least two subsites of the pVHL-HIF1 α interface. This work contrasted with the previous study that fragments had higher ligand efficiency than the larger compounds they were part of and the results pointed to the possibility that current fragment screens against PPIs may be missing interesting fragments because of the inherently low ligand efficiencies associated with binding small molecules at protein surfaces.

NRF2-KEAP1 The nuclear factor erythroid 2-related factor 2 (NRF2) has emerged as a master regulator of cellular resistance to oxidants, mediating the upregulation of multiple phase 2 and cytoprotective enzymes and proteins. The protein Kelch-like ECH-associated protein 1 (KEAP1) plays a key role in the regulation of NRF2. Davies and his colleagues [115] applied a crystallographic screening of approximately 330 fragments, then identified three discrete hot spots within the NRF2 site and found the three novel fragments bound to three hot spots independently (Fig. 6.26). Fragment 1 with a carboxylic acid group were identified as a promising anchor fragment engaged in a key electrostatic interaction with

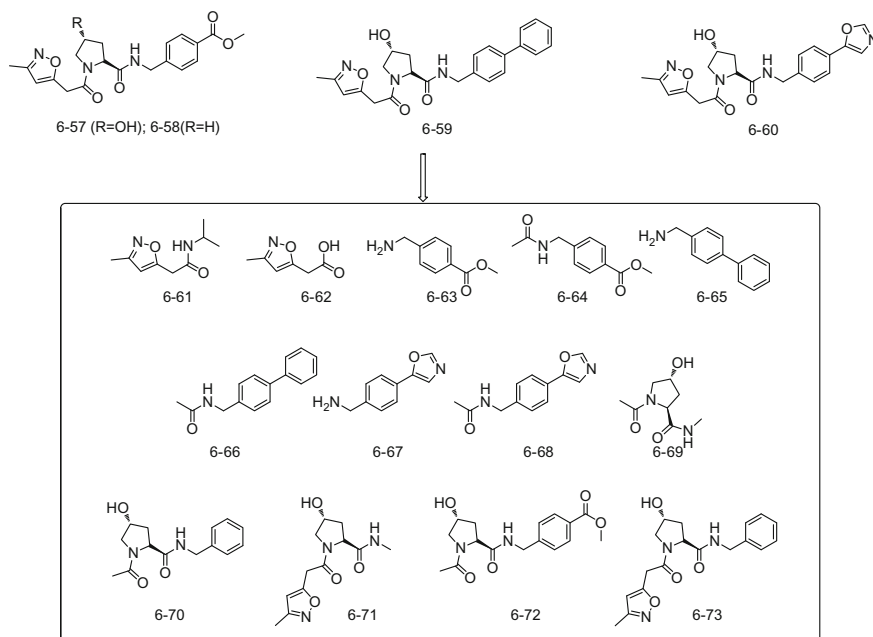


Fig. 6.25 The deconstruction of pVHL–HIF1 α inhibitors

Arg483 on the KEAP1 Kelch domain. Starting from fragment 6-74, fragment growth from the benzylic carbon would add more interactions with the hot spot occupied by fragment 6-75, while growth from the phenyl ring, at the direction ortho to the chlorine, would allow access to the subsite bound by the sulfonamide fragment 6-76. The fragment linking method was then adopted for the subsequent modification. The benzotriazole moiety was chosen for attachment directly to the benzylic carbon of the phenyl acetic acid and showed a dramatic increase in affinity to allow detection using the FP assay and ITC ($IC_{50} = 61 \mu\text{M}$; $ITC K_d = 59 \mu\text{M}$), growth from the 3-position of the chlorophenyl ring with a sulfonamide group, and replacement of the para-chloro-phenyl with methyl led to the identification of a very potent compound 6-77 ($ITC K_d = 1.3 \text{ nM}$). This compound fulfills the three-point pharmacophore identified from the fragment screen, suggesting the utility of their fragment-based approach.

RAD51-BRCA2 Scott et al. [116] described a fragment-based approach targeting the interaction between the tumor suppressor BRCA2 and the recombination enzyme RAD51. The first step in the biophysical screening of the fragment library was a thermal-shift screen against the MAYSAM mutant of RadA by monitoring the thermal unfolding temperature (T_m) of the protein by using a sensitive dye that fluoresces when the protein unfolds. Two compounds (6-78 and 6-79), which gave thermal shifts of +2 and +1.5 $^{\circ}\text{C}$, respectively, were selected for the saturation transfer difference (STD) NMR spectroscopy experiments to confirm the ability of

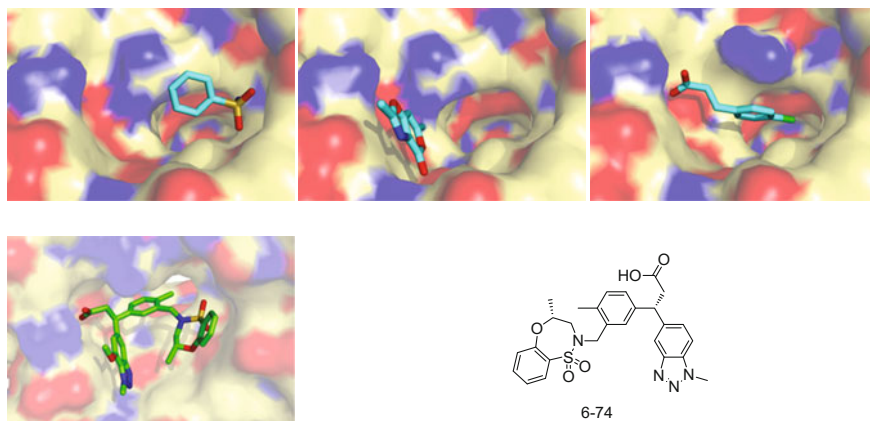
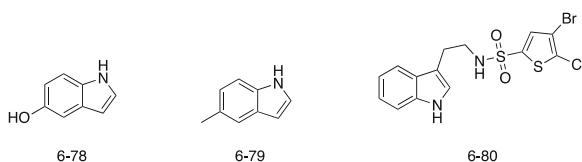


Fig. 6.26 The development of NRF2 inhibitors. Fragment **6-74** (PDB code: 5FNQ); fragment **6-75** (PDB code:5FZJ); fragment **6-76** (PDB code:5FZN); co-crystal structure of compound **6-77** (PDB code:5FNU)

Fig. 6.27 The development of RAD51 inhibitors



ligand binding (Fig. 6.27). And these two compounds were found to bind with a K_d of 2.1 mM with ligand efficiencies of 0.36, consistent with the competition experiment performed by ITC method. Based on the evidences for the binding site of the fragments, the indole scaffold was chosen as the starting point for SAR study, and finally compound 6-80 was discovered as the most potent compound with K_D of 1.3 μ M, demonstrating a successful optimization with 1000-fold improvement over the original fragment.

6.3 Conclusion

The approval of the first Bcl2 inhibitor venetoclax has been an important milestone for developing PPIs with fragment-based methodology. Currently, there are a large number of drugs in clinical trials that were discovered using fragment-based methods, reinforcing the utility of this efficient approach. Although the protein-protein interaction placed a big obstacle to develop small molecular drugs, over several decades of evolution, the fragment-based drug discovery can not only aid to identify the hot spots at the interface of PPIs, also provide novel starting points for

elaboration into drug candidates. In order to integrate the FBDD in developing drugs of PPIs, the researchers need to incorporate more 3D-type molecules in the fragment library to meet the complex surface of PPIs. The sensitivity of biophysical tools in fragment assay has been improved constantly, empowering us to find more fragment hits even for difficult targets. As interface of PPIs is usually containing several hot spots, the fragment linking approach will be increased in use for optimization. Giving many successful case studies we have introduced, we expect the combination of PPI with FBDD will expand our ability to tackle difficult targets and provide novel bioactive compounds for the next generation of therapeutics.

References

1. Yamada T, Bork P (2009) Evolution of biomolecular networks: lessons from metabolic and protein interactions. *Nat Rev Mol Cell Biol* 10(11):791–803. <https://doi.org/10.1038/nrm2787>
2. Ryan CJ, Cimermancic P, Szpiech ZA, Sali A, Hernandez RD, Krogan NJ (2013) High-resolution network biology: connecting sequence with function. *Nat Rev Genet* 14(12):865–879. <https://doi.org/10.1038/nrg3574>
3. Chakraborty C, Doss CG, Chen L, Zhu H (2014) Evaluating protein-protein interaction (PPI) networks for diseases pathway, target discovery, and drug-design using ‘in silico pharmacology’. *Curr Protein Pept Sci* 15(6):561–571
4. Szklarczyk D, Franceschini A, Wyder S, Forslund K, Heller D, Huerta-Cepas J, Simonovic M, Roth A, Santos A, Tsafou KP, Kuhn M, Bork P, Jensen LJ, von Mering C (2015) STRING v10: protein-protein interaction network, integrated over the tree of life. *Nucleic Acids Res* 43(Database issue):D447–D452. <https://doi.org/10.1093/nar/gku1003>
5. Higuero AP, Jubb H, Blundell TL (2013) TIMBAL v2: update of a database holding small molecules modulating protein-protein interactions. *Database: J Biol Databases Curation* 2013:bat039. <https://doi.org/10.1093/database/bat039>
6. Basse MJ, Betzi S, Morelli X, Roche P (2016) 2P2Idb v2: update of a structural database dedicated to orthosteric modulation of protein-protein interactions. *Database: J Biol Databases Curation* 2016. <https://doi.org/10.1093/database/baw007>
7. Bickerton GR, Higuero AP, Blundell TL (2011) Comprehensive, atomic-level characterization of structurally characterized protein-protein interactions: the PICCOLO database. *BMC Bioinform* 12:313. <https://doi.org/10.1186/1471-2105-12-313>
8. Coelho ED, Arrais JP, Oliveira JL (2013) From protein-protein interactions to rational drug design: are computational methods up to the challenge? *Curr Top Med Chem* 13(5):602–618
9. Kar G, Kuzu G, Keskin O, Gursoy A (2012) Protein-protein interfaces integrated into interaction networks: implications on drug design. *Curr Pharm Des* 18(30):4697–4705
10. DeLano WL (2002) Unraveling hot spots in binding interfaces: progress and challenges. *Curr Opin Struct Biol* 12(1):14–20
11. Moreira IS, Fernandes PA, Ramos MJ (2007) Hot spots—a review of the protein-protein interface determinant amino-acid residues. *Proteins* 68(4):803–812. <https://doi.org/10.1002/prot.21396>
12. Chen J, Ma X, Yuan Y, Pei J, Lai L (2014) Protein-protein interface analysis and hot spots identification for chemical ligand design. *Curr Pharm Des* 20(8):1192–1200
13. Winter A, Higuero AP, Marsh M, Sigurdardottir A, Pitt WR, Blundell TL (2012) Biophysical and computational fragment-based approaches to targeting protein-protein interactions: applications in structure-guided drug discovery. *Q Rev Biophys* 45(4):383–426. <https://doi.org/10.1017/s0033583512000108>

14. Scott DE, Coyne AG, Hudson SA, Abell C (2012) Fragment-based approaches in drug discovery and chemical biology. *Biochemistry* 51(25):4990–5003. <https://doi.org/10.1021/bi3005126>
15. Joseph-McCarthy D, Campbell AJ, Kern G, Moustakas D (2014) Fragment-based lead discovery and design. *J Chem Inf Model* 54(3):693–704. <https://doi.org/10.1021/ci400731w>
16. Erlanson DA, Fesik SW, Hubbard RE, Jahnke W, Jhoti H (2016) Twenty years on: the impact of fragments on drug discovery. *Nat Rev Drug Discovery* 15(9):605–619. <https://doi.org/10.1038/nrd.2016.109>
17. Jencks WP (1981) On the attribution and additivity of binding energies. *Proc Natl Acad Sci USA* 78(7):4046–4050
18. Verlinde CL, Rudenko G, Hol WG (1992) In search of new lead compounds for trypanosomiasis drug design: a protein structure-based linked-fragment approach. *J Comput Aided Mol Des* 6(2):131–147
19. Shuker SB, Hajduk PJ, Meadows RP, Fesik SW (1996) Discovering high-affinity ligands for proteins: SAR by NMR. *Science (New York, NY)* 274(5292):1531–1534
20. Rees DC, Congreve M, Murray CW, Carr R (2004) Fragment-based lead discovery. *Nat Rev Drug Discov* 3(8):660–672. <https://doi.org/10.1038/nrd1467>
21. Carr R, Jhoti H (2002) Structure-based screening of low-affinity compounds. *Drug Discov Today* 7(9):522–527
22. van Deursen R, Reymond JL (2007) Chemical space travel. *ChemMedChem* 2(5):636–640. <https://doi.org/10.1002/cmdc.200700021>
23. Hann MM, Leach AR, Harper G (2001) Molecular complexity and its impact on the probability of finding leads for drug discovery. *J Chem Inf Comput Sci* 41(3):856–864
24. Wilde F, Link A (2013) Advances in the design of a multipurpose fragment screening library. *Expert Opin Drug Discov* 8(5):597–606. <https://doi.org/10.1517/17460441.2013.780022>
25. Ray PC, Kiczun M, Huggett M, Lim A, Prati F, Gilbert IH, Wyatt PG (2017) Fragment library design, synthesis and expansion: nurturing a synthesis and training platform. *Drug Discov Today* 22(1):43–56. <https://doi.org/10.1016/j.drudis.2016.10.005>
26. Keseru GM, Erlanson DA, Ferenczy GG, Hann MM, Murray CW, Pickett SD (2016) Design principles for fragment libraries: maximizing the value of learnings from pharma fragment-based drug discovery (FBDD) programs for use in academia. *J Med Chem* 59(18):8189–8206. <https://doi.org/10.1021/acs.jmedchem.6b00197>
27. Congreve M, Carr R, Murray C, Jhoti H (2003) A ‘rule of three’ for fragment-based lead discovery? *Drug Discov Today* 8(19):876–877
28. Baell JB, Holloway GA (2010) New substructure filters for removal of pan assay interference compounds (PAINS) from screening libraries and for their exclusion in bioassays. *J Med Chem* 53(7):2719–2740. <https://doi.org/10.1021/jm901137j>
29. Huth JR, Mendoza R, Olejniczak ET, Johnson RW, Cothron DA, Liu Y, Lerner CG, Chen J, Hajduk PJ (2005) ALARM NMR: a rapid and robust experimental method to detect reactive false positives in biochemical screens. *J Am Chem Soc* 127(1):217–224. <https://doi.org/10.1021/ja0455547>
30. Morley AD, Pugliese A, Birchall K, Bower J, Brennan P, Brown N, Chapman T, Drysdale M, Gilbert IH, Hoelder S, Jordan A, Ley SV, Merritt A, Miller D, Swarbrick ME, Wyatt PG (2013) Fragment-based hit identification: thinking in 3D. *Drug Discov Today* 18(23–24):1221–1227. <https://doi.org/10.1016/j.drudis.2013.07.011>
31. Hennig M, Ruf A, Huber W (2012) Combining biophysical screening and X-ray crystallography for fragment-based drug discovery. *Top Curr Chem* 317:115–143. https://doi.org/10.1007/128_2011_225
32. Harner MJ, Frank AO, Fesik SW (2013) Fragment-based drug discovery using NMR spectroscopy. *J Biomol NMR* 56(2):65–75. <https://doi.org/10.1007/s10858-013-9740-z>
33. Navratilova I, Hopkins AL (2011) Emerging role of surface plasmon resonance in fragment-based drug discovery. *Future Med Chem* 3(14):1809–1820. <https://doi.org/10.4155/fmc.11.128>

34. Zhang R, Monsma F (2010) Fluorescence-based thermal shift assays. *Curr Opin Drug Discov Devel* 13(4):389–402
35. Pedro L, Quinn RJ (2016) Native mass spectrometry in fragment-based drug discovery. *Molecules* (Basel, Switzerland) 21(8). <https://doi.org/10.3390/molecules21080984>
36. Gossert AD, Jahnke W (2016) NMR in drug discovery: a practical guide to identification and validation of ligands interacting with biological macromolecules. *Prog Nucl Magn Reson Spectrosc* 97:82–125. <https://doi.org/10.1016/j.pnmrs.2016.09.001>
37. Davies TG, Tickle IJ (2012) Fragment screening using X-ray crystallography. *Top Curr Chem* 317:33–59. https://doi.org/10.1007/128_2011_179
38. Murray CW, Berdini V, Buck IM, Carr ME, Cleasby A, Coyle JE, Curry JE, Day JE, Day PJ, Hearn K, Iqbal A, Lee LY, Martins V, Mortenson PN, Munck JM, Page LW, Patel S, Roomans S, Smith K, Tamanini E, Saxty G (2015) Fragment-based discovery of potent and selective DDR1/2 inhibitors. *ACS Med Chem Lett* 6(7):798–803. <https://doi.org/10.1021/acsmedchemlett.5b00143>
39. Larsson EA, Jansson A, Ng FM, Then SW, Panicker R, Liu B, Sangthongpitag K, Pendharkar V, Tai SJ, Hill J, Dan C, Ho SY, Cheong WW, Poulsen A, Blanchard S, Lin GR, Alam J, Keller TH, Nordlund P (2013) Fragment-based ligand design of novel potent inhibitors of tankyrases. *J Med Chem* 56(11):4497–4508. <https://doi.org/10.1021/jm400211f>
40. Chavanieu A, Pugniere M (2016) Developments in SPR Fragment Screening. *Expert Opin Drug Discov* 11(5):489–499. <https://doi.org/10.1517/17460441.2016.1160888>
41. Neumann T, Junker HD, Schmidt K, Sekul R (2007) SPR-based fragment screening: advantages and applications. *Curr Top Med Chem* 7(16):1630–1642
42. Crawford TD, Ndubaku CO, Chen H, Boggs JW, Bravo BJ, Delatorre K, Giannetti AM, Gould SE, Harris SF, Magnuson SR, McNamara E, Murray LJ, Nonomiya J, Sambrone A, Schmidt S, Smyczek T, Stanley M, Vitorino P, Wang L, West K, Wu P, Ye W (2014) Discovery of selective 4-Amino-pyridopyrimidine inhibitors of MAP4K4 using fragment-based lead identification and optimization. *J Med Chem* 57(8):3484–3493. <https://doi.org/10.1021/jm500155b>
43. Navratilova I, Aristotelous T, Picaud S, Chaikuad A, Knapp S, Filappakopoulos P, Hopkins AL (2016) Discovery of New Bromodomain Scaffolds by Biosensor Fragment Screening. *ACS Med Chem Letters* 7(12):1213–1218. <https://doi.org/10.1021/acsmedchemlett.6b00154>
44. Riccardi Sirtori F, Caronni D, Colombo M, Dalvit C, Paolucci M, Regazzoni L, Visco C, Fogliatto G (2015) Establish an automated flow injection ESI-MS method for the screening of fragment based libraries: Application to Hsp90. *Eur J Pharm Sci: Off J Eur Fed Pharm Sci* 76:83–94. <https://doi.org/10.1016/j.ejps.2015.05.001>
45. Drinkwater N, Vu H, Lovell KM, Criscione KR, Collins BM, Prinszano TE, Poulsen SA, McLeish MJ, Grunewald GL, Martin JL (2010) Fragment-based screening by X-ray crystallography, MS and isothermal titration calorimetry to identify PNMT (phenylethanolamine N-methyltransferase) inhibitors. *Biochem J* 431(1):51–61. <https://doi.org/10.1042/bj20100651>
46. Wang L, Pratt JK, Soltwedel T, Sheppard GS, Fidanze SD, Liu D, Hasvold LA, Mantei RA, Holms JH, McClellan WJ, Wendt MD, Wada C, Frey R, Hansen TM, Hubbard R, Park CH, Li L, Magoc TJ, Albert DH, Lin X, Warder SE, Kovar P, Huang X, Wilcox D, Wang R, Rajaraman G, Petros AM, Hutchins CW, Panchal SC, Sun C, Elmore SW, Shen Y, Kati WM, McDaniel KF (2017) Fragment-Based structure-enabled discovery of novel pyridones and pyridone macrocycles as potent bromodomain and extra-terminal domain (BET) family bromodomain inhibitors. *J Med Chem* 60(9):3828–3850. <https://doi.org/10.1021/acs.jmedchem.7b00017>
47. Fjellström O, Akkaya S, Beisel HG, Eriksson PO, Erixon K, Gustafsson D, Jurva U, Kang D, Karis D, Knecht W, Nerme V, Nilsson I, Olsson T, Redzic A, Roth R, Sandmark J, Tigerström A, Öster L (2015) Creating novel activated factor XI inhibitors through fragment based lead generation and structure aided drug design. *PLoS One* 10(1):e0113705. <https://doi.org/10.1371/journal.pone.0113705>

48. Chilingaryan Z, Yin Z, Oakley AJ (2012) Fragment-based screening by protein crystallography: successes and pitfalls. *Int J Mol Sci* 13(10):12857–12879. <https://doi.org/10.3390/ijms131012857>
49. Sharff A, Jhoti H (2003) High-throughput crystallography to enhance drug discovery. *Curr Opin Chem Biol* 7(3):340–345
50. Caliandro R, Belviso DB, Aresta BM, de Candia M, Altomare CD (2013) Protein crystallography and fragment-based drug design. *Future Med Chem* 5(10):1121–1140. <https://doi.org/10.4155/fmc.13.84>
51. Saalau-Bethell SM, Woodhead AJ, Chessari G, Carr MG, Coyle J, Graham B, Hiscock SD, Murray CW, Pathuri P, Rich SJ, Richardson CJ, Williams PA, Jhoti H (2012) Discovery of an allosteric mechanism for the regulation of HCV NS3 protein function. *Nat Chem Biol* 8(11):920–925. <https://doi.org/10.1038/nchembio.1081>
52. Gill A, Cleasby A, Jhoti H (2005) The discovery of novel protein kinase inhibitors by using fragment-based high-throughput x-ray crystallography. *Chembiochem: Eur J Chem Biol* 6(3):506–512. <https://doi.org/10.1002/cbic.200400188>
53. Saalau-Bethell SM, Berdini V, Cleasby A, Congreve M, Coyle JE, Lock V, Murray CW, O'Brien MA, Rich SJ, Sambrook T, Vinkovic M, Yon JR, Jhoti H (2014) Crystal structure of human soluble adenylate cyclase reveals a distinct, highly flexible allosteric bicarbonate binding pocket. *ChemMedChem* 9(4):823–832. <https://doi.org/10.1002/cmdc.201300480>
54. Ludlow RF, Verdonk ML, Saini HK, Tickle IJ, Jhoti H (2015) Detection of secondary binding sites in proteins using fragment screening. *Proc Natl Acad Sci USA* 112(52):15910–15915. <https://doi.org/10.1073/pnas.1518946112>
55. Nikiforov PO, Surade S, Blaszczyk M, Delorme V, Brodin P, Baulard AR, Blundell TL, Abell C (2016) A fragment merging approach towards the development of small molecule inhibitors of *Mycobacterium tuberculosis* EthR for use as ethionamide boosters. *Org Biomol Chem* 14(7):2318–2326. <https://doi.org/10.1039/c5ob02630j>
56. Borsi V, Calderone V, Fragai M, Luchinat C, Sarti N (2010) Entropic contribution to the linking coefficient in fragment based drug design: a case study. *J Med Chem* 53(10):4285–4289. <https://doi.org/10.1021/jm901723z>
57. Edink E, Rucktooa P, Retra K, Akdemir A, Nahar T, Zuiderveld O, van Elk R, Janssen E, van Nierop P, van Muijlwijk-Koezen J, Smit AB, Sixma TK, Leurs R, de Esch IJ (2011) Fragment growing induces conformational changes in acetylcholine-binding protein: a structural and thermodynamic analysis. *J Am Chem Soc* 133(14):5363–5371. <https://doi.org/10.1021/ja110571r>
58. Potter A, Oldfield V, Nunns C, Fromont C, Ray S, Northfield CJ, Bryant CJ, Scrase SF, Robinson D, Matosova N, Baker L, Dokurno P, Surgenor AE, Davis B, Richardson CM, Murray JB, Moore JD (2010) Discovery of cell-active phenyl-imidazole Pin1 inhibitors by structure-guided fragment evolution. *Bioorg Med Chem Lett* 20(22):6483–6488. <https://doi.org/10.1016/j.bmcl.2010.09.063>
59. Mattos C, Bellamacina CR, Peisach E, Pereira A, Vitkup D, Petsko GA, Ringe D (2006) Multiple solvent crystal structures: probing binding sites, plasticity and hydration. *J Mol Biol* 357(5):1471–1482. <https://doi.org/10.1016/j.jmb.2006.01.039>
60. Brenke R, Kozakov D, Chuang GY, Beglov D, Hall D, Landon MR, Mattos C, Vajda S (2009) Fragment-based identification of druggable ‘hot spots’ of proteins using Fourier domain correlation techniques. *Bioinformatics (Oxford, England)* 25(5):621–627. <https://doi.org/10.1093/bioinformatics/btp036>
61. Kozakov D, Grove LE, Hall DR, Bohnuud T, Mottarella SE, Luo L, Xia B, Beglov D, Vajda S (2015) The FTMap family of web servers for determining and characterizing ligand-binding hot spots of proteins. *Nat Protoc* 10(5):733–755. <https://doi.org/10.1038/nprot.2015.043>
62. Randjelovic J, Eric S, Savic V (2014) In silico design of small molecule inhibitors of CDK9/cyclin T1 interaction. *J Mol Graph Model* 50:100–112. <https://doi.org/10.1016/j.jmgm.2014.04.002>

63. Arkin MR, Tang Y, Wells JA (2014) Small-molecule inhibitors of protein-protein interactions: progressing toward the reality. *Chem Biol* 21(9):1102–1114. <https://doi.org/10.1016/j.chembiol.2014.09.001>
64. Kim I, Xu W, Reed JC (2008) Cell death and endoplasmic reticulum stress: disease relevance and therapeutic opportunities. *Nat Rev Drug Discovery* 7(12):1013–1030. <https://doi.org/10.1038/nrd2755>
65. Kepp O, Galluzzi L, Lipinski M, Yuan J, Kroemer G (2011) Cell death assays for drug discovery. *Nat Rev Drug Discov* 10(3):221–237. <https://doi.org/10.1038/nrd3373>
66. Lessene G, Czabotar PE, Colman PM (2008) BCL-2 family antagonists for cancer therapy. *Nat Rev Drug Discov* 7(12):989–1000. <https://doi.org/10.1038/nrd2658>
67. Ashkenazi A, Fairbrother WJ, Leverson JD, Souers AJ (2017) From basic apoptosis discoveries to advanced selective BCL-2 family inhibitors. *Nat Rev Drug Discov* 16(4):273–284. <https://doi.org/10.1038/nrd.2016.253>
68. Fulda S, Vucic D (2012) Targeting IAP proteins for therapeutic intervention in cancer. *Nat Rev Drug Discov* 11(2):109–124. <https://doi.org/10.1038/nrd3627>
69. Vazquez A, Bond EE, Levine AJ, Bond GL (2008) The genetics of the p53 pathway, apoptosis and cancer therapy. *Nat Rev Drug Discov* 7(12):979–987. <https://doi.org/10.1038/nrd2656>
70. Oltersdorf T, Elmore SW, Shoemaker AR, Armstrong RC, Augeri DJ, Belli BA, Bruncko M, Deckwerth TL, Dinges J, Hajduk PJ, Joseph MK, Kitada S, Korsmeyer SJ, Kunzer AR, Letai A, Li C, Mitten MJ, Nettekheim DG, Ng S, Nimmer PM, O'Connor JM, Oleksijew A, Petros AM, Reed JC, Shen W, Tahir SK, Thompson CB, Tomaselli KJ, Wang B, Wendt MD, Zhang H, Fesik SW, Rosenberg SH (2005) An inhibitor of Bcl-2 family proteins induces regression of solid tumours. *Nature* 435(7042):677–681. <https://doi.org/10.1038/nature03579>
71. Friberg A, Vigil D, Zhao B, Daniels RN, Burke JP, Garcia-Barrantes PM, Camper D, Chauder BA, Lee T, Olejniczak ET, Fesik SW (2013) Discovery of potent myeloid cell leukemia 1 (Mcl-1) inhibitors using fragment-based methods and structure-based design. *J Med Chem* 56(1):15–30. <https://doi.org/10.1021/jm301448p>
72. Petros AM, Swann SL, Song D, Swinger K, Park C, Zhang H, Wendt MD, Kunzer AR, Souers AJ, Sun C (2014) Fragment-based discovery of potent inhibitors of the anti-apoptotic MCL-1 protein. *Bioorg Med Chem Lett* 24(6):1484–1488. <https://doi.org/10.1016/j.bmcl.2014.02.010>
73. Huang JW, Zhang Z, Wu B, Cellitti JF, Zhang X, Dahl R, Shiao CW, Welsh K, Emdadi A, Stebbins JL, Reed JC, Pellecchia M (2008) Fragment-based design of small molecule X-linked inhibitor of apoptosis protein inhibitors. *J Med Chem* 51(22):7111–7118. <https://doi.org/10.1021/jm8006992>
74. Chessari G, Buck IM, Day JE, Day PJ, Iqbal A, Johnson CN, Lewis EJ, Martins V, Miller D, Reader M, Rees DC, Rich SJ, Tamanini E, Vitorino M, Ward GA, Williams PA, Williams G, Wilsher NE, Woolford AJ (2015) Fragment-based drug discovery targeting inhibitor of apoptosis proteins: discovery of a non-alanine lead series with dual activity against cIAP1 and XIAP. *J Med Chem* 58(16):6574–6588. <https://doi.org/10.1021/acs.jmedchem.5b00706>
75. Estrada-Ortiz N, Neochoritis CG, Domling A (2016) How to design a successful p53-MDM2/X interaction inhibitor: a thorough overview based on crystal structures. *ChemMedChem* 11(8):757–772. <https://doi.org/10.1002/cmdc.201500487>
76. Fry DC, Wartchow C, Graves B, Janson C, Lukacs C, Kammloft U, Belunis C, Palme S, Klein C, Vu B (2013) Deconstruction of a nutlin: dissecting the binding determinants of a potent protein-protein interaction inhibitor. *ACS Med Chem Lett* 4(7):660–665. <https://doi.org/10.1021/ml400062c>
77. Boltjes A, Huang Y, van de Velde R, Rijkee L, Wolf S, Gaugler J, Lesniak K, Guzik K, Holak TA, Domling A (2014) Fragment-based library generation for the discovery of a peptidomimetic p53-Mdm4 inhibitor. *ACS Comb Sci* 16(8):393–396. <https://doi.org/10.1021/co500026b>

78. Wilson CY, Tolias P (2016) Recent advances in cancer drug discovery targeting RAS. *Drug Discov Today* 21(12):1915–1919. <https://doi.org/10.1016/j.drudis.2016.08.002>
79. Papke B, Der CJ (2017) Drugging RAS: know the enemy. *Science* 355(6330):1158–1163. <https://doi.org/10.1126/science.aam7622>
80. Spiegel J, Cromm PM, Zimmermann G, Grossmann TN, Waldmann H (2014) Small-molecule modulation of Ras signaling. *Nat Chem Biol* 10(8):613–622. <https://doi.org/10.1038/nchembio.1560>
81. Keeton AB, Salter EA, Piazza GA (2017) The RAS-Effector Interaction as a Drug Target. *Science* (New York, NY) 77 (2):221–226. <https://doi.org/10.1126/science.aam7622>. <https://doi.org/10.1158/0008-5472.can-16-0938>
82. Martin-Gago P, Fansa EK, Wittinghofer A, Waldmann H (2017) Structure-based development of PDEdelta inhibitors. *Biol Chem* 398(5–6):535–545. <https://doi.org/10.1515/hsz-2016-0272>
83. Maurer T, Wang W (2013) NMR study to identify a ligand-binding pocket in Ras. *The Enzymes* 33 Pt A:15–39. <https://doi.org/10.1016/b978-0-12-416749-0.00002-6>
84. Maurer T, Garrenton LS, Oh A, Pitts K, Anderson DJ, Skelton NJ, Fauber BP, Pan B, Malek S, Stokoe D, Ludlam MJ, Bowman KK, Wu J, Giannetti AM, Starovasnik MA, Mellman I, Jackson PK, Rudolph J, Wang W, Fang G (2012) Small-molecule ligands bind to a distinct pocket in Ras and inhibit SOS-mediated nucleotide exchange activity. *Proc Natl Acad Sci USA* 109(14):5299–5304. <https://doi.org/10.1073/pnas.1116510109>
85. Winter JJ, Anderson M, Blades K, Brassington C, Breeze AL, Chresta C, Embrey K, Fairley G, Faulder P, Finlay MR, Kettle JG, Nowak T, Overman R, Patel SJ, Perkins P, Spadola L, Tart J, Tucker JA, Wrigley G (2015) Small molecule binding sites on the Ras: SOS complex can be exploited for inhibition of Ras activation. *J Med Chem* 58(5):2265–2274. <https://doi.org/10.1021/jm501660t>
86. Wittinghofer A, Waldmann H, Bastiaens PI, Zimmermann G, Papke B, Ismail S, Vartak N, Chandra A, Hoffmann M, Hahn SA, Triola G, Wittinghofer A, Bastiaens PI, Waldmann H (2013) Small molecule inhibition of the KRAS-PDEdelta interaction impairs oncogenic KRAS signalling. *Nat Commun* 497(7451):638–642. <https://doi.org/10.1038/ncomms11360>. <https://doi.org/10.1038/nature12205>
87. Papke B, Murarka S, Vogel HA, Martin-Gago P, Kovacevic M, Truxius DC, Fansa EK, Ismail S, Zimmermann G, Heinelt K, Schultz-Fademrecht C, Al Saabi A, Baumann M, Nussbaumer P (2016) Identification of pyrazolopyridazinones as PDEdelta inhibitors. *Identification of pyrazolopyridazinones as PDEdelta inhibitors* 7:11360. <https://doi.org/10.1038/ncomms11360>
88. Martin-Gago P, Fansa EK, Klein CH, Murarka S, Janning P, Schurmann M, Metz M, Ismail S, Schultz-Fademrecht C, Baumann M, Bastiaens PI, Wittinghofer A, Waldmann H (2017) A PDE6delta-KRas inhibitor chemotype with up to seven H-bonds and picomolar affinity that prevents efficient inhibitor release by Arl2. *Angew Chem Int Ed Engl* 56 (9):2423–2428. <https://doi.org/10.1002/anie.201610957>
89. Tough DF, Tak PP, Tarakhovskiy A, Prinjha RK (2016) Epigenetic drug discovery: breaking through the immune barrier. *Nat Rev Drug Discov* 15(12):835–853. <https://doi.org/10.1038/nrd.2016.185>
90. Shortt J, Ott CJ, Johnstone RW, Bradner JE (2017) A chemical probe toolbox for dissecting the cancer epigenome. *Nat Rev Cancer* 17(3):160–183. <https://doi.org/10.1038/nrc.2016.148>
91. Arrowsmith CH, Bountra C, Fish PV, Lee K, Schapira M (2012) Epigenetic protein families: a new frontier for drug discovery. *Nat Rev Drug Discovery* 11(5):384–400. <https://doi.org/10.1038/nrd3674>
92. Kaniskan HU, Jin J (2015) Chemical probes of histone lysine methyltransferases. *ACS Chem Biol* 10(1):40–50. <https://doi.org/10.1021/cb500785t>
93. He Y, Korboukh I, Jin J, Huang J (2012) Targeting protein lysine methylation and demethylation in cancers. *Acta Biochim Biophys Sin* 44(1):70–79. <https://doi.org/10.1093/abbs/gmr109>

94. Scheufler C, Mobitz H, Gaul C, Ragot C, Be C, Fernandez C, Beyer KS, Tiedt R, Stauffer F (2016) Optimization of a fragment-based screening hit toward potent DOT1L inhibitors interacting in an induced binding pocket. *ACS Med Chem Lett* 7(8):730–734. <https://doi.org/10.1021/acsmchemlett.6b00168>
95. Ferreira de Freitas R, Eram MS, Szewczyk MM, Steuber H, Smil D, Wu H, Li F, Senisterra G, Dong A, Brown PJ, Hitchcock M, Moosmayer D, Stegmann CM, Egner U, Arrowsmith C, Barysyt-Lovejoy D, Vedadi M, Schapira M (2016) Discovery of a potent Class I protein arginine methyltransferase fragment inhibitor. *J Med Chem* 59(3):1176–1183. <https://doi.org/10.1021/acs.jmedchem.5b01772>
96. Jiao L, Liu X (2015) Structural basis of histone H3K27 trimethylation by an active polycomb repressive complex 2. *Science (New York, NY)* 350 (6258):aac4383. <https://doi.org/10.1126/science.aac4383>
97. Lingel A, Sendzik M, Huang Y (2017) Structure-guided design of EED binders allosterically inhibiting the epigenetic polycomb repressive complex 2 (PRC2) methyltransferase. *60* (1):415–427. <https://doi.org/10.1021/acs.jmedchem.6b01473>
98. Fujisawa T, Filippakopoulos P (2017) Functions of bromodomain-containing proteins and their roles in homeostasis and cancer. *Nat Rev Mol Cell Biol* 18(4):246–262. <https://doi.org/10.1038/nrm.2016.143>
99. Filippakopoulos P, Knapp S (2014) Targeting bromodomains: epigenetic readers of lysine acetylation. *Nat Rev Drug Discovery* 13(5):337–356. <https://doi.org/10.1038/nrd4286>
100. Zeng L, Li J, Muller M, Yan S, Mujtaba S, Pan C, Wang Z, Zhou MM (2005) Selective small molecules blocking HIV-1 Tat and coactivator PCAF association. *J Am Chem Soc* 127 (8):2376–2377. <https://doi.org/10.1021/ja044885g>
101. Filippakopoulos P, Qi J, Picaud S, Shen Y, Smith WB, Fedorov O, Morse EM, Keates T, Hickman TT, Felletar I, Philpott M, Munro S, McKeown MR, Wang Y, Christie AL, West N, Cameron MJ, Schwartz B, Heightman TD, La Thangue N, French CA, Wiest O, Kung AL, Knapp S, Bradner JE (2010) Selective inhibition of BET bromodomains. *Nature* 468(7327):1067–1073. <https://doi.org/10.1038/nature09504>
102. Mirguet O, Gosmini R, Toum J, Clement CA, Barnathan M, Brusq JM, Mordaunt JE, Grimes RM, Crowe M, Pineau O, Ajakane M, Daugan A, Jeffrey P, Cutler L, Haynes AC, Smithers NN, Chung CW, Bamborough P, Uings JJ, Lewis A, Witherington J, Parr N, Prinjha RK, Nicodeme E (2013) Discovery of epigenetic regulator I-BET762: lead optimization to afford a clinical candidate inhibitor of the BET bromodomains. *J Med Chem* 56(19):7501–7515. <https://doi.org/10.1021/jm401088k>
103. Chung CW, Dean AW, Woolven JM, Bamborough P (2012) Fragment-based discovery of bromodomain inhibitors part I: inhibitor binding modes and implications for lead discovery. *J Med Chem* 55(2):576–586. <https://doi.org/10.1021/jm201320w>
104. Zhao L, Cao D, Chen T, Wang Y, Miao Z, Xu Y, Chen W, Wang X, Li Y, Du Z, Xiong B, Li J, Xu C, Zhang N, He J, Shen J (2013) Fragment-based drug discovery of 2-thiazolidinones as inhibitors of the histone reader BRD4 bromodomain. *J Med Chem* 56(10):3833–3851. <https://doi.org/10.1021/jm301793a>
105. Spiliotopoulos D, Caffisch A (2016) Fragment-based in silico screening of bromodomain ligands. *Drug Discov Today Technol* 19:81–90. <https://doi.org/10.1016/j.ddtec.2016.06.003>
106. Vidler LR, Brown N, Knapp S, Hoelder S (2012) Druggability analysis and structural classification of bromodomain acetyl-lysine binding sites. *J Med Chem* 55(17):7346–7359. <https://doi.org/10.1021/jm300346w>
107. Harner MJ, Chauder BA, Phan J, Fesik SW (2014) Fragment-based screening of the bromodomain of ATAD2. *J Med Chem* 57(22):9687–9692. <https://doi.org/10.1021/jm501035j>
108. Miller TC, Rutherford TJ, Birchall K, Chugh J, Fiedler M, Bienz M (2014) Competitive binding of a benzimidazole to the histone-binding pocket of the Pygo PHD finger. *ACS Chem Biol* 9(12):2864–2874. <https://doi.org/10.1021/cb500585s>
109. Tsao DH, Sutherland AG, Jennings LD, Li Y, Rush TS 3rd, Alvarez JC, Ding W, Dushin EG, Dushin RG, Haney SA, Kenny CH, Malakian AK, Nilakantan R, Mosyak L

- (2006) Discovery of novel inhibitors of the ZipA/FtsZ complex by NMR fragment screening coupled with structure-based design. *Bioorg Med Chem* 14(23):7953–7961. <https://doi.org/10.1016/j.bmc.2006.07.050>
110. Yin Z, Whittell LR, Wang Y, Jergic S, Liu M, Harry EJ, Dixon NE, Beck JL, Kelso MJ, Oakley AJ (2014) Discovery of lead compounds targeting the bacterial sliding clamp using a fragment-based approach. *J Med Chem* 57(6):2799–2806. <https://doi.org/10.1021/jm500122r>
111. Latham CF, La J, Tinetti RN, Chalmers DK, Tachedjian G (2016) Fragment based strategies for discovery of novel HIV-1 reverse transcriptase and integrase inhibitors. *Curr Top Med Chem* 16(10):1135–1153
112. Serrao E, Debnath B, Otake H, Kuang Y, Christ F, Debyser Z, Neamati N (2013) Fragment-based discovery of 8-hydroxyquinoline inhibitors of the HIV-1 integrase-lens epithelium-derived growth factor/p75 (IN-LEDGF/p75) interaction. *J Med Chem* 56(6):2311–2322. <https://doi.org/10.1021/jm301632e>
113. Ziarek JJ, Liu Y, Smith E, Zhang G, Peterson FC, Chen J, Yu Y, Chen Y, Volkman BF, Li R (2012) Fragment-based optimization of small molecule CXCL12 inhibitors for antagonizing the CXCL12/CXCR4 interaction. *Curr Top Med Chem* 12(24):2727–2740
114. Van Molle I, Thomann A, Buckley DL, So EC, Lang S, Crews CM, Ciulli A (2012) Dissecting fragment-based lead discovery at the von Hippel-Lindau protein: hypoxia inducible factor 1 α protein-protein interface. *Chem Biol* 19(10):1300–1312. <https://doi.org/10.1016/j.chembiol.2012.08.015>
115. Davies TG, Wixted WE, Coyle JE, Griffiths-Jones C, Hearn K, McMenamin R, Norton D, Rich SJ, Richardson C, Saxty G, Willems HM, Woolford AJ, Cottom JE, Kou JP, Yonchuk JG, Feldser HG, Sanchez Y, Foley JP, Bolognese BJ, Logan G, Podolin PL, Yan H, Callahan JF, Heightman TD, Kerns JK (2016) Monoacidic inhibitors of the Kelch-like ECH-associated protein 1: nuclear factor erythroid 2-related factor 2 (KEAP1: NRF2) protein-protein interaction with high cell potency identified by fragment-based discovery. *J Med Chem* 59(8):3991–4006. <https://doi.org/10.1021/acs.jmedchem.6b00228>
116. Scott DE, Ehebauer MT, Pukala T, Marsh M, Blundell TL, Venkitaraman AR, Abell C, Hyvonen M (2013) Using a fragment-based approach to target protein-protein interactions. *Chembiochem: Eur J Chem Biol* 14(3):332–342. <https://doi.org/10.1002/cbic.201200521>

Part II
Case Studies of Small-Molecule Inhibitors
of Protein-Protein Interactions

Chapter 7

Small Molecule Inhibitors Targeting New Targets of Protein-Protein Interactions



Liyan Yue, Wei Wan, Pan Xu, Linjuan Li, Chen Wang,
Yuanyuan Zhang, Heng Xu, Rukang Zhang, Junchi Hu, Wenchao Lu,
Hao Jiang and Cheng Luo

7.1 Introduction

Protein-protein interactions (PPIs) have long been considered as ‘undruggable’ targets due to their unique properties such as the large and flat interfaces, the lack of desirable endogenous ligands, or the involvement in large protein complexes. However, recent advances in technology and renewed understanding of PPIs mechanisms have led to notable successes in the development of small molecule inhibitors targeting PPIs [1].

Several databases are available to search inhibitors of protein-protein interactions (2P2Is or i-PPIs) based on information of targets as well as inhibitors, such as the 2P2I DB (<http://2p2idb.cnrs-mrs.fr>), the TIMBAL (<http://mordred.bioc.cam.ac.uk/timbal/>) and the iPPI-DB (<http://www.ippidb.cdithem.fr/>). PPIs included in these databases or other literature studies are usually categorized in terms of their structural information. In this chapter, we provided a list of PPIs and their inhibitors (Table 7.1) that would be useful for researchers to get a quick overview of this area. We divided these targets into six main categories according to their biological functions or the superfamilies that they belong to: (a) PPIs involve in epigenetic modifications; (b) components of the ubiquitin-mediated protein degradation processes; (c) PPIs in apoptosis pathways (and some apoptosis-related proteins are E3 ligases); (d) immune-related PPIs targets; (e) interactions between RAS superfamily proteins and their partners; and (f) PPIs in other pathways. Of course, it is impossible to cover all PPIs in our list, and we will focus on the development of small molecules against newly established and important targets in the following description.

L. Yue · W. Wan · P. Xu · L. Li · C. Wang · Y. Zhang
H. Xu · R. Zhang · J. Hu · W. Lu · H. Jiang · C. Luo (✉)
State Key Laboratory of Drug Research, Shanghai Institute of Materia Medica, Chinese
Academy of Sciences, 555 Zu chongzhi Road, Shanghai 201203, China
e-mail: cluo@simm.ac.cn

Table 7.1 PPIs and their small molecule inhibitors

Function/ superfamily	PPIs	Related disease	Inhibitors (and highest phase reached)	Key references
Epigenetics	EED-EZH2	Cancer	Astemizole, EED226, A-395	[2–4]
	MENIN-MLL	Cancer	MI-2, MI-2-2, MI-463, MI-503, MI-538, MIV-6R, DCZ_M123, ML227, Neomycin, Tobramycin, DC_YM21, Cpd8, 1a, MCP-1	[5–12]
Ubiquitin-mediated protein degradation	WDR5-MLL	Cancer	Peptidomimetic inhibitors (MM-101 and derivatives), WDR5-0101 and derivatives, OICR-9429, WDR5-47 and derivatives, biphenyl compounds (DDO-2117)	[10, 13–17]
	BRD2-4-T-H4KAc	Cancer	(+)-JQ1, I-BET762, MT1, dBET1, DUAL946(1), BI-2536, etc.	[18–23]
	L3MBTL1/2/3-H3K4me1 or -H4K20me2	Cancer	UNC669, UNC926, UNC928, UNC1679, UNC1215, UNC2533	[24–27]
	53BP1-H4K20me1/2 Spindlin1-H3K4me3	Cancer	UNC2170, UNC2892, A366	[28, 29]
	CBX7-H3K27me2/3	Cancer	MS37452, MS351	[30, 31]
	JARID1A PHD3-H3K4me3	Cancer	Compounds 25-28, desethylamiodorone, IS19, CF1, CF2, CF4, CF16, CF18	[32, 33]
	Pygo-PHD-H3K4me2			
	Ubc13-Uev1A	Cancer	Leucettamol A, Manasterols A and B	[34]
	SCF	Cancer, inflammation, circadian-related disorders	Compound A, C1 series, etc.	[35]
	N-acetyl-UBC12-DCN1	Cancer	NAcM-HIT, NAcM-OPT, NAcM-COV	[36]
VHL-HIF1A	Cancer, chronic anemia, Ischemia	Hydroxyproline analogs, optimized compound 5 and compound 7	[37–40]	
MDM2-p53	Parkinson disease	Many molecules in clinic trials phase I-III	[1, 41]	

(continued)

Table 7.1 (continued)

Function/ superfamily	PPIs	Related disease	Inhibitors (and highest phase reached)	Key references
Apoptosis	MDM4(MDMX)-p53	Cancer, eye disorders, hematologic diseases	1,4,5-Trisubstituted imidazole-based compounds (MDM2/MDMX-p53), WK298, SI-172550, EEF1A2, ALRN-6924 (phase II, target both MDM2/p53 and MDMX/p53)	[42–46]
	IAPs-SMAC IAPs-CASPASE-9	Cancer	Birinapant (phase II), CUDC-427, LCL-161 (phase II), GDC-0152 (terminated), HGS-1029 (terminated), AT-406 (phase II), AEG-35156 (terminated), ASTX-660 (phase II), APG-1387	[1, 47]
Immune response	BCL2-Bax	Cancer	Many molecules in clinic trials, Venclexta (ABT-199, approved)	[1]
	MCL1-BH3	Cancer	Compound 8 (preclinical), 62, 60, 61, UMI-77	[48–50]
	S100B-p53	Cancer	SBi1-7 (SBi1, phase II), SBi132, SBi279, SBi523, SBi4211, SC0067, SC0332, SC0844, SC1982, SC124, SBi4172, SC1475, 10a	[51–55]
	CD4-gp120	HIV infection	NBD-556, NBD-557, (+)-DMJ-I-228, (+)-DMJ-II-121, other NBD-class and DMJ-class	[56, 57]
	Integrase-LEDGF	HIV infection	Acylhydrazone and hydrazine-based compounds, NPD series, CHEMBL2311902	[58–60]
Immune response	CD80/CD28	Autoimmune diseases	JBS2007_1, JBS2007_6, JBC277_2, BOMD11_6q	[61]
	LFA-ICAM (CD54)	Dry eye disease, anti-inflammatory	Lifitegrast (approved), statins like Lovastatin, Cinnamides, hydantoin-based compounds like BIRT-377, BMS-587101 (phase II), etc.	[62, 63]
	IL-2-IL-2R	Cancer, infectious disease, autoimmune disease	Ro26-4550, SP-4206	[64]
	TNF- α			[65–69]

(continued)

Table 7.1 (continued)

Function/ superfamily	PPIs	Related disease	Inhibitors (and highest phase reached)	Key references	
RAS superfamily		Cancer, neurologic diseases cardiovascular diseases; pulmonary diseases; diabetes; autoimmune and inflammatory disorders	SPD 304; C87; Quinclidine 15; Indoquinilididine 16; Erythrosine B; Japonicone A; IW927; AP-906/41640035; AG-690/11190044; AG-690/15438091	[70, 71]	
		Cancer	Sulfonamide derivatives (1) and (2), BMS and derivatives, peptidomimetic compounds, CA-170 (phase I)	[72–77]	
		Cancer	NSC-658497, compounds 1–14, DCAL, compounds 8–13, compound 6 and its analogs, SML-8-73-1	[78, 79]	
		Cancer	Rigosertib (phase III), MPI and its derivatives	[80–84]	
		Cancer	Deltazinone 1, benzimidazole derivatives, Pyridazinone inhibitors, Pyrazolopyridazinone derivatives	[85, 86]	
		Various disorders	EHT 1864, NSC23766	[87–89]	
		Cancer, asthma, pulmonary hypertension, type 2 diabetes, idiopathic pulmonary fibrothersis	G04, Y16, Compound A13		
	Others	VEGF–NRP1	Cancer	4 compounds with chlorobenzoyloxy alkyl/loxy halogenobenzyl amine scaffold, compound 1	[90, 91]
		VEGF–VEGFR	Cancer	Compound 4321, compound Y	[92]
		FAK–VEGFR3	Cancer	C4 and its analog 29	[93, 94]
ZipA–FtsZ		Bacterial infection	Indolo[2,3-a]quinolizin-7-one; carboxybiphenylindole inhibitors	[95–99]	
KEAP1–NRF2		Cancer, Alzheimer, neurodegeneration, diabetes, atherosclerosis, chronic obstructive pulmonary disease, cardiomyopathy, Ulcerative colitis,	CPUY192018, LH601A, benzenesulfonyl-pyrimidone, N-phenyl-benzenesulfonamide, AN-465/144580; cpd15, cpd16; Tetrahydroisoquinoline compounds;	[1, 100–105]	
Beta catenin–TCF-4		Cancer		[106–108]	

(continued)

Table 7.1 (continued)

Function/ superfamily	PPIs	Related disease	Inhibitors (and highest phase reached)	Key references
			PNU74654, LF3, PKF115-584, PKF118-310, PKF118-744, CGP049090, ZTM000990, iCRT3, iCRT5, iCRT14, TMP-D-27 ~ 38	
	SUR2-ESX	Cancer	Adamanolol, Wrenchmolol, Amphipathic-isoxazolidine, A-62176, CHO10	[109–113]
	Atox1, CCS	Cancer	DC_AC50	[114]
	Integrins	Bone diseases, Thrombosis, Psoriasis, Multiple sclerosis, ulcerative colitis, Asthma,	6-B345TTQ (preclinical), IPS-02001 (preclinical), Tirofiban (Aggrastat, approved), BMS-587101 (terminated), Firategrast (SB-683699, phase II), AJM300 (phase II), IVL745 (terminated), BIRT 377 (terminated), JSM6427 (phase I)	[115–121]
	RAD51–BRCA2	Cancer	Compound 7p	[122]
	Gα/RGS4	Schizophrenia	CCG-4986 (preclinical, 2014)	[123]
	PLK1 PDB domain	Cancer	Poloxin (approved), Purpurogallin (approved), Poloxipan (approved), etc.	[124–127]
	HPV–E2/E1	Cervical cancer, genital warts, condyloma	Indanedione-containing E1–E2 interaction inhibitors, AP611074 (phase II)	[128, 129]

7.2 PPIs in Epigenetics: The PRC2 Complex

Epigenetic signaling can be controlled by key protein families that write, erase, or read specific post-translational modifications (PTMs). While most epigenetic inhibitors are designed to directly target catalytic pockets of enzymes, the ‘reader’-histone targeting represents a unique therapeutic strategy to modulate both the chromatin state and activities of epigenetic ‘writers’ and ‘erasers.’ Especially, this strategy may provide inhibitors with fewer side effects due to the specificity in targets’ recognition of their substrates. The bromodomain and extraterminal (BET) subfamily proteins (BRD2-4 and BRDT) are well-characterized acetyl-lysine (KAc) ‘readers’ targets, and lots of inhibitors have emerged since the discovery of (+)-**JQ1** and **I-BET762** [130–132]. Moreover, efforts have been made to inhibit epigenetic enzymes through interfering with the protein complexes they constitute, the forms in which enzymes actually function.

The polycomb repressive complex 2 (PRC2) is so far the sole mammalian histone lysine methyltransferase (HKMT) complex that catalyzes histone H3 at lysine 27 (H3K27me1 to H3K27me3), a marker of gene silence [133]. Three core proteins are strictly required for the HKMT activity of PRC2: the enhancer of zeste (EZH1 or EZH2) that contains a SET domain and functions as methyltransferase, the embryonic ectoderm development (EED), and the suppressor of zeste 12 (SUZ12) (Fig. 7.1a–c). The complex containing EZH1 (PRC2–EZH1) shows lower methyltransferase activity than PRC2–EZH2 [133]. EED acts as both a scaffold and an H3K27 me3-binding protein in PRC2 complex [3].

7.2.1 EED–EZH2^{EBD}

Deregulated PRC2 and EZH2 are associated with the genesis and progression of various cancers, and the pharmaceutical industry has strived to develop small molecule inhibitors targeting the enzyme catalytic domain of EZH2 (to some extent EZH1) [134–136]. Recently, studies presented a new strategy to disable the complex that disrupting the interactions between the EBD domain of EZH2 and the EED protein (Fig. 7.1a), which is required for the integrity and methyltransferase activity of PRC2 [2, 137]. This has been achieved by a stabilized peptide or the small molecule **Astemizole**. Using a structure-based virtual screening (SBVS) method, Kong et al. identified **Astemizole**, an FDA-approved antihistamine drug for seasonal allergic rhinitis, to bind EED and inhibit EZH2–EED interactions (Fig. 7.1d) [2]. Several assays were applied, validating the competition with the EZH2 peptide by **Astemizole** on the EED surface. The disruption of EZH2–EED interactions by **Astemizole** destabilized PRC2 complex and led to PRC2’s methyltransferase activity inhibition in cancer cells. This finding emphasized the unique mechanism of inhibiting PRC2 by EZH2–EED disruptors that the degradation of core components contained in PRC2 were accelerated by the

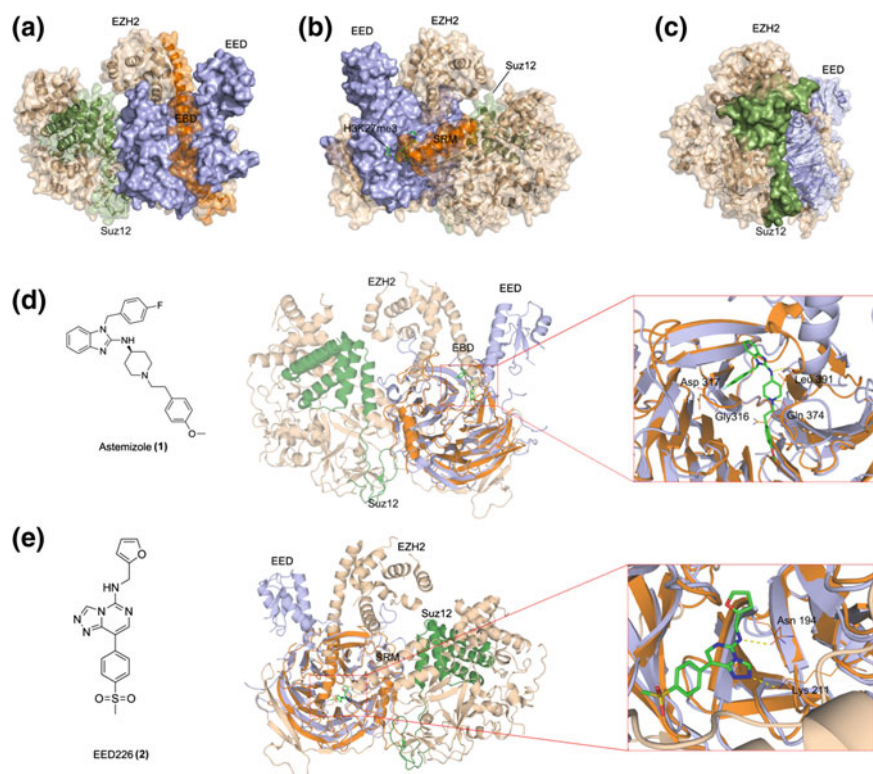


Fig. 7.1 Structure analysis and PPI inhibitors of PRC2 complex. **a** Structure analysis of the interface between EED and EBD domain of EZH2 (EZH2, wheat; EBD domain is shown in dashed oval, orange; EED, light blue; Suz12, forest; PDB ID: 5KJH). **b** Interface between EED and SRM domain of EZH2 (EZH2, wheat; SRM domain is shown in dashed oval, orange; EED, light blue; Suz12, forest; PDB ID: 5KJH). **c** Interface between EZH2 and Suz12 (EZH2, wheat; Suz12, forest; PDB ID: 5KJH). **d** The chemical structure of Astemizole and predicted binding model of Astemizole to EED by docking, which aligns to 5KJH, indicating Astemizole blocks the interactions between EED and EBD domain of EZH2 (Astemizole, green; predicted binding model, orange; EZH2, wheat; EED, light blue; Suz12, forest; PDB ID: 5KJH). **e** The chemical structure of EED226 and co-crystal structure of EED-EED226, which aligns to 5KJH, indicating EED226 blocks the interaction between EED and SRM domain of EZH2 (EED226, green; co-crystal structure of EED-EED226, orange; PDB ID 5GSA; EZH2, wheat; EED, light blue; Suz12, forest; PDB ID: 5KJH)

disassociation of the complex. Molecular modeling studies predicted the overlap of EED binding model between **Astemizole** and the EZH2 peptide (Fig. 7.1d) [2]; however, further structural work remains needed.

7.2.2 *EED–EZH2^{SRM} (or EED-Histone)*

In more recent time, several new structures of PRC2 components and sub-complexes were published and shed light on how proteins in the complex function together [138–140]. Structure determination also accelerated the structure-based drug design and discovery for PRC2. A new targetable protein-protein interaction interface formed by EED and the SRM domain of EZH2 was revealed (Fig. 7.1b). Using a high-throughput thermal shift assay (TSA) against EED protein, researchers have identified a series of small molecules that bound to EED and inhibited the PRC2 activity, such as **EED226** and **A-395** that with IC_{50} values of nanomolar level (Fig. 7.1e). The binding of inhibitors to EED didn't cause a dramatic conformational change at the EBD binding site. However, the well superimposition of inhibitor-bound EED and that of the activating H3K27 peptide bound PRC2 structure suggested the occupation of this compound in the H3K27me3-binding pocket of EED [4]. As the H3K27me3 recognition by EED induced a conformational change of the stimulation-responsive motif (SRM) in EZH2, which enhanced the PRC2 activity, the binding of these inhibitors competed with the activating peptide and thus prevented the allosteric activation of PRC2 [3]. This type of PPIs probes are distinct from and highly complementary to the current generation of EZH2 catalytic inhibitors, as cell lines with acquired resistance to SAM-competitive EZH2 inhibitors are still potently arrested [3]. These inhibitors were very close to SRM of EZH2 when composited to the PRC2 structure, but notice that it is still unclear whether they directly interfere with the EZH2^{SRM} [4].

Profited from the determination of complex structures, researchers are able to identify new targetable PPIs involved in epigenetic regulations, such as WDR5–MLL1 [10, 13–17, 141], MENIN–MLL [5–12, 141], and many methyl-lysine (Kme) 'readers' [141] (see Table 7.1). For the PRC2 complex, an extensive and characteristic hydrophobic surface that serves as the interface of SUZ12 with EZH2 has also been revealed (Fig. 7.1c), yet no inhibitor targeting this interface has ever been developed.

7.3 E3 Ligases

Ubiquitination is an evolutionarily conserved process that transfers the ubiquitin (Ub) to a wide array of substrate proteins through an E1–E2–E3 enzymatic cascade [142, 143]. It subsequently leads to signaling events or protein degradation through the proteasome [144–146]. The ubiquitin-mediated process has been reported to correlate with various pathological disorders [147] but is difficult to target by small molecules because of its dependence on a complex dynamic of multiple protein-protein interactions. In the last decade, drug developments focused heavily on proteasome inhibitors but serious non-specific side effects and drug resistance were observed in clinic. Recently, increasing efforts are devoted to discovering inhibitors

of specific components in the ubiquitin cascade system [148]. Compared with E1 and E2 inhibition, targeting the E3 related steps such as E2–E3 and the E3–substrate interactions or the binding of substrate to E3 adaptor proteins (Fig. 7.2a) may provide better specificity due to the high diversities of E3 ligase complexes. E3s can be divided into two types based on their mechanism of action and assembly: the RING family and the HECT family. Most of the human E3s belong to the RING family, which bring the E2 near the substrates to transfer of ubiquitin directly from E2 to the substrate, and there are only dozens of HECT E3s [149]. Several E3s involved PPIs and their inhibitors are listed in category (b), among which the IAPs, MDM2, and MDMX interact with proteins that are critical in apoptosis signaling pathways. What we mainly discussed below are achievements in two new targets: VHL–HIF1 α (E3–substrate) and SPOP–substrate (E3 adaptor–substrate) interactions.

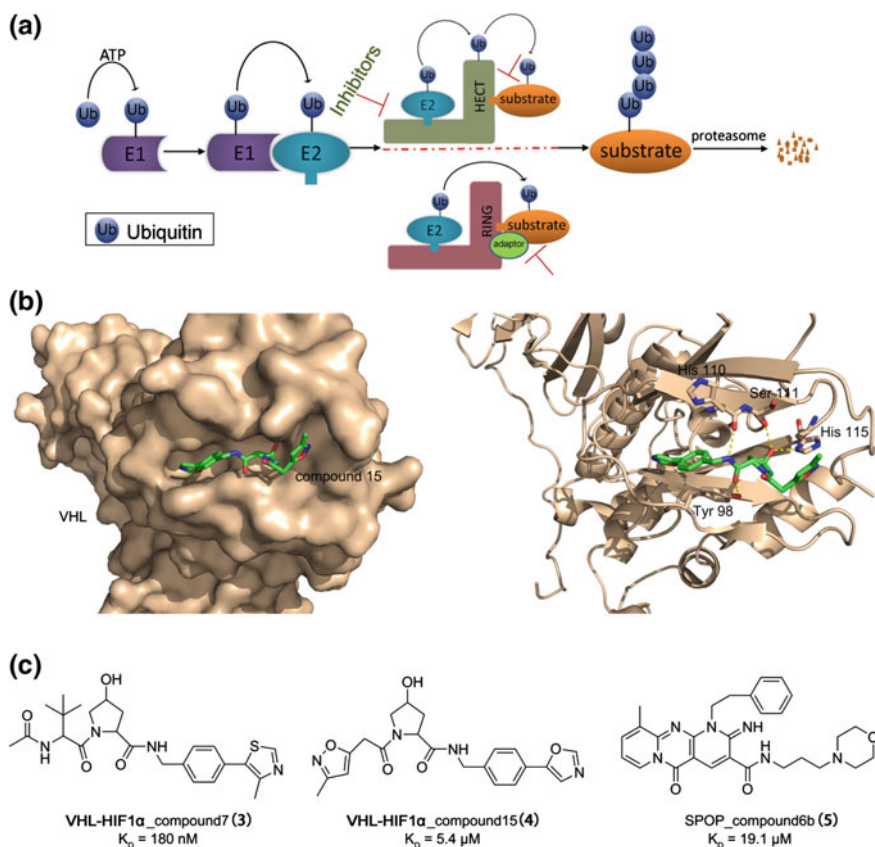


Fig. 7.2 Small molecule inhibitors targeting PPIs of E3 ligases. **a** Schema of ubiquitin-proteasome system and strategies for PPIs inhibitors of E3. **b** The co-crystal structure of compound 15 (green) bound to VHL (PDB ID: 3ZRC). **c** Representative small molecule inhibitors targeting the VHL–HIF1 α and SPOP–substrate interactions

7.3.1 VHL–HIF1 α Interaction

Von Hippel–Lindau disease (VHL) protein is the substrate recognition subunit of the E3 ubiquitin ligase VHL that consists of VHL, elongins B and C, cullin 2, and ring box protein 1 (Rbx1) [150]. The transcription factor hypoxia-inducible factor isoform 1 α (HIF1 α), which activates various genes such as vascular endothelial growth factor (VEGF), GLUT1, and erythropoietin [150], is a primary substrate of VHL. Under normoxic conditions, HIF1 α is activated by the prolyl hydroxylases domain (PHD) enzymes and provides a binding site for VHL, resulting in ubiquitination and proteasomal degradation [150, 151], thus keeping the very low level of HIF1 α in cells. In hypoxia, however, the hydroxylation processes are suppressed, leading to HIF1 α accumulation and genes upregulation [150]. Several PHD inhibitors are under examination in clinic trials for the treatment of chronic anemia or ischemia associated disorders. Whereas these inhibitors have caused the HIF-independent off-target effects [152], targeting the VHL–HIF1 α interactions would be an alternative or even better way to modulate HIF1 α .

Inspired by the key interaction formed by the hydroxyl-proline (Hyp564) of HIF1 α and VHL, Buckley et al. designed several hydroxyproline analogs using de novo design software BOMB [37]. After validation, two small hydroxyproline fragments were identified to bind VHL and were capable of disrupting the interaction between VHL and a HIF1 α peptide ($IC_{50} = 120 \mu\text{M}$). Chemistry optimization, especially the incorporation of halogenated benzylamines, led to **compound 15** ($K_D = 5.4 \mu\text{M}$, determined by ITC). Crystal structures of VHL-inhibitor complex revealed that the small molecule mimicked the binding mode of the HIF1 α peptide with VHL (Fig. 7.2b). Notably, a fragment-based lead discovery (FBLD) method was applied to analyze the key features of compounds that interacted with the hot spots of VHL [39]. Further structure–activity relationships (SAR) analyzation and structure-based drug design successfully improved the binding affinity of the molecule to the nanomolar level (**compound 7**, $K_D = 180 \text{ nM}$) [38, 40]. This work offered an excellent probe to validate VHL as a druggable target and emphasized the importance of using parallel structure-driven and metrics-driven design to target other E3 PPIs [40].

7.3.2 SPOP–Substrate Protein Interactions

The BTB domain-containing speckle-type POZ (pox virus and zinc finger protein) protein (SPOP) is an adaptor of the E3 ubiquitin ligase Cul3 [153, 154]. SPOP plays important roles in cancer development and tumorigenesis by mediating the ubiquitination of multiple substrates. Three domains are contained in SPOP: an N-terminal meprin and TRAF homology (MATH) domain, the internal BTB/POZ domain, and a C-terminal nuclear localization sequence. SPOP interacts with Cul3 using its BTB domain and mediates the specific substrate recognition through the

MATH sequences. Inhibition of the ubiquitin signal might be achieved through interfering with either the SPOP^{BTB}-Cul3 or SPOP^{MATH}-substrate interactions. Furthermore, overexpression of SPOP is found in 99% of the most common form of kidney cancer cell, clear cell renal cell carcinomas (RCCs) [155], thus making SPOP a potential antitumor target for treating ccRCC [156].

As structural studies revealed that SPOP^{MATH} specifically bound the SBC motif of its substrate [153], Guo et al. initiated the drug design based on one of the SPOP-substrate^{SBC} complex structures, SPOP-puc_SBC1 (PDB: 3HQL). The first small molecule inhibitors of SPOP-substrate, the compound **6a** [157] (IC₅₀ = 62 μM in FP assay), was identified using a combinative method of virtual screening, pharmacophore modeling, and molecular docking, and synthetic optimization subsequently led to the **compound 6b** (IC₅₀ = 35 μM). **6b** disrupted the SPOP-mediated protein interactions, inhibited the ubiquitination and degradation of tumor repressors PTEN and DUSP7, and decreased the downstream phosphorylation of AKT and ERK [157]. Especially, **compound 6b** displayed well specificity for killing human ccRCC cells and reduced the growth of ccRCC xenograft in nude mice [157], validating the SPOP-substrate interactions as an attractive drug target specific for ccRCC treatment. However, it remains to reveal whether the inhibitor target the MATH domain of SPOP or both MATH and BTB domain.

A lot of E3 ligase are discovered and investigated in recent years; for instance, the N-acetyl-UBC12-DCN1 interaction has already attracted much attention for drug development [36]. In addition, deubiquitinases (UBDs) are also essential targets for PPI drug discoveries. And no doubt the emergence of compounds targeting ubiquitin cascades will provide therapeutic benefits in the future.

7.4 Immune-Related New Targets

Protein-protein interactions are tightly regulated for proper functioning in diverse facets of immune response, such as signaling, antigen recognition, and cell-cell communication [158]. Lymphocyte function-associated antigen (LFA)-1, presented on the cell surface of immune cells, binds to the intracellular adhesion molecule (ICAM)-1 that located on the surface of endothelial cells, further enabling immune cells to migrate into neighboring tissue to initiate inflammation [159, 160]. Hence, Lifitegrast, an antagonist of ICAM-1/LFA-1, has been approved for the treatment of dry eye disease (DED), a common disorder associated with inflammation [62]. Another well-known case is the drug discovery that targets the tumor necrosis factor (TNF)-α [65–69]. Moreover, several new PPI targets in immune-related therapy have emerged during the last couple of years. Herein we will take gp120-CD4 and PD-1-PD-L1 interactions as examples to elaborate the essential roles of PPIs in anti-HIV therapy and oncology treatment, respectively.

7.4.1 CD4–gp120

The HIV-1 gp120 is a vital component of envelope (Env) glycoprotein. It binds to host CD4 receptor and mediates the attachment and entry of virus to the host cells, and thus, disrupting the CD4–gp120 interactions represents an efficient way to stop the virus in the early entry process [161]. The interaction interface formed by CD4 and gp120 buries a total surface of 742 Å² from CD4, and 802 Å² from gp120 [162], which are considerably smaller than the common protein-protein interaction contacts (vary from 1000 to 6000 Å²) [163]. More precisely, hydrophobic contacts, as well as electrostatic interactions, stabilize the binding of CD4 with gp120. Phe43 and Arg59 of CD4 contribute most to this interface; accordingly, the Phe43 cavity and Asp368 of gp120 are considered as hotspot residues [162]. All of these structural features throw light on the design of small molecules targeting the CD4–gp120 interactions.

Using an HIV-1 syncytium formation screening assay, Zhao et al. identified the first small molecules **NBD-556** and **NBD-557** disrupting CD4–gp120 interactions in 2005 [164]. Evidence suggested the binding of these two compounds at the ‘Phe 43 cavity’ of gp120 protein [165]. Especially, co-crystal structures of **NBD-556** with gp120 provided details of binding model that **NBD-556** bound gp120 and fixed the gp120 conformation of the CD4-bound state, with its phenyloxalamide moiety projecting deep into the Phe43 pocket [165, 166] (Fig. 7.3a). As the HIV fusion process requires two major conformational transitions of gp120: an unliganded to CD4-bound transition and a CD4-bound to co-receptor (CCR5)-triggered transition, **NBD-556** fixes the gp120 at its CD4-bound state and blocks the viral entry [166]. Combining ligand- and structure-based drug design methods, researchers were able to develop compounds with new scaffold and increased activity. The **NBD-09027** and **NBD-10007** (Fig. 7.3b), two representative compounds of the new-generation inhibitors, showed more potent antiviral activity than the precursors **NBD-556** and **NBD-557** [167]. Unfortunately, NBD-derived compounds effectively blocked the CD4-dependent viral entry but activated viral infectivity in CD4-negative cells [165], which hindered their further development. Since the CD4–gp120 interface is dominated by Phe43_{CD4} as well as the electrostatic interaction between Arg59_{CD4} and Asp368_{gp120}, efforts of dual hotspot design were made and a guanidinium moiety was added to the scaffold, yielding **AWS-I-169**, **DMJ-I-228**, and other DMJ series (Fig. 7.3b). Interestingly, these compounds are fully antagonists independent of CD4 expression [57, 168].

7.4.2 PD1–PD-L1

Cancer immunotherapy has made breakthrough progress in blocking immunologic checkpoints on immune cells with antibodies, for example targeting the interactions between the programmed death receptor 1 (PD-1) and its ligand PD-L1. PD-L1 is

expressed on the surface of immune cells and certain human cancer cells, whereas PD-1 is presented on the surface of immune effector cells. Binding of PD-1 to PD-L1 induces the exhaustion of antigen-specific effector T cells within the tumor microenvironment [169], so-called the cancer-induced immunosuppression. Blockage of PD-1–PD-L1 interactions can reverse the exhausted T cell phenotype and reactivate the antitumor response, providing the rationale for cancer targeted therapy [170]. In 2014, FDA approved two humanized monoclonal antibodies that target PD-1 and block its interaction with PD-L1: **Pembrolizumab** for treatment of metastatic melanoma and **Nivolumab** for non-small cell lung cancer [171]. The exciting clinic success of antibodies encourages the development of small molecule regulators, which would definitely be a next magic bullet. Moreover, small molecules are likely to overcome the typical drawbacks like limited tissue penetration, lacking oral bioavailability, and high expense in antibody-based immunotherapy [70].

However, the research into small molecule inhibitors targeting PD-1–PD-L1 interactions is hindered partly due to the insufficient structural information of this complex. Till 2015, Zak et al. determined the co-crystal structure of human PD-1–PD-L1 complex and provided a detailed molecular mechanism of this binding, including the hotspot residues in the interaction interface [172]. PD-1 and PD-L1 form a substantially flat and large surface extended to a total area of 1970 Å², which is rather difficult for small ligand binding (Fig. 7.4a). Even so, academic institutions and corporations have disclosed several small molecules, peptide mimics, and cyclo-peptides targeting PD-1–PD-L1 [70].

Bristol-Myers Squibb (BMS) has been working on designing small molecules targeting PD-1–PD-L1 interactions for years. In 2015, BMS disclosed a scaffold binding to PD-L1, resulting in PD-1 blockade [173]. The claimed compounds were investigated using a PD-1–PD-L1 homogenous time-resolved fluorescence (HTRF) assay and inhibited the PD-1–PD-L1 interactions with IC₅₀ values ranging from 6 nM to 10 μM. In the same year, BMS patented a series of compounds derived from the initial scaffold [174]. More recently, a new patent was applied by the same company, providing inhibitors of a more complicated scaffold [175]. Among these BMS compounds, **BMS-8** and **BMS-202** (Fig. 7.4b) bind directly to PD-L1 and block the formation of PD-1–PD-L1 complex. Moreover, they can induce the dimerization of PD-L1, thus keeping PD-L1 away from PD-1 [71].

Two heterocyclic-based scaffolds were termed by Incyte Corporation as immunomodulators capable of targeting the PD-1–PD-L1 interaction [176, 177]. However, no further biological activity was provided. Besides, researchers from Aurigene disclosed a oxadiazole compound and a thiadiazole compound inhibiting the PD1 signaling pathway [178]. More impressively, Curis licensed a first-in-class oral small molecule designated as **CA-170**. It can target the PD-1–PD-L1 and V-domain Ig suppressor or T cell activation (VISTA) pathways, and serves as a combination therapy. **CA-170** is now in phase I trials for patients with lymphomas and advanced solid tumor (NCT02812875).

PD-1–PD-L1 antagonists are proven useful in more indications, such as various cancers, viral or bacterial infections, and even the Alzheimers disease (AD).

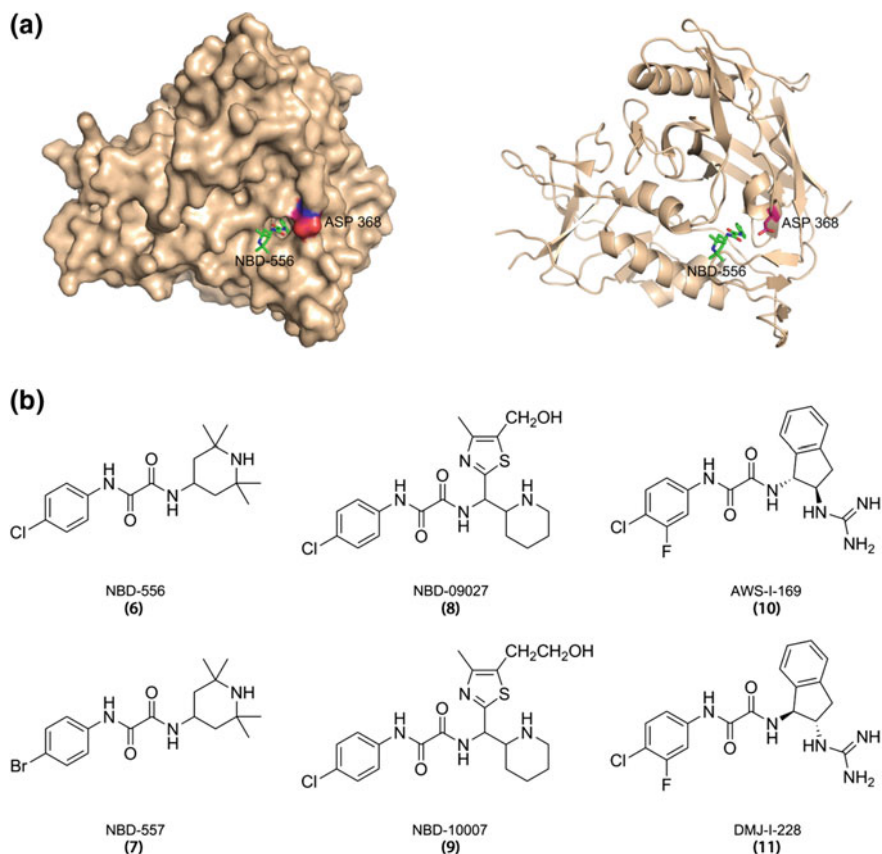


Fig. 7.3 Small molecule inhibitors of CD4–gp120 interactions. **a** The co-crystal structure of NBD-556 (green) bound to gp120 (PDB ID: 3TGS). **b** Representative small molecule inhibitors targeting CD4–gp120 interactions

Especially, small molecules might be advantageous in AD due to their blood–brain penetration [169]. However, the development of small molecules targeting PD-1–PD-L1 is at the very early stage, and it will take time to further validate the effectiveness of these inhibitors.

7.5 RTK Signaling Pathway

Vascular endothelial growth factor (VEGF) tyrosine kinase receptor system is a major driver of the angiogenesis process, which is essential for tumor invasion and metastasis [179–182]. There are five VEGF ligands in mammals: VEGF (VEGF-A), VEGF-B, VEGF-C, FIGF (VEGF-D), and PIGF. They bind with different specificity to the endothelial receptor tyrosine kinases (RTKs): VEGFR1-3,

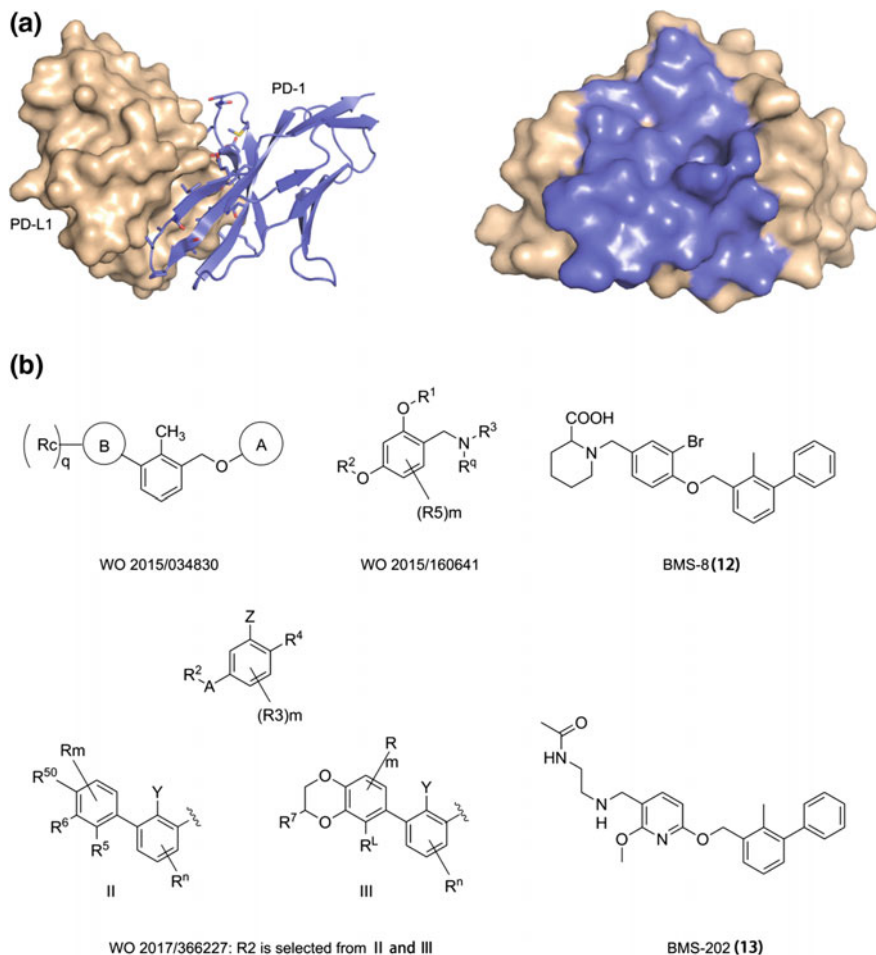


Fig. 7.4 Small molecule inhibitors targeting PD-1–PD-L1 interface. **a** The crystal structure of PD-1 (light blue)–PD-L1 (wheat) complex (PDB ID: 4ZQK) and the interface of PD-L1 (light blue). **b** Representative small molecules targeting PD-1–PD-L1 interactions

the co-receptors neuropilins (NRPs) and heparan sulfate proteoglycans (HSPG). Among these RTKs, VEGFR1, and VEGFR2 are primarily involved in angiogenesis [183]. VEGFR signaling is activated upon ligand binding and transmitted through MAPK, FAK, and PI3K pathways to promote cell proliferation, migration, and survival [184]. Nowadays, cancer therapies are usually conducted using monoclonal antibodies to neutralize VEGF or small molecule tyrosine kinase inhibitors to target the VEGF receptors [184]. The high price of antibodies and poor selectivity of tyrosine kinase inhibitors put forward the demand for small molecule inhibitors of novel mechanism, such as compounds targeting the VEGFR1/2/NRP–VEGF interfaces or the interactions between VEGFR3 and the extracellular tyrosine kinase FAK.

7.5.1 VEGFR1/2/NRP-VEGF

VEGFR1 acts as a receptor for VEGF-A, VEGF-B, PlGF, and TfsvVEGF, expressed in vascular endothelial and lots of non-endothelial cells [179, 180]. For angiogenesis, VEGFR1 is a negative regulator during early development, but an activator under pathological conditions. Gautier et al. carried out a theoretical prediction of potential pockets around the VEGF-VEGFR1 interaction interface but found that the surface was very large and flat. However, they defined three small sub-pockets that might be favorable to ligand binding (Fig. 7.5a) [92]. A total of 8,000 chemical compounds from a library were then docked onto the pockets for screening, validated by chemiluminescence assays and Water LOGSY NMR experiments. They finally identified 20 compounds disrupting the VEGF-VEGFR1 interactions, among which the best inhibitor **compound 4321** ($IC_{50} = 10 \mu M$, Fig. 7.5b) bound to VEGFR1 D2 (the second Ig domain) and inhibited the formation of the VEGF-VEGFR1 complex. Impressively, the inhibition of signaling pathway by **compound 4321** is more specific for VEGFR1 than VEGFR2.

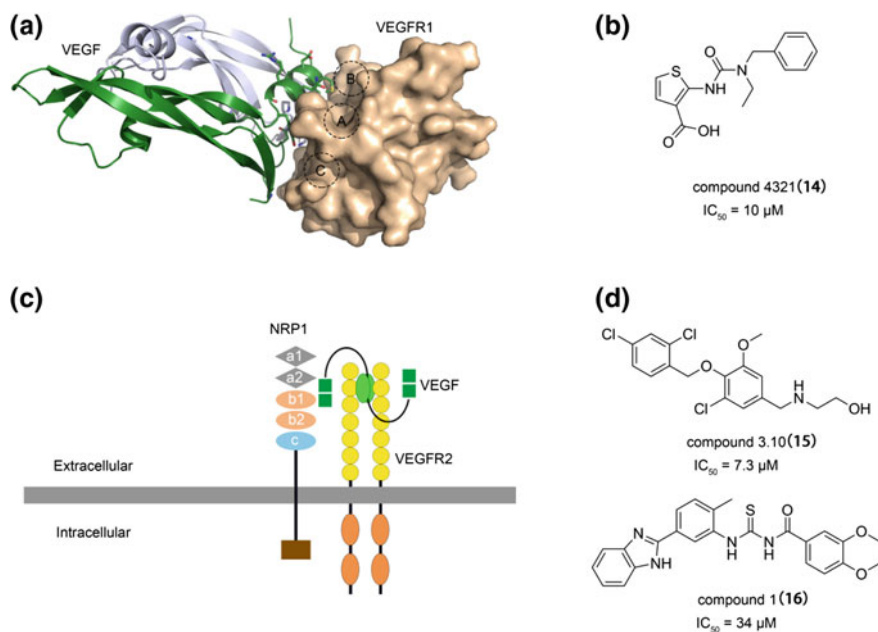


Fig. 7.5 VEGFR1/NRP1-VEGF interactions and their small molecule inhibitors. **a** Structure analysis of VEGF and VEGFR1. The interface of VEGF-VEGFR1 interactions is flat, but there are three small sub-pockets near (pockets A, B, and C are shown as dashed circles; surface of VEGFR1's D2 domain, wheat; cartoon of dimeric VEGF, forest and light blue; PDB ID: 1FLT). **b** Representative inhibitor of VEGF-VEGFR1. **c** Extracellular domain of NRP1 interaction with VEGF-A₁₆₅, in association with VEGFR2. **d** Small molecule inhibitors of VEGF-A₁₆₅-NRP1

VEGFR2 is the receptor for VEGF-A, and also binds to VEGF-E, the processed form of VEGF-C and VEGF-D. Compared with VEGFR-1, a kinase-impaired RTK, VEGFR-2 has a highly active kinase activity [183]. The role of VEGFR2 in angiogenesis, especially in cancer cell, is broadly recognized. A small molecule, **compound Y**, targeting the VEGF-VEGFR interactions is on the pipeline of a company named Interprotein in Japan. Interprotein indentified **compound Y** using a structure-based drug design method. With a desirable in vitro inhibitory activity against human umbilical vein endothelial cells, **compound Y** (40 mg/kg) showed a comparable efficacy with Avastin (5 mg/kg) in human colon adenocarcinoma cell strains (LS174T)-inoculated xenograft nude mice model. (Presentation of Hirotsugu KOMATSU, Ph.D. 'Drug discovery research for small molecule protein-protein interaction (PPI) modulators with unique in silico drug design strategy.' January 30, 2013.)

Neuropilins (NRPs) are transmembrane glycoproteins, non-tyrosine kinase receptors, and comprise of two homologues: NRP1 and NRP2 [90]. NRP1 binds VEGF-A₁₆₅, VEGF-B, PIGF-2 and some variants of VEGF-E in association with tyrosine kinase receptors like VEGFR2 (Fig. 7.5c). The formation of VEGFR2-NRP1 complex enhances the VEGF-A₁₆₅-induced cell proliferation and migration effects. Overexpression of NRP1 is found to correlate with the development of several cancer types [182, 185], making it an attractive target in cancer therapy. Structural studies revealed a VEGF-A₁₆₅ binding pocket on NRP1 surface that is deep enough for an arginine occupation. Two groups independently conducted structure-based virtual screenings for small molecule inhibitors disrupting the interactions between NRP1 and VEGF-A₁₆₅. Starzec et al. identified 4 compounds with a Ki about 10 μM in a biotinylated VEGF-A₁₆₅ displacement assay. These compounds share a chlorobenzoyloxy alkyloxy halogenobenzyl amine scaffold (**compound 3.10** as an example, Fig. 7.5d) [91]. In another virtual screening experiment, Borriello et al. monitored the blockage of VEGF-A₁₆₅-NRP1 protein-protein interactions by **compound 1** ($\text{IC}_{50} = 34 \mu\text{M}$, Fig. 7.5d). **Compound 1** showed potent anti-proliferative activity in breast cancer cells and was efficient to block angiogenesis and tumor growth in the MDA-MB-231-NOG xenografted mouse model of breast cancer [90].

7.5.2 FAK-VEGFR3

Focal adhesion kinase (FAK) is a protein tyrosine kinase, localized to focal contacts of extracellular matrix-integrin junctions, and is associated with cancer progression. It interacts with lots of binding partners, serving as a scaffold to direct many signaling pathways [186]. Compared with the FAK kinase inhibitors that target the FAK catalytic pocket (several inhibitors are being tested in clinical trials), compounds disabling the FAK complex might provide more potent inhibitory efficacy and less toxicity.

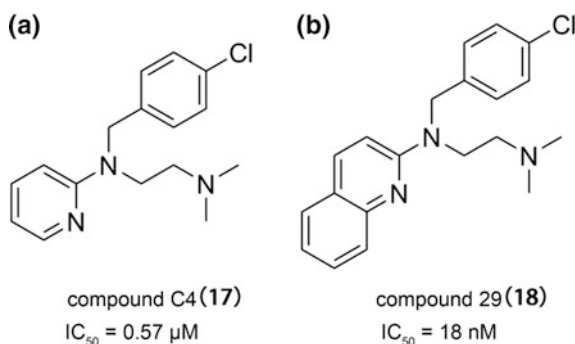


Fig. 7.6 Small molecule inhibitors of FAK–VEGFR3 interactions

VEGFR3, the receptor for VEGF-C and VEGF-D, binds to FAK at the C-terminal FAT domain. Garces et al. demonstrated that the interaction between VEGFR3 and FAK suppressed apoptosis of breast cancer cells [187], and they sought to develop small molecule inhibitors targeting this interaction site. Using a structure-based drug design method, they successfully discovered a **compound C4** (chloropyramine hydrochloride, Fig. 7.6a) that blocked the FAK–VEGFR3 binding and subsequent the phosphorylation of FAK [93]. The compound selectively induced apoptosis in many tumor cell lines and reduced tumor growth in breast cancer xenograft models [93]. A series of **C4** analogs were synthesized and evaluated for their binding affinities to FAK and anti-cancer activities, yielding the most potent analog **29** (Fig. 7.6b). **29** showed a binding constant of 18 nM and an enhanced anti-proliferative effect in multiple cancer cell lines [94]. Furthermore, studies of **29** validated its selectivity for VEGFR3 overexpressed cells [186]. Still, no co-crystal structure of FAK–PPI inhibitor complex has been reported and the analog **29** is currently under further development.

7.6 Copper-Trafficking Target: Atox1 and CCS

Functions as a catalytic cofactor for various enzymes, copper is essential for many life processes. The intracellular free copper is limited strictly under normal conditions, and the uncontrolled copper accumulation may cause serious toxicity. Once entering cells, copper binds to copper chaperone proteins such as Atox1 (antioxidant 1 copper chaperone) and CCS (copper chaperone for superoxide dismutase) and is then transferred to specific destinations through protein-protein interactions and ligand exchange between chaperones and target proteins [188]. These copper chaperones are essential for tumor cell survival, as the knockdown of Atox1 inhibits copper-stimulated proliferation in cancer cells but not normal cells [189]. Noticing this, Wang et al. aimed to develop small molecules targeting the protein-protein

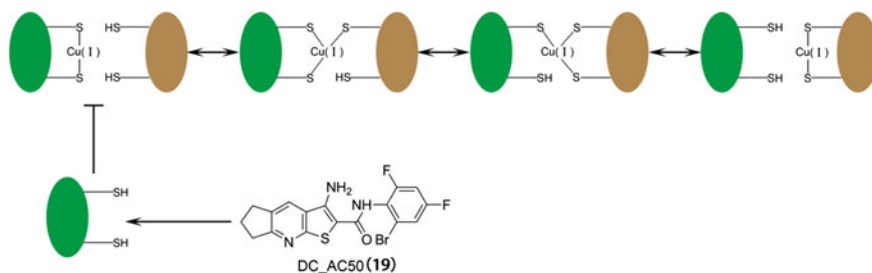


Fig. 7.7 Copper-trafficking in eukaryotes and the selective inhibition by the small molecule inhibitor DC_AC50. Green represents copper chaperone proteins, and brown represents proteins that receive copper from the chaperones

interactions mediated copper-trafficking processes, which may provide novel strategy for copper regulation and cancer therapy.

Based on the structure of copper chaperones and the established copper-transfer mechanism, they firstly applied a virtual screening on the Specs database containing more than 200,000 compounds and subsequently discovered a series of compounds that targeted the interface of Atox1 and CCS [114]. Compounds selected from the screening were subjected to a FRET-based assay for evaluating their inhibitory activity against the interactions between Atox1 and domain 4 of its copper-binding partner protein ATP7B (WD4). Finally, six potent compounds were identified, among which DC_AC50 (Fig. 7.7) stood out in both the FRET screening and the subsequent anti-cancer assays. DC_AC50 bound directly to potential copper-transfer interfaces of Atox1 and CCS proteins with the K_d about 6.8 μM for Atox1 and 8.2 μM for CCS, blocked copper-trafficking and resulted in cellular copper accumulation. This blockage induced cellular oxidative stress and a series of biochemical effects, which contributed to a specific proliferation inhibition in cancer cells and a significant reduction in tumor growth of mouse models. While the copper chelators commonly used have caused severe side effects, this finding provided a new and selective approach to regulate cellular copper transport that targeting the copper chaperones and their interactions with target proteins (Fig. 7.7).

7.7 Conclusion and Discussion

PPIs are difficult-to-drug targets but are clearly druggable (or at least inhibitable), and exciting achievements have gained in this area over the past decade. Many small molecule inhibitors of PPIs have reached clinic trails and several approved. For instance, Venetoclax (also named Venclexta or ABT-199), the inhibitor of BCL2 family, was approved for cancer treatment by FDA very recently in 2016. New progresses also made in bromodomain family, of which polypharmacological

agents such as dual kinase/BDT inhibitors and dual HDAC/BET inhibitors were developed [19, 22, 190], as well as proteolysis-targeting chimeras (PROTACs) that degrade BET family proteins [191, 192].

Impressively, many important PPIs were identified and well characterized as we discussed above. Novel strategies such as computational approaches (structure-based design or virtual screening) and the fragment-based design method contributed a lot to their successes. Another critical way to interfere with PPIs is the development of allosteric inhibitors (and to some extent means covalent inhibitor discovery). Researchers may learn a lot from RAS family (Table 7.1), of which most inhibitors don't directly target the protein-protein interfaces but bind to small G proteins and cause allosteric change in protein conformations, thus blocking the interactions between RAS and their cofactors and resulting in signaling inhibition [72, 73, 75–77, 193]. These findings also highlight the PPI disruption as an alternative and efficient way to target proteins with substrates of high binding affinity and hardly competed by inhibitors. Furthermore, targeting specific protein-protein interfaces may provide compounds with better selectivity, but notice that the target engagement of these inhibitors should be carefully evaluated.

New targets of PPIs and their small molecule inhibitors are continuing to emerge, providing benefits for mechanism researches and disease therapies. Meanwhile, targets that are of great clinical significance deserve further investigation, for example, the well-known PCSK9–LDLR interactions, an essential drug target for the treatment of familial hypercholesterolemia [194]. Though two monoclonal antibodies (**Evolocumab** and **Alirocumab**) targeting the PCSK9–LDLR interfaces are already available, small molecule inhibitors with better oral availability and lower cost may be more easily accepted by patients. However, no such inhibitor or probe has ever been reported. For drug developers, there is still a long way to go.

References

1. Scott DE, Bayly AR, Abell C, Skidmore J (2016) Small molecules, big targets: drug discovery faces the protein-protein interaction challenge. *Nat Rev Drug Discov* 15(8):533–550. <https://doi.org/10.1038/nrd.2016.29>
2. Kong X, Chen L, Jiao L, Jiang X, Lian F, Lu J, Zhu K, Du D, Liu J, Ding H, Zhang N, Shen J, Zheng M, Chen K, Liu X, Jiang H, Luo C (2014) Astemizole arrests the proliferation of cancer cells by disrupting the EZH2-EED interaction of polycomb repressive complex 2. *J Med Chem* 57(22):9512–9521. <https://doi.org/10.1021/jm501230c>
3. He Y, Selvaraju S, Curtin ML, Jakob CG, Zhu H, Comess KM, Shaw B, The J, Lima-Fernandes E, Szewczyk MM, Cheng D, Klinge KL, Li HQ, Pliushchev M, Algire MA, Maag D, Guo J, Dietrich J, Panchal SC, Petros AM, Sweis RF, Torrent M, Bigelow LJ, Senisterra G, Li F, Kennedy S, Wu Q, Osterling DJ, Lindley DJ, Gao W, Galasinski S, Barsyte-Lovejoy D, Vedadi M, Buchanan FG, Arrowsmith CH, Chiang GG, Sun C, Pappano WN (2017) The EED protein-protein interaction inhibitor A-395 inactivates the PRC2 complex. *Nat Chem Biol* 13(4):389–395. <https://doi.org/10.1038/nchembio.2306>

4. Qi W, Zhao K, Gu J, Huang Y, Wang Y, Zhang H, Zhang M, Zhang J, Yu Z, Li L, Teng L, Chuai S, Zhang C, Zhao M, Chan H, Chen Z, Fang D, Fei Q, Feng L, Feng L, Gao Y, Ge H, Ge X, Li G, Lingel A, Lin Y, Liu Y, Luo F, Shi M, Wang L, Wang Z, Yu Y, Zeng J, Zeng C, Zhang L, Zhang Q, Zhou S, Oyang C, Atadja P, Li E (2017) An allosteric PRC2 inhibitor targeting the H3K27me3 binding pocket of EED. *Nat Chem Biol* 13(4):381–388. <https://doi.org/10.1038/nchembio.2304>
5. Grembecka J, He S, Shi A, Purohit T, Muntean AG, Sorenson RJ, Showalter HD, Murai MJ, Belcher AM, Hartley T, Hess JL, Cierpicki T (2012) Menin-MLL inhibitors reverse oncogenic activity of MLL fusion proteins in leukemia. *Nat Chem Biol* 8(3):277–284. <https://doi.org/10.1038/nchembio.773>
6. Huang J, Gurung B, Wan B, Matkar S, Veniaminova NA, Wan K, Merchant JL, Hua X, Lei M (2012) The same pocket in menin binds both MLL and JUND but has opposite effects on transcription. *Nature* 482(7386):542–546. <https://doi.org/10.1038/nature10806>
7. He S, Senter TJ, Pollock J, Han C, Upadhyay SK, Purohit T, Gogliotti RD, Lindsley CW, Cierpicki T, Stauffer SR, Grembecka J (2014) High-affinity small-molecule inhibitors of the menin-mixed lineage leukemia (MLL) interaction closely mimic a natural protein-protein interaction. *J Med Chem* 57(4):1543–1556. <https://doi.org/10.1021/jm401868d>
8. Li L, Zhou R, Geng H, Yue L, Ye F, Xie Y, Liu J, Kong X, Jiang H, Huang J, Luo C (2014) Discovery of two aminoglycoside antibiotics as inhibitors targeting the menin-mixed lineage leukaemia interface. *Bioorg Med Chem Lett* 24(9):2090–2093. <https://doi.org/10.1016/j.bmcl.2014.03.055>
9. Borkin D, Pollock J, Kempinska K, Purohit T, Li X, Wen B, Zhao T, Miao H, Shukla S, He M, Sun D, Cierpicki T, Grembecka J (2016) Property focused structure-based optimization of small molecule inhibitors of the protein-protein interaction between menin and mixed lineage leukemia (MLL). *J Med Chem* 59(3):892–913. <https://doi.org/10.1021/acs.jmedchem.5b01305>
10. Getlik M, Smil D, Zepeda-Velazquez C, Bolshan Y, Poda G, Wu H, Dong A, Kuznetsova E, Marcellus R, Senisterra G, Dombrovski L, Hajian T, Kiyota T, Schapira M, Arrowsmith CH, Brown PJ, Vedadi M, Al-Awar R (2016) Structure-based optimization of a small molecule antagonist of the interaction between WD repeat-containing protein 5 (WDR5) and mixed-lineage leukemia 1 (MLL1). *J Med Chem* 59(6):2478–2496. <https://doi.org/10.1021/acs.jmedchem.5b01630>
11. Ren J, Xu W, Tang L, Su M, Chen D, Chen YL, Zang Y, Li J, Shen J, Zhou Y, Xiong B (2016) Design and synthesis of benzylpiperidine inhibitors targeting the menin-MLL1 interface. *Bioorg Med Chem Lett* 26(18):4472–4476. <https://doi.org/10.1016/j.bmcl.2016.07.074>
12. Xu Y, Yue L, Wang Y, Xing J, Chen Z, Shi Z, Liu R, Liu YC, Luo X, Jiang H, Chen K, Luo C, Zheng M (2016) Discovery of novel inhibitors targeting the menin-mixed lineage leukemia interface using pharmacophore- and docking-based virtual screening. *J Chem Inf Model* 56(9):1847–1855. <https://doi.org/10.1021/acs.jcim.6b00185>
13. Bolshan Y, Getlik M, Kuznetsova E, Wasney GA, Hajian T, Poda G, Nguyen KT, Wu H, Dombrovski L, Dong A, Senisterra G, Schapira M, Arrowsmith CH, Brown PJ, Al-Awar R, Vedadi M, Smil D (2013) Synthesis, Optimization, and Evaluation of Novel Small Molecules as Antagonists of WDR5-MLL Interaction. *ACS Med Chem Lett* 4(3):353–357. <https://doi.org/10.1021/ml300467n>
14. Senisterra G, Wu H, Allali-Hassani A, Wasney GA, Barsyte-Lovejoy D, Dombrovski L, Dong A, Nguyen KT, Smil D, Bolshan Y, Hajian T, He H, Seitova A, Chau I, Li F, Poda G, Couture JF, Brown PJ, Al-Awar R, Schapira M, Arrowsmith CH, Vedadi M (2013) Small-molecule inhibition of MLL activity by disruption of its interaction with WDR5. *Biochem J* 449(1):151–159. <https://doi.org/10.1042/BJ20121280>
15. Grebien F, Vedadi M, Getlik M, Giamb Bruno R, Grover A, Avellino R, Skucha A, Vittori S, Kuznetsova E, Smil D, Barsyte-Lovejoy D, Li F, Poda G, Schapira M, Wu H, Dong A, Senisterra G, Stukalov A, Huber KV, Schonegger A, Marcellus R, Bilban M, Bock C, Brown PJ, Zuber J, Bennett KL, Al-Awar R, Delwel R, Nerlov C, Arrowsmith CH,

- Superti-Furga G (2015) Pharmacological targeting of the Wdr5-MLL interaction in C/EBPalpha N-terminal leukemia. *Nat Chem Biol* 11(8):571–578. <https://doi.org/10.1038/nchembio.1859>
16. Li DD, Chen WL, Wang ZH, Xie YY, Xu XL, Jiang ZY, Zhang XJ, You QD, Guo XK (2016) High-affinity small molecular blockers of mixed lineage leukemia 1 (MLL1)-WDR5 interaction inhibit MLL1 complex H3K4 methyltransferase activity. *Eur J Med Chem* 124:480–489. <https://doi.org/10.1016/j.ejmech.2016.08.036>
 17. Li DD, Chen WL, Xu XL, Jiang F, Wang L, Xie YY, Zhang XJ, Guo XK, You QD, Sun HP (2016) Structure-based design and synthesis of small molecular inhibitors disturbing the interaction of MLL1-WDR5. *Eur J Med Chem* 118:1–8. <https://doi.org/10.1016/j.ejmech.2016.04.032>
 18. Filippakopoulos P, Qi J, Picaud S, Shen Y, Smith WB, Fedorov O, Morse EM, Keates T, Hickman TT, Felletar I, Philpott M, Munro S, McKeown MR, Wang Y, Christie AL, West N, Cameron MJ, Schwartz B, Heightman TD, La Thangue N, French CA, Wiest O, Kung AL, Knapp S, Bradner JE (2010) Selective inhibition of BET bromodomains. *Nature* 468(7327):1067–1073. <https://doi.org/10.1038/nature09504>
 19. Atkinson SJ, Soden PE, Angell DC, Bantscheff M, C-w Chung, Giblin KA, Smithers N, Furze RC, Gordon L, Drewes G, Rioja I, Witherington J, Parr NJ, Prinjha RK (2014) The structure based design of dual HDAC/BET inhibitors as novel epigenetic probes. *MedChemComm* 5(3):342. <https://doi.org/10.1039/c3md00285c>
 20. Ciceri P, Muller S, O'Mahony A, Fedorov O, Filippakopoulos P, Hunt JP, Lasater EA, Pallares G, Picaud S, Wells C, Martin S, Wodicka LM, Shah NP, Treiber DK, Knapp S (2014) Dual kinase-bromodomain inhibitors for rationally designed polypharmacology. *Nat Chem Biol* 10(4):305–312. <https://doi.org/10.1038/nchembio.1471>
 21. Nicodeme E, Jeffrey KL, Schaefer U, Beinke S, Dewell S, Chung CW, Chandwani R, Marazzi I, Wilson P, Coste H, White J, Kirilovsky J, Rice CM, Lora JM, Prinjha RK, Lee K, Tarakhovskiy A (2010) Suppression of inflammation by a synthetic histone mimic. *Nature* 468(7327):1119–1123. <https://doi.org/10.1038/nature09589>
 22. Tanaka M, Roberts JM, Seo HS, Souza A, Paulk J, Scott TG, DeAngelo SL, Dhe-Paganon S, Bradner JE (2016) Design and characterization of bivalent BET inhibitors. *Nat Chem Biol* 12(12):1089–1096. <https://doi.org/10.1038/nchembio.2209>
 23. Winter GE, Buckley DL, Paulk J, Roberts JM, Souza A, Dhe-Paganon S, Bradner JE (2017) Phthalimide conjugation as a strategy for in vivo target protein degradation. *Science* 348(6241):1376–1391–1381
 24. Herold JM, Wigle TJ, Norris JL, Lam R, Korboukh VK, Gao C, Ingerman LA, Kireev DB, Senisterra G, Vedadi M, Tripathy A, Brown PJ, Arrowsmith CH, Jin J, Janzen WP, Frye SV (2011) Small-molecule ligands of methyl-lysine binding proteins. *J Med Chem* 54(7):2504–2511. <https://doi.org/10.1021/jm200045v>
 25. Herold JM, James LI, Korboukh VK, Gao C, Coil KE, Bua DJ, Norris JL, Kireev DB, Brown PJ, Jin J, Janzen WP, Gozani O, Frye SV (2012) Structure–activity relationships of methyl-lysine reader antagonists. *MedChemComm* 3(1):45–51. <https://doi.org/10.1039/c1md00195g>
 26. Camerino MA, Zhong N, Dong A, Dickson BM, James LI, Baughman BM, Norris JL, Kireev DB, Janzen WP, Arrowsmith CH, Frye SV (2013) The structure-activity relationships of L3MBTL3 inhibitors: flexibility of the dimer interface. *MedChemComm* 4(11):1501–1507. <https://doi.org/10.1039/C3MD00197K>
 27. James LI, Korboukh VK, Krichevsky L, Baughman BM, Herold JM, Norris JL, Jin J, Kireev DB, Janzen WP, Arrowsmith CH, Frye SV (2013) Small-molecule ligands of methyl-lysine binding proteins: optimization of selectivity for L3MBTL3. *J Med Chem* 56(18):7358–7371. <https://doi.org/10.1021/jm400919p>
 28. Sweis RF, Pliushchev M, Brown PJ, Guo J, Li F, Maag D, Petros AM, Soni NB, Tse C, Vedadi M, Michaelides MR, Chiang GG, Pappano WN (2014) Discovery and development of potent and selective inhibitors of histone methyltransferase g9a. *ACS Med Chem Lett* 5(2):205–209. <https://doi.org/10.1021/ml400496h>

29. Perfetti MT, Baughman BM, Dickson BM, Mu Y, Cui G, Mader P, Dong A, Norris JL, Rothbart SB, Strahl BD, Brown PJ, Janzen WP, Arrowsmith CH, Mer G, McBride KM, James LI, Frye SV (2015) Identification of a fragment-like small molecule ligand for the methyl-lysine binding protein, 53BP1. *ACS Chem Biol* 10(4):1072–1081. <https://doi.org/10.1021/cb500956g>
30. Ren C, Morohashi K, Plotnikov AN, Jakoncic J, Smith SG, Li J, Zeng L, Rodriguez Y, Stojanoff V, Walsh M, Zhou MM (2015) Small-molecule modulators of methyl-lysine binding for the CBX7 chromodomain. *Chem Biol* 22(2):161–168. <https://doi.org/10.1016/j.chembiol.2014.11.021>
31. Ren C, Smith SG, Yap K, Li S, Li J, Mezei M, Rodriguez Y, Vincek A, Aguilo F, Walsh MJ, Zhou MM (2016) Structure-guided discovery of selective antagonists for the chromodomain of polycomb repressive protein CBX7. *ACS Med Chem Lett* 7(6):601–605. <https://doi.org/10.1021/acsmchemlett.6b00042>
32. Wagner EK, Nath N, Flemming R, Feltenberger JB, Denu JM (2012) Identification and characterization of small molecule inhibitors of a plant homeodomain finger. *Biochemistry* 51(41):8293–8306. <https://doi.org/10.1021/bi3009278>
33. Miller TC, Rutherford TJ, Birchall K, Chugh J, Fiedler M, Bienz M (2014) Competitive binding of a benzimidazole to the histone-binding pocket of the Pygo PHD finger. *ACS Chem Biol* 9(12):2864–2874. <https://doi.org/10.1021/cb500585s>
34. Tsukamoto S (2016) Search for inhibitors of the ubiquitin-proteasome system from natural sources for cancer therapy. *Chem Pharm Bull* 64(2):112–118. <https://doi.org/10.1248/cpb.c15-00768>
35. Liu Y, Mallampalli RK (2016) Small molecule therapeutics targeting F-box proteins in cancer. *Semin Cancer Biol* 36:105–119. <https://doi.org/10.1016/j.semcancer.2015.09.014>
36. Scott DC, Hammill JT, Min J, Rhee DY, Connelly M, Sviderskiy VO, Bhasin D, Chen Y, Ong SS, Chai SC, Goktug AN, Huang G, Monda JK, Low J, Kim HS, Paulo JA, Cannon JR, Shelat AA, Chen T, Kelsall IR, Alpi AF, Pagala V, Wang X, Peng J, Singh B, Harper JW, Schulman BA, Guy RK (2017) Blocking an N-terminal acetylation-dependent protein interaction inhibits an E3 ligase. *Nat Chem Biol*. <https://doi.org/10.1038/nchembio.2386>
37. Buckley DL, Van Molle I, Gareiss PC, Tae HS, Michel J, Noblin DJ, Jorgensen WL, Ciulli A, Crews CM (2012) Targeting the von Hippel-Lindau E3 ubiquitin ligase using small molecules to disrupt the VHL/HIF-1 α interaction. *J Am Chem Soc* 134(10):4465–4468. <https://doi.org/10.1021/ja209924v>
38. Buckley DL, Gustafson JL, Van Molle I, Roth AG, Tae HS, Gareiss PC, Jorgensen WL, Ciulli A, Crews CM (2012) Small-molecule inhibitors of the interaction between the E3 ligase VHL and HIF1 α . *Angew Chem* 51(46):11463–11467. <https://doi.org/10.1002/anie.201206231>
39. Van Molle I, Thomann A, Buckley DL, So EC, Lang S, Crews CM, Ciulli A (2012) Dissecting fragment-based lead discovery at the von Hippel-Lindau protein: hypoxia inducible factor 1 α protein-protein interface. *Chem Biol* 19(10):1300–1312. <https://doi.org/10.1016/j.chembiol.2012.08.015>
40. Galdeano C, Gadd MS, Soares P, Scaffidi S, Van Molle I, Birced I, Hewitt S, Dias DM, Ciulli A (2014) Structure-guided design and optimization of small molecules targeting the protein-protein interaction between the von Hippel-Lindau (VHL) E3 ubiquitin ligase and the hypoxia inducible factor (HIF) α subunit with in vitro nanomolar affinities. *J Med Chem* 57(20):8657–8663. <https://doi.org/10.1021/jm5011258>
41. Nguyen D, Liao W, Zeng SX, Lu H (2017) Reviving the guardian of the genome: Small molecule activators of p53. *Pharmacol Ther*. <https://doi.org/10.1016/j.pharmthera.2017.03.013>
42. Popowicz GM, Czarna A, Wolf S, Wang K, Wang W, Domling A, Holak TA (2010) Structures of low molecular weight inhibitors bound to MDMX and MDM2 reveal new approaches for p53-MDMX/MDM2 antagonist drug discovery. *Cell Cycle* 9(6):1104–1111. <https://doi.org/10.4161/cc.9.6.10956>

43. Reed D, Shen Y, Shelat AA, Arnold LA, Ferreira AM, Zhu F, Mills N, Smithson DC, Regni CA, Bashford D, Cicero SA, Schulman BA, Jochemsen AG, Guy RK, Dyer MA (2010) Identification and characterization of the first small molecule inhibitor of MDMX. *J Biol Chem* 285(14):10786–10796. <https://doi.org/10.1074/jbc.M109.056747>
44. Twarda-Clapa A, Krzanik S, Kubica K, Guzik K, Labuzek B, Neochoritis CG, Khoury K, Kowalska K, Czub M, Dubin G, Domling A, Skalniak L, Holak TA (2017) 1,4,5-trisubstituted imidazole-based p53-MDM2/MDMX antagonists with aliphatic linkers for conjugation with biological carriers. *J Med Chem* 60(10):4234–4244. <https://doi.org/10.1021/acs.jmedchem.7b00104>
45. Wang H, Ma X, Ren S, Buolamwini JK, Yan C (2011) A small-molecule inhibitor of MDMX activates p53 and induces apoptosis. *Mol Cancer Ther* 10(1):69–79. <https://doi.org/10.1158/1535-7163.MCT-10-0581>
46. Pellegrino R, Calvisi DF, Neumann O, Kolluru V, Wesely J, Chen X, Wang C, Wuestefeld T, Ladu S, Elgohary N, Bermejo JL, Radlwimmer B, Zornig M, Zender L, Dombrowski F, Evert M, Schirmacher P, Longerich T (2014) EEF1A2 inactivates p53 by way of PI3 K/AKT/mTOR-dependent stabilization of MDM4 in hepatocellular carcinoma. *Hepatology* 59(5):1886–1899. <https://doi.org/10.1002/hep.26954>
47. Fulda S, Vucic D (2012) Targeting IAP proteins for therapeutic intervention in cancer. *Nat Rev Drug Discov* 11(2):109–124. <https://doi.org/10.1038/nrd3627>
48. Abulwerdi F, Liao C, Liu M, Azmi AS, Aboukameel A, Mady AS, Gulappa T, Cierpicki T, Owens S, Zhang T, Sun D, Stuckey JA, Mohammad RM, Nikolovska-Coleska Z (2014) A novel small-molecule inhibitor of mcl-1 blocks pancreatic cancer growth in vitro and in vivo. *Mol Cancer Ther* 13(3):565–575. <https://doi.org/10.1158/1535-7163.MCT-12-0767>
49. Pelz NF, Bian Z, Zhao B, Shaw S, Tarr JC, Belmar J, Gregg C, Camper DV, Goodwin CM, Arnold AL, Sensintaffar JL, Friberg A, Rossanese OW, Lee T, Olejniczak ET, Fesik SW (2016) Discovery of 2-Indole-acylsulfonamide Myeloid Cell Leukemia 1 (Mcl-1) Inhibitors Using Fragment-Based Methods. *J Med Chem* 59(5):2054–2066. <https://doi.org/10.1021/acs.jmedchem.5b01660>
50. Liu J, Tian Z, Zhou N, Liu X, Liao C, Lei B, Li J, Zhang S, Chen H (2017) Targeting the apoptotic Mcl-1-PUMA interface with a dual-acting compound. *Oncotarget*. <https://doi.org/10.18632/oncotarget.17294>
51. Yoshimura C, Miyafusa T, Tsumoto K (2013) Identification of small-molecule inhibitors of the human S100B–p53 interaction and evaluation of their activity in human melanoma cells. *Bioorg Med Chem* 21(5):1109–1115. <https://doi.org/10.1016/j.bmc.2012.12.042>
52. McKnight LE, Raman EP, Bezawada P, Kudrimoti S, Wilder PT, Hartman KG, Godoy-Ruiz R, Toth EA, Coop A, MacKerell AD, Weber DJ (2012) Structure-based discovery of a novel pentamidine-related inhibitor of the calcium-binding protein S100B. *ACS Med Chem Lett* 3(12):975–979. <https://doi.org/10.1021/ml3001665>
53. Wilder PT, Charpentier TH, Liriano MA, Gianni K, Varney KM, Pozharski E, Coop A, Toth EA, MacKerell AD (2010) Weber DJ (2010) In vitro screening and structural characterization of inhibitors of the S100B–p53 interaction. *Int J High Throughput Screen* 1:109–126. <https://doi.org/10.2147/IJHTS.S8210>
54. Charpentier TH, Wilder PT, Liriano MA, Varney KM, Zhong S, Coop A, Pozharski E, MacKerell AD, Toth EA, Weber DJ (2009) Small molecules bound to unique sites in the target protein binding cleft of calcium-bound S100B as characterized by nuclear magnetic resonance and X-ray crystallography. *Biochemistry* 48(26):6202–6212. <https://doi.org/10.1021/bi9005754>
55. Markowitz J, Chen I, Gitti R, Baldisseri DM, Pan Y, Udan R, Carrier F, MacKerell AD, Weber DJ (2004) Identification and characterization of small molecule inhibitors of the calcium-dependent S100B–p53 tumor suppressor interaction. *J Med Chem* 47(21):5085–5093. <https://doi.org/10.1021/jm0497038>
56. Acharya P, Lusvarghi S, Bewley CA, Kwong PD (2015) HIV-1 gp120 as a therapeutic target: navigating a moving labyrinth. *Expert Opin Ther Targets* 19(6):765–783. <https://doi.org/10.1517/14728222.2015.1010513>

57. Courter JR, Madani N, Sodroski J, Schon A, Freire E, Kwong PD, Hendrickson WA, Chaiken IM, LaLonde JM, Smith AB 3rd (2014) Structure-based design, synthesis and validation of CD4-mimetic small molecule inhibitors of HIV-1 entry: conversion of a viral entry agonist to an antagonist. *Acc Chem Res* 47(4):1228–1237. <https://doi.org/10.1021/ar4002735>
58. Sanchez TW, Debnath B, Christ F, Otake H, Debyser Z, Neamati N (2013) Discovery of novel inhibitors of LEDGF/p75-IN protein-protein interactions. *Bioorg Med Chem* 21(4):957–963. <https://doi.org/10.1016/j.bmc.2012.12.012>
59. Hu G, Li X, Zhang X, Li Y, Ma L, Yang LM, Liu G, Li W, Huang J, Shen X, Hu L, Zheng YT, Tang Y (2012) Discovery of inhibitors to block interactions of HIV-1 integrase with human LEDGF/p75 via structure-based virtual screening and bioassays. *J Med Chem* 55(22):10108–10117. <https://doi.org/10.1021/jm301226a>
60. Christ F, Voet A, Marchand A, Nicolet S, Desimmié BA, Marchand D, Bardiot D, Van der Veken NJ, Van Remoortel B, Strelkov SV, De Maeyer M, Chaltin P, Debyser Z (2010) Rational design of small-molecule inhibitors of the LEDGF/p75-integrase interaction and HIV replication. *Nat Chem Biol* 6(6):442–448. <https://doi.org/10.1038/nchembio.370>
61. Erbe DV, Wang S, Xing Y, Tobin JF (2002) Small molecule ligands define a binding site on the immune regulatory protein B7.1. *J Biol Chem* 277(9):7363–7368. <https://doi.org/10.1074/jbc.M110162200>
62. Pflugfelder SC, Stern M, Zhang S, Shojaei A (2017) LFA-1/ICAM-1 interaction as a therapeutic target in dry eye disease. *J Ocular Pharm Ther: Off J Assoc Ocular Pharm Ther* 33(1):5–12. <https://doi.org/10.1089/jop.2016.0105>
63. Zimmerman T, Blanco FJ (2008) Inhibitors targeting the LFA-1/ICAM-1 cell-adhesion interaction: design and mechanism of action. *Curr Pharm Des* 14(22):2128–2139
64. Wilson CGM, Arkin MR (2011) Small-molecule inhibitors of IL-2/IL-2R: lessons learned and applied. In: Vassilev L, Fry D (eds) *Small-molecule inhibitors of protein-protein interactions*. Springer, Berlin, Heidelberg
65. Campa M, Ryan C, Menter A (2015) An overview of developing TNF- α targeted therapy for the treatment of psoriasis. *Expert Opin Investig Drugs* 24(10):1343–1354. <https://doi.org/10.1517/13543784.2015.1076793>
66. Chen S, Feng Z, Wang Y, Ma S, Hu Z, Yang P, Chai Y, Xie X (2017) Discovery of novel ligands for TNF- α and TNF Receptor-1 through structure-based virtual screening and biological assay. *J Chem Inf Model* 57(5):1101–1111. <https://doi.org/10.1021/acs.jcim.6b00672>
67. He MM, Smith AS, Oslob JD, Flanagan WM, Braisted AC, Whitty A, Cancilla MT, Wang J, Lugovskoy AA, Yoburn JC, Fung AD, Farrington G, Eldredge JK, Day ES, Cruz LA, Cachero TG, Miller SK, Friedman JE, Choong IC, Cunningham BC (2005) Small-molecule inhibition of TNF- α . *Science* 310(5750):1022
68. Ma L, Gong H, Zhu H, Ji Q, Su P, Liu P, Cao S, Yao J, Jiang L, Han M, Ma X, Xiong D, Luo HR, Wang F, Zhou J, Xu Y (2014) A novel small-molecule tumor necrosis factor α inhibitor attenuates inflammation in a hepatitis mouse model. *J Biol Chem* 289(18):12457–12466
69. Richmond V, Michelini FM, Bueno CA, Alche LE, Ramirez JA (2015) Small molecules as anti-TNF drugs. *Curr Med Chem* 22(25):2920–2942
70. Zarganes-Tzitzikas T, Konstantinidou M, Gao Y, Krzemien D, Zak K, Dubin G, Holak TA, Domling A (2016) Inhibitors of programmed cell death 1 (PD-1): a patent review (2010–2015). *Expert Opin Ther Pat* 26(9):973–977. <https://doi.org/10.1080/13543776.2016.1206527>
71. Zak KM, Grudnik P, Guzik K, Zieba BJ, Musielak B, Domling A, Dubin G, Holak TA (2016) Structural basis for small molecule targeting of the programmed death ligand 1 (PD-L1). *Oncotarget* 7(21):30323–30335. <https://doi.org/10.18632/oncotarget.8730>
72. Winter JJ, Anderson M, Blades K, Brassington C, Breeze AL, Chresta C, Embrey K, Fairley G, Faulder P, Finlay MR, Kettle JG, Nowak T, Overman R, Patel SJ, Perkins P, Spadola L, Tart J, Tucker JA, Wrigley G (2015) Small molecule binding sites on the Ras:

- SOS complex can be exploited for inhibition of Ras activation. *J Med Chem* 58(5):2265–2274. <https://doi.org/10.1021/jm501660t>
73. Evelyn CR, Duan X, Biesiada J, Seibel WL, Meller J, Zheng Y (2014) Rational design of small molecule inhibitors targeting the Ras GEF, SOS1. *Chem Biol* 21(12):1618–1628. <https://doi.org/10.1016/j.chembiol.2014.09.018>
 74. Maurer T, Garrenton LS, Oh A, Pitts K, Anderson DJ, Skelton NJ, Fauber BP, Pan B, Malek S, Stokoe D, Ludlam MJC, Bowman KK, Wu J, Giannetti AM, Starovasnik MA, Mellman I, Jackson PK, Rudolph J, Wang W, Fang G (2012) Small-molecule ligands bind to a distinct pocket in Ras and inhibit SOS-mediated nucleotide exchange activity. *Proc Natl Acad Sci USA* 109(14):5299–5304. <https://doi.org/10.1073/pnas.1116510109>
 75. Sun Q, Burke JP, Phan J, Burns MC, Olejniczak ET, Waterson AG, Lee T, Rossanese OW, Fesik SW (2012) Discovery of small molecules that bind to K-Ras and inhibit Sos-mediated activation. *Angew Chem* 51(25):6140–6143. <https://doi.org/10.1002/anie.201201358>
 76. Ostrem JM, Peters U, Sos ML, Wells JA, Shokat KM (2013) K-Ras(G12C) inhibitors allosterically control GTP affinity and effector interactions. *Nature* 503(7477):548–551. <https://doi.org/10.1038/nature12796>
 77. Hunter JC, Gurbani D, Ficarro SB, Carrasco MA, Lim SM, Choi HG, Xie T, Marto JA, Chen Z, Gray NS, Westover KD (2014) In situ selectivity profiling and crystal structure of SML-8-73-1, an active site inhibitor of oncogenic K-Ras G12C. *Proc Natl Acad Sci USA* 111(24):8895–8900. <https://doi.org/10.1073/pnas.1404639111>
 78. Kato-Stankiewicz J, Hakimi I, Zhi G, Zhang J, Serebriiskii I, Guo L, Edamatsu H, Koide H, Menon S, Eckl R, Sakamuri S, Lu Y, Chen QZ, Agarwal S, Baumbach WR, Golemis EA, Tamanoi F, Khazak V (2002) Inhibitors of Ras/Raf-1 interaction identified by two-hybrid screening revert Ras-dependent transformation phenotypes in human cancer cells. *Proc Natl Acad Sci USA* 99(22):14398–14403. <https://doi.org/10.1073/pnas.222226999>
 79. Athuluri-Divakar SK, Vasquez-Del Carpio R, Dutta K, Baker SJ, Cosenza SC, Basu I, Gupta YK, Reddy MV, Ueno L, Hart JR, Vogt PK, Mulholland D, Guha C, Aggarwal AK, Reddy EP (2016) A small molecule RAS-mimetic disrupts RAS association with effector proteins to block signaling. *Cell* 165(3):643–655. <https://doi.org/10.1016/j.cell.2016.03.045>
 80. Murarka S, Martin-Gago P, Schultz-Fademrecht C, Al Saabi A, Baumann M, Fansa EK, Ismail S, Nussbaumer P, Wittinghofer A, Waldmann H (2017) Development of pyridazinone chemotypes targeting the PDEdelta prenyl binding site. *Chemistry* 23(25):6083–6093. <https://doi.org/10.1002/chem.201603222>
 81. Martin-Gago P, Fansa EK, Wittinghofer A, Waldmann H (2017) Structure-based development of PDEdelta inhibitors. *Biol Chem* 398(5–6):535–545. <https://doi.org/10.1515/hsz-2016-0272>
 82. Kim J, Kwon J, Kim M, Do J, Lee D, Han H (2016) Low-dielectric-constant polyimide aerogel composite films with low water uptake. *Polym J* 48(7):829–834. <https://doi.org/10.1038/pj.2016.37>
 83. Zimmermann G, Schultz-Fademrecht C, Kuchler P, Murarka S, Ismail S, Triola G, Nussbaumer P, Wittinghofer A, Waldmann H (2014) Structure guided design and kinetic analysis of highly potent benzimidazole inhibitors targeting the PDEdelta prenyl binding site. *J Med Chem* 57(12):5435–5448. <https://doi.org/10.1021/jm500632s>
 84. Zimmermann G, Papke B, Ismail S, Vartak N, Chandra A, Hoffmann M, Hahn SA, Triola G, Wittinghofer A, Bastiaens PIH, Waldmann H (2013) Small molecule inhibition of the KRAS–PDE δ interaction impairs oncogenic KRAS signalling. *Nature* 497(7451):638–642. <https://doi.org/10.1038/nature12205>
 85. Shutes A, Onesto C, Picard V, Leblond B, Schweighoffer F, Der CJ (2007) Specificity and mechanism of action of EHT 1864, a novel small molecule inhibitor of Rac family small GTPases. *J Biol Chem* 282(49):35666–35678. <https://doi.org/10.1074/jbc.M703571200>
 86. Ferri N, Corsini A, Bottino P, Clerici F, Contini A (2009) Virtual screening approach for the identification of new Rac1 inhibitors. *J Med Chem* 52(14):4087–4090. <https://doi.org/10.1021/jm8015987>

87. Shang X, Marchioni F, Sipes N, Evelyn CR, Jerabek-Willemsen M, Duhr S, Seibel W, Wortman M, Zheng Y (2012) Rational design of small molecule inhibitors targeting RhoA subfamily Rho GTPases. *Chem Biol* 19(6):699–710. <https://doi.org/10.1016/j.chembiol.2012.05.009>
88. Shang X, Marchioni F, Evelyn CR, Sipes N, Zhou X, Seibel W, Wortman M, Zheng Y (2013) Small-molecule inhibitors targeting G-protein-coupled Rho guanine nucleotide exchange factors. *Proc Natl Acad Sci* 110(8):3155–3160. <https://doi.org/10.1073/pnas.1212324110>
89. Diviani D, Raimondi F, Del Vescovo CD, Dreyer E, Reggi E, Osman H, Ruggieri L, Gonano C, Cavin S, Box CL, Lenoir M, Overduin M, Bellucci L, Seeber M, Fanelli F (2016) Small-molecule protein-protein interaction inhibitor of oncogenic Rho signaling. *Cell Chem Biol* 23(9):1135–1146. <https://doi.org/10.1016/j.chembiol.2016.07.015>
90. Borriello L, Montes M, Lepelletier Y, Leforban B, Liu WQ, Demange L, Delhomme B, Pavoni S, Jarray R, Boucher JL, Dufour S, Hermine O, Garbay C, Hadj-Slimane R, Raynaud F (2014) Structure-based discovery of a small non-peptidic Neuropilins antagonist exerting in vitro and in vivo anti-tumor activity on breast cancer model. *Cancer Lett* 349(2):120–127. <https://doi.org/10.1016/j.canlet.2014.04.004>
91. Starzec A, Miteva MA, Ladam P, Villoutreix BO, Perret GY (2014) Discovery of novel inhibitors of vascular endothelial growth factor-A-Neuropilin-1 interaction by structure-based virtual screening. *Bioorg Med Chem* 22(15):4042–4048. <https://doi.org/10.1016/j.bmc.2014.05.068>
92. Gautier B, Miteva Maria A, Goncalves V, Huguenot F, Coric P, Bouaziz S, Seijo B, Gaucher J-F, Broutin I, Garbay C, Lesnard A, Rault S, Inguibert N, Villoutreix Bruno O, Vidal M (2011) Targeting the proangiogenic VEGF-VEGFR protein-protein interface with drug-like compounds by in silico and in vitro screening. *Chem Biol* 18(12):1631–1639. <https://doi.org/10.1016/j.chembiol.2011.10.016>
93. Kurenova EV, Hunt DL, He D, Magis AT, Ostrov DA, Cance WG (2009) Small molecule chloropyramine hydrochloride (C4) targets the binding site of focal adhesion kinase and vascular endothelial growth factor receptor 3 and suppresses breast cancer growth in vivo. *J Med Chem* 52(15):4716–4724. <https://doi.org/10.1021/jm900159g>
94. Gogate PN, Ethirajan M, Kurenova EV, Magis AT, Pandey RK, Cance WG (2014) Design, synthesis, and biological evaluation of novel FAK scaffold inhibitors targeting the FAK-VEGFR3 protein-protein interaction. *Eur J Med Chem* 80:154–166. <https://doi.org/10.1016/j.ejmech.2014.04.041>
95. Jennings LD, Foreman KW, Rush TS, Tsao DHH, Mosyak L, Li Y, Sukhdeo MN, Ding W, Dushin EG, Kenny CH, Moghazeh SL, Petersen PJ, Ruzin AV, Tuckman M, Sutherland AG (2004) Design and synthesis of indolo[2,3-a]quinolizin-7-one inhibitors of the ZipA–FtsZ interaction. *Bioorg Med Chem Lett* 14(6):1427–1431. <https://doi.org/10.1016/j.bmcl.2004.01.028>
96. Hurley KA, Santos TMA, Nepomuceno GM, Huynh V, Shaw JT, Weibel DB (2016) Targeting the bacterial division protein FtsZ. *J Med Chem* 59(15):6975–6998. <https://doi.org/10.1021/acs.jmedchem.5b01098>
97. Tsao DHH, Sutherland AG, Jennings LD, Li Y, Rush TS, Alvarez JC, Ding W, Dushin EG, Dushin RG, Haney SA, Kenny CH, Karl Malakian A, Nilakantan R, Mosyak L (2006) Discovery of novel inhibitors of the ZipA/FtsZ complex by NMR fragment screening coupled with structure-based design. *Bioorg Med Chem* 14(23):7953–7961. <https://doi.org/10.1016/j.bmc.2006.07.050>
98. Kenny CH, Ding W, Kelleher K, Benard S, Dushin EG, Sutherland AG, Mosyak L, Kriz R, Ellestad G (2003) Development of a fluorescence polarization assay to screen for inhibitors of the FtsZ/ZipA interaction. *Anal Biochem* 323(2):224–233. <https://doi.org/10.1016/j.ab.2003.08.033>
99. Sutherland AG, Alvarez J, Ding W, Foreman KW, Kenny CH, Labthavikul P, Mosyak L, Petersen PJ, Rush Iii TS, Ruzin A, Tsao DHH, Wheless KL (2003) Structure-based design of

- carboxybiphenylindole inhibitors of the ZipA-FtsZ interaction. *Org Biomol Chem* 1 (23):4138–4140. <https://doi.org/10.1039/B312016C>
100. Zhuang C, Wu Z, Xing C, Miao Z (2017) Small molecules inhibiting Keap1-Nrf2 protein-protein interactions: a novel approach to activate Nrf2 function. *MedChemComm* 8 (2):286–294. <https://doi.org/10.1039/C6MD00500D>
 101. Lu M, Ji J, Jiang Y, Chen Z, Yuan Z, You Q, Jiang Z (2016) An inhibitor of the Keap1-Nrf2 protein-protein interaction protects NCM460 colonic cells and alleviates experimental colitis. *Sci Rep* 6:26585. <https://doi.org/10.1038/srep26585>
 102. Abed DA, Goldstein M, Albanyan H, Jin H, Hu L (2015) Discovery of direct inhibitors of Keap1–Nrf2 protein–protein interaction as potential therapeutic and preventive agents. *Acta Pharmaceutica Sinica B* 5(4):285–299. <https://doi.org/10.1016/j.apsb.2015.05.008>
 103. Scott DE, Bayly AR, Abell C, Skidmore J (2016) Small molecules, big targets: drug discovery faces the protein-protein interaction challenge. *Nat Rev Drug Discov* 15(8):533–550. <https://doi.org/10.1038/nrd.2016.29>
 104. Marcotte D, Zeng W, Hus J-C, McKenzie A, Hession C, Jin P, Bergeron C, Lugovskoy A, Enyedy I, Cuervo H, Wang D, Atmanene C, Roecklin D, Vecchi M, Vivat V, Kraemer J, Winkler D, Hong V, Chao J, Lukashev M, Silvian L (2013) Small molecules inhibit the interaction of Nrf2 and the Keap1 Kelch domain through a non-covalent mechanism. *Bioorg Med Chem* 21(14):4011–4019. <https://doi.org/10.1016/j.bmc.2013.04.019>
 105. Jiang Z, Lu M, Xu L, Yang T, Xi M, Xu X, Guo X, Zhang X, You Q, Sun H (2014) Discovery of potent Keap1–Nrf2 protein-protein interaction inhibitor based on molecular binding determinants analysis. *J Med Chem* 57(6):2736–2745. <https://doi.org/10.1021/jm5000529>
 106. Fang L, Zhu Q, Neuenschwander M, Specker E, Wulf-Goldenberg A, Weis WI, von Kries JP, Birchmeier W (2016) A small-molecule antagonist of the β -Catenin/TCF4 interaction blocks the self-renewal of cancer stem cells and suppresses tumorigenesis. *Cancer Res* 76(4):891
 107. Yan M, Li G, An J (2017) Discovery of small molecule inhibitors of the Wnt/ β -catenin signaling pathway by targeting β -catenin/Tcf4 interactions. *Exp Biol Med* 242(11):1185–1197. <https://doi.org/10.1177/1535370217708198>
 108. Lepourcelet M, Chen Y-NP, France DS, Wang H, Crews P, Petersen F, Bruseo C, Wood AW, Shivdasani RA (2004) Small-molecule antagonists of the oncogenic Tcf/ β -catenin protein complex. *Cancer Cell* 5(1):91–102. [https://doi.org/10.1016/S1535-6108\(03\)00334-9](https://doi.org/10.1016/S1535-6108(03)00334-9)
 109. Nam JM, Jeon KH, Kwon H, Lee E, Jun KY, Jin YB, Lee YS, Na Y, Kwon Y (2013) Dithiiranylmethoxy azaxanthone shows potent anti-tumor activity via suppression of HER2 expression and HER2-mediated signals in HER2-overexpressing breast cancer cells. *Eur J Pharm Sci* 50(2):181–190. <https://doi.org/10.1016/j.ejps.2013.06.014>
 110. Kim H-L, Jeon K-H, Jun K-Y, Choi Y, Kim D-K, Na Y, Kwon Y (2012) A-62176, a potent topoisomerase inhibitor, inhibits the expression of human epidermal growth factor receptor 2. *Cancer Lett* 325(1):72–79. <https://doi.org/10.1016/j.canlet.2012.06.004>
 111. Lee LW, Taylor CEC, Desaulniers J-P, Zhang M, Højfeldt JW, Pan Q, Mapp AK (2009) Inhibition of ErbB2(Her2) expression with small molecule transcription factor mimics. *Bioorg Med Chem Lett* 19(21):6233–6236. <https://doi.org/10.1016/j.bmcl.2009.08.090>
 112. Shimogawa H, Kwon Y, Mao Q, Kawazoe Y, Choi Y, Asada S, Kigoshi H, Uesugi M (2004) A wrench-shaped synthetic molecule that modulates a transcription factor–coactivator interaction. *J Am Chem Soc* 126(11):3461–3471. <https://doi.org/10.1021/ja038855+>
 113. Asada S, Choi Y, Uesugi M (2003) A gene-expression inhibitor that targets an α -Helix-Mediated protein interaction. *J Am Chem Soc* 125(17):4992–4993. <https://doi.org/10.1021/ja0292703>
 114. Wang J, Luo C, Shan C, You Q, Lu J, Elf S, Zhou Y, Wen Y, Vinkenborg JL, Fan J, Kang H, Lin R, Han D, Xie Y, Karpus J, Chen S, Ouyang S, Luan C, Zhang N, Ding H, Merx M, Liu H, Chen J, Jiang H, He C (2015) Inhibition of human copper trafficking by a

- small molecule significantly attenuates cancer cell proliferation. *Nat Chem* 7(12):968–979. <https://doi.org/10.1038/nchem.2381>
115. Park D, Park CW, Choi Y, Lin J, Seo DH, Kim HS, Lee SY, Kang IC (2016) A novel small-molecule PPI inhibitor targeting integrin alphavbeta3-osteopontin interface blocks bone resorption in vitro and prevents bone loss in mice. *Biomaterials* 98:131–142. <https://doi.org/10.1016/j.biomaterials.2016.05.007>
 116. Kummer C, Petrich BG, Rose DM, Ginsberg MH (2010) A small molecule that inhibits the interaction of paxillin and alpha 4 integrin inhibits accumulation of mononuclear leukocytes at a site of inflammation. *J Biol Chem* 285(13):9462–9469. <https://doi.org/10.1074/jbc.M109.066993>
 117. Cox D, Brennan M, Moran N (2010) Integrins as therapeutic targets: lessons and opportunities. *Nat Rev Drug Discov* 9(10):804–820. <https://doi.org/10.1038/nrd3266>
 118. Tilley JW (2008) Very late antigen-4 integrin antagonists. *Expert Opin Ther Pat* 18(8):841–859. <https://doi.org/10.1517/13543776.18.8.841>
 119. Stragies R, Osterkamp F, Zischinsky G, Vossmeier D, Kalkhof H, Reimer U, Zahn G (2007) Design and synthesis of a new class of selective integrin $\alpha 5 \beta 1$ antagonists. *J Med Chem* 50(16):3786–3794. <https://doi.org/10.1021/jm070002v>
 120. Potin D, Launay M, Monatik F, Malabre P, Fabreguettes M, Fouquet A, Maillet M, Nicolai E, Dorgeret L, Chevallier F, Besse D, Dufort M, Caussade F, Ahmad SZ, Stetsko DK, Skala S, Davis PM, Balimane P, Patel K, Yang Z, Marathe P, Postelneck J, Townsend RM, Goldfarb V, Sheriff S, Einspahr H, Kish K, Malley MF, DiMarco JD, Gougoutas JZ, Kadiyala P, Cheney DL, Tejwani RW, Murphy DK, McIntyre KW, Yang X, Chao S, Leith L, Xiao Z, Mathur A, Chen B-C, Wu D-R, Traeger SC, McKinnon M, Barrish JC, Robl JA, Iwanowicz EJ, Suchard SJ, Dhar TGM (2006) Discovery and development of 5-[(5S,9R)-9-(4-Cyanophenyl)-3-(3,5-dichlorophenyl)-1-methyl-2,4-dioxo-1,3,7-triazaspiro[4.4]non-7-yl-methyl]-3-thiophenecarboxylic Acid (BMS-587101). A small molecule antagonist of leukocyte function associated Antigen-1. *J Med Chem* 49(24):6946–6949. <https://doi.org/10.1021/jm0610806>
 121. Kelly TA, Jeanfavre DD, McNeil DW, Woska JR, Reilly PL, Mainolfi EA, Kishimoto KM, Nabozny GH, Zinter R, Bormann B-J, Rothlein R (1999) Cutting edge: a small molecule antagonist of LFA-1-mediated cell adhesion. *J Immunol* 163(10):5173–5177
 122. Scott DE, Coyne AG, Venkitaraman A, Blundell TL, Abell C, Hyvonen M (2015) Small-molecule inhibitors that target protein-protein interactions in the RAD51 family of recombinases. *ChemMedChem* 10(2):296–303. <https://doi.org/10.1002/cmdc.201402428>
 123. Roman DL, Talbot JN, Roof RA, Sunahara RK, Traynor JR, Neubig RR (2006) Identification of small-molecule inhibitors of RGS4 using a high-throughput flow cytometry protein interaction assay. *Mol Pharmacol* 71(1):169–175. <https://doi.org/10.1124/mol.106.028670>
 124. Yun SM, Moulaei T, Lim D, Bang JK, Park JE, Shenoy SR, Liu F, Kang YH, Liao C, Soung NK, Lee S, Yoon DY, Lim Y, Lee DH, Otaka A, Appella E, McMahon JB, Nicklaus MC, Burke TR Jr, Yaffe MB, Wlodawer A, Lee KS (2009) Structural and functional analyses of minimal phosphopeptides targeting the polo-box domain of polo-like kinase 1. *Nat Struct Mol Biol* 16(8):876–882. <https://doi.org/10.1038/nsmb.1628>
 125. Watanabe N, Sekine T, Takagi M, Iwasaki J, Imamoto N, Kawasaki H, Osada H (2009) Deficiency in chromosome congression by the inhibition of Plk1 polo box domain-dependent recognition. *J Biol Chem* 284(4):2344–2353. <https://doi.org/10.1074/jbc.M805308200>
 126. Reindl W, Yuan J, Kramer A, Strebhardt K, Berg T (2009) A pan-specific inhibitor of the polo-box domains of polo-like kinases arrests cancer cells in mitosis. *Chembiochem* 10(7):1145–1148. <https://doi.org/10.1002/cbic.200900059>
 127. Reindl W, Yuan J, Kramer A, Strebhardt K, Berg T (2008) Inhibition of polo-like kinase 1 by blocking polo-box domain-dependent protein-protein interactions. *Chem Biol* 15(5):459–466. <https://doi.org/10.1016/j.chembiol.2008.03.013>

128. White PW, Faucher A-M, Goudreau N (2011) Small molecule inhibitors of the human papillomavirus E1-E2 interaction. In: Vassilev L, Fry D (eds) Small-molecule inhibitors of protein-protein interactions. Springer, Berlin, Heidelberg, pp 61–88. https://doi.org/10.1007/82_2010_92
129. A study to assess the safety, tolerability, pharmacokinetics and efficacy of twice daily topical applications of AP611074 5% gel for up to 16 weeks in condyloma patients. <https://clinicaltrials.gov/ct2/show/NCT02724254>
130. Andrieu G, Belkina AC, Denis GV (2016) Clinical trials for BET inhibitors run ahead of the science. *Drug Discov Today Technol* 19:45–50. <https://doi.org/10.1016/j.ddtec.2016.06.004>
131. Delmore JE, Issa GC, Lemieux ME, Rahl PB, Shi J, Jacobs HM, Kastiris E, Gilpatrick T, Paranal RM, Qi J, Chesi M, Schinzel AC, McKeown MR, Heffernan TP, Vakoc CR, Bergsagel PL, Ghobrial IM, Richardson PG, Young RA, Hahn WC, Anderson KC, Kung AL, Bradner JE, Mitsiades CS (2011) BET bromodomain inhibition as a therapeutic strategy to target c-Myc. *Cell* 146(6):904–917. <https://doi.org/10.1016/j.cell.2011.08.017>
132. Romero FA, Taylor AM, Crawford TD, Tsui V, Cote A, Magnuson S (2016) Disrupting acetyl-lysine recognition: progress in the development of bromodomain inhibitors. *J Med Chem* 59(4):1271–1298. <https://doi.org/10.1021/acs.jmedchem.5b01514>
133. Margueron R, Reinberg D (2011) The Polycomb complex PRC2 and its mark in life. *Nature* 469(7330):343–349. <https://doi.org/10.1038/nature09784>
134. Xu B, Konze KD, Jin J, Wang GG (2015) Targeting EZH2 and PRC2 dependence as novel anticancer therapy. *Exp Hematol* 43(8):698–712. <https://doi.org/10.1016/j.exphem.2015.05.001>
135. Knutson SK, Wigle TJ, Warholic NM, Sneeringer CJ, Allain CJ, Klaus CR, Sacks JD, Raimondi A, Majer CR, Song J, Scott MP, Jin L, Smith JJ, Olhava EJ, Chesworth R, Moyer MP, Richon VM, Copeland RA, Keilhack H, Pollock RM, Kuntz KW (2012) A selective inhibitor of EZH2 blocks H3K27 methylation and kills mutant lymphoma cells. *Nat Chem Biol* 8(11):890–896. <https://doi.org/10.1038/nchembio.1084>
136. Comet I, Riising EM, Leblanc B, Helin K (2016) Maintaining cell identity: PRC2-mediated regulation of transcription and cancer. *Nat Rev Cancer* 16(12):803–810. <https://doi.org/10.1038/nrc.2016.83>
137. Kim W, Bird GH, Neff T, Guo G, Kerenyi MA, Walensky LD, Orkin SH (2013) Targeted disruption of the EZH2-EED complex inhibits EZH2-dependent cancer. *Nat Chem Biol* 9(10):643–650. <https://doi.org/10.1038/nchembio.1331>
138. Brooun A, Gajiwala KS, Deng YL, Liu W, Bolanos B, Bingham P, He YA, Diehl W, Grable N, Kung PP, Sutton S, Maegley KA, Yu X, Stewart AE (2016) Polycomb repressive complex 2 structure with inhibitor reveals a mechanism of activation and drug resistance. *Nat Commun* 7:11384. <https://doi.org/10.1038/ncomms11384>
139. Jiao L, Liu X (2015) Structural basis of histone H3K27 trimethylation by an active polycomb repressive complex 2. *Science* 350 (6258):aac4383. <https://doi.org/10.1126/science.aac4383>
140. Jiao L, Liu X (2016) Structural analysis of an active fungal PRC2. *Nucleus* 7(3):284–291. <https://doi.org/10.1080/19491034.2016.1183849>
141. Teske KA, Hadden MK (2017) Methyllysine binding domains: structural insight and small molecule probe development. *Eur J Med Chem* 136:14–35. <https://doi.org/10.1016/j.ejmech.2017.04.047>
142. Hershko A, Ciechanover A (1998) The ubiquitin system. *Ann Rev Biochem* 67(1):425–479. <https://doi.org/10.1146/annurev.biochem.67.1.425>
143. Pickart CM (2001) Mechanisms underlying ubiquitination. *Ann Rev Biochem* 70(1):503–533. <https://doi.org/10.1146/annurev.biochem.70.1.503>
144. Rubin DM, Finley D (1995) Proteolysis: The proteasome: a protein-degrading organelle? *Curr Biol* 5(8):854–858. [https://doi.org/10.1016/S0960-9822\(95\)00172-2](https://doi.org/10.1016/S0960-9822(95)00172-2)
145. Ravid T, Hochstrasser M (2008) Diversity of degradation signals in the ubiquitin-proteasome system. *Nat Rev Mol Cell Biol* 9(9):679–689

146. Scheffner M, Nuber U, Huibregtse JM (1995) Protein ubiquitination involving an E1-E2-E3 enzyme ubiquitin thioester cascade. *Nature* 373(6509):81–83. <https://doi.org/10.1038/373081a0>
147. Xolalpa W, Perez-Galan P, Rodriguez MS, Roue G (2013) Targeting the ubiquitin proteasome system: beyond proteasome inhibition. *Curr Pharm Des* 19(22):4053–4093
148. Zhang W, Sidhu SS (2014) Development of inhibitors in the ubiquitination cascade. *FEBS Lett* 588(2):356–367. <https://doi.org/10.1016/j.febslet.2013.11.003>
149. Li W, Bengtson MH, Ulbrich A, Matsuda A, Reddy VA, Orth A, Chanda SK, Batalov S, Joazeiro CAP (2008) Genome-wide and functional annotation of human E3 ubiquitin ligases identifies MULAN, a mitochondrial E3 that regulates the organelle's dynamics and signaling. *PLoS ONE* 3(1):e1487. <https://doi.org/10.1371/journal.pone.0001487>
150. Kaelin WG Jr (2002) Molecular basis of the VHL hereditary cancer syndrome. *Nat Rev Cancer* 2(9):673–682. <https://doi.org/10.1038/nrc885>
151. Salama R, Masson N, Simpson P, Sciesielski LK, Sun M, Tian YM, Ratcliffe PJ, Mole DR (2015) Heterogeneous effects of direct hypoxia pathway activation in kidney cancer. *PLoS ONE* 10(8):e0134645. <https://doi.org/10.1371/journal.pone.0134645>
152. Muchnik E, Kaplan J (2011) HIF prolyl hydroxylase inhibitors for anemia. *Expert Opin Investig Drugs* 20(5):645–656. <https://doi.org/10.1517/13543784.2011.566861>
153. Zhuang M, Calabrese MF, Liu J, Waddell MB, Nourse A, Hammel M, Miller DJ, Walden H, Duda DM, Seyedin SN, Hoggard T, Harper JW, White KP, Schulman BA (2009) Structures of SPOP-substrate complexes: insights into molecular architectures of BTB-Cul3 ubiquitin ligases. *Mol Cell* 36(1):39–50. <https://doi.org/10.1016/j.molcel.2009.09.022>
154. Kwon JE, La M, Oh KH, Oh YM, Kim GR, Seol JH, Baek SH, Chiba T, Tanaka K, Bang OS, Joe CO, Chung CH (2006) BTB domain-containing speckle-type POZ protein (SPOP) serves as an adaptor of DAXX for ubiquitination by Cul3-based ubiquitin ligase. *J Biol Chem* 281(18):12664–12672. <https://doi.org/10.1074/jbc.M600204200>
155. The Cancer Genome Atlas Research N (2013) Comprehensive molecular characterization of clear cell renal cell carcinoma. *Nature* 499(7456):43–49. <https://doi.org/10.1038/nature12222>
156. Li G, Ci W, Karmakar S, Chen K, Dhar R, Fan Z, Guo Z, Zhang J, Ke Y, Wang L, Zhuang M, Hu S, Li X, Zhou L, Li X, Calabrese Matthew F, Watson Edmond R, Prasad Sandip M, Rinker-Schaeffer C, Eggener Scott E, Stricker T, Tian Y, Schulman Brenda A, Liu J, White Kevin P (2014) SPOP promotes tumorigenesis by acting as a key regulatory hub in kidney cancer. *Cancer Cell* 25(4):455–468. <https://doi.org/10.1016/j.ccr.2014.02.007>
157. Guo ZQ, Zheng T, Chen B, Luo C, Ouyang S, Gong S, Li J, Mao LL, Lian F, Yang Y, Huang Y, Li L, Lu J, Zhang B, Zhou L, Ding H, Gao Z, Zhou L, Li G, Zhou R, Chen K, Liu J, Wen Y, Gong L, Ke Y, Yang SD, Qiu XB, Zhang N, Ren J, Zhong D, Yang CG, Liu J, Jiang H (2016) Small-molecule targeting of E3 ligase adaptor SPOP in kidney cancer. *Cancer Cell* 30(3):474–484. <https://doi.org/10.1016/j.ccell.2016.08.003>
158. Srinivasan M, Dunker AK (2012) Proline rich motifs as drug targets in immune mediated disorders. *Int J Peptides* 2012:634769. <https://doi.org/10.1155/2012/634769>
159. Teijeira A, Hunter MC, Russo E, Proulx ST, Frei T, Debes GF, Coles M, Melero I, Detmar M, Rouzaut A, Halin C (2017) T Cell migration from inflamed skin to draining lymph nodes requires intralymphatic crawling supported by ICAM-1/LFA-1 interactions. *Cell Rep* 18(4):857–865. <https://doi.org/10.1016/j.celrep.2016.12.078>
160. Arkin MR, Tang Y, Wells JA (2014) Small-molecule inhibitors of protein-protein interactions: progressing toward the reality. *Chem Biol* 21(9):1102–1114. <https://doi.org/10.1016/j.chembiol.2014.09.001>
161. Tintori C, Brai A, Fallacara AL, Fazi R, Schenone S, Botta M (2014) Protein-protein interactions and human cellular cofactors as new targets for HIV therapy. *Curr Opin Pharmacol* 18:1–8. <https://doi.org/10.1016/j.coph.2014.06.005>
162. Kwong PD, Wyatt R, Robinson J, Sweet RW, Sodroski J, Hendrickson WA (1998) Structure of an HIV gp120 envelope glycoprotein in complex with the CD4 receptor and a neutralizing human antibody. *Nature* 393(6686):648–659. <https://doi.org/10.1038/31405>

163. Scott DE, Bayly AR, Abell C, Skidmore J (2016) Small molecules, big targets: drug discovery faces the protein–protein interaction challenge. *Nat Rev Drug Discov* 15(8):533–550. <https://doi.org/10.1038/nrd.2016.29>
164. Zhao Q, Ma L, Jiang S, Lu H, Liu S, He Y, Strick N, Neamati N, Debnath AK (2005) Identification of N-phenyl-N'-(2,2,6,6-tetramethyl-piperidin-4-yl)-oxalamides as a new class of HIV-1 entry inhibitors that prevent gp120 binding to CD4. *Virology* 339(2):213–225. <https://doi.org/10.1016/j.virol.2005.06.008>
165. Kwon YD, LaLonde JM, Yang Y, Elban MA, Sugawara A, Courter JR, Jones DM, Smith AB 3rd, Debnath AK, Kwong PD (2014) Crystal structures of HIV-1 gp120 envelope glycoprotein in complex with NBD analogues that target the CD4-binding site. *PLoS ONE* 9(1):e85940. <https://doi.org/10.1371/journal.pone.0085940>
166. Kwon YD, Finzi A, Wu X, Dogo-Isonagie C, Lee LK, Moore LR, Schmidt SD, Stuckey J, Yang Y, Zhou T, Zhu J, Vivic DA, Debnath AK, Shapiro L, Bewley CA, Mascola JR, Sodroski JG, Kwong PD (2012) Unliganded HIV-1 gp120 core structures assume the CD4-bound conformation with regulation by quaternary interactions and variable loops. *Proc Natl Acad Sci USA* 109(15):5663–5668. <https://doi.org/10.1073/pnas.1112391109>
167. Curreli F, Choudhury S, Pyatkin I, Zagorodnikov VP, Bulay AK, Altieri A, Kwon YD, Kwong PD, Debnath AK (2012) Design, synthesis, and antiviral activity of entry inhibitors that target the CD4-binding site of HIV-1. *J Med Chem* 55(10):4764–4775. <https://doi.org/10.1021/jm3002247>
168. LaLonde JM, Kwon YD, Jones DM, Sun AW, Courter JR, Soeta T, Kobayashi T, Princiotta AM, Wu X, Schon A, Freire E, Kwong PD, Mascola JR, Sodroski J, Madani N, Smith AB 3rd (2012) Structure-based design, synthesis, and characterization of dual hotspot small-molecule HIV-1 entry inhibitors. *J Med Chem* 55(9):4382–4396. <https://doi.org/10.1021/jm300265j>
169. Domling A, Holak TA (2014) Programmed death-1: therapeutic success after more than 100 years of cancer immunotherapy. *Angewandte Chemie* 53(9):2286–2288. <https://doi.org/10.1002/anie.201307906>
170. Sakuishi K, Apetoh L, Sullivan JM, Blazar BR, Kuchroo VK, Anderson AC (2010) Targeting Tim-3 and PD-1 pathways to reverse T cell exhaustion and restore anti-tumor immunity. *J Exp Med* 207(10):2187–2194. <https://doi.org/10.1084/jem.20100643>
171. Wolchok JD (2015) PD-1 blockers. *Cell* 162(5):937. <https://doi.org/10.1016/j.cell.2015.07.045>
172. Zak KM, Kitel R, Przetocka S, Golik P, Guzik K, Musielak B, Domling A, Dubin G, Holak TA (2015) Structure of the complex of human programmed death 1, PD-1, and its ligand PD-L1. *Structure* 23(12):2341–2348. <https://doi.org/10.1016/j.str.2015.09.010>
173. Chupak LS, Zheng X (2015) Compounds useful as immunomodulators. WO2015034820
174. Chupak LS, Ding M, Martin SW, Zheng X, Hewawasam P, Connolly TP, Xu N, Yeung K-S, Zhu J, Langley DR, Tenney DJ, Scola PM (2015) Compounds useful as immunomodulators. WO2015160641A2
175. Yeung K-S, Connolly TP, Frennesson DB, et al (2017) Compounds useful as immunomodulators. WO2017066227
176. Li J, Wu L, Yao W (2017) Heterocyclic compound as immunomodulators. WO2017087777
177. Wu L, Shen B, Li j, Li Z, Liu K, Zhang F, Yao W (2017) Heterocyclic compounds as immunomodulators. WO2017070089
178. Sasikumar PGN, Ramachandra M, Naremaddepalli SSS (2014) 1,3,4-oxadiazole and 1,3,4-thiadiazole derivatives as immunomodulators. WO2015033301
179. Sawano A, Iwai S, Sakurai Y, Ito M, Shitara K, Nakahata T, Shibuya M (2001) Flt-1, vascular endothelial growth factor receptor 1, is a novel cell surface marker for the lineage of monocyte-macrophages in humans. *Blood* 97(3):785
180. Kanno S, Oda N, Abe M, Terai Y, Ito M, Shitara K, Tabayashi K, Shibuya M, Sato Y (2000) Roles of two VEGF receptors, Flt-1 and KDR, in the signal transduction of VEGF effects in human vascular endothelial cells. *Oncogene* 19(17):2138–2146. <https://doi.org/10.1038/sj.onc.1203533>

181. Su JL, Yang PC, Shih JY, Yang CY, Wei LH, Hsieh CY, Chou CH, Jeng YM, Wang MY, Chang KJ, Hung MC, Kuo ML (2006) The VEGF-C/Flt-4 axis promotes invasion and metastasis of cancer cells. *Cancer Cell* 9(3):209–223. <https://doi.org/10.1016/j.ccr.2006.02.018>
182. Pellet-Many C, Frankel P, Jia H, Zachary I (2008) Neuropilins: structure, function and role in disease. *Biochem J* 411(2):211–226. <https://doi.org/10.1042/bj20071639>
183. Rahimi N (2006) VEGFR-1 and VEGFR-2: two non-identical twins with a unique physiognomy. *Front Biosci: J Virtual Library* 11:818–829
184. Sia Daniela, Alsinet Clara, Newell Pippa, Villanueva A (2014) VEGF signaling in cancer treatment. *Current Pharm Des* 20(17):2834–2842. <https://doi.org/10.2174/13816128113199990590>
185. Miao HQ, Lee P, Lin H, Soker S, Klagsbrun M (2000) Neuropilin-1 expression by tumor cells promotes tumor angiogenesis and progression. *FASEB J: Off Publ Fed Am Soc Exp Biol* 14(15):2532–2539. <https://doi.org/10.1096/fj.00-0250com>
186. Gogate PN, Kurenova EV, Ethirajan M, Liao J, Yemma M, Sen A, Pandey RK, Cance WG (2014) Targeting the C-terminal focal adhesion kinase scaffold in pancreatic cancer. *Cancer Lett* 353(2):281–289. <https://doi.org/10.1016/j.canlet.2014.07.032>
187. Garces CA, Kurenova EV, Golubovskaya VM, Cance WG (2006) Vascular endothelial growth factor receptor-3 and focal adhesion kinase bind and suppress apoptosis in breast cancer cells. *Cancer Res* 66(3):1446
188. <wang2015.pdf>. <https://doi.org/10.1038/nchem.2381>
189. Cai H, Peng F (2013) Knockdown of copper chaperone antioxidant-1 by RNA interference inhibits copper-stimulated proliferation of non-small cell lung carcinoma cells. *Oncol Rep* 30(1):269–275. <https://doi.org/10.3892/or.2013.2436>
190. Waring MJ, Chen H, Rabow AA, Walker G, Bobby R, Boiko S, Bradbury RH, Callis R, Clark E, Dale I, Daniels DL, Dulak A, Flavell L, Holdgate G, Jowitt TA, Kikhney A, McAlister M, Mendez J, Ogg D, Patel J, Petteruti P, Robb GR, Robers MB, Saif S, Stratton N, Svergun DI, Wang W, Whittaker D, Wilson DM, Yao Y (2016) Potent and selective bivalent inhibitors of BET bromodomains. *Nat Chem Biol* 12(12):1097–1104. <https://doi.org/10.1038/nchembio.2210>
191. Neklesa TK, Winkler JD, Crews CM (2017) Targeted protein degradation by PROTACs. *Pharmacol Ther* 174:138–144. <https://doi.org/10.1016/j.pharmthera.2017.02.027>
192. Ottis P, Crews CM (2017) Proteolysis-targeting chimeras: induced protein degradation as a therapeutic strategy. *ACS Chem Biol* 12(4):892–898. <https://doi.org/10.1021/acschembio.6b01068>
193. Maurer T, Garrenton LS, Oh A, Pitts K, Anderson DJ, Skelton NJ, Fauber BP, Pan B, Malek S, Stokoe D, Ludlam MJ, Bowman KK, Wu J, Giannetti AM, Starovasnik MA, Mellman I, Jackson PK, Rudolph J, Wang W, Fang G (2012) Small-molecule ligands bind to a distinct pocket in Ras and inhibit SOS-mediated nucleotide exchange activity. *Proc Natl Acad Sci USA* 109(14):5299–5304. <https://doi.org/10.1073/pnas.1116510109>
194. Cunningham D, Danley DE, Geoghegan KF, Griffior MC, Hawkins JL, Subashi TA, Varghese AH, Ammirati MJ, Culp JS, Hoth LR, Mansour MN, McGrath KM, Seddon AP, Shenolikar S, Stutzman-Engwall KJ, Warren LC, Xia D, Qiu X (2007) Structural and biophysical studies of PCSK9 and its mutants linked to familial hypercholesterolemia. *Nat Struct Mol Biol* 14(5):413–419. <https://doi.org/10.1038/nsmb1235>

Chapter 8

The Development of New Spirooxindoles Targeting the p53–MDM2 Protein-Protein Interactions for Cancer Therapy



Bin Yu and Hong-Min Liu

8.1 Significance and Structures of p53–MDM2 Interactions

8.1.1 Biological Roles of p53

The TP53 gene-encoded p53 tumor suppressor protein is a transcriptional factor, which plays pivotal roles in regulating cellular processes and suppressing tumor development [1]. In cells, p53 and MDM2 (also known as HDM2 in humans) are tightly regulated through the auto-regulatory negative feedback loop, thus maintaining normal physiological functions (Fig. 8.1) [2, 3]. This auto-regulatory feedback loop operates from the transcription of MDM2 initiated by the p53 activation, leading to the increase in MDM2 mRNA and protein expression. In unstressed cells, because of the low cellular levels and the MDM2-mediated degradation (leading to instability of p53, $T_{1/2} < 30$ min), the growth-suppressing activity of p53 is inhibited [4]. By contrast, the rapid stabilization and expression of p53 induced by cellular stress such as DNA damage, oncogenic activation, hypoxia prevent unwanted propagation and kill defective cells via a dual transcription-dependent/-independent function [5]. However, almost 50% of human cancers fail to express p53 protein as a consequence of the mutation or deletion of TP53 gene

B. Yu · H.-M. Liu (✉)

Ministry of Education, Key Laboratory of Advanced Drug Preparation Technologies, Zhengzhou University, 100 Kexue Avenue, Zhengzhou 450001, Henan, China
e-mail: liuhm@zzu.edu.cn

B. Yu

e-mail: zzyubin@hotmail.com

B. Yu · H.-M. Liu

Co-innovation Center of Henan Province for New Drug Research & Development and Preclinical Safety, School of Pharmaceutical Sciences, Zhengzhou University, 100 Kexue Avenue, Zhengzhou 450001, Henan, China

© Springer Nature Singapore Pte Ltd. 2018

C. Sheng and G. I. Georg (eds.), *Targeting Protein-Protein Interactions by Small Molecules*, https://doi.org/10.1007/978-981-13-0773-7_8

213

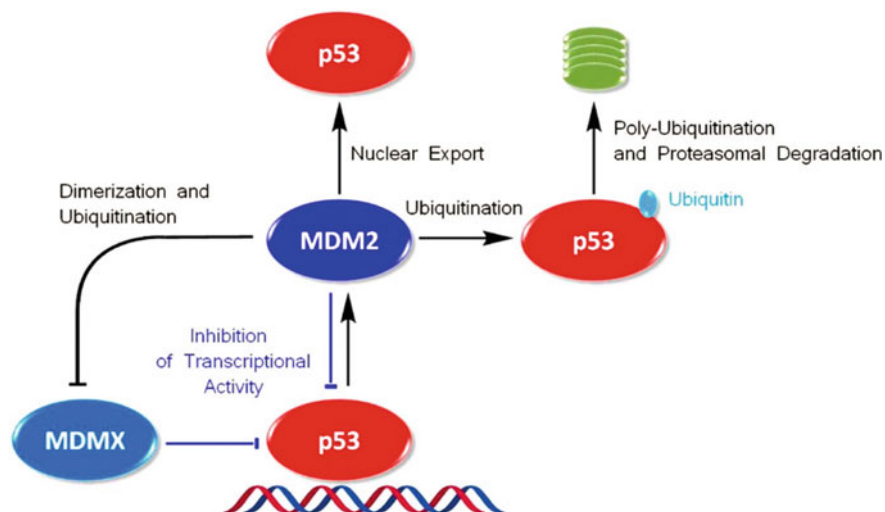


Fig. 8.1 Auto-regulatory feedback loop between p53 and MDM2. Reprinted with permission from Ref. [13]. Copyright © 2014, American Chemical Society

[6]. For those tumors expressing wild-type (wt) p53, their p53 functions are always inhibited through multiple different mechanisms [7–10]: (1) MDM2, as an E3 ubiquitin ligase, promotes ubiquitin-dependent p53 degradation on nuclear and cytoplasmic 26S proteasomes; (2) MDM2 promotes the nuclear export of p53 into the cytoplasm, thereby reducing its transcriptional ability; (3) The binding ability of p53 to its targeted DNA is attenuated by the MDM2–p53 interaction, rendering p53 non-functional [11]. Besides, MDM2 can also bind to p53 directly and inhibits p53 function without leading to p53 degradation. Tumor suppressor ARF stabilizes p53 by binding to MDM2 and sequestering MDM2 into the nucleolus. MDMX, as a regulator of MDM2, inhibits degradation of MDM2 through their interactions at the C-terminal RING finger domains [12].

8.1.2 Structures of p53–MDM2 Interactions

In structure, the functional p53 is a homo-tetramer, in which each monomer contains the *N*-terminal transactivation domain, proline-rich domain, sequence-specific DNA-binding domain, and oligomerization domain (Fig. 8.2a), while the MDM2 protein consists of an *N*-terminal p53 interaction domain, a central acidic domain, a zinc-finger domain, and a C-terminal RING domain (Fig. 8.2b) [14]. The *N*-terminal transactivation domain in p53 shows a stable helical conformation, where the π – π interaction between Phe19 and Trp23 has proven to be crucial in maintaining its structural stability and functional roles (Fig. 8.2c) [15]. Historically,

the protein-protein interactions (PPIs) have long been recognized as undruggable targets because PPIs usually involve large and flat interfaces that are difficult to break by small molecules [16, 17]. Differently, the co-crystal structure of MDM2–p53 complex in 1996 shows that the interactions between MDM2 and p53 are primarily mediated by a small range of amino acid residues (namely the first ~120 *N*-terminal amino acid residues of MDM2 and the first 30 *N*-terminal residues of p53 [13]) and the MDM2-bound p53 peptide adopts a α -helical conformation and interacts with MDM2 primarily through the Phe19, Trp23, and Leu23 residues, which are inserted into the well-defined hydrophobic cleft in MDM2 (Fig. 8.2d) [13, 18]. The structural features of MDM2–p53 complex provide a basis for designing small molecules that mimic the key residues to block the MDM2–p53 interactions [19]. Substantial efforts have been devoted to developing small molecules and peptides that can disrupt the MDM2–p53 interactions, making p53 a potential target for cancer therapy [11, 20–29].

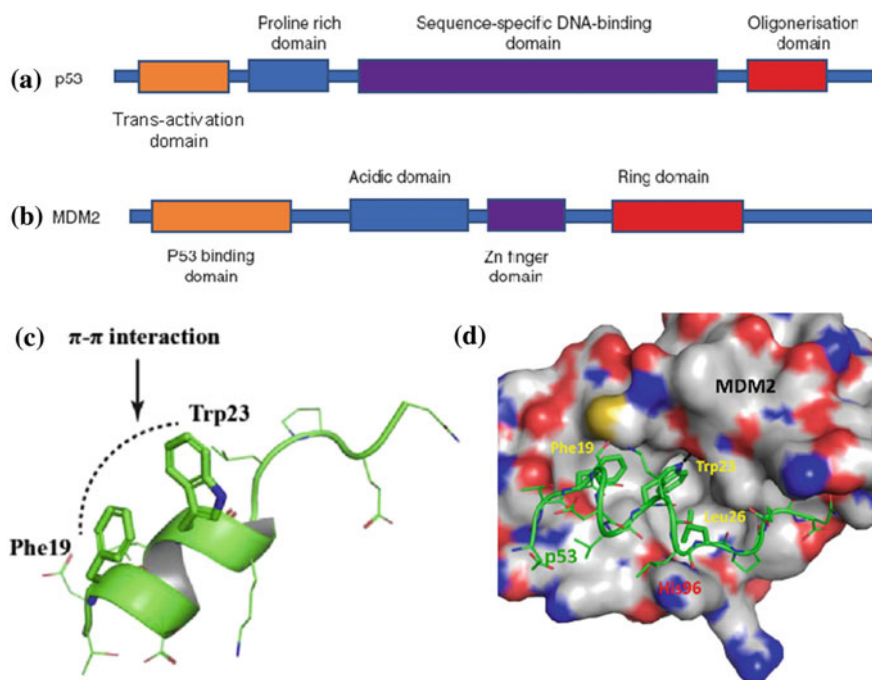


Fig. 8.2 a, b Major functional domains of p53 and MDM2 proteins, respectively; c The *N*-terminal domain of p53; d The co-crystal structure of MDM2–p53 complex (PDB code: 1YCR). a and b were reprinted with permission from Ref. [14]. Copyright © 2010, Elsevier Ltd; c was reprinted with permission from Ref. [15]. Copyright © 2015, Elsevier Ltd; d was reprinted with permission from Ref. [13]. Copyright © 2014, American Chemical Society

8.1.3 Small Molecules in Clinical Trials Targeting p53–MDM2 Interactions

To date, a large number of small-molecule inhibitors targeting the MDM2–p53 interactions have been identified, and these inhibitors can be divided into several chemotypes including imidazolines (e.g., Nutlin series [30], RG-7112), benzodiazepinediones (e.g., TDP665759 [31]), spirooxindoles (e.g., SAR405838 [32, 33]), piperidinones (e.g., AMG232 [34–36] and CGM097 [37]), isoindolinones. Some of them have advanced into clinical trials for anticancer assessment [13], such as SAR405838 [32, 33], MK-8242, DS-3032b, NVP-CGM097 [37–39], RG7112, [40, 41] RG7388, [42] AMG 232 [34–36], and APG-115 [43] (Fig. 8.3). Among them, the structures of MK-8242 and DS-3032b are not available to date.

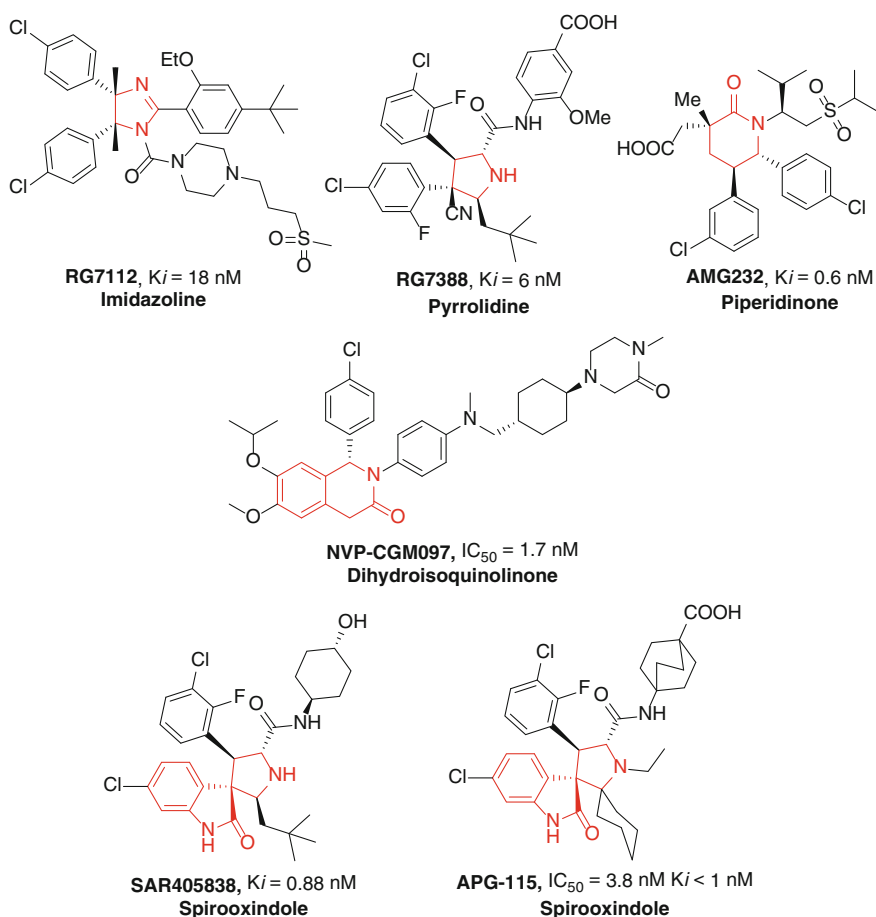


Fig. 8.3 Small-molecule MDM2 inhibitors in clinical trials

In this chapter, we highlight the identification of spirooxindole containing small-molecule inhibitors, strategies employed for optimizations, structure–activity relationship studies (SARs) as well as preclinical data of those undergoing clinical assessment. Based on the SARs and the co-crystal structures of p53–MDM2 complexes, we first propose the prolinamide-based ‘3+1’ model that may be utilized for designing potent MDM2 inhibitors.

8.2 The Development of Spirooxindoles as MDM2–p53 Protein-Protein Interaction Inhibitors

8.2.1 Structure-Based Design and Optimization of Spirooxindoles Targeting MDM2–p53 Interactions

Spirooxindole fragments have recently drawn extensive attention because of their prevalence in natural products (e.g., spirotryprostatin A and B) [44] and biologically active agents (e.g., CFI-400945 [45], KAE609 [46–49], and SAR405838) and have been proved to possess diverse biological activities [45, 50–57]. The structural characteristics of spirooxindoles lie in their spiro scaffolds with other heterocyclic moieties fused at the C3 position of oxindole core. The 3D structural features of spirocycles make spirooxindole scaffolds promising as templates in drug discovery programs, as observed in identifying potent and selective MDM2 inhibitors.

As shown in Fig. 8.2d, the hydrophobic cleft on the surface of MDM2 is occupied by Phe19, Trp23, and Leu26 residues of p53 in a compact and well-defined fashion. Of these three residues, Trp23 is deeply buried inside the narrow and deep hydrophobic cavity in MDM2 and the NH unit of Trp23 residue forms an additional hydrogen bond with the carbonyl group of MDM2. A pioneering work in designing MDM2 inhibitors was carried out by the Wang group, generating a library of potent MDM2 inhibitors, such as the anticancer drug candidate SAR405838 ($K_i = 0.88$ nM) and the second-generation inhibitor MI-1061 ($K_i = 0.16$ nM) (Fig. 8.4) [58]. Initially, they found that the oxindole group can closely mimic the Trp23 residue of p53 to occupy the hydrophobic pocket in MDM2, where the amide NH in place of NH in Trp23 served as the hydrogen bond donor [59]. The spiropyrrolidinyl oxindole core (highlighted in Red in Fig. 8.4) was then used as substructure for designing MDM2 inhibitors; another two hydrophobic groups around the pyrrolidinyl ring were projected in a certain manner to mimic Phe19 and Leu26 because of the spatial repulsion of adjacent hydrophobic groups.

Based on the spiropyrrolidinyl oxindole-based substructure, compound **1** (MI-5, $K_i = 8.46$ μ M) was designed to mimic three key residues in p53, but was less potent than natural p53 peptide ($K_i = 1.52$ μ M). Docking studies showed that the phenyl and isopropyl groups of compound **1** mimicked the Phe19 and Leu26 in p53, respectively, to occupy two hydrophobic pockets in MDM2, while the oxindole

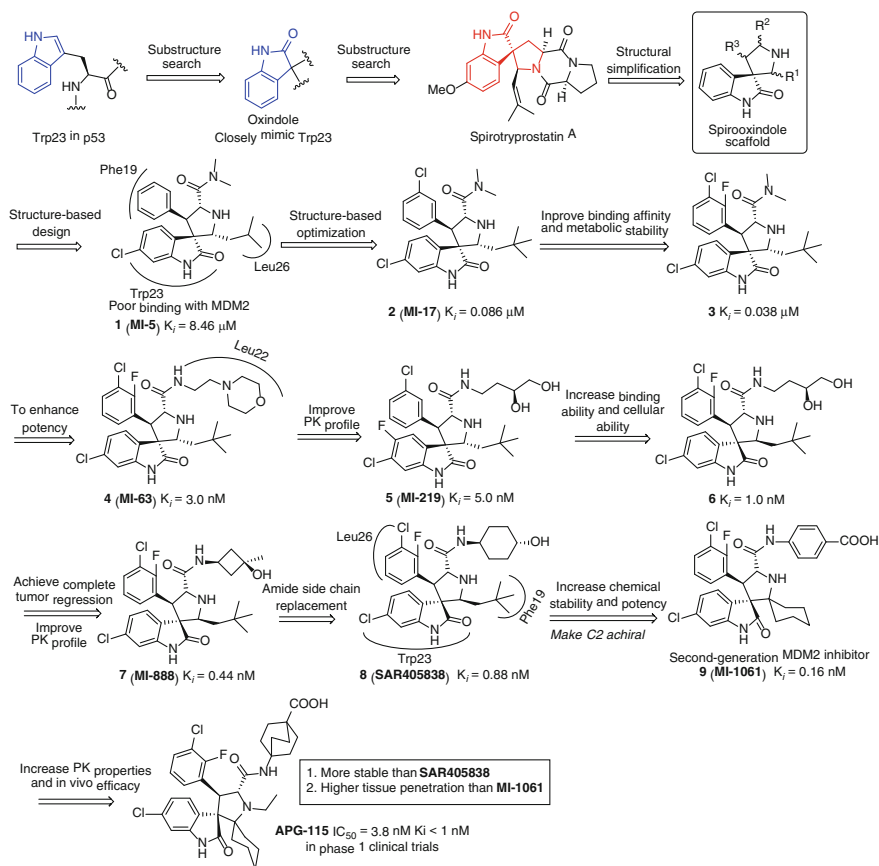


Fig. 8.4 Substructure-based discovery of spirooxindole-derived MDM2 inhibitors **SAR405838** and **APG-115** in clinical trials

core was inserted into the Trp23 cavity. Variations of substituents on the phenyl ring coupled with replacement of isopropyl with larger neopentyl group generated compound **2** (MI-17), which showed significantly increased binding affinity ($K_i = 0.086 \mu\text{M}$, about 100-fold more potent than MI-5) [59]. It is well believed that adding fluorine atom to the parent compounds can improve the physicochemical properties (the acidity, lipophilicity, etc.), thus affecting the ADME properties [60]. Therefore, the fluorine atom was introduced into the phenyl ring of compound **2**, yielding compound **3**, which displayed improved binding affinity to MDM2 ($K_i = 0.038 \mu\text{M}$) [61]. Although compounds **1–3** displayed high binding affinities to MDM2, they were still less potent than the most potent p53-based peptide inhibitor ($K_i = 1 \text{ nM}$) [59]. This suggests compound **3** may fail to occupy additional cavities that are crucial for the MDM2–p53 interactions. The X-ray analysis of MDM2–p53 complex together with mutant analysis [62] and alanine

scanning of p53 peptide [63] proved that aside from Trp23, Phe19, and Leu26, Leu22 was another important residue that was involved in the overall MDM2–p53 interactions. To mimic this additional Leu22 residue, the dimethylamine group in compound **3** was replaced with more hydrophilic morpholin-4-yl-ethylamine group to form MI-63 (compound **4**, $K_i = 3.0$ nM), where the carbon atoms in morphine ring and carbon linker closely mimicked Leu22 in p53 and the oxygen atom in morphine ring provided an additional hydrogen bond with positively charged Lys90 in MDM2. However, MI-63 had a poor PK profile, which hampered further in vivo evaluation [64]. Further modifications of the amide side chain and substituents on the phenyl ring and oxindole core of MI-63 yielded compound **5** (MI-219), which was endowed with increased oral bioavailability. Interestingly, although MI-219 potently inhibited MDM2 and reactivated p53 in cells expressing p53, there was no remarkable toxicity against normal cells with minimal p53 accumulation [64].

Compared to MI-219, compound **6** showed better binding affinity to MDM2 ($K_i = 1$ nM, comparable binding affinity with the most potent p53-based peptide inhibitor) and improved cellular ability, highlighting the importance of substituents on the phenyl rings and the stereochemistry [65]. Both MI-219 and compound **6**, however, failed to achieve complete tumor regression. In order to improve its PK profiles and in vivo antitumor potency, the diol side chain was replaced with the conformationally constrained *tert*-alcohol, yielding orally active compound **7** (MI-888, $K_i = 0.44$ nM), which achieved complete and durable tumor regression in two types of xenograft models [66]. Besides, the *tert*-alcohol group in MI-888 was proven to be able to block the CYP450 oxidation.

The stereochemistry, in some cases, plays an important role in the activity. Different enantiomer may have remarkably different binding affinity to their targets as observed in many drug molecules [45]. It is evident that spirooxindoles have multiple adjacent stereocenters, and different diastereoisomers may exist in the buffer solution of the biological testing. From the structural point of view, the diastereoisomer with all *trans*-configuration should be the most stable one because of the spatial repulsion of adjacent large groups. Indeed, isomerizations through the reversible ring-opening cyclization reaction of spirooxindoles in protic solvents such as MeOH, MeCN, H₂O were observed by some research groups [65–67], resulting in an equilibrium mixture of four diastereoisomers, as shown in MI-888 (Fig. 8.5). Compared to compound **10** ($K_i = 4.5$ nM), MI-888 had about tenfold binding affinity toward MDM2 ($K_i = 0.44$ nM), which suggests that three *trans*-configured hydrophobic substituents attached to the pyrrolidine ring in MI-888 may better mimic three key amino acid residues in p53 to occupy three hydrophobic cavities in MDM2. The structural requirement of all *trans*-configuration for optimal binding ability is probably due to the α -helical structure of *N*-domain of p53, in which Phe19, Trp23, and Leu26 residues may have similar *trans*-like spatial projection.

Replacement of the *tert*-alcohol group with a *trans*-4-hydroxycyclohexylamino group yielded SAR405838 (compound **8**, $K_i = 0.88$ nM), which is currently undergoing phase I clinical assessment for the treatment of human tumors retaining p53 (ClinicalTrials.gov Identifier for SAR405838: NCT01636479 and

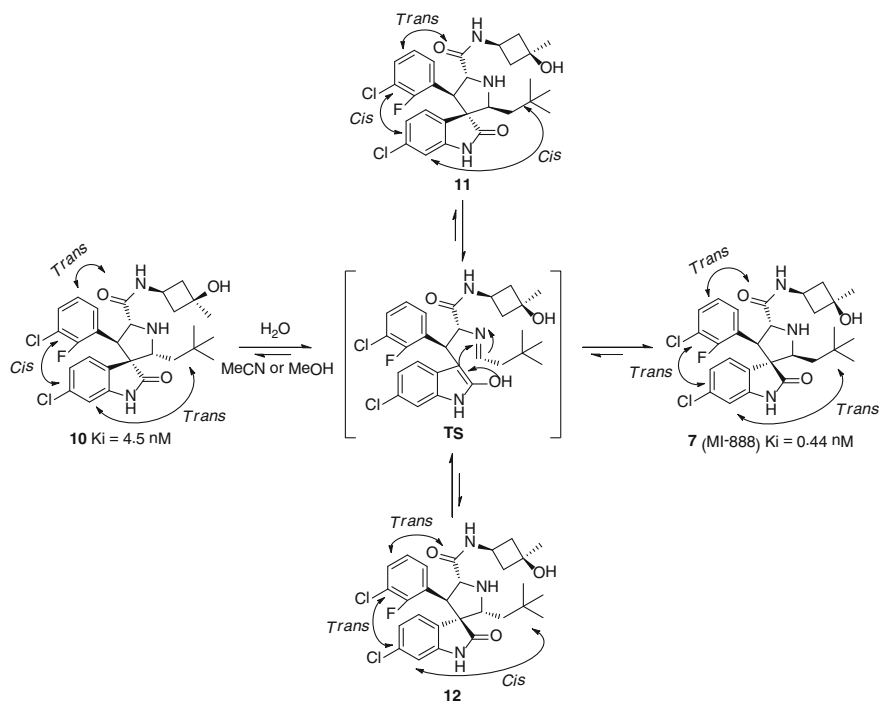


Fig. 8.5 Isomerization of spirooxindole **10** in protic solvents

NCT01985191) [33]. SAR405838 achieved complete and durable tumor regression in four types of xenograft models and induced strong apoptosis by up-regulating PUMA transcription. Very recently, Wang's group found that prolonged treatment of SJS-A-1 tumor cells with SAR405838 induced different degrees of acquired resistance *in vitro* and *in vivo*, and the *in vitro* resistance was due to the mutation of DNA-binding domain of p53 and cannot be further activated by SAR405838 [68]. This type of acquired resistance *in vitro* and *in vivo* in acute leukemia RS4;11 and MV4;11 cell lines through mutation of the TP53 gene was also observed [69].

In terms of the binding model, the co-crystal structure of SAR405838-MDM2 complex showed that SAR405838 not only mimicked the three key residues (Phe19, Trp23, and Leu26) in p53, but also captured additional interactions that were not observed in MDM2-p53 interactions. The Cl atom in the oxindole ring was beneficial for its hydrophobic interaction with MDM2. The π - π interaction between His96 and the 2-fluoro-3-chlorophenyl group was observed, along with a hydrogen bond between the imidazole side chain of His96 and the amide carbonyl group of the hydrophilic chain (Fig. 8.6a). Besides, SAR405838 can also induce refolding of the *N*-terminal domain of MDM2 (residues 10–18) to achieve high binding through Val14 and Thr16 [33]. By contrast, structurally different MI-219 had different binding model with MDM2. The neopentyl and 3-Cl phenyl groups in

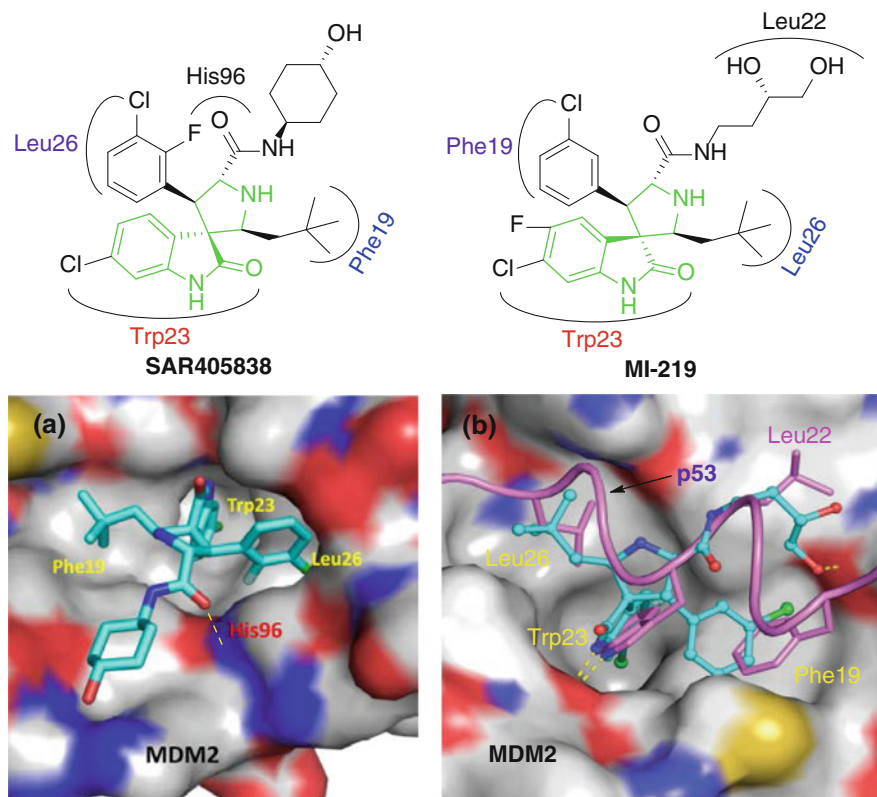


Fig. 8.6 Binding models of MI-219 and SAR405838 with MDM2 (PDB code: 1YCR). Reprinted with permission from Ref. [13]. Copyright © 2014, American Chemical Society

MI-219 mimicked Leu26 and Phe19 residues, respectively, to occupy corresponding cavities in MDM2 (Fig. 8.6b) [64]. Clearly, SAR405838 and MI-219 possessed the same structural scaffold (highlighted in green in Fig. 8.6). Carlos Garcia-Echeverria et al. also observed this kind of difference in binding models of spirooxindoles to MDM2 [70]. This different binding model of MI-219 may explain the suboptimal binding affinity to MDM2 compared to SAR405838 (5.0 nM for MI-219 vs. 0.88 nM for SAR405838).

As shown in Fig. 8.5, spirooxindoles can isomerize through the ring-opening retro-Mannich reaction in protic solvents to give a mixture of four diastereoisomers. Among them, the most potent MDM2 inhibitor is the one with all *trans*-configuration as shown in SAR405838. Based on this, Wang et al. designed a series of second-generation spirooxindoles as MDM2 inhibitors by introducing symmetric C2 substitution on the pyrrolidine ring [58]. Further modifications focusing on variations of C2 substituents and hydrophilic amide chains led to the discovery of MI-1061 (compound **9**, Fig. 8.4), which exhibited excellent chemical stability in

solutions and improved binding affinity to MDM2 ($K_i = 0.16$ nM), and induced apoptosis in the SJSA-1 xenograft model. Compared to the first-generation inhibitors, the second-generation possessed better binding affinity to MDM2. PK studies showed that MI-1061 had considerably lower C_{max} and AUC values than compound SAR405838 upon oral administration, indicating that further improvement of oral PK is needed for stronger in vivo antitumor activity [43]. Further structural modifications for improving tissue penetration were then carried out through decreasing the lipophilicity, reducing the acidity of carboxylic acids, increasing the basicity of the nitrogen atom in the pyrrolidine core, and finally leading to the discovery of APG-115, which is currently undergoing clinical assessment in patients with advanced solid tumor or lymphoma (ClinicalTrials.gov identifier for APG-115: NCT02935907). APG-115 showed extremely high binding affinity to MDM2 with the IC_{50} and K_i of 3.8 nM and <1 nM, respectively, and activated p53 in the SJSA-1 xenograft mice models following a single oral administration. Significantly, APG-115 achieved complete and long-lasting growth inhibition of the SJSA-1 xenograft tumors in mice and demonstrated strong antitumor efficacy in the RS4;11 acute leukemia model.

In addition to Wang's work, Yuuichi et al. also designed a series of spiro-pyrrolidinyl oxindole-based MDM2 inhibitors [71]. Their modifications focused on the variations of amide side chains and C2 substituents, as well as the bioisosteric replacement of phenyl ring with the pyridine ring, generating a library of structurally interesting and biologically important molecules as shown in Fig. 8.7. Apparently, these structures are highly similar to the drug candidates SAR405838, RO8994 (as shown in Fig. 8.4 and Fig. 8.8, respectively), and their second-generation inhibitors (MI-1061, RO2468, and RO5353), reported by Wang and Graves's group in 2013–2014. Intriguingly, all these structures had symmetric C2 substituents (highlighted in bold in scaffold **13** in Fig. 8.7), which were subsequently proved to be crucial for improving chemical stability of such scaffolds and binding affinities to MDM2, leading to the identification of second-generation MDM2 inhibitors such as MI-1061 [58, 72]. However, the inventors of this patent just claimed these compounds can be used as antitumor agents through disrupting MDM2–p53 interactions without detailed biological data reported.

Apart from the spirooxindole-based MDM2 inhibitors (known as MI series), the Graves group identified another series of MDM2 inhibitors, such as RG7388, RO8994, RO2468, and RO5353 (Fig. 8.8). Among them, RG7388 is currently undergoing phase 1 clinical evaluation for the treatment of solid and hematological tumors (ClinicalTrials.gov Identifier for RG7388: NCT02407080).

This program was initiated to identify new MDM2 inhibitors with novel scaffolds, in which two aryl groups (A and B in compound **21**) are 'trans' to each other, different from that in RG7112 (a drug candidate in phase 1 clinical trials belonging to Nutlin family as shown in Fig. 8.2) and MI-219. Much less is known regarding the effect of this trans-configuration of pyrrolidine core toward the binding affinity to MDM2. Based on the structures of RG7112 and MI-219 (A and B rings in both compounds are 'cis' to each other), they designed and synthesized the MDM2 inhibitor compound **21** ($IC_{50} = 196$ nM), which was less potent than RG7112 ($IC_{50} = 18$ nM) but

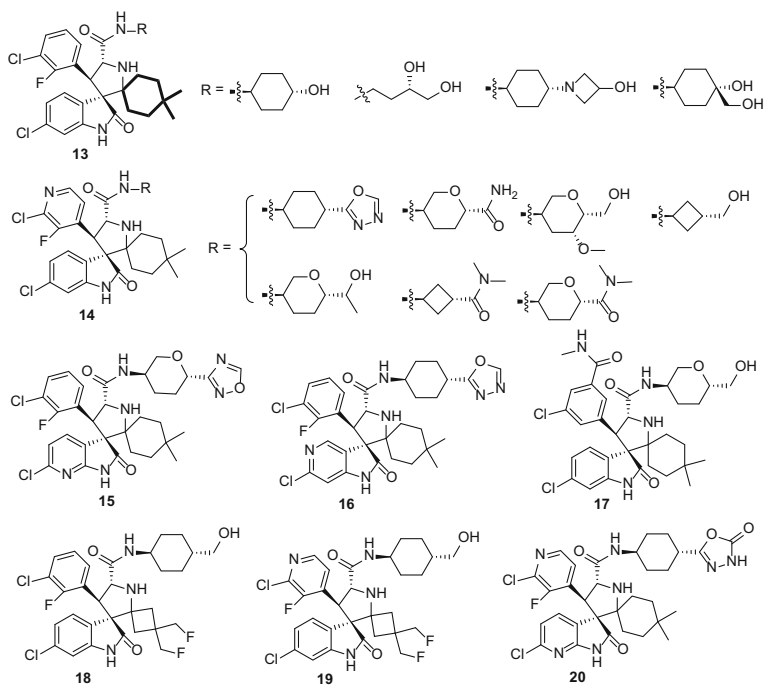


Fig. 8.7 Spirooxindoles and their bioisosteres as MDM2 inhibitors

significantly more potent than its enantiomer ($IC_{50} > 10,000$ nM) [42]. The introduction of fluorine atom to both phenyl rings yielded compound **22** with improved binding affinity to MDM2 ($IC_{50} = 74$ nM). Unfortunately, compounds **21** and **22** were found to have poor oral bioavailability and high clearance rates in mouse PK studies. The diol side chain could be oxidized in the metabolic process, so further modifications focusing on the diol side chain were performed, generating a new series of analogs with diverse amide side chains. Of these compounds, compound **23** with the *p*-benzoic acid group showed markedly increased PK profiles and cellular potency/selectivity ($IC_{50} = 22$ nM), showing promise for further optimizations. Subsequent modifications by introducing electron-donating or withdrawing groups to the phenyl ring eventually led to the discovery of RG7388 (compound **24**, $IC_{50} = 6$ nM).

Very recently, RG7388 was reported to be able to enhance the activity of ionizing radiation (XRT) in xenograft models of childhood sarcoma without inducing extra local XRT skin toxicity [73]. Combination of the key structural units of RG7388 with the oxindole scaffold gave compound **25**, which shared the same structural architecture with SAR405838 with a slight difference in the amide side chain [74]. However, compound **25** was also found to have a high clearance rate (34.6 mL/min/kg) and suboptimal oral bioavailability ($F = 21$), albeit with impressive cellular potency ($IC_{50} = 5$ nM). In order to improve the PK properties,

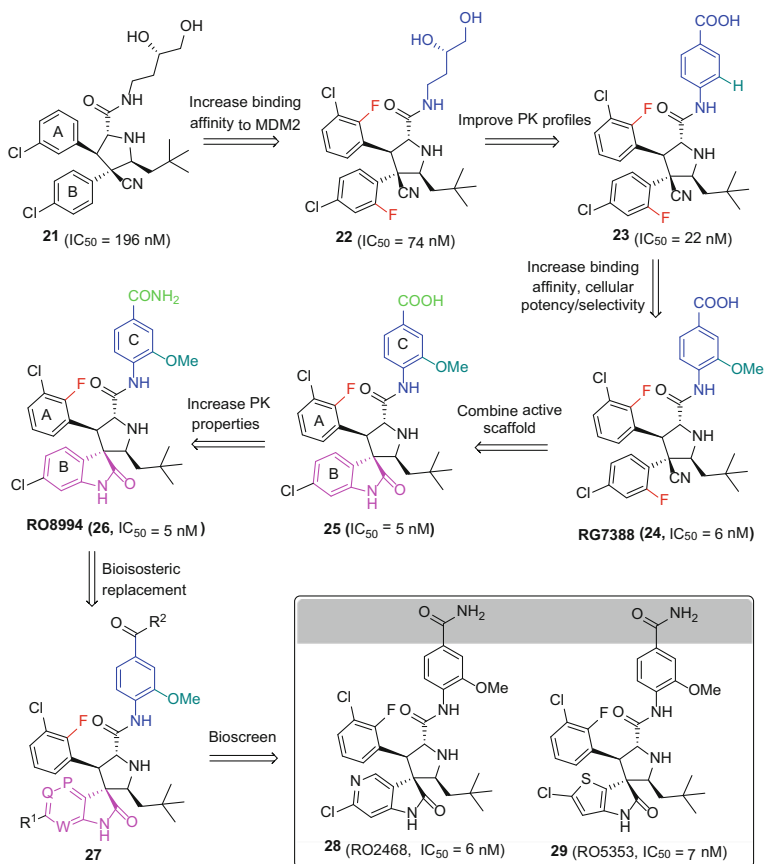


Fig. 8.8 Identification of drug candidate RG7388 and further optimizations

further optimization of compound **25** by converting the terminal carboxylic acid group to carboxamide group yielded RO8994 (compound **26**), which exhibited significantly decreased clearance rate (5.8 mL/min/kg) and improved oral bioavailability ($F = 92$). Besides, the aromatic group C in both RG7388 and RO8994 can markedly improve the metabolic stability, PK properties, cellular potency/selectivity, and in vivo efficacy, compared to MI-888 with an aliphatic amide side chain [62, 63]. RG7388 and RO8994 dose-dependently and non-genotoxically induced p53 stabilization, cell cycle arrest, and apoptosis in tumor cells retaining wt p53. An impressive in vivo efficacy for RG7388 and RO8994 against human SJS1 tumor xenografts was observed at significantly lower doses and exposures, more efficacy than RG7112 and MI-888. The interaction between 6-chlorooxindole group and the Trp23 subpocket is believed to be the most crucial. Further derivatizations of RO8994 on the 6-chlorooxindole motif using bioisosteric replacement strategies were carried out in the Graves group,

generating a new series of RO8994 analogs as shown in **27** (Fig. 8.8) [75]. Among this series, RO2468 (compound **28**) and RO5353 (compound **29**) showed promise for clinical development with excellent PK profiles, impressive in vivo efficacy in SJSA1 xenograft models, and excellent cellular potency/selectivity. Additionally, computational docking studies showed that this series of compounds had similar binding models with SAR405838. The 6-chlorooxindole motif occupied the Trp23 pocket with the NH forming a hydrogen bond with the backbone carbonyl of MDM2, while the 2-fluoro-3-chloro phenyl group and the neopentyl group were filled into Leu26 and Phe19 hydrophobic pockets, respectively. In order to exhibit their anticancer potential for clinical development, the preclinical data of RG7388, RO8994, RO2468, and RO5353 are summarized in Table 8.1.

Apart from those discussed above, the Graves group also designed other series of spirooxindoles as MDM2 inhibitors (Fig. 8.9). Initially, they found that only the (*S*)-**30** was active with an IC₅₀ of 3.9 μM in a biochemical binding assay [76]. This moderate binding affinity may be attributed to the suboptimal binding of acylated piperidine group to the Phe19 pocket, although the 6-chlorooxindole motif can occupy the deep and narrow Trp23 pocket in MDM2. Further structural rigidization through cyclization strategies gave a library of small molecules with different scaffolds [77–82]. Of these scaffolds, scaffolds 2 and 4 (highlighted in blue in Fig. 8.9) failed to progress because of unfavorable physicochemical or pharmaceutical properties, albeit with enhanced binding affinities. For the remaining scaffolds, they just claimed that these compounds can serve as antitumor agents by targeting MDM2, but no further information has been reported since then. Compared to those with pyrrolidine core such as SAR405838 and RG7388, the suboptimal binding affinities of these scaffolds to MDM2 in Fig. 8.9 are probably attributed to their structural features. In contrast to 6- or 7-membered ring systems, 5-membered pyrrolidine ring systems are generally more flexible because of their

Table 8.1 Preclinical data of RG7388, RO8994, RO2468, and RO5353

Compound	RG7388	RO8994	RO2468	RO5353
MTT IC ₅₀ (μM) ^a	0.03	0.02	0.015	0.007
HTRF IC ₅₀ (nM) ^b	6	5	6	7
HLM_CL (mL/min/kg)	4.3	7.5	10.2	2.0
PO dose (mg/kg)	50	25	5	10
PO AUC/dose (μg h/mL/mg/kg)	1.3	3.7	4.2	1.5
PO C _{max} (μg/mL)	9.9	5.8	2.1	1.3
IV dose (mg/kg)	5	0.64	2	2.5
CL (mL/min/kg)	10.3	5.8	1.8	9.9
t _{1/2} (h)	1.6	7.1	3.0	3.0
F (%)	80	92	46	92

^aMean IC₅₀ of three wt p53 cancer cell lines (SJSA, RKO, and HCT116)

^bThe binding affinity was determined by the homogeneous time-resolved fluorescence (HTRF) binding assay

^cF represents oral bioavailability

pseudorotational mobility [83–87] and have two predominant puckering modes, namely the ‘*Cis–Cis*’ and ‘*trans–trans*’ models [88]. The ‘*trans–trans*’ model has been proved to be crucial for optimal binding to MDM2 as shown in SAR405838 and RG7388, where the two aromatic rings (A and B rings in Fig. 8.8) adopt a *trans*-configuration. Evidently, scaffolds in Fig. 8.9 are rigid and cannot maintain a ‘*trans–trans*’ configuration.

Aside from those discussed above that can inhibit MDM2–p53 interactions at nanomolar levels, other MDM2 inhibitors with different core structures (highlighted in red in Fig. 8.10) were also reported before. These MDM2 inhibitors may help us gain deeper insights into the structure–activity relationships (SARs) and design novel small-molecule inhibitors with excellent potency, selectivity, and low toxicity although these inhibitors showed moderate MDM2 inhibition ($K_i > 1 \mu\text{M}$). Isabel Gomez-Monterrey et al. designed a new series of indoline-3, 2'-thiazolidines as possible MDM2 inhibitors from the imidazo-[1, 5-*c*] thiazole scaffold (Fig. 8.10), similar to scaffold 7 in Fig. 8.9 [89]. Initially, they proposed that the imidazo-[1, 5-*c*] thiazole scaffolds such as compound **32** could define the orientation of oxindole, aryl, and alkyl groups to mimic the three key residues (Trp23, Phe19, and Leu26) in p53. Compound **32** showed good cytotoxicity against HEK, M14, and U937 cancer cell lines ($\text{IC}_{50} < 1 \mu\text{M}$) and increased p53 expression. NMR studies showed compound **32** can block MDM2–p53 interactions, but was less potent than Nutlin-3. Subsequent modifications with the aim of reducing conformational constraints by the ring-opening of imidazolone gave compound **33**, which exhibited excellent cytotoxicity against a panel of human cancer cell lines, especially for

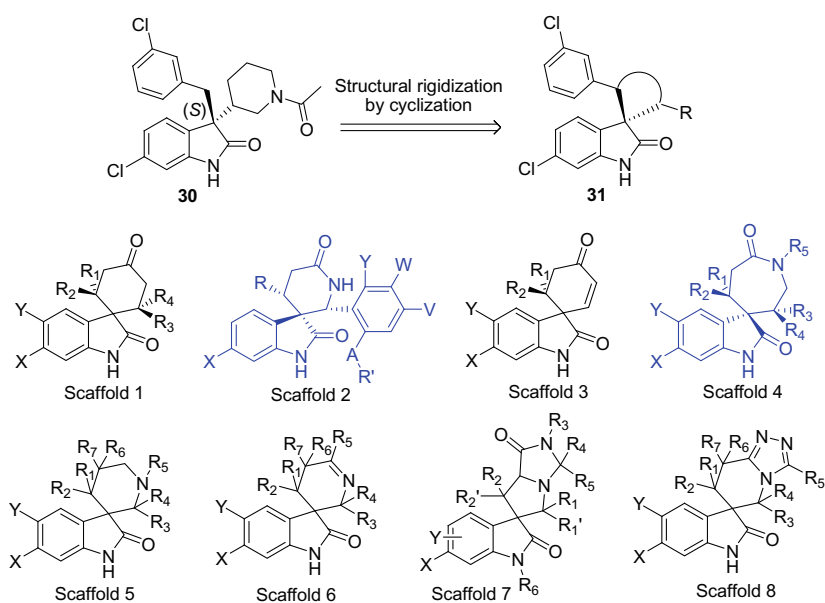


Fig. 8.9 Structurally rigid spirooxindoles as possible MDM2 inhibitors

MCF-7, U937, and HT29 cell lines with the IC_{50} values of 0.04, 0.07, and 0.07 μM , respectively. However, certain cytotoxicity against human normal cell line HGF was also observed ($IC_{50} = 1.60 \mu\text{M}$). The immunoprecipitation assay indicated that compound **33** inhibited 30% of MDM2-p53 interactions. Docking studies showed that the cyclohexyl carbonyl and ethyl ester groups occupied the Trp23 and Phe19 pockets, respectively, while the oxindole core was inserted into the Leu54 pocket, not the Leu26. The hydrolysis of ester group resulted in a loss of activity as the hydrophilic acid group cannot be filled into the hydrophobic Phe19 cavity.

Very recently, Ivanenkov and co-workers designed dispiro-indolinones by combining the spirooxindole and 2-thiohydantoin moiety [90]. The most potent compound **34** (diastereomeric mixture) among this series showed good inhibitory activity against several cancer cell lines of different origins with the IC_{50} values

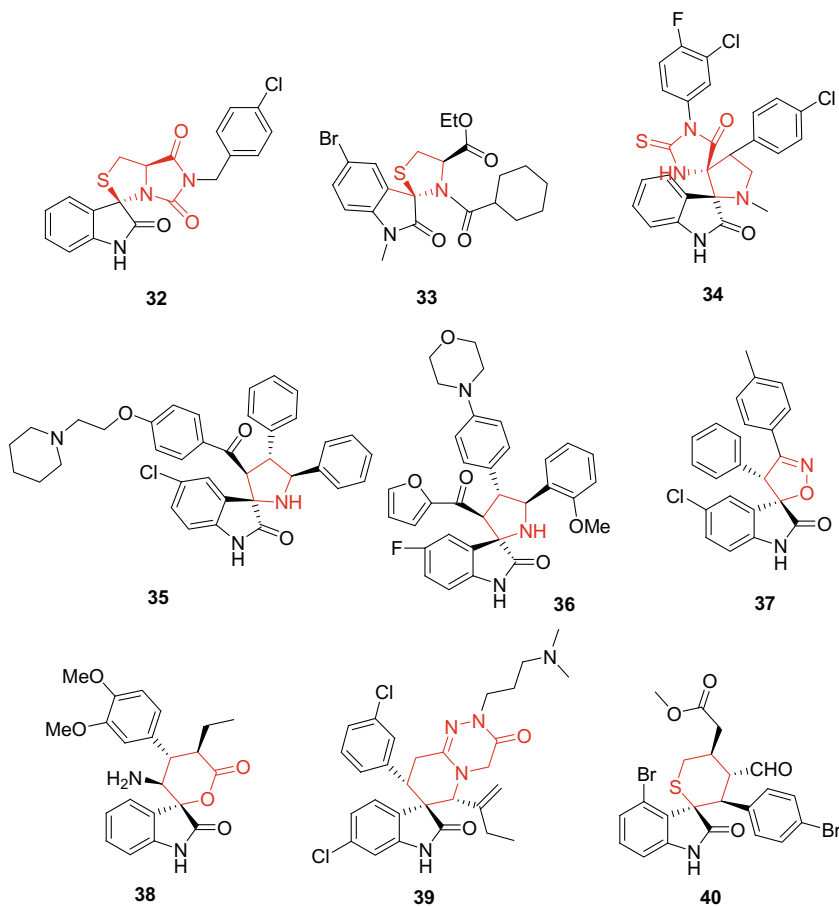


Fig. 8.10 Other reported spirooxindole-based MDM2 inhibitors

ranging from 4.88 to 9.08 μM ($\text{IC}_{50} = 4.88 \mu\text{M}$ against MCF-7 cells). No selectivity, however, toward HCT116 ($\text{p53}^{+/+}$) and HCT116 ($\text{p53}^{-/-}$) was observed. Compound **34** was less potent and selective than Nutlin-3a. Based on the 2D structural similarity analysis of reported MDM2 inhibitors and docking results, the authors proposed that MDM2 could be the main target of their compounds.

Previously reported potent MDM2 inhibitors such as Nutlins, AM8553, MI family, and RG7388 possess diaryl substituents around the pyrrolidine ring. Based on the structural features, Kumar et al. designed a series of diaryl-spirooxindoles having the spiro [indoline-3, 2'-pyrrolidin]-2-one scaffold, which were bioisosteres of MI-63 (as shown in Fig. 8.4) [91]. Of this series, compound **35** (Fig. 8.10) exhibited the best inhibition against breast cancer cell lines MCF-7 and MDA-MB 231 with the IC_{50} values of 3.7 and 6.5 μM , respectively, more potent than Nutlin-3 and OH-Tamoxifen. Also, good selectivity was observed ($\text{IC}_{50} > 50 \mu\text{M}$ against HEK-293 and VERO cells). Further mechanism studies showed that compound **35** displayed excellent *in vivo* antitumor activity in wt p53 containing MCF-7 xenograft model in nude mice by restoring p53 function (66% lower in tumor volume and size than that of vehicle group at 20 mg/kg after 14-day treatment) and modulated downstream proteins p21, pRb, and CCND1. Structurally similar compound **36** designed by He and co-workers inhibited growth of MDM2 overexpressed LNCaP cells with an IC_{50} value of 0.35 $\mu\text{g/mL}$ [92].

Santos's group synthesized spiroisoxazoline oxindoles, where three hydrophobic groups (two phenyl rings and the oxindole core) were designed to mimic three key residues Phe19, Leu26, and Trp23 in p53 [93]. Compound **37** was found to be the most potent one against HepG2 expressing wt p53 with an GI_{50} value of 29.11 μM , about twice potent than Nutlin-3 ($\text{GI}_{50} = 51.31 \mu\text{M}$). The BiFC (venus-based bimolecular fluorescence complementation) assay indicated compound **37** inhibited MDM2-p53 interactions and dose-dependently induced expression of cleaved PARP and active caspase-3.

Compound **38** designed by Peng et al. bonded to MDM2 moderately ($K_i = 0.21 \mu\text{M}$) and selectively inhibited growth of HCT116 ($\text{p53}^{+/+}$) and PC-3 ($\text{p53}^{-/-}$) cells with the IC_{50} values of 2.26 and 25.16 μM , respectively, while compound **39** was found to be able to dock into MDM2 pockets [94]. Very recently, Han et al. reported that chroman-fused spirooxindoles with spirohexyl oxindole scaffold can potentially inhibit growth of an array of cancer cells ($\text{IC}_{50} = 1.7 \mu\text{M}$ against MCF-7) by blocking the MDM2-p53 interactions and downstream pathways [95]. Sheng et al. identified a series of structurally novel tetrahydrothiopyran fused spirooxindoles using the organocatalysis strategy, which showed good cytotoxicity through interrupting the p53-MDM2 interactions [96]. Among these compounds, compound **40** potentially inhibited growth of A549, HCT116, and MDA-MB-231 cells with the IC_{50} values ranging from 1.57 to 3.55 μM . The MDM2 inhibition of compound **40** was further confirmed by the fluorescence polarization and Western blotting assays, showing that compound **40** inhibited MDM2 with a K_D value of 2.2 μM and up-regulated expression of p53 and MDM2 in A549 cells concentration-dependently. Docking simulations showed that the oxindole, methyl ester, and bromophenyl groups occupied the Leu26,

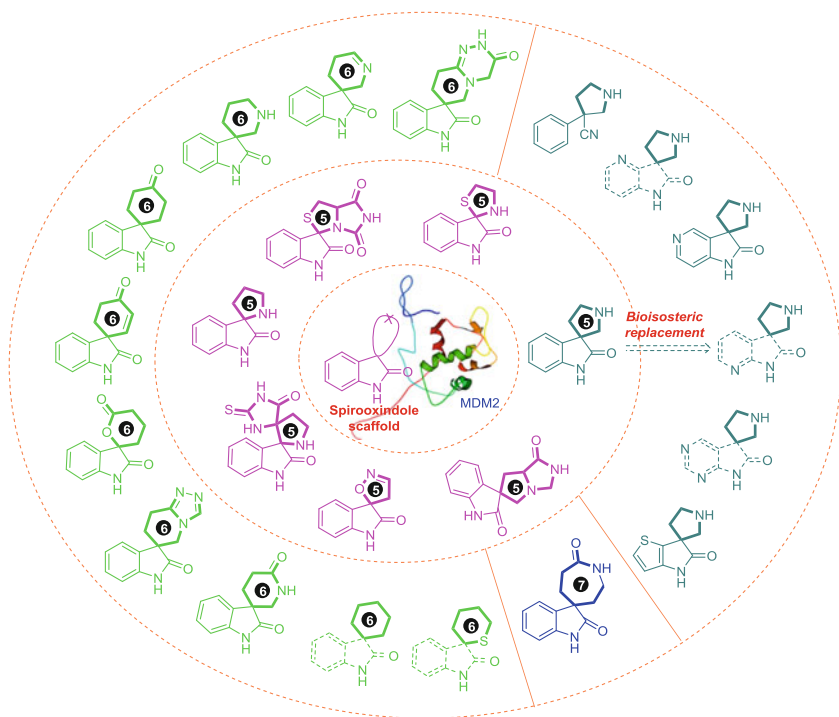


Fig. 8.11 An overview of spirooxindole-based scaffolds as MDM2 inhibitors

Phe19, and Trp23 cavity of MDM2, respectively. It is worth noting that this series of compounds also possessed modifiable synthetic handles (e.g., the ester and aldehyde moiety), which could be utilized for late-stage structural modifications to search more potent MDM2 inhibitors for anticancer treatment.

Based on previously reported small-molecule inhibitors of MDM2–p53 interactions discussed above, the structural scaffolds of spirooxindole-based MDM2 inhibitors are summarized in Fig. 8.11 (substituents attached to the scaffolds are omitted).

8.2.2 Summary on SARs

On the basis of above analysis, it is evident that potent spirooxindole-based MDM2 inhibitors such as SAR405838, APG-115, RO8994, and RG7388 possess scaffolds **41** and **42**. Scaffold **42** can be regarded as the ring-opening biosisostere of scaffold **41** (Fig. 8.12). The general trend of SARs related to scaffold **41** was consistent with that of scaffold **42**, and the cyano group of scaffold **42** was found to be critical for maintaining the *trans*-configuration of A and B rings [42].

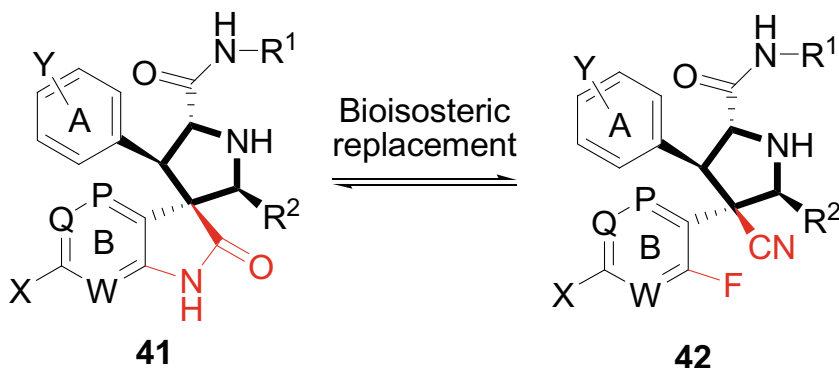


Fig. 8.12 General scaffolds of spirooxindoles and their bioisosteres as MDM2 inhibitors

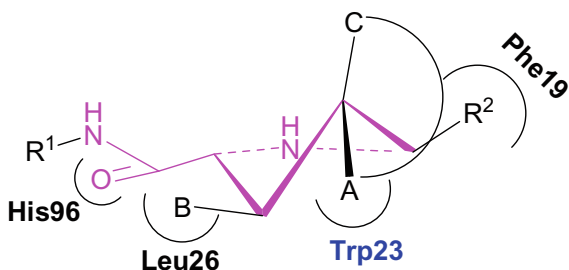
For spirooxindole-based MDM2 inhibitors and their bioisosteres, the SARs are summarized below, although this summary may be not comprehensive.

- The structure scaffold** (highlighted in bold in scaffolds **41** and **42**). The saturated 5-membered rings, the pyrrolidine ring in particular, are more preferred than structurally rigid 6-/7-membered rings (as shown in Fig. 8.9) and unsaturated 5-membered rings (as shown in compound **37** in Fig. 8.10) as saturated 5-membered rings are more flexible to maintain the ‘*trans-trans*’ configuration (as shown in SAR405838, RG7388, etc.), which has been proved to be crucial for optimal binding to MDM2. The pyrrolidine ring seems to be the optimal structural unit for designing spirooxindole-based MDM2 inhibitors to date. However, much less is known about the function of NH unit in pyrrolidine in binding affinity to MDM2. Recent work by Wang et al. showed the addition of ethyl group to the nitrogen atom improved the chemical stability [43]. Other 5-membered rings such as tetrahydrofuran, tetrahydrothiophene, cyclopentane have not yet been investigated.
- The stereochemistry**. Substituents around the pyrrolidine core should be ‘*trans*’ to each other for optimal binding. Variations of configurations may result in suboptimal binding affinities to MDM2 ($K_i = 4.5$ and 0.44 nM for compound **10** and MI-888, respectively, as shown in Fig. 8.5) and different binding models with MDM2 (as shown in Fig. 8.6). The *trans*-substituents can better mimic three key residues (Phe19, Trp23, and Leu26) in p53 to occupy hydrophobic subpockets on the surface of MDM2. This preferred *trans*-configuration could be explained by the α -helical structure of *N*-terminal domain of p53, where three key residues are ‘*trans*’ to each other. Besides, compounds with all *trans*-configurations are more chemically stable in protic solvents.
- The R² group**. Larger aliphatic groups may be preferred over smaller ones. The binding affinities of inhibitors to MDM2 increase following the order: cyclohexyl (in MI-1061) > neopentyl (in SAR405838) > 2-isobutyl (in MI-5). Large groups may fit well into the Phe19 hydrophobic pocket with improved binding

affinities. Little known is about the effect of aromatic rings on the binding affinities, although the aromatic ring can better mimic the Phe19 residue (as depicted in Fig. 8.3c). Also, the introduction of symmetric substituents (e.g., the cyclohexyl group in MI-1061) can increase the chemical stability by irreversible isomerization in protic solvents.

- (d) **The oxindole core.** The oxindole core in scaffold **41** or the phenyl ring (B) in scaffold **42** occupies the deep and narrow Trp23 pocket, which is the most crucial for blocking MDM2–p53 interactions. The NH in the oxindole core forms a hydrogen bond with the backbone carbonyl in MDM2. Modifications on the NH position may result in decreased binding affinity. The chlorine atom at the 6-position of the oxindole core is beneficial for enhancing binding affinity because of the additional interaction of 6-Cl with the Trp23 cavity. Bioisosteric replacement of the phenyl ring with pyridine or thiophene gives comparable binding affinity but with improved cytotoxicity as shown in Table 8.1 (RO8994 vs RO2468 and RO5353) [75]. Replacement of phenyl ring with pyridinyl ring leads to significantly decreased oral bioavailability (RO8994 vs. RO2468). The position of nitrogen atom in the pyridine ring in scaffold **41** is important for the binding affinity and cytotoxicity. When P or W in scaffold **41** is the nitrogen atom, the binding ability and cytotoxicity decrease accordingly. The fluorine atom in scaffold **42** can improve binding ability to MDM2.
- (e) **The A ring in Scaffolds 41 and 42.** The phenyl ring (A) in these two types of scaffolds has been proved to be inserted into the Leu26 pocket in MDM2. Also, the π – π interaction between His96 and the phenyl ring has been observed and is crucial for enhancing binding affinity to MDM2. Therefore, the substituent without the π -system would be less favored. The introduction of fluorine and chlorine atoms into the 2- and 3-position, respectively, can improve binding affinity and metabolic stability.
- (f) **The amide side chain.** In contrast to the aliphatic amide side chains (as shown in MI series), the introduction of the aromatic side chain (as shown in RO8994 in Fig. 8.8) can markedly improve the metabolic stability, PK properties, cellular potency/selectivity, and in vivo efficacy. Among the aromatic groups, the introduction of the terminal benzamide group can reduce the clearance rates and improve oral bioavailability compared to the benzoic acid group (RO8994 vs. compound **25** in Fig. 8.8). Besides, the amide carbonyl group forms a hydrogen bond with His96. The ester group may be less preferred than the amide group as the ester group is not stable enough and may undergo the enzymatic hydrolysis under the physiological conditions. More importantly, a hydrophilic amide side chain (solvent-exposed polar group) is necessary to protect the hydrophobic interface between MDM2 and inhibitors from surrounding solvent [97]. Lack of this hydrophilic moiety may cause suboptimal binding affinity. Most of the potent small molecules that disrupt MDM2–p53 interactions possess a hydrophilic amide side chain as shown in drug candidates in Fig. 8.2. It is believed that the solvent-exposed polar group can provide additional interactions that are outside the MDM2–p53 interactions. For example, the diol group in MI-219 can contact with Leu22 as shown in Fig. 8.6.

Fig. 8.13 Prolinamide-based ‘3+1’ model for designing potent MDM2 inhibitors



On the basis of above SARs analysis, we tentatively propose the prolinamide (highlighted in purple in Fig. 8.13)-based ‘3+1’ model for designing potent MDM2 inhibitors based on the following considerations: (1) the amide carbonyl group in prolinamide has an additional interaction with His96 through a hydrogen bond, which is beneficial for improving binding affinity; (2) the pyrrolidine ring of prolinamide can maintain the required ‘*trans-trans*’ configuration for optimal binding to MDM2 due to its pseudorotational mobility. The ‘3’ refers to the three hydrophobic moieties (R^2 , A, and B) that are designed to occupy the Phe19, Trp23, and Leu26 subpockets, respectively, in MDM2. The ‘B’ group with a π -system can interact with His96 near the Leu26 pocket through the π - π stacking. It should be noted that a cyclic unit (e.g., the oxindole core in SAR405838) formed by A and C can also fit well into the Trp23 cavity. The ‘1’ refers to the hydrophilic amide side chain (R^1), which may capture additional interactions.

8.3 Conclusions and Outlooks

Spiro compounds have drawn unprecedented attention in drug discovery because of its prevalence in natural products and the 3D structural features. It is well believed that non-flat spiro compounds can specifically bind to biological targets with reduced conformational entropy. All these features make spiro scaffolds attractive starting points in drug discovery programs.

Historically, disruption of PPIs is always challenging as PPIs generally involve a large and flat interface. Differently, the MDM2–p53 interactions are primarily mediated by three key residues (Trp23, Phe19, and Leu26), and this well-defined fashion has provided a rationale for designing non-peptide small-molecule inhibitors. Particularly, spirooxindole scaffolds have shown diverse bioactivities and have been observed in drug leads such as SAR405838 (MDM2 inhibitor), CFI-400945 (the first PLK4 inhibitor), and KAE609 (antimalarial agent) as well as natural products. Interestingly, spirooxindoles are privileged scaffolds in identifying potent MDM2 inhibitors, and several potent MDM2 inhibitors (SAR405838, RO8994, etc.) derived from spirooxindoles are currently in preclinical or clinical trials. After scaffold analysis, we found that 5-membered rings fused at C-3 position,

the pyrrolidine ring in particular, are more preferred than structurally rigid 6/7-membered rings for optimal binding affinity to MDM2 because of the pseudorotational mobility of pyrrolidine ring. Based on the SARs analysis and binding models of MDM2 inhibitors to MDM2 protein, we tentatively proposed the prolinamide-based '3+1' model, which may be regarded as the general template for designing small molecules interrupting the MDM2–p53 interactions.

In general, potent MDM2 inhibitors should possess three hydrophobic groups and one hydrophilic group. The hydrophobic groups mimic three key residues Phe19, Trp23, and Leu26 in p53 to occupy cavities in MDM2, while the hydrophilic group exposed to the solvent region can protect the hydrophobic interaction surface between MDM2 and potent inhibitors from surrounding solvent and provide extra interactions that are out of MDM2–p53 interaction for optimal binding ability. Although several MDM2 inhibitors have entered phase I clinical trials for anti-cancer treatment, challenges still exist and should be addressed further. Acquired resistance to these MDM2 inhibitors has been observed after prolonged treatment. Therefore, the development of new MDM2 antagonists for the newly occurred mutations and combinations of MDM2 inhibitors with other agents that are effective against p53-mutated cancer cells are promising strategies against the acquired resistance. Another challenge is the toxicity of these MDM2 inhibitors to normal tissues as p53 is expressed in all proliferative cells and plays pivotal roles in regulating normal cellular processes. The activation of p53 in normal cells may result in unwanted side effects or even toxicity. Appropriate dose regimes that maintain strong inhibitory activity but with less toxicity to normal tissues would alleviate the toxicity.

Acknowledgements This work was supported by the National Natural Science Foundation of China (No. 81430085, 21372206, and 81703326, National Key Research Program of Proteins (No. 2016YFA0501800), Key Research Program of Henan Province (No. 1611003110100), Scientific Program of Henan Province (No. 182102310123), China Postdoctoral Science Foundation (No. 2018M630840), Key Research Program of Higher Education of Henan Province (No.18B350009), and the Starting Grant of Zhengzhou University (No. 32210533).

References

1. Biegging KT, Mello SS, Attardi LD (2014) Unravelling mechanisms of p53-mediated tumour suppression. *Nat Rev Cancer* 14:359–370
2. Wu X, Bayle JH, Olson D et al (1993) The p53-mdm-2 autoregulatory feedback loop. *Genes Dev* 7:1126–1132
3. Harris SL, Levine AJ (2005) The p53 pathway: positive and negative feedback loops. *Oncogene* 24:2899–2908
4. Chen F, Wang W, El-Deiry WS (2010) Current strategies to target p53 in cancer. *Biochem Pharmacol* 80:724–730
5. Moll UM, Petrenko O (2003) The MDM2-p53 Interaction. *Mol Cancer Res* 1:1001–1008
6. Feki A, Irminger-Finger I (2004) Mutational spectrum of p53 mutations in primary breast and ovarian tumors. *Crit Rev Oncol Hematol* 52:103–116

7. Momand J, Jung D, Wilczynski S et al (1998) The MDM2 gene amplification database. *Nucleic Acids Res* 26:3453–3459
8. Forslund A, Zeng Z, Qin L-X et al (2008) MDM2 gene amplification is correlated to tumor progression but not to the presence of SNP309 or TP53 mutational status in primary colorectal cancers. *Mol Cancer Res* 6:205–211
9. Dickens MP, Fitzgerald R, Fischer PM (2010) Small-molecule inhibitors of MDM2 as new anticancer therapeutics. *Semin Cancer Biol* 20:10–18
10. Barakat K, Mane J, Friesen D et al (2010) Ensemble-based virtual screening reveals dual-inhibitors for the p53–MDM2/MDMX interactions. *J Mol Graph Model* 28:555–568
11. Shangary S, Wang S (2009) Small-molecule inhibitors of the MDM2–p53 protein-protein interaction to reactivate p53 function: a novel approach for cancer therapy. *Annu Rev Pharmacol Toxicol* 49:223–241
12. Tanimura S, Ohtsuka S, Mitsui K et al (1999) MDM2 interacts with MDMX through their RING finger domains. *FEBS Lett* 447:5–9
13. Zhao Y, Aguilar A, Bernard D et al (2015) Small-molecule inhibitors of the MDM2–p53 protein-protein interaction (MDM2 inhibitors) in clinical trials for cancer treatment. *J Med Chem* 58:1038–1052
14. Brown CJ, Cheok CF, Verma CS et al (2011) Reactivation of p53: from peptides to small molecules. *Trends Pharmacol Sci* 32:53–62
15. Saha T, Kar RK, Sa G (2015) Structural and sequential context of p53: a review of experimental and theoretical evidence. *Prog Biophys Mol Biol* 117:250–263
16. Nero TL, Morton CJ, Holien JK et al (2014) Oncogenic protein interfaces: small molecules, big challenges. *Nat Rev Cancer* 14:248–262
17. Guo W, Wisniewski JA, Ji H (2014) Hot spot-based design of small-molecule inhibitors for protein–protein interactions. *Bioorg Med Chem Lett* 24:2546–2554
18. Kussie PH, Gorina S, Marechal V et al (1996) Structure of the MDM2 oncoprotein bound to the p53 tumor suppressor transactivation domain. *Science* 274:948–953
19. Vassilev LT, Vu BT, Graves B et al (2004) In vivo activation of the p53 pathway by small-molecule antagonists of MDM2. *Science* 303:844–848
20. Vassilev LT (2007) MDM2 inhibitors for cancer therapy. *Trends Mol Med* 13:23–31
21. Lv P-C, Sun J, Zhu H-L (2015) Recent advances of p53-MDM2 small molecule inhibitors (2011–Present). *Curr Med Chem* 22:618–626
22. Zak K, Pecak A, Rys B et al (2013) Mdm2 and MdmX inhibitors for the treatment of cancer: a patent review (2011–present). *Expert Opin Ther Pat* 23:425–448
23. Wang W, Hu Y (2012) Small molecule agents targeting the p53-MDM2 pathway for cancer therapy. *Med Res Rev* 32:1159–1196
24. Liu L, Bernard D, Wang S (2015) Case study: discovery of inhibitors of the MDM2–p53 protein-protein interaction. In: Meyerkord CL, Fu H (eds) *Protein-protein interactions*, vol 1278. *Methods in molecular biology*. Springer, New York, pp 567–585
25. Zhang B, Golding BT, Hardcastle IR (2015) Small-molecule MDM2-p53 inhibitors: recent advances. *Future Med Chem* 7:631–645
26. Hardcastle IR (2014) Targeting the MDM2–p53 protein-protein interaction: design, discovery, and development of novel anticancer agents. In: Neidle S (ed) *Cancer drug design and discovery*, 2nd edn. Academic Press, San Diego, pp 391–426
27. Popowicz GM, Dömling A, Holak TA (2011) The structure-based design of Mdm2/Mdmx–p53 inhibitors gets serious. *Angew Chem Int Ed* 50:2680–2688
28. Khoury K, Popowicz GM, Holak TA et al (2011) The p53-MDM2/MDMX axis—a chemotype perspective. *MedChemComm* 2:246–260
29. Lemos A, Leão M, Soares J et al (2016) Medicinal chemistry strategies to disrupt the p53–MDM2/MDMX interaction. *Med Res Rev* 36:789–844
30. Secchiero P, Bosco R, Celeghini C et al (2011) Recent advances in the therapeutic perspectives of Nutlin-3. *Curr Pharm Design* 17:569–577

31. Koblisch HK, Zhao S, Franks CF et al (2006) Benzodiazepinedione inhibitors of the Hdm2: p53 complex suppress human tumor cell proliferation in vitro and sensitize tumors to doxorubicin in vivo. *Mol Cancer Ther* 5:160–169
32. Rew Y, Sun D, Yan X et al (2014) Discovery of AM-7209, a potent and selective 4-amidobenzoic acid inhibitor of the MDM2–p53 interaction. *J Med Chem* 57:10499–10511
33. Wang S, Sun W, Zhao Y et al (2014) SAR405838: an optimized inhibitor of MDM2–p53 interaction that induces complete and durable tumor regression. *Cancer Res* 74:5855–5865
34. Sun D, Li Z, Rew Y et al (2014) Discovery of AMG 232, a potent, selective, and orally bioavailable MDM2–p53 inhibitor in clinical development. *J Med Chem* 57:1454–1472
35. Canon J, Osgood T, Olson SH et al (2015) The MDM2 inhibitor AMG 232 demonstrates robust anti-tumor efficacy and potentiates the activity of p53-inducing cytotoxic agents. *Mol Cancer Ther* 14:649–658
36. Wang Y, Zhu J, Liu J et al (2014) Optimization beyond AMG 232: Discovery and SAR of sulfonamides on a piperidinone scaffold as potent inhibitors of the MDM2–p53 protein–protein interaction. *Bioorg Med Chem Lett* 24:3782–3785
37. Valat T, Masuya K, Baysang F et al (2014) Mechanistic study of NVP-CGM097: a potent, selective and species specific inhibitor of p53–Mdm2. *Cancer Res* 74:1798
38. Gessier F, Kallen J, Jacoby E et al (2015) Discovery of dihydroisoquinolinone derivatives as novel inhibitors of the p53–MDM2 interaction with a distinct binding mode. *Bioorg Med Chem Lett* 25:3621–3625
39. Holzer P, Masuya K, Furet P et al (2015) Discovery of a dihydroisoquinolinone derivative (NVP-CGM097): a highly potent and selective MDM2 inhibitor undergoing phase 1 clinical trials in p53wt tumors. *J Med Chem* 58:6348–6358
40. Tovar C, Graves B, Packman K et al (2013) MDM2 small-molecule antagonist RG7112 activates p53 signaling and regresses human tumors in preclinical cancer models. *Cancer Res* 73:2587–2597
41. Vu B, Wovkulich P, Pizzolato G et al (2013) Discovery of RG7112: a small-molecule MDM2 inhibitor in clinical development. *ACS Med Chem Lett* 4:466–469
42. Ding Q, Zhang Z, Liu J-J et al (2013) Discovery of RG7388, a potent and selective p53–MDM2 inhibitor in clinical development. *J Med Chem* 56:5979–5983
43. Aguilar A, Lu J, Liu L et al (2017) Discovery of 4-((3'R,4'S,5'R)-6"-Chloro-4'-(3-chloro-2-fluorophenyl)-1'-ethyl-2"-oxodispiro[cyclohexane-1,2'-pyrrolidine-3',3"-indoline]-5'-carboxamido)bicyclo[2.2.2]octane-1-carboxylic Acid (AA-115/APG-115): a potent and orally active Murine Double Minute 2 (MDM2) inhibitor in clinical development. *J Med Chem* 60:2819–2839
44. Over B, Wetzel S, Grütter C et al (2013) Natural-product-derived fragments for fragment-based ligand discovery. *Nat Chem* 5:21–28
45. Galliford CV, Scheidt KA (2007) Pyrrolidinyl-spirooxindole natural products as inspirations for the development of potential therapeutic agents. *Angew Chem Int Ed* 46:8748–8758
46. Yu B, Yu Z, Qi P-P et al (2015) Discovery of orally active anticancer candidate CFI-400945 derived from biologically promising spirooxindoles: Success and challenges. *Eur J Med Chem* 95:35–40
47. Yeung BKS, Zou B, Rottmann M et al (2010) Spirotetrahydro β -Carbolines (Spiroindolones): a new class of potent and orally efficacious compounds for the treatment of malaria. *J Med Chem* 53:5155–5164
48. Rottmann M, McNamara C, Yeung BKS et al (2010) Spiroindolones, a potent compound class for the treatment of malaria. *Science* 329:1175–1180
49. White NJ, Pukrittayakamee S, Phyo AP et al (2014) Spiroindolone KAE609 for falciparum and vivax malaria. *N Engl J Med* 371:403–410
50. van Pelt-Koops JC, Pett HE, Graumans W et al (2012) The spiroindolone drug candidate NITD609 potently inhibits gametocytogenesis and blocks Plasmodium falciparum transmission to anopheles mosquito vector. *Antimicrob Agents Chemother* 56:3544–3548
51. Yu B, Qi P-P, Shi X-J et al (2014) Discovery of novel steroidal pyran–oxindole hybrids as cytotoxic agents. *Steroids* 88:44–52

52. Yu B, Shi X-J, Qi P-P et al (2014) Design, synthesis and biological evaluation of novel steroidal spiro-oxindoles as potent antiproliferative agents. *J Steroid Biochem Mol Biol* 141:121–134
53. Yu B, Yu D-Q, Liu H-M (2015) Spirooxindoles: promising scaffolds for anticancer agents. *Eur J Med Chem* 97:673–698
54. Yu B, Sun X-N, Shi X-J et al (2015) Efficient synthesis of novel antiproliferative steroidal spirooxindoles via the [3+2] cycloaddition reactions of azomethine ylides. *Steroids* 102: 92–100
55. Bin Y, Yi-Chao Z, Xiao-Jing S et al (2016) Natural product-derived spirooxindole fragments serve as privileged substructures for discovery of new anticancer agents. *Anticancer Agents Med Chem* 16:1315–1324
56. Zhang Y-L, Li Y-F, Wang J-W et al Multicomponent assembly of novel antiproliferative steroidal dihydropyridinyl spirooxindoles. *Steroids* 109:22–28
57. Shi X-J, Yu B, Wang J-W et al (2016) Structurally novel steroidal spirooxindole by241 potently inhibits tumor growth mainly through ROS-mediated mechanisms. *Sci Rep* 6:31607
58. Yu B, Xing H, Yu D-Q et al (2016) Catalytic asymmetric synthesis of biologically important 3-hydroxyoxindoles: an update. *Beilstein J Org Chem* 12:1000–1039
59. Aguilar A, Sun W, Liu L et al (2014) Design of chemically stable, potent, and efficacious MDM2 inhibitors that exploit the retro-mannich ring-opening-cyclization reaction mechanism in spiro-oxindoles. *J Med Chem* 57:10486–10498
60. Ding K, Lu Y, Nikolovska-Coleska Z et al (2005) Structure-based design of potent non-peptide MDM2 inhibitors. *J Am Chem Soc* 127:10130–10131
61. Smart BE (2001) Fluorine substituent effects (on bioactivity). *J Fluor Chem* 109:3–11
62. Ding K, Lu Y, Nikolovska-Coleska Z et al (2006) Structure-based design of spiro-oxindoles as potent, specific small-molecule inhibitors of the MDM2–p53 interaction. *J Med Chem* 49:3432–3435
63. Lin J, Chen J, Elenbaas B et al (1994) Several hydrophobic amino acids in the p53 amino-terminal domain are required for transcriptional activation, binding to MDM-2 and the adenovirus 5 E1B 55-kD protein. *Genes Dev* 8:1235–1246
64. Picksley SM, Vojtesek B, Sparks A et al (1994) Immunochemical analysis of the interaction of p53 with MDM2:—fine mapping of the MDM2 binding site on p53 using synthetic peptides. *Oncogene* 9:2523–2529
65. Shangary S, Qin D, McEachern D et al (2008) Temporal activation of p53 by a specific MDM2 inhibitor is selectively toxic to tumors and leads to complete tumor growth inhibition. *Proc Natl Acad Sci USA* 105:3933–3938
66. Zhao Y, Liu L, Sun W et al (2013) Diastereomeric spirooxindoles as highly potent and efficacious MDM2 inhibitors. *J Am Chem Soc* 135:7223–7234
67. Zhao Y, Yu S, Sun W et al (2013) A Potent small-molecule inhibitor of the MDM2–p53 interaction (MI-888) achieved complete and durable tumor regression in mice. *J Med Chem* 56:5553–5561
68. Shu L, Li Z, Gu C et al (2013) Synthesis of a spiroindolinone pyrrolidinecarboxamide MDM2 antagonist. *Org Proc Res Dev* 17:247–256
69. Hoffman-Luca CG, Yang C-Y, Lu J et al (2015) Significant differences in the development of acquired resistance to the MDM2 inhibitor SAR405838 between in vitro and in vivo drug treatment. *PLoS ONE* 10:e0128807
70. Hoffman-Luca CG, Ziazadeh D, McEachern D et al (2015) Elucidation of acquired resistance to Bcl-2 and MDM2 inhibitors in acute leukemia in vitro and in vivo. *Clin Cancer Res* 21:2558–2568
71. Carry J-C, Garcia-Echeverria C (2013) Inhibitors of the p53/hdm2 protein–protein interaction —path to the clinic. *Bioorg Med Chem Lett* 23:2480–2485
72. Miyazaki M, Setoguchi M, Sugimoto Y et al (2012) Dispiropyrrolidine derivative. EP20120755073
73. Wang S, Sun W, Aguilar A et al (2014) Spiro-oxindole MDM2 antagonists. US 14/485,054

74. Phelps D, Bondra K, Seum S et al (2015) Inhibition of MDM2 by RG7388 confers hypersensitivity to X-radiation in xenograft models of childhood sarcoma. *Pediatr Blood Cancer* 62:1345–1352
75. Zhang Z, Ding Q, Liu J-J et al (2014) Discovery of potent and selective spiroindolinone MDM2 inhibitor, RO8994, for cancer therapy. *Bioorg Med Chem* 22:4001–4009
76. Zhang Z, Chu X-J, Liu J-J et al (2013) Discovery of potent and orally active p53-MDM2 inhibitors RO5353 and RO2468 for potential clinical development. *ACS Med Chem Lett* 5:124–127
77. Luk KC, So SS, Zhang J et al (2006) Oxindole derivatives. PCT/EP2006/063475
78. Ding Q, Jiang N, Yang S et al (2009) Spiroindolinone derivatives. US 12/272,870
79. Ding Q, Liu JJ, Zhang Z (2007) Spiroindolinone derivatives. PCT/EP2007/052038
80. Liu JJ, Tilley JW, Zhang Z (2009) 3,3-spiroindolinone derivatives. CN 200880016425
81. Liu JJ, Tilley JW, Zhang Z (2010) 3,3-spiroindolinone derivatives as anticancer agents. PCT/EP2010/051757
82. Liu JJ, Zhang Z (2008) Spiroindolinone derivatives. PCT/EP2008/055831
83. Chu XJ, Ding Q, Jiang N et al (2012) Substituted Spiro[3H-Indole-3,6'(5'H)-[1H]Pyrrolo [1,2c]Imidazole-1',2(1H,2'H)-diones. US 20120071499
84. Pfafferott G, Oberhammer H, Boggs JE et al (1985) Geometric structure and pseudorotational potential of pyrrolidine. An ab initio and electron diffraction study. *J Am Chem Soc* 107:2305–2309
85. Cremer D, Pople JA (1975) General definition of ring puckering coordinates. *J Am Chem Soc* 97:1354–1358
86. Madison V (1977) Flexibility of the pyrrolidine ring in proline peptides. *Biopolymers* 16:2671–2692
87. Ramachandran GN, Lakshminarayanan AV, Balasubramanian R et al (1970) Studies on the conformation of amino acids XII. Energy calculations on prolyl residue. *Biochim Biophys Acta (BBA)—Protein Struct* 221:165–181
88. DeTar DF, Luthra NP (1977) Conformations of proline. *J Am Chem Soc* 99:1232–1244
89. Bertamino A, Soprano M, Musella S et al (2013) Synthesis, in vitro, and in cell studies of a new series of [Indoline-3,2'-thiazolidine]-based p53 modulators. *J Med Chem* 56:5407–5421
90. Ivanenkov YA, Vasilevski SV, Beloglazkina EK et al (2015) Design, synthesis and biological evaluation of novel potent MDM2/p53 small-molecule inhibitors. *Bioorg Med Chem Lett* 25:404–409
91. Kumar A, Gupta G, Bishnoi AK et al (2015) Design and synthesis of new bioisosteres of spirooxindoles (MI-63/219) as anti-breast cancer agents. *Bioorg Med Chem* 23:839–848
92. Li Bo ZR, He Gu, Li Guo, Wei Huang (2013) Molecular docking, QSAR and molecular dynamics simulation on spiro-oxindoles as MDM2 inhibitors. *Acta Chim Sinica* 71: 1396–1403
93. Ribeiro CJA, Amaral JD, Rodrigues CMP et al (2014) Synthesis and evaluation of spiroisoxazoline oxindoles as anticancer agents. *Bioorg Med Chem* 22:577–584
94. Huang W, Cai L, Chen C et al (2015) Computational analysis of spiro-oxindole inhibitors of the MDM2-p53 interaction: insights and selection of novel inhibitors. *J Biomol Struct Dyn* 34:1–11
95. Zhou R, Wu Q, Guo M et al (2015) Organocatalytic cascade reaction for the asymmetric synthesis of novel chroman-fused spirooxindoles that potently inhibit cancer cell proliferation. *Chem Commun* 51:13113–13116
96. Wang S, Jiang Y, Wu S et al (2016) Meeting organocatalysis with drug discovery: asymmetric synthesis of 3,3'-Spirooxindoles fused with tetrahydrothiopyrans as novel p53-MDM2 inhibitors. *Org Lett* 18:1028–1031
97. Patil SP (2013) FOLICation: engineering approved drugs as potential p53–MDM2 interaction inhibitors for cancer therapy. *Med Hypotheses* 81:1104–1107

Chapter 9

Small-Molecule Inhibitors for the β -Catenin/T Cell Factor Protein-Protein Interaction



Yongqiang Zhang and Wei Wang

9.1 Introduction

The canonical Wnt signaling has been proven to play a crucial role in directing cell proliferation, differentiation, and cell–cell communication [1–5]. An overview of this signaling pathway is shown in Fig. 9.1 [6, 7]. In the absence of Wnt signal, β -catenin is actively phosphorylated by the destruction box, which is formed by Axin, adenomatous polyposis coli (APC), casein kinase 1 α (CK-1 α), and glycogen synthase kinase 3 β (GSK-3 β). Phosphorylated β -catenin is ubiquitinated by β -transducin repeat-containing protein (β -TRCP). In the presence of Wnt signal, Wnt interacts with the frizzled (Fzd)–lipoprotein receptor-related proteins 5 and 6 (LRP5/6) complex. Disheveled (Dvl) recruitment by Fzd leads to LRP5/6 phosphorylation and Axin recruitment. This then inactivates the destruction box and allows β -catenin to accumulate in the cell nucleus, where it interacts with the member of the T cell factor (Tcf)/lymphoid enhancer factor (Lef) family, and recruits co-activators B cell lymphoma 9 (BCL-9), CREB binding protein (CBP)/p300 [8]. This results in the expression of Wnt target genes. Furthermore, the cytosolic β -catenin also fulfills important regulatory functions in cell–cell adhesions, maintaining cell shape and regulating cell movement through interaction with cytoplasmic domain of E-cadherin, α -catenin, and cytoskeleton actin [9].

Y. Zhang (✉) · W. Wang (✉)
School of Pharmacy, East China University of Science & Technology,
130 Mei-Long Rd, Shanghai 200237, China
e-mail: yongqiangzhang@ecust.edu.cn

W. Wang
e-mail: wwang@unm.edu

W. Wang
Department of Chemistry & Chemical Biology, University of New Mexico,
MSC03 2060, Albuquerque, NM 87131, USA

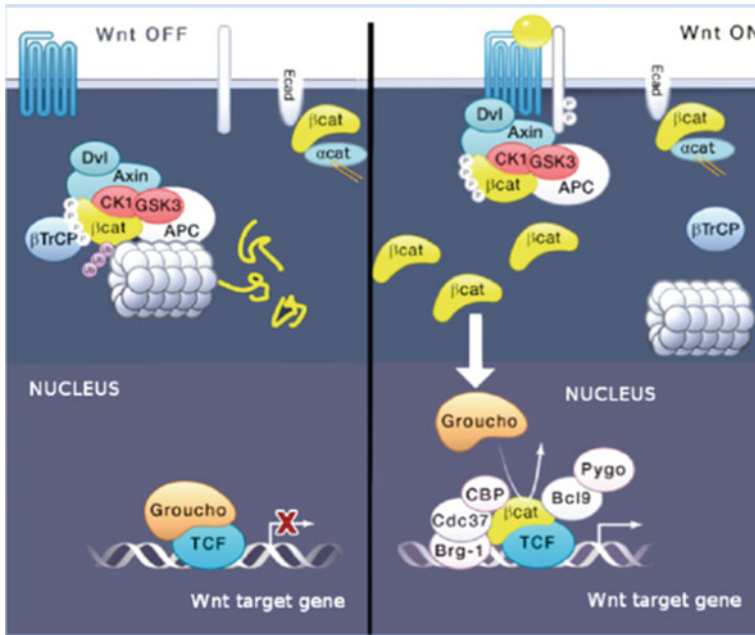


Fig. 9.1 An overview of the canonical Wnt signaling pathway. Adapted from Ref. [7], Copyright 2012, with permission from Elsevier

The aberrant activation of canonical Wnt signaling promotes the transcription of cell proliferation, migration, and survival genes, such as cyclin D1, c-myc, and survivin, and is strongly associated with the initiation and progression of many cancers including colorectal carcinoma [10, 11], hepatocellular carcinoma [12], leukemia [13], and multiple myeloma [14]. Cancer stem cells, which are resistant to conventional chemo- and radiotherapies and especially virulent, are also controlled by the hyperactivation of canonical Wnt signaling [3–5]. Therefore, the disruption of canonical Wnt signaling is an attractive strategy for cancer therapy. However, the inhibition of the upstream sites is less desirable because they can cause cross-regulatory effects on the β -catenin-dependent Wnt pathways or perturb the function of β -catenin in cell–cell adhesion. It would be advantageous to identify inhibitors for the downstream sites of the canonical Wnt signaling pathway.

The formation of the β -catenin/Tcf complex in the cell nucleus is the penultimate step of canonical Wnt signaling. Transcriptional overactivation of canonical Wnt target genes is solely dependent on the formation of this complex. The deletion of the β -catenin gene can significantly reduce the growth of cancer cells [15]. Overexpression of dominant-negative Tcf [16], or the use of siRNAs [17] and inducible shRNAs [18] against β -catenin, can markedly decrease β -catenin-dependent gene expression and diminish the growth of many cancer cells in vitro and in vivo. Therefore, selective disruption of β -catenin/Tcf protein–protein interactions (PPIs)

represents an appealing therapeutic target for cancer therapy. Furthermore, it would be ideal that the inhibitor binds to coactivator β -catenin rather than transcriptional factor Tcf, as Tcf is essential in other signaling pathways, while β -catenin is specific for Wnt/ β -catenin signaling [19].

Crystal structures of β -catenin in complexes with *Xenopus* Tcf [20], human Tcf4 [21–23], and mouse Lef-1 [24] have been reported. As a typical PPI, β -catenin/Tcf has a flat, featureless, and large protein-protein contacting surface ($\geq 2800 \text{ \AA}^2$). Three hot spots on β -catenin are critical for binding to Tcf which were revealed by crystallographic and biochemical analyses [24, 25]. One is K435/K508 where D16/E17 of Tcf4 binds. The second one involves the interaction of K312/K345 with E24/E29 of Tcf4 in two alternative conformations. The third one is a hydrophobic pocket lined with F253, I256, F293, A295, and I296. V44 and L48 of Tcf4 bind to this pocket. Further study of the binding mode indicates that D16/E17 of human Tcf4 is much more important than E24/E29 and V44/L48 when binding to β -catenin (Fig. 9.2). This enables the discovery of small-molecule inhibitors via virtual screening and hot spots-based rational design. In addition, high throughput screening (HTS), as a rapid approach to identify hit compounds that modulate a particular biomolecular pathway, was also employed to identify small-molecule inhibitors of β -catenin/Tcf PPI. Many small-molecule inhibitors of β -catenin/Tcf PPI discovered via these strategies have been reported and are the focus of this chapter.

1. The discovery of small-molecule inhibitors of β -catenin/Tcf PPI through high throughput screening (HTS)

By using surface plasmon resonance (SPR) assay and enzyme-linked immunosorbent assay (ELISA), HTS of natural product collections identified six β -catenin/Tcf

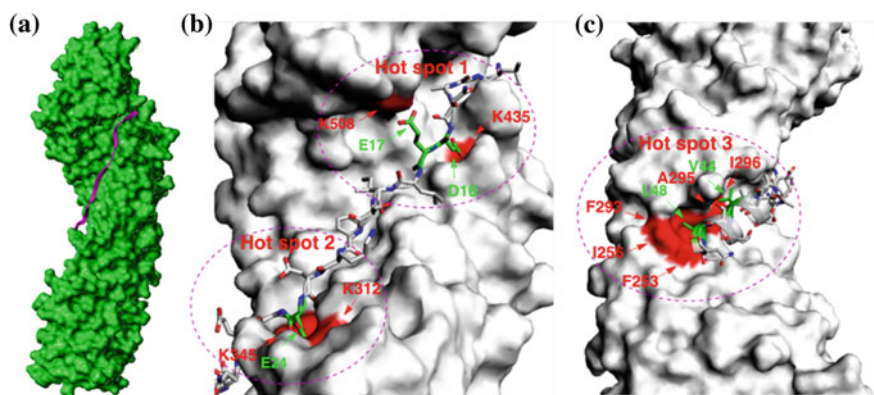


Fig. 9.2 Structure of the β -catenin/Tcf complex (PDB id: 2GL7 [21]). **a** β -catenin is shown as a surface model (green), and Tcf is shown as a ribbon (purple). **b** “Hot spots” 1 and 2. β -catenin: surface model (gray), and Tcf: stick model. “Hot spot” 1: K435 and K508 of β -catenin. “Hot spot” 2: K312 and K345 of β -catenin. **c** “Hot spot” 3: F253, I256, F293, A295, and I296 of β -catenin. Adapted with the permission from Ref. [36]. Copyright 2013 American Chemical Society

PPI small-molecule inhibitors (Fig. 9.3) [26]. These compounds can inhibit β -catenin/Tcf interaction at a low micromolar IC_{50} (0.64–8.7 μ M). Among them, three inhibitors from fungal derivatives, **4** (PKF115-584), **5** (CGP049090), and **6** (PKF118-310), exhibit high potency to inhibit the growth of many cancer cells in vitro and in vivo, including colorectal cancer, prostate cancer, and multiple myeloma. Furthermore, **4** (PKF115-584) and **5** (CGP049090) effectively block the expression of Wnt target genes. The exact mechanisms of how these inhibitors interfere with the target interaction are unclear. However, strong interference with β -catenin/APC interactions was observed for these compounds, suggesting that β -catenin is likely the target of the interaction.

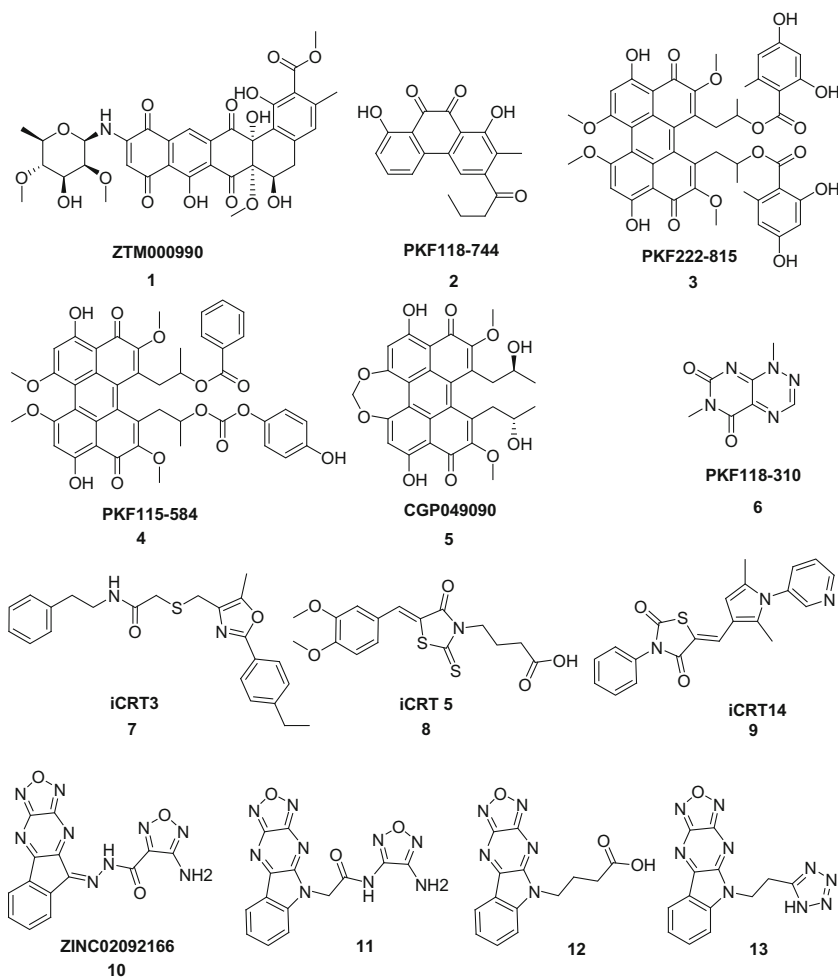


Fig. 9.3 Small-molecule inhibitors identified through HTS

In 2011, Gonsalves et al. identified three small-molecule inhibitors **7** (iCRT3), **8** (iCRT5), and **9** (iCRT14) out of 14,977 compounds using HTS (Fig. 9.3) [27]. The HTS methods employed an Axin-specific dsRNA to address the selectivity for β -catenin/Tcf interaction over β -catenin/E-cadherin and other proteins. These compounds inhibited the expression of Wnt target genes and the growth of colorectal cancers in vitro and in vivo through direct inhibition of β -catenin/Tcf4 interaction. The binding mode with β -catenin was initially disclosed via in silico studies. The pocket lined by K435 and R469 was considered the most important binding site for the iCRT compounds, because these two residues are crucial for stabilizing the interaction for β -catenin/Tcf4 [24].

Recently, Ji and colleagues identified a new small-molecule inhibitor for β -catenin/Tcf PPI, **10** (ZINC02092166) ($IC_{50} = 1.2 \pm 0.39 \mu\text{M}$, AlphaScreen result), through HTS of commercially available small-molecule libraries using AlphaScreen and FP assays [28]. However, this hit compound contains the acyl hydrazone moiety, which has been recognized as a substructure of pan assay interference compounds (PAINS) or causing false positives in bioassays [29, 30]. It exhibits higher inhibitory activity in cell-based assays than biochemical assays, which suggests the off-target effect. Further, optimization resulted in chemically stable derivatives **11–13** (**11**, $IC_{50} = 2.7 \pm 0.45 \mu\text{M}$; **12**, $IC_{50} = 1.0 \pm 0.43 \mu\text{M}$; **13**, $IC_{50} = 18 \pm 2.2 \mu\text{M}$; AlphaScreen result) with a new scaffold exhibit improved selectivity for β -catenin/Tcf over β -catenin/cadherin and β -catenin/APC PPIs. The binding mode of new inhibitors **12** and **13** was initially disclosed by site-directed mutagenesis and structure–activity relationship studies. The tetracyclic ring of **12**

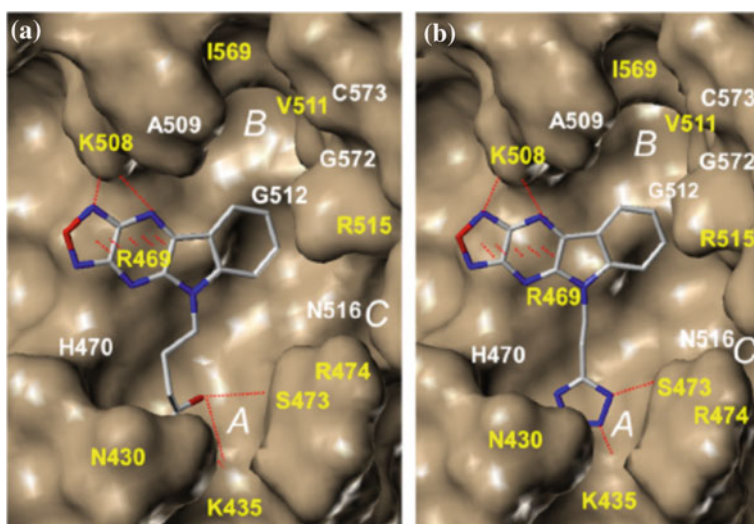


Fig. 9.4 Binding mode of inhibitors from Ji group with β -catenin. **a** Glide docking mode of inhibitor **14** with β -catenin; **b** Glide docking mode of inhibitor **15** with β -catenin. Reprinted with the permission from Ref. [28]. Copyright 2015 American Chemical Society

and **13** was predicted to form a cation– π interaction with the positively charged guanidino group of R469. The benzene moiety of the tetracyclic ring was located in hydrophobic pocket B, while two nitrogen atoms of the oxadiazolopyrazine ring of **12** and **13** formed H-bonds with K508. The carboxylic group of **12** and the tetrazole ring of **13** created a salt bridge with K435 and H-bonds with the backbone NH group of N470 and the hydroxyl group of S473 (Fig. 9.4). Further study indicates that the inhibitor **13** is able to suppress canonical Wnt signaling, downregulate the expression of Wnt target genes, and inhibit the growth of cancer cells (IC_{50} , $2.7 \pm 4.1 \mu\text{M}$; colorectal cancer cells SW480). This compound represents a good starting point for the development of potent and selective β -catenin/Tcf inhibitors.

2. The discovery of small-molecule inhibitors of β -catenin/Tcf PPI through virtual screening

In 2006, Trosset et al. reported a small-molecule inhibitor **14** (PNU74654), identified through virtual screening and medium-throughput biophysical (NMR and ITC) assays (Fig. 9.5) [31]. The isothermal titration calorimetry (ITC) experiments confirmed that the small molecule binds to β -catenin with a K_d of 450 nM (ITC). In 2012, Tian et al. reported an organocopper inhibitor **15** (BC21) (Fig. 9.5), from virtual screening and subsequent luciferase reporter assays [32]. Its inhibitory activity against β -catenin/Tcf interactions was confirmed by the fluorescence polarization (FP) assay. BC21 also exhibits direct interruption of β -catenin/Tcf4 interaction and downregulates the Wnt target genes, resulting in cancer cell death. It is suggested that PNU74654 is likely to bind to the K435/R469 “hot spot” area on the β -catenin, and the binding site for BC21 is the pocket around K435. However, no experimental support was given to verify the binding mode. This makes difficult to optimize their activities. Moreover, none of the above compounds is selective for β -catenin/Tcf over β -catenin/E-cadherin and β -catenin/APC interactions.

3. The discovery of small-molecule inhibitors of β -catenin/Tcf PPI through hot spots-based rational design

Studies suggest that not all interfaces between the two proteins are equally important for PPIs [33]. Small subsets of residues on protein surface contribute to most of the free energy of binding, termed as “hot spots,” which can serve as the

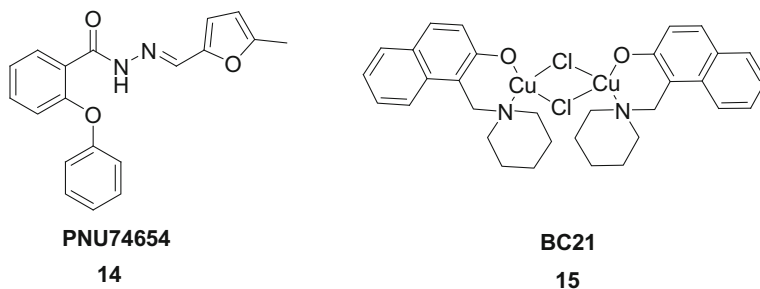


Fig. 9.5 Small-molecule inhibitors identified through virtual screening

crucial targeting sites for inhibitor design [34, 35]. The identification of hot spot regions of β -catenin/Tcf PPIs enables the direct extracting of key substructures from the hot spot residues and guides to design small-molecule inhibitors. D16/E17 of Tcf (bind with hot spot 1 of β -catenin, Fig. 9.2) was proved to be the most important residues to bind with β -catenin via alanine scanning and SPR experiments. This study indicates that mimicking D16/E17 was a rational starting point and feasible approach to designing small-molecule inhibitors for β -catenin/Tcf PPI. Therefore, a nonpeptidic small-molecule inhibitor **16** (UU-T01) was designed and synthesized by employing a bioisostere replacement strategy [36]. The K_i value was determined by competitive fluorescence polarization (FP) assay to be $3.14 \pm 0.48 \mu\text{M}$, which shows a high ligand efficiency (molecule weight, 230). This hit compound serves as a starting point for further lead generation and optimization. The binding mode of the designed inhibitors was validated by the site-directed mutagenesis and structure-activity relationship (SAR) studies. The results imply

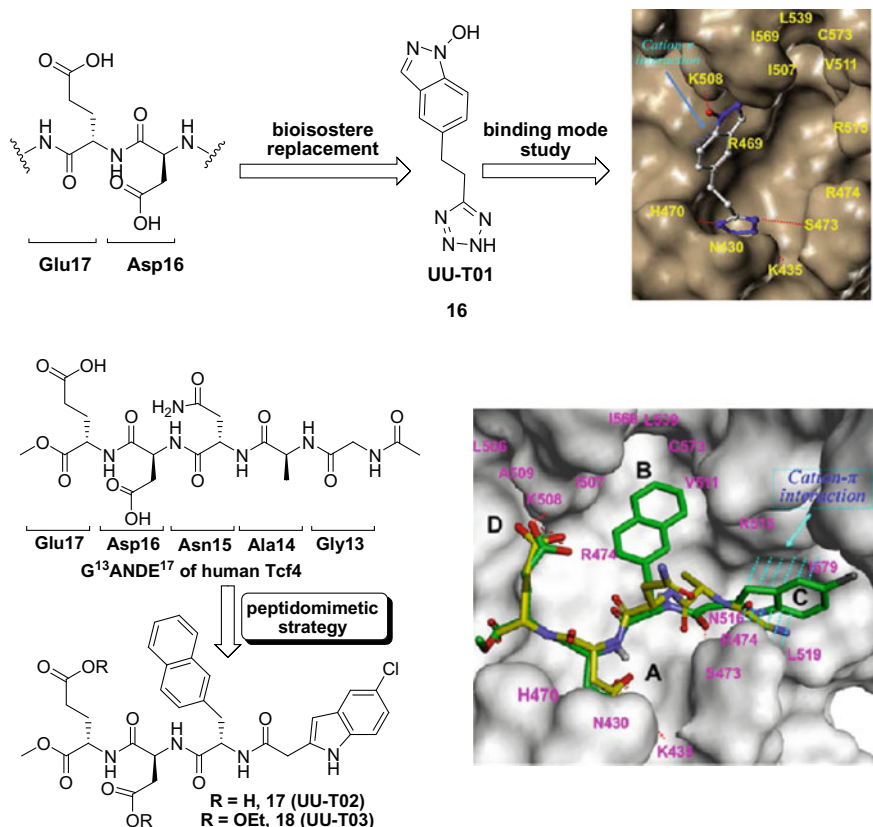


Fig. 9.6 Small-molecule inhibitor identified through hot spots-based rational design. Adapted with the permission from Refs. [36, 37]. Copyright 2013 and 2014 American Chemical Society

that cation- π interaction with the positively charged guanidino group of R469 might be involved for the interaction of this inhibitor with β -catenin, which was not present in β -catenin/Tcf PPI (Fig. 9.6). It was also found to be selective for β -catenin/Tcf over β -catenin/E-cadherin and β -catenin/APC interactions (Tcf/Cadherin = 33.0; Tcf/APC = 56.0). However, the cell-based anti-tumor activity was not reported, which might attribute to its poor membrane permeability.

β -catenin uses the same interface to bind with APC, Axin, and E-cadherin. Therefore, the designing of a selective inhibitor of β -catenin/Tcf remained a challenge. In 2013, Ji group identified a selective binding site of β -catenin that can differentiate β -catenin/Tcf, β -catenin/cadherin, and β -catenin/APC interactions by employing alanine scanning and biochemical assays. G¹³ANDE¹⁷ of human Tcf4 was proved to bind this site, which enables the rational design of selective inhibitors by peptidomimetic strategy and leads to the generation of a peptidic inhibitor **17** (UU-T02) with excellent binding affinity (FP, $3.14 \pm 0.48 \mu\text{M}$) [37]. It should be noted that excellent dual-selectivity for β -catenin/Tcf over β -catenin/E-cadherin and β -catenin/APC interactions was achieved (Tcf/Cadherin = 175.1; Tcf/APC = 63.7). The binding mode study reveals the hydrophobic interaction of naphthalene in pocket B, and the cation- π interaction in pocket C (Arginine channel, R474 and R515) might contribute to the high potency and selectivity (Fig. 9.6). Interestingly, the diethyl ester of **18** (UU-T03) can effectively penetrate the cell membrane and inhibit canonical Wnt signaling and the growth of colorectal cancer cells. This compound provides another excellent starting point for developing more potent and selective inhibitors specific for β -catenin/Tcf interactions.

The design of a selective inhibitor for β -catenin/Tcf PPI is an attractive strategy for cancer therapy. However, as a typical protein-protein interaction, β -catenin/Tcf has a flat, featureless, and large protein-protein contacting surface ($\geq 2800 \text{ \AA}^2$), and the biochemical analyses indicate the dissociation constant (K_d) value of β -catenin/Tcf interactions is in a 7–10 nM range. Furthermore, β -catenin uses the same interface to bind with APC, Axin, and E-cadherin. Therefore, the selective disruption of such a large and tightly binding complex with small molecular represents a great challenge. In the past decades, various strategies, such as HTS, virtual screening, and hot spots-based rational design, have been explored for the development of potent inhibitor specific for β -catenin/Tcf interactions. Varieties of inhibitors were reported. However, most of the small-molecule inhibitors identified from HTS and virtual screening have PAINS substructures (quinone, toxoflavin, and rhodanine) and are frequent hits in biochemical assays [30, 31]. Hot spots-based rational design initiated by Ji group represents an efficient strategy to generate selective small-molecule inhibitor for β -catenin/Tcf. Three types of inhibitors were thus developed, which provide a good starting point for further research. However, further improvement of the binding potency and selectivity remains a great challenge. The generation of drug-like inhibitors for cell-based and in vivo studies will also be a critical issue to be addressed in the future.

Acknowledgements We thank the National Natural Science Foundation of China (21602060, Y.-Q. Z. and 21372073, 21738002 and 21572055, W. W.) for the financial support of the research.

References

1. Clevers H (2006) Wnt/ β -Catenin signaling in development and disease. *Cell* 127:469–480
2. Hartmann C (2006) A Wnt canon orchestrating osteoblastogenesis. *Trends Cell Biol* 16:151–158
3. Logan CY, Nusse R (2004) The Wnt signaling pathway in development and disease. *Annu Rev Cell Dev Biol* 20:781–810
4. Okamura RM, Sigvardsson M, Galceran J, Verbeek S, Clevers H, Grosschedl R (1998) Redundant regulation of T-cell differentiation and TCR α gene expression by the transcription factors LEF-1 and TCF-1. *Immunity* 8:11–20
5. Reya T, Clevers H (2005) Wnt signalling in stem cells and cancer. *Nature* 434:843–850
6. MacDonald BT, Tamai K, He X (2009) Wnt/ β -catenin signaling: components, mechanisms, and diseases. *Dev Cell* 17:9–26
7. Clevers H, Nusse R (2012) Wnt/ β -catenin signaling and disease. *Cell* 149:1192–1205
8. Behrens J, von Kries JP, Kuhl M, Bruhn L, Wedlich D, Grosschedl R, Birchmeier W (1996) Functional interaction of β -catenin with the transcription factor LEF-1. *Nature* 382:638–642
9. Molenaar M, van de Wetering M, Oosterwegel M, Peterson-Maduro J, Godsave S, Korinek V, Roose J, Destree O, Clevers H (1996) XTcf-3 transcription factor mediates β -Catenin-induced axis formation in xenopus embryos. *Cell* 86:391–399
10. Morin PJ, Sparks AB, Korinek V, Barker N, Clevers H, Vogelstein B, Kinzler KW (1997) Activation of *beta*-catenin-Tcf signaling in colon cancer by mutations in β -catenin or APC. *Science* 275:1787–1790
11. Tetsu O, McCormick F (1999) β -Catenin regulates expression of cyclin D1 in colon carcinoma cells. *Nature* 398:422–426
12. de La Coste A, Romagnolo B, Billuart P, Renard CA, Buendia MA, Soubrane O, Fabre M, Chelly J, Beldjord C, Kahn A, Perret C (1998) Somatic mutations of the β -catenin gene are frequent in mouse and human hepatocellular carcinomas. *Proc Natl Acad Sci USA* 95:8847–8851
13. Lu D, Zhao Y, Tawatao R, Cottam HB, Sen M, Leoni LM, Kipps TJ, Corr M, Carson DA (2004) Activation of the Wnt signaling pathway in chronic lymphocytic leukemia. *Proc Natl Acad Sci USA* 101:3118–3123
14. Sukhdeo K, Mani M, Zhang Y, Dutta J, Yasui H, Rooney MD, Carrasco DE, Zheng M, He H, Tai YT, Mitsiades C, Anderson KC, Carrasco DR (2007) Targeting the *beta*-catenin/Tcf transcriptional complex in the treatment of multiple myeloma. *Proc Natl Acad Sci USA* 104:7516–7521
15. Kim JS, Crooks H, Foxworth A, Waldman T (2002) Proof-of-principle: oncogenic *beta*-catenin is a valid molecular target for the development of pharmacological inhibitors. *Mol Cancer Ther* 1:1355–1359
16. van de Wetering M, Sancho E, Verweij C, de Lau W, Oving I, Hurlstone A, van der Horn K, Battle E, Coudreuse D, Haramis AP, Tjon-Pon-Fong M, Moerer P, van den Born M, Soete G, Pals S, Eilers M, Medema R, Clevers H (2002) The *beta*-catenin/Tcf-4 complex imposes a crypt progenitor phenotype on colorectal cancer cells. *Cell* 111:241–250
17. Ashihara E, Kawata E, Nakagawa Y, Shimazaki C, Kuroda J, Taniguchi K, Uchiyama H, Tanaka R, Yokota A, Takeuchi M, Kamitsuji Y, Inaba T, Taniwaki M, Kimura S, Maekawa T (2009) *beta*-Catenin small interfering RNA successfully suppressed progression of multiple myeloma in a mouse model. *Clin Cancer Res: An Official J Am Assoc Cancer Res* 15:2731–2738
18. Scholer-Dahirel A, Schlabach MR, Loo A, Bagdasarian L, Meyer R, Guo R, Woolfenden S, Yu K, Markovits J, Killary K, Sonkin D, Yao Y, Warmuth M, Sellers WR, Schlegel R, Stegmeier F, Mosher RE, McLaughlin ME (2011) Maintenance of adenomatous polyposis

- coli (APC)-mutant colorectal cancer is dependent on Wnt/*beta*-catenin signaling. Proc Natl Acad Sci USA 108:17135–17140
19. Weber BN, Chi A, Chavez A, Yashiro-Ohtani Y, Yang Q, Shestova O, Bhandoola A (2011) A critical role for Tcf-1 in T-lineage specification and differentiation. Nature 476:63–68
 20. Graham TA, Weaver C, Mao F, Kimelman D, Xu W (2000) Crystal structure of a β -catenin/Tcf complex. Cell 103:885–896
 21. Sampietro J, Dahlberg CL, Cho US, Hinds TR, Kimelman D, Xu W (2006) Crystal structure of a β -catenin/Bcl9/Tcf4 complex. Mol Cell 24:293–300
 22. Poy F, Lepourcelet M, Shivdasani RA, Eck MJ (2001) Structure of a human Tcf4- β -catenin complex. Nat Struct Biol 8:1053–1057
 23. Graham TA, Ferkey DM, Mao F, Kimelman D, Xu W (2001) Tcf4 can specifically recognize β -catenin using alternative conformations. Nat Struct Biol 8:1048–1052
 24. von Kries JP, Winbeck G, Asbrand C, Schwarz-Romond T, Sochnikova N, Dell’Oro A, Behrens J, Birchmeier W (2000) Hot spots in *beta*-catenin for interactions with LEF-1, conductin and APC. Nat Struct Biol 7:800–807
 25. Gail R, Frank R, Wittinghofer A (2005) Systematic peptide array-based delineation of the differential *beta*-catenin interaction with Tcf4, E-cadherin, and adenomatous polyposis coli. J Mol Biol 280:7107–7117
 26. Lepourcelet M, Chen Y, France DS, Wang H, Crews P, Petersen F, Bruseo C, Wood AW, Shivdasani RA (2004) Small-molecule antagonists of the oncogenic Tcf/*beta*-catenin protein complex. Cancer Cell 5:91–102
 27. Gonsalves FC, Klein K, Carson BB, Katz S, Ekas LA, Evans S, Nagourney R, Cardozo T, Brown AM, DasGupta R (2011) An RNAi-based chemical genetic screen identifies three small-molecule inhibitors of the Wnt/wingless signaling pathway. Proc Natl Acad Sci USA 108:5954–5963
 28. Catrow JL, Zhang Y, Zhang M, Ji H (2015) Discovery of selective small-molecule inhibitors for the β -Catenin/T-cell factor protein-protein interaction through the optimization of the acyl hydrazone moiety. J Med Chem 58:4678–4692
 29. Baell JB, Holloway GA (2010) New substructure filters for removal of pan assay interference compounds (PAINS) from screening libraries and for their exclusion in bioassays. J Med Chem 53:2719–2740
 30. Malvezzi A, de Rezende L, Izidoro M A, Cezari M H S, Juliano L, do Amaral A T (2008) Uncovering false positives on a virtual screening search for cruzain inhibitors. Bioorg Med Chem Lett 18:350–354
 31. Trosset JY, Dalvit C, Knapp S, Fasolini M, Veronesi M, Mantegani S, Gianellini LM, Catana C, Sundstrom M, Stouten PF, Moll JK (2006) Inhibition of protein-protein interactions: the discovery of druglike *beta*-catenin inhibitors by combining virtual and biophysical screening. Proteins 64:60–67
 32. Tian W, Han X, Yan M, Xu Y, Duggineni S, Lin N, Luo G, Li YM, Han X, Huang Z, An J (2012) Structure-based discovery of a novel inhibitor targeting the *beta*-catenin/Tcf4 interaction. Biochemistry 51:724–731
 33. Villoutreix BO, Kuenemann MA, Poyet JL, Bruzzoni-Giovanelli H, Labbé C, Lagorce D, Sperandio O, Miteva MA (2014) Drug-like protein-protein interaction modulators: challenges and opportunities for drug discovery and chemical biology. Mol Inform 33:414–437
 34. Clackson T, Wells JA (1995) A hot spot of binding energy in a hormone-receptor interface. Science 267:383–386
 35. Guo W, Wisniewski JA, Ji H (2014) Hot spot-based design of small-molecule inhibitors for protein-protein interactions. Bioorg Med Chem Lett 24:2546–2554
 36. Yu B, Huang Z, Zhang M, Dillard DR, Ji H (2013) Rational design of small-molecule inhibitors for *beta*-catenin/T-cell factor protein-protein interactions by bioisostere replacement. ACS Chem Biol 8:524–529
 37. Huang Z, Zhang M, Burton SD, Katsakhyan LN, Ji H (2014) Targeting the Tcf4 G13ANDE17 binding site to selectively disrupt β -catenin/T-cell factor protein-protein interactions. ACS Chem Biol 9:193–201

Chapter 10

Discovery and Development of Keap1-Nrf2 Protein-Protein Interaction Inhibitors



Zhengyu Jiang and Qidong You

10.1 Introduction

Human body is constantly exposed to the oxidative and electrophilic chemicals from both extrinsic and intrinsic sources [1]. These reactive chemicals can damage cell lipids, proteins, and nucleic acids, leading to the dysfunction of mammalian cells. The accumulation of the damages is closely related to aging and age-related diseases such as cancer, neurodegenerative, and cardiovascular diseases [2–5]. To counteract these threats, cells are equipped with the fine-tuned defending system that can adapt to the cellular environment. At normal conditions, the system will be kept at a basal state, while it can be activated at once the harmful chemicals emerge in the cell environment. The Keap1-Nrf2-ARE signaling is a key component of the defending system. Nrf2 (nuclear factor erythroid 2-related factor 2), a basic-leucine zipper (bZIP) transcription factor, mediates the transcription of more than 100 stress-related genes by binding the ARE (antioxidant response element). These genes encode a battery of cryoprotective proteins, including antioxidant proteins, phase I and II detoxification enzymes, transport proteins, proteasome subunits, chaperones, growth factors, and their receptors, as well as some transcription factors [6–8]. Thus, activation of Nrf2 can switch on the cellular defending mechanism. Keap1 (Kelch-like ECH-associated protein) is the main regulator of Nrf2 (Fig. 10.1). It can mediate the ubiquitination of Nrf2 by acting as an adaptor component of ubiquitin E3 ligase. The ubiquitinated Nrf2 will be degraded by proteasome. Besides acting as the negative regulator of Nrf2, Keap1 plays the role

Z. Jiang (✉) · Q. You (✉)

Jiangsu Key Laboratory of Drug Design and Optimization, Department of Medicinal Chemistry, School of Pharmacy, China Pharmaceutical University, Nanjing, Jiangsu, People's Republic of China
e-mail: jiangzhengyucpu@163.com

Q. You

e-mail: youqd@163.com

© Springer Nature Singapore Pte Ltd. 2018

C. Sheng and G. I. Georg (eds.), *Targeting Protein-Protein Interactions by Small Molecules*, https://doi.org/10.1007/978-981-13-0773-7_10

249

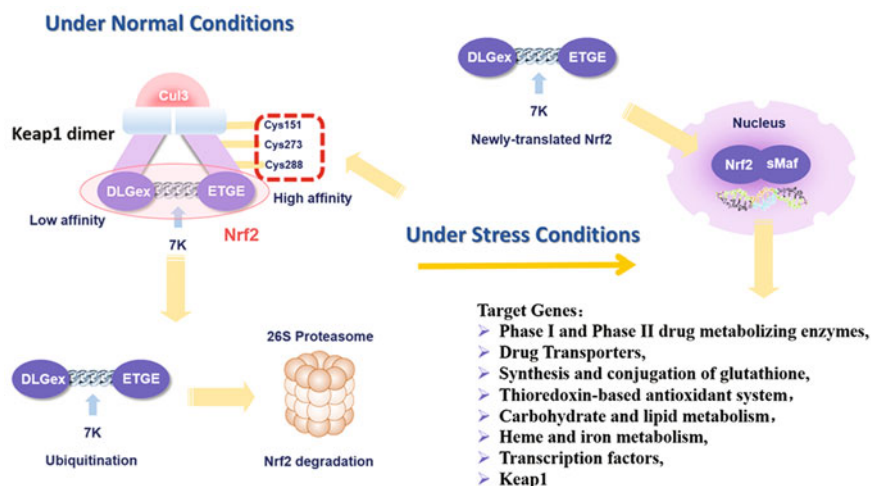


Fig. 10.1 Schematic diagram for the regulation of Nrf2 activity

of a switch in this signaling. Keap1 is a cysteine-rich protein that contains 25 (mouse) or 27 (human) cysteine residues. Some of these cysteines are quite sensitive to the cellular oxidative state and can be covalently modified by electrophilic and/or oxidative assault. These cysteines have been identified as sensors of cellular microenvironment [9–13]. Under stress conditions, the sulfhydryl groups of these cysteine residues are oxidized to disulfides or conjugated to electrophiles [8]. These covalent modifications can affect the structure of Keap1, hindering the precise assembly of E3 ligase complex and suppressing the ubiquitination of Nrf2. The newly synthesized Nrf2 will be accumulated, and then Nrf2 will translocate into the nucleus and induce the transcription of a battery of cytoprotective genes, which ultimately lead to the activation of the defending system. Generally, the inactivation of Keap1-involved E3 ligase finally results in the activation of Nrf2 [14, 15]. This fine-tuned regulating mechanism can efficiently adjust the Nrf2-regulated cell-defending system adapting to the cellular stress state.

In recent years, the research on biological functions of Nrf2 has made much progress. Besides the oxidative stress-related genes, Nrf2 controls the transcription of wider range genes, including the lipid and glucose metabolism, heme and iron metabolism, and gene transcription [16–20]. Nrf2 has been traditionally considered as a tumor suppressor because of its cytoprotective function [21–23]. However, recent studies demonstrate that hyperactivation of the Nrf2 pathway can enhance the survival of malignant cells and protect them against oxidative stress, chemotherapeutic agents, and radiotherapy [24, 25]. Thus, Nrf2 inhibition could be a possible strategy in cancer treatment [26–28]. Besides acting as a therapeutic target in cancer treatment, Nrf2 has also been emerging as a potential therapeutic target for various diseases, especially these chronic age-related and inflammatory diseases, including neurodegenerative diseases [29], cardiovascular diseases, acute lung injury [30],

chronic obstructive pulmonary disease [31], kidney diseases [32], and inflammation [33]. However, Nrf2 is a transcription factor, and directly modulating its transcription function is quite difficult. Identifying an optimal way to affect Nrf2 activity is a precondition for developing Nrf2-targeting therapeutic agents.

10.2 Keap1-Nrf2 Protein-Protein Interaction

10.2.1 *Regulating Mechanism of Keap1-Nrf2 PPI*

As described above, Nrf2 activity is tightly regulated by Keap1. In this process, Keap1-Nrf2 PPI (protein-protein interaction) plays a central role. It ensures the recognition of Nrf2 by Keap1-involved E3 ligase complex. Thus, disrupting Keap1-Nrf2 PPI can deprive Nrf2 from Keap1-mediated inhibitory effects, which can elevate protein level of Nrf2. It provides a feasible way for modulating Nrf2 activity. Discovery of potent PPI inhibitors is the hanging fruit in drug discovery community. Keap1-Nrf2 PPI is no exception.

Nrf2 has six highly conserved regions, named as Neh1 to Neh6 [34]. Neh1, Neh3, and Neh6 locate in the C-terminal half of Nrf2. Neh1 is responsible for forming heterodimer with members of the small Maf protein family by its CNC-type basic-leucine zipper DNA binding motif. It is indispensable for DNA binding and nuclear import and export. Neh3 harbors a critical activity required for activation of transcription, along with the Neh4 and Neh5 domains. This domain is important for interaction with CHD6 (a chromo-ATPase/helicase DNA binding protein) in a yeast two-hybrid screen [35]. Neh6 contains a serine-rich conserved region, involving in the Keap1-independent negative regulation of Nrf2. In the N-terminal half, Neh4 and Neh5 are transactivation domains that bind to the KIX and CH3 domains of CBP (CREB binding protein) for transactivation [36]. Neh2 domain is in charge of the interaction with Keap1, and it has two binding sites for binding with Keap1, namely ETGE motif and DLG motif.

For Keap1, it has five characteristic domains (Fig. 10.2): N-terminal domain (NTD, 1–60); the Broad complex, Tramtrack, and Bric-à-brac (BTB, 61–178); the intervening region (IVR, 179–321); the double glycine repeat (DGR, 322–608) or the Kelch domain; and the C-terminal region (CTR, 609–625). The DGR and CTR can be named as DC domain, and it is responsible for recognizing and binding with Nrf2 [37, 38]. BTB domain is responsible for the homodimerization of Keap1, and the dimerization of Keap1 has been confirmed as the key step for Nrf2 ubiquitination [39]. Besides it also mediates the interaction with Cul3.

The detailed binding model of Keap1-Nrf2 has been intensively investigated. Existing achievements have fully confirmed that Nrf2 contains two Keap1 binding motifs, called ETGE and DLG. It has been widely accepted that two molecule Keap1 proteins form a homodimer and interact with these two motifs in one-molecule Nrf2 protein. The early experimental proof for this PPI model is from the isothermal titration calorimetry (ITC) experiment between the Keap1 DC

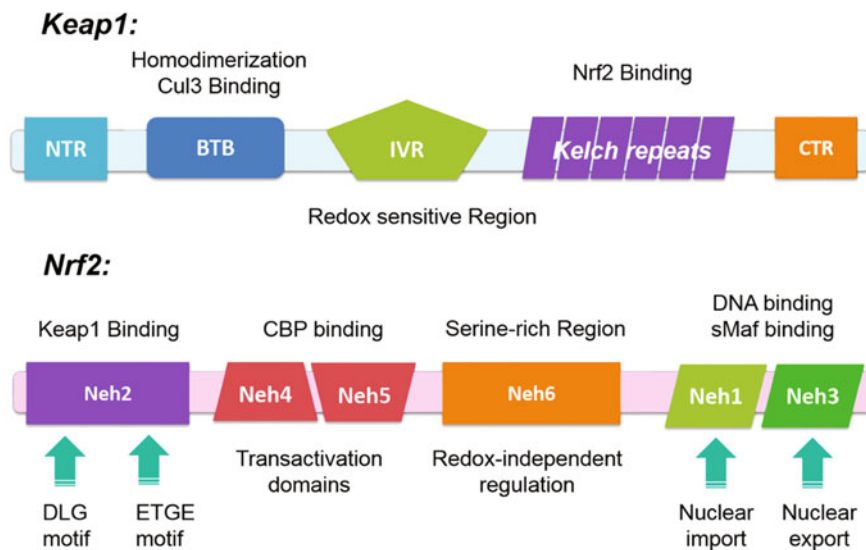


Fig. 10.2 Protein domains of Nrf2 and Keap1. Nrf2 domains: Nrf2 possesses 6 highly conserved domains called Nrf2-ECH homology (Neh) domains. Neh1 contains a CNC-type basic-leucine zipper DNA binding motif, which is required for heterodimer formation with members of the small Maf protein family, for DNA binding and nuclear import and export. The Neh2 domain binds with Keap1. The Neh3 domain contributes to stabilization of the Nrf2 protein and is also reported as transactivation domain. Neh4 and Neh5 are transcriptional activation domains. Neh6 contains a serine-rich conserved region, which has a function of Keap1-independent negative regulation of Nrf2; Keap1 domains: NTR, N-terminal region; BTB, bric-à-brac domain that binds with Nrf2 ubiquitin factors Cul3-Rbx1; IVR, intervening region; Kelch repeats region (also known as double glycine repeat) that binds with Nrf2; CTR, C-terminal region

domain and the Nrf2 Neh2 domain [40]. The obtained titration curve exhibits a biphasic curve, which is fitted best with a two-site binding model. Then the co-crystal structures of the Keap1-Nrf2 ETGE peptide and the Keap1-Nrf2 DLG peptide [41] were reported, which confirmed that Nrf2 contains two Keap1 binding sites. In addition, the experimental results showed that Keap1 protein exists as a stable dimer, but not as a monomer, in mammalian cells and the dimerization of Keap1 is indispensable for its interaction with Cul3 [42]. The direct structure evidence for the Keap1 homodimer is the results from the single particle electron microscopy that clearly showed two large spheres attached by short linker arms to the sides of a small forked-stem structure, resembling a cherry-bob [43]. On the basis of these research results, the “hinge and latch” model was raised to elucidate the detailed mechanism of Keap1-Nrf2 PPI [41]. In this model, the high binding affinity ETGE motif acts as the hinge to tightly link Nrf2 with the Keap1 dimer and the weak binding affinity DLG motif acts as the latch to switch the ubiquitination. Only when both two motifs bind with Keap1 dimer will the ubiquitination of Nrf2 be carried out. The intracellular oxidative stress signals mainly induce the disassociation of the Keap1-Nrf2 DLG motif and block the ubiquitination of Nrf2.

However, recent studies gave some new insights into the Keap1-Nrf2-Cul3 regulation pattern. Dinkova-Kostova's group developed a quantitative Förster resonance energy transfer-based system using multiphoton fluorescence lifetime imaging microscopy to investigate the interaction between Nrf2 and Keap1 in single live cells [44]. Their research results showed that the complex of Keap1 dimer with Nrf2 adopts two distinct conformations under homeostatic conditions: the “open” conformation, in which Nrf2 binds to Keap1 dimer through the high binding affinity ETGE motif, and the “closed” conformation, in which both of the two motifs in Nrf2 bind with Keap1 dimer. The conformation of the Keap1-Nrf2 complex switched between the two states, the ubiquitination of Nrf2 only occurs when the “closed” conformation formed, which is termed the “conformation cycling model” (as shown in Fig. 10.3) [45]. Under induced conditions, the accumulation of the complex in the closed conformation instead of the open conformation was observed. It is probably because the inducers disrupted the ubiquitination step and the closed conformation of the complex cannot enter the cycling. Thus, intracellular Keap1 is anchored with Nrf2 and newly translated Nrf2 accumulates and translocates into the nucleus, which finally turns on the expression of cytoprotective genes. It declared that the inducers activate Nrf2 by inhibiting the regeneration of free Keap1 rather than releasing Nrf2 from Keap1 dimer.

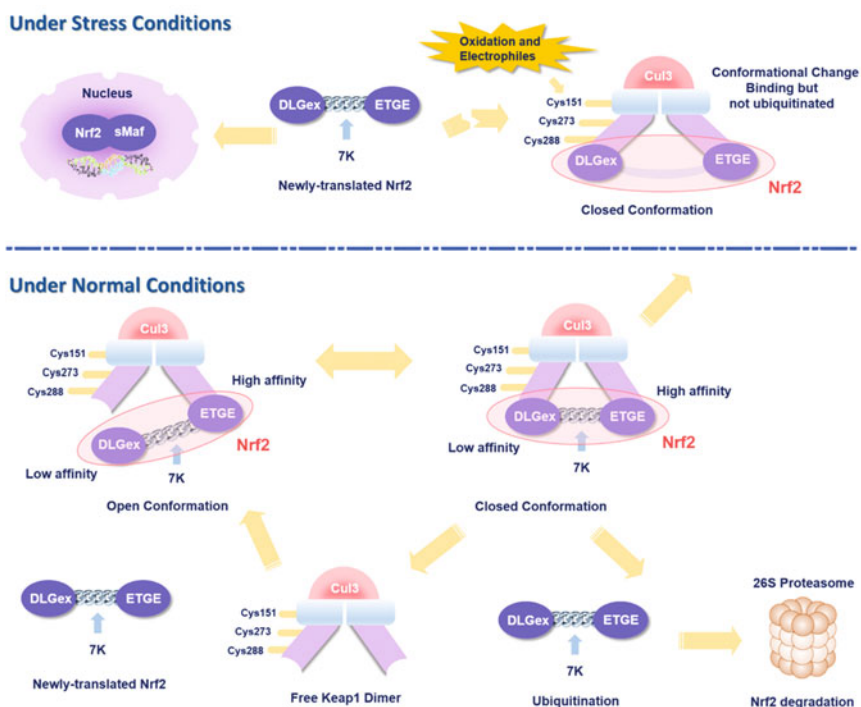


Fig. 10.3 Conformation cycling model of Keap1-Nrf2 regulation

Recent studies about the Nrf2 DLG motif further confirmed the conformation cycling model (Fig. 10.3). Previous obtained minimal DLG motif-derived peptide showed weaker binding affinity and was poorly tolerated with the ETGE-like residue optimization. This ambiguity was revealed by the further investigation of Masayuki Yamamoto's group about the minimum Keap1-binding sequence of the Nrf2 DLG motif. They defined a new DLGex motif that covers a sequence much longer than that was previously defined [46]. The binding affinity of DLGex motif-derived peptide is inconsistent with the second binding constant of the Nrf2 Neh2 domain. Moreover, in kinetic analyses, Keap1-DLGex binding follows a fast association and fast dissociation model, while Keap1-ETGE binding contains a slow-reaction step that leads to a stable conformation. This research indicated that the disassociation of Keap1-DLGex may occur spontaneously, which fits the "conformation cycling" model rather than the "hinge and latch" model.

10.2.2 Structural Characteristics of Keap1-Nrf2 PPI

The progress in structural biology of Keap1-Nrf2 interaction set the stage for the discovery of Keap1-Nrf2 PPI inhibitor. The reported structures showed that the binding pocket in Keap1 is open, which is similar to the most PPIs, but it is well defined. The size of the binding site is relatively small. The interface area of the Keap1-Nrf2 ETGE motif is about 529 Å² (calculated from PDB code: 1X2R), and that of the Keap1-Nrf2 DLGex motif is a bit larger, about 820 Å² (calculated from PDB code: 3WN7). The contact surfaces involved in Keap1-Nrf2 PPI are more typical of those involved in protein–small-molecule interactions (300–1000 Å²), than of PPIs (1500–3000 Å²) [47, 48]. Previously, our group have divided the Keap1 substrate binding cavity into five sub-pockets (P1–P5) based on the co-crystal structures of the Keap1-Nrf2 ETGE motif (Fig. 10.4a). However, the co-crystal structure of Keap1-Nrf2 DLGex complex showed that a P6 sub-pocket should be included in the Keap1-Nrf2 interface (as shown in Fig. 10.4b). Although

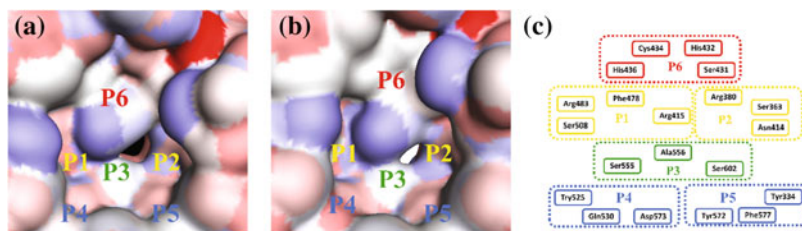


Fig. 10.4 Sub-pocket analysis of Keap1 substrate binding cavity. On the basis of the Keap1-Nrf2 crystal structures, Keap1 substrate binding cavity can be divided into six sub-pockets. **a** Sub-pocket analysis of Keap1 substrate binding cavity based on the Keap1-Nrf2 ETGE complex (PDB code: 1X2R); **b** sub-pocket analysis of Keap1 substrate binding cavity based on the Keap1-Nrf2 DLGex complex (PDB code: 3WN7); **c** summary of key residues in each sub-pocket

the interface surface area of Keap1-Nrf2 is not large, the binding strength between Keap1-Nrf2 is quite potent. Even the 9-mer Nrf2 ETGE peptide can get a K_d of about 20 nM [49]. This information indicated that the substrate binding cavity of Keap1 has more well-characterized hotspots on the one hand and is strict with the ligands on the other hand. It indicated that the discovery of hotspots in Keap1-Nrf2 interface is key issues in developing modulators.

In general, PPIs are classified into two categories: domain-domain pattern that is mediated by the interaction between two protein domains and peptide-domain pattern that is mediated by the interaction between a linear sequence of residues of one of the partners and a domain of the other one [50, 51]. From this perspective, the Keap1-Nrf2 ETGE interaction and the Keap1-Nrf2 DLGex interaction belong to the two types, respectively (as shown in Fig. 10.5a, e). The Keap1-Nrf2 ETGE interaction is a typical example of peptide-domain pattern. The Nrf2 ETGE peptide possesses a tight four-residue β -hairpin conformation that is comprised of the conservative DXETGE motif, specifically the residues Asp77, Glu78, Glu79, Thr80, Gly81, and Glu82. This conformation was stabilized by intramolecular hydrogen bonds involving the side chains of Asp77 and Thr80 and the peptide backbone. Glu79 and Glu82 inserted into the P1 and P2 sub-pockets and formed multiple electrostatic interactions with key arginine residues in Keap1, including Arg483, Arg415, and Arg380 (Fig. 10.5b).

As to the Keap1-Nrf2 DLGex interaction, it is more consistent with domain-domain pattern. The co-crystal structure showed that the DLGex region constitutes three helices, helix 1 (Leu19 to Arg25), helix 2 (Ile28 to Leu30), and helix 3 (Arg34 to Phe37) which form a U shape, and the overall conformation is distinctly different from the β -hairpin conformation of the ETGE region [46]. The helix 1 and helix 3 covered the outside surface of the P1 and P2 sub-pockets in Keap1, and helix 2 and the surrounding linking residues located on the central part of the cavity. This binding pattern is also significantly different from that of the previously reported short DLG peptide (as shown in Fig. 10.5). In the case of the DLGex motif, the side chain of Gln27 moved from the inside to the outside of the P1 sub-pocket and occupied a shallow groove composed of Ser431, Gly433, Cys434, His436, and Arg380. The side-chain amide group of Gln26 supplies hydrogen bonds to the imidazole group of His436 and the main-chain carbonyl group of Gly433 in Keap1, which is not found among other Keap1 ligands. Besides, the side-chain carbonyl oxygen atom of Gln26 can form hydrogen bonds with Arg380 in Keap1. Asp29 was inserted into the P1 sub-pocket and formed multiple hydrogen bonds with Arg415 and Arg483 simultaneously, while the short DLG peptide occupied this cavity with Gln27. Because of the negatively charged character, Asp29 can make a firm salt bridge with Arg415 in Keap1. Closer examination revealed that the positions of Asp27 also adopted a displacement, which allowed the side-chain carboxyl group to form multiple interactions with Arg415, Arg380, Asn382, and Asn414. Only the interaction with Arg415 can be observed in the Keap1-Nrf2 DLG complex. It indicated that the binding strength was also improved in the P2 sub-pocket. Overall, the incorporation of two helices on both sides of the DLG peptide significantly changed positions of the polar

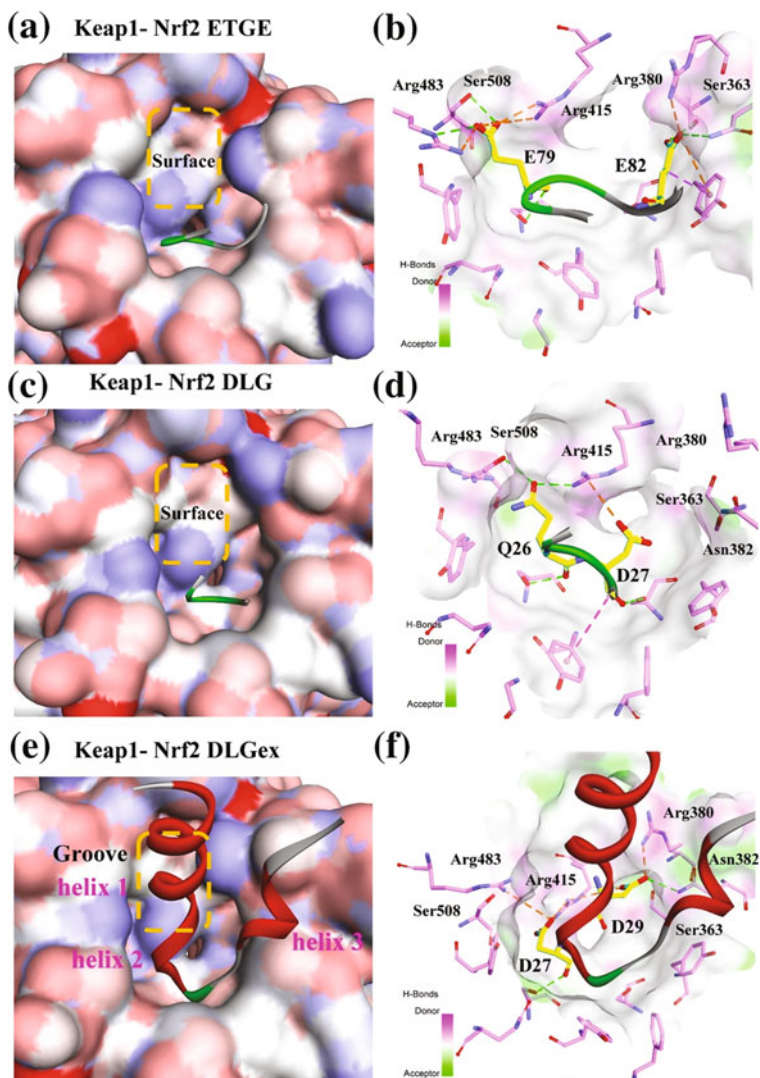


Fig. 10.5 Co-crystal structures of Keap1-Nrf2 PPI. **a** and **b** Binding surface and key polar residue interactions of the Keap1-Nrf2 ETGE motif (PDB code: 1X2R); **c** and **d** binding surface and key polar residue interactions of the Keap1-Nrf2 DLG motif (PDB code: 2DYH); **e** and **f** binding surface and key polar residue interactions of the Keap1-Nrf2 DLGex motif (PDB code: 3WN7). The hydrogen bonds are represented as green dashed lines, and the electrostatic interactions are represented as yellow dashed lines. The carbon atoms of Nrf2 residues and Keap1 residues are colored cyan and purple, respectively

residues, especially the Asp27 and Asp29, which remarkably strengthened the key polar interactions in the P1 and P2 sub-pockets. Compared with the Nrf2 ETGE peptide, the DLGex peptide can form similar polar interactions in the P1 and P2

sub-pockets by a completely different sequence (the DLG and ETGE sequence). Not only did it stress the importance of the polar interactions in the Keap1 substrate recognition, but also provide new thoughts for both novel natural ligand finding and design of potent modulators.

Besides the interacting pattern, the binding thermodynamics and kinetics profiling of the two regions also showed significant differences. Several studies elucidated that the Keap1-ETGE binding is a single enthalpy-driven process [40, 52], which is consistent with the key role of the polar interactions in the Keap1-ETGE binding. Our computational studies also showed that the polar sub-pockets, P1 and P2, contributed the major part of the total binding energy [53]. The ITC results of Keap1 DC domain with a deletion mutant of Nrf2 Neh2, in which the residues of ETGE was removed, showed that the total entropy effects were beneficial for binding [40]. It showed that the second binding site may have distinct binding thermodynamic behavior. The recent identification of the DLGex motif further confirmed this suggestion. The ITC experiment between the DLGex peptide and Keap1 clearly showed a synergistic enthalpy-/entropy-driven process [46]. This finding declared that even though the binding cavity of Keap1 has plenty polar residues, the overall entropy effects can benefit the binding and stressed that both polar and hydrophobic interactions contribute to anchoring small molecules and peptides. The binding kinetics of Keap1-ETGE and Keap1-DLGex also have great differences. The k_{on} and k_{off} determined from both surface plasmon resonance (SPR) [49] and biolayer interferometry (BLI) [52] assay showed that the Nrf2 ETGE peptide has a very slow dissociation rate, confirming the recognition and anchoring effects of this region in the conformation cycling model. Besides, Masayuki Yamamoto group's recent study raised a two-state binding model of Keap1-ETGE that Nrf2-ETGE binds to Keap1-DC by two steps: In the first step, Keap1 DC recognize Nrf2 ETGE by a fast association and dissociation step, then the complex adopted the fully optimized conformation by a slow conformational adjustment reaction in the second step. It provides a reasonable explanation for the current findings. On the contrary, the kinetic analysis results from the SPR experiment showed that the Keap1-DLGex binding follows a fast association and fast dissociation model [46], which allows other signaling pathways to regulate Nrf2 activity. Without a doubt, the in-depth investigation of Keap1-Nrf2 PPI, coupled with the co-crystal structures, can facilitate the discovery of Keap1-Nrf2 PPI antagonists.

10.2.3 Assays for Evaluating the Keap1-Nrf2 PPI Inhibitors

The fast identification and accurate assessment of PPI inhibitors is another hurdle in the PPI drug discovery. Unlike the traditional drug targets, especially the enzymes, PPIs did not involve in the enzymatic activity in most cases. Nowadays, various interdisciplinary techniques, especially the biochemical and biophysical techniques, can be used to develop screening assays to find active hits from small arrays to large

compound library. Cell-based high content screening, cellular downstream phenotype examination and in vivo imaging monitor of PPIs have also been used to further evaluate the biological effects of PPI modulators. Now, various methods have been developed to meet the needs in the discovery of Keap1-Nrf2 PPI inhibitors, including the high-throughput screening (HTS) of hits, the improvement of PPI inhibition activity, and the optimization process for drug-like properties.

Hereafter, we will describe the current available assays for the identification and evaluation of Keap1-Nrf2 inhibitors (Table 10.1). The basic principles and the advantages as well as strengths and weaknesses of these different assay types will be included.

10.2.4 *In Vitro Assays*

Appropriate in vitro assays are the basis for discovery and development of Keap1-Nrf2 PPI inhibitors. Both Keap1 binding affinity and Keap1-Nrf2 PPI inhibition activity should be accurately measured to discover potent agents.

10.2.4.1 Assessment of Keap1 Binding

The equilibrium dissociation constant K_d is a universal parameter for reflecting the binding strength, which can be used for comparing the potency of different Keap1-Nrf2 PPI inhibitors directly. The estimation of K_d also plays an important role in the PPI biology, and thus, there are many methods that can be used for evaluating PPI modulators. The K_d can be obtained via two distinct ways: binding thermodynamic method and binding kinetic method. The most commonly used technique for the binding thermodynamic method is ITC assay, and as described above it has been used in the evaluation of Keap1-Nrf2 interaction. ITC assay can give the quantitative contribution of enthalpy and entropy simultaneously, and these parameters are quite useful in the drug-like optimization process [66, 67]. The values of both ΔG and ΔH can be obtained from the ITC titration profiles, and entropic contribution ($T\Delta S$) can be calculated using the fundamental equation $\Delta G = \Delta H - T\Delta S$. Our group have successfully used this method to optimize the peptide Keap1-Nrf2 inhibitors and obtained the most potent peptide inhibitor with a K_d value of about 10 nM [52]. SPR and BLI are the commonly used binding kinetic methods. Besides the K_d value, binding kinetic assay can monitor the association and disassociation process in real time and get the association rate constant k_{on} and the dissociation rate constant k_{off} . As described above, these kinetic results further enhanced the understanding of the Keap1-Nrf2 interaction mechanism. In the optimization process of the inhibitors, the kinetic profile is also an important drug-like index, which directly impacts drug efficacy and safety [68]. Longqin Hu's group used SPR to carry out the kinetic analyses of the Keap1-Nrf2 interaction and determine the minimal Nrf2 ETGE peptide for Keap1 binding [49]. By using the

Table 10.1 Summary of assays for evaluating the Keap1-Nrf2 PPI inhibitors

Assay type	Assay principle	Biological effect	Notes	References
<i>In vitro system</i>				
Biolayer interferometry (BLI)	Biophysics-optics	Keap1 binding	Binding kinetic analysis Quantitative methods Medium throughput	[52, 54]
Isothermal titration calorimetry (ITC)	Physical chemistry-calorimetry	Keap1 binding	Label-free; quantitative methods; binding thermodynamics analysis Low throughput	[52]
Competitive Fluorescence polarization (FP)	Molecular size-based luminescence	Keap1-Nrf2 ETGE peptide disruption	High throughput Quantitative methods	[55]
SPR-based competition assay	Biophysics-optics	Keap1-Nrf2 ETGE peptide disruption	Wide applicability for compounds; Competition assay; Medium throughput	[49]
Fluorescence resonance energy transfer assay	Proximity-based luminescence	Keap1-Nrf2 ETGE peptide disruption	High throughput Quantitative methods	[56]
Tracer displacement assay	Fluorescence anisotropy and Van't Hoff analysis	Keap1-Nrf2 ETGE peptide disruption	Medium throughput Binding thermodynamics analysis	[57]
Differential scanning fluorimetry (DSF) assay	Melting temperatures of Keap1 protein	Keap1 binding	High throughput	[58]
<i>Cellular and in vivo system</i>				
ARE-Luciferase Reporter Gene Assay	Luciferase enzymatic activity	Nrf2 transcription activity	High throughput High false positives	[59, 60]
ARE- β -lactamase Reporter Gene Assay	β -lactamase enzymatic activity	Nrf2 transcription activity	High throughput Provided by Invitrogen	
Nrf2-MafK or Keap1-RunX2 luciferase enzyme fragment complementation	Luciferase enzymatic activity	Nrf2 translocation and Nrf2-MafK or Nrf2-RunX binding	High throughput Low false positives	[61]

(continued)

Table 10.1 (continued)

Assay type	Assay principle	Biological effect	Notes	References
Nrf2–Keap1 Luciferase enzyme fragment complementation (EFC) assay	Luciferase enzymatic activity	Keap1-Nrf2 Disruption	Works in vivo	[62]
FRET and multiphoton fluorescence lifetime imaging microscopy	fluorescence lifetime	Keap1-Nrf2 Disruption	Direct detection of Keap1-Nrf2 interaction	[44, 63]
Enzymatic assay of Nrf2-dependent protein	Enzymatic activity (NQO1, HO1, etc.)	Protein level Nrf2-regulated genes	High throughput	[63]
β -gal enzyme fragment complementation	β -gal enzymatic activity	Nrf2 translocation	High throughput Low false positives Provided by DiscoverX	
Gene expression	qRT-PCR Detection of mRNA	mRNA level Nrf2-regulated genes	Cells and in vivo tissue; Low throughput	[64]
Protein expression	antigen-antibody reaction Detection of protein	Protein level Nrf2-regulated genes	Cells and in vivo tissue; Low throughput	[65]

BLI technique, we accessed the kinetic profile of the potent small-molecule Keap1-Nrf2 inhibitor and found that the inhibitor followed the binding behavior of the ETGE peptide, which has quite a slow disassociation rate. Generally, the binding kinetic and thermodynamic profile together ensures the precise assessment of Keap1-ligand binding and provides useful tips for further optimization of inhibitors.

The advantages of these methods are obvious, such as the label-free detection, real-time monitoring of binding interactions and quantitative evaluation of the binding strength. The shortcomings are also conspicuous. These assays need separate operation for each test sample, which restricts the throughput of the assay. These assays can only be used to validate and step-by-step optimize the inhibitors, rather than to carry out high-throughput screening to find novel hits. In recent years, the differential scanning fluorimetry (DSF) has been developed to detect ligand–receptor binding interactions that promote protein stability [69]. The main advantage of DSF is that it can be done with higher throughput without requiring large amounts of protein, and Chunlin Zhuang et al. used this method to confirm the binding interaction of the lead compounds with Keap1 [58].

10.2.4.2 Keap1-Nrf2 Inhibition Activity

The *in vitro* Keap1-Nrf2 interaction inhibition activity is the most important character reflecting the potency of the compounds. Because the PPI itself cannot induce the biological effects directly in most cases, the extra reporter groups, especially the fluorescent groups, should be introduced. Among these fluorescent-based techniques, the fluorescence polarization (FP) is the simplest and most widely used. The basic principle of FP is that fluorescent molecules emit light of a different plane as before when excited with linear polarized light [70]. This effect is induced by the movement of the molecules in solution between excitation and emission, which can be significantly affected by the molecular size. The difference in polarization can be observed for fluorescently labeled species of different sizes that essentially relies on a mass difference (preferably $\sim 10\times$). Thus, the FP assay is often used in a competition format: A short peptide derived from the binding motif of one protein will be fluorescently labeled, and the binding partner will be treated as the receptor. Only in this way, the mass of fluorophore-bearing peptide can get the sufficient difference between the unbound and bound state, which can induce a strong difference in FP. Thus, it is more suitable for the peptide-domain PPI, which the Keap1-Nrf2 ETGE PPI belongs to. Longqin Hu's group firstly reported the FP assay conditions for Keap1-Nrf2 PPI inhibitors using the optimized fluorescently labeled Nrf2 ETGE peptide [55]. They also used this assay to carry out an HTS and discovered the first-in-class small-molecule Keap1-Nrf2 inhibitor [71]. And now, the FP assay has been widely used in evaluating Keap1-Nrf2 inhibitors [54, 58, 63, 72, 73]. The main advantage of the FP assay is that it can quantitatively evaluate the activity of inhibitors with the biological reagents and compound-saving system, simple operation process ("mix-and-read assay"), and high screening throughput. The FP assay also has some weakness. Besides the size-dependent nature mentioned above, FP assay cannot be conducted in a time-resolving way and lacks the time stability. The further improvement of the FP method, the two-dimensional fluorescence intensity distribution analysis (2D-FIDA) [74] has also been used to set up the HTS assay of the Keap1-Nrf2 PPI inhibitors, and it also identified the active hits [75].

To overcome the drawbacks of FP assays, some proximity-based fluorescent methods have also been established. Among them, fluorescence resonance energy transfer (FRET)-based assay is the most widely used. FRET is the radiationless transmission of energy from a donor molecule that initially absorbs the energy to an acceptor molecule which the energy is subsequently transferred. The efficiency of this energy transfer is inversely proportional to the sixth power of the distance between donor and acceptor, making FRET extremely sensitive to small changes in distance. Thus, it is a proximity-based method, which can be adapted to detect the distance of two proteins and avoid the process of minimizing one binding partner to a short peptide, which facilitates the setting-up of the screening assay. Besides, the time stability of FRET over FP can facilitate HTS. Geoff Wells's group has successfully developed a steady-state FRET-based assay to identify inhibitors of the Keap1-Nrf2 PPI [56]. Besides evaluating the PPI inhibition, the fluorescent tracer

displacement assay can also be used to rapidly access thermodynamic parameters for target-ligand binding [76]. The main advantage of this kind of binding thermodynamic assay is that it can reach the medium throughput, which can be used in the hit-to-lead programs [77]. The research group from Evotec AG reported the protocol for the determination of the thermodynamic parameters of the Keap1-Nrf2 PPI inhibitors and tested the small-molecule inhibitors obtained from HTS [57].

The Keap1-Nrf2 inhibition assays mentioned above are all fluorescence related, which may not work on the compounds themselves bearing fluorescence. The SPR-based solution competition assay can be used to exam the Keap1-Nrf2 PPI inhibition activity of the fluorescent compounds [49]. In this assay, the biotin-labeled Nrf2 ETGE peptide was captured on the streptavidin chip and competitively bound Keap1 with the inhibitors in the solution. Because of the nature of SPR technique, it will not be disturbed by the compound's fluorescence and the throughput is also limited.

10.2.5 Cellular and In Vivo Assays

10.2.5.1 Assays for the Keap1-Nrf2 PPI Inhibition

Compared with determining Keap1-Nrf2 PPI inhibition activity *in vitro*, directly evaluating Keap1-Nrf2 PPI inhibition activity in live cells or *in vivo* is more difficult. Recently, a cell-based luciferase enzyme fragment complementation (EFC) assay has been reported to measure the dissociation of the Keap1-Nrf2 complex [62]. The authors generated the HEK293T cells which stably express the Nrf2 protein with the N-terminal luciferase fragment (CLuc-Nrf2) and the Keap1 protein with C-terminal luciferase fragment (NLuc-Keap1). When Keap1 interacts with Nrf2, the complemented luciferase enzymes will become an active form. Once the Keap1-Nrf2 complex is disrupted, the complemented luciferase enzymes will be disassembled, leading to a decrease in luciferase activity. Thus, the disruption of the Keap1-Nrf2 PPI can be related to the decrease of the luciferase activity, which can be easily detected and used in a high-throughput intact cell-imaging platform. Moreover, with the help of the non-invasive molecular imaging approach, this assay can also be used to evaluate compounds in small animal models. The FRET-based assay system is an alternative to evaluate the Keap1-Nrf2 inhibition activity in live cells. As mentioned above, Geoff Wells's group has successfully established and used this kind of assay to investigate the Keap1-Nrf2 PPI regulating mechanism [44, 45]. They also applied it to the evaluation of small-molecule inhibitors [63].

10.2.5.2 Assays for Nrf2 Activation

On account of transcriptional activation activity of Nrf2, it is much easier to construct the assay to estimate the potency of Nrf2 activation qualitatively and

quantitatively. Among these methods, the most straightforward way is the Nrf2-ARE-luciferase reporter gene assay. Nrf2 induces a battery of cytoprotective genes through binding to ARE that locates in the promoter regions, and thus, a luciferase gene under the control of ARE promoters can reflect the Nrf2 activation. Moreover, the luminescence signal affected by the luciferase activity can be easily detected, which provides a rapid and convenient quantification of Nrf2-ARE induction. Therefore, the cellular ARE-luciferase reporter gene assay can be used in HTS and several HTS using this assay have been reported [59, 60]. Apart from using the luciferase as the reporter gene, some other ARE-controlled reporter system is also commercially available. For example, Invitrogen provided the Cell Sensor™ ARE-bla HepG2 Cell-based Assay which used the β -lactamase as the reporter. The main disadvantage of ARE-luciferase reporter gene assay is the false positive. The cell-based luciferase enzyme fragment complementation assay (EFC), to a certain extent, can overcome this shortcoming. This method depends on the reconstitution of a “split” luciferase. Based on the interaction of Nrf2 with its nuclear partner MafK or runt-related transcription factor 2 (RunX2), a research group from GlaxoSmithKline developed such an approach, in which firefly luciferase is split into two fragments, which are genetically fused to Nrf2 and MafK or RunX2, respectively [61]. Thus, non-transcriptional readout is needed to minimize false positives and the luminescence signal can provide information directly on the level of Nrf2 protein and its function, which is a clear advantage over the classical ARE-luciferase reporter assay. The commercially available PathHunter® U2OS Keap1-Nrf2 Nuclear Translocation Cell Line from DiscoverX used the very similar mechanism. Nrf2 also controls the transcription of several enzymes, and thus, enzyme activity of these downstream enzymes can be used as the reporters directly. The examination of NQO1 enzyme activity is widely used in both classic Nrf2 activators [78] and the Keap1-Nrf2 PPI inhibitors [63]. This kind of assay is a good complement to the ARE-luciferase reporter gene assay to eliminate the false positives.

Compared with these medium- to high-throughput assays to evaluate the activation of Nrf2, there are many low-throughput but direct methods to validate the activation of Nrf2 and its function at the cellular level and *in vivo*, including the Western blot and the qRT-PCR analysis of Nrf2 and its downstream genes. As the prototypical Nrf2-target genes, NQO-1 (NAD(P)H:quinone oxidoreductase-1) [64, 79, 80] and HO-1 (heme-oxygenase-1) [81–83] are the most widely evaluated. However, it is noticed that the basal expression of NQO-1 is considerably high in certain cell lines, especially the tumor cell lines, for example, the HCT116 cells [54, 65, 73, 83]. Thus, a variety of downstream genes should be used to accurately evaluate the compound's effects on the Nrf2-regulated genes.

The current suite of available assay technologies, some of which are available as commercial kits, allows the discovery scientist to efficiently identify activators, confirm mechanism of action *in vitro*, and demonstrate pathway engagement *in vivo* in a tissue of interest. As such, the tools are available for robust drug discovery efforts.

10.3 Discovery and Optimization of Keap1-Nrf2 PPI Inhibitors

10.3.1 Peptide Keap1-Nrf2 Antagonists

The unknown of hotspots and characterized interactions is the main hurdle for targeting PPIs. Peptides are the ideal candidates to explore the PPI interface as they are able to closely mimic the principle features and proper conformation of a protein but can be easily synthesized and modified for functional fine-tuning [50]. Besides, the sequence of the nature protein can directly guide the design of peptides. It is feasible to discover the first-in-class PPI inhibitors from peptides and to explore the action mechanisms of PPI using peptides [51], as was the process of discovering the Keap1-Nrf2 PPI inhibitors (Table 10.2) [84].

10.3.2 Exploration of the Minimal Nrf2 Peptide Sequence Required for Keap1 Binding

As mentioned previously, the strong binding motif, the Nrf2 ETGE region, which is a typical peptide-domain PPI pattern, provided the primary sequence for discovering the peptide antagonists. Searching for the minimal peptide sequence from the primary sequence is a general approach for peptide PPI inhibitors in early stages. The identification of the minimal sequence can help the understanding of PPI hotspots. Besides, the minimal peptide can be derived to useful tools to investigate the PPI chemical biology and set up the screening assay that has been mentioned in Sect. 10.2.4.2. The reported co-crystal structures of Keap1-Nrf2 ETGE provide the direct guidance for the research. In the two reported structures, the Nrf2 ETGE region is the 9-mer and 16-mer ETGE-containing peptides, respectively. It indicated that the 9-mer peptide (LDEETGEFL) may be the good start point for the search of the minimal peptide. Two different groups carried out similar research using quite different evaluation methods. Using the competitive SPR assay, Longqin Hu's group found that the 10-mer to 14-mer Nrf2 peptides had similar binding affinities to the Keap1 Kelch domain while the 9-mer Nrf2 peptide had a moderate binding affinity of 352 nM and Nrf2 peptides < 9 amino acid residues failed to bind to the Keap1 Kelch domain [49]. Besides, the acetylation of the N-terminal could significantly improve the binding affinity to about 20 nM. The binding affinities of FITC-labeled Nrf2 peptides also gave similar results, the FITC-9-mer Nrf2 peptide can maintain the binding affinity (peptide **1**, FITC-LDEETGEFL-NH₂), while the FITC-8-mer Nrf2 peptide only showed a moderate binding affinity (835 nM). Thus, peptide **1** was chosen as the tracer to construct the FP assay. Using this assay, they found that the 8-mer Nrf2 peptide (H-DEETGEFL-OH) also had moderate inhibition activity, which indicated that the 8-mer peptide can interact with Keap1. Geoff Wells's group used the FP method that can get an apparent K_d value to

Table 10.2 Representative peptide Keap1-Nrf2 PPI inhibitors

No.	Sequence	Keap1-Nrf2 inhibition activity	Keap1-binding affinity	References
Peptide 1	FITC-LDEETGEFL-NH ₂	Fluorescent tracer	25.6 nM	[55]
Peptide 2	FITC-β-Ala-DEETGEF-OH		95.7 nM (K_d^{apparent})	[85]
Peptide 3	LQLDEETGEFLPQGGK(MR121)-OH		Not reported	[75]
Peptide 4	LDEETGEFL-NH ₂	3.57 μM	355 nM	[49]
Peptide 5	Ac-LDEETGEFL-NH ₂	0.194 μM	21.4 nM	
Peptide 6	Ac-DEETGEF-OH	5.39 μM	NA	[85]
Peptide 7	Ac-DPETGEL-OH	0.115 μM		
Peptide 8	Ac-DPETGEL-NH ₂	0.634 μM		[86]
Peptide 9	Ac-NPETGEL-OH	0.875 μM		
Peptide 10	St-DPETGEL-OH	0.022 μM		
Peptide 11	Ac-LDPETGEYL-OH	29.6 nM	46.5 nM	[52]
Peptide 12	Ac-c[CLDPETGEYLC]-OH	9.45 nM	10.4 nM	
Peptide 13	YGRKKRRQRRRLQLDEETGEFLPIQ	Cell penetrating		[87]
Peptide 14	RKKRRQRRR-PLFAER-LDEETGEFLP-NH ₂	Cell penetrating and target activation		[88]

determine the minimal peptide. Their results showed that the FITC-labeled 7-mer ETGE-containing peptide (peptide **2**, FITC- β -Ala-DEETGEF-OH) is the shortest peptide that can maintain the binding affinity, which showed an apparent K_d of 95.7 nM. The results seem different from the Lonqin Hu's group. However, the FITC-labeled 7-mer peptide contains a β -Ala to act as the linker between the FITC and the N-terminal. This β -Ala has similar effects compared with the leucine at the N-terminal of the 9-mer peptide, and thus, the FITC-labeled 7-mer peptide should be treated as the 8-mer peptide. Therefore, the main difference occurs at the leucine of the C-terminal. In the co-crystal structure, this residue did not form obvious interaction with the Keap1 protein, and only its terminal carboxyl acid can form intramolecular hydrogen bond with the amine at the N-terminal, which may have slight effects on maintaining the peptide conformation. It is reasonable that it can be simplified to obtain the minimal fluorescent peptide tracer for Keap1 binding. Using this tracer, Hancock et al. found that another 7-mer Nrf2 peptide (peptide **6**, Ac-DEETGEF-OH) also has moderate peptide inhibition activity, which indicated that such kind of 7-mer Nrf2 peptide is the minimal sequence for Keap1 binding [85]. Taken together, we can conclude that the 7-mer Nrf2 peptide (Ac-DEETGEF-OH) is the shortest Keap1 binding peptide that can retain the proper conformation and most Keap1 binding interactions, the FITC-labeled "8-mer" ETGE-containing peptide (FITC- β -Ala-DEETGEF-OH) is the simplest fluorescent peptide tracer for the FP assay, and the 9-mer peptide (Ac-LDEETGEFL-OH) is the optimal peptide inhibitor with potent Keap1-Nrf2 inhibition activity.

10.3.2.1 Structure-Based Optimization of the Nrf2 ETGE Peptide

Although the 9-mer peptide showed fair Keap1 binding affinity and Keap1-Nrf2 inhibition activity, its Keap1 binding affinity is still lower than the Nrf2 protein. Besides, the four acidic residues strongly disfavor cellular penetration. Further optimization is necessary to improve the activity, shorten the length of the peptide, and replace the unnecessary acidic residues. The SAR study around the Ac-DEETGEF-OH sequence was carried out. The first glutamic acid in the peptide can be optimized, and changing it to alanine improved the IC_{50} to 0.73 μ M. Moreover, inspired by the primary sequence of another Keap1 substrate protein, p62, the proline replacement of the glutamic acid further increased the activity to an IC_{50} of 0.248 μ M. The core ETGE motif is highly conserved for the activity and changing the glutamic acid to glutamine and asparagine is intolerant for activity. Even changing the second glutamic acid in ETGE to aspartic acid could abolish the activity and only the first glutamic acid in ETGE can be replaced by aspartic acid which caused threefold loss in activity. The serine which can form hydrogen bond with Keap1 is also sensitive for the residue-altering, and only the serine derivative retained some activity. The phenylalanine at the right side of ETGE gave high tolerance for the residue change. Replacement with tryptophan, leucine or tyrosine can maintain the activity, and the leucine is the optimal which can result in the most

potent peptide (peptide **7**, Ac-DPETGEL-OH) with an IC_{50} of 0.115 μ M in this research [85]. In the following study, Wells's group found that transforming first aspartic acid to asparagine is also acceptable though it will induce the eightfold activity loss (peptide **9**). Besides, they found the terminal modifications have dramatic effects on the activity. In order to promote the lipophilic of the peptide, the C18 fatty acid stearic acid was introduced at the N-terminal. This conjugate (peptide **10**) showed a fivefold greater activity (0.022 μ M vs. 0.115 μ M), while the introduction of the benzoyl group almost did not affect the activity. Their research also showed that the C-terminal carboxyl group is important for Keap1-Nrf2 inhibition activity and changing the carboxyl group to carboxamide caused a six- to tenfold decrease of the activity (peptides **7** and **8** as an example) [86].

Our group further investigated this activity loss by molecular dynamics (MD) simulation and found that the C-terminal carboxyl group can form extra multiple hydrogen bonds with Arg483, while only the terminal carboxyl oxygen atom of peptide forms much weaker interaction with Asn382. The terminal carboxyl group at this site can form favorable electrostatic interaction with the Arg483 in the P2 sub-pocket, which can strengthen the multiple polar interaction networks in the P2 sub-pocket [89]. It indicated that the C-terminal carboxyl group should be retained when this 7-mer residue scaffold was used, but when the growth of residue occurs at the C-terminal, the terminal carboxyl will be far away from key arginine. On the basis of Hu's study [49], the terminal amide analog will be optimal. Besides explaining this activity change, we also used systematic MD approach to set up a computational workflow to investigate the peptide Keap1-Nrf2 PPI inhibitors. We found that the terminal leucines residues in the 9-mer Nrf2 peptide could contribute to Keap1 binding through favorable hydrophobic interactions at an additive manner, and it is also consistent with the positive results of introducing the C18 fatty acid stearic acid at the N-terminal. According to this result, the Leu residues were added to the optimal 7-mer peptide inhibitor and gave a more potent inhibitor (Ac-LDPETGEFL-OH) with an IC_{50} of 42.6 nM. Further MD simulation of this peptide indicated that replacing the Phe with Tyr may be beneficial for activity, and the experimental results also proved that this replacement (peptide **11**) can further enhance the activity.

10.3.2.2 Conformational Restriction

During the optimization process of the ETGE-containing peptide inhibitors, the most dramatic finding is that the Pro replacement significantly improved the activity of the peptide which has been described above. Although the Pro has limited effects in forming interaction, it has been proven to be helpful for mimicking the β -hairpin secondary conformation for a long time [90, 91]. Our computational results stressed this thought. MD simulation results showed that the Pro replacement can significantly stabilize the β -hairpin conformation and enhance the hydrogen bond network formed by the key glutamates in the ETGE motif [89]. The dramatic effect of Pro in

stabilizing the peptide conformation further indicated conformation restriction as a valuable strategy in PPI inhibitor design.

Terminal cyclization is another conformational restriction method. Besides the remarkable effects on the conformation locking, cyclic peptide also has enhanced peptide stability against both exo- and endo-proteases, which significantly strengthens the therapeutic potential of this class of peptides. The secondary structure of the ETGE region is a typical β -hairpin, which comprises two antiparallel β -strands connected by a turn sequence. It is suitable for using the head-to-tail cyclizing or disulfide bridges to develop the conformation stable cyclic peptides [92]. Previously, based on the optimized peptide Keap1-Nrf2 inhibitors, we introduced a terminal disulfide linkage to stabilize the peptide, resulting the most potent peptide inhibitor (peptide 12, Ac-c[CLDPETGEYLC]-OH) with a K_d value of 2.8 nM binding to Keap1 and an IC_{50} value of 9.4 nM in the FP assay [52]. It proved that the terminal cyclization is quite useful in the design of Keap1-Nrf2 PPI inhibitors. Another head-to-tail cyclized Nrf2-derived peptide (cycloGDEETGE) has been reported and its structure in complex with the Keap1 Kelch domain is also available in the PDB [93]. Although the activity of this peptide is still unknown, it provides valuable thoughts in the further development of peptide inhibitors.

10.3.2.3 Cellular Activity of Peptide Inhibitors

The two glutamate residues of the Nrf2 ETGE peptide are important for Keap1-Nrf2 inhibition activity. While these acidic residues have important roles in both conformation stabilization and Keap1 binding, they strongly disfavor cell membrane permeability. Thus, reducing the acid residues and enhancing the lipophilicity is the main goal for improving the cellular activity of peptide inhibitors. Hancock et al. demonstrated that the introduction of the lipophilic stearic acid group can significantly improve the cellular activity. However, restricted by the key roles of the Glu residues in Keap1 binding, the net charge of peptide can hardly be higher than -2 . Thus, the cellular activity is still limited.

Directly conjugating to a cell penetrating peptide (CPP) to the primary sequence is a more direct way to develop cell penetrating probe to investigate the PPI inhibition effects. Steel et al. used the trans-activating transcriptional activator (TAT) peptide that was derived from HIV as the CPP to construct the cell penetrating Nrf2 ETGE peptides [87]. The resulted activate peptide (peptide 13) can elevate the protein level of Nrf2 and up-regulate its downstream target gene HO-1 at both mRNA and protein levels in a dose-dependent manner in the intact human THP-1 monocytes. Moreover, this research also proved that this peptide Keap1-Nrf2 inhibitor can also inhibit the production of the pro-inflammatory cytokine TNF, which indicates the potential anti-inflammatory usages of the Keap1-Nrf2 PPI inhibitors.

Jing et al. also used the same strategy to construct the similar peptide, but found it did not work in the brain-injured mice. They further introduced a calpain cleavage

sequence (PLFAER) between the TAT sequence and the Nrf2 ETGE motif, which makes the peptide sensitive to Ca^{2+} increase and allows injury-specific activation of Nrf2. This new peptide (peptide **14**) significantly increased the mRNA levels of Nrf2-regulated genes. Moreover, it attenuated blood–brain barrier (BBB) compromise following TBI that is beneficial for reducing neurovascular dysfunction in the injured brain [94]. This research not only indicated the potential therapeutic application of the Keap1-Nrf2 PPI inhibitor, but also provided an enlightening thought for the design of target-activated Nrf2 activators. The very recent study further confirmed that this peptide induced Nrf2-regulated cytoprotective genes, reduced oxidative stress, and induced strong neuroprotection and marked preservation of hippocampal-dependent cognitive function after global cerebral ischemia (GCI) at an injury-specific manner [88]. This study further confirmed the Keap1-Nrf2 PPI inhibitors as the potentially promising new therapeutic modality for the treatment of GCI.

10.3.2.4 Searching for Novel Peptide Sequence

Despite these peptide antagonists based on the primary sequences of natural binding partner, display methods, in particular the phage display method, are a good source for the discovery of antagonists with novel binding sequences [95]. Brian Kuhlman et al. used the phage display combining with computational loop grafting protocol to discover a engineered monobody that is a potent competitive inhibitor of the Keap1-Nrf2 PPI, which bound to Keap1 with a K_d of 300 pM [96]. However, this study could not find the novel Keap1 binding sequence, and the core binding sequence is RDEETGEFHWP, which also included the primary Nrf2 sequence DEETGEF. Geoff Wells's group also set up a phage display library approach to discover peptide ligands with non-native sequence motifs, but only weak peptides were discovered [85]. The hurdles in discovering novel peptide Keap1-Nrf2 inhibitors further confirmed the conservatism of the core ETGE motif.

Taken together, the development of peptide Keap1-Nrf2 inhibitors has made much progress [84]. It confirmed that this PPI can be disrupted by the artificial compounds and directly disrupting Keap1-Nrf2 PPI could be an effective way to activate Nrf2. Besides, the potential uses of Keap1-Nrf2 inhibitors as the anti-inflammatory and organ-protective agents have also been validated. The SAR study of the peptides also pointed out that the P1 and P2 sub-pockets occupied by the two Glu residues are the hotspots, which can give the direct guidance for the design of small molecules.

10.3.3 Small-Molecule Keap1-Nrf2 Inhibitors

Compared to the discovery of peptide inhibitors, finding small-molecule Keap1-Nrf2 PPI inhibitors is more challenging. With the help of progress in both

screening methods and peptide inhibitors, a number of small-molecule inhibitors have been identified and the detailed binding mode of some inhibitors has been clarified by crystal structures (Table 10.3) [97, 98].

10.3.3.1 Experimental HTS of Hit Compounds

Similar to the most cases, the first hits targeting Keap1-Nrf2 PPI were obtained from the HTS. Hu et al. used the FP assay to screen the NIH MLPCN library of small molecules (containing about 330,000 compounds) and identified a small-molecule hit, **1** (Fig. 10.6), as a first-in-class direct small-molecule inhibitor of Keap1-Nrf2 PPI [71]. Because this compound contains three chiral centers, the authors further investigated the effects of chirality on activity through combination of flash and chiral chromatographic separation. They finally got one stereoisomer which is predominantly responsible for Keap1 binding activity ($K_d = 1 \mu\text{M}$), and the stereochemistry of this stereoisomer **2** was assigned by the X-ray crystal structures. This compound also showed fair activity in the cellular ARE gene reporter assay and Nrf2 nuclear translocation assay, with an EC_{50} of 18 μM and 12 μM , respectively.

Another group from Biogen Idec carried out an HTS of Evotec Lead Discovery library using the 2D-FIDA assay. They got 18 active hit compounds which can be divided into two subclasses based on the chemical structures, specifically the N-phenyl-benzenesulfonamide class and the benzenesulfonyl-pyrimidone class. The representatives **4** and **5** (Fig. 10.7) with an IC_{50} of 118 μM and 2.7 μM , respectively, were chosen to carry out the following hits validation process. The NMR and native mass spectrometry results together confirmed the direct interaction between the Keap1 DC domain and the small molecules. Moreover, this group obtained the co-crystal structures of the two inhibitors with the Keap1 DC domain, providing useful information for the structure-based design (Fig. 10.8). The cellular ARE-luciferase cell reporter assay was also used to measure the action of Nrf2, and only compound **5** upregulated Nrf2 response genes. Western blot measuring Nrf2 stabilization also gave the similar results. It could be due to the extremely weak Keap1-Nrf2 PPI inhibition activity of **4**.

10.3.3.2 Virtual Screening of the Keap1-Nrf2 PPI Inhibitors

Besides the HTS method, the virtual screening (VS) is another commonly used hit screening method with high efficiency and low costs. In the previous study, we reported the first hierarchical structure-based virtual screening utilizing the receptor-ligand binding model of Keap1-Nrf2 [72]. In this study, we used the co-crystal structure of the Keap1-Nrf2 ETGE peptide to construct the pharmacophore. Considering the ETGE motif displays multiple acidic residues that form strong electrostatic interactions with Keap1, the database was pre-filtered using the criteria that the molecules should have a calculated formal charge ≤ 1 . Using this

Table 10.3 Summary of the available crystal structures of Keap1 and Keap1 with ligands

Keap1	Ligand	PDB code	References
mKeap1-DC domain; residues 309–624		1U6D	[99]
mKeap1-DC domain; residues 309–624		1ZGK	[100]
mKeap1-DC domain; residues 309–624		1X2 J	[101]
hKeap1 DC domain; residues 321–609		4IFJ	
hKeap1 BTB domain; residues 48–180		4CXI	[102]
hKeap1 BTB domain C151 W mutant; residues 48–180		4CXJ	
Keap1 BTB domain C151 W mutant; residues 48–180	CDDO	4CXJ	
hKeap1 DC domain; residues 321–609	Nrf2/Neh2 DLGex; residues 17–51	3WN7	[46]
mKeap1-DC domain; residues 309–624	Nrf2/Neh2 ETGE; residues 76–84	1X2R	[101]
hKeap1 DC domain; residues 321–609	Nrf2/Neh2 ETGE; residues 69–84	4IFL	
hKeap1 DC domain; residues 325–609	Nrf2/Neh2 ETGE; residues 69–84	2FLU	[103]
mKeap1-DC domain	Nrf2/Neh2 DLG; residues 24–29	2DYH	[41]
mKeap1-DC domain; residues 309–607	Prothymosin α residues 39–54	2Z32	
mKeap1-DC domain; residues 309–624	p62 peptide residues 346–359	3ADE	[104]
mKeap1-DC domain; residues 309–624	phosphorylated p62 residues 346–359	3WDZ	[105]
hKeap1 DC domain; residues 321–609	21	3VNG	[106]
hKeap1 DC domain; residues 321–609		3VNH	
mKeap1-DC domain; residues 309–624	10 (RA389)	5CGJ	[107]
hKeap1 DC domain; residues 321–609	9	4XMB	[108]
hKeap1 DC domain; residues 321–611	Keap1-Nrf2 inhibitors with THIQ scaffold	4L7B, 4L7C, 4L7D, 4N1B	[109]
hKeap1 DC domain; residues 321–609	2 with THIQ scaffold	4IFN	

(continued)

Table 10.3 (continued)

Keap1	Ligand	PDB code	References
hKeap1 DC domain; residues 321–609; Mutation: E540A, E542A	cycloGDEETGE	3ZGC	[93]
hKeap1 DC domain; residues 321–609; Mutation: E540A, E542A		3ZGD	
hKeap1 DC domain; residues 321–609	4	4IN4	[75]
hKeap1 DC domain; residues 321–609	5	4IQK	
mKeap1-DC domain; residues 309–607	Fragments and hits used in the design of 24	5FNQ, 5FNR, 5FNS, 5FNT, 5FNU, 5FZJ, 5FZN	[110]

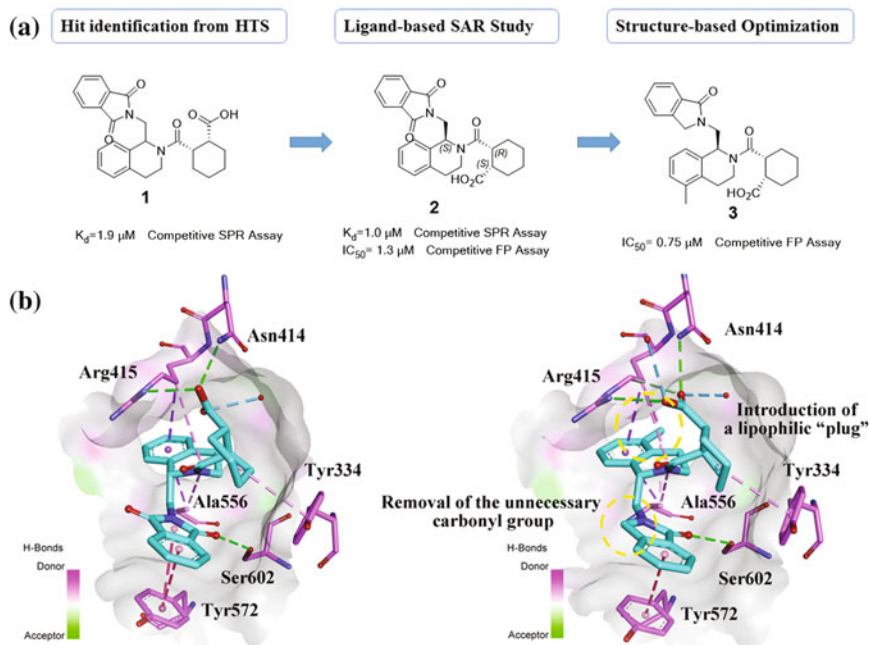


Fig. 10.6 Discovery and optimization of Keap1-Nrf2 inhibitors with tetrahydroisoquinoline (THIP) scaffold. **a** The developing process of the Keap1-Nrf2 inhibitors with THIP scaffold. **b** The binding mode differences between the hit and optimal compound. Key modifications are labeled by yellow dashed lines. The hydrogen bonds are represented as green dashed lines, and the electrostatic interactions are represented as yellow dashed lines. The carbon atoms of small molecules and Keap1 residues are colored cyan and purple, respectively. Key water molecules are represented as red dots

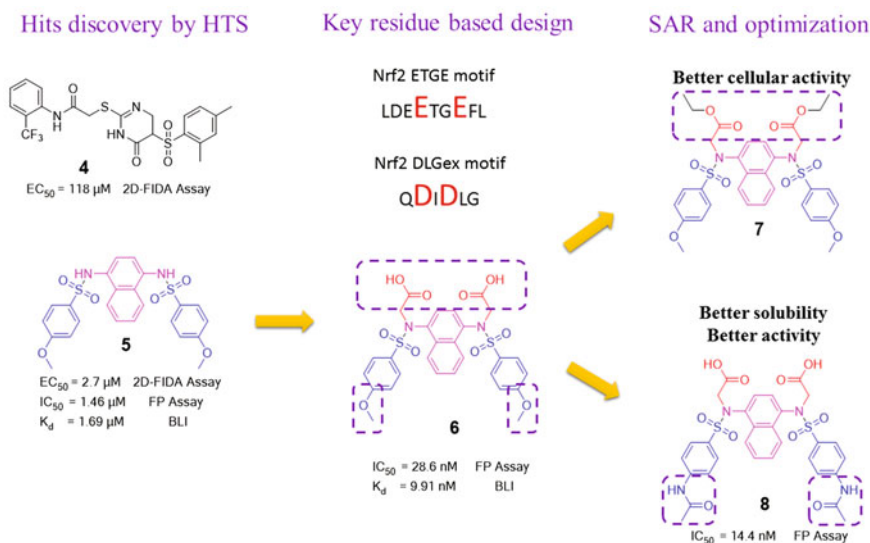


Fig. 10.7 The developing process for the naphthalene sulfonamide class of the Keap1-Nrf2 PPI inhibitors. Hit structure **5** was discovered from HTS. Hotspots-based design gave the first nanomole small-molecule inhibitor **6**. The SAR and optimization further enhanced the cell activity and solubility

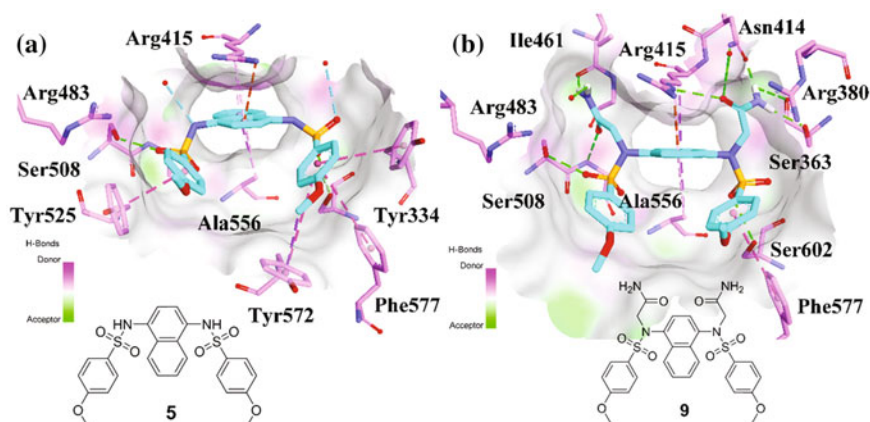


Fig. 10.8 Binding mode of the naphthalene sulfonamide class of the Keap1-Nrf2 PPI inhibitors. **a** The binding mode of **5** (PDB code: 4IQK); **b** the binding mode of **9** (PDB code: 4XMB). The hydrogen bonds are represented as green dashed lines, and the electrostatic interactions are represented as yellow dashed lines. The carbon atoms of small molecules and Keap1 residues are colored cyan and purple, respectively

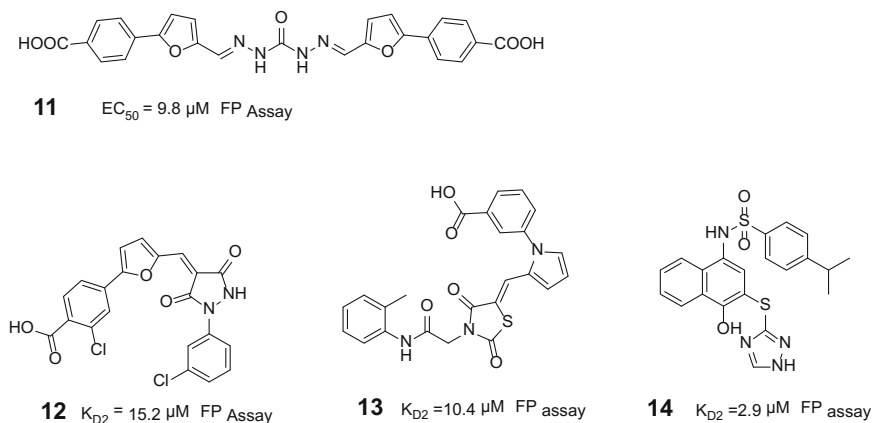


Fig. 10.9 Active hits from virtual screening

pharmacophore together with molecular docking method, we screened the SPECS database and obtained an active hit, **11** (Fig. 10.9) with an EC_{50} of $9.80 \mu\text{M}$ in FP assay. This compound also elevated the Nrf2 transcription activity in the cell-based ARE-luciferase reporter assays at a concentration-dependent manner. Zhuang et al. also carried out a VS of SPECS database using the cascade docking method integrated in Schrodinger's Glide module. The previously reported active hit **5** was chosen as the control, and only these compounds that gave the better performance than **5** were retained. The maximum chemical diversity was used as the criteria to select compounds, and clustering based on the calculated Tanimoto coefficient using the 2D fingerprint [111] was carried out to get the final purchasing list. They obtained nine compounds representing three chemotypes of the Keap1-Nrf2 PPI inhibitors (Fig. 10.9), which possessed good inhibitory activity with K_{D2} ranging from 2.9 to $75.48 \mu\text{M}$. Then the author used the hit-based substructure search method to investigate the preliminary SAR of the new scaffold. Among these compounds, compound **14** is the most potent, and it also contains the naphthalene sulfonamide scaffold.

10.3.3.3 Structure-Based SAR and Optimization of Hit Compounds

The emergence of the pioneer small-molecule inhibitors inspired the further SAR and optimization work around these hits. And now, the activity of the inhibitors can reach the nanomole range and the SAR of certain scaffolds has been clarified.

Tetrahydroisoquinolines

After the discovery of the hit compound **1**, Hu's group conducted some preliminary SAR study. Their research indicated that the acidic functionality on the cycloalkane ring is important for Keap1 binding and the amide or ester analog could induce the significant loss or even abolish the activity. The aryl ring at tetrahydroisoquinoline

(THIQ) scaffold is also indispensable and the one-carbon linker between the THIQ and phthalimido group is naturally optimal. The further optimization site may be the phthalimido group that can tolerate the simplification.

This compound also attracted the interests of UCB Pharma. They obtained the co-crystal structure of the Keap1-compound **2** complex, which clarified the binding mode. Based on this co-crystal structure, they first conducted detailed SAR study around the cyclohexane carboxylic acid. Both the cyclohexane and cyclopentane were optimal and further reducing the size of the ring harmed the activity. The removal of the carboxylic acid or its replacement by carboxamide or nitrile totally abolished the activity, and only the tetrazole analog was active with a small decrease in potency. Introducing a polar nitrogen atom in the cyclohexane significantly reduced the activity. These results together stated the cyclohexane carboxylic acid as a privileged fragment in this site. The phthalimido group has also been investigated, and their research results were consistent with the previous study. One of the carbonyls can be moved, but the amide group was necessary. The removal of phenyl ring in the phthalimido group was also feasible, which had nearly no effects on potency. The research on the THIQ also had some positive finding, and the methylation of the 5-position of the THIQ further improved the activity, leading to the most potent compound **3** in this study ($IC_{50} = 0.75 \mu M$). This research group only investigated the physicochemical and DMPK properties, they found that compound **2** is a P-gp substrate and restricted to the peripheral compartment in mice, while the isoxindole analog **3** with reducing PSA exhibited a trend toward decreased efflux. It gave the guidance for improving drug-like properties and making it brain available.

Naphthalene sulfonamides

Another active hit **5**, which was reported by Biogen Idec, attracted our research interests. The co-crystal structure of this compound showed that it adopted a unique binding mode, quite different from the Nrf2 ETGE motif. The naphthalene ring inserted into central cavity, and the two side-chain aryl rings occupied the P4 and P5 sub-pockets. These aromatic rings can form multiple cation- π and π - π interactions with the side chains of Tyr334, Tyr572, Tyr525, and Arg415, which cannot be observed in the Keap1-Nrf2 ETGE structures. With the help of these hydrophobic interactions, compound **5** can effectively compete with Nrf2 ETGE peptide with an EC_{50} of $2.7 \mu M$ without the tight polar interactions in the P1 and P2 polar sub-pockets. However, in our computational analysis, the electrostatic interactions with the polar residues in the P1 and P2 sub-pockets, especially the key arginines, are pivotal for Keap1 binding. Accordingly, we introduced the polar recognition group, di-acetic moiety, to mimic the binding mode of the ETGE motif. Based on the crystal structure of Keap1-**5** complex, the nitrogen atom of the sulfonamide was chosen as the linking site, resulting a potent Keap1-Nrf2 PPI inhibitor **6**, with a K_d of 9.91 nM to Keap1 and an IC_{50} of 28.6 nM in the FP assay. This is the first nanomole small-molecule Keap1-Nrf2 PPI inhibitor, which confirmed that the Keap1-Nrf2 PPI can be effectively regulated by small molecules. Then, we further optimized the substituents on the side-chain aryl rings and found that p-acetamido substituents were the best choice for balancing PPI inhibition

activity, physicochemical properties, and cellular Nrf2 activity [73]. Besides, in this study, we also found that the core naphthalene ring played an important role in Keap1 binding, and simplifying the naphthalene to a phenyl ring caused about 50-fold decrease in activity. Moore et al. also investigated the structural requirements of naphthalene sulfonamide-based Keap1-Nrf2 inhibitors. Their study showed that the 1,4-disubstitution pattern of the naphthalene scaffold is important for the Keap1-Nrf2 PPI inhibition and singly substituted acetic acid analog can maintain the most part of the activity. Besides, the di-amide analog **9** also showed good potency, and its X-ray structure with Keap1 fully confirmed the binding pattern, especially the water displacement effects. In this study, they also found the ethyl ester **7** is more potent in the cellular assays, exhibiting ex vivo efficacy similar to the well-known electrophilic activator, sulforaphane. It provided a valuable thought to develop prodrugs for improving drug-like properties.

Very recently, Schmoll et al. also reported a novel Keap1-Nrf2 PPI inhibitor (**10**, RA839), which contains the naphthalene sulfonamide scaffold. It also has a 1,4-disubstitution pattern of the naphthalene scaffold, but just one sulfonamide group. The other substituent is the pyrrolidine-3-carboxylic acid, which can form key polar interaction with Arg483 in the crystal structure. This compound gave a K_d of 6 μM to the Keap1 Kelch domain in the ITC experiment, partly because it cannot fully occupy the Keap1 binding cavity.

Other structure classes

Geoff Wells's group reported a series of 1,4-diphenyl-1,2,3-triazole compounds that inhibit the Keap1-Nrf2 PPI (Fig. 10.10a). The design of this series of compounds was inspired by the docking-based design. The two functionalized phenyl rings can mimic the side chain of the key Glu residues, while the triazole ring acted as the scaffold which can be easily synthesized. The SAR study showed that the benzoic acid moiety was optimal in the in vitro FP assay, but not preferable in the cell-based NQO1 assays (compound **18**). The nitro-substituted compounds were more potent in the cell-based activity, and a meta-nitro group on the 4-phenyl ring and a meta-nitro, methyl, or halogen on the 1-phenyl unit are the best combinations (compound **15–17**) [63]. It provided an alternative choice for the polar recognition group that can be further investigated. Recently, our group reported a series of Nrf2

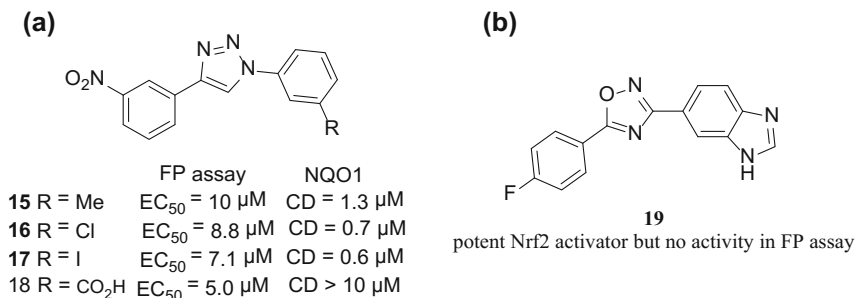


Fig. 10.10 The discovery of 1,4-diphenyl-1,2,3-triazole compounds as the Keap1-Nrf2 PPI inhibitor

activators with similar overall shape but the 1,2,4-oxadiazole core (**19** as an example) [112]. However, these compounds did not show the Keap1-Nrf2 PPI inhibition activity. It further indicated that the Keap1 cavity is strict with the substrate structures.

In another study, Mochizuki et al. reported another Nrf2 activator **20**, NK-252, which can interact with the Keap1 DC domain [113]. It may be a Keap1-Nrf2 PPI inhibitor, but the detailed study was absent. This scaffold has also been reported by Kunishima's group recently. However, their ligands contain an acidic group that can interact with key arginine. In addition, their study found that the small molecule could adopt two different binding modes with the Keap1 DC domain in the soaking and the co-crystallization forms (Fig. 10.11b, c). In the co-crystallization form, the 2-phenoxyacetic acid moiety deeply inserted into the P2 sub-pocket and formed multiple hydrogen bonds with Ser363, Arg380, and Asn382. In this binding, the phenyl ring can form two pi-pi interactions with Tyr572 and Tyr334

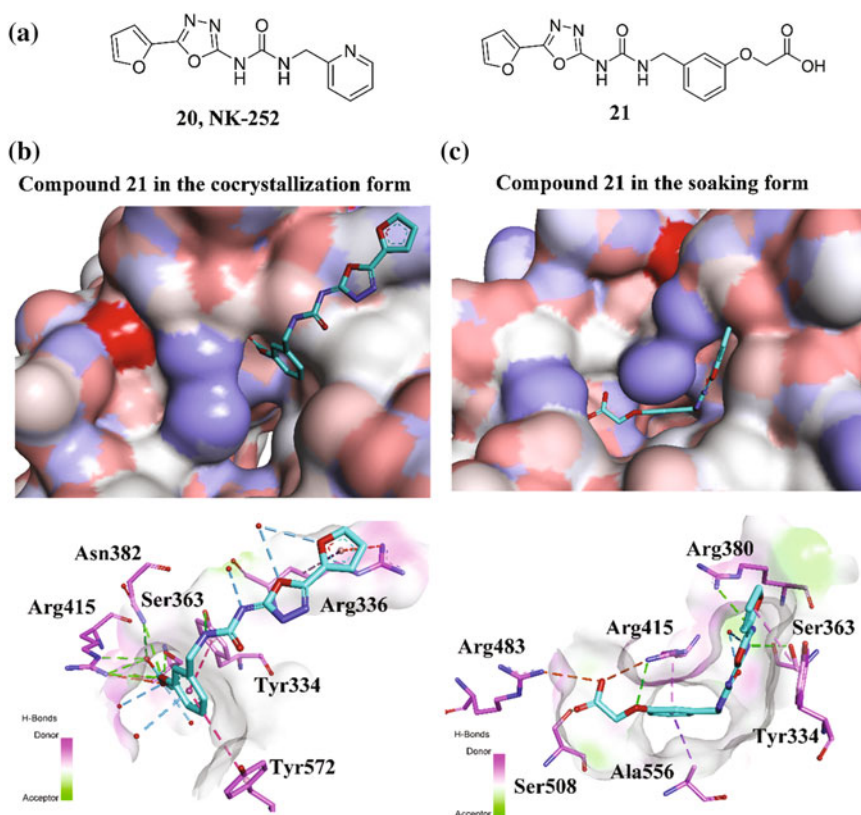


Fig. 10.11 Binding mode investigation of the Keap1 ligands with urea fragment. **a** Chemical structures of the Keap1 ligands with urea fragment; **b** binding mode of **21** with Keap1 in the co-crystallization form (PDB code: 3VNG); **c** binding mode of **21** with Keap1 in the soaking form (PDB code: 3VNH)

simultaneously, while the biaryl moiety located on the outside of the central cavity and interacted with Arg336. The soaking experiment gave a distinct binding mode that the molecule approximately located on the central hole of Keap1. The phenyl ring occupied the P3 sub-pocket similar to the naphthalene ring of the Compound **21**. The acetic acid group extended to the P1 sub-pocket and formed multiple polar interactions with Arg483, Arg415, and Ser508. The carbamide linker and the biaryl moiety occupied the P2 sub-pocket by a novel pattern. They also used the MD simulation to further investigate the differences between the two forms, and the binding pattern from co-crystallization form tended to dissociate more easily compared to the structure from the soaking form. Although the Keap1-Nrf2 inhibition activity of this compound was unknown, it gave the fresh binding pattern with Keap1 that facilitates the design of novel Keap1-Nrf2 PPI inhibitors.

Very recently, researchers from Astex Pharmaceuticals and GlaxoSmithKline Pharmaceuticals identified a series of novel Keap1-Nrf2 PPI inhibitors with high cell potency by fragment-based approach [110]. At the beginning of their research, a crystallographic screen of fragments library was carried out and three fragments were identified that occupied three discrete hotspots within the Keap1 cavity (as shown in Fig. 10.12). Fragment **1** showed a similar binding pattern with

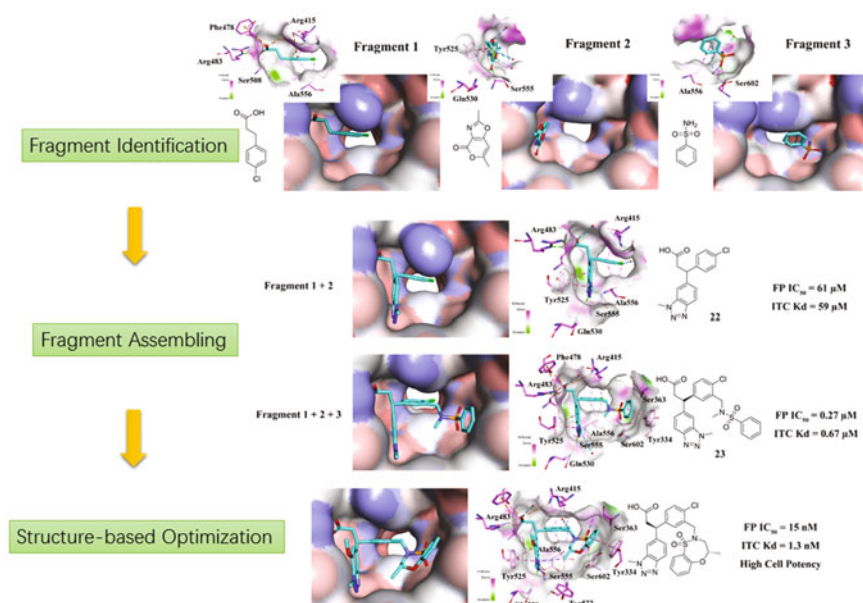


Fig. 10.12 Fragment-based discovery of novel Keap1-Nrf2 PPI inhibitors with high cell potency. Three distinct fragments were identified through a crystallographic screen of fragments library (fragment 1: PDB code 5FNQ; fragment 2: PDB code 5FZJ, and fragment 3: PDB code 5FZN). The first hit in fragment to hit process, **22**, was designed based on the binding mode of fragments **1** and **2** (PDB code: 5FNR). The structure of fragment **3** was integrated into **22**, resulting in a good hit **23** (PDB code: 5FNT). Further structure-based optimization gave the nanomolar inhibitor **24**, with a quite ingenious seven-member heterocyclic structure (PDB code: 5FNU)

compound **21** in the soaking form. The aliphatic acid of fragment **1** inserted into sub-pocket P1, forming electrostatic interactions with Arg483 and Arg415, and the core phenyl ring located in the P3 pocket. Fragment **2** formed a pi-pi interaction with Tyr525 and several hydrogen bonds with Gln530 and Ser555. On the basis of the crystal structure, the fragment **1** was chosen as the template, and the benzotriazole moiety is that similar to fragment **2** was attached directly to the benzylic carbon of the phenyl acetic acid. This modification gave the first hit structure **22**, which showed the inhibition activity in the FP assay. The crystal structure also proved that **22** retained the Keap1-binding interactions that can be found in fragments **1** and **2**. Besides, the chlorophenyl ring of **22** provided the site for the introduction of privileged fragments. The benzenesulfonamide was linked to 3-position of the chlorophenyl ring of **22** by using the methylene group as the linker, which gave a good hit **23**, with an IC₅₀ of 0.27 μM in the FP assay. This hit structure showed some outstanding characteristics. It used the two anchoring characters: It formed hydrogen bonds with Ser555 and Ser602 as same as the Nrf2 ETGE peptide and the core phenyl ring inserted into the P3 sub-pocket similar to the naphthalene sulfonamide inhibitors. Further structure-based optimization gave the nanomole inhibitor **24**, which contains a quite ingenious seven-member heterocyclic structure. It further locked the binding conformation of the benzulfamide, and the extra methyl group in the ring can form favorable hydrophobic interaction with Tyr572. This compound also showed good potency in activating the Nrf2 antioxidant response in cellular and in vivo models.

10.4 Future Directions and Concerns of Keap1-Nrf2 Inhibitors

The development of Keap1-Nrf2 inhibitors has made much progress. Now, the potent Keap1-Nrf2 inhibitors are available and the in vivo therapeutic effects of Keap1-Nrf2 inhibitors have been explored. However, the chemical diversity of small-molecule Keap1-Nrf2 inhibitors is quite limited and the clinical application of Keap1-Nrf2 inhibition is still obscure. These issues should be further investigated. Besides, the intact mechanism of Keap1-Nrf2 inhibitors also needs to be intensively investigated. Keap1 can mediate the ubiquitination of multiple substrates, including, IKKβ [114, 115], Bcl-2 [116], and PGAM5 [117]. Some other proteins, including heat-shock protein 90 (Hsp90) [118], DJ-1 [119, 120], P62 [104, 105], and p65 [121] also can modulate Keap1-Nrf2 PPI. Thus, Keap1-Nrf2 may also have a concern in selectivity, and it has also attracted some research interests [122]. The overall outcome of Keap1-Nrf2 PPI inhibitors on Keap1-related interactome should be investigated both in vitro and in vivo. It is also a common problem in the study of PPI inhibitors.

References

1. Finkel T, Holbrook NJ (2000) Oxidants, oxidative stress and the biology of ageing. *Nature* 408(6809):239–247
2. Barnham KJ, Masters CL, Bush AI (2004) Neurodegenerative diseases and oxidative stress. *Nat Rev Drug Discov* 3(3):205–214
3. Hu R, Saw CL, Yu R, Kong AN (2010) Regulation of NF-E2-related factor 2 signaling for cancer chemoprevention: antioxidant coupled with antiinflammatory. *Antioxid Redox Signal* 13(11):1679–1698
4. Kensler TW, Wakabayashi N, Biswal S (2007) Cell survival responses to environmental stresses via the Keap1-Nrf2-ARE pathway. *Annu Rev Pharmacol Toxicol* 47:89–116
5. Benz CC, Yau C (2008) Ageing, oxidative stress and cancer: paradigms in parallax. *Nat Rev Cancer* 8(11):875–879
6. Kobayashi M, Yamamoto M (2005) Molecular mechanisms activating the Nrf2-Keap1 pathway of antioxidant gene regulation. *Antioxid Redox Signal* 7(3–4):385–394
7. Stepkowski TM, Kruszewski MK (2011) Molecular cross-talk between the NRF2/KEAP1 signaling pathway, autophagy, and apoptosis. *Free Radic Biol Med* 50(9):1186–1195
8. Taguchi K, Motohashi H, Yamamoto M (2011) Molecular mechanisms of the Keap1-Nrf2 pathway in stress response and cancer evolution. *Genes Cells* 16(2):123–140
9. Egglar AL, Liu G, Pezzuto JM, van Breemen RB, Mesecar AD (2005) Modifying specific cysteines of the electrophile-sensing human Keap1 protein is insufficient to disrupt binding to the Nrf2 domain Neh2. *Proc Natl Acad Sci USA* 102(29):10070–10075
10. Holland R, Fishbein JC (2010) Chemistry of the cysteine sensors in Kelch-like ECH-associated protein 1. *Antioxid Redox Signal* 13(11):1749–1761
11. Hong F, Sekhar KR, Freeman ML, Liebler DC (2005) Specific patterns of electrophile adduction trigger Keap1 ubiquitination and Nrf2 activation. *J Biol Chem* 280(36):31768–31775
12. Saito R, Suzuki T, Hiramoto K, Asami S, Naganuma E, Suda H, Iso T, Yamamoto H, Morita M, Furusawa Y, Negishi T, Ichinose M, Yamamoto M (2015) Characterizations of three major cysteine sensors of Keap1 in stress response. *Mol Cell Biol*
13. Zhang DD, Hannink M (2003) Distinct cysteine residues in Keap1 are required for Keap1-dependent ubiquitination of Nrf2 and for stabilization of Nrf2 by chemopreventive agents and oxidative stress. *Mol Cell Biol* 23(22):8137–8151
14. Itoh K, Mimura J, Yamamoto M (2010) Discovery of the negative regulator of Nrf2, Keap1: a historical overview. *Antioxid Redox Signal* 13(11):1665–1678
15. Kansanen E, Kuosmanen SM, Leinonen H, Levonen AL (2013) The Keap1-Nrf2 pathway: mechanisms of activation and dysregulation in cancer. *Redox Biol* 1:45–49
16. Chartoupekis DV, Wakabayashi N, Kensler TW (2015) Keap1/Nrf2 pathway in the frontiers of cancer and non-cancer cell metabolism. *Biochem Soc Trans* 43(4):639–644
17. Yates MS, Tran QT, Dolan PM, Osburn WO, Shin S, McCulloch CC, Silkworth JB, Taguchi K, Yamamoto M, Williams CR, Liby KT, Sporn MB, Sutter TR, Kensler TW (2009) Genetic versus chemoprotective activation of Nrf2 signaling: overlapping yet distinct gene expression profiles between Keap1 knockout and triterpenoid-treated mice. *Carcinogenesis* 30(6):1024–1031
18. Kitteringham NR, Abdullah A, Walsh J, Randle L, Jenkins RE, Sison R, Goldring CE, Powell H, Sanderson C, Williams S, Higgins L, Yamamoto M, Hayes J, Park BK (2010) Proteomic analysis of Nrf2 deficient transgenic mice reveals cellular defence and lipid metabolism as primary Nrf2-dependent pathways in the liver. *J Proteomics* 73(8):1612–1631
19. Hirotsu Y, Katsuoka F, Funayama R, Nagashima T, Nishida Y, Nakayama K, Engel JD, Yamamoto M (2012) Nrf2-MafG heterodimers contribute globally to antioxidant and metabolic networks. *Nucleic Acids Res* 40(20):10228–10239

20. Chorley BN, Campbell MR, Wang X, Karaca M, Sambandan D, Bangura F, Xue P, Pi J, Kleeberger SR, Bell DA (2012) Identification of novel NRF2-regulated genes by ChIP-Seq: influence on retinoid X receptor alpha. *Nucleic Acids Res* 40(15):7416–7429
21. Sporn MB, Liby KT (2012) NRF2 and cancer: the good, the bad and the importance of context. *Nat Rev Cancer* 12(8):564–571
22. Jaramillo MC, Zhang DD (2013) The emerging role of the Nrf2-Keap1 signaling pathway in cancer. *Genes Dev* 27(20):2179–2191
23. Lee JH, Khor TO, Shu L, Su ZY, Fuentes F, Kong AN (2013) Dietary phytochemicals and cancer prevention: Nrf2 signaling, epigenetics, and cell death mechanisms in blocking cancer initiation and progression. *Pharmacol Ther* 137(2):153–171
24. Menegon S, Columbano A, Giordano S (2016) The dual roles of NRF2 in cancer. *Trends Mol Med* 22(7):578–593
25. Ngo HKC, Kim DH, Cha YN, Na HK, Surh YJ (2017) Nrf2 mutagenic activation drives hepatocarcinogenesis. *Cancer Res*
26. Singh A, Venkannagari S, Oh KH, Zhang YQ, Rohde JM, Liu L, Nimmagadda S, Sudini K, Brimacombe KR, Gajghate S, Ma J, Wang A, Xu X, Shahane SA, Xia M, Woo J, Mensah GA, Wang Z, Ferrer M, Gabrielson E, Li Z, Rastinejad F, Shen M, Boxer MB, Biswal S (2016) Small molecule inhibitor of NRF2 selectively intervenes therapeutic resistance in KEAP1-deficient NSCLC tumors. *ACS Chem Biol* 11(11):3214–3225
27. Zhu J, Wang H, Chen F, Fu J, Xu Y, Hou Y, Kou HH, Zhai C, Nelson MB, Zhang Q, Andersen ME, Pi J (2016) An overview of chemical inhibitors of the Nrf2-ARE signaling pathway and their potential applications in cancer therapy. *Free Radic Biol Med* 99:544–556
28. Choi EJ, Jung BJ, Lee SH, Yoo HS, Shin EA, Ko HJ, Chang S, Kim SY, Jeon SM (2017) A clinical drug library screen identifies clobetasol propionate as an NRF2 inhibitor with potential therapeutic efficacy in KEAP1 mutant lung cancer. *Oncogene*
29. Bhakkiyalakshmi E, Sireesh D, Rajaguru P, Paulmurugan R, Ramkumar KM (2015) The emerging role of redox-sensitive Nrf2-Keap1 pathway in diabetes. *Pharmacol Res* 91:104–114
30. Cho HY, Jedlicka AE, Reddy SP, Kensler TW, Yamamoto M, Zhang LY, Kleeberger SR (2002) Role of NRF2 in protection against hyperoxic lung injury in mice. *Am J Respir Cell Mol Biol* 26(2):175–182
31. Biswal S, Thimmulappa RK, Harvey CJ (2012) Experimental therapeutics of Nrf2 as a target for prevention of bacterial exacerbations in COPD. *Proc Am Thorac Soc* 9(2):47–51
32. Shelton LM, Lister A, Walsh J, Jenkins RE, Wong MH, Rowe C, Ricci E, Ressel L, Fang Y, Demougis P, Vukojevic V, O'Neill PM, Goldring CE, Kitteringham NR, Park BK, Odermatt A, Copple IM (2015) Integrated transcriptomic and proteomic analyses uncover regulatory roles of Nrf2 in the kidney. *Kidney Int* 88(6):1261–1273
33. Copple IM (2012) The Keap1-Nrf2 cell defense pathway—a promising therapeutic target? *Adv Pharmacol* 63:43–79
34. Itoh K, Wakabayashi N, Katoh Y, Ishii T, Igarashi K, Engel JD, Yamamoto M (1999) Keap1 represses nuclear activation of antioxidant responsive elements by Nrf2 through binding to the amino-terminal Neh2 domain. *Genes Dev* 13(1):76–86
35. Nioi P, Nguyen T, Sherratt PJ, Pickett CB (2005) The carboxy-terminal Neh3 domain of Nrf2 is required for transcriptional activation. *Mol Cell Biol* 25(24):10895–10906
36. Katoh Y, Itoh K, Yoshida E, Miyagishi M, Fukamizu A, Yamamoto M (2001) Two domains of Nrf2 cooperatively bind CBP, a CREB binding protein, and synergistically activate transcription. *Genes Cells* 6(10):857–868
37. Pintard L, Willis JH, Willems A, Johnson J-LF, Srayko M, Kurz T, Glaser S, Mains PE, Tyers M, Bowerman B (2003) The BTB protein MEL-26 is a substrate-specific adaptor of the CUL-3 ubiquitin-ligase. *Nature* 425(6955):311–316
38. Xu L, Wei Y, Reboul J, Vaglio P, Shin T-H, Vidal M, Elledge SJ, Harper JW (2003) BTB proteins are substrate-specific adaptors in an SCF-like modular ubiquitin ligase containing CUL-3. *Nature* 425(6955):316–321

39. Zipper LM, Mulcahy RT (2002) The Keap1 BTB/POZ dimerization function is required to sequester Nrf2 in cytoplasm. *J Biol Chem* 277(39):36544–36552
40. Tong KI, Katoh Y, Kusunoki H, Itoh K, Tanaka T, Yamamoto M (2006) Keap1 recruits Nrf2 through binding to ETGE and DLG motifs: characterization of the two-site molecular recognition model. *Mol Cell Biol* 26(8):2887–2900
41. Tong KI, Padmanabhan B, Kobayashi A, Shang C, Hirotsu Y, Yokoyama S, Yamamoto M (2007) Different electrostatic potentials define ETGE and DLG motifs as hinge and latch in oxidative stress response. *Mol Cell Biol* 27(21):7511–7521
42. McMahan M, Thomas N, Itoh K, Yamamoto M, Hayes JD (2006) Dimerization of substrate adaptors can facilitate cullin-mediated ubiquitylation of proteins by a “Tethering” mechanism. *J Biol Chem* 281(34):24756
43. Ogura T, Tong KI, Mio K, Maruyama Y, Kurokawa H, Sato C, Yamamoto M (2010) Keap1 is a forked-stem dimer structure with two large spheres enclosing the intervening, double glycine repeat, and C-terminal domains. *Proc Natl Acad Sci USA* 107(7):2842–2847
44. Baird L, Lleres D, Swift S, Dinkova-Kostova AT (2013) Regulatory flexibility in the Nrf2-mediated stress response is conferred by conformational cycling of the Keap1-Nrf2 protein complex. *Proc Natl Acad Sci USA* 110(38):15259–15264
45. Baird L, Swift S, Lleres D, Dinkova-Kostova AT (2014) Monitoring Keap1-Nrf2 interactions in single live cells. *Biotechnol Adv* 32(6):1133–1144
46. Fukutomi T, Takagi K, Mizushima T, Ohuchi N, Yamamoto M (2014) Kinetic, thermodynamic, and structural characterizations of the association between Nrf2-DLGex degron and Keap1. *Mol Cell Biol* 34(5):832–846
47. Keskin O, Gursoy A, Ma B, Nussinov R (2008) Principles of protein-protein interactions: what are the preferred ways for proteins to interact? *Chem Rev* 108(4):1225–1244
48. Jones S, Thornton JM (1996) Principles of protein-protein interactions. *Proc Natl Acad Sci USA* 93(1):13–20
49. Chen Y, Inoyama D, Kong ANT, Beamer LJ, Hu L (2011) Kinetic analyses of Keap1-Nrf2 interaction and determination of the minimal Nrf2 peptide sequence required for Keap1 binding using surface plasmon resonance. *Chem Biol Drug Des* 78(6):1014–1021
50. Nevala L, Giralt E (2015) Modulating protein-protein interactions: the potential of peptides. *Chem Commun (Camb)* 51(16):3302–3315
51. London N, Raveh B, Schueler-Furman O (2013) Druggable protein-protein interactions— from hot spots to hot segments. *Curr Opin Chem Biol* 17(6):952–959
52. Lu M-C, Chen Z-Y, Wang Y-L, Jiang Y-L, Yuan Z-W, You Q-D, Jiang Z-Y (2015) Binding thermodynamics and kinetics guided optimization of potent Keap1-Nrf2 peptide inhibitors. *RSC Adv* 5(105):85983–85987
53. Jiang Z-Y, Xu L-L, Lu M-C, Pan Y, Huang H-Z, Zhang X-J, Sun H-P, You Q-D (2014) Investigation of the intermolecular recognition mechanism between the E3 ubiquitin ligase Keap1 and substrate based on multiple substrates analysis. *J Comput-Aided Mol Des* 28(12):1233–1245
54. Jiang Z-Y, Lu M-C, Xu LL, Yang T-T, Xi M-Y, Xu X-L, Guo X-K, Zhang X-J, You Q-D, Sun H-P (2014) Discovery of potent Keap1-Nrf2 protein-protein interaction inhibitor based on molecular binding determinants analysis. *J Med Chem* 57(6):2736–2745
55. Inoyama D, Chen Y, Huang X, Beamer LJ, Kong AN, Hu L (2012) Optimization of fluorescently labeled Nrf2 peptide probes and the development of a fluorescence polarization assay for the discovery of inhibitors of Keap1-Nrf2 interaction. *J Biomol Screen* 17(4):435–447
56. Schaap M, Hancock R, Wilderspin A, Wells G (2013) Development of a steady-state FRET-based assay to identify inhibitors of the Keap1-Nrf2 protein-protein interaction. *Protein Sci* 22(12):1812–1819
57. Nasiri HR, Linge S, Ullmann D (2016) Thermodynamic profiling of inhibitors of Nrf2: Keap1 interactions. *Bioorg Med Chem Lett* 26(2):526–529

58. Zhuang C, Narayanapillai S, Zhang W, Sham YY, Xing C (2014) Rapid identification of Keap1-Nrf2 small-molecule inhibitors through structure-based virtual screening and hit-based substructure search. *J Med Chem* 57(3):1121–1126
59. Hur W, Sun Z, Jiang T, Mason DE, Peters EC, Zhang DD, Luesch H, Schultz PG, Gray NS (2010) A small-molecule inducer of the antioxidant response element. *Chem Biol* 17(5):537–547
60. Wu KC, McDonald PR, Liu JJ, Chaguturu R, Klaassen CD (2012) Implementation of a high-throughput screen for identifying small molecules to activate the Keap1-Nrf2-ARE pathway. *PLoS ONE* 7(10):e44686
61. Xie W, Pao C, Graham T, Dul E, Lu Q, Sweitzer TD, Ames RS, Li H (2012) Development of a cell-based high throughput luciferase enzyme fragment complementation assay to identify nuclear-factor- κ B-related transcription factor 2 activators. *Assay Drug Dev Technol* 10(6):514–524
62. Ramkumar KM, Sekar TV, Foygel K, Elango B, Paulmurugan R (2013) Reporter protein complementation imaging assay to screen and study Nrf2 activators in cells and living animals. *Anal Chem* 85(15):7542–7549
63. Bertrand HC, Schaap M, Baird L, Georgakopoulos ND, Fowkes A, Thiollier C, Kachi H, Dinkova-Kostova AT, Wells G (2015) Design, synthesis, and evaluation of triazole derivatives that induce Nrf2 dependent gene products and inhibit the Keap1-Nrf2 protein-protein interaction. *J Med Chem* 58(18):7186–7194
64. Kumar V, Kumar S, Hassan M, Wu H, Thimmulappa RK, Kumar A, Sharma SK, Parmar VS, Biswal S, Malhotra SV (2011) Novel chalcone derivatives as potent Nrf2 activators in mice and human lung epithelial cells. *J Med Chem* 54(12):4147–4159
65. Xi MY, Jia JM, Sun HP, Sun ZY, Jiang JW, Wang YJ, Zhang MY, Zhu JF, Xu LL, Jiang ZY, Xue X, Ye M, Yang X, Gao Y, Tao L, Guo XK, Xu XL, Guo QL, Zhang XJ, Hu R, You QD (2013) 3-Aroylmethylene-2,3,6,7-tetrahydro-1H-pyrazino[2,1-a]isoquinolin-4(11bH)-ones as potent Nrf2/ARE inducers in human cancer cells and AOM-DSS treated mice. *J Med Chem* 56(20):7925–7938
66. Freire E (2008) Do enthalpy and entropy distinguish first in class from best in class? *Drug Discov Today* 13(19–20):869–874
67. Klebe G (2015) Applying thermodynamic profiling in lead finding and optimization. *Nat Rev Drug Discov* 14(2):95–110
68. Pan AC, Borhani DW, Dror RO, Shaw DE (2013) Molecular determinants of drug-receptor binding kinetics. *Drug Discov Today*
69. Niesen FH, Berglund H, Vedadi M (2007) The use of differential scanning fluorimetry to detect ligand interactions that promote protein stability. *Nat Protoc* 2(9):2212–2221
70. Milroy LG, Grossmann TN, Hennig S, Brunsveld L, Ottmann C (2014) Modulators of protein-protein interactions. *Chem Rev* 114(9):4695–4748
71. Hu L, Magesh S, Chen L, Wang L, Lewis TA, Chen Y, Khodier C, Inoyama D, Beamer LJ, Emge TJ, Shen J, Kerrigan JE, Kong AN, Dandapani S, Palmer M, Schreiber SL, Munoz B (2013) Discovery of a small-molecule inhibitor and cellular probe of Keap1-Nrf2 protein-protein interaction. *Bioorg Med Chem Lett* 23(10):3039–3043
72. Sun H-P, Jiang Z-Y, Zhang M-Y, Lu M-C, Yang T-T, Pan Y, Huang H-Z, Zhang X-J, Q-d You (2014) Novel protein-protein interaction inhibitor of Nrf2-Keap1 discovered by structure-based virtual screening. *MedChemComm* 5(1):93–98
73. Jiang ZY, Xu LL, Lu MC, Chen ZY, Yuan ZW, Xu XL, Guo XK, Zhang XJ, Sun HP, You QD (2015) Structure-activity and structure-property relationship and exploratory in vivo evaluation of the nanomolar Keap1-Nrf2 protein-protein interaction inhibitor. *J Med Chem* 58(16):6410–6421
74. Kask P, Palo K, Fay N, Brand L, Mets U, Ullmann D, Jungmann J, Pschorr J, Gall K (2000) Two-dimensional fluorescence intensity distribution analysis: theory and applications. *Biophys J* 78(4):1703–1713

75. Marcotte D, Zeng W, Hus J-C, McKenzie A, Hession C, Jin P, Bergeron C, Lugovskoy A, Enyedy I, Cuervo H, Wang D, Atmanene C, Roecklin D, Vecchi M, Vivat V, Kraemer J, Winkler D, Hong V, Chao J, Lukashov M, Silvan L (2013) Small molecules inhibit the interaction of Nrf2 and the Keap1 Kelch domain through a non-covalent mechanism. *Bioorg Med Chem* 21(14):4011–4019
76. Neumann L, von Konig K, Ullmann D (2011) HTS reporter displacement assay for fragment screening and fragment evolution toward leads with optimized binding kinetics, binding selectivity, and thermodynamic signature. *Methods Enzymol* 493:299–320
77. Tarcsay A, Keseru GM (2015) Is there a link between selectivity and binding thermodynamics profiles? *Drug Discov Today* 20(1):86–94
78. Li W, Zheng S, Higgins M, Morra RP Jr, Mendis AT, Chien CW, Ojima I, Mierke DF, Dinkova-Kostova AT, Honda T (2015) New monocyclic, bicyclic, and tricyclic ethynylcyanodienones as activators of the Keap1/Nrf2/ARE pathway and inhibitors of inducible nitric oxide synthase. *J Med Chem* 58(11):4738–4748
79. Munday R, Zhang Y, Paonessa JD, Munday CM, Wilkins AL, Babu J (2010) Synthesis, biological evaluation, and structure-activity relationships of dithiolethiones as inducers of cytoprotective phase 2 enzymes. *J Med Chem* 53(12):4761–4767
80. Zheng S, Laxmi YR S, David E, Dinkova-Kostova AT, Shrivastava KH, Ren Y, Zheng Y, Trevino I, Bumeister R, Ojima I (2012) Synthesis, chemical reactivity as Michael acceptors, and biological potency of monocyclic cyanoenones, novel and highly potent anti-inflammatory and cytoprotective agents. *J Med Chem*
81. Nikam A, Ollivier A, Rivard M, Wilson JL, Mebarki K, Martens T, Dubois-Randé JL, Motterlini R, Foresti R (2016) Diverse Nrf2 activators coordinated to cobalt carbonyls induce heme oxygenase-1 and release carbon monoxide in vitro and in vivo. *J Med Chem*
82. Chang KM, Chen HH, Wang TC, Chen IL, Chen YT, Yang SC, Chen YL, Chang HH, Huang CH, Chang JY, Shih C, Kuo CC, Tzeng CC (2015) Novel oxime-bearing coumarin derivatives act as potent Nrf2/ARE activators in vitro and in mouse model. *Eur J Med Chem* 106:60–74
83. M-y Xi, Z-y Sun, H-p Sun, J-m Jia, Z-y Jiang, Tao L, Ye M, Yang X, Y-j Wang, Xue X, J-j Huang, Gao Y, X-k Guo, S-l Zhang, Y-r Yang, Guo Q-l HuR, Q-d You (2013) Synthesis and bioevaluation of a series of α -pyrone derivatives as potent activators of Nrf2/ARE pathway (part I). *Eur J Med Chem* 66:364–371
84. Zhuang C, Miao Z, Sheng C, Zhang W (2014) Updated research and applications of small molecule inhibitors of Keap1-Nrf2 protein-protein interaction: a review. *Curr Med Chem* 21(16):1861–1870
85. Hancock R, Bertrand HC, Tsujita T, Naz S, El-Bakry A, Laoruchpong J, Hayes JD, Wells G (2012) Peptide inhibitors of the Keap1-Nrf2 protein-protein interaction. *Free Radic Biol Med* 52(2):444–451
86. Hancock R, Schaap M, Pfister H, Wells G (2013) Peptide inhibitors of the Keap1-Nrf2 protein-protein interaction with improved binding and cellular activity. *Org Biomol Chem* 11(21):3553–3557
87. Steel R, Cowan J, Payerne E, O'Connell MA, Searcey M (2012) Anti-inflammatory effect of a cell-penetrating peptide targeting the Nrf2/Keap1 interaction. *ACS Med Chem Lett* 3(5):407–410
88. Tu J, Zhang X, Zhu Y, Dai Y, Li N, Yang F, Zhang Q, Brann DW, Wang R (2015) Cell-permeable peptide targeting the Nrf2-Keap1 interaction: a potential novel therapy for global cerebral ischemia. *J Neurosci* 35(44):14727–14739
89. Lu M-C, Yuan Z-W, Jiang Y-L, Chen Z-Y, You Q-D, Jiang Z-Y (2016) A systematic molecular dynamics approach to the study of peptide Keap1-Nrf2 protein-protein interaction inhibitors and its application to p62 peptides. *Mol Biosyst* 12(4):1378–1387
90. Nair CM, Vijayan M, Venkatachalapathi YV, Balam P (1979) X-Ray crystal structure of pivaloyl-D-Pro-L-Pro-L-Ala-N-methylamide; observation of a consecutive [small beta]-turn conformation. *J Chem Soc Chem Commun* 24:1183–1184

91. Bean JW, Kopple KD, Peishoff CE (1992) Conformational analysis of cyclic hexapeptides containing the D-Pro-L-Pro sequence to fix beta-turn positions. *J Am Chem Soc* 114(13):5328–5334
92. Robinson JA (2008) Beta-hairpin peptidomimetics: design, structures and biological activities. *Acc Chem Res* 41(10):1278–1288
93. Horer S, Reinert D, Ostmann K, Hoevels Y, Nar H (2013) Crystal-contact engineering to obtain a crystal form of the Kelch domain of human Keap1 suitable for ligand-soaking experiments. *Acta Crystallogr Sect F: Struct Biol Cryst Commun* 69(Pt 6):592–596
94. Zhao J, Redell JB, Moore AN, Dash PK (2011) A novel strategy to activate cytoprotective genes in the injured brain. *Biochem Biophys Res Commun* 407(3):501–506
95. Sidhu SS, Fairbrother WJ, Deshayes K (2003) Exploring protein-protein interactions with phage display. *ChemBioChem* 4(1):14–25
96. Guntas G, Lewis SM, Mulvaney KM, Cloer EW, Tripathy A, Lane TR, Major MB, Kuhlman B (2016) Engineering a genetically encoded competitive inhibitor of the KEAP1-NRF2 interaction via structure-based design and phage display. *Protein Eng Des Sel* 29(1):1–9
97. Richardson BG, Jain AD, Speltz TE, Moore TW (2015) Non-electrophilic modulators of the canonical Keap1/Nrf2 pathway. *Bioorg Med Chem Lett* 25(11):2261–2268
98. Wells G (2015) Peptide and small molecule inhibitors of the Keap1-Nrf2 protein-protein interaction. *Biochem Soc Trans* 43(4):674–679
99. Li X, Zhang D, Hannink M, Beamer LJ (2004) Crystal structure of the Kelch domain of human Keap1. *J Biol Chem* 279(52):54750–54758
100. Beamer LJ, Li X, Bottoms CA, Hannink M (2005) Conserved solvent and side-chain interactions in the 1.35 Angstrom structure of the Kelch domain of Keap1. *Acta Crystallogr D Biol Crystallogr* 61 (Pt 10):1335–1342
101. Padmanabhan B, Tong KI, Ohta T, Nakamura Y, Scharlock M, Ohtsuji M, Kang M-I, Kobayashi A, Yokoyama S, Yamamoto M (2006) Structural basis for defects of Keap1 activity provoked by its point mutations in lung cancer. *Mol Cell* 21(5):689–700
102. Cleasby A, Yon J, Day PJ, Richardson C, Tickle IJ, Williams PA, Callahan JF, Carr R, Concha N, Kerns JK, Qi H, Sweitzer T, Ward P, Davies TG (2014) Structure of the BTB domain of Keap1 and its interaction with the triterpenoid antagonist CDDO. *PLoS ONE* 9(6):e98896
103. Lo S-C, Li X, Henzl MT, Beamer LJ, Hannink M (2006) Structure of the Keap1:Nrf2 interface provides mechanistic insight into Nrf2 signaling. *EMBO J* 25(15):3605–3617
104. Komatsu M, Kurokawa H, Waguri S, Taguchi K, Kobayashi A, Ichimura Y, Sou YS, Ueno I, Sakamoto A, Tong KI, Kim M, Nishito Y, Iemura S, Natsume T, Ueno T, Kominami E, Motohashi H, Tanaka K, Yamamoto M (2010) The selective autophagy substrate p62 activates the stress responsive transcription factor Nrf2 through inactivation of Keap1. *Nat Cell Biol* 12(3):213–223
105. Ichimura Y, Waguri S, Sou YS, Kageyama S, Hasegawa J, Ishimura R, Saito T, Yang Y, Kouno T, Fukutomi T, Hoshii T, Hirao A, Takagi K, Mizushima T, Motohashi H, Lee MS, Yoshimori T, Tanaka K, Yamamoto M, Komatsu M (2013) Phosphorylation of p62 activates the Keap1-Nrf2 pathway during selective autophagy. *Mol Cell* 51(5):618–631
106. Satoh M, Saburi H, Tanaka T, Matsuura Y, Naitow H, Shimozone R, Yamamoto N, Inoue H, Nakamura N, Yoshizawa Y, Aoki T, Tanimura R, Kunishima N (2015) Multiple binding modes of a small molecule to human Keap1 revealed by X-ray crystallography and molecular dynamics simulation. *FEBS Open Bio* 5:557–570
107. Winkel AF, Engel CK, Margerie D, Kannt A, Szillat H, Glombik H, Kallus C, Ruf S, Gussregen S, Riedel J, Herling AW, von Knethen A, Weigert A, Brune B, Schmoll D (2015) Characterization of RA839, a noncovalent small molecule binder to Keap1 and selective activator of Nrf2 signaling. *J Biol Chem* 290(47):28446–28455
108. Jain AD, Potteti H, Richardson BG, Kingsley L, Luciano JP, Ryuzoji AF, Lee H, Kronic A, Mesecar AD, Reddy SP, Moore TW (2015) Probing the structural requirements of non-electrophilic naphthalene-based Nrf2 activators. *Eur J Med Chem* 103:252–268

109. Jnoff E, Albrecht C, Barker JJ, Barker O, Beaumont E, Bromidge S, Brookfield F, Brooks M, Bubert C, Ceska T, Corden V, Dawson G, Duclos S, Fryatt T, Genicot C, Jigorel E, Kwong J, Maghames R, Mushi I, Pike R, Sands ZA, Smith MA, Stimson CC, Courade JP (2014) Binding mode and structure-activity relationships around direct inhibitors of the Nrf2-Keap1 complex. *ChemMedChem* 9(4):699–705
110. Davies TG, Wixted WE, Coyle JE, Griffiths-Jones C, Hearn K, McMenamin R, Norton D, Rich SJ, Richardson C, Saxty G, Willems HMG, Woolford AJA, Cottom JE, Kou J-P, Yonchuk JG, Feldser HG, Sanchez Y, Foley JP, Bolognese BJ, Logan G, Podolin PL, Yan H, Callahan JF, Heightman TD, Kerns JK (2016) Monoacidic inhibitors of the Kelch-like ECH-associated protein 1: nuclear factor erythroid 2-related factor 2 (KEAP1: NRF2) protein-protein interaction with high cell potency identified by fragment-based discovery. *J Med Chem* 59(8):3991–4006
111. Maggiora G, Vogt M, Stumpfe D, Bajorath J (2014) Molecular similarity in medicinal chemistry. *J Med Chem* 57(8):3186–3204
112. Xu L-L, Zhu J-F, Xu X-L, Zhu J, Li L, Xi M-Y, Jiang Z-Y, Zhang M-Y, Liu F, M-c Lu, Bao Q-C, Li Q, Zhang C, Wei J-L, Zhang X-J, Zhang L-S, You Q-D, Sun H-P (2015) Discovery and modification of in vivo active Nrf2 activators with 1,2,4-Oxadiazole core: hits identification and structure-activity relationship study. *J Med Chem* 58(14):5419–5436
113. Shimozono R, Asaoka Y, Yoshizawa Y, Aoki T, Noda H, Yamada M, Kaino M, Mochizuki H (2013) Nrf2 activators attenuate the progression of nonalcoholic steatohepatitis-related fibrosis in a dietary rat model. *Mol Pharmacol* 84(1):62–70
114. Jiang Z-Y, Chu H-X, Xi M-Y, Yang T-T, Jia J-M, Huang J-J, Guo X-K, Zhang X-J, You Q-D, Sun H-P (2013) Insight into the intermolecular recognition mechanism between Keap1 and IKK β combining homology modelling, protein-protein docking, molecular dynamics simulations and virtual alanine mutation. *PLoS ONE* 8(9):e75076
115. Lee DF, Kuo HP, Liu M, Chou CK, Xia W, Du Y, Shen J, Chen CT, Huo L, Hsu MC, Li CW, Ding Q, Liao TL, Lai CC, Lin AC, Chang YH, Tsai SF, Li LY, Hung MC (2009) KEAP1 E3 ligase-mediated downregulation of NF-kappaB signaling by targeting IKKbeta. *Mol Cell* 36(1):131–140
116. Lo SC, Hannink M (2006) PGAM5, a Bcl-XL-interacting protein, is a novel substrate for the redox-regulated Keap1-dependent ubiquitin ligase complex. *J Biol Chem* 281(49):37893–37903
117. Niture SK, Jaiswal AK (2011) INrf2 (Keap1) targets Bcl-2 degradation and controls cellular apoptosis. *Cell Death Differ* 18(3):439–451
118. Niture SK, Jaiswal AK (2010) Hsp90 interaction with INrf2(Keap1) mediates stress-induced Nrf2 activation. *J Biol Chem* 285(47):36865–36875
119. Clements CM, McNally RS, Conti BJ, Mak TW, Ting JP (2006) DJ-1, a cancer- and Parkinson's disease-associated protein, stabilizes the antioxidant transcriptional master regulator Nrf2. *Proc Natl Acad Sci USA* 103(41):15091–15096
120. Bitar MS, Liu C, Ziaei A, Chen Y, Schmedt T, Jurkunas UV (2012) Decline in DJ-1 and decreased nuclear translocation of Nrf2 in Fuchs endothelial corneal dystrophy. *Invest Ophthalmol Vis Sci* 53(9):5806–5813
121. Yu M, Li H, Liu Q, Liu F, Tang L, Li C, Yuan Y, Zhan Y, Xu W, Li W, Chen H, Ge C, Wang J, Yang X (2011) Nuclear factor p65 interacts with Keap1 to repress the Nrf2-ARE pathway. *Cell Signal* 23(5):883–892
122. Yasuda D, Nakajima M, Yuasa A, Obata R, Takahashi K, Ohe T, Ichimura Y, Komatsu M, Yamamoto M, Imamura R, Kojima H, Okabe T, Nagano T, Mashino T (2016) Synthesis of Keap1-phosphorylated p62 and Keap1-Nrf2 protein-protein interaction inhibitors and their inhibitory activity. *Bioorg Med Chem Lett* 26(24):5956–5959

Chapter 11

BRDT Inhibitors for Male Contraceptive Drug Discovery: Current Status



Zhenyuan Miao, Xianghong Guan, Jiewei Jiang and Gunda I. Georg

11.1 Introduction: BET Bromodomains Are Epigenetic Reader Proteins that Represent Therapeutic Targets for Diverse Diseases and Male Contraception

Epigenetics refers to the investigation of inherited traits that are unrelated to changes in DNA sequences and that affect gene expression [1]. Epigenetic processes include chemical modifications of histones and nucleic acids, and chromatin remodeling. Dysregulations of these processes are implicated in the development and progression of a variety of disorders including cancer, inflammation, viral infections, and cardiovascular and neurological diseases [2]. Therefore, targeting epigenetic proteins has become an active area of research for the development of novel therapeutic agents. Among the histone post-translational modifications (PTMs), modification of the lysine acetylation status is one of the key mechanisms modulating gene expression and histone compaction. Acetylation initiates gene transcription and allows for the interaction with other proteins such as transcription factors, whereas deacetylation leads to chromatin compaction and repression of gene expression (Fig. 11.1). Acetylation of the lysine ϵ -amino groups of histones neutralizes their positive charge and also introduces steric constraints that both can influence interactions with nucleic acids and proteins, PTM regulatory enzymes, and the control of protein subcellular location [1]. The acetylation of lysine is carried out by acetyltransferases (KATs, writer proteins) using acetyl-CoA.

Z. Miao

Second Military Medical University, Shanghai, China

X. Guan · J. Jiang · G. I. Georg (✉)

Department of Medicinal Chemistry and Institute for Therapeutics
Discovery and Development, University of Minnesota, Minneapolis,
MN 55414, USA

e-mail: georg@umn.edu

© Springer Nature Singapore Pte Ltd. 2018

C. Sheng and G. I. Georg (eds.), *Targeting Protein-Protein Interactions
by Small Molecules*, https://doi.org/10.1007/978-981-13-0773-7_11

287

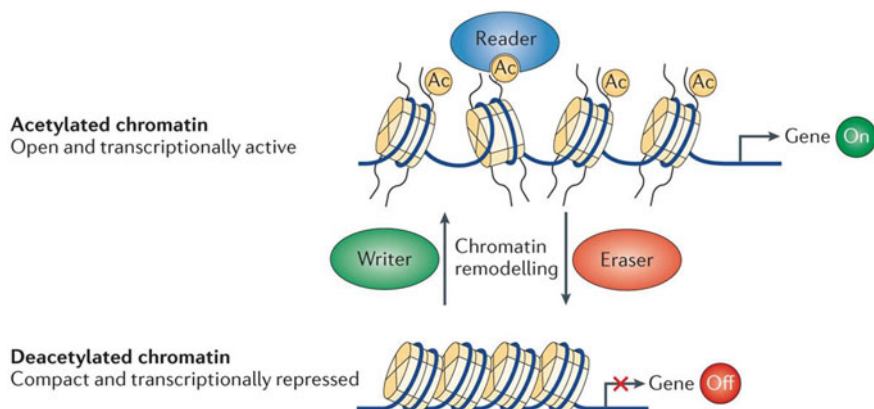


Fig. 11.1 Effects of lysine acetylation on chromatin. Reprinted with permission from Ref. [5] by permission of Springer Nature © 2014

Deacetylation is performed by lysine deacetylases (HDAC, eraser proteins). Bromodomains (BRD, reader proteins) recognize acetylated lysine residues [1]. Examples of successfully launched epigenetic drugs are the histone deacetylase inhibitors vorinostat, romidepsin, belinostat, and panobinostat that were approved by the FDA for various cancer indications. Many other epigenetic therapeutics are currently undergoing clinical trials [3, 4].

Among the epigenetic reader proteins, the bromodomains have been most comprehensively characterized. Since the aberrant expression of the BET subfamily of bromodomain proteins has been linked to cancer, they have become targets for anticancer drug discovery [3, 6–8]. To date, 61 bromodomains in 46 proteins have been identified in the human genome and are classified into eight families based on sequence alignments (Fig. 11.2). The bromodomain and extra-terminal domain (BET) family (family II) consists of four proteins, BRD2, BRD3, BRD4, and BRDT, all of which have two tandem bromodomains, referred to as BD1 and BD2. The testis-specific bromodomain (BRDT) protein has an important role in normal physiology of spermatogenesis and has been validated as a target for male contraception by gene knockout studies in mice, demonstrating that the first bromodomain of Brdt is essential for spermatogenesis [9, 10]. In addition, a GWAS study in men of European descent showed that a single nucleotide polymorphism of BRDT is associated with severe oligozoospermia (low concentration of sperm in semen) [11]. Taken together, these results and the fact that BRDT is exclusively expressed in the human testis provide persuasive evidence that a selective BRDT inhibitor could be an efficient male contraceptive agent free of unwanted side effects.

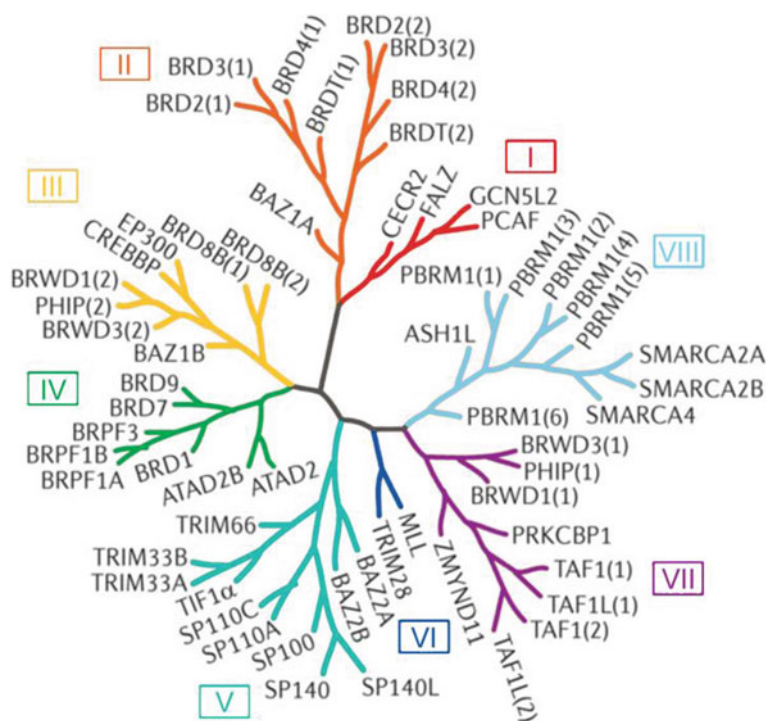


Fig. 11.2 Phylogenetic tree of the human bromodomain family consists of 61 modules in eight families (I–VIII). Adapted with permission from Ref. [1] by permission of Springer Nature © 2014

11.2 Bromodomain Inhibitors in Clinical Trials

The availability of approximately 80 X-ray crystal structures of bromodomains in complex with small molecules and the development of a variety of assay methods, such as the BROMOScanTM assay by DiscoverX for selectivity screening, have accelerated discovery of chemical probes and drug development [12–15]. Inhibitors based on a variety of scaffolds have been discovered, and several comprehensive reviews have summarized those findings [13, 16–20]. The charge-neutralized acetylated lysine residues often have relatively weak interactions with the mostly hydrophobic binding pocket, and therefore, inhibitors targeting this protein-protein interaction have become attractive for small-molecule drug discovery [6]. Examples of inhibitor scaffolds (Fig. 11.3) include triazolothienodiazepin present in JQ1 and OTX-015, a triazolodiazepin in I-BET762, benzoazepin in CPI-0610, isoxazolquinoline present in I-BET151 and pyrrolopyridone in ABBV-75. I-BET762 (Fig. 11.3), a potent inhibitor of BRD2, BRD3, BRD4, and BRDT that does not interact with other bromodomains, was the first bromodomain inhibitor to enter clinical trials for the treatment of midline carcinoma [21]. Several other compounds

are being investigated in phase I/II trials for cancer indications. They were developed by GSK, Tensha and Dana Faber Cancer Institute, Bayer, Gilead, Incyte, AbbVie, and BMS [1, 17]. OTX-015 is a representative compound in the oncology field. The first clinical trial started in December 2012. Following early clinical success, phase Ib and phase IIa trials were launched in 2014. In addition to OTX-015, other BET inhibitors are in clinical trials, including ABBV-075 (mivebresib) (Fig. 11.3) [22], and RO6870810/TEN-010, BAY 1238097, GS-5829, INCB054329, and BMS-9861158, but their structures remain undisclosed [23].

Some of these compounds have shown BET-selective activities. OTX-015 is a potent inhibitor of BRD2, BRD3, and BRD4 ($IC_{50} = 10\text{--}19\text{ nM}$) [24] that was found to be selective for cancer cells and decreased expression of BRD2, BRD4, and c-Myc at sub-micromolar concentrations but did not change BRD3 expression when tested in over 50 leukemia cell lines and patient-derived leukemia cell lines [25]. Another selective inhibitor is RVX-208 from OncoEthix that binds preferentially to BD2 of the BET bromodomains [26], increases apolipoprotein A1 production and HDL-C levels, and has advanced to a phase III clinical trial [27]. A statistically significant reduction of major adverse cardiovascular events was observed in patients treated with RVX-208 compared with placebo [28].

11.3 BRDT Structure

Structural analysis of the bromodomain architecture from multiple X-ray structures revealed that they possess a shared fold, consisting of four left-handed α -helix bundles (αA , αB , αC , and αZ) that are linked by highly variable ZA and BC loop regions that enclose the centrally located conserved acetylated lysine (KAc) binding site (Fig. 11.4a). The KAc site is located at one end of the four helices and away

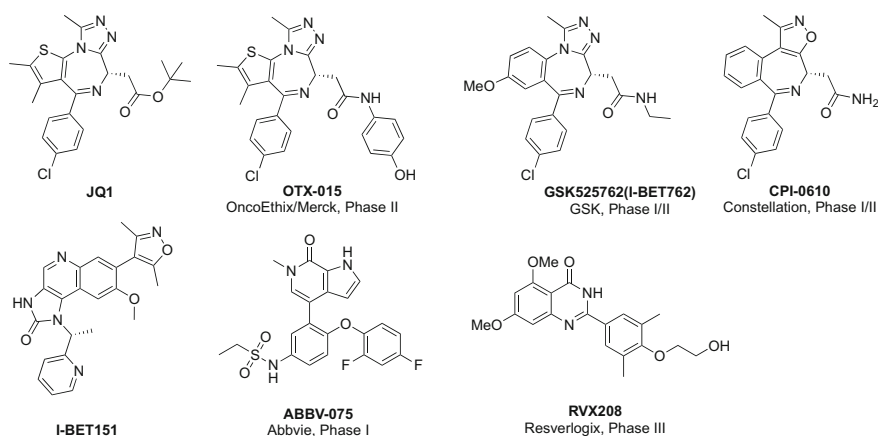


Fig. 11.3 Structures of BET inhibitor JQ1 and select bromodomain inhibitors in clinical trials

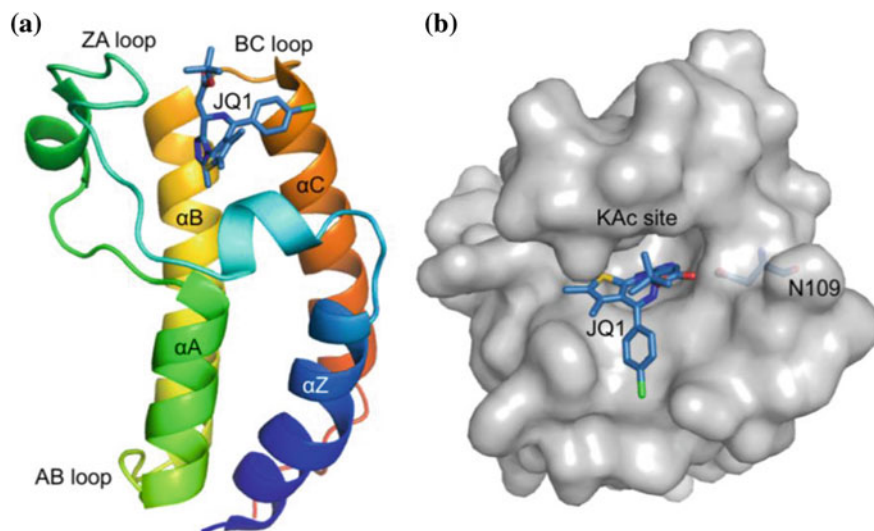


Fig. 11.4 **a** Overall structure of BRDT-1 with the secondary structure elements labeled. **b** Co-crystal structure of a small-molecule inhibitor JQ1 in complex with BRDT-1 (PDB: 4FLP)

from both the C- and N-termini. Acetylated lysines of histones bind to conserved asparagine residues, Asn140 in BRD4 and Asn109 in BRDT (Fig. 11.4b) of the bromodomains by forming a hydrogen bond between the carbonyl group of the acetyl-lysine and the side chain amide hydrogen of the asparagine. A network of conserved water molecules (Fig. 11.5), reaching deep into the binding site, contributes to the stability of the proteins and extends into a channel framed by the ZA loop that is termed the ZA channel. Specific interactions of small-molecule inhibitors with the ZA channel, the tryptophan-proline-phenylalanine (WPF) shelf (Fig. 11.5, green), and the gatekeeper residue confer potency and selectivity [29].

11.4 Selectivity of Bromodomain Inhibitors

The development of a specific inhibitor targeting a single BET protein such as BRDT, which is critical for male contraceptive drug development, however, also poses a significant challenge because of the highly conserved lipophilic binding pocket (Fig. 11.6) [27]. Most of the currently known BET inhibitors show little selectivity between the individual BET proteins. The sequence alignment of human BET proteins (Fig. 11.6) shows the very high homology between the four BET proteins within the histone binding site. The WPF shelf is highlighted in green. Highlighted in red are the asparagine (Asn140 in BRD4 and Asn109 in BRDT) and the conserved tyrosine (Y), residues that are critical for recognition of the acetylated lysine. One difference between BRDT-1 and the other BET bromodomains that

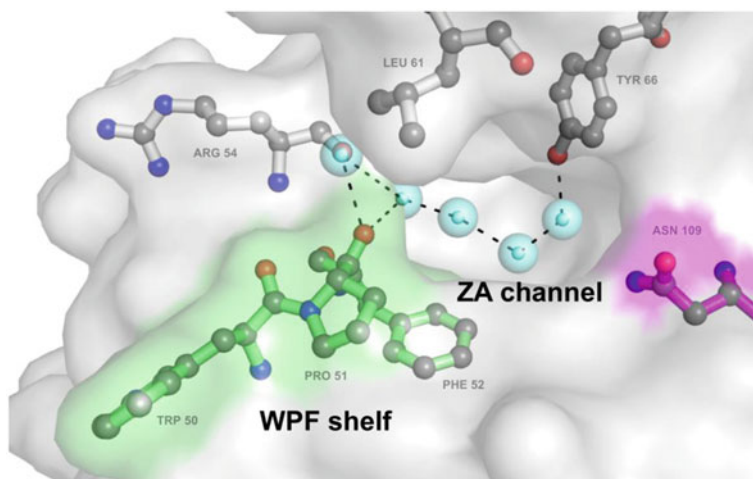


Fig. 11.5 BRDT-1 KAc binding site (4KCX) with conserved water network (cyan), WPF shelf (green), conserved asparagine (magenta), and other residues surrounding the KAc site (gray)

could be explored to engender selectivity is the unique positively charged arginine residue (Arg54) at the end of the ZA channel, that is not present in other BET proteins (Figs. 11.5 and 11.6). They instead have neutral residues at that position: BRD2-1, BRD3-1, and BRD4-1 have a glutamine (Gln101, Gln61, and Gln85, respectively), BRD2-2, BRD3-2, and BRD4-2 have a lysine, and BRDT-2 has an asparagine. Arginine residues in proteins can form nonpolar aromatic and aliphatic interactions with residues above and below the plane of the guanidine and can form hydrogen bonds in an in-plane arrangement. Salt bridge formation between a positively charged guanidinium moiety and a negatively charged group such as a phosphate approaches the strength of a covalent bond [30, 31]. If it was possible to develop an inhibitor that tightly binds Arg54, a selective inhibitor for BRDT-1 could potentially be developed.

Figure 11.7 depicting the domain structure of the BET bromodomains shows that the bromodomains have different length and that the distances between the tandem bromodomains are also different. The BRDT tandem bromodomain distance is the shortest, spanning 169 amino acids, followed by BRD2 with 199 amino acids, BRD3 with 200 amino acids, and BRD4 with the longest distance of 219 amino acids. The differences in the distance between the tandem bromodomains could hold promise for the design of selective bivalent inhibitors, including those for BRDT.

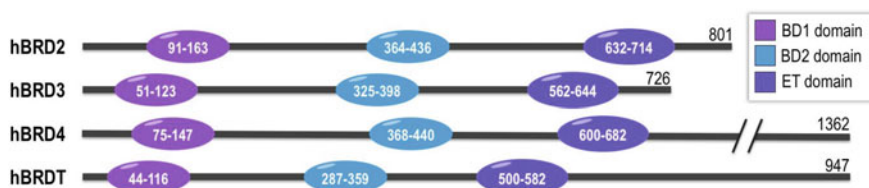
Another approach to develop a selective BRDT inhibitor could be based on recently reported differences for the interactions of BRDT compared to the other BET proteins with histones H3 and H4 and chromatin (Fig. 11.8). Miller et al. reported that BD1 of BRDT initially interacts with DNA, which then guides and orients the KAc binding pocket of BD1 toward acetyl-lysines H4K8_{ac} and H4K5_{ac}

			~~~ ~~~~ $\alpha$ Z ~~~~			ZA loop		~~~ $\alpha$ A
BRD2_BD1	61	PPPEVSNPK	KPGRVNLQ	YLHKVVMKAL	WK---HQFAW	PPRQPVDAVK	LGLPDYHKII	KQPMMDMTIK
BRD3_BD1	21	PPPEVSNPK	KPGRKTNLQ	YMQNVVVKTL	WK---HQFAW	PPYQPVDAIK	LNLDPYHKII	KNPMDMTIK
BRD4_BD1	45	PPPEVSNPN	KPKRQTNLQ	YLLRVVLKTL	WK---HQFAW	PPQQPVDAVK	LNLDPYHKII	KTPMDMTIK
BRDT_BD1	14	PPPEYINTK	KNGRLTNLQ	YLQKVVLKDL	WK---HSFSW	PPQRVDAVK	LKLPDYHTII	KNPMDLNTIK
BRD2_BD2	339	-----QS	SKKGLSEQL	KHCNGILKEL	LSKKHAAYAW	PPYKPVDAVA	LGLHDYHDII	KHPMDLSTVK
BRD3_BD2	301	-----HA	GKKGKLSLHL	RYCDSILREM	LSKKHAAYAW	PPYKPVDAEA	LELHDYHDII	KHPMDLSTVK
BRD4_BD2	343	-----AP	EKSSKVSEQL	KCCSGILKEM	FAKKHAAYAW	PPYKPVDAEA	LGLHDYHDII	KHPMDMSTIK
BRDT_BD2	262	-----NV	VKTVKVTEQL	RHCSEILKEM	LAKKHFSYAW	PPYNPVVDVA	LGLHDYHDYV	KNPMDLSTIK
CREBBP	1084	-----	--IFKPEELR	QALMPTLEAL	YR---QDPESL	PPRQPVPDQL	LGLIPDYFDIV	KNPMDLSTIK
GCN5/KAT2A	729	-----	---DPDQLY	TTLKNLLAQI	KS---HPSAW	PFMEPVKKS-	---EAPDYVEVI	RFPIDLKTMT
ATAD2	981	-----	QEDDTFRELR	IFLRNVTHRL	AI---DKRFR	VFTKVPVDPD-	---EVPDYVTVI	KQFMDLSSVI

		$\alpha$ A ~~~	~~~~~ $\alpha$ B ~~~~~	BC loop	~~~ ~~~~ $\alpha$ C ~~~ ~~~~		
BRD2_BD1	128	RRLENNYYWA	ASECMDQFNT	MFTNCYIYNK	P---TDDIV	LMAQLEKIF	LQKVASMPQE
BRD3_BD1	88	KRLENNYYWS	ASECMDQFNT	MFTNCYIYNK	P---TDDIV	LMAQALEKIF	LQKVASMPQE
BRD4_BD1	112	KRLENNYYWN	AQECIQDFNT	MFTNCYIYNK	P---GDDIV	LMAEALKEKF	LQKINELPTE
BRDT_BD1	81	KRLENNYYAK	ASECIEDFNT	MFSNCYLYNK	P---GDDIV	LMAQALEKLF	MQKLSQMPQE
BRD2_BD2	401	RKMNDRDYRD	AQEFADVRL	MFSNCYKYNP	P---DHEVV	AMARKLDQVF	EMFRYAKMPDE
BRD3_BD2	363	RKMGREYPD	AQGFADVRL	MFSNCYKYNP	P---DHEVV	AMARKLDQVF	EMFRYAKMPDE
BRD4_BD2	405	SKLEAREYRD	AQEFADVRL	MFSNCYKYNP	P---DHEVV	AMARKLDQVF	EMFRYAKMPDE
BRDT_BD2	324	EKMDNQEYKD	AYKFAADVRL	MFNNCYKYNP	P---DHEVV	TMARMLQDVF	ETHFSKIPIE
CREBBP	1140	RKLDTGQYQE	PWQYVDDVWL	MFNNAWLYNR	K---TSRYV	KFCSKLAEVF	EQEIDPVMQS
GCN5/KAT2A	780	ERLRSRYVVT	RKLFVADLQR	VIANCREYNP	P---DSEYK	RCASALEKEFF	YFKLKEGGII
ATAD2	1036	SKIDLHXYLT	VKDYLRDIDL	ICSNALRYNP	DRDPGDRILR	HRACALRDTA	YAIIEKEELDE

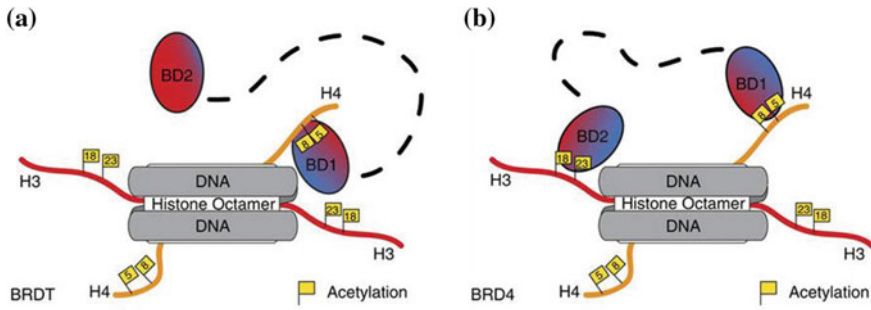
**Fig. 11.6** Sequence homology of the KAc binding site of BET bromodomains. Reprinted with permission from Ref. [21]. Copyright © 2011, American Chemical Society



**Fig. 11.7** Domain structures of BRD2, BRD3, BRD4, and BRDT


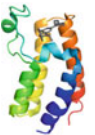
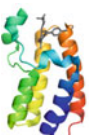
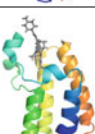
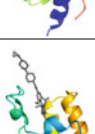
of the histone 4 tail [32]. Binding affinity is thus enhanced by binding to both DNA and histone H4. BD2 of BRDT did not show any interactions with DNA or histone H3. It was suggested that the lack of BD2 interaction with histone H3 could be traced to the negative electrostatic surface of BD2, which would result in electrostatic repulsion from the negatively charged DNA, thereby preventing binding (Fig. 11.8a). The authors suggested that BRDT-2 may have interactions with acetylated lysines of transition proteins and protamines (sperm-specific nuclear proteins) that are critical for spermatogenesis. No interactions were observed between BRD4-1 and DNA (Fig. 11.8b). BD1 of BRD4 binds to H4K8_{ac} and H4K5_{ac} of the H4 tail and to H3K18_{ac} and H3K23_{ac} of BD2 in a bivalent manner. By simultaneously binding both its bromodomains, binding affinity for BRD4 is enhanced [33]. Furthermore, they found that BRD3-1 does not interact with DNA, while BRD2-1, BRD2-2, and BRD4-2 do interact with DNA.

Five high-resolution co-crystal structures of human BRDT-1 (Table 11.1, entries 1–5), and two for mouse Brdt (Table 11.1, entries 6 and 7) have been deposited into the PDB. Six crystal structures of BD1 (entries 1–6) and one of BD2 are reported (entry 7). Four are co-crystal structures of BD1 with small molecules dinaciclib



**Fig. 11.8** Binding modes for BRDT (a) and BRD4 (b) to H3 and H4. Reprinted with permission from Ref. [32]


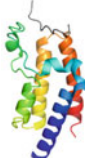
**Table 11.1** BRDT/Brdt crystal structures in the PDB^a

No.	PDB code	Resolution (Å)	Structure	Short description	References
1	2RFJ	2.05		Crystal structure of human BRDT-1	[29]
2	4KCX	2.0		Human BRDT-1 in complex with dinaciclib	[34]
3	4FLP	2.23		Human BRDT-1 in complex with JQ1	[9]
4	5VBQ	1.65		Human BRDT-1 in complex with BI2536	BDB: 5VBQ
5	5VBR	1.9		Human BRDT-1 in complex with Volasertib	BDB: 5VBR

(continued)



**Table 11.1** (continued)

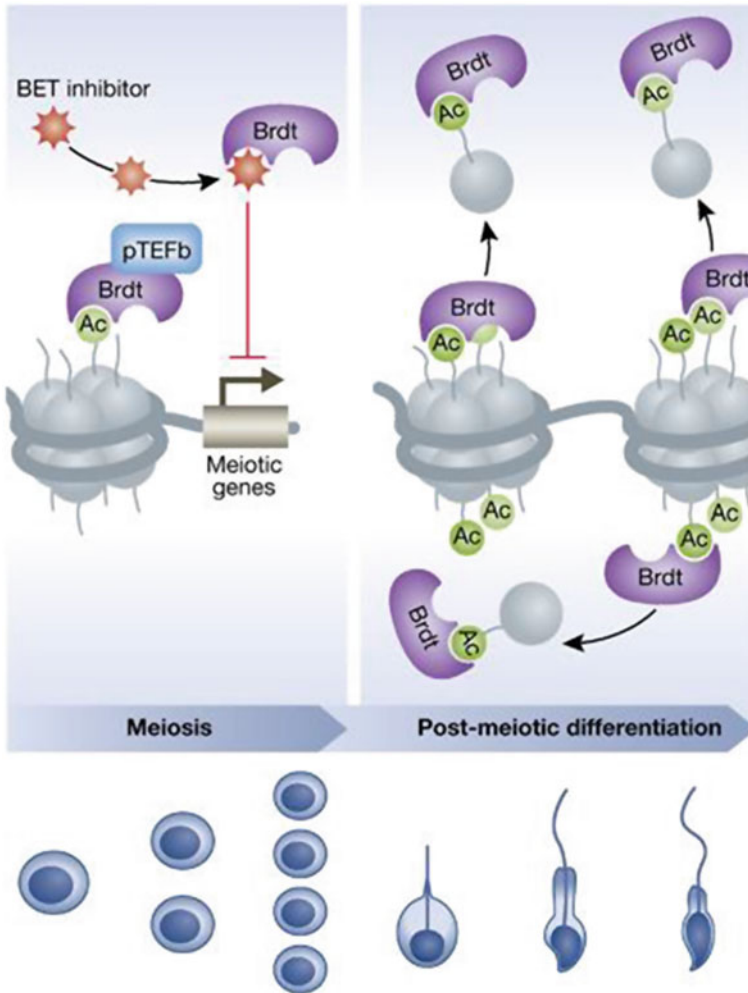
No.	PDB code	Resolution (Å)	Structure	Short description	References
6	2WP2	2.37		Mouse Brdt-1 bound in complex with a histone H4 peptide	[33]
7	2WP1	2.1		Mouse Brdt-2 in complex with an acetylated histone H3 peptide	[33]

^aAll proteins expressed in *E. coli*

(entry 2), JQ1 (entry 3), BI2536 (entry 4), and Volasertib (entry 5). Two co-crystal structures have been solved with histone-type ligands (entries 6 and 7). A tandem BET bromodomain crystal structure has not been solved yet, but once available, it is expected to be important for the future design of selective BET inhibitors.

## 11.5 The Role of BRDT in Spermatogenesis [35]

BRDT is an attractive pharmacological target for male contraception because it is exclusively expressed in male germ cells. *Brdt-1* knockout mice were shown to be viable but completely sterile and produced fewer and abnormal sperm [10]. The knockout of both bromodomains of *Brdt* in mice resulted in an even more severe disruption of spermatogenesis [36]. A genetic knockout model is not available for any of the other BET bromodomains. In humans, BRDT is the only BET bromodomain expressed in the germ line of the testis [37] and was found in spermatocytes, including ejaculated sperm [38], whereas in mice, Brdt was found in stages ranging from pachytene spermatocytes to round spermatids [38]. In contrast to humans, mouse germ cells express all four BET proteins. *Brdt* knockout mice showed delayed puberty, and therefore, it was posited that BRDT also plays a role in the timing of puberty [37]. Brdt is a transcriptional regulator that controls the initiation of meiotic division after histone hyperacetylation and recruitment of positive transcription elongation factor (P-TEFb) [36], a kinase that initiates RNA polymerase II-mediated transcriptional elongation, which leads to meiotic gene expression (Fig. 11.9). Brdt later regulates post-meiotic genome repackaging by removing histones from DNA, which are subsequently replaced with other proteins [36]. Thus, Brdt has dual functions as an activator and repressor of transcription (Fig. 11.9) at the appropriate time [36, 39]. In addition, Brdt-1 was shown to form a



**Fig. 11.9** Two-stage role of Brdt in spermatogenesis. Reproduced from Ref. [41] by permission of John Wiley & Sons, Ltd.

complex with the transcription repressor proteins histone deacetylase 1 (HDAC1), arginine-specific histone methyltransferase 5 (PRMT5), and the tripartite motif-containing 28 protein (TRIM28) [40]. These proteins bind to the promoter of histone H1t and repress its expression in round spermatids. In BD1 knockout mice, it was shown that Brdt and the associated proteins were not recruited to histone H1t, confirming the essential role of Brdt-1 in spermatogenesis [10].



## 11.6 Small-Molecule Monovalent Inhibition of BRDT for Male Contraception

Compared to female contraceptive methods, options for men are generally limited to vasectomy, condoms, and withdrawal [42]. Hormonal contraception with testosterone and related analogs, which lead to reversible infertility, have been studied since the 1960s, but potential untoward cardiovascular side effects, mood changes, acne, and weight gain have thus far prevented commercialization [43]. Globally, surveys have demonstrated that about 50% of men have an interest in a pharmacological approach for fertility control with daily oral administration as the preferred method [44]. Some agents currently undergoing preclinical studies include CBD-402, adjudin, H2-gamendazole, WIN 18446, BMS 189453, eppin antagonists, CatSper blockers, and Na,K-ATPase inhibitors [45], which may eventually offer a male contraceptive agent [42, 46, 47].

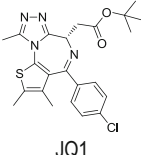
In 2012, Matzuk et al. first established the feasibility of targeting BRDT with bromodomain inhibitor JQ1 [9]. Treatment of mice with JQ1 revealed reduction in testis size, number of spermatozoa, and sperm motility. Hormonal levels of follicle-stimulating hormone, luteinizing hormone, and testosterone were not affected, and the mice mated normally. The fertility of the JQ1-treated male mice was fully reversed after treatment was halted, and the first- and second-generation offspring of the JQ1-treated mice had normal testes and sperm. The results by Matzuk et al. provided further validation of BRDT as a potential target for male contraception and encouraged further drug discovery efforts. However, evaluation of JQ1 in a mouse model demonstrated toxic effects on lymphocytes and at higher doses led to significant weight loss [48]. Another study showed that JQ1 caused cognitive defects in mice [49]. It is possible that these side effects could hamper the development of JQ1 analogs for contraception, and therefore, it is important to discover and develop novel chemical matter for specific BRDT inhibition.

JQ1 is the most widely studied BET bromodomain inhibitor. As shown in Table 11.2, JQ1 is a potent BET bromodomain inhibitor with little intra-BET selectivity. Generally, inhibitory activity for BRDT is the lowest among all BET proteins, which has been traced in several cases to the presence of Arg54 interfering with inhibitor binding to BRDT, as will be discussed below.

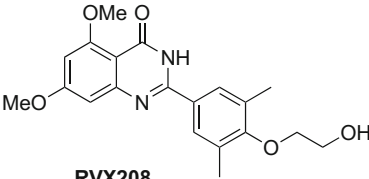
Some selectivity among BET bromodomain inhibitors has been achieved. For example, RVX208 (Fig. 11.10) [26] is selective (up to 23-fold) for BD2 over BD1 of the four BET bromodomains. RVX208 did not bind to other bromodomain proteins that were investigated in a thermal shift assay. Co-crystal structures revealed that binding of RVX208 to BD2 caused a conformational change, leading to differences in binding mode. These results suggest that dynamic properties of the BET proteins could hold a key to obtaining selective inhibitors. This example clearly demonstrates that selectivity can be achieved among the BET bromodomains.

Raux et al. describe several inhibitors with a xanthine scaffold that target BRD4-1 (Fig. 11.11) [56]. The most potent compound in this series,

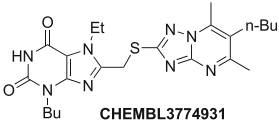
**Table 11.2** Assay data for pan-BET inhibitor JQ1 [9, 50–55]

Structure and name	Protein	IC ₅₀ (μM)	K _d (μM)	K _i (μM)
 JQ1	BRDT-1		0.047 ² 0.19 ³	
	BRDT-2		0.035 ²	
	BRDT-1,2		0.046 ²	
	BRD4-1	0.077 ¹ , 0.029 ⁴	0.014 ² 0.049 ³	0.0076 ⁴
	BRD4-2	0.033 ¹ 0.036 ⁴	0.0082 ² 0.0901 ³	0.011 ⁴
	BRD4-1,2		0.0073 ²	
	BRD3-1		0.014 ² 0.0595 ³	0.0066 ⁴
	BRD3-2		0.019 ² 0.082 ³	0.0089 ⁴
	BRD3-1, 2		0.014 ²	
	BRD2-1		0.027 ² 0.128 ³	0.013 ⁴
	BRD2-2		0.018 ²	0.013 ⁴
	BRD2-1,2		0.0056 ²	

Where determination methods are: ¹TR-FRET, ²BROMOscan, ³ITC, and ⁴FP

 RVX208	Δ Tm (°C)		K _d nM	
		BRDT-1	0.6	BRDT-1
	BRDT-2	4.0	BRDT-2	637
	BRD4-1	1.3	BRD4-1	1142
	BRD4-2	3.4	BRD4-2	135
	BRD3-1	0.8	BRD3-1	4065
	BRD3-2	4.0	BRD3-2	195
	BRD2-1	0.9	BRD2-1	5780
	BRD2-2	4.0	BRD2-2	251

**Fig. 11.10** Structure of BD2-selective inhibitor RVX208 and assay data. ΔTm by thermal shift, K_d by ITC**Fig. 11.11** Structure of BRD-1 inhibitor CHEMBL3774931, devoid of BRDT-1 activity; data from HTRF assay

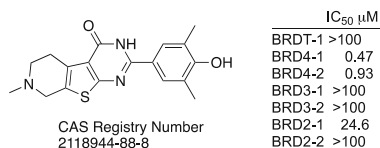
 CHEMBL3774931	IC ₅₀ μM
	BRDT-1
BRD4-1	5.0
BRD3-1	62
BRD2-1	59

CHEMBL377493, was a weak inhibitor ( $IC_{50} = 5 \mu M$ ) but shows >ten fold selectivity for BRD4-1 over other tested BET bromodomains and was not active against BRDT-1. The co-crystal structure showed that the xanthine core mimics acetyl-lysine and forms the canonical hydrogen bond with the conserved asparagine. The BET-BD1 selectivity was derived from two interactions: the hydrogen bond between the triazolo moiety of the side chain and the conserved Asp88 as well as van der Waals interaction between the pyrimidine and Gln85 in the ZA loop. They attributed the lack of BRDT-1 inhibition to a steric clash between the compound's triazolopyrimidine moiety with the unique Arg54 residue. Analogs devoid of the triazolopyrimidine moiety inhibited all investigated BET proteins, including BRDT. The steric hindrance caused by a group such as the triazolopyrimidine group with Arg54 in BRDT-1 could be considered as a general approach to obtain BET inhibitors that will not inhibit BRDT and cause infertility in male patients. It also supports the hypothesis that a BRDT-selective compound could be developed that has strong interactions with Arg54, as discussed above.

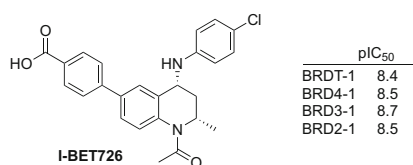
Ouyang and collaborators employed virtual HTS to discover BET bromodomain inhibitors [57]. Hit optimization provided a selective BRD4 inhibitor (Fig. 11.12) that did not inhibit BRDT-1, BRD3-1, BRD3-2, and BRD2-2 at 100  $\mu M$ . MD simulation and calculated binding free energies of the docked poses with the lead compound showed the strongest binding affinity for BRD4. The authors traced the selectivity of their compound for BRD4-1 to hydrogen bonding between the carbonyl group to Gln85 in BRD4-1 (PDB: 4ZW1). When they evaluated docking poses, they did not observe hydrogen bonding between Gln61 in BRD3-1 or Gln101 with BRD2-1. As discussed before, BRDT-1 has Arg54 instead of a Gln at that same position. The docking pose did not predict an interaction between the lead compound and Arg54. The results suggest that this region in the proteins is important for BET bromodomain selectivity.

Gosmini et al. reported a tetrahydroquinoline series of compounds (Fig. 11.13) that upregulate ApoA1 and selectively inhibit BET bromodomains with potent anti-inflammatory effects and in vivo activity in a septic shock mouse model. I-BET726 is a potent BET inhibitor with no intra-BET selectivity [58].

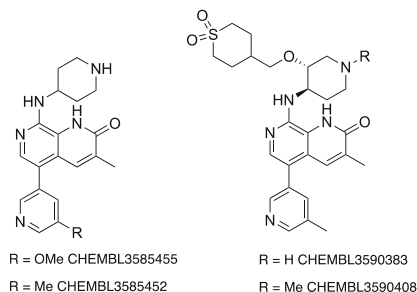
**Fig. 11.12** Structure of optimized virtual screening hit CAS Registry Number 2118944-88-8 selective for BRD4; data from TR-FRET



**Fig. 11.13** Structure of non-selective BET inhibitor I-BET726; data from BROMOscan™ assay



**Fig. 11.14** Structures of BET and ADAT2 inhibitors CHEMBL3585452 and CHEMBL3585455 and selective ATAD2 inhibitors CHEMBL3590383 and CHEMBL3590408

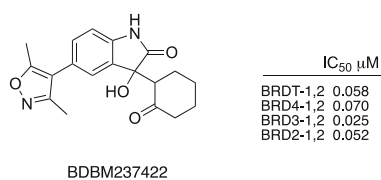


In their search for an ATAD2 selective inhibitor, a GSK group identified a quinolinone scaffold (Fig. 11.14) as a hit for inhibitors of bromodomain-containing proteins [59, 60]. CHEMBL3585452 and CHEMBL3585455 were lead compounds that inhibited ATAD2 and BET bromodomains, including BRDT with similar potencies. CHEMBL3590383 and CHEMBL3590408 with optimized ATAD2 selectivity profiles were discovered by adding an additional side chain at the 3' position of the piperidine ring. CHEMBL3590383 is a <100 nM inhibitor ATAD2 with 100-fold selectivity over BET proteins.

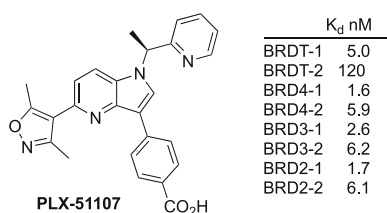
BeiGene patented a series of compounds based on isoxazoles [61]. A representative example BDBM237422 is shown in Fig. 11.15. The compounds are potent BET inhibitors with no intra-BET selectivity.

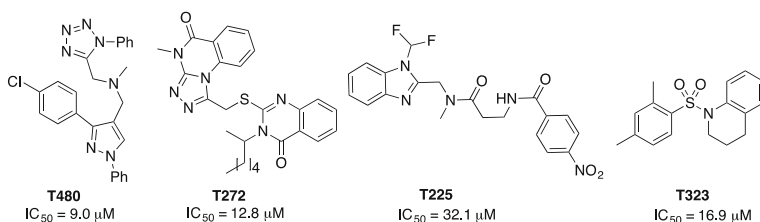
Ozer et al. profiled BET inhibitor PLX051107 (Fig. 11.16) in chronic lymphocytic leukemia in vitro and in vivo [62]. The binding affinities revealed that PLX051107 was a potent inhibitor of all BET bromodomains. However, it is of note that this compound had a 24-fold less affinity for BRDT-2, which could be a result of electrostatic repulsion between the negatively charged BRDT-2 and the carboxylic acid present in PLX051107.

**Fig. 11.15** Structure of non-selective isoxazole BRD inhibitor BDBM237422 from BeiGene; data from TRF assay



**Fig. 11.16** Structure of isoxazole BET inhibitor PLX-51107, with weak BRDT-2 affinity; data from TRF assay. Reprinted with permission from Ref. [62]. Copyright © 2013, American Chemical Society

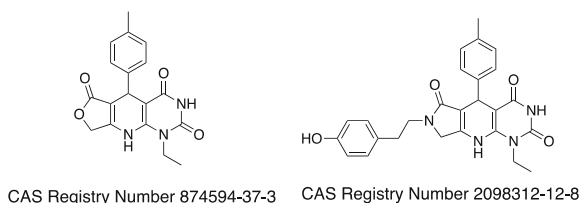




**Fig. 11.17** Structure of isoxazole BET inhibitor PLX-51107, with weak BRDT-2 affinity; data from TRF assay. Reprinted with permission from Ref. [63]

To identify novel potent BRDT inhibitors, Gao et al. performed structure-based virtual screening [63, 64], employing the co-crystal complex of BRDT and JQ1 (4FLP). A total of 125 compounds were selected for biochemical assays, and four new scaffolds (Fig. 11.17) were identified as BRDT-1 inhibitors with IC₅₀ values of 9.02–32.12 μM. The most active compound, T480, was predicted to form two hydrogen bonds with the key Asn109 residue. However, none of the compounds were evaluated for interactions with other bromodomains or in cellular assays.

Ayoub et al. reported the discovery of BET bromodomain inhibitors from virtual high throughput screening of the six million compounds in the ZINC library using the BRDT-1 co-crystal structure with JQ1 (4FLP) [65]. Out of the top 200 identified hits, 22 commercially available compounds were tested initially in a fluorescent anisotropy assay. Of the nine compounds with verified binding, a dihydropyridopyrimidine was the most potent BRDT-1 inhibitor with an IC₅₀ of 2.3 μM (Fig. 11.18, left). BRD4-1 was inhibited with an IC₅₀ of 1.0 μM. Verification of binding to BRDT-1 was confirmed by differential scanning fluorimetry (DSF) and protein-based ¹⁹F NMR assay (PrOF NMR). A BROMOScan indicated that this compound is selective for the BET family proteins. A brief SAR study identified a lactam analog (Fig. 11.18, right) with sub-micromolar cellular activity (IC₅₀ = 0.46 μM) against MM1.S cells. The IC₅₀ values for inhibition of BRDT-1 and BRD4-1 were 0.750 and 0.390 μM, respectively, demonstrating again that selectivity of BET inhibition is difficult to achieve.

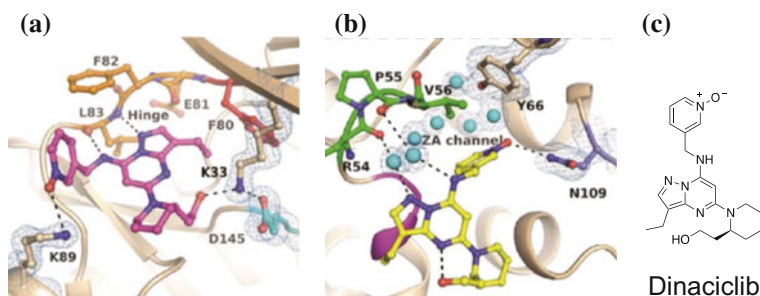


**Fig. 11.18** Structures of virtual screening hit CAS #87494-37-3 and optimized lactam analog

## 11.7 Dual BET Bromodomain–Kinase Inhibitors [66]

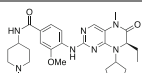
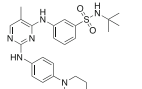
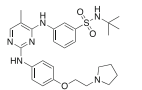
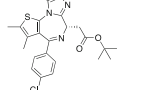
Since it was reported that BRD4 functions as an atypical kinase [67], Martin et al. investigated whether kinase inhibitors could also function as bromodomain inhibitors. The first report to validate this hypothesis showed that the potent cyclin-dependent kinase inhibitor dinaciclib, which is in phase III clinical trials for the treatment of refractory chronic lymphocytic leukemia, is a weak inhibitor of BRDT (Fig. 11.19) [34].

The high-resolution co-crystal structures of dinaciclib bound to CDK2, and BRDT-1 revealed the binding modes for the two proteins (Fig. 11.19). Dinaciclib is a potent ATP site binder that binds tightly to the hinge region and gains its potency and selectivity from a network of hydrogen bonding and hydrophobic interactions that rigidify the molecule and the normally flexible activation loop. Dinaciclib interactions with BRDT are characterized by binding to the KAc recognition site Asn109, forming a hydrogen bond between the N-oxide moiety and Asn109, binding to water molecules in the ZA channel that establish interactions with Pro55 and Val56 in the pseudo-hinge region, and hydrophobic interactions with Pro51 and Phe52 of the WPF shelf. However, dinaciclib is only a weak inhibitor of BRDT-1 ( $K_d = 37 \mu\text{M}$ ). This discovery, nevertheless, provided the first evidence for the cross-reactivity of kinase inhibitors with BRDT and suggested a novel strategy for the discovery of bromodomain inhibitors by examining kinase inhibitors. Subsequent studies [68, 69] demonstrated that kinase inhibitors can bind to bromodomains in a variety of binding modes and that these compounds act as dual kinase–bromodomain inhibitors. The results have recently been summarized in a comprehensive review [66]. Table 11.3 summarizes findings from the Ember et al. high throughput crystallographic study that identified 14 compounds as bromodomain inhibitors from a library of 581 known kinase inhibitors. While most of them were micromolar inhibitors, BI2536, TG101209, and TG101348 were sub-micromolar inhibitors.



**Fig. 11.19** Dual kinase BRD4-1 inhibitor dinaciclib. **a** Crystal structure of dinaciclib bound to CDK2 (PDB: 4KD1). **b** Crystal structure of dinaciclib bound to BRDT (PDB: 4KCX). **c** Structure of dinaciclib. From Ref. [34]

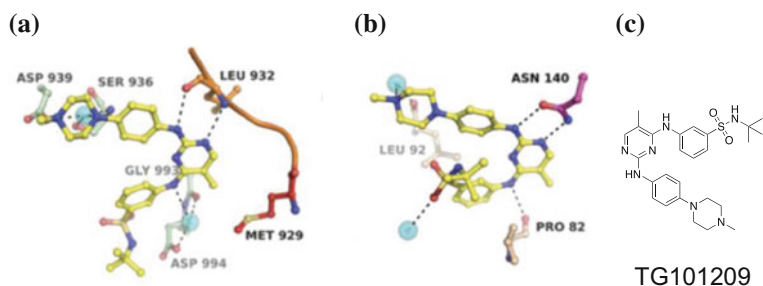
**Table 11.3** IC₅₀ data for BRD4 and BRDT inhibition

Compound name	Structure	BRDT-1 (nM) ^a	BRD4-1 (nM) ^a
BI2536		260	25
TG101209		230	103
TG101348		340	290
JQ1		110	35

^aIC₅₀ determined with AlphaScreen

TG101209 utilizes its aminopyrimidine moiety to bind the hinge region of JAK2 and with Asn140 of BRD4-1 (Fig. 11.20). None of the inhibitors revealed significant differences in the inhibition of BRD4 and BRDT. Furthermore, in cases where a difference was observed, such as for BI2536, inhibition of BRD4-1 was more potent than inhibition of BRDT-1. The results indicated that these structurally novel BRD inhibitors can be explored and optimized in the future for BRD inhibition or as dual kinase/BET inhibitors. However, the results from these studies indicate again the difficulties to generate selective intra-BET bromodomain inhibitors.

Subsequent studies using TG101209 as the lead compound and preparing reverse amides provided potent and cellularly active BRD4 and BRDT inhibitors [70]. BROMOScans for compounds **2** and **4** (Table 11.4) showed high selectivity for BET bromodomains but no differentiation among the BET proteins. Compounds **1–4** inhibited BRDT-1 and BRD4-1 with double-digit nanomolar IC₅₀ values. Compounds **1–3** were also highly active for BRD4-2. Given the double-digit nanomolar activities of compounds **1–4**, they are among the most potent BRDT-1 inhibitors known.

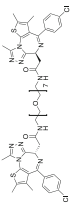
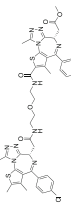


**Fig. 11.20** Dual kinase BRD4-1 inhibitor TG101209. **a** TG101209 binding to the JAK2 hinge region. **b** TG101209 binding to BRD4-1. **c** Structure of TG101209. From Ref. [34]



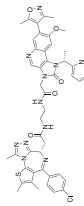


**Table 11.5** Structures and data for bivalent BRD inhibitors

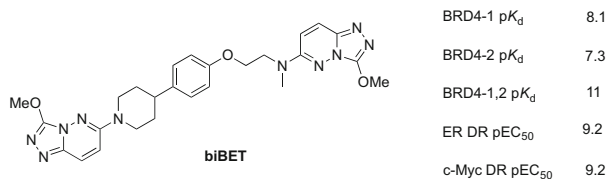
Name	Structure	Protein	IC ₅₀ (nM)	K _d (nM)	K _i (nM)	Assay method	References				
MTI (6S)-JQ1-PEG7		BRDT-1			0.560	AlphaScreen/ BROMOscan	[53]				
		BRDT-2			0.086						
		BRDT-1,2			0.076						
		BRD2-1			0.160						
		BRD2-2			0.033						
		BRD2-1,2			0.024						
		BRD3-1			0.059						
		BRD3-2			0.070						
		BRD3-1,2			0.012						
		BRD4-1		3.09	0.099						
		BRD4-2			0.053						
		BRD4-1,2			0.087						
		(6S+2S)-PEG1		BRDT-1	0.574				0.290	AlphaScreen/ BROMOscan	[53]
				BRDT-2					0.066		
BRDT-1,2	0.039				0.420						
BRD2-1					0.014						
BRD2-2					0.0069						
BRD2-1,2					0.010						
BRD3-1					0.130						
BRD3-2					0.0027						
BRD3-1,2					0.110						
BRD4-1	0.758			0.0100, 16.7 ^a	0.180						
BRD4-2				0.0240	0.0043						

(continued)

Table 11.5 (continued)

Name	Structure	Protein	IC ₅₀ (nM)	K _d (nM)	K _i (nM)	Assay method	References
6S+IBET-PEGO		BRD4-1,2 BRDT-1 BRD4-1	148 404	0.00470	0.012	AlphaScreen	[53]

All K_i and K_d values were determined by qPCR/BROMOscan™, except when indicated by ^a, where K_d was determined by ITC. All IC₅₀ values were determined by AlphaScreen



**Fig. 11.21** Structure and cellular data for biBET probe (DR = downregulation)

exhibited BRDT selectivity. Notably, BROMOscan assays showed that (6S+2S)-PEG1 had 2- to 50-fold selectivity for the second bromodomain of different bromodomains. IBET 151 was then used to replace (6S)-JQ1 or (2S)-JQ1. The (6S+IBET)-PEG heterodimer with the shortest linker, (6S+IBET)-PEG0 ( $IC_{50}$  = 148 nM), was found to be a weaker threefold selective BRDT-1 inhibitor (Table 11.5) over BRD4-1, compared with other (6S+IBET)-PEG heterodimers ( $IC_{50}$  = 5.1–13 nM). Similar results were observed for the 2S+IBET-PEG series and the IBETx2-PEG series. Notably, almost all (6S+IBET)-PEG heterodimers exhibited approximately fivefold selectivity for BRD4-1 over BRDT-1. Most of the 2S+IBET-PEG heterodimers showed two- to fourfold specificity for BRD4-1. IBETx2-PEG heterodimers failed to show any selectivity for BRDT-1 or BRD4-1.

Waring et al. described a focused SAR study and the characterization of biBET, a bivalent triazolopyridazine probe compound (Fig. 11.21) [71]. The X-ray co-crystal structure between biBET and BRD4-1 showed the ability of biBET to induce protein dimerization. NMR experiments with the tandem BRD4 protein demonstrated bivalent and intramolecular cis-binding mode of biBET to BD1 and BD2. The cellular potency of the bivalent probe was significantly higher than those of monovalent ligands as shown by the significant increase of BRD4 inhibition, potency in cancer cells, and downregulation of c-Myc (MM.1S cells) and ER $\alpha$  (MCF-7 cells). A molecular weight of 531 and a  $\log D_{7.4}$  of 2.9 suggest that this probe molecule may have potential as a lead for drug discovery.

## 11.9 Heterobifunctional PROTAC Degraders

Protein degradation is a novel drug discovery approach that has already been validated in vivo for BRD4 and may also hold promise for male contraceptive target proteins such as BRDT. Several groups reported a proteolysis-targeting chimera (PROTAC) approach to degrade BRD4 by linking BET inhibitors to either a thalidomide analog, which binds cereblon or a von Hippel–Lindau binder such as VHL-1 (Fig. 11.21). They are ligands for E3 ubiquitin ligases that target proteins for ubiquitination and proteasomal degradation [54, 72–75]. A recent review has summarized these findings [76]. PROTAC-induced protein degradation is an

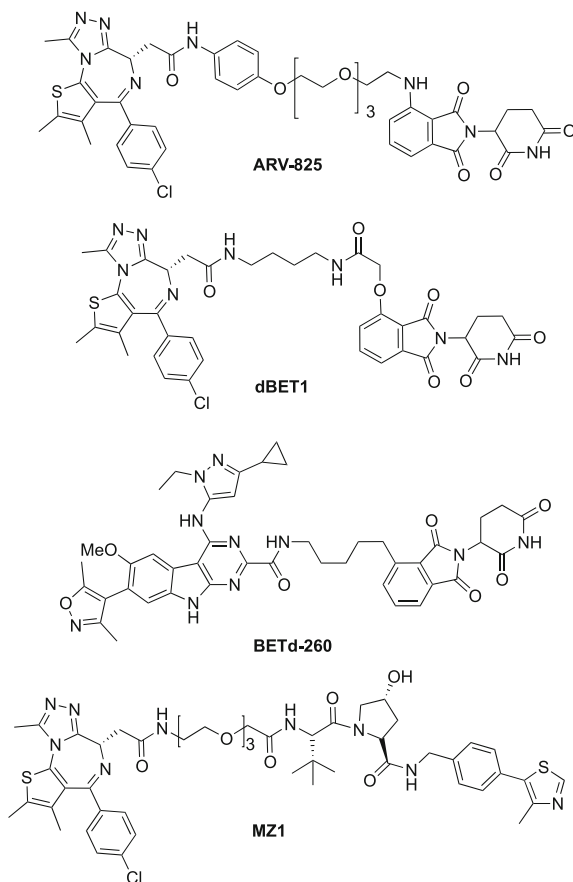
emerging strategy that constitutes a paradigm shift from traditional drug discovery approaches because proteins are degraded rather than inhibited [77]. Protein degradation closely mimics the knockout phenotype, which is a method used to validate drug targets. The effect is catalytic, and low levels of target protein occupancy can still be quite effective. This approach could be a promising strategy for developing a male contraceptive agent, because the degradation of a protein requires its resynthesis, which therefore can lead to a long-lasting effect that might not require daily dosing. This is especially true for proteins with a relatively long half-life such as the BET proteins. Less frequent dosing could also limit side effects. However, the relatively large molecular weight of these PROTAC conjugates is a concern for oral bioavailability that needs to be addressed either by medicinal chemistry approaches or by the use of dermal or intramuscular drug delivery.

It had been shown that BRD4 inhibitors such as JQ1 and OTX015 cause an accumulation of BRD4 in several cancer cell lines, which prevents the complete suppression of c-Myc levels. This effect could be an impediment to effective cancer chemotherapy because transcriptional activation could be restored quickly after discontinuation of treatment. In addition, effects are cytostatic and no significant apoptosis was observed. For these reasons, the Crews group selected BRD4 for PROTAC targeting [72]. They prepared ARV-825 (Fig. 11.22), a pan-BET inhibitor, using a PEG linker to connect JQ1 to lenalidomide and demonstrated that this compound effectively degraded BRD4 in BL cancer cells ( $DC_{50} < 1$  nM) and reduced c-Myc levels much more significantly than JQ1 or OTX015.

The Bradner group investigated the JQ1-thalidomide conjugate dBET1 [73], which is a potent ( $IC_{50} = 20$  nM) BET-selective inhibitor. Immunoblotting showed pronounced loss of BRD4 in human AML MV4;11 cells ( $DC_{50} = <100$  nM) after 18 h, as well as multiple myeloma MM1.S and SUM149 breast cancer cell lines. In vivo studies with dBET1 in a human xenograft mouse model of MV4;11 demonstrated reduction of leukemia progression and tumor weight. Downregulation of c-Myc was also observed. The data supported the validity of the PROTAC approach to bromodomains in vivo.

Wang and collaborators linked azacarbazole-based BRD4 inhibitors to a thalidomide derivative [74]. They carried out SAR studies that included linkers of different length and composition, and discovered that analog BETd-260 is a picomolar (0.051 nM) inhibitor of RS4;11 cell line proliferation. BETd-260 efficiently downregulated c-Myc and induced apoptosis in the RS4;11 cell line. Antitumor activity was established in a xenograft RS4;11 mouse model that demonstrated >90% tumor regression without any toxic side effects. BRD2, BRD3, BRD4, and c-Myc were downregulated, and apoptosis was observed in the tumor tissue.

The Ciulli group designed and investigated compound MZ1, composed of JQ1 connected by a PEG linker to a drug-like VHL-1 ligand [54]. The  $K_d$  values for BD1 and BD2 for BRD4, BRD3, and BRD2 were similar (120–380 nM) or slightly lower than for JQ1. However, after 24 h at a concentration of 1  $\mu$ M MZ1, BRD4

**Fig. 11.22** Structures of PROTAC BRD degraders

was selectively degraded over BRD2 and BRD3 in HeLa cells [54]. The removal of BRD4 in HeLa cells was reversible and long lasting. Importantly, BET selectivity was achieved with this approach. The authors hypothesize that this effect could come from preferential or more efficient polyubiquitination of BRD4 or a steric effect that allows a tighter formation of the VHL-PROTAC-BRD4 complex. They were able to obtain a crystal structure of MZ1 in complex with human VHL and BRD4-2, and based on these results, they propose that not only ligand-induced proximity but also surface complementarity between the proteins as induced by the bivalent ligand is of importance for effective complex formation and subsequent protein degradation [78].

The downregulation of BRDT using the PROTAC approach has not been reported yet because a suitable cell line expressing BRDT is not available.

## 11.10 Concluding Remarks

BRDT has been genetically validated as a promising target for the development of a male contraceptive agent. Potent BRDT inhibitors have been discovered; however, selective inhibition of BRDT over other BET proteins has not been realized and poses a significant challenge to overcome because of the high similarity of the BET protein binding sites. However, some success for selective inhibition of BET bromodomains has been achieved in cellular environments. Possibilities that could be explored to obtain selective BRDT inhibitors are the engagement of Arg54, a unique residue in the ZA channel of BRDT, the lack of BRDT-2 binding to DNA and histone H3. The exploration of bivalent homodimeric or heterodimeric inhibitors that selectively engage BD1 and BD2 of BRDT is a promising approach, as are protein degradation (PROTAC) strategies. The design of inhibitors that displace or modify the conserved network of water molecules in the BET inhibitor-binding domain is another possibility [79]. Obtaining a selective inhibitor in light of the highly conserved binding site is reminiscent of the kinase field, where selectivity has historically been a major challenge. The discovery of allosteric inhibitors that bind outside of the ATP-binding site has led to some success, with one drug approved and more than 10 allosteric inhibitors in clinical trials [80]. An allosteric inhibitor approach could be considered for bromodomains as well. Solving the crystal structure of a BET tandem bromodomain and related co-crystal structures with inhibitors, along with the availability of a cell line expressing BRDT, would also be helpful in achieving progress toward the development of selective BRDT inhibitors. In addition to the usual drug discovery and development process that includes pharmacokinetic, pharmacodynamic, and ADMET studies, the ability of compounds to cross the blood–testis barrier needs to be considered for a male contraceptive agent. While significant knowledge is available about design strategies for blood–brain barrier penetration, little is known about the blood–testis barrier, which is considered a challenge for the development of any male contraceptive agent.

**Acknowledgements** We gratefully acknowledge the support of our program by the Contraception Research Branch of the Eunice Kennedy Shriver National Institute of Child Health and Human Development (1 U54 HD093540 and HHSN275201300017C). We thank Dr. C. Leigh Allen for editorial assistance and for generating Figs. 11.2, 11.4, 11.5, and 11.7.

## References

1. Filippakopoulos P, Knapp S (2014) Targeting bromodomains: epigenetic readers of lysine acetylation. *Nat Rev Drug Discov* 13(5):337–356
2. Prinjha RK, Witherington J, Lee K (2012) Place your BETs: the therapeutic potential of bromodomains. *Trends Pharmacol Sci* 33(3):146–153
3. Ahuja N, Sharma AR, Baylin SB (2016) Epigenetic therapeutics: a new weapon in the war against cancer. *Annu Rev Med* 67:73–89

4. Bennett RL, Licht JD (2018) Targeting epigenetics in cancer. *Annu Rev Pharmacol Toxicol* 58(1):187–207
5. Verdin E, Ott M (2014) 50 years of protein acetylation: from gene regulation to epigenetics, metabolism and beyond. *Nat Rev Mol Cell Biol* 16:258
6. Muller S, Filippakopoulos P, Knapp S (2011) Bromodomains as therapeutic targets. *Expert Rev Mol Med* 13:e29
7. Scanlan MJ, Altorki NK, Gure AO, Williamson B, Jungbluth A, Chen Y-T, Old LJ (2000) Expression of cancer-testis antigens in lung cancer: definition of bromodomain testis-specific gene (BRDT) as a new CT gene, CT9. *Cancer Lett* 150(2):155–164
8. Pérez-Salvia M, Esteller M (2017) Bromodomain inhibitors and cancer therapy: From structures to applications. *Epigenetics* 12(5):323–339
9. Matzuk MM, McKeown MR, Filippakopoulos P, Li Q, Ma L, Agno JE, Lemieux ME, Picaud S, Yu RN, Qi J, Knapp S, Bradner JE (2012) Small-molecule inhibition of BRDT for male contraception. *Cell* 150(4):673–684
10. Shang E, Nickerson HD, Wen D, Wang X, Wolgemuth DJ (2007) The first bromodomain of Brdt, a testis-specific member of the BET sub-family of double-bromodomain-containing proteins, is essential for male germ cell differentiation. *Development* 134(19):3507–3715
11. Barda S, Yogev L, Paz G, Yavetz H, Lehavi O, Hauser R, Doniger T, Breitbart H, Kleiman SE (2014) BRDT gene sequence in human testicular pathologies and the implication of its single nucleotide polymorphism (rs3088232) on fertility. *Andrology* 2:641–647
12. Filippakopoulos P, Knapp S (2014) Targeting bromodomains: epigenetic readers of lysine acetylation. *Nat Rev Drug Discov* 13:337–356
13. Hewings DS, Rooney TPC, Jennings LE, Hay DA, Schofield CJ, Brennan PE, Knapp S, Conway SJ (2012) Progress in the development and application of small molecule inhibitors of bromodomain–acetyl-lysine interactions. *J Med Chem* 55(22):9393–9413
14. Chun-wa C, Jason W (2011) Progress in the discovery of small-molecule inhibitors of bromodomain–histone interactions. *J Biomol Screen* 16(10):1170–1185
15. Arntson KE, Pomerantz WCK (2016) Protein-observed fluorine NMR: a bioorthogonal approach for small molecule discovery. *J Med Chem* 59(11):5158–5171
16. Zhang G, Smith SG, Zhou M-M (2015) Discovery of chemical inhibitors of human bromodomains. *Chem Rev* 115(21):11625–11668
17. Romero FA, Taylor AM, Crawford TD, Tsui V, Cote A, Magnuson S (2016) Disrupting acetyl-lysine recognition: progress in the development of bromodomain inhibitors. *J Med Chem* 59(4):1271–1298
18. Liu Z, Wang P, Chen H, Wold EA, Tian B, Brasier AR, Zhou J (2017) Drug discovery targeting bromodomain-containing protein 4. *J Med Chem* 60(11):4533–4558
19. Smith SG, Zhou M-M (2016) The bromodomain: a new target in emerging epigenetic medicine. *ACS Chem Biol* 11(3):598–608
20. Gallenkamp D, Gelato KA, Haendler B, Weinmann H (2014) Bromodomains and their pharmacological inhibitors. *ChemMedChem* 9(3):438–464
21. C-w Chung, Coste H, White JH, Mirguet O, Wilde J, Gosmini RL, Delves C, Magny SM, Woodward R, Hughes SA, Boursier EV, Flynn H, Bouillot AM, Bamborough P, Brusq J-MG, Gellibert FJ, Jones EJ, Riou AM, Homes P, Martin SL, Uings IJ, Toum J, Clément CA, Boullay A-B, Grimley RL, Blandel FM, Prinjha RK, Lee K, Kirilovsky J, Nicodeme E (2011) Discovery and characterization of small molecule inhibitors of the BET family bromodomains. *J Med Chem* 54(11):3827–3838
22. McDaniel KF, Wang L, Soltwedel T, Fidanze SD, Hasvold LA, Liu D, Mantei RA, Pratt JK, Sheppard GS, Bui MH, Faivre EJ, Huang X, Li L, Lin X, Wang R, Warder SE, Wilcox D, Albert DH, Magoc TJ, Rajaraman G, Park CH, Hutchins CW, Shen JJ, Edalji RP, Sun CC, Martin R, Gao W, Wong S, Fang G, Elmore SW, Shen Y, Kati WM (2017) Discovery of N-(4-(2,4-difluorophenoxy)-3-(6-methyl-7-oxo-6,7-dihydro-1H-pyrrolo[2,3-c]pyridin-4-yl)phenyl)ethanesulfonamide (ABBV-075/Mivebresib), a potent and orally available bromodomain and extraterminal domain (BET) family bromodomain inhibitor. *J Med Chem* 60(20):8369–8384

23. Theodoulou NH, Tomkinson CO, Prinjha RK, Humphreys PG (2016) Clinical progress and pharmacology of small molecule bromodomain inhibitors. *Curr Opin Chem Biol* 33:58–66
24. Noel JK, Iwata K, Ooike S, Sugahara K, Nakamura H, Daibata M (2013) Abstract C244: development of the BET bromodomain inhibitor OTX015. *Mol Cancer Ther* 12(11 Supplement):C244
25. Coudé M-M, Braun T, Berrou J, Mélanie Dupont I, Bertrand S, Masse A, Raffoux E, Itzykson R, Delord M, Riveiro ME, Herait P, Baruchel A, Dombret H, Gardin C (2015) Progress in the discovery of small-molecule inhibitors of bromodomain–histone interactions. *Oncotarget* 6:17698–17712
26. Picaud S, Wells C, Felletar I, Brotherton D, Martin S, Savitsky P, Diez-Dacal B, Philpott M, Bountra C, Lingard H, Fedorov O, Müller S, Brennan PE, Knapp S, Filippakopoulos P (2013) RVX-208, an inhibitor of BET transcriptional regulators with selectivity for the second bromodomain. *Proc Natl Acad Sci USA* 110(49):19754–19759
27. Gilham D, Wasiak S, Tsujikawa LM, Halliday C, Norek K, Patel RG, Kulikowski E, Johannson J, Sweeney M, Wong NCW (2016) RVX-208, a BET-inhibitor for treating atherosclerotic cardiovascular disease, raises ApoA-I/HDL and represses pathways that contribute to cardiovascular disease. *Atherosclerosis* 247:48–57
28. Nicholls SJ, Gordon A, Johannson J, Ballantyne CM, Barter PJ, Brewer HB, Kastelein JJP, Wong NC, Borgman MRN, Nissen SE (2012) ApoA-I induction as a potential cardioprotective strategy: Rationale for the SUSTAIN and ASSURE studies. *Cardiovasc Drugs Ther* 26(2):181–187
29. Filippakopoulos P, Picaud S, Mangos M, Keates T, Lambert JP, Barsyte-Lovejoy D, Felletar I, Volkmer R, Müller S, Pawson T, Gingras AC, Arrowsmith CH, Knapp S (2012) Histone recognition and large-scale structural analysis of the human bromodomain family. *Cell* 149(1):214–231
30. Woods AS, Ferre S (2005) Amazing stability of the arginine-phosphate electrostatic interaction. *J Proteome Res* 4(4):1397–1402
31. Woods AS, Moyer SC, Jackson SN (2008) Amazing stability of phosphate-quaternary amine interactions. *J Proteome Res* 7(8):3423–3427
32. Miller TCR, Simon B, Rybin V, Grötsch H, Curtet S, Khochbin S, Carlomagno T, Müller CW (2016) A bromodomain–DNA interaction facilitates acetylation-dependent bivalent nucleosome recognition by the BET protein BRDT. *Nat Commun* 7:13855
33. Moriniere J, Rousseaux S, Steuerwald U, Soler-Lopez M, Curtet S, Vitte AL, Govin J, Gaucher J, Sadoul K, Hart DJ, Krijgsveld J, Khochbin S, Muller CW, Petosa C (2009) Cooperative binding of two acetylation marks on a histone tail by a single bromodomain. *Nature* 461(7264):664–668
34. Martin MP, Olesen SH, Georg GI, Schonbrunn E (2013) Cyclin-dependent kinase inhibitor dinaciclib interacts with the acetyl-lysine recognition site of bromodomains. *ACS Chem Biol* 8(11):2360–2365
35. Berkovits BD, Wolgemuth DJ (2013) The role of the double bromodomain-containing BET genes during mammalian spermatogenesis. *Curr Top Dev Biol* 102:293–326
36. Gaucher J, Boussouar F, Montellier E, Curtet S, Buchou T, Bertrand S, Hery P, Jounier S, Depaux A, Vitte AL, Guardiola P, Pernet K, Debernardi A, Lopez F, Holota H, Imbert J, Wolgemuth DJ, Gerard M, Rousseaux S, Khochbin S (2012) Bromodomain-dependent stage-specific male genome programming by Brdt. *EMBO J* 31(19):3809–3820
37. Barda S, Yogev L, Paz G, Yavetz H, Hauser R, Breitbart H, Kleiman SE (2016) New insights into the role of the Brdt protein in the regulation of development and spermatogenesis in the mouse. *Gene Expr Patterns* 20(2):130–137
38. Barda S, Paz G, Yogev L, Yavetz H, Lehavi O, Hauser R, Botchan A, Breitbart H, Kleiman SE (2012) Expression of BET genes in testis of men with different spermatogenic impairments. *Fertil Steril* 97(1):46–52.e45
39. Berkovits BD, Wang L, Guarnieri P, Wolgemuth DJ (2012) The testis-specific double bromodomain-containing protein BRDT forms a complex with multiple spliceosome



- components and is required for mRNA splicing and 3'-UTR truncation in round spermatids. *Nucleic Acids Res* 40(15):7162–7175
40. Wang L, Wolgemuth DJ (2016) BET protein BRDT complexes with HDAC1, PRMT5, and TRIM28 and functions in transcriptional repression during spermatogenesis. *J Cell Biochem* 117(6):1429–1438
  41. Bryant JM, Berger SL (2012) Low-hanging fruit: targeting Brdt in the testes. *EMBO J* 31(19):3788–3789
  42. Kogan P, Wald M (2014) Male contraception: history and development. *Urol Clin North Am* 41(1):145–161
  43. Blithe D (2016) Pipeline for contraceptive development. *Fertil Steril* 106:1295–1302
  44. Heinemann K, Saad F, Wiesemes M, White S, Heinemann L (2005) Attitudes toward male fertility control: results of a multinational survey on four continents. *Hum Reprod* 20(2):549–556
  45. Syeda SS, Sánchez G, Hong KH, Hawkinson JE, Georg GI, Blanco G (2018) Design, synthesis, in vitro and in vivo evaluation of ouabain analogs as potent and selective Na, K-ATPase  $\alpha 4$  isoform inhibitors for male contraception. *J Med Chem*. <https://doi.org/10.1021/acs.jmedchem.1027b00925>
  46. Murdoch FE, Goldberg E (2014) Male contraception: Another holy grail. *Bioorg Med Chem Lett* 24(2):419–424
  47. Zdrojewicz Z, Konieczny R, Papier P (2015) Brdt bromodomain Inhibitors and other modern means of male contraception. *Adv Clin Exp Med* 24:705–714
  48. Lee DU, Katavolos P, Palanisamy G, Katewa A, Sioson C, Corpuz J, Pang J, DeMent K, Choo E, Ghilardi N, Diaz D, Danilenko DM (2016) Nonselective inhibition of the epigenetic transcriptional regulator BET induces marked lymphoid and hematopoietic toxicity in mice. *Toxicol Appl Pharmacol* 300:47–54
  49. Korb E, Herre M, Zucker-Scharff I, Darnell RB, Allis CD (2015) BET protein Brd4 activates transcription in neurons and BET inhibitor JQ1 blocks memory in mice. *Nat Neurosci* 18(10):1464–1473
  50. Brand M, Measures AM, Wilson BG, Cortopassi WA, Alexander R, Höss M, Hewings DS, Rooney TPC, Paton RS, Conway SJ (2015) Small molecule inhibitors of bromodomain–acetyl-lysine interactions. *ACS Chem Biol* 10(1):22–39
  51. Ran X, Zhao Y, Liu L, Bai L, Yang C-Y, Zhou B, Meagher JL, Chinnaswamy K, Stuckey JA, Wang S (2015) Structure-based design of  $\gamma$ -carboline analogues as potent and specific bet bromodomain inhibitors. *J Med Chem* 58(12):4927–4939
  52. Sasaki K, Ito A, Yoshida M (2012) Development of live-cell imaging probes for monitoring histone modifications. *Bioorg Med Chem* 20(6):1887–1892
  53. Tanaka M, Roberts JM, Seo HS, Souza A, Paulk J, Scott TG, DeAngelo SL, Dhe-Paganon S, Bradner JE (2016) Design and characterization of bivalent BET inhibitors. *Nat Chem Biol* 12(12):1089–1096
  54. Zengerle M, Chan KH, Ciulli A (2015) Selective small molecule induced degradation of the BET bromodomain protein BRD4. *ACS Chem Biol* 10(8):1770–1777
  55. Bryant J, Donahue G, Wang X, Meyer-Ficca M, Luense L, Weller A, Bartolomei M, Blobel G, Meyer R, Garcia B, Berger S (2015) Characterization of BRD4 during mammalian postmeiotic sperm development. *Mol Cell Biol* 35:1433–1448
  56. Raux B, Voitovich Y, Derviaux C, Lugari A, Rebuffet E, Milhas S, Priet S, Roux T, Trinquet E, Guillemot JC, Knapp S, Brunel JM, Fedorov AY, Collette Y, Roche P, Betzi S, Combes S, Morelli X (2016) Exploring selective inhibition of the first bromodomain of the human bromodomain and extra-terminal domain (BET) proteins. *J Med Chem* 59(4):1634–1641
  57. Ouyang L, Zhang L, Liu J, Fu L, Yao D, Zhao Y, Zhang S, Wang G, He G, Liu B (2017) Discovery of a small-molecule bromodomain-containing protein 4 (BRD4) Inhibitor that induces AMP-activated protein kinase-modulated autophagy-associated cell death in breast cancer. *J Med Chem* 60(24):9990–10012

58. Gosmini R, Nguyen VL, Toum J, Simon C, Brusq JM, Krysa G, Mirguet O, Riou-Eymard AM, Boursier EV, Trottet L, Bamborough P, Clark H, Chung CW, Cutler L, Demont EH, Kaur R, Lewis AJ, Schilling MB, Soden PE, Taylor S, Walker AL, Walker MD, Prinjha RK, Nicodem E (2014) The discovery of I-BET726 (GSK1324726A), a potent tetrahydroquinoline ApoA1 up-regulator and selective BET bromodomain inhibitor. *J Med Chem* 57(19):8111–8131
59. Demont EH, Chung CW, Furze RC, Grandi P, Michon AM, Wellaway C, Barrett N, Bridges AM, Craggs PD, Diallo H, Dixon DP, Douault C, Emmons AJ, Jones EJ, Karamshi BV, Locke K, Mitchell DJ, Mouzon BH, Prinjha RK, Roberts AD, Sheppard RJ, Watson RJ, Bamborough P (2015) Fragment-based discovery of low-micromolar ATAD2 bromodomain inhibitors. *J Med Chem* 58(14):5649–5673
60. Bamborough P, Chung CW, Furze RC, Grandi P, Michon AM, Sheppard RJ, Barnett H, Diallo H, Dixon DP, Douault C, Jones EJ, Karamshi B, Mitchell DJ, Prinjha RK, Rau C, Watson RJ, Werner T, Demont EH (2015) Structure-based optimization of naphthyridones into potent ATAD2 bromodomain inhibitors. *J Med Chem* 58(15):6151–6178
61. B. R, Wang C (US9393232, 2017) Substituted 5-(3,5-dimethylisoxazol-4-yl)indoline-2-ones
62. Ozer HG, El-Gamal D, Powell B, Hing ZA, Blachly JS, Harrington B, Mitchell S, Grieselhuber NR, Williams K, Lai T-H, Alinari L, Baiocchi RA, Brinton L, Baskin E, Cannon M, Beaver L, Goettl VM, Lucas DM, Woyach JA, Sampath D, Lehman AM, Yu L, Zhang J, Ma Y, Zhang Y, Spevak W, Shi S, Severson P, Shelloe R, Carias H, Tsang G, Dong K, Ewing T, Marimuthu A, Tantoy C, Walters J, Sanftner L, Rezaei H, Nespi M, Matusow B, Habets G, Ibrahim P, Zhang C, Mathé EA, Bollag G, Byrd JC, Lapalombella R (2018) BRD4 profiling identifies critical chronic lymphocytic leukemia oncogenic circuits and reveals sensitivity to PLX51107, a novel structurally distinct BET inhibitor. *Cancer Discov*. <https://doi.org/10.1158/2159-8290.CD-1117-0902>
63. Gao N, Ren J, Hou L, Zhou Y, Xin L, Wang J, Yu H, Xie Y, Wang H (2016) Identification of novel potent human testis-specific and bromodomain-containing protein (BRDT) inhibitors using crystal structure-based virtual screening. *Int J Mol Med* 38(1):39–44
64. N-n Gao, Hou L, Zhou Y, Xin L, Yang D, Li N, Wang H (2016) Discovery of male anti-fertility inhibitors target BRDT through structure-based virtual screening. *Shengzhi Yixue Zazhi* 25(6):550–555
65. Ayoub AM, Hawk LML, Herzig RJ, Jiang J, Wisniewski AJ, Gee CT, Zhao P, Zhu J-Y, Berndt N, Offei-Addo NK, Scott TG, Qi J, Bradner JE, Ward TR, Schönbrunn E, Georg GI, Pomerantz WCK (2017) BET bromodomain inhibitors with one-step synthesis discovered from virtual screen. *J Med Chem* 60(12):4805–4817
66. Carlino L, Rastelli G (2016) Dual kinase-bromodomain inhibitors in anticancer drug discovery: a structural and pharmacological perspective. *J Med Chem* 59(20):9305–9320
67. Devaiah BN, Lewis BA, Cherman N, Hewitt MC, Albrecht BK, Robey PG, Ozato K, Sims RJ, Singer DS (2012) BRD4 is an atypical kinase that phosphorylates Serine2 of the RNA polymerase II carboxy-terminal domain. *PNAS* 109(18):6927–6932
68. Ember SWJ, Zhu J-Y, Olesen SH, Martin MP, Becker A, Berndt N, Georg GI, Schönbrunn E (2014) Acetyl-lysine binding site of bromodomain-containing protein 4 (BRD4) interacts with diverse kinase inhibitors. *ACS Chem Biol* 9(5):1160–1171
69. Ciceri P, Müller S, O'Mahony A, Fedorov O, Filippakopoulos P, Hunt JP, Lasater EA, Pallares G, Picaud S, Wells C, Martin S, Wodicka LM, Shah NP, Treiber DK, Knapp S (2014) Dual kinase-bromodomain inhibitors for rationally designed polypharmacology. *Nat Chem Biol* 10(4):305–312
70. Ember SW, Lambert QT, Berndt N, Gunawan S, Ayaz M, Tauro M, Zhu J-Y, Cranfill PJ, Greninger P, Lynch CC, Benes CH, Lawrence HR, Reuther GW, Lawrence NJ, Schönbrunn E (2017) Potent dual BET bromodomain-kinase inhibitors as value-added multitargeted chemical probes and cancer therapeutics. *Mol Cancer Ther* 16(6):1054–1067
71. Waring MJ, Chen H, Rabow AA, Walker G, Bobby R (2016) Potent and selective bivalent inhibitors of BET bromodomains. *Nat Chem Biol* 12(12):1097–1104

72. Lu J, Qian Y, Altieri M, Dong H, Wang J, Raina K, Hines J, Winkler JD, Crew AP, Coleman K, Crews CM (2015) Hijacking the E3 ubiquitin ligase cereblon to efficiently target BRD4. *Chem Biol* 22(6):755–763
73. Winter GE, Buckley DL, Paulk J, Roberts JM, Souza A, Dhe-Paganon S, Bradner JE (2015) Phthalimide conjugation as a strategy for in vivo target protein degradation. *Science* 348(6241):1376–1381
74. Zhou B, Hu J, Xu F, Chen Z, Bai L, Fernandez-Salas E, Lin M, Liu L, Yang C-Y, Zhao Y, McEachern D, Przybranowski S, Wen B, Sun D, Wang S (2017) Discovery of a small-molecule degrader of bromodomain and extra-terminal (BET) proteins with picomolar cellular potencies and capable of achieving tumor regression. *J Med Chem* 61(2):462–481
75. Wurz RP, Dellamaggiore K, Dou H, Javier N, Lo M-C, McCarter JD, Mohl D, Sastri C, Lipford JR, Cee VJ (2017) A “click chemistry platform” for the rapid synthesis of bispecific molecules for inducing protein degradation. *J Med Chem*. <https://doi.org/10.1021/acs.jmedchem.1026b01781>
76. Kharenko OA, Hansen HC (2017) Novel approaches to targeting BRD4. *Drug Discov Today Technol* 24:19–24
77. Churcher I (2017) PROTAC-induced protein degradations in drug discovery: breaking the rules or just making new ones? *J Med Chem* 61(2):444–452
78. Gadd MS, Testa A, Lucas X, Chan K-H, Chen W, Lamont DJ, Zengerle M, Ciulli A (2017) Structural basis of PROTAC cooperative recognition for selective protein degradation. *Nat Chem Biol* 13:514
79. Crawford TD, Tsui V, Flynn EM, Wang S, Taylor AM, Côté A, Audia JE, Beresini MH, Burdick DJ, Cummings R, Dakin LA, Duplessis M, Good AC, Hewitt MC, Huang H-R, Jayaram H, Kiefer JR, Jiang Y, Murray J, Nasveschuk CG, Pardo E, Poy F, Romero FA, Tang Y, Wang J, Xu Z, Zawadzke LE, Zhu X, Albrecht BK, Magnuson SR, Bellon S, Cochran AG (2016) Diving into the water: Inducible binding conformations for BRD4, TAF1 (2), BRD9, and CECR2 bromodomains. *J Med Chem* 59(11):5391–5402
80. Wu P, Clausen MH, Nielsen TE (2015) Allosteric small-molecule kinase inhibitors. *Pharmacol Ther* 156:59–68

# Chapter 12

## Targeting Protein-Protein Interactions in Small GTPases



Jiahui Liu, Ning Kang, Yaxue Zhao and Mingyan Zhu

Protein-protein interactions (PPIs) are significant in all biological processes including cell growth, survival, and differentiation, while they are often dysregulated in pathological states. PPIs are attractive targets for the development of therapeutics, and it is important to discover or design small molecules which regulate the PPIs (Fig. 12.1). However, PPIs are once considered as undruggable targets because of the following reasons: First, the PPI interfaces are much larger than the small and deep pockets in enzymes or receptors. Jones and Thornton found that the protein-protein interface varies widely from 368 to 4746 Å² in the homodimers and 639 to 3228 Å² in the heterocomplexes by analysis of 59 protein complexes [1]. Smith and Gestwicki found protein-protein interface varies between 1000 and 5850 Å² by measurement of the buried surface area for which inhibitors have been discovered [2]. In contrast, the pockets on enzymes or receptors, which typical for small molecules binding, vary from 300 to 500 Å² [3]. Second, PPIs lack typical binding pocket, and the PPI interface is often a flat and featureless region instead of a well-defined pocket. Third, the current collection of small molecule compound libraries and databases are often specific to deep and small binding pockets on proteins but few targeted to PPIs.

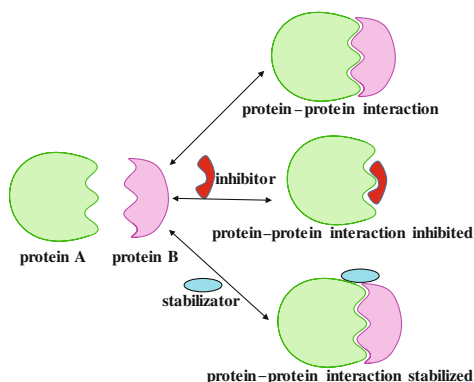
### 12.1 Critical Residues of PPI Interface

Although it has seemed to be challenging to target the generally large and flat PPI interfaces, recent progress in targeting PPIs has been achieved through a combination of high-resolution structure analysis and identification of critical residues at

---

J. Liu · N. Kang · Y. Zhao · M. Zhu (✉)  
School of Pharmacy, Shanghai Jiao Tong University, Shanghai 200240, People's  
Republic of China  
e-mail: myzhu@sjtu.edu.cn

**Fig. 12.1** Illustration of protein-protein interactions and their inhibitors/stabilizers



the PPI interfaces. Mutational analysis showed that not all residues at the PPI interface are critical for protein-protein complex formation. The energetically essential residues for protein-protein complex formation usually locate near the center of the protein-protein interfaces [4]. Alanine scanning mutagenesis offers an effective approach for identification of critical residues: Residues whose substitution with alanine leads to a decrease in binding energy by  $\Delta\Delta G$  more than 1.0 kcal/mol are considered important contributors [5]. For example, Clackson and Wells determined the critical residues at the binding interface of human growth hormone (hGH) and its first bound receptor (hGHbp) through mutation of each of these residues individually to alanine: There are 11 out of 33 buried hGHbp residues whose mutation leads to more than 1.0 kcal/mol binding energy decrease; 8 out of the 31 buried hGH residues account for approximately 85% of binding energy [6]. Computational methods such as molecular mechanics–Poisson–Boltzmann surface area (MM-PBSA) and molecular mechanics–generalized Born surface area (MM-GBSA) have been successfully used in the prediction of critical residues in the protein-protein interface [7] and gained attentions because of their low cost. Identification of the critical residues at protein-protein interfaces provides a powerful starting point for targeting PPIs.

In recent decades, with the advances in proteomics, computational chemistry, and ligand designs, targeting PPIs have drawn more attentions in research and development for novel drugs and several achievements have been made. For example, inhibitors which target X-linked inhibitor of apoptosis protein (XIAP)/Smac, murine double minute 2 (MDM2)/p53, bromodomain/histone, HIV1 integrase/lens endothelial growth factor (LEDGF) are now in clinical trials to treat pathologies from cancer to inflammation and HIV infection [3].

## 12.2 Inhibition Mechanisms of Small Molecules on PPIs

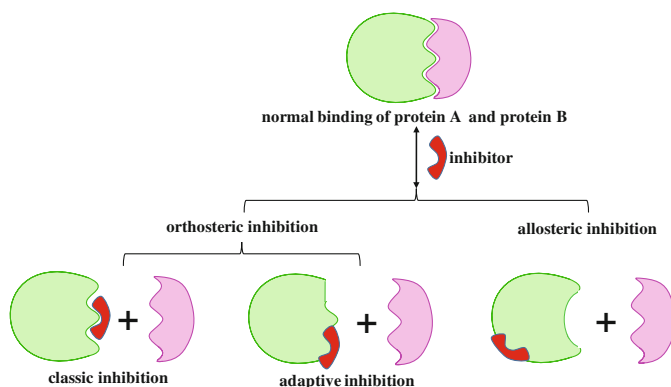
There are several different inhibition mechanisms of small molecules on PPIs (Fig. 12.2). The orthosteric inhibitor can either directly bind to the protein-protein interface of one protein or can take advantage of an adaptive protein interface to

stabilize a protein conformer to inhibit PPIs. The allosteric inhibitor binds a site distal from the PPI interface, leads to structural rearrangement in the target protein, and ultimately inhibits the formation of protein-protein complexes [8].

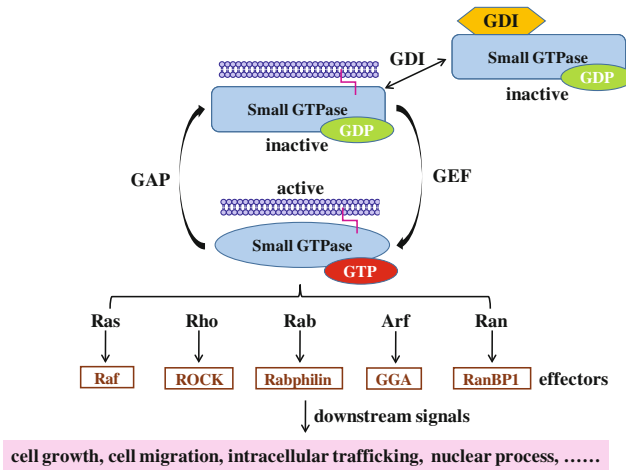
### 12.3 PPIs in Signal Transduction of Small GTPase

As an example, small GTPases (small guanine nucleotide-binding proteins, approximately 21 kDa) are very rich in PPIs in their signal transduction pathways. Small GTPases are a family of guanosine triphosphate (GTP)/guanosine diphosphate (GDP) binding proteins, basically function as hydrolase enzymes to bind to and hydrolyze GTP to GDP. They behave as molecular switches for signal transduction from external stimuli to control a variety of essential cellular processes which is critical in a variety of physiological or disease states [9]. So as a case study of modulators of PPIs, GTPase has attracted broad interests.

Regulation of small GTPase activities depends on PPIs, and small GTPases are cycled between an active conformation (GTP-bound) and an inactive conformation (GDP-bound) (Fig. 12.3). There are three regulators in the small GTPase activation–inactivation cycle: guanine nucleotide exchange factors (GEFs), GTPase activating proteins (GAPs), and guanine nucleotide dissociation inhibitors (GDIs). The binding of GEFs to small GTPases catalyzes the dissociation of GDP to allow the binding of GTP [10]. The GAPs deactivate small GTPases by binding with small GTPases and enhancing their ability to hydrolyze the bound GTP to GDP [11]. They are important in the maintenance of an appropriate basal level of small GTPases activity. The GDIs are named due to their ability to inhibit the dissociation of bound GDP from their partner GTPases. They clamp the inactive GDP bound conformation of small GTPase to prevent GDP-GTP exchange [12].



**Fig. 12.2** Mechanisms of small molecule inhibition of PPIs



**Fig. 12.3** Regulation and signal transduction pathways of small GTPases

Once activated, small GTPases interact with a variety of downstream effector proteins and activate them.

Signal transduction of small GTPases also involves many PPIs. There are five subfamilies of small GTPases (Ras, Rho, Rab, Arf, Ran), and they have various downstream effectors to control highly diverse cellular roles. The Ras GTPases have at least 11 catalytically diverse downstream effector families, which ultimately turn on genes involved in cell growth, differentiation, and survival. Among them, the RAF-MEK-ERK and PI3K-AKT-mTOR pathways whose alteration is highly related to human cancer have attracted the greatest attentions [13]. The Rho GTPases have more than 60 known downstream effectors including Rho-associated protein kinase (ROCK) and Wiskott–Aldrich syndrome protein (WASP), which play essential roles in the regulation of cell shape changes, cytokinesis, cell adhesion, and cell migration [14]. The Rab GTPases which contains approximately 60 members regulate intracellular trafficking through various effector proteins such as Rabphilin and Rabenosyn5 [15]. The Arf GTPases consist of about 30 members. They also regulate intracellular trafficking through effectors including Golgi-localized, gamma-ear-containing, ARF-binding (GGA) proteins and binder of ARL2 (BART) [16]. Ran has been implicated in a variety of nuclear processes, including the maintenance of nuclear structure, protein import, mRNA processing and export, and cell cycle regulation through various downstream effectors such as RanBP1 and RanBP2 [17].

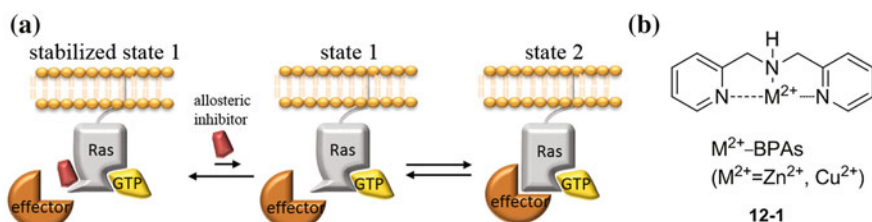
Small GTPases achieve their functions through huge PPI networks including their cycling regulators and the numerous downstream effector proteins. Targeting PPIs of small GTPases provided a promising strategy to the effective regulation of their function and the development of new drugs for related diseases. We would illustrate the progress of targeting PPIs in small GTPase with several different methods through examples from recent five years in this field.

## 12.4 Examples of Inhibitors of PPIs of Small GTPase

### 12.4.1 Allosteric Inhibitor of Ras and Raf-RBD

In 2012, Kalbitzer and coworkers reported Ras–effector binding inhibitors which targeted the low effector-binding conformational state of the activated Ras [18]. GTP-bound Ras exists in two conformational states (Fig. 12.4a), state 1 is a weak effector-binding conformational state of Ras and has about two orders of magnitude lower affinity for effectors than state 2. Two states are in dynamic equilibrium, interconvert on millisecond timescale, and  $^{31}\text{P}$  NMR can be used to identify the two distinct conformational states of Ras. In state 1, Ras reveals a unique surface pocket since the region around the  $\gamma$ -phosphate is accessible, which can be explored for Ras inhibitors. Metal(II)–bis(2-picolyl)amines ( $\text{M}^{2+}$ –BPAs, Fig. 12.4b) were identified as state 1 stabilizer with millimolar binding affinity, which could disrupt PPI between Ras and effector and could prevent Ras transform to state 2.

$\text{M}^{2+}$ –BPAs (**12-1**) were allosteric inhibitors and bound outside of nucleotide binding cleft in state 1 of Ras.  $^{31}\text{P}$  NMR illustrated that presence of  $\text{M}^{2+}$ –BPAs did not change the chemical shift of phosphate in GppNHP, suggesting  $\text{M}^{2+}$ –BPAs did not interact with nucleotide binding pocket. To define binding site of  $\text{M}^{2+}$ –BPAs,  $[^1\text{H}, ^{15}\text{N}]$  HSQC and NOE spectra of Ras-(T35A)- $\text{Mg}^{2+}$ -GppNHP with  $\text{Cu}^{2+}$ –BPA and  $\text{Zn}^{2+}$ –BPA were measured. Asp38, Ser39, Tyr40, Ile163, Gln165, and His166 showed the largest chemical shift changes. These residues could be divided into two binding sites on Ras, site 2 with residues 163, 165, 166 was near the C-terminal of Ras, which did not stabilize state 1. Site 1 with residues 38–40 was located near the active center, which was related to the stabilization of state 1. Interestingly, the site 1 was not in proximity to nucleotide binding pocket, showing  $\text{M}^{2+}$ –BPAs bound allosterically to state 1. These organometallic complexes provide a proof-of-concept of targeting the dynamic conformational states of small GTPase, as the equilibrium of different conformational states also exist in other small GTPases [19].

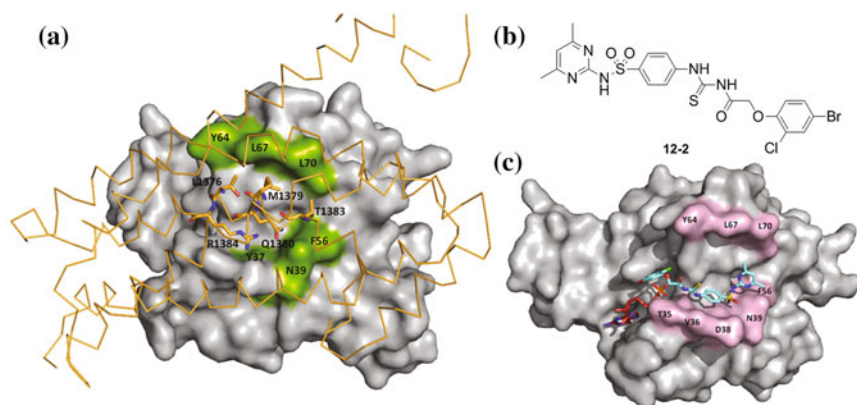


**Fig. 12.4** Allosteric inhibitor of Ras–effector binding and mechanism for inhibition of Ras–effector binding. **a** State 1 is formed after nucleotide exchange reaction, and in a dynamic equilibrium with state 2, state 2 is accessible for effector. Inhibitor stabilized the state 1 and reduced the affinity of Ras to effector, **b** chemical structure of  $\text{M}^{2+}$ –BPAs. Reprinted from Ref. [19], Copyright 2012, with permission from John Wiley & Sons, Inc.



### 12.4.2 Inhibition of Cdc42 Bioactivity by Disruption of Cdc42–ITSN Interactions

Cell division control protein 42 homolog (Cdc42), a Rho-family GTPase, regulates diverse cellular functions including cell morphology, migration, and cell cycle progression and has also been shown to be involved in cancer cell metastasis and transformation. In 2013, Zhou and Lu reported small molecule targeting Cdc42–GEF interaction [20]. Intersectin (ITSN) is a specific GEF for Cdc42, which accelerates GDP release and prompts GTP binding to Cdc42, ITSN interacted with Cdc42 at a large interface (PDB ID: 1KI1). After analysis of key residues of Cdc42–ITSN interaction, a main binding region was revealed (Fig. 12.5a). Through virtual screen from 197,000 compounds, ZCL278 (**12-2**) was identified as a Cdc42 inhibitor (Fig. 12.5b). ZCL278 showed micromolar binding affinity with Cdc42 in fluorescence titration ( $K_d = 6.4 \mu\text{M}$ ) and surface plasma resonance (SPR) measurements ( $K_d = 11.4 \mu\text{M}$ ). It disrupted Cdc42-mediated microspike formation in fibroblastic cell, disrupted Cdc42 perinuclear distribution, and GM130 docked Golgi organization. The results of wound healing assay and trypan blue dye exclusion assay demonstrated that ZCL278 inhibited Cdc42-dependent cell motility without affecting cell viability. ZCL278 also showed efficacy on neuronal cell, treatment of ZCL278 to cortical neuronal growth cone lead to retraction of microspikes or filopodia.

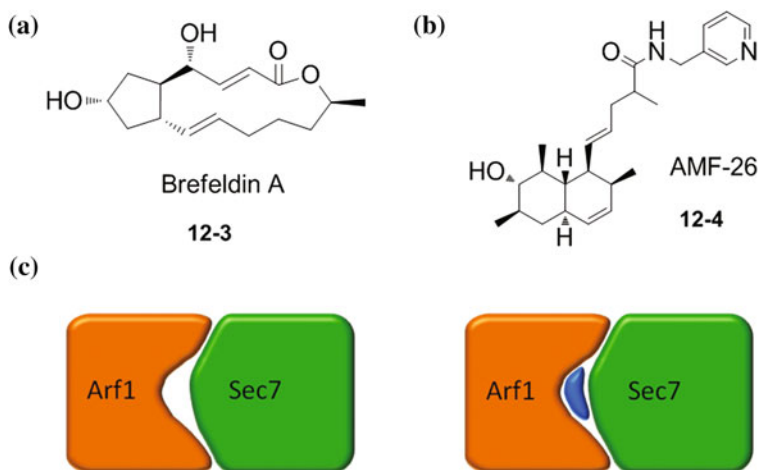


**Fig. 12.5** Structure of Cdc42 (gray) and ITSN (yellow) and ZCL278 (blue) binding to Cdc42 with GDP (red). **a** Cdc42 and ITSN complex (PDB ID: 1KI1), hydrogen bonds formed between residues Gln1380, Arg1384 of ITSN and Asn39, Phe37 of Cdc42, hydrophobic interactions formed between residues Leu1376, Met1379, Thr1383 of ITSN and Phe56, Tyr64, Leu67, Leu70 of Cdc42 (residues shown as sticks on ITSN and colored in green on Cdc42), **b** chemical structure of ZCL278 (**12-2**), **c** binding pocket of ZCL278 on Cdc42 is a groove, outside the nucleotide binding site surrounded by residues shown in pink. Adapted from Ref. [20], with permission from National Academy of Sciences

Binding conformation of ZCL278 in Cdc42 was simulated through docking, which showed ZCL278 lied in a groove at protein-protein interface of Cdc42–ITSN outside the nucleotide binding site of Cdc42 (Fig. 12.5c). Since the wide functions and high affinity to Cdc42, ZCL278 will be a promising lead compound for metastasis inhibition.

### 12.4.3 Stabilizer of Arf1–ARNO

ADP-ribosylation factor 1 (Arf1) is localized in Golgi apparatus and plays a key role in vesicle transport and cargo selection. Arf1 is activated by Sec7 domain of GEF that catalyzes nucleotide exchange [21]. The first small molecule inhibitor targeting PPI of Arf–ArfGEF is brefeldin A (BFA, 12-3), which stabilized the complex of Arf1–GEF, but due to poor bioavailability and cytotoxicity, BFA failed at pre-clinical stage of drug development. In 2012, Yamori and coworkers reported a novel small molecule AMF-26 (12-4), as Golgi inhibitor and showing anti-cancer activity [22]. The structure of AMF-26 was quite different from BFA (Fig. 12.6a and Fig. 12.6b), but it also worked as a Arf1–GEF stabilizer. The molecule was discovered through bioinformatics approach, which compared the growth inhibition patterns of 4000 test compounds on JFCR39 (a panel of 39 cell lines) with anti-cancer drugs and inhibitors in database by a COMPARE algorithm, AMF-26 showed the highest correlation to BFA in the COMPARE analysis. AMF-26 could induce Golgi disruption reversibly and decrease the signals of endogenous pan-Arf-GTP in human cells, which was same as BFA. Molecular dynamics



**Fig. 12.6** Brefeldin A and AMF-26, and schematic mechanism of inhibition. **a, b** Chemical structure of Brefeldin A and AMF-26, **c** AMF-26 or Brefeldin A (blue) stabilized the complex of Arf1 (orange) with Sec7 domain (green) of its GEF

(MD) simulation on complex of Arf1–AMF-26–Sec7 starting with structure of Arf1–BFA–Sec7 (PDB: 1R8Q) showed that AMF-26 bound to the same pocket of BFA and interacted with surrounding hydrophobic residues. The Arg19 in Arf1 formed a hydrogen bond with the hydroxyl oxygen of AMF-26 and the carbonyl oxygen of BFA, respectively. Besides the inhibition against JFCR39 cell lines in vitro, AMF-26 also showed in vivo anti-tumor activity with inhibition of tumor growth of BSY-1 (human breast cancer cell line) xenografts via oral administration in mice.

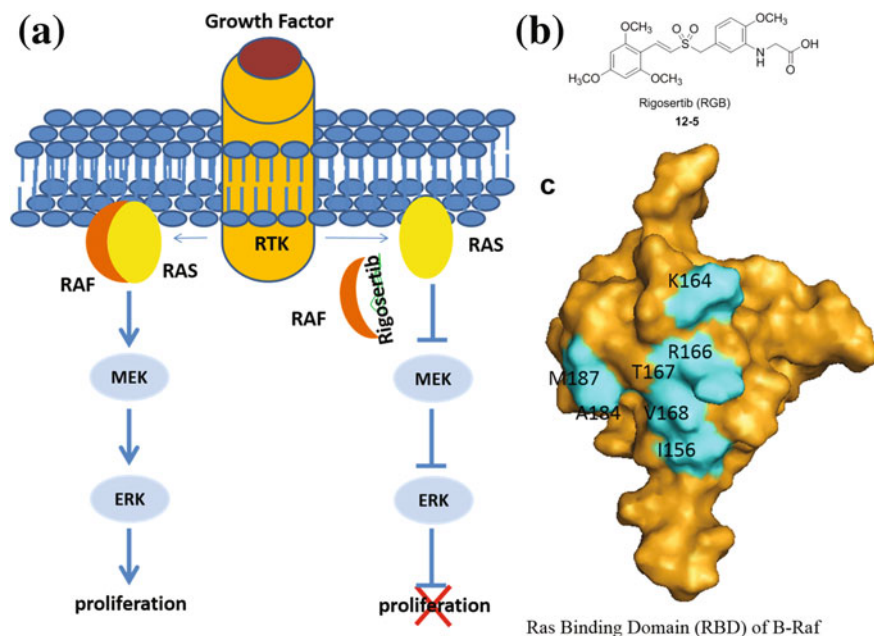
#### 12.4.4 Inhibitor of RAS–RBDs

In 2016, Reddy and coworkers reported that rigosertib (RGS, **12-5**), a benzyl styryl sulfone, which is in phase III clinical trials for the treatment of myelodysplastic syndrome (MDS), was the first small molecule inhibitor targeting the interactions between RAS and RAS binding domains (RBDs) of RAS effectors [23]. Oncogenic RAS serves to activate and mediate the signal pathways related to cell survival, metastasis and apoptosis in oncogenesis via the binding of its switch I and switch II domains to RBD, which is a relatively conserved-structured motif shared by RAS effectors such as RAF proteins, RalGDS and PI3 kinases. Rigosertib could bind to RBDs of c-RAF and B-RAF with a considerable affinity, whose  $K_d$  obtained from microscale thermophoresis (MST) is 0.18 nM and 0.71 nM, respectively. It served as a mimicry of RAS, precluding its interaction with RAF RBDs, thereby blocked the RAS-RAF-MEK-ERK signal pathway (Fig. 12.7a).

The NMR data of the solution structures of B-RAF RBD and B-RAF RBD:RGS complex implied the mode of the rigosertib–RBDs interaction. HSQC showed that rigosertib mainly bound to the  $\beta_1$ ,  $\beta_2$  strands and  $\alpha_1$  helix of RBD, where residues I156, K164, R166, T167, V168, A184, and M187 contributed largely to binding (Fig. 12.7c). Since the residues above are conserved within RAF RBDs, c-RAF and A-RAF probably share the same binding details. The NOE spectra revealed that rigosertib bound to B-RAF RBD in two different orientations evenly but in the same interface, having the same occluding effect. RAS downstream effectors have similar tertiary ubiquitin-like structure of RBDs, which facilitates the effective binding of rigosertib to other effectors including RalGDS and some of PI3 kinases. That indicates the potential of rigosertib to inhibit multiple RAS driven pathways and that explains why rigosertib showed great inhibitory activities on tumor, like pancreatic, colorectal, and lung cancers.

#### 12.4.5 Stapled Peptide as Inhibitor of Ral

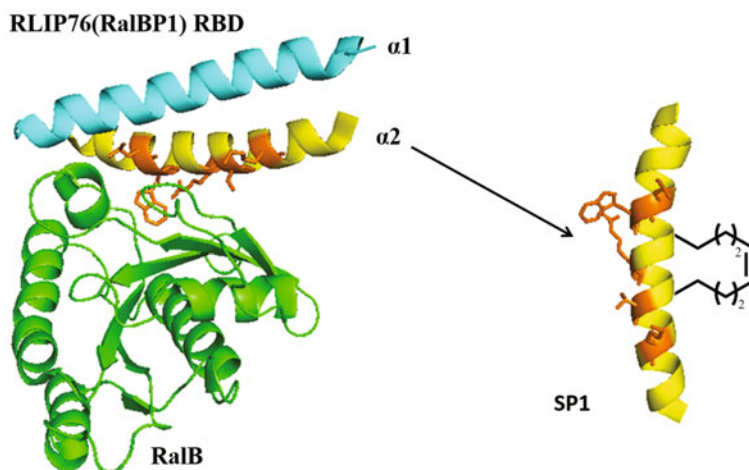
Progress in inhibitor development targeting the RAS downstream signal protein Ral was reported in 2016 by Mott and coworkers. They discovered a stapled peptide could selectively bind to Ral protein, in GTP-bound state [24]. The aberrant



**Fig. 12.7** **a** Binding of rigosertib to RAF blocked RAF association with RAS and impaired the RAS-RAF-MEK-ERK signal pathway, **b** chemical structure of the rigosertib, **c** crystal structure of Ras Binding Domain (RBD) of B-Raf (PDB ID: 5J17), the residues critical for rigosertib binding is colored in cyan. Reprinted from Ref. [23], Copyright 2016, with permission from Elsevier

activation of RalA and RalB has been proven to be critical impetus of oncogenesis such as the development of bladder, melanoma, colorectal, and pancreatic cancer. The downstream effectors of RalA and RalB include RLIP76 (or RalBP1), the exocyst complex subunits Sec5 and Exo84, and the transcription factor ZO-1-associated nucleic acid-binding protein (ZONAB).

Solution structure of RalB in complex with the RLIP76 showed that the Ral binding domain of RLIP76 (RLIP76 RBD) employed a coiled-coil motif, which consisted of two  $\alpha$  helices, to bind to Ral (Fig. 12.8). The helices did not undergo significant conformational changes upon binding to the Ral protein. Inspired by the rigid structure of the motif, an idea of developing stapled peptide simulating such helices was brought up. By synthesizing peptides of full-length  $\alpha 2$  helix and the remaining residues of RLIP76 RBD and testing their binding affinity to RalB using isothermal titration calorimetry (ITC), they proved that the  $\alpha 2$  helix contributed predominantly and overwhelmingly to the Ral-RBD binding, which is in accordance with the analysis result of the solution structure above. NMR experiments were used to prove that the single  $\alpha 2$  peptide bound to the Ral proteins in the same manner as RLIP76 RBD. And then the strategy of stapled peptide was adopted to improve the binding affinity. Alanine scanning mutagenesis data revealed that L429, W430, R434, T437, and K440 of helix  $\alpha 2$  are key residues for binding to the



**Fig. 12.8** RalB in complex with RLIP76 (RalBP1) (PDB ID: 2KWI) and the structure of stapled peptide. RalB is colored green, Ral binding domain of RLIP76 (RLIP76 RBD) is shown as follows: the N-terminal helix  $\alpha 1$  is colored cyan, the C-terminal helix  $\alpha 2$  is colored yellow, the side chains of residues whose mutation reduced the binding to RalB more than fivefold are colored orange. The stapled peptide based on  $\alpha 2$  was named SP1. Reprinted with the permission from Ref. [24]. Copyright 2016, by the American Society for Biochemistry and Molecular Biology

switch regions of Ral (Fig. 12.8); therefore, two residues less important for binding were mutated to form the staple. In ITC measurement, the affinity of stapled peptide, SP1 (Fig. 12.8), was proven to be increased, with  $K_d$  value of 4.7  $\mu\text{M}$ , compared with 30  $\mu\text{M}$  of the unstapled one. Subsequent fluorescence polarization (FP) assays indicated that SP1 bound preferentially to the GTP-bound Ral over the GDP-bound one.

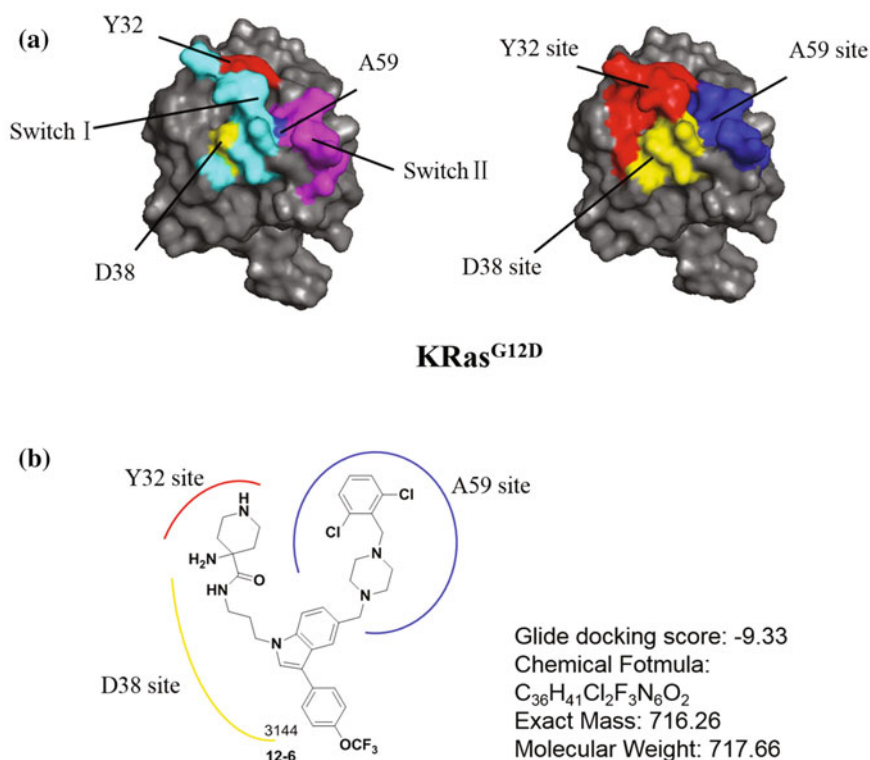
While RalA and RalB are 82% identical in full sequence, and 100% identical in switch I and switch II, SP1 based on the structure of RalB-RLIP76 RBD could bind to both RalA and RalB effectively, but with a slightly higher affinity for RalB. The SP1 could enter mammalian cells with a cellular lifetime of more than 16 h, which was proven by the cellular uptake assays. Moreover, because of the overlap of binding sites among Ral effectors, SP1 could compete with RLIP76, Sec5, and Exo84 upon binding to Ral, showing that it blocked RalB pathways by function as a pan RalB-effector complex inhibitor with micromolar activity.

#### 12.4.6 RAS Inhibitors Discovered by Fragment-Based Screening

Although structure-based molecule design seems to be more challenging when applied to small GTPase, some individual shallow sites on RAS proteins have been

found through fragment-based screening. Stockwell and his coworkers were motivated by such previous efforts and reported in 2017, that compound 3144 (**12-6**) which consist of three fragments bound to disparate sites lead to higher selectivity and affinity to KRAS [25]. Mutagenesis was performed to reveal that the mutation of certain residues (I36-S39 in switch I) can result in weaker interaction between KRAS^{G12D} and its primary effectors, like RAF, PI3K, and RALGDS. Three adjacent sites that are critical for binding were chosen, one site centered on D38 in switch I region, one centered on A59 between switch I and switch II, and one centered on Y32 on the other side of D38, as potential binding pockets (Fig. 12.9a).

Virtual screening of fragments and molecules that were designed for targeting one or more of the three sites was done. Compound 3144 was selected as the most promising inhibitor with high docking scores and acceptable predicted physiochemical properties. Although its molecular weight and the predicted logP were large, other properties were suitable. The low docking scores of 3144 into analogous sites of other proteins belonging to RAS superfamily also assured its good selectivity. MST, ITC,



**Fig. 12.9** **a** Crystal structure of KRAS^{G12D} (PDB ID: 4DSN), switch I is shown in cyan and switch II is shown in magenta, residues chosen for site identification are highlighted in red, yellow, and blue colors, while the binding sites centered on the three residues are shown the same color, **b** chemical structure, docking score, chemical formula, mass, and molecular weight of the small molecule 3144. Reprinted from Ref. [25], Copyright 2017, with permission from Elsevier

NMR, and mutagenesis assays indicated that the mechanism of 3144 binding to KRAS^{G12D} is just as designed (Fig. 12.9b). The lethality of 3144 in different cell lines varied a lot, partially dependent on RAS expression. Although the toxicity, low solubility, and off-target activity of 3144 in vitro, it was proven to inhibit tumor growth and RAS signaling pathways in mouse cancer models, cells, and mice results implied the big room for modification to develop a more promising RAS inhibitor.

## 12.5 Conclusion

Small GTPases control various cellular processes which contains many challenging and interesting targets in drug development. The complex and dynamic interaction network for small GTPase provides us with rich PPIs which is a valuable source for investigation. Importantly, PPIs can be useful for targeting “undruggable” proteins since protein complex might offer additional pockets for binding [9]. The main success of targeting PPIs in small GTPase includes, such as examples shown in this chapter, inhibition of small GTPase-GEF interactions, inhibition of small GTPase–effector interactions, and stabilization of small GTPase–protein complexes. For the large family numbers of small GTPase, targeting PPIs could modulate activities of small GTPases effectively and selectively. The outcome of this field keeps growing with the application of various strategies such as structure-guided and fragment-based approaches, stabilized peptide structures and transition state stabilization methods. Although small GTPase are very challenging as drug target and up to now no clinically relevant inhibitor of small GTPase has been discovered, as the development of crystal structures, screen and computational approaches and our understanding of context of PPIs in small GTPase, novel PPIs of small GTPases could be identified and more modulators for PPIs could be discovered which could be utilized in the research of small GTPase and could promote progress for drug discovery for small GTPases.

## References

1. Jones S, Thornton JM (1996) Principles of protein-protein interactions. *Proc Natl Acad Sci* 93 (1):13–20
2. Smith MC, Gestwicki JE (2012) Features of protein-protein interactions that translate into potent inhibitors: topology, surface area and affinity. *Expert Rev Mol Med* 14:e16
3. Arkin MR, Tang Y, Wells JA (2014) Small-molecule inhibitors of protein-protein interactions: progressing toward the reality. *Chem Biol* 21(9):1102–1114
4. (a) Bogan AA, Thorn KS (1998) Anatomy of hot spots in protein interfaces. *J Mol Biol* 280 (1):1–9; (b) Guo W, Wisniewski JA, Ji H (2014) Hot spot-based design of small-molecule inhibitors for protein-protein interactions. *Bioorg Med Chem Lett* 24(11):2546–2554
5. Modell AE, Blosser SL, Arora PS (2016) Systematic targeting of protein-protein interactions. *Trends Pharmacol Sci* 37(8):702–713



6. Clackson T, Wells JA (1995) A hot spot of binding energy in a hormone-receptor interface. *Science* 267(5196):383–386
7. (a) Gohlke H, Kiel C, Case DA (2003) Insights into protein–protein binding by binding free energy calculation and free energy decomposition for the Ras-Raf and Ras-RalGDS complexes. *J Mol Biol* 330(4):891–913; (b) Zhao Y, Li W, Zeng J, Liu G, Tang Y (2008) Insights into the interactions between HIV-1 integrase and human LEDGF/p 75 by molecular dynamics simulation and free energy calculation. *Proteins: Struct Funct Bioinform* 72(2): 635–645
8. Cesa LC, Mapp AK, Gestwicki JE (2015) Direct and propagated effects of small molecules on protein–protein interaction networks. *Front Bioeng Biotechnol* 3
9. Cromm PM, Spiegel J, Grossmann TN, Waldmann H (2015) Direct modulation of small GTPase activity and function. *Angew Chem Int Ed* 54(46):13516–13537
10. Cherfils J, Chardin P (1999) GEFs: structural basis for their activation of small GTP-binding proteins. *Trends Biochem Sci* 24(8):306–311
11. Tcherkezian J, Lamarche-Vane N (2007) Current knowledge of the large RhoGAP family of proteins. *Biol Cell* 99(2):67–86
12. DerMardirossian C, Bokoch GM (2005) GDIs: central regulatory molecules in Rho GTPase activation. *Trends Cell Biol* 15(7):356–363
13. Papke B, Der CJ (2017) Drugging RAS: know the enemy. *Science* 355(6330):1158–1163
14. Lu Q, Longo FM, Zhou H, Massa SM, Chen YH (2009) Signaling through Rho GTPase pathway as viable drug target. *Curr Med Chem* 16(11):1355–1365
15. Hutagalung AH, Novick PJ (2011) Role of Rab GTPases in membrane traffic and cell physiology. *Physiol Rev* 91(1):119–149
16. Khan AR, Ménétrey J (2013) Structural biology of Arf and Rab GTPases’ effector recruitment and specificity. *Structure* 21(8):1284–1297
17. Avis JM, Clarke PR (1996) Ran, a GTPase involved in nuclear processes: its regulators and effectors. *J Cell Sci* 109(10):2423–2427
18. Spoerner M, Hozsa C, Poetzl JA et al (2010) Conformational states of human rat sarcoma (RAS) protein complexed with its natural ligand GTP and their role for effector interaction and GTP hydrolysis. *J Biol Chem* 285(51):39768–39778
19. Rosnizeck IC, Spoerner M, Harsch T et al (2012) Metal-bis(2-picolyl)amine complexes as state 1(T) inhibitors of activated Ras protein. *Angew Chem Int Ed* 51(42):10647–10651
20. Friesland A, Zhao Y, Chen YH, Wang L, Zhou H, Lu Q (2013) Small molecule targeting Cdc42-intersectin interaction disrupts Golgi organization and suppresses cell motility. *Proc Natl Acad Sci* 110(4):1261–1266
21. Dell’Angelica EC, Puertollano R, Mullins C, Hartnell LM et al (2000) GGas a family of ADP ribosylation factor-binding proteins related to adaptors and associated with the Golgi complex. *J Cell Biol* 149(1):81–94
22. Ohashi Y, Iijima H, Yamaotsu N, Yamazaki K, Sato S, Okamura M, Yamori T et al (2012) AMF-26, a novel inhibitor of the Golgi system, targeting ADP-ribosylation factor 1 (Arf1) with potential for cancer therapy. *J Biol Chem* 287(6):3885–3897
23. Athuluri-Divakar SK, Vasquez-Del Carpio R, Dutta K, Baker SJ, Cosenza SC, Basu I, Gupta YK, Reddy MVR, Ueno L, Hart JR, Vogt PK, Mulholland D, Guha C, Aggarwal AK, Reddy EP (2016) A small molecule RAS-mimetic disrupts RAS association with effector proteins to block signaling. *Cell* 165(3):643–655
24. Thomas JC, Cooper JM, Clayton NS, Wang C, White MA, Abell C, Owen D, Mott HR (2016) Inhibition of Ral GTPases using a stapled peptide approach. *J Biol Chem* 291(35): 18310–18325
25. Welsch ME, Kaplan A, Chambers JM, Stokes ME, Bos PH, Zask A, Zhang Y, Martin MS, Badgley MA, Huang CS, Tran TH, Akkiraju H, Brown LM, Nandakumar Renu, Cremers S, Yang WS, Tong L, Olive KP, Ferrando A, Stockwell BR (2017) Multivalent small-molecule pan-RAS inhibitors. *Cell* 168(5):878–889